

Geothermal Well Test Analysis

Geothermal Well Test Analysis

Fundamentals, Applications and
Advanced Techniques

SADIQ J. ZARROUK

Senior Lecturer of Geothermal Engineering, Department of
Engineering Science, The University of Auckland, New Zealand

KATIE MCLEAN

Geothermal Reservoir Engineer, Contact Energy Ltd., New Zealand



ACADEMIC PRESS

An imprint of Elsevier

Academic Press is an imprint of Elsevier
125 London Wall, London EC2Y 5AS, United Kingdom
525 B Street, Suite 1650, San Diego, CA 92101, United States
50 Hampshire Street, 5th Floor, Cambridge, MA 02139, United States
The Boulevard, Langford Lane, Kidlington, Oxford OX5 1GB, United Kingdom

Copyright © 2019 Elsevier Inc. All rights reserved.

No part of this publication may be reproduced or transmitted in any form or by any means, electronic or mechanical, including photocopying, recording, or any information storage and retrieval system, without permission in writing from the publisher. Details on how to seek permission, further information about the Publisher's permissions policies and our arrangements with organizations such as the Copyright Clearance Center and the Copyright Licensing Agency, can be found at our website: www.elsevier.com/permissions.

This book and the individual contributions contained in it are protected under copyright by the Publisher (other than as may be noted herein).

Notices

Knowledge and best practice in this field are constantly changing. As new research and experience broaden our understanding, changes in research methods, professional practices, or medical treatment may become necessary.

Practitioners and researchers must always rely on their own experience and knowledge in evaluating and using any information, methods, compounds, or experiments described herein. In using such information or methods they should be mindful of their own safety and the safety of others, including parties for whom they have a professional responsibility.

To the fullest extent of the law, neither the Publisher nor the authors, contributors, or editors, assume any liability for any injury and/or damage to persons or property as a matter of products liability, negligence or otherwise, or from any use or operation of any methods, products, instructions, or ideas contained in the material herein.

British Library Cataloguing-in-Publication Data

A catalogue record for this book is available from the British Library

Library of Congress Cataloging-in-Publication Data

A catalog record for this book is available from the Library of Congress

ISBN: 978-0-12-819266-5

For Information on all Academic Press publications
visit our website at <https://www.elsevier.com/books-and-journals>

Publisher: Katie Hammon
Acquisition Editor: Raquel Zanol
Editorial Project Manager: Peter Adamson
Production Project Manager: Nirmala Arumugam
Cover Designer: Mark Rogers

Typeset by MPS Limited, Chennai, India



About the authors

Dr. Sadiq J. Zarrouk

Senior lecturer of Geothermal Engineering and the course coordinator of the Postgraduate Certificate in Geothermal Energy Technology programme at the Department of Engineering Science, The University of Auckland, New Zealand. Dr. Zarrouk has an applied approach to geothermal energy training and research with on-going collaboration with several universities and research institutions worldwide. He has more than 130 publications in journals and conference proceedings, three patents and two books. In 2007 he was instrumental in the restart of the geothermal training programme at the University of Auckland, which was stopped in 2002.

Dr. Zarrouk has passion for geothermal energy with an extensive commercial field experience in geothermal and reservoir engineering since 1997. He has worked on more than 40 geothermal fields in New Zealand, Australia, Asia, Europe and North America. His roles involved the assessment of the resource, well targeting, well test analysis and reservoir modelling. He also participated in several due diligence projects, his role also included all the engineering aspects of the field development (steam field equipment, flow measurements, two-phase flow, power stations design, scaling, corrosion and direct use). Dr. Zarrouk has run several advanced professional training courses and provided expert evidence on several occasions. He was elected into the boards of directors of the New Zealand Geothermal Association 2011–17 and the International Geothermal Association (IGA) in 2013–20. He is a member of the organising committee of the New Zealand Geothermal Workshop since 2006.

Affiliation and expertise

Senior Lecturer, Geothermal Engineering, Department of Engineering Science, The University of Auckland, Auckland, New Zealand

Katie McLean

Katie McLean has been a Geothermal Reservoir Engineer at Contact Energy Ltd. since 2010, based at the Wairakei Power Station in Taupo, New Zealand. She is also currently completing her doctoral thesis on the subject of geothermal well testing at the University of Auckland and holds a prestigious New Zealand scholarship, the Todd Foundation Postgraduate Scholarship in Energy Research. Ms. McLean's work has encompassed many aspects of characterising geothermal well and reservoir behaviour, including completion testing and output testing, with the integration of cross-disciplinary data. A particular focus has been on pressure transient analysis by numerical methods and how the results of this analysis inform the conceptual model of the

geothermal field. Her work has encompassed data from geothermal wells in several geothermal fields in New Zealand, Asia, North America and Europe. In the field of geothermal reservoir engineering, she has 15 publications in journals and conference proceedings. Ms. McLean has bachelor of engineering and bachelor of science (geology) degrees from the Australian National University, and a Postgraduate Certificate in Geothermal Energy Technology from the Geothermal Institute, the University of Auckland. She was elected to the board of directors of the New Zealand Geothermal Association (NZGA) in 2018. She was on the organising committee for the World Geothermal Congress short course programme in 2015. Prior to moving to New Zealand for a career shift into the geothermal energy industry, she worked as a project geologist in mineral exploration in Canada's Northwest Territories.

Affiliation and expertise

Geothermal Reservoir Engineer, Contact Energy Ltd., Wellington, New Zealand

Preface

Geothermal energy is proven to be clean and renewable. It is the most abundant energy source on the Earth and has the potential to provide all of humanity's energy needs for generations to come. However, geothermal energy development is very challenging and involves high risk and high upfront investment. Development must start with understanding the type of geothermal system under consideration, which can help with identifying the possibilities for utilisation of the system and making the project commercially viable. Geothermal development is not only about using efficient equipment but also adapting the geothermal resource to a reliable and tested technology.

The wells are the arteries of the geothermal energy development; they provide access to the fluid containing the thermal energy and are the main insight into the reservoir. Despite this, testing and analysis of geothermal wells are the least understood and least studied part of the geothermal system by the majority of researchers in the field.

The motivation for this work came from observing a significant knowledge gap on geothermal well testing methods in general, and pressure transient analysis (PTA) in particular. Most PTA methods are adapted from the petroleum and ground water industries. It has been a combination of applied science and more of a black art.

The book starts by giving an overview to geothermal energy, its potential, its challenges and some of the many misconceptions. The authors use their experience to highlight what is practically possible and what is not.

The challenges, risk and cost of drilling geothermal wells and the different well designs are presented. Also discussed are wells drilled by other industries and their potential use for geothermal energy production.

In the past, geothermal system classifications have always been considered based on the geological setting, type of rock and the geological event that led to the formation of the system, with several methods found in the literature. The book recommends and provides justification for a more reservoir engineering-based method for system classification, which encompasses the resource temperature, method of heat transfer and reservoir permeability. It covers both conventional and enhanced geothermal systems and relates to the way the system is explored, developed, operated and managed long term.

Comprehensive cover of existing analytically based PTA theory from the petroleum and ground water industries follows. Following this, and more suitable to the geothermal industry, is the new numerically based PTA methodology using a modelling

framework developed by the second author. Numerical PTA is revolutionising geothermal PTA, allowing interpretation of data sets that were previously not possible.

PTA is only one aspect of geothermal well testing. Practical aspects of geothermal completion testing, downhole equipment used and interpretation of the results are covered in detail with field examples. The initial output/production testing is covered, and then operation and management of geothermal wells during long-term production. Stimulation of geothermal wells and long-term operational challenges including mineral scaling and well casing corrosion and its mechanical integrity are outlined.

Several field examples are given in the final chapter, which use numerical PTA and incorporate other aspects of geothermal well testing from this book. Most of the data sets used in the book were collected with approval from companies within the geothermal industry, and references are provided to most claims and observations when possible. However, the authors' own experiences are used when it was not possible to provide a reference. This is necessary in the effort to make this book more applied and practically useful.

We hope that the book will be a good source of information and guidance on industry techniques and practices: to students, researchers and the practicing engineers in the field of geothermal engineering.

Sadiq J. Zarrouk and Katie McLean

Auckland-Taupo, New Zealand

December 2018

Acknowledgements

The publication of this work would not have been possible without the support of the geothermal industry both in New Zealand and around the world.

We thank the staff and management of Contact Energy New Zealand Ltd for their support and access to geothermal well test data and information. In particular, we express our gratitude to Dr Mike Dunstall and Mr Warren Mannington.

Mr Marcel Manders and Mr Richard Adams from MB Century New Zealand Ltd for sharing their experience and providing technical information on downhole measurement tools, pictures and diagrams.

The staff and management of the following:

Mercury Limited, New Zealand

Energy Development Corporation, Philippines

Pertamina Geothermal Energy, Indonesia

Star Energy, Indonesia

Veto, Belgium

Jacobs, New Zealand

Students and graduates of the Geothermal Institute, University of Auckland, who provided technical information, access to data and help in preparing some of the diagrams including the following:

Mrs Shanti R. A. Sugiono, Mr Julian Lopez, Mr Arvin Aqui, Mr James Nogara, Mr Mohamad Husni Mubarok, Mr Dorman Purba, Mr Anthony Ciraco, Mr Carlo Paul P. Moranten and Mr Mark Angelo O. Malibiran.

Mr Jafar Zarrouk for proof reading the manuscript, Miss Josephine Claudia Halim for the book cover design and Prof. Mike O'Sullivan for his help with AWTAS. Mrs Christine Siega, Dr Ramonchito Cedric M. Malate, Mr Mulyadi, Mr Hagen Hole and Mr Gábor Szita for sharing their work.

Our appreciation to the former staff of the Geothermal Institute: A. Prof. Arnold Watson, Dr Mike Dunstall, A. Prof. Pat Browne, A. Prof. Stuart Simmons, A. Prof. Manfred Hochstein, Dr Supri Soengkono and Mr K.C. Lee.

Our deep gratitude to the International Geothermal Association for developing the world geothermal conference database, which made geothermal literature search a simple and a pleasant experience.

The University of Auckland for granting the first author a paid sabbatical to develop the book proposal.

Finally and most importantly, our families for their support and encouragement in making such a long project possible.

CHAPTER 1

Introduction

Contents

1.1 Background	2
1.2 Geothermal energy	3
1.3 Power production	5
1.4 Direct use of geothermal energy	7
1.5 Scope of this book	9

Earth is a large powerhouse continuously generating approximately 46 ± 3 TW of thermal power (Jaupart et al., 2007), by the radioactive decay of heavy nuclei ^{238}U , ^{232}Th and ^{40}K inside the crust and mantle (Dickson and Fanelli, 2003). This energy manifests itself at the surface from time to time through seismic and volcanic activities mainly along tectonic plate boundaries. Earth also has a massive stored thermal energy (inertia) estimated around 12.6×10^{24} MJ. Of these, 5.4×10^{21} MJ (1.5×10^{12} TW h) of energy is in the Earth's crust (Armstead, 1978). Knowing that the total world energy consumption in 2012 was 154,795 TW h (USEIA, 2017), geothermal energy can effectively provide all of humanity's energy needs for many generations to come. Theoretically, the geothermal energy stored and generated underground is more than all other (fossil and renewable) energy sources combined. However, the technology needed to harness geothermal energy faces many technical and commercial challenges. The main challenge is the high cost and commercial risks associated with drilling deep geothermal wells to produce this energy.

Geothermal energy developments are known for their high availability and independence from weather conditions compared to the other renewable sources (Zarrouk and Moon, 2015). Unlike solar or wind energy, geothermal energy does not need to be integrated with energy storage systems because the geothermal energy is naturally stored underground and can be directly accessed when needed through the geothermal well. On the other (down) side, unlike other renewable energy sources (such as solar and wind), geothermal energy can be site specific, require longer development time and involve high upfront cost and risk associated with drilling into permeable hot fluid targets.

The historic trends in geothermal power development since the 1950s show that the growth in geothermal power development is highly affected by the fluctuation in the price of oil; and since the late 2000s, geothermal energy has been challenged by

low-cost solar energy (Zarrouk, 2017). However, geothermal energy will always have a role to play as the world moves toward a low-carbon economy by reducing greenhouse gas emissions and phasing out fossil-fuelled thermal and thermal–nuclear plants. Geothermal energy is an integral part of the strategy in many countries to achieve energy independence and reduce reliance on fossil fuels.

Geothermal wells are the veins and arteries of any geothermal development, allowing both the production of hot geothermal fluid to the surface and the reinjection of the utilised fluids back into the reservoir. Geothermal projects become commercially viable (bankable) only after the drilling and testing of large and deep wells and when the power potential/output of each well is measured and quantified. The behaviour of geothermal wells can also change with time; generally, the power output of production wells reduces with time, which makes it necessary to drill make-up wells. Reinjection wells can suffer from reduction in their injectivity, which will require intervention. Well testing can help identify the reasons for changes in well behaviour and help guide the reservoir engineers to the potential solution or well intervention.

1.1 Background

The motivation for this book came through our observation that the worldwide boom in the applications and research in geothermal energy have mainly focussed on enhanced geothermal systems (EGS), above ground geothermal technology (e.g. Organic Rankin Cycles), low temperature direct use and ground source heat pump applications. However, there is not much published work or research on testing, assessing and understanding the behaviour of geothermal wells, despite the fact they are critical for any geothermal development and are a major investment. One reason is the lack of understanding of – and appreciation for – the importance of geothermal well testing by researchers from different backgrounds venturing into geothermal energy.

Geothermal energy training is very specialised with only a few established institutions in the world offering internationally recognised academic training (Zarrouk, 2017). Only a handful of these courses cover geothermal well test analysis in some detail, since well test analysis practices differ between regions depending on the types of geothermal systems being dealt with. In addition the well test data are normally commercially sensitive (confidential) and only available to geothermal reservoir engineers working in the industry. Therefore unlike the petroleum industry, geothermal well test expertise and skills are not commonly found in research institutions or academia.

Geothermal well test analysis has sprung from analytical methods developed by the petroleum and groundwater industries. Geothermal well test data largely do not satisfy the fundamental assumptions upon which these techniques were developed. Therefore it is common that geothermal well test analysis leads to incorrect interpretations or

behaviour that is difficult to interpret. For this reason, there is low confidence in well test analysis and it is common for reservoir engineers not to report well test results.

From our experience in analysing data from a host of geothermal wells from around the world, it became obvious that testing and analysing the well test data should be carried out differently from petroleum and groundwater wells. The two-phase condition (steam and water) and high temperature of the geothermal fluid can lead to false effects when using techniques developed for single-phase isothermal conditions (McLean and Zarrouk, 2015a). This undermines the accuracy and the findings of the transient geothermal well test analysis. As a result, geothermal well test analysis is to some extent perceived as a black art. Young geothermal engineers and scientists find it difficult to understand and master well testing without making mistakes on the way as they try to develop their skills in the absence of specialised training or experienced mentors.

1.2 Geothermal energy

The thermal power that is generated in Earth's mantle travels to the ground surface through the rock formations of the crust by thermal conduction. This generates an average conductive temperature gradient between 20 and 30°C/km (Armstead, 1978), which results in a heat flux of about 40–60 mW/m². In some parts of the world the local thermal gradient is higher than 30°C/km, for example the measured thermal gradient of Huntly, New Zealand, ranges between 52 and 55°C/km (Zarrouk and Moore, 2007). The geothermal gradient is also affected by the thermal conductivity of the different rock formations that it passes through, following Fourier's law of thermal conduction.

The thermal gradient is often thought of as linear, though in reality a higher thermal gradient is expected through less conductive rock, and a lower gradient expected through rock that is more conductive. For example the deep EGS well of the Habanero project in Australia has a local thermal gradient that ranges between 32.3 and 63.3°C/km depending on the rock type (Fig. 1.1). It is known that coal, coal measures and rocks bearing hydrocarbons are less conductive than other rock types and can act as thermal insulators, trapping heat underneath. In addition, some deep volcanic rocks (e.g. granite) generate heat by radioactive decay which can also result in an above average thermal gradient through these rock types. Natural state numerical modelling shows that the temperature gradient of Fig. 1.1 can be reproduced with natural heat flux of 125 mW/m² and heat generation of 10 μW/m³ (Llanos et al., 2015).

In areas along Earth's plate tectonic boundaries the natural thermal gradient can be as high as 100°C/km. When there is reasonable permeability in the surrounding rocks and good natural supply of water (meteoric or seawater), the thermal gradient will become unstable giving way to convective heat transfer through water movement, which carries much more thermal energy than thermal conduction. Natural thermal convection can result in significantly elevated temperatures close to the ground surface (Fig. 1.2), and this high energy density can be accessed by drilling into these convective upflows of fluid. It is at plate boundaries that most geothermal heat manifests itself

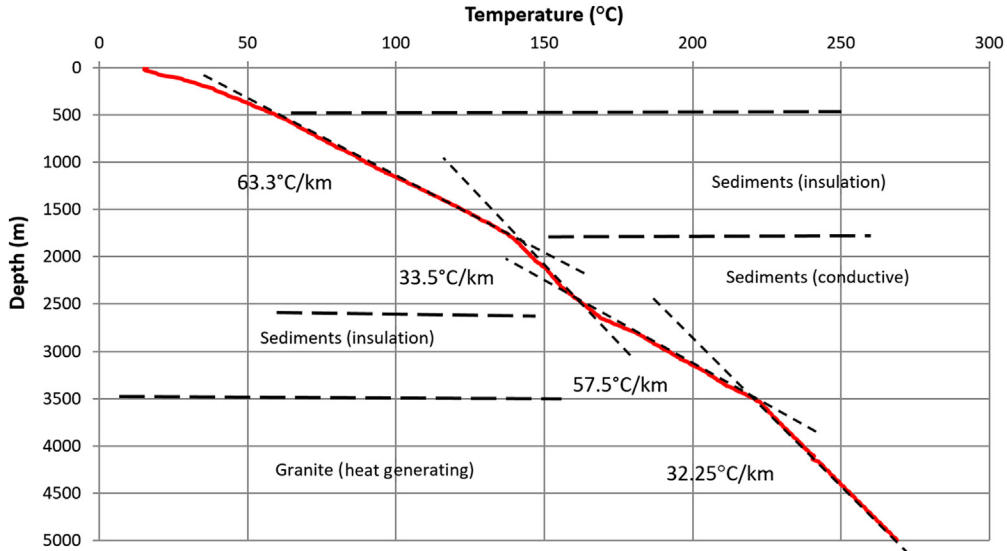


Figure 1.1 The geothermal gradient of the H01 Habanero well. *Data source from Llanos, E.M., Zarrouk, S.J., Hogarth, R., 2015. Simulation of the habanero geothermal reservoir, Australia. Geothermics 53, 308–319.*

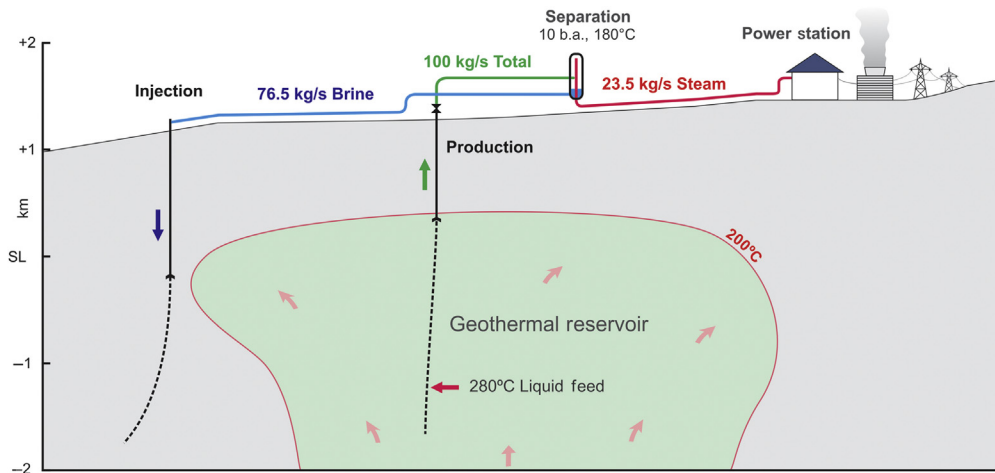


Figure 1.2 Cross section through a convective geothermal system utilised for power production. *From Brian Lovelock, Jacobs Ltd. with kind permission.*

in the form of thermal springs, hot pools, geysers, steaming ground and bubbling mud pools. These are referred to as conventional geothermal systems and have been extensively studied and commercially developed for energy production in many parts of the world. Most of the geothermal power generated around the world comes from conventional systems. Effectively these systems are much easier to develop (low-hanging fruit) than the nonconventional systems (e.g. EGS, geopressed systems) that will be discussed later in this book.

1.3 Power production

Geothermal electric power generation first commenced in 1904 at Larderello, Italy. The first generation used reciprocating steam engines which soon failed due to corrosion problems, after which clean steam was generated in heat exchangers. Development of new technology and materials enabled the heat exchanger to be dispensed with, and a 250 kWe power station was put into operation in 1913. By 1940, 130 MWe was feeding the Italian railway system. This was later destroyed in the Second World War but has since been rebuilt and is still generating successfully.

It was not until the early 1950s that New Zealand started to plan a geothermal plant. The first geothermal electricity in New Zealand was at the Spa Hotel in Taupo on 13 February 1952. The steam engine did not run for long due to the deposition of mineral scale carried by the wet steam. In 1958 the first power unit was commissioned at Wairakei. Then the United States was next to produce geothermal power in 1960 at The Geysers in California. Many countries have followed in geothermal power development, which was reported in 26 countries around the world in 2015 with a total installed capacity of more than 12.7 GWe, with a forecast of 21.0 GWe in 51 countries by 2020 (Bertani, 2016).

Wairakei, New Zealand, was the first low enthalpy liquid-dominated geothermal system to be developed, as wells at Larderello and The Geysers produced dry steam. Two-phase fluid produced from wells at Wairakei required the development of new technology for separating steam from water and disposing of the separated water (brine).

Thermal power generation requires satisfying the second law of thermodynamics, which limits the maximum theoretical power conversion efficiency to the Carnot cycle. The efficiency for geothermal power plants are significantly lower than other thermal power plants as they operate at much lower input temperature and reject geothermal fluid still at high temperatures in order to control mineral scaling. There are also energy losses inside the well and long transmission pipelines from well to plant (Fig. 1.2).

There are different measures for assessing the actual efficiency of a geothermal power development. The overall conversion efficiency, which is the net produced power to the input thermal power, is lower than all other thermal power plants (Zarrouk and Moon, 2014). However, geothermal power development should not be considered based on their thermodynamic efficiency but rather their commercial efficiency since the energy source is effectively free, clean and renewable when compared with conventional thermal power plants, which require an ongoing fuel supply at high cost and produce large amounts of greenhouse gases.

Since the development of the early geothermal plants in Italy, New Zealand and the United States, no geothermal field has been abandoned even after exceeding their commercial life.

The design of geothermal power station equipment (e.g. turbines, condensers, pumps) is greatly influenced by the characteristics and chemistry of the available geothermal fluid. The chemistry of the fluids influences the choice of operating parameters and material selection for the plant construction, and the gas content and its constituents affect the choice and design of the gas extraction system. The type of resource (dry or wet field) in general determines the surface equipment necessary to utilise the fluid. For example in a dry or vapour-dominated geothermal field, dry saturated or slightly superheated steam is produced from the wells, and generally this can be transmitted by pipeline directly to the steam turbine without further conditioning. However, in wet fields, two-phase fluid is produced at the surface, and before being sent to the turbine it is necessary to separate the water from the steam. Lower temperature (enthalpy) geothermal fluid is utilised using binary power plants. One advantage to geothermal steam plants is that these power plants do not require cooling water like all other thermal plants as they generate their own water from geothermal steam condensates. While binary plants normally use air for cooling to minimise their impact on natural resources (water) and the environment, steam plants generally have economy of scale compared with binary plants, as there is higher cost associated with testing and health and safety precautions from using the hydrocarbon binary fluid (e.g. pentane, isopentane). However, binary plants are more suited for staged development in new geothermal fields. Binary turbines are also less prone to moisture and mineral scaling damage.

Regarding the type of wells, self-discharging or pumped wells also affect the choice of power generation technology. Pumped wells can only be utilised using binary plants, while self-discharging wells allow the use of both steam and binary technologies. Dry steam wells make steam plants a much more attractive option.

Unlike clean steam from a boiler in a conventional thermal power plant, geothermal steam contains noncondensable gases (NCG) ranging from almost zero up to about 15% by weight in some geothermal fields (Nogara et al., 2018). The gases not only degrade the quality of the steam but also require the consumption of work to remove it from the condenser to achieve vacuum in steam plants. For this reason a geothermal power plant requires a large capacity NCG extraction system, which forms a significant portion of total capital cost and can consume a large amount of auxiliary power. Moreover, the presence of NCG also reduces the heat transfer coefficient of heat exchangers and requires larger surface area condensers.

Hudson (1988) suggested that the effect of NCG on the gross power output could be corrected using the following equation:

$$W_g = W_o(1 - G \times 0.59) \quad (1.1)$$

where W_g is the gross power with $G\%$ NCG by weight, W_o is the gross power with zero NCG, G is the percentage of NCG content by weight in total flow (steam plus NCG).

It can be observed from Eq. (1.1) that for every 1% increase in NCG content, the gross turbine work is decreased by 0.59%. This can affect the choice of equipment used for NCG extraction.

In countries with young volcanic systems the geothermal fluid can be very acidic with pH averaging 3–4 (Nogara and Zarrouk, 2018a), with a pH as low as two observed in one field (Zarrouk, 2004). Hypersaline sedimentary deep aquifers can have fluid salinity of 100–200 parts per thousand (Llanos et al., 2015). These highly corrosive geothermal fluids require advanced well construction material that can significantly increase the cost of geothermal development (Nogara and Zarrouk, 2018a,b).

The selection of an appropriate generation technology, construction material, gas extraction system, etc. are therefore of particular importance in geothermal power plants. This can only be done once the geothermal wells are drilled and tested. Funding geothermal power development is normally carried out by governments or large companies that can afford the risk of exploration drilling. Commercial lending (e.g. banks) is only possible after proving 62% of the potential power development through well testing.

1.4 Direct use of geothermal energy

Direct use of geothermal energy refers to all applications other than electricity production. It involves – but is not limited to – space heating, recreation, greenhouse heating, aquaculture, agricultural drying, industrial uses, cooling and snow melting.

Direct use simply applies the first law of thermodynamics, which involves energy transfer/conversion from the geothermal fluid to a secondary fluid. High conversion efficiency between 80% and 90% is possible in direct use. The key concept in the application of direct use is to quantify the thermal power load needed for a given application under normal and peak demand. Then testing and understanding the geothermal source output (hot natural pond or a geothermal well) and matching this to the demand. In some cases the geothermal resource can match the full energy demand and in others may require a supplementary heat source during peak (e.g. winter) demand time.

For centuries, natural hot springs have been used for bathing and healing properties by ancient civilisations, from the balneology industry developed from the Roman spas and Turkish baths to present-day spas and pools. The use of hot pools for domestic purposes (cooking, washing, etc.) has long been part of the Maori way of life in New Zealand.

Mineral extraction in the early 19th century started at what is now known as Larderello in Italy, where a boric acid industry was founded. Today, elemental sulphur is recovered from fumaroles in Indonesia, Japan and Taiwan, and sulphuric acid and

ammonium salts in Italy and Japan. Gold and silver mines are mainly extinct geothermal reservoirs, where the geothermal fluid dissolved and transported the gold and silver from deeper formations then deposited and concentrated them in shallower rocks.

Iceland exploits its geothermal resources for district heating and domestic hot water. A pilot district-heating scheme was established in 1930 in Reykjavik to supply about 70 homes, 2 public swimming pools, a school and a hospital. The scheme was so successful that the engineers drilled for hot water 15 km outside the city boundaries, and by 1943, 2300 houses were supplied. New areas were drilled and by 1975, all but 1% of the buildings in Reykjavik were supplied with domestic heat. Further systems were developed across the country and by 1980, two-thirds of the population enjoyed the benefits of geothermal heating.

In the United States, at Boise, Idaho, the residential area associated with the warm springs was geothermally heated in 1980. At Klamath Falls, Oregon, contemporaneous development provided many houses with geothermal heat. In Japan and New Zealand, geothermal space heating has been developed on individual lines, with each householder building their own systems, although in recent years, group schemes have developed as costs have risen. In 1962 space heating was developed in Hungary and the former USSR, and in the early 1970s, public heat supplies were made available in the Paris Basin, France.

Farming and aquaculture uses have developed over the years. In 1920 greenhouses in Iceland were heated to grow vegetables, fruits and flowers and by 1980, 11,000 m² of greenhouses were being used. Russia and Hungary have exploited their geothermal fields for greenhouse heating, 420,000 m² and 1,900,000 m², respectively, accounting for over 600 MWth of thermal power. Over recent years, geo-heat has been used for animal husbandry, soil heating, fish farming, etc.

The first large-scale industrial application was initiated in the 1950s at Kawerau, New Zealand, where pulp and paper production utilises over 200 T/h of steam for processing. In Iceland, at Namafjall, geothermal steam has been used in a diatomite plant since 1967, and elsewhere in the world, uses are being found for both high- and low-temperature geothermal fluids. The worldwide installed direct use of geothermal energy in 2015 stands at 70.9 GWth with annual growth of 7.9% and has been reported in 82 countries (Lund and Boyd, 2016). However, all countries in the world will have some natural thermal springs that are traditionally used for cultural or industrial applications.

The future for geothermal energy is very promising; however, there are still a number of challenges. The cost and risk of drilling geothermal wells is the main challenge. Potential developers are easily put off when they understand that there is no guaranteed well success when investing in the drilling of geothermal wells.

Environment is also a major concern, and the control of waste gases and liquids is of considerable importance. ReInjection has become necessary and mandatory at almost all recently constructed projects. The technique is theoretically simple, but the implementation is fraught with problems including mineral depositions in pipes and formations, and breakthrough of cold fluids into the production wells, to mention just a few. The technique is also 'site specific', so each field requires considerable study, drilling and well testing before a successful reInjection program can be devised.

1.5 Scope of this book

Geothermal wells are an expensive and high-risk component of any geothermal development. Wells are the main window into the underground reservoir, via well testing which provides insight into the reservoir conditions and enables the assessment of production well output or reInjection well capacity.

This book provides a comprehensive review of well test practices and methodology starting from the brief introduction to geothermal energy and its applications in this chapter. This chapter demonstrates that the choice of utilisation technology and construction material is dependent on understanding the geothermal well behaviour and measuring the brine and gas chemistry.

To develop any geothermal prospect, one needs to understand the characteristics of the geothermal system. There are several classifications of geothermal systems which mainly depend on the natural geological setting and the geological events that lead to the creation of such systems. These types of classifications are more relevant during the field exploration phase. Therefore in Chapter 2, Geothermal Systems, we will focus on an alternative reservoir engineering – and thermodynamic – classification that can be identified from well testing. The classification can then be related to the way the system is going to be developed and operated and will have a major impact on choosing the appropriate technology and reInjection strategy.

Chapter 3, Geothermal Wells, will introduce geothermal well drilling and casing design and then discuss the different types of geothermal wells based on their operation and application. This encompasses self-discharging wells, wells with downhole pumps, airlifted wells and wells with downhole heat exchangers, and then reInjection wells. For comparison, well design and testing methods from other industries (petroleum, groundwater, coalbed methane, mineral exploration wells and waste disposal wells) are also discussed and compared with geothermal wells.

Chapter 4, Introduction to Pressure Transient Analysis, gives a detailed review of the fundamental concepts of pressure transient analysis (PTA), starting from the earliest well test theory developed for groundwater wells and reviews existing graphical analytical well test analysis methods and their limitations in the geothermal context.

Then in Chapter 5, *Advanced Analytical PTA Relevant to Geothermal Wells*, advanced analytical models developed for the petroleum industry are presented and their use in geothermal well testing is examined. This is including reservoir boundaries, multiphase reservoirs, non-Darcy flow and fractured reservoirs. Extending these analytical methods to the geothermal environment can result in some unrealistic behaviour and incorrect interpretations. These effects are identified and their impact to geothermal well test analysis is discussed.

In Chapter 6, *Completion and Output Testing*, the practical considerations during geothermal well testing are provided based on current industry practices. A detailed description is given of the different stages of completion testing, including water loss surveys, injectivity, pressure falloff, and heat-up surveys. This chapter also outlines the interpretation of the data from different stages of testing, the downhole equipment used and their setups. Then the output testing methods are given and the methods used for discharge prediction, output estimation and discharge simulation. Finally, downhole flowing surveys and their application are described.

Chapter 7, *Downhole Tools and Other Practical Considerations*, gives the practical issues associated with geothermal well testing that should be taken into consideration when analysing geothermal well test data. These includes slow valve closure, multi-stage pump shutdown, cold water injection into a hot reservoir, thermal expansion of the downhole wire line, boiling in two-phase wellbores and high pressure drop inside EGS wells. Wellbore simulators are also described, and their applications in geothermal reservoir engineering are outlined.

In Chapter 8, *Numerical PTA Modelling Framework*, a framework for PTA is given, which uses numerical reservoir simulation software coupled with inverse modelling tools for matching of the well test behaviour. This has been shown to be the optimum technique for the accurate assessment of the geothermal reservoir properties from transient well test data. The framework matches the pressure derivatives of the transient well test response, identifying well effects and events that cannot be handled by existing interpretation techniques.

Chapter 9, *Operation and Management of Geothermal Wells*, focuses on production data analysis and well stimulation methods, which are directly related to geothermal field management. Moreover, well integrity and the effects of mineral scaling, corrosion and mechanical damage in geothermal wells are covered.

Finally, in Chapter 10, *Field Studies*, several field case studies are presented using well test field data from around the world. This includes cement damaged wells, acid-stimulated wells, fractured reservoirs, wells with mechanical workover, wells with single and double impermeable boundaries, fracture closure after injection testing, chemical tracer testing and slug testing.

The appendices give common geothermal engineering terminology. The book uses SI units and all existing equations and models found in literature are converted

and presented in the SI unit system (many are currently published in oilfield units only). However, wells and pipelines' nominal diameters are presented in inches, as it is the industry practice.

The book focuses on applied rather than theoretical well testing techniques and analysis, which we feel to be of more use to practicing engineers and researchers. The focus will not be on the derivation and solution of governing equations, as this is comprehensively covered by other publications, and references are given to them.

CHAPTER 2

Geothermal systems

Contents

2.1	Classification of geothermal systems	13
2.1.1	Geological circumstances (play type)	14
2.1.2	Temperature classification	16
2.1.3	Enthalpy classification	17
2.1.4	Exergy classification	18
2.1.5	United Nations Framework Classification for Resources	20
2.2	Conventional geothermal systems	21
2.2.1	Warm water systems	21
2.2.2	Hot water systems	23
2.2.3	Low-enthalpy two-phase systems	26
2.2.4	Medium-enthalpy two-phase systems	28
2.2.5	High-enthalpy two-phase systems	29
2.2.6	Dry steam (vapour-dominated) systems	31
2.3	Nonconventional geothermal systems	32
2.3.1	Supercritical (deep volcanic) systems	33
2.3.2	Geo-pressured systems	33
2.3.3	Enhanced geothermal systems	34
2.3.4	Alternative geothermal (man-made) systems	36
2.4	Summary	37

2.1 Classification of geothermal systems

Geothermal systems are different from oil and gas (petroleum) systems where the fluids are stored in the pores of permeable formations and confined by impermeable rock. They are also different from groundwater systems, which can be either confined, unconfined or perched aquifers. Geothermal systems are more complex, less defined, and their type and extent can only be asserted through exploration drilling and well testing.

There are several geological and engineering classifications of geothermal systems. Geothermal geologists classify the geothermal systems based on their geological setting and how these systems were formed. In this work we are going to use a reservoir engineering classification, which is based on the dominant heat transfer mechanism, how these systems are assessed during well testing and how they are going to response to long term production. Understanding the type of geothermal system is crucial to the success of any commercial development. This is when the technology

implemented to utilise the geothermal energy can be finalised. Three main requirements must be fulfilled to have a geothermal system that can be developed commercially for energy production. These are: high temperatures, water in the deep rocks and permeable/fractured rock to allow this energy to flow into the production wells. Different classification systems are discussed, then focus is given to the system classification based on the production enthalpy of geothermal wells. It is demonstrated that this enthalpy classification system in conventional geothermal systems lends itself very well to non-conventional systems.

The objective of classification is to allow easy comparison to similar systems. This aids the selection of exploration strategy, development strategy and power generation system, hopefully sidestepping issues which have already been overcome elsewhere. Classification is a common and important concept not just for geothermal systems but also for the petroleum and mineral industries. In some contexts, the word ‘classification’ can have a very specific definition; however, in this text, it is used more generally to refer to any systematic division of geothermal systems into groups based on some criterion.

There is no consensus on the best method for classification of geothermal systems, and there are classifications based on a variety of criteria including geological circumstances, reservoir temperature, enthalpy, exergy, economic and social viability, project status and feasibility and level of geological knowledge. The choice of classification system depends ultimately on the purpose for which it will be used – each is potentially useful at different stages from exploration through to assessment, development and for global reporting.

2.1.1 Geological circumstances (play type)

The terminology ‘play’ is common within the petroleum and minerals industries but introduced more recently to the geothermal industry. It is a large regional area, which is controlled by the same set of geological circumstances. For example, the ‘Taupo Volcanic Zone (TVZ) play’ would refer to the entire TVZ region in New Zealand, within which the controlling set of geological circumstances is that this is a back-arc basin associated with nearby subduction and is hence an area of extension and active volcanism. The objective of exploration companies would then be to identify the economic geothermal reservoirs within the ‘TVZ play’, currently there are 23 identified geothermal systems.

There are a variety of geological circumstances (other ‘play types’) which can host economic geothermal reservoirs. Identifying this range of geothermal play types has been the subject of work by Moeck (2014) and Moeck et al. (2015). One reason a classification based on geological play type was not attempted until relatively recently is that it was not considered to be practical, and there would be no consistent set of geological attributes to divide geothermal systems into useful groups (Sanyal, 2005). Others did not agree and Moeck (2014) published a scheme with two major groups,

Table 2.1 Geothermal play types defined by Moeck et al. (2015).

CV		CD	
CV1	<i>Magmatic</i> Heat source is relatively shallow liquid magma activity (either extrusive or intrusive)	CD1	<i>Intracratonic basin</i> In a sedimentary sequence in an extensional or thermal sag basin
CV2	<i>Plutonic</i> Heat source is a young crystallised intrusive body (either associated with recent volcanism or not)	CD2	<i>Orogenic belt/foreland basin</i> In a sediment within a wedge-shaped foreland basin adjacent to an orogenic mountain belt
CV3	<i>Fault-controlled in extensional domains</i> Heat source is the elevated mantle, and fluid circulation is deep faults	CD3	<i>Basement (crystalline rock)</i> In hot fractured crystalline (e.g. granitic) rock with low natural permeability and porosity

CD, Conduction-dominated; CV, convection-dominated.

‘convection-dominated (CV)’ and ‘conduction-dominated (CD)’ systems, according to the dominant method of heat transfer within the system. These are divided into subgroups based on geological features (Table 2.1). CV systems are divided according to the nature of the heat source and tectonic setting into ‘magmatic’, ‘plutonic’ or ‘fault-controlled in extensional domains’. CD systems are divided into ‘intracratonic’, ‘orogenic belt/foreland basin’ and ‘basement (crystalline rock)’.

The primary drawback to this concept of classification by geological play type is that within a single play the individual geothermal reservoirs can have a wide variety of characteristics. For example, within the TVZ play, the Rotokawa geothermal reservoir has a much higher enthalpy (1750 kJ/kg) than the Wairakei geothermal reservoir (1050 kJ/kg). Hence, the systems have completely different extraction/reinjection strategies and above ground equipment/plant design, and the play type will not be of use during the development and operational phases.

Another major drawback is that a large number of geothermal regions fit more than one play type from Table 2.1. Moeck et al. (2015) discuss the TVZ, which has magmatic and plutonic bodies, as well as crustal extension, an elevated mantle and deep fault-control on fluid movement, and so the TVZ is a ‘hybrid’ of CV1, CV2 and CV3. If a single play type is not of practical use during development and operation then a hybrid play type will be even less so.

More recent work by Wallis et al. (2017) groups geothermal systems not by their geological setting but by the degree to which the geological features in the system influence fluid flow and hence the shape of the convection plume. This is a spectrum: from ‘focused’ flow, which is highly restricted by features such as faults and lithological boundaries to ‘unconstrained’ where flow is practically independent of geological features. In between these is a group where flow is ‘influenced’ by geological features

in some places, but they do not control the plume overall. This classification has a bearing on practical decisions such as production and reinjection strategy and so will have relevance beyond the exploration stage.

2.1.2 Temperature classification

Reservoir temperature is the most common criterion for classification, partly due to the fact that temperature is easy to measure and to understand (Lee, 2001). Another reason for this is that the reservoir temperature is available very early in the exploration phase, even predrilling, as it can be approximated from geothermometry (Hochstein, 1988).

There are a variety of temperature classification schemes, which use the reservoir temperature to divide geothermal systems into ‘low-temperature’, ‘intermediate-temperature’ and ‘high-temperature’ resources (Muffler and Cataldi, 1978; Rybach, 1981; Hochstein, 1988; Benderitter and Corny, 1990) (Table 2.2).

A more detailed classification scheme is proposed by Sanyal (2005), which divides geothermal systems into seven groups (Table 2.3). This was done for commercial purposes, as part of a national inventory in the United States.

The temperature ranges are inconsistent between the different classification schemes (Fig. 2.1), and there is no consensus. A major drawback to using only temperature as the basis for classification is that the actual condition of fluid at the wellhead is not accounted for. Two geothermal systems at the same reservoir temperature can produce either steam or water, depending on pressure. Fluid from the steam reservoir

Table 2.2 Summary of classification schemes based on reservoir temperature.

	Low-temperature resources (°C)	Intermediate-temperature resources (°C)	High-temperature resources (°C)
Muffler and Cataldi (1978)	< 90	90–150	> 150
Rybach (1981)	< 150	–	> 150
Hochstein (1988)	< 125	125–225	> 225
Benderitter and Corny (1990)	< 100	100–200	> 200

Table 2.3 Sanyal (2005) classification scheme based on reservoir temperature.

Nonelectrical grade (°C)	Very low temperature (°C)	Low temperature (°C)	Moderate temperature (°C)	High temperature (°C)	Ultra-high temperature (°C)	Steam fields ^a (°C)
< 100	100–150	150–190	190–230	230–300	> 300	~ 240

^aSpecial case of reservoirs in which steam is the only mobile phase.

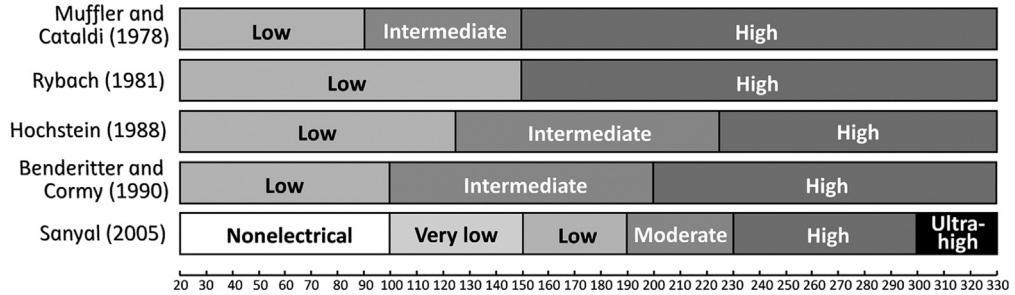


Figure 2.1 Graphical summary of temperature classification schemes.

will have a significantly higher enthalpy than the water reservoir and requires a different development and management strategy.

It should be noted that as temperature and enthalpy are closely related, the terms are often used interchangeably, for example ‘low-enthalpy’ resources instead of ‘low-temperature’ resources. This gives the misleading impression that enthalpy is being considered when in fact it is not the basis of the classification.

2.1.3 Enthalpy classification

Before discussing the enthalpy classifications of geothermal systems, it is important to discuss the different heat transfer mechanisms underground:

1. Heat is predominantly transferred by conduction following Fourier’s law of thermal conduction through the Earth’s crust.
2. In areas of higher temperature gradient and good rock permeability, the natural conductive thermal gradient can become unstable, giving rise to natural thermal (hydrothermal) convection following Newton’s law of cooling. Convection will allow the transfer of much more thermal energy towards the ground surface than conduction, and this is in a localised plume called an upflow.
3. When gravity forces fluid through the permeable rock, it is called advection, and these are referred to as downflows. Advection (forced convection) can create fluid movement in subhorizontal (down-sloped) aquifers or can provide downflow (counterflow) recharge at the top of some geothermal systems.

Examples can be found in nature with multiple concurrent heat transfer mechanisms. This forms the basis of the enthalpy classification system (Kaya et al., 2011; Diaz et al., 2016) and will have implications for both production and reinjection in geothermal development.

Note that the maximum temperature in both [Fig. 2.1](#) and [Table 2.4](#) is limited to 330°C, while many geothermal wells have encountered higher temperatures. This is simply because conventional/commercial geothermal fluid production has not been reported from higher temperatures.

Table 2.4 Enthalpy classification scheme and heat transfer.

Category (system type)		Temperature (T) (°C)	Enthalpy (h) (kJ/kg)	Heat transfer
Warm water (low temperature)		$T < 120$	$h < 504$	Conduction Possible advection No convection
Hot water (intermediate temperature)		$120 < T < 220$	$h < 943$	Convection Some conduction
Two phase, liquid dominated	Low enthalpy	$220 < T < 250$	$943 < h < 1100$	Strong convection Some advection (counterflow) Some conduction
	Medium enthalpy	$250 < T < 300$	$1100 < h < 1500$	Moderate convection Moderate advection (counterflow) Some conduction
	High enthalpy	$250 < T < 330$	$1500 < h < 2600$	Moderate convection High advection (counterflow) Some conduction
Two phase, vapour dominated		$220 < T < 300$	$2600 < h < 2800$	Negligible convection High advection (counterflow), Conduction

Source: Modified from Kaya, E., Zarrouk, S.J., O'Sullivan, M.J., 2011. Reinjection in geothermal fields: a review of worldwide experience. *Renew. Sustain. Energy Rev.* 15 (1), 47–68.

The enthalpy method allows a very simple estimation of the geothermal well power output immediately after production testing when the reservoir enthalpy and mass flow rate are measured (Eq. 2.1):

$$\text{Power(kWe)} = \eta_c \times \dot{m}_t \times h_r \quad (2.1)$$

where η_c is the conversion (enthalpy) efficiency (%) (Fig. 2.2), \dot{m}_t is the total mass flow rate from the well (kg/s) and h_r is the measured reservoir enthalpy (kJ/kg).

Alternatively, Zarrouk and Moon (2014) provided similar conversion efficiency as a function of enthalpy for three different geothermal power plant design: single-flash, double-flash and binary plants.

2.1.4 Exergy classification

A classification scheme based on the exergy of fluid at the wellhead is proposed by Lee (2001). The thermodynamic property ‘exergy’ is the maximum work available in the fluid, which excludes energy in the fluid below a certain temperature (the ‘sink

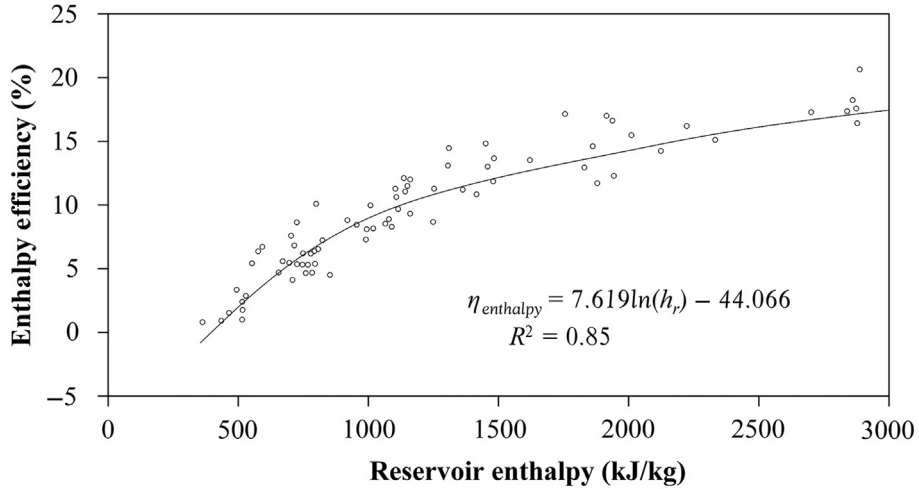


Figure 2.2 Enthalpy (conversion) efficiency versus reservoir enthalpy. After Varney, J., Zarrouk, S.J., Bean, N., Bendall, B., 2017. Performance measures in geothermal power developments. *Renew. Energy* 101, 835–844.

condition’, usually defined as ambient temperature). Exergy is hence a measure of the quality of the energy content of the fluid (Eq. 2.2).

$$e = h - h_0 - T_0(s - s_0) \quad (2.2)$$

where e is the specific exergy (kJ/kg), h is the specific enthalpy of geothermal fluid (kJ/kg), h_0 is the specific enthalpy at sink condition (kJ/kg), T_0 is the absolute temperature at sink condition (K), s is the specific entropy of geothermal fluid (kJ/kg K) and s_0 is the specific entropy at sink condition (kJ/kg K).

The Lee (2001) classification is based on a dimensionless specific exergy index (SExI) (Eq. 2.3) which is then plotted on an enthalpy–entropy diagram to classify the system as ‘low-exergy’, ‘medium-exergy’ or ‘high-exergy’ (Fig. 2.3).

$$\text{SExI} = \frac{h - 273.16 \times s}{1192} \quad (2.3)$$

Then the specific power output (SPO) and the specific fluid consumption (SFC) are

$$\text{SPO} = e \times \text{SExI}, \quad \text{SFC} = \frac{3.6}{(\eta_u \times \text{SExI})} \quad (2.4)$$

where SPO is in kW_e/(kg/s), SFC is in (t/h)/MW_e and η_u (%) is the power plant efficiency based on exergy also known as the utilisation efficiency (Zarrouk and Moon, 2015; Varney et al., 2017).

Lee (2001) used a fixed $\eta_u = 50\%$ however DiPippo (2015) showed that it could vary with enthalpy between 15% and 65%.

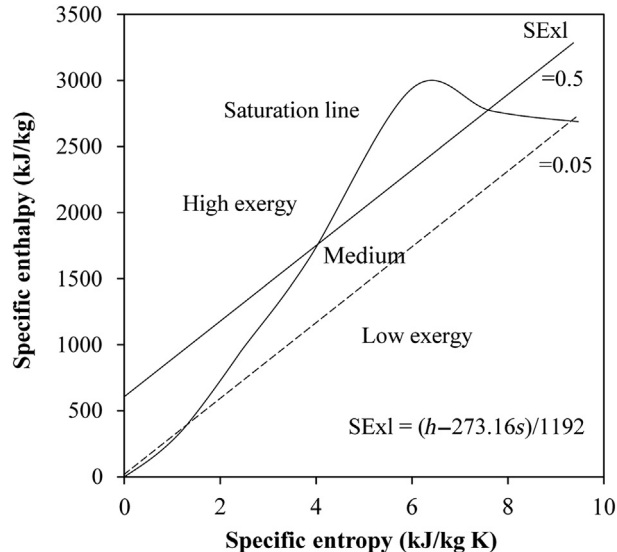


Figure 2.3 Enthalpy–entropy diagram for exergy classification scheme. Modified after Lee, K.C., 2001. Classification of geothermal resources by exergy. *Geothermics* 30(4), 431–442.

We feel that the exergy classification is a step in the right direction, and it is somewhat similar to the enthalpy classification as it uses fluid (liquid) enthalpy referenced to the triple point of water (0.01°C, 0.006116 bar).

The advantage of an exergy classification is that it does take account of the actual fluid condition at the wellhead. However, the main drawback is that exergy tends to overestimate the utilisation efficiency of the power plant (Zarrouk and Moon, 2015). Varney et al. (2017) showed that fitting published power plant data gives a low utilisation efficiency accuracy (Fig 2.4) compared with the enthalpy efficiency method (Fig. 2.2).

The enthalpy and exergy classifications can only be used after the wells have been drilled and tested, as it is not possible to estimate the reservoir enthalpy by other exploration methods.

2.1.5 United Nations Framework Classification for Resources

The United Nations Framework Classification for Resources (UNFC) (2009) was developed as an internationally applicable scheme for classification and reporting of both energy and mineral resources. Standardisation of the classification of renewable energy resources is required, including geothermal energy. To facilitate this, the International Geothermal Association (IGA) developed specifications to apply the UNFC to geothermal resources (IGA-UNFC, 2016). This classification is multifaceted and has three categories: economic and social viability (E), field project status and feasibility (F) and geological knowledge (G), each with subgroups. In the case of geothermal systems, ‘geological knowledge’ refers also to the results of well testing and reservoir simulation. This classification is useful in a high-level global reporting context.

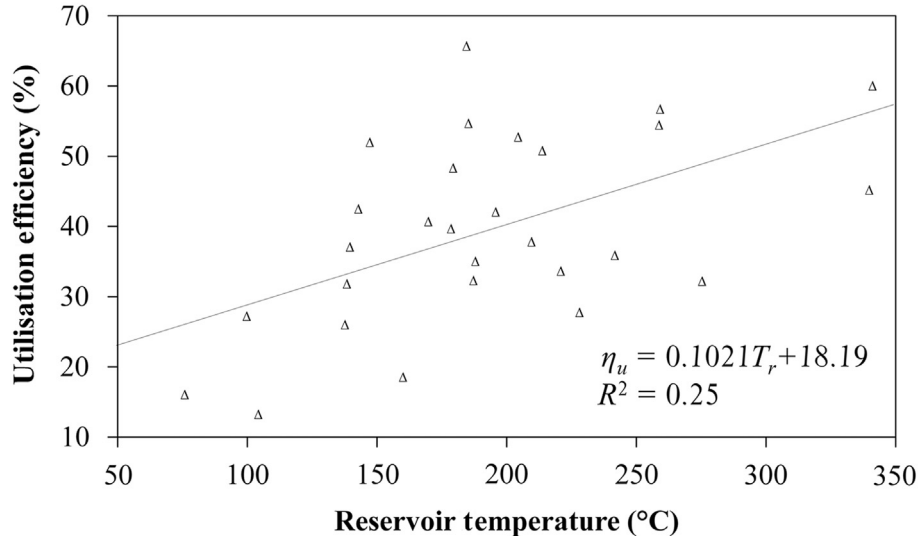


Figure 2.4 Utilisation efficiency function of temperature based on exergy. After Varney, J., Zarrouk, S.J., Bean, N., Bendall, B., 2017. *Performance measures in geothermal power developments. Renew. Energy* 101, 835–844.

2.2 Conventional geothermal systems

The term ‘conventional’ refers here to geothermal systems that have been in commercial use for many years. These systems are reasonably understood and can be found around the world. Three main parameters are essential to have a conventional geothermal system: high underground temperatures, the presence of fluids to recover this energy and good rock permeability for the fluid to flow from the reservoir to the well-bore. The main feature of conventional systems is that the development relies primarily on the natural (in situ) reservoir permeability to produce the geothermal energy. The enthalpy classification of Table 2.4 is implemented and discussed in this section. The use of this classification is not about strictly applying the temperature or enthalpy ranges given in Table 2.4, but more about understanding the setting which gave rise to these conditions, the extent of these systems and the way they should be managed during long-term development. It is also related to the dominant heat transfer mechanisms taking place in the geothermal reservoir (conduction, convection and advection).

2.2.1 Warm water systems

This is the most commonly encountered geothermal system in nature ($T < 120^\circ\text{C}$, i.e. $h < 504 \text{ kJ/kg}$). ‘Low-temperature systems’ in sedimentary basins are simply warm water systems. In these systems, deep ground water is heated by the local natural thermal gradient, mainly through conductive heating (Fig. 2.5). However, some aquifers can have a subhorizontal flow of liquid water by advection if the permeable host formation dips.

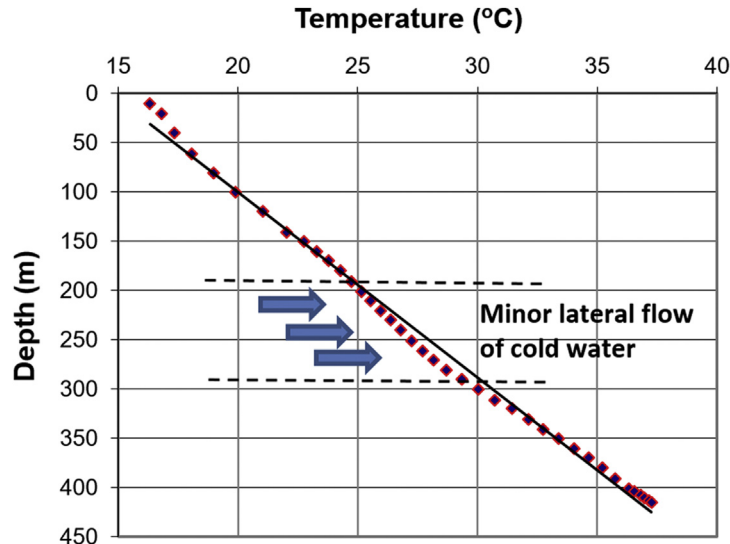


Figure 2.5 Thermal gradient showing a slight drop in temperature with depth due to shallow lateral flow. From Zarrouk, S.J., Moore, T., 2007. *Preliminary assessment of the geothermal signature and ECBM potential of the Huntly Coal bed methane field, New Zealand*. In: *Proceedings of the 29th NZ Geothermal Workshop, Auckland, New Zealand*.

Warm water systems include the largest geothermal systems with some extending between several countries [e.g. the Pannonian Basin extends between Austria, Croatia, Hungary and Slovenia (Raman et al., 2015)]. Historically, most of these systems have been identified through their natural thermal signature (hot springs) or from shallow ground water drilling. More recently, many new systems have been encountered through deeper petroleum or mineral exploration drilling (Fig. 2.6).

Warm water wells generally encounter reservoir pressures that are less than the hydrostatic head of water, temperatures much lower than the boiling point for depth (BPD) and with not much gas content. These wells are not likely to be self-discharging and down-hole pumps are required in most cases to produce the geothermal fluid. In some cases, water quality is reasonably potable (e.g. Vietnam and China). It is common that the reservoir includes some unconsolidated sand or silt formations, which complicates drilling but provides good permeability.

In some shallow wells 800–1500 m depth, sand removal from the produced geothermal water is crucial. The upper-Pannonian sandstones (45°C–55°C) in Hungary have some badly cemented, heterogeneous and argilliferous formations (Gábor Szita, personal communication). The production of sand reduces the life of the down-hole pump, and so multistage sand removal systems are required sometimes to prevent damage to the pump and the reservoir permeability around the reinjection wells.

Warm water systems are likely to be used for direct-use applications; however, electricity production from 79°C water has been reported in the United States using a

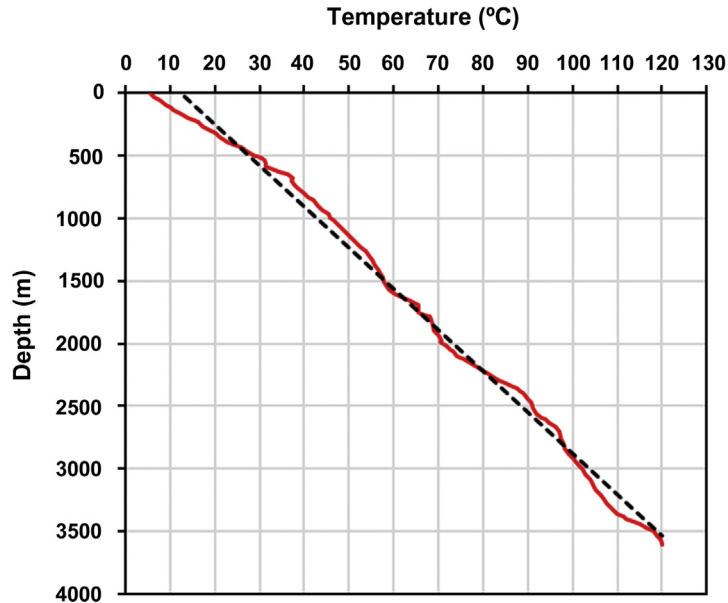


Figure 2.6 Temperature profile of a well from the Peace River Arch area, Canada. Data from Bachu, S., 1994. Geothermal regime in the Western Canada sedimentary basin. In: Mossop, G.D., Shetsen, I. (Comp.), *Geological Atlas of the Western Canada Sedimentary Basin*. Canadian Society of Petroleum Geologists and Alberta Research Council (Bachu, 1994).

binary unit at a very low conversion efficiency (Zarrouk and Moon, 2014). There is a boom in developing these systems mainly in Europe for large-scale district heating schemes, recreation, commercial greenhouse heating and industrial applications. Since large amounts of geothermal fluid are required due to the relatively low-energy content (low-energy quality), the fluid should be reinjected not far from the production well to minimise reservoir drawdown. Produced fluids from ~ 3000 m deep sediments can have a very high salinity (hypersaline) plus other dissolved minerals. Heijnen et al. (2015) reported an equivalent NaCl salinity of 280 g/L in 100.8°C reservoir fluid from 2748 m depth, which is highly corrosive. Heat exchangers are commonly used to heat a secondary fluid (fresh water) to control corrosion and mineral scaling in the surface production facilities. It is important to note here that even for a relatively low-temperature gradient of 20°C/km, drilling to great depths of 5–6 km will result in reservoir temperatures $>120^\circ\text{C}$. The criteria set in Table 2.4 considers the use of realistic drilling depths, technology and cost.

2.2.2 Hot water systems

These systems produce higher temperatures than warm water systems ($120^\circ\text{C} < T < 220^\circ\text{C}$) with the enthalpy of liquid water at the measured temperature

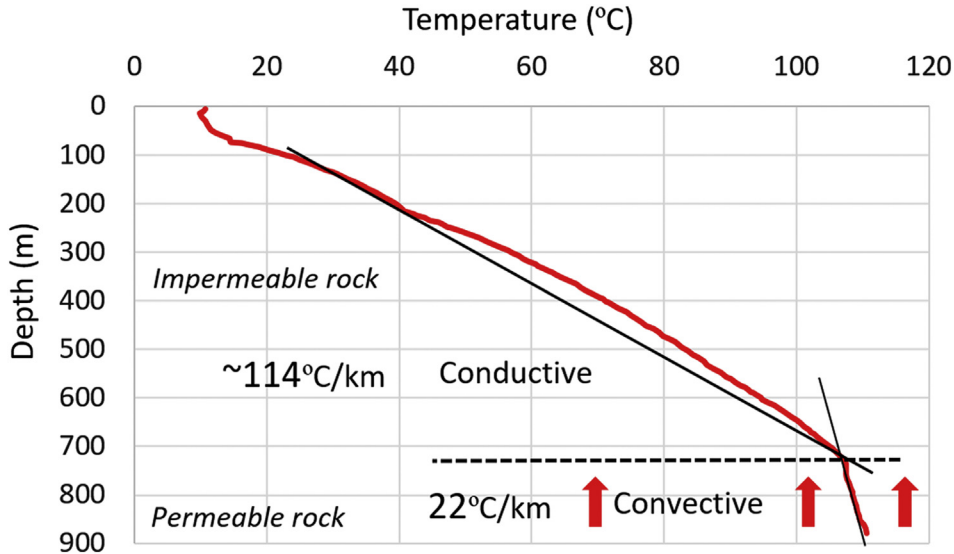


Figure 2.7 Temperature versus depth for a convective flow through the Alpine fault, New Zealand. Data from Sutherland, R., Townend, J., Toy, T., Upton, Ph., Coussens, J., Allen, M., et al., 2017. *Extreme hydrothermal conditions at an active plate-bounding fault. Nature 546 (7656) 137–140 (Sutherland et al., 2017).*

(504 kJ/kg < h < 943 kJ/kg). Generally, they have higher temperature gradients than warm water systems, which can result in convective heat transfer when the thermal gradient becomes unstable and gives way to natural convection. When the geothermal fluid ascends (in the convective plume ‘upflow’) through permeable rocks or fault zones, above this upflow near the ground surface the result will be both higher temperatures and a much higher thermal gradient ($> 100^{\circ}\text{C}/\text{km}$) than is practically possible through conduction alone (Fig. 2.7). Fig. 2.7 shows the conductive temperature profile to be relatively gentle, transitioning to a much steeper convective profile where there is fluid movement in the upflow. The slightly curved conductive profile of Fig. 2.7 is due to a deviated (nonvertical) drilled well profile.

Hot water systems are used for direct-use application, and for power generation, they are more suited to binary power plants, but steam flash technology can be used for the higher temperature end.

In hot water systems, no boiling occurs in the natural state or after production commences. Fig. 2.8 shows the temperature profile of well 6-2 in East Mesa plotted against the boiling hydrostat (Watson, 2013) or the ‘BPD’ curve. It is clear that no boiling is taking place in this well as at all depths temperatures are \ll those required for boiling (BPD).

To distinguish between a variable conductive temperature gradient (Fig. 1.1) and a profile with the conductive–convective transition (Figs 2.7 and 2.8), the decrease in temperature gradient (steepening) should be greater than four times to indicate a

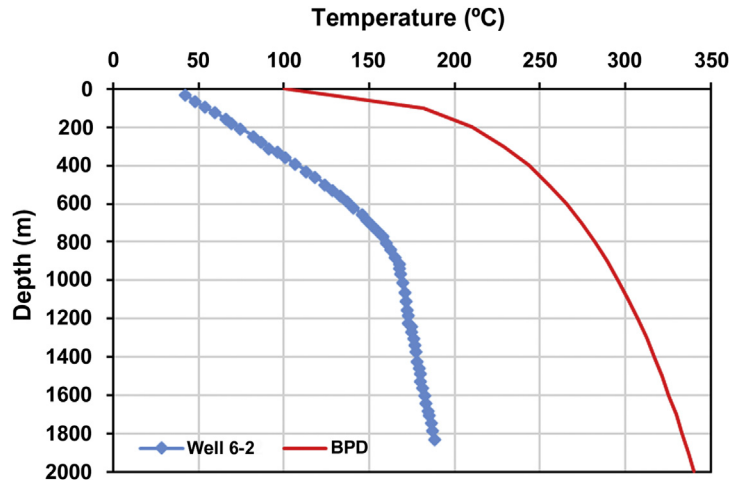


Figure 2.8 East Mesa hot water well 6-2. Data from Goldstein, E.N., Carle, S., 1986. *Faults and gravity anomaly over the east mesa hydrothermal-geothermal system. Geotherm. Resour. Council Trans. 10, 223–228 (Goldstein and Carle, 1986).*

transition to convection. In addition, only deep convective heat transfer will bring enough thermal energy to allow the development of shallow temperature gradients $>100^{\circ}\text{C}/\text{km}$ (Figs 2.7 and 2.8). These simple criteria should be useful to identify the presence of high-enthalpy (hot water or higher enthalpy) geothermal systems from examining shallow ($\sim 600\text{--}700$ m deep) exploration wells. However, these exploration wells will not help to distinguish between the upflow or outflow of a conventional system, for this purpose deeper wells are needed.

Some hot water wells are self-discharging when the reservoir pressure is higher than the hydrostatic head of water, but most wells require the installation of down-hole pumps to produce the geothermal fluid. Many of the geothermal systems utilised in the United States (e.g. Brady, East Mesa), Turkey (Aydin, Buharkent) and Russia (Pauzhetsky) are simply hot water systems. They have been referred to elsewhere as ‘low-temperature liquid-dominated’ systems (Aksoy, 2007) since the geothermal fluid has a low temperature (Table 2.3) and is in the liquid phase in the reservoir.

Kaya et al. (2011) and Diaz et al. (2016) showed that in hot water systems, more mass is produced per MWe generated when compared to the other higher enthalpy (two-phase or vapour-dominated) systems. Therefore as for warm water systems, without any injection the pressure will continue to decline until there is an induced recharge (from above, below and laterally) matching the overall production rate. In many cases, without reinjection, the pressure will drop too low to allow the self-producing wells to continue operation, and some may require the installation of down-hole pumps later in their life or possibly be converted to reinjection wells to recharge the surrounding production wells. Hence, reinjection should take place

relatively close to production wells. However, there is the fundamental tension between the benefit of pressure maintenance and chemical and/or thermal breakthrough when the cooled injected water reaches the production wells. In some fields, particularly those with large faults, thermal breakthrough has occurred rapidly, and injection has to be relocated further away from the production wells (Kaya et al., 2011).

2.2.3 Low-enthalpy two-phase systems

These systems are generally much more fractured than all the other system types, with high reservoir permeability surrounded by permeable formation allowing plenty of cold water recharge. Typically, vertical permeability is also high, resulting in flow of cold recharge fluid down into the reservoir from above. This also results in generally larger natural thermal output at the ground surface (more natural thermal features) than the other higher enthalpy systems. These systems are also larger in the extent of their upflow and outflow zone compared with the higher enthalpy systems. The natural thermal features in low-enthalpy systems are dominated by extensive boiling chloride water and less steam heated features in its natural state. Excessive exploitation commonly leads to an increase in steam-heated features and reduction in deep chloride water discharge as reservoir pressure decline.

Recharge of hot fluid will flow into the reservoir from below, induced by production and pressure drawdown. Wairakei witnessed >100% increase in deep fluid mass recharge in response to production between 1958 and 1997; this induced deep recharge slightly slowed down when infield reinjection started in 1997 (Zarrouk and Simiyu, 2013).

When production begins in this type of system, the pressure does not drop as much, as compared to higher enthalpy systems, and less boiling occurs. On the other hand the presence of noncondensable gases (NCG) (mainly CO₂) results in the lowering of the boiling point of water and boiling may occur after production.

Generally, wells in two-phase systems will self-discharge after drilling (during completion/production testing) or may have to be discharge stimulated (see Chapter 6: Completion and Output Testing), but the use of down-hole pumps is uncommon in these systems. Due to the presence of gas, to prevent corrosion of casing and to maintain it at a high temperature, two-phase wells are kept on a small bleed line when they are not in use.

Production enthalpies are typically at (or not much above) the enthalpy of hot water at the reservoir temperature. A good example of a low-enthalpy well is Wairakei well WK317 (Fig. 2.9)

The shut in temperature profile of these wells can be complicated by the formation of gas and steam caps (Fig. 2.10) and internal flows. Fig. 2.10 shows the

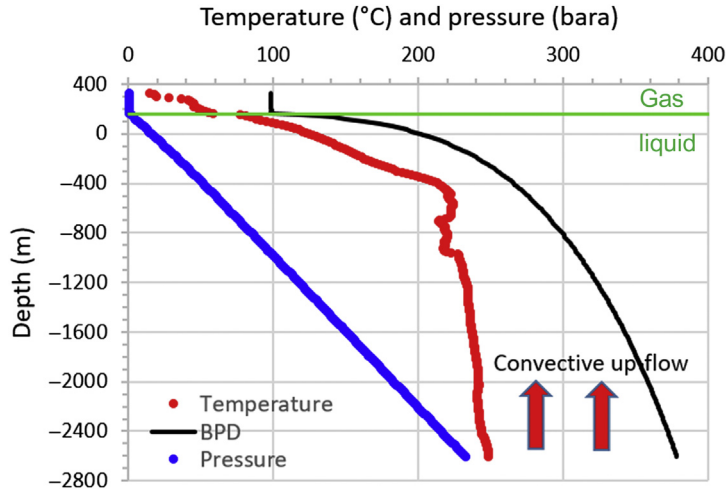


Figure 2.9 Shut-in temperature and pressure profile of well WK317. Data from Contact Energy Ltd., with kind permission.

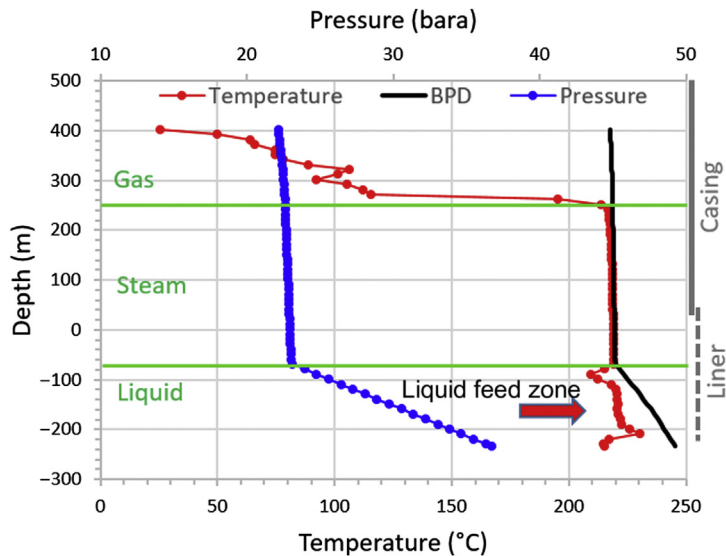


Figure 2.10 Shut-in temperature and pressure profile of well WK27. Data from Contact Energy Ltd., with kind permission.

formation of a gas and steam cap on top of the hot liquid in Wairakei well WK27, with a production enthalpy of just above 1000 kJ/kg, which is just above the enthalpy of water at the feed zone of 220°C. Fig. 2.10 also shows that Wairakei has a shallow vapour-dominated zone in a predominantly low-enthalpy, two-phase system. If this well is cased to say 400 m and drilled to

<800 m, it can produce dry steam with an enthalpy of ~ 2800 kJ/kg (enthalpy of steam at 220°C).

Steam flash power plant technology is historically used for low-enthalpy systems. However, binary units and hybrid steam and binary can also be used (Zarrouk and Moon, 2014). For every MWe of generation, less mass flow rate is needed in low-enthalpy systems than for hot water systems (Diaz et al., 2016), but in general a large number of reinjection wells are needed to ensure all the produced fluids are reinjected back. The common experience of infield injection in this type of geothermal field is that it has caused degradation of the resource by thermal breakthrough, and so injection has been moved outfield (Kaya et al., 2011; Diaz et al., 2016). The large fluid take in these systems can result in major subsidence, and reinjection can also play an important role in controlling/managing subsidence.

2.2.4 Medium-enthalpy two-phase systems

In their preexploitation or natural state, these systems are comprised almost entirely of hot water, with boiling zones which are nonexistent or small (Fig. 2.11). However, when production starts, the two-phase zone will expand and discharge medium-enthalpy fluid (in the range $1100\text{--}1500$ kJ/kg). These wells are also called ‘excess enthalpy’ because the produced enthalpy is higher than the enthalpy of water/liquid at the measured reservoir temperature (Kaya et al., 2011). Mubarok and Zarrouk (2017) demonstrated that even low-enthalpy (liquid-dominated) two-phase systems have some level of excess enthalpy.

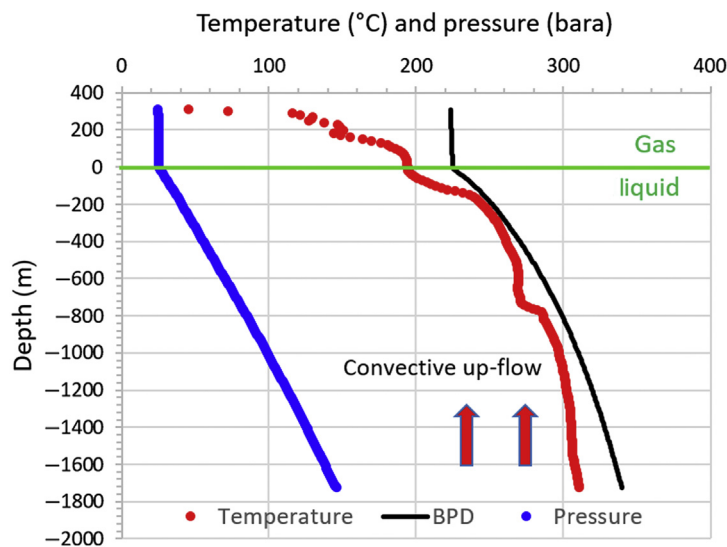


Figure 2.11 Medium-enthalpy Ohaaki west bank well showing close to boiling conditions (-200 to -300 m) in preexploitation state. *Data from Contact Energy Ltd., with kind permission.*

These systems have a lower reservoir permeability and less fracturing than low-enthalpy systems, with permeability of the rock surrounding the hot reservoir similar to that inside the reservoir, that is there is not necessarily any permeability contrast between the inside (the hot part) and outside (the cold part) of the reservoir (Kaya et al., 2011). These systems will have lower natural thermal output than low-enthalpy systems but have more steam-heated features. The size of the upflow zone is smaller than for low-enthalpy systems.

Medium-enthalpy two-phase ‘large diameter’ wells can potentially produce 35–40 MWe power output per well. This is because these wells have relatively higher enthalpy than low-enthalpy systems and produce more mass flow rate (more permeable reservoirs) than high-enthalpy systems. However, this is not very common with only a few such wells reported by the industry (Quinao et al., 2015).

Single and double steam flash power plant technology is historically used for medium enthalpy systems (Zarrouk and Moon, 2014). However, binary plant is used in the more recent power development at Ngatamariki (Quinao and Zarrouk, 2018).

In two-phase medium-enthalpy systems, the boiling zones which are developed as a result of production are more localised and have a higher steam fraction than low-enthalpy systems. The large pressure drop at production wells and the boiling induced in the reservoir are desirable effects from a reservoir engineering point of view as it results in high enthalpies. When production first starts, the pressure declines rapidly until boiling occurs and then the pressure declines more slowly.

In some cases, induced hot deep recharge due to rapid pressure drop may offset the cold recharge to some extent. However, depending on the balance between lateral and vertical permeabilities, natural cold recharge from both top and sides of the reservoir will help to sustain production. Infield injection of cold water will cause faster cooling of the production wells. Experience at a number of fields shows that a reinjection strategy of combined infield and outfield is essential. Often full reinjection infield in two-phase medium-enthalpy geothermal systems has resulted in thermal breakthrough. Moving reinjection outfield can reverse the damage (Kaya et al., 2011; Diaz et al., 2016).

2.2.5 High-enthalpy two-phase systems

These systems are very similar to the medium-enthalpy systems discussed earlier, but with a higher temperature range (250°C–330°C). They consist of a few major fractures in a low-permeability rock matrix with fracture volume and/or permeability somewhat smaller, and a boiling zone surrounding the production wells which is larger and dryer (Fig. 2.12) and thus the production enthalpies are higher (1500–2600 kJ/kg). These wells definitely produce excess enthalpy fluid. Multiple (double and triple) steam flash power plant technology is used in the lower

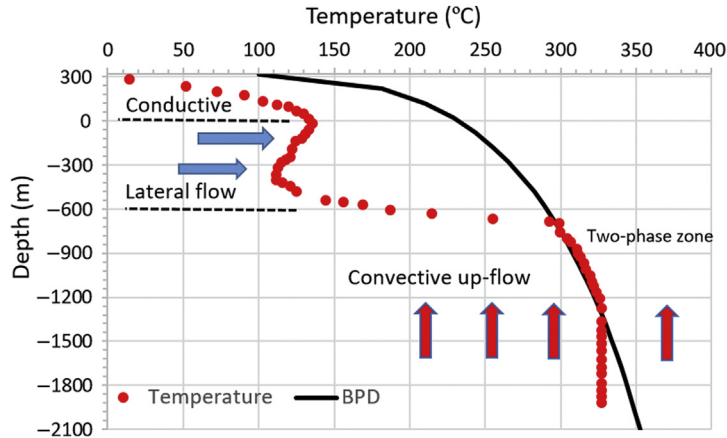


Figure 2.12 High-enthalpy two-phase Rotokawa Eastern well showing large >700 m thick two-phase zone. Hernandez, D., Clearwater, J., Burnell, J., Franz, P., Azwar, L., Marsh, A., 2015. *Update on the modeling of the Rotokawa Geothermal System: 2010–2014*. In: *Proceedings of the World Geothermal Congress, Melbourne, Australia*. © World Geothermal Congress (Hernandez et al., 2015).

enthalpy range (1500–1900 kJ/kg), but only single steam flash is used for the higher enthalpy (1900–2600 kJ/kg) wells (Zarrouk and Moon, 2014). This is because not much liquid remains after the first flash of the high-enthalpy fluid to be used in the second flash. At the same time, higher enthalpy wells can eventually dry with time, and single-flash (single pressure) technology lends itself better to dry steam by simply removing the steam separator (e.g. Kamojang). Hybrid steam and binary power plant technology have been used in medium (Mokai) and high-enthalpy (Rotokawa) systems. While it can be higher in conversion efficiency than flash steam technology, hybrid technology is less adaptive to changes in the geothermal reservoir and will likely need shutdown and plant modifications with time (Zarrouk and Moon, 2014).

Steam-heated features typically dominate the natural thermal discharge, with little or no chloride water discharging at the surface. The natural fluid recharge is limited by low permeability, and infield reinjection is essential to the sustainability of production (Kaya et al., 2011). More of the produced fluid should be injected infield compared with medium and low-enthalpy two-phase systems. A good example is the Rotokawa geothermal system, New Zealand, where all the reinjection is taking place infield. Note that all heat transfer mechanisms (conduction, convection and advection) are present in the system given in Fig. 2.12.

Some medium and high-enthalpy systems develop multiple upflow (convection) zones known as sectors, controlled by permeability and geological setting (Herrera et al., 1996; Aleman and Saw, 2000; Ramos, 2002; Sta Ana et al., 2002; Fajardo and Malate, 2005). Medium and high-enthalpy wells are generally self-discharging, and no

down-hole pumps are used. Non-self-discharging wells that cannot be discharge stimulated are likely to be on the system margins. These wells are normally used for reinjection or monitoring or are abandoned.

2.2.6 Dry steam (vapour-dominated) systems

Vapour-dominated systems are the prime geothermal systems with only a handful found in nature (Diaz et al., 2016). These wells produce dry (high-enthalpy) steam 2600–2800 kJ/kg, which can be sent directly to the steam turbines without separation to produce electricity with the highest conversion efficiency (Zarrouk and Moon, 2014). Dry steam wells are relatively shallow (<2000 m) compared to conventional wells, with most dry steam wells producing from a narrow reservoir temperature range of 220°C–250°C, for example Kamojang (Darwis et al., 1995), Matsukawa (Hanano and Matsuo, 1990) and Darajat (Simatupang et al., 2015). However, higher temperatures have been reported at >3000 m in the Geysers (Hulen et al., 2001) and Travale (Cei et al., 2009).

These systems are made of low-permeability reservoirs with even lower permeability rock surrounding the reservoir. If the surrounding rock were permeable, cold water would flow into the low-pressure vapour-dominated reservoir and cool the system (reducing the enthalpy). Therefore there is no natural convection taking place in these systems, and the dominant heat transfer mechanisms are thermal conduction from below plus advection (counterflow) from the top. The term ‘counterflow’ is used here to refer to the upwards travel of the low-density steam through the system to the ground surface (feeding the natural features), the downward travel of steam condensates and cold ground water under gravity to recharge the reservoir (Kaya et al., 2011).

The water level in a dry steam well is commonly below the steam feed zone (Fig. 2.13), and warmed up temperature, and pressure profiles are almost vertical and less than that the BPD pressure and temperature.

Vapour-dominated wells are always self-discharging (while there is hot fluid in the reservoir), and down-hole pumps are never used. Vapour-dominated wells commonly produce a relatively high gas content and a relatively low mineral content, since minerals have almost no solubility in steam.

Vapour-dominated systems generally have limited natural thermal output on the ground surface compared with low and medium-enthalpy two-phase systems. These natural features are strictly steam heated (e.g. steaming ground, mud and acid pools) with no deep (chloride) waters discharging at the ground surface.

As the reservoir pressure decreases during production, the immobile water in the reservoir boils to form steam. The water in a vapour-dominated reservoir is not replenished by natural recharge, and so after some years of production, parts of the reservoir may run out of immobile water and become superheated (i.e. the temperature

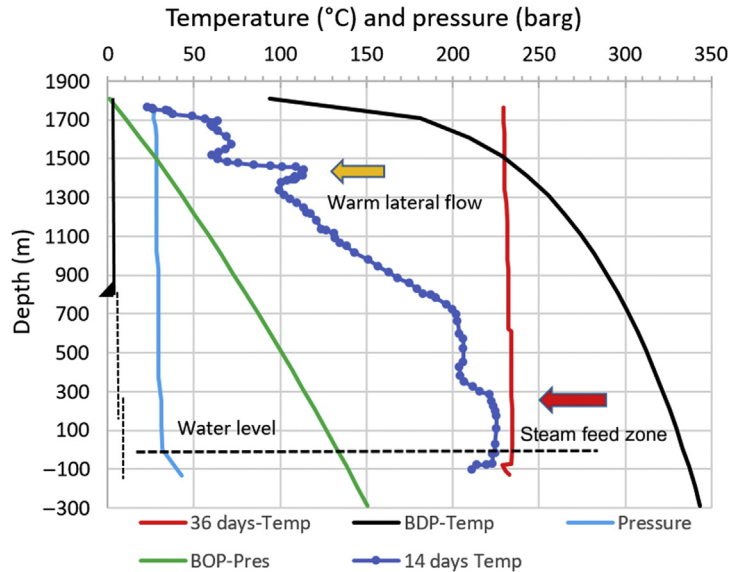


Figure 2.13 Temperature and pressure profiles of well DRJ-CA, Darajat, Indonesia. *Simatupang, C. H., Intani, R.G., Suryanta, M.R., Irfan, R., Golla, G. Cease, C., et al., 2015. Evaluation of water produced from a steam dominated system, a case study from the Darajat field. In: Proceedings of the World Geothermal Congress, Melbourne, Australia. © World Geothermal Congress.*

of the steam is above the boiling point) and eventually dry out completely. Infield reinjection is most critical for the management of these systems. It is beneficial to inject water directly above the depleted reservoir and close to the production wells as at Kamojang and Darajat (Diaz et al., 2016). Since 75%–90% of the steam leaving the turbine evaporates in the cooling towers (Kaya et al., 2011), little water will be available for reinjection. In most cases, extra water is sourced externally for addition to the steam condensate before reinjection. This strategy has been successfully implemented at the Geysers and Larderello (Kaya et al., 2011) to maintain steam production. The need for external fresh water can pressure field operators to tap into natural water resources and possibly affect other users. This is because lack of external water for reinjection can affect the sustainable operation of these vapour-dominated reservoirs and result in rapid well decline.

2.3 Nonconventional geothermal systems

The term ‘nonconventional’ refers here to geothermal systems that are in research and development and field-testing stages but have not achieved the full mainstream commercial use of conventional geothermal systems.

2.3.1 Supercritical (deep volcanic) systems

This involves drilling much deeper wells into conventional two-phase geothermal systems to access geothermal fluid with temperatures of 450°C–600°C from 4 to 5 km depths (Elders and Fridleifsson, 2009). These temperatures are above the critical point of water (373.946°C and 220.64 bar), hence the name ‘supercritical’. At these conditions, the phase difference between water and steam will disappear, and the fluid will be a single-phase supercritical fluid with enthalpy of >3000 kJ/kg. The power potential of such wells will be in the order of 50–70 MWe, which is much higher than any conventional geothermal well. Drilling these systems pushes drilling, material and well test technology to new limits. The Icelandic deep drilling project (IDDP) is the only active supercritical exploration programme in the world. The first well IDDP-1 was drilled in 2008–09 and encountered molten magma at a depth of ~2100 m. In 2010–11 a series of measurements and flow testing showed that IDDP-1 has a measured temperature of 452°C and shut in wellhead pressure (WHP) of 140 bar/g (Friðleifsson, 2017) with a flowing enthalpy of 3200 kJ/kg and mass flow rate of 20–40 kg/s (Ingason et al., 2014) sufficient to generate 35 MWe (Friðleifsson, 2017). However, acidic condensate associated with the volcanic steam resulted in severe corrosion and erosion damage to the casing (Ingason et al., 2014). The second well IDDP-2 drilled at Reykjanes in 2016–17 to a total depth (TD) of 4659 m with production casing cemented to 2931 m. IDDP-2 encounters supercritical conditions with measured temperature of 426°C and pressure of 340 bar at TD after only 6 days of heating. Cold water stimulation was undertaken in 2017–18 to enhance the permeability of the well with plans to flow test the well in 2018 (Friðleifsson, 2017).

There are no pilots or commercial implementation of supercritical power systems yet, but the potential for utilising these systems can take geothermal power production to new horizons in the future.

2.3.2 Geo-pressured systems

Geo-pressured systems are highly pressurised sedimentary aquifers with water containing significant quantities of dissolved gases. These gases are different from the NCG (Kaya and Zarrouk, 2017) found in conventional systems, which are dominated by CO₂. The main gas components are CH₄ (Garg et al., 1986), with N₂, CO₂ and H₂S in lesser quantities (Yanagisawa et al., 2013).

The heat transfer mechanism in geo-pressured systems is mainly thermal conduction (see Fig. 1.1) with possible advection in some settings, for example warm water systems. In some of these systems, heat is generated by radioactive decay in granites underlying the sedimentary sequence, for example the granite reservoir in the

Cooper Basin, Australia, has measured $7\text{--}10\ \mu\text{W}/\text{m}^3$ of ongoing heat generation (Llanos et al., 2015).

Geo-pressured systems have been encountered during petroleum explorations in Australia (Llanos et al., 2015), Hungary (Antics, 1998; Toth, 2010), Indonesia (Hochstein and Sudarman, 2010), Japan (Yanagisawa et al., 2013) and the United States (Rudesill, 1978; Garg et al., 1986). Antics (1998) reported from the Pannonian Basin, Hungary, 190°C fluid from 3165 m depth, a reservoir pressure of 638 bar and WHP of 320 bar, with an equivalent pressure gradient of 210 bar/km (which is more than twice the hydrostatic head of cold water).

Hochstein and Sudarman (2010) described the uncontrolled Lusi mud-volcano discharge, Java, Indonesia, from geo-pressured and under-compacted Pleistocene sediments. The system has a $40^\circ\text{C}/\text{km}$ thermal gradient and a pressure gradient twice as high as the normal hydrostatic head of water. It was encountered during petroleum exploration drilling and resulted in gas (CH_4 , CO_2 and H_2S) and hot mud discharge of $1.5\ \text{m}^3/\text{s}$ covering an area of $6\ \text{km}^2$, the displacement of 40,000 people, and a subsidence area of over $7\ \text{km}^2$.

Geo-pressured systems can have all the necessary elements of conventional geothermal systems with the added potential to utilise the methane gas. Given the high reservoir pressures, these wells are definitely self-discharging, and down-hole pumps are not required. However, the very high reservoir pressure and operating WHP make them technically difficult to develop commercially. The main challenges are the high-pressure rating of all the utilisation equipment, and the associated cost and environmental risks. In addition, there is a high parasitic load required to operate the reinjection pumps to return the used geothermal fluid back into the pressurised reservoir. The production of both (high salinity) geothermal fluid and methane gas has been investigated since the 1970s (Garg et al., 1986). However, currently, there are no commercially operating geothermal geo-pressured developments.

2.3.3 Enhanced geothermal systems

Enhanced geothermal systems (EGS) are also known as engineered geothermal systems, and in the past the term hot dry rock (HDR) was used (Kruger, 1995) and the term hot sedimentary aquifers is also used by some authors (Bendall et al., 2014). In general, these systems may not have all three requirements of a conventional geothermal system (high temperature, fluid and reservoir permeability). They will normally have the high temperatures but lack the natural reservoir permeability and/or the presence of water in the rock. However, recent experience has shown that water should in fact exist at great depths almost everywhere on earth, but very low rock permeability and lack of fractures make some of these wells appear dry during testing, which is where the term HDR has originated. Since the 1970s there have been several field

trials of enhanced geothermal systems (EGSs)/HDR in many parts of the world (Kruger, 1995).

The Soultz EGS project, France, is the most widely studied EGS field in the world. Line shaft down-hole pumps produce 160°C fluid from ~5000 m deep fracture-stimulated wells (Ravier et al., 2015). The geothermal fluid has a natural Na–Cl–Ca rich brine with a high salinity of 100 g/L (ppt) and high gas content (mainly 85% CO₂, 10% N₂ and 2.5% CH₄) causing major corrosion problems with the down-hole pump assembly (Ravier et al., 2015). Temperature profiles of these wells (Held et al., 2014) show that the reservoir is effectively a hot water (convective) geothermal system. It is the only successfully stimulated EGS with an operating pilot power plant since 2011 (Vernier et al., 2015).

Careful examination of recent literature shows that the term EGS is also used to refer to improvement or stimulation of geothermal fluid production from practically all types of systems mentioned earlier, both conventional and nonconventional. Some examples are:

1. The Landau EGS project, Germany, is simply a conventional hot water system (160°C) with natural fault and fracture permeability in sedimentary and crystalline rock, with naturally existing (highly saline) fluid. The geothermal fluid is produced with a down-hole pump from a ~3000 m deep well and reinjected back under gravity into another well (doublet arrangement).
2. The Habanero EGS project in Australia (Llanos et al., 2015) is effectively a geopressured system, it has a reservoir temperature of >240°C from a depth of >4200 m, with shut in WHP of 337 bar. Hydraulic fracturing (using water only) is used to ‘improve’ the existing natural fracture permeability to allow commercial levels of power production. Geothermal fluid is reinjected back in to the reservoir using a high-pressure 160 bar reinjection pump (Hogarth and Baur, 2015).
3. Friðleifsson (2017) described production from a magma EGS, also called deep EGS, referring to the production of steam from the supercritical wells IDDP-1 and IDDP-2. Water is injected into these wells to enhance permeability then allowed to heat up to produce superheated steam. Given the low reservoir permeability at these high temperatures (> 400°C), it effectively means that deep geothermal or volcanic systems are simply EGS, or deep EGS as referred to by Friðleifsson (2017).

Therefore the term EGS is used when fluid is introduced to the geothermal reservoir or when the reservoir permeability is enhanced. It is also used at times to refer to developing geothermal energy in areas where no conventional two-phase systems exist. However, the most common EGS under investigation around the world mainly comprises warm and hot water systems.

The well test analysis concepts and applied techniques discussed in this book are valid for all types of geothermal system, and examples will be provided to their

applications in EGS. Permeability enhancement techniques used for improving the production from EGS and conventional geothermal wells (well intervention methods) will be discussed in detail in Chapter 9, Operation and Management of Geothermal Wells.

The development of EGS technology has the potential to bring geothermal energy utilisation to many parts of the world where none currently exists, and to boost energy production in a similar manner to the boom in nonconventional shale oil and gas production, which has resulted in a significant drop in oil and gas prices since late 2014.

2.3.4 Alternative geothermal (man-made) systems

Armstead (1978) proposed using an explosion from a thermonuclear weapon to create a geothermal system in areas where none exists. The explosion will trap the thermal energy and create a large cylindrical rubble zone, with high permeability. The size of the rubble zone is proportional to the power of the thermonuclear weapon. The geothermal development concept involves drilling into this rubble zone and injecting cold water to allow the recovery of the released energy plus the natural thermal gradient in production wells similar to EGS. However, the produced fluid will bring to the surface all the highly radioactive material from the thermonuclear explosion, which presents major environmental, health and safety risks. Therefore it is not recommended for any future research, field trials or consideration for commercial development.

Bär et al. (2017) investigated seasonal underground heat storage in middle-to-deep (100–1500 m) down-hole heat exchangers (or bottom-hole exchanger, see Chapter 3: Geothermal Wells) to store solar energy in summer to be utilised in winter for district heating. Numerical modelling showed that this is a promising technology that can potentially dispense of heat pumps (Bär et al., 2017). Energy storage between summer and winter helps reduce energy demand, decrease the use of fossil fuel and the release of greenhouse gases from burning of fossil fuels. We believe that man-made underground storage requires deep understanding of the local geological setting (e.g. having a permeable reservoir and an insulating cap rock formation) and the impact on ground water (e.g. heat migration). The cost of such system will limit the application of this technology to countries with specific optimum weather conditions and energy market setting, given the potentially low load factor. It should also be compared with the cost and risk of simply developing the local geothermal warm water systems, which can provide the required energy and storage system at the same time. Note that even in conventional geothermal systems, not all the energy in place can be extracted, hence a recovery factor (0.1–0.48) is used during estimation of a geothermal resource potential (Zarrouk and Simiyu, 2013).

Therefore it is anticipated that most (> 50%) of the energy stored in summer may not be recovered in winter.

Pruess (2006) proposed the use of CO₂ as a working fluid to recover the geothermal energy from EGS with the ancillary benefit of some CO₂ sequestration. However, CO₂ gas has much lower thermal transfer properties (e.g. enthalpy) compared to water or steam at the same temperatures. When the CO₂ mixes with any water in the formations, it will form a weak carbonic acid that causes ongoing corrosion problems to the geothermal wells in these developments (Zarrouk, 2004).

Several authors discussed using hybrid systems of combined solar, biomass and geothermal (DiMarzio et al., 2015; Thain and DiPippo, 2015). The concept is very valid and dates back to 1924 (Thain and DiPippo, 2015). A 30 MWe hybrid wood waste (biomass) plant with geothermal preheat has been running since 1989 near Honey Lake, California. Skiba (1985) discussed the drilling and testing of the self-discharging warm water wells at Honey Lake; however, there is no information on performance evaluation of the whole utilisation system.

Grijalva (1978), Rigby (1979) and Tiangco et al. (1996) investigated theoretical hybrid fossil fuel-geothermal power generation, but there is no field implementation of such systems.

In our opinion the industrial application of hybrid systems is attractive and possible but will be more technically challenging and site specific than using a single energy source.

Ground source heat pumps or geothermal heat pumps (GHP) that use the shallow conductive stable ground temperature as a heat source in winter, and a heat sink in summer have witnessed increasing growth worldwide (Lund and Boyd, 2016). Several authors have reported the results of field trials and long-term implementation of GHP. Rosen and Koochi-Foyegh (2017) discussed results of field trials of a GHP system in Alberta, Canada that uses 144 wells 35 m deep to store the solar energy in summer for use space heating in winter that resulted in significant saving in natural gas conventionally used in heating.

GHP is simply heat pump technology with the shallow underground as a heat source and sink. It can be applied anywhere on Earth and will be outside the scope of this book.

2.4 Summary

At the very early stage of regional exploration, the geological play type is of use, as other classification systems are precluded by a lack of data. During the exploration phase a temperature classification is possible at an early stage and is useful for planning further exploration strategy. After drilling and well testing, a classification based on thermodynamic fluid properties (enthalpy or exergy) is possible and the most useful

moving forward into the development phase. The influence of geological features on the fluid flow is also potentially useful during the production phase (and may not be apparent until this time). In a high-level global reporting context, the multifaceted United Nations classification is of use at any stage.

The classification based on enthalpy is preferred from a reservoir engineering point of view and was the focus of this chapter. This classification is based on experience in conventional geothermal systems; it takes into consideration the heat transfer modes and the permeability structure of the geothermal reservoir and surrounding rock. The enthalpy classification will not only influence the utilisation technology but also the reinjection strategy and will be referred to in the following chapters.

Alternative geothermal systems (deep geothermal, geo-pressured and EGS) and emerging and proposed technologies were also discussed. The work demonstrates that the term EGS is used differently by different authors, but generally, it refers to permeability enhancement and is most commonly applied to warm and hot water systems, while deep geothermal (volcanic systems) can simply be classified as deep EGS.

CHAPTER 3

Geothermal wells

Contents

3.1	Drilling and casing design	39
3.1.1	Drilling and the types of geothermal system	43
3.2	Self-discharging wells	44
3.3	Pumped wells	46
3.4	Airlifted wells	48
3.5	Down-hole heat exchangers	50
3.6	Reinjection wells	54
3.7	Monitoring wells	54
3.8	Other well types	56
3.8.1	Petroleum wells	56
3.8.2	Ground-water wells	58
3.8.3	Coal bed methane wells	59
3.8.4	Waste-water disposal wells	60
3.9	Summary	61

3.1 Drilling and casing design

Drilling a geothermal well in a new field is the most critical step in any geothermal development, due to the investment risk compared to all the other investigation studies and field surveys (geology, geochemistry and geophysics). From our experience, many geothermal projects stop at this stage when the developer/investor lacks the will or incentive to take this risk.

Geothermal drilling is not different in concept from petroleum or other deep drilling. However, there are certain differences specific to geothermal drilling and some modifications are required to allow petroleum rigs to be used for drilling geothermal wells. The main challenge is the high temperature, which affects the equipment used and the drilling string design. It also dictates geothermal well control practices that prevent uncontrolled well discharge (blowout), which are very different from those applied to petroleum well drilling.

Drilling effectively telescopes downwards from larger to smaller holes/casings in three to four stages depending on the well size, depth and target. The final cemented casing is called the production casing, and drilling for production extends downwards from there, and is usually protected from collapse by running perforated or slotted steel liner. In some shallow direct-use wells, it is common to keep an open hole

Table 3.1 Conventional self-discharging geothermal well casing designs.

Casing	Large well size	Standard well size	Small well size
Conductor casing	40" Casing cemented to 24 m, drilled with auger	30" Casing cemented to 24 m, drilled with auger	20" Casing cemented to 24 m, drilled with auger or in 26" drilled hole
Surface casing	30" casing cemented in 36" drilled hole	20" casing cemented in 26" drilled hole	13.375" Casing cemented in 17.5" drilled hole
Anchor casing	20" or 18.625" Casing cemented in 20" drilled hole	13.375" Casing cemented in 17.5" drilled hole	9.625" Casing cemented in 12.25" drilled hole
Production casing	13.375" Casing cemented in 17.5" drilled hole	9.625" Casing cemented in 12.25" drilled hole	7" Casing cemented in 8.5" drilled hole
Open hole (liner)	9.625" Perforated liner in 12.25" drilled hole	7" or 7.625" Perforated liner in 8.5" drilled hole	Open 5.5" drilled hole Or possibly installed with 4.5" perforated liner

Source: From Hole, H., 2013. Geothermal drilling-keep it simple. In: Proceedings the 35th New Zealand Geothermal Workshop, Rotorua, New Zealand; Hodson-Clarke, A., Rudoff, R., Bour, D., Russell, P., 2016. Key factors to successful drilling and completion of EGS well in Cooper Basin. In: Proceedings 41st Workshop on Geothermal Reservoir Engineering, Stanford University, Stanford, CA.

without running the liner. Geothermal wells are generally larger in diameter than wells drilled by all other industries. This is to enable the production of more fluid (mass flow rate) and hence more thermal power [following Eq. (2.1)]. Table 3.1 gives the common conventional geothermal well casing designs used by the industry.

Well sites are chosen to allow access to specific permeable geological targets in the reservoir. Common targets are permeable formations, contact zones between different formations, and faults and fractures. Experience shows that certain rock types (e.g. andesite) usually make good reservoir targets in conventional geothermal systems. The final well-site location may be constrained by land access and ground surface setting. Therefore deviated wells are common as they allow the intersection of multiple targets by a single well and the drilling of multiple wells from the same drilling pad, thus reducing the length of surface pipelines and fluid-handling facilities. The two common deviated well profiles (well tracks) are the J and S shapes (Fig. 3.1). Deviated wells can travel horizontally (throw) >1000 m which increases their chance of intersecting targets (e.g. faults), especially during exploration drilling. Vertical wells, on the other hand, are lower cost and are the simple option when possible or when the targets are reasonably constrained.

Deviated wells are drilled vertically at first, and then after setting the anchor casing, the mud motor is used from the kick off point to build angle in the chosen direction

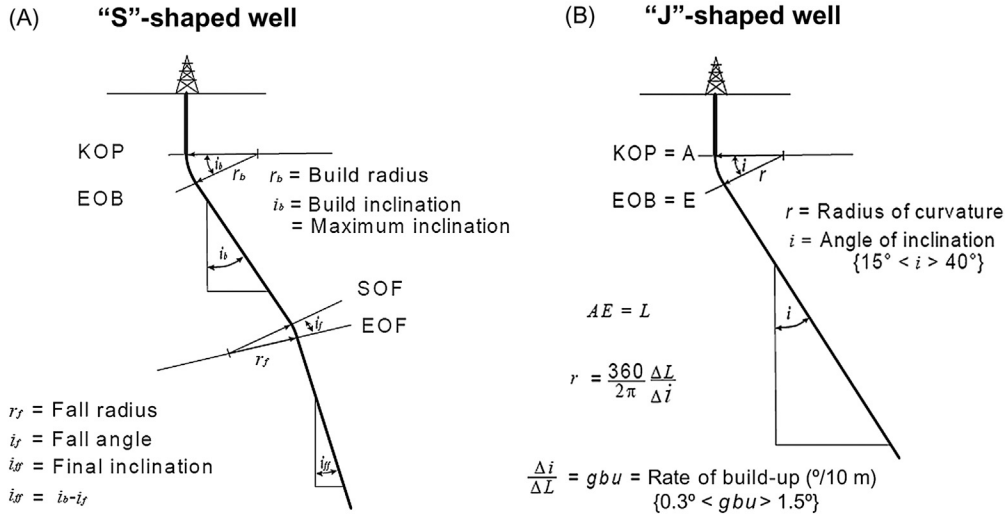


Figure 3.1 Showing deviated geothermal well tracks (A) S-shaped well and (B) J-shaped well. From Mr. Hagen Hole with kind permission.

until the end of build-up. J-shaped wells maintain this angle to total depth (Fig 3.1B), while S-shaped wells can change their angle or direction if needed (Fig. 3.1A). The change in well direction (azimuth) requires the use of the mud motor, while changing the fall angle can be done with modification to the bottom-hole assembly. An important point to make when working with down-hole data from deviated wells is to distinguish between drilled depth or measured depth, which are always greater than the true vertical depth (VD).

Horizontal drilling is common in sedimentary formations in petroleum and other industries but is not used in conventional two-phase systems with fractured volcanic rock due to hole stability risks. However, it could be an option for warm and hot water systems in sedimentary basins when there are favourable commercial terms.

Well pad (site) preparation is also a very important step as the pad is designed to protect the drilling rig from an accidental uncontrolled well kick during drilling. If the wells are not predicted/expected to self-discharge (e.g. in warm or hot water systems), this will significantly simplify well design, drilling and reduce the site preparation cost.

Since production from conventional geothermal wells relies on the natural reservoir permeability, care is taken to prevent damage to the target formations. The shallow part of a conventional well is drilled with heavy (high-density) fluid (mud) to block/isolate ground-water aquifers and any permeable shallow formations, then a carbon steel casing is cemented through this section. Drilling with mud allows the drilling engineers to put higher pressure than the hydrostatic head of water on the formations while drilling. This allows them to manage the well through cooling, help maintain a clean hole and prevent the flow of hot fluid to the surface.

Historically, wells were drilled with mud even in the productive part of the reservoir and then switched to drilling with water when circulation was lost. This method can cause build-up of cuttings (fill) and mud damage to the reservoir near the wellbore, which affects future production. Recent drilling practice involves underbalanced (aerated or foam) drilling in the productive part of the reservoir, which means the pressure in the well during drilling is kept slightly below the formation pressure. This prevents formation damage and allows the well to flow (kick) when the production target is intersected.

Elaborate site preparation and blowout prevention systems are required to control the well at any stage in the drilling programme (Watson, 2013; NZS 2403, 2015).

Commonly-used casing programmes for conventional wells are given in [Table 3.1](#). These casing sizes and their specifications originated from the oil industry standards (see NZS 2403, 2015) and have been adapted by the geothermal industry. Therefore despite the widespread use of SI units, casing diameters [in inches (")] are the only British Standards unit reported in use.

Deep EGS wells (> 4000 m) are commonly drilled vertically and often follow the smallest well size ([Table 3.1](#)). Sometimes however the production casing and open hole (liner) sections are drilled continuously, to the same size (8.5"), and then only the top part of this section is cemented (with the 7" production casing), leaving the bottom part open (Hodson-Clarke et al., 2016). Relatively shallow exploration slim holes are drilled to investigate the geothermal resource (temperature, geology, chemistry and permeability), and are generally drilled up to 1000–1200 m using a small mobile rig and typically cased with 7" intermediate casing, 4.5" production casing and a 3.5" perforated liner (common practice in New Zealand). However, other dimensions for slim holes are used in other countries (Nielson & Garg, 2016; Kaspereit & Osborn 2017).

Hole (2013) reported the cost of drilling a standard geothermal well ([Table 3.1](#)) at \$NZ 8.5 M (~\$US 6.0 M) with a calculated annual inflation of 19% between 2003 and 2013. Therefore the drilling cost is expected to increase with time. Geothermal exploration wells are normally drilled in a multiple-well campaign to reduce the mobilisation cost per well. From experience, it is not possible for all these wells to be successful. Developers venturing into the geothermal industry should be prepared for the possibility of walking away with nothing, as there is no method to guarantee the success of a well.

Geothermal well drilling is a wide engineering discipline and discussing all the detail involved is outside the scope of this book. The main point we would like to make is that engaging a qualified and experienced 'geothermal drilling engineer' is critical to success of any geothermal drilling and exploration programme. There are also different drilling techniques (schools) which can vary from one country to another. An excellent worldwide-recognised guide on geothermal drilling is the code of practice for deep geothermal wells (NZS 2403, 2015).

3.1.1 Drilling and the types of geothermal system

Understanding the type of geothermal system is very important when planning geothermal drilling operations. The main concerns are: well control during drilling through the productive part of the geothermal reservoir, ensuring maximum well productivity/injectivity and the long-term well integrity.

When drilling into warm and hot water systems, it is less likely that wells will self-discharge, which simplifies well control. These systems also have less warm and steaming ground and gas hazards on the surface (or none at all). This should simplify and reduce the cost of site preparation if cement grouting is not mandated. The low temperature and pressure conditions reduce the mechanical and thermal stresses and simplify well construction.

When drilling into two-phase systems, there is a higher chance of self-discharge (kick) during drilling. In the up-flow part of the system, the depth of the two-phase zone generally increases with the increase in reservoir enthalpy (see Figs 2.9, 2.11 and 2.12). The risk of blowout in two-phase systems is high not only in the productive part of the reservoir but also while drilling into the shallow steam cap (200–600 m) on top of the up-flow zone. The risk of a well kick increases with the increase in the gas content of the field. Expensive site preparations are required due to the relative prevalence of natural thermal activity (hot pools, steaming ground etc.) compared to warm or hot water systems.

On the other hand, drilling in vapour-dominated (dry steam) systems has a lower risk than two-phase systems. Although vapour-dominated wells will definitely self-discharge (see Section 2.2.6) and can effectively kick during drilling, the low reservoir pressure makes it easy to control the well by simply quenching (cooling) the steam by pumping cold water.

The highest risks for blowouts during geothermal drilling are in geo-pressured systems, since the reservoir pressure is much higher than the hydrostatic head of water. Toth (2010) reported a blowout of a geo-pressured geothermal system during the drilling of an oil-exploration well in Hungary in the 1980s. The well intersected a highly pressurised formation at a depth of 3880 m with a temperature of 199.6°C and pressure of 73.1 MPa (estimated from a wellhead pressure (WHP) of 36 MPa and by adding the hydrostatic head of water). Petroleum drilling and well control practices did not prepare the drilling engineers to control this scenario with almost double the hydrostatic pressure gradient at high-temperature conditions.

Drilling engineers generally know from experience that some fields have a higher likelihood of a kick (shallow or deep) during drilling than others. This effectively comes down to the type of geothermal system discussed in Chapter 2, Geothermal Systems.

3.2 Self-discharging wells

It is very desirable that all production wells are self-discharging. However, this is unlikely in warm and hot water systems, while most two-phase and all vapour-dominated wells are self-discharging (Chapter 2: Geothermal Systems). Reservoir pressure, rock permeability and depth of the feed zone play an important role in determining the ability of the well to self-discharge. Good permeability and relatively high reservoir pressure will result in good production from a geothermal well with high temperature and enthalpy. However, these wells generally have lower reservoir pressure than the hydrostatic head of cold water; it is a common misconception that geothermal wells discharge as a result of high pressure underground. Rather, the flashing (to steam and water) of the geothermal fluid inside the reservoir or casing causes the fluid to reduce in density and expand in volume, allowing the fluid to travel to the surface. Of course, the higher the reservoir pressure, the higher the WHP will be. Higher flowing WHP allows the use of different generation technology (double and triple flash) and gives more operational flexibility.

Predicting whether the well will self-discharge after drilling and the techniques employed to stimulate discharge will be addressed in Chapter 6, Completion and Output Testing.

Self-discharging wells generally produce more energy than the other well types. In geothermal power development, they effectively replace both the circulating pump and the boiler in conventional (Rankine cycle) thermal power plants.

Self-discharging wells are designed following the casing designs given in Table 3.1. Conventional wells in two-phase and vapour-dominated systems are generally drilled to around 1000–2500 m VD, deeper wells are drilled in some fields but it is not common to drill beyond 3000 m. EGS wells (hot and warm water systems) are commonly drilled deeper (> 3000 m) and for this reason, the small well size is used in some cases.

The wellhead assembly for a standard well size commonly includes two side valves of at least 3" through bore diameter (NZS 2403, 2015). Also one master valve which is commonly 10" with material and flange sizes chosen depending on the expected service temperature, pressure and down-hole conditions (NZS 2403, 2015). The master valve function is only to open or shut the well. It is not to be used for flow control (throttling). An additional flow control valve is installed downstream to manage the well.

The wellhead assembly is either attached to the production casing (Fig. 3.2A), which is also called single-skin assembly, or to the anchor casing (Fig. 3.2B) via an expansion spool, which is also called double-skin assembly. The expansion spool allows the production casing to thermally expand or contract with minimum movement of the wellhead assembly. A permanent thrust frame is used to support the wellhead assembly in the axial direction while allowing the well to thermally expand vertically (Fig. 3.3).

Fig. 3.3 also shows the service valve on the top of the assembly, which is used to run down-hole measurement tools in the well. The flange that connects the master

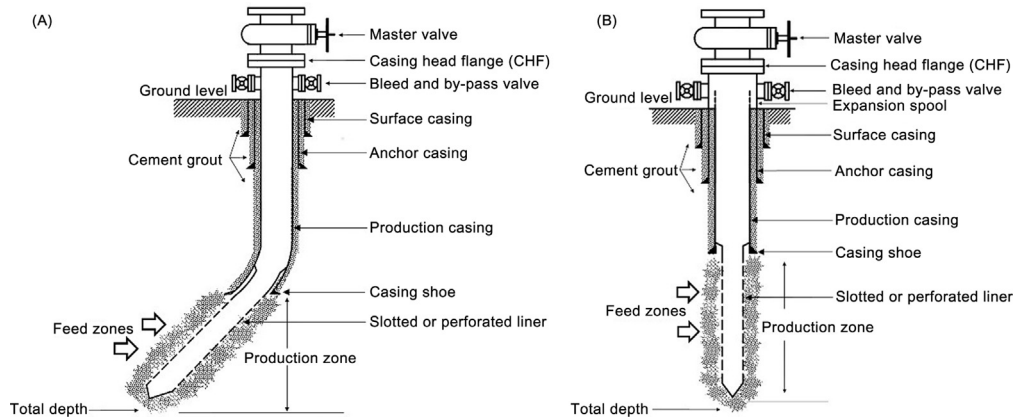


Figure 3.2 Self-discharge wells design (A) deviated (J-shaped) with no expansion spool and (B) vertical well with expansion spool.

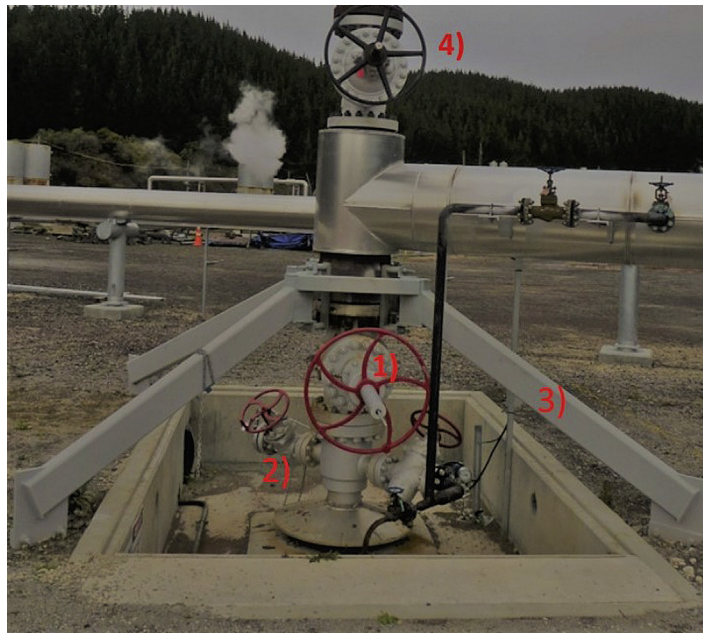


Figure 3.3 Producing conventional wellhead assembly showing: (1) master valve, (2) side valves, (3) thrust frame and (4) service valve.

valve to the well casing (Fig. 3.2) is called the casing head flange (CHF), which is used as the reference for all down-hole measurements, referred to as metres from casing head flange (m CHF) or simply “measured depth”.

In direct-use applications, shallow (100–150 m) wells drilled into lateral flows (outflow) with geothermal fluid temperatures exceeding 150°C are known to be

self-discharging (Narasimhan and Witherspoon, 1979). These wells can transfer a significant amount of energy to the surface in the range of 3–30 MW_{th} depending on well size and reservoir temperature. In New Zealand, direct-use wells are commonly designed with 6" or 4" production casing and with open-hole completion (Dunstall, 1992).

3.3 Pumped wells

Geothermal production wells that do not self-discharge (even after discharge-stimulation) are converted into reinjection or monitoring wells or are abandoned. However, production may be enabled by running down-hole pumps. Pumped wells are generally less commercially attractive than self-discharging wells because of the added investment and maintenance costs and the added parasitic load of the pump motors (Hochwimmer et al., 2015), and the most critical factor which is the short lifetime of the pumps (Held et al., 2014).

Nevertheless, geothermal resources requiring the use of pumps are potentially more widespread. These include warm and hot water systems (discussed in Chapter 2: Geothermal Systems), as well as lateral outflows from higher temperature (two-phase) systems (Hochwimmer et al., 2015) and EGS systems (Held et al., 2014). The production casings are cemented at relatively shallow depths (100–200 m) when producing from lateral outflows of two-phase systems (Steins and Zarrouk, 2012; Febrianto et al., 2016). These wells are commonly designed with an open hole without perforated liner.

Deeper (> 600 m) wells with liners are commonly needed when targeting hot water systems and much deeper wells (> 2000 m) for warm water systems (Hochwimmer et al., 2015).

Pumped wells are used with Organic Rankine cycle (ORC) power plants or for direct-use applications. The produced fluid goes through heat exchangers and is then reinjected into the reservoir. Note that it is not common to have pumped wells and self-discharging wells serving the same ORC power plant and definitely not steam flash plants.

There are two types of down-hole pumps: submersible (down-hole motor) (Fig. 3.4) and line-shaft (top drive) pumps (Fig. 3.5), each design has advantages and disadvantages (Hochwimmer et al., 2015). Geothermal down-hole pumps can operate at $T < 240^{\circ}\text{C}$ (Hochwimmer et al., 2015) and the selection and installation of these pumps depends on the well design, fluid chemistry, production flow rate, reservoir pressure (water level) and permeability. Table 3.2 from Johannesson (2015) gives the common line-shaft pump flow capacity for different size casings. The pump size is determined after knowing the production casing size.

It is possible to install a down-hole pump inside existing wells originally designed for self-discharge (Fig. 3.4A). However, dedicated pumped wells are designed

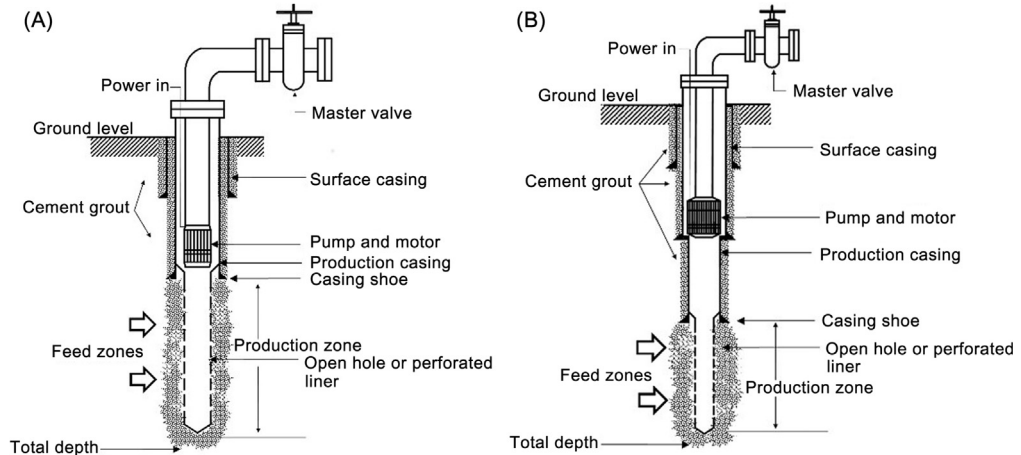


Figure 3.4 Down-hole pump with motor (A) standard well design and (B) dedicated pumped well design.

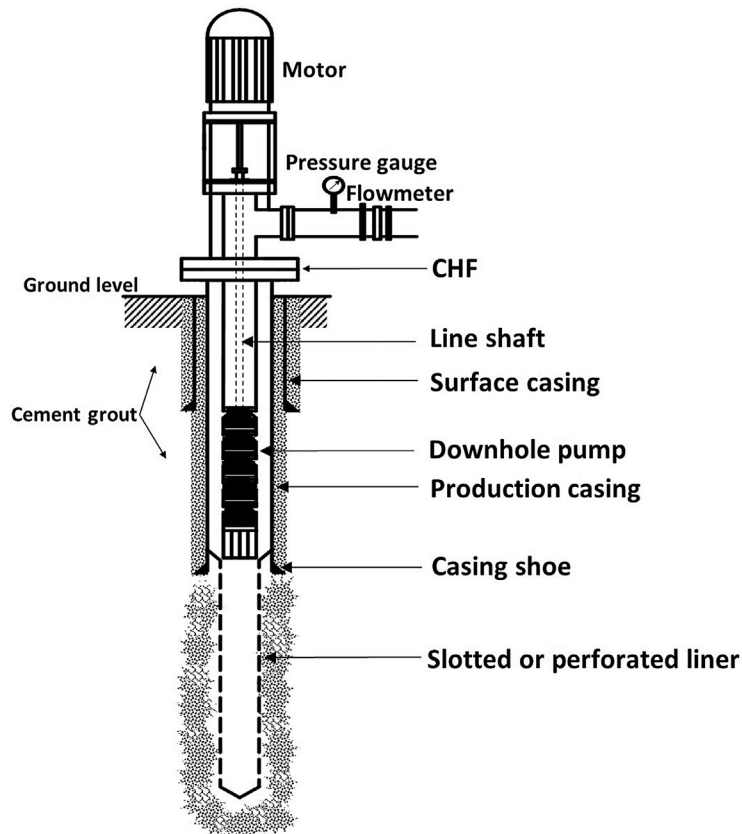


Figure 3.5 Line-shaft (multistage) down-hole pump with top electrical motor. After Niyazi, A., 2007. *Optimization of downhole pump setting depths in liquid dominated geothermal systems: a case study on the Balcova-Narlıdere field, Turkey. Geothermics 36, 436–458 (Niyazi, 2007).*

Table 3.2 Common line-shaft pumps using in geothermal power production.

Pump size OD (in.)	Flow rate (L/s)	Pump bowl diameter (mm)	Casing OD (in)	Casing ID (mm)
8	36	196.9	9.625"	210
10	63	249.2	13.375	315
12	100	298.5	13.375	315
16	181	406.4	20	470

Source: After Johannesson, Th., 2015. Low temperature geothermal wells. In: Lecture at the IGA academy, World Geothermal Congress, Melbourne, Australia.

differently (Fig. 3.4B) to allow the installation of larger diameter pumps for greater fluid flow rate (Table 3.2).

Line-shaft pumps (Fig. 3.5) require ongoing lubrication of the line shaft bearings, which keeps the shaft in the centre of the rising pipe and prevents mechanical erosion. Lubrication oil (~15–20 litres/day) is pumped through the shaft to the bearing; this oil does not circulate back to the surface and is lost to the fluid.

To protect the down-hole pump from possible hole collapse, the down-hole pump is always installed within the cased part of the well (Figs. 3.4 and 3.5). Hochwimmer et al. (2015) provided simple calculations for setting the pump depth and the required pump shaft power to produce a constant flow rate at the required discharge pressure.

Experience with large-capacity down-hole geothermal pumps indicates an operational life of 1–2 years, after which the pump needs major maintenance or possible replacement (Hochwimmer et al., 2015). However, this can be sufficient and Held et al. (2014) used a pump lifetime of 1 year in his business model of the Soultz EGS demonstration project. Febrianto et al. (2016) reported a down-hole pump (motor) failure within 2.4 years from a relatively warm, lateral outflow fluid at 105°C. In power development, it may be viable to have some redundant production capacity or have spare pumps ready to install in such events. However, for direct-use applications, a backup (alternative) energy supply might be more economical than having standby wells and pumps.

3.4 Airlifted wells

Airlift wells work by blowing air into the shallow well from a compressor (Fig. 3.6). Hot water and air mix below the water level in the well, consequently decreasing the density of the mixed water–air fluid, allowing it to discharge to the surface for utilisation.

Many airlift geothermal wells are utilised in Rotorua, New Zealand, for domestic purposes such as bathing, mineral pools and space heating. Airlifted geothermal wells are not used in power production since they have a relatively lower power

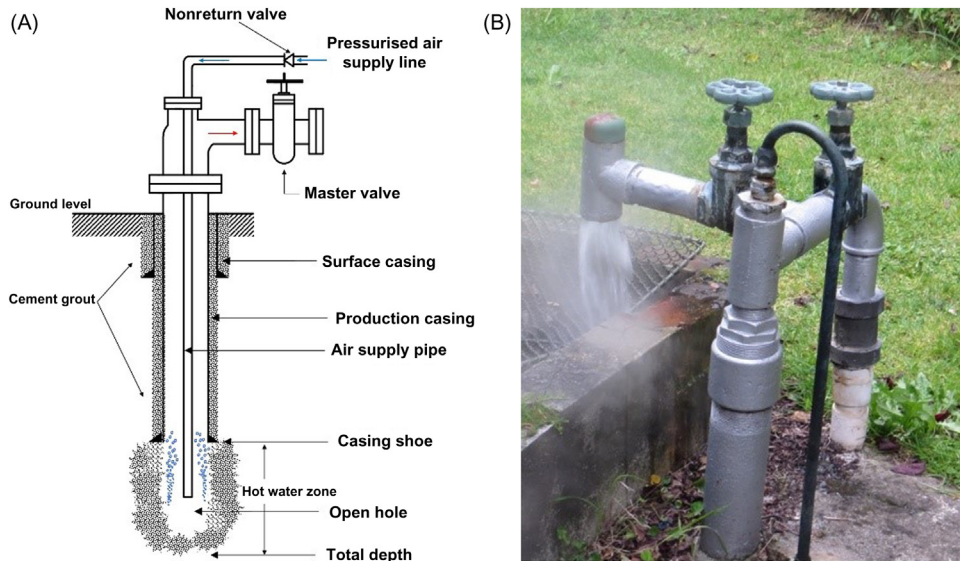


Figure 3.6 (A) Schematic of an airlifted production well. (B) Picture of airlifted well RR447, Rotorua, during discharge testing. (A) After Thain, I., Reyes, A., Hunt, T., 2006. *A Practical Guide to Exploiting Low Temperature Geothermal Resources*. Technical Report. Institute of Geological and Nuclear Sciences Limited, Lower Hutt; (B) from Candra, S.A., Zarrouk, S.J., 2013. *Testing direct use geothermal wells in Rotorua, New Zealand*. In: *Proceedings the 35th New Zealand Geothermal Workshop, Rotorua, New Zealand* (Candra and Zarrouk, 2013) with permission.

output 1–4 MW_{th} (Thain et al., 2006) compared to self-discharging or pumped wells in lateral outflows from two-phase systems. This makes these wells more suitable for small-to-medium-scale domestic purposes that generally do not require large flow rates.

The common problems with airlift geothermal wells are mineral deposition and corrosion, which can occur due to the introduction of oxygen into the well. This will cause deposition in the inner surface pipe and later in surface heat exchangers. Drew (1988) recommended reducing the air-to-water ratio (thus increasing the geothermal water flow) to reduce these problems. It is also possible to use nitrogen gas to lift the geothermal fluid; however, this comes at an added cost. Artificial gas lift is used by the petroleum industry to enhance oil recovery (Hammadh et al., 2015).

The maximum well output and the optimum air/water ratio are normally measured by trial and error, which involves changing the air flow rate and the depth of the air supply pipe to water level (submergence ratio). It is also possible to optimise these parameters to estimate the maximum potential well output (Zenz, 1993; Cho et al., 2009).

3.5 Down-hole heat exchangers

Also known as bottom-hole exchangers, down-hole heat exchangers (DHEs) are an environment-friendly method of extracting thermal power from shallow geothermal wells. This is because using DHEs will eliminate the production and disposal of the geothermal fluid, since only heat is extracted from the well (Lund, 2003). DHEs are used extensively at Klamath Falls, USA, and Rotorua, New Zealand, for both domestic hot water heating in dwellings and institutional buildings, and they have also been reported in use in other countries (Dunstall, 1992).

The DHE consists of a U-tube (Fig. 3.7) or pipe laid inside the geothermal production well. Clean (fresh) water is circulated inside the pipe or tube, and the heat is

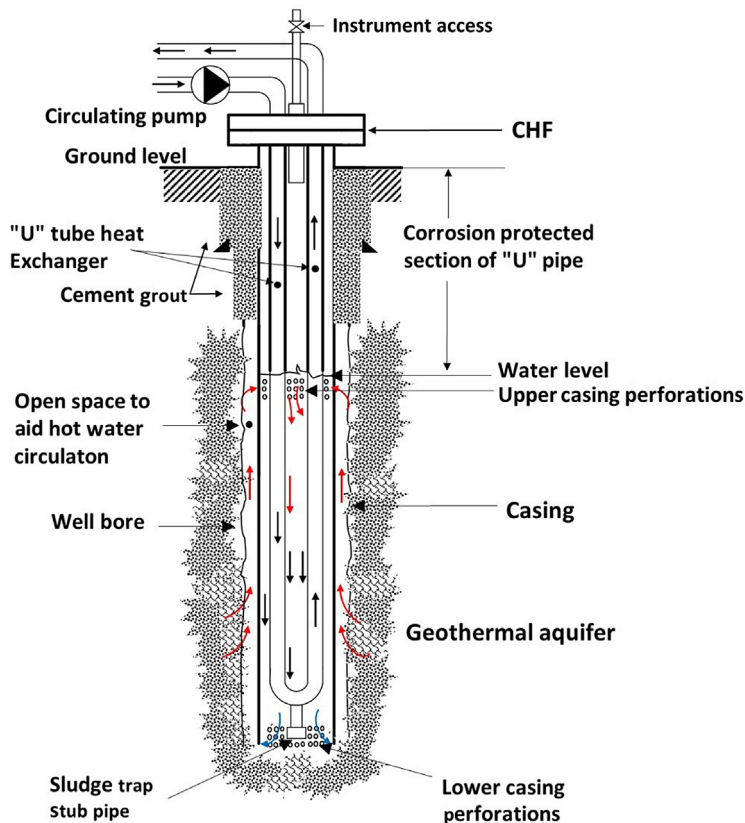


Figure 3.7 Geothermal well with a DHE designed to promote natural convection between the well and the open hole. DHE, Down-hole heat exchanger. Modified after Thain, I., Reyes, A., Hunt, T., 2006. *A Practical Guide to Exploiting Low Temperature Geothermal Resources*. Technical Report. Institute of Geological and Nuclear Sciences Limited, Lower Hutt.

extracted from the geothermal well by forced convection while the heat is brought from the reservoir into the well by natural convection and conduction.

Installing the U-tube DHE inside of the geothermal well is more economical compared with the other methods, because it does not require drilling a reinjection well, mitigates the risk of scale deposition and pump maintenance costs. However, the thermal power output of a DHE is relatively small, typically 200 kW_{th} maximum (Thain et al., 2006) compared with all the other well designs previously discussed. The amount of energy recovered strongly depends on the type of geothermal system.

Some DHEs are designed to promote (enhance) natural convection between the drilled open hole (bore) and the perforated well casing (Fig. 3.7). An alternative design involves installing promoter pipe inside the well casing to promote natural convection from the open bottom part of the well up to the water level inside the casing (Fig. 3.8A).

The common casing size for domestic dwelling sized direct-use wells with DHE is 4" (100 mm). The standard DHE pipe size is 1" (25.4 mm) for both the hot and cold legs, and this can limit the use of the promoter pipeline. Therefore having a promoter pipe built into the cold leg (Fig. 3.8B) allows more space for both instrument access and natural fluid circulation.

Dunstall (1992) reported that the promoter pipe of Fig. 3.8B has two main functions: (1) provides a path for bulk circulation in the well and (2) provides additional barrier to the thermal interference between the DHE tubes.

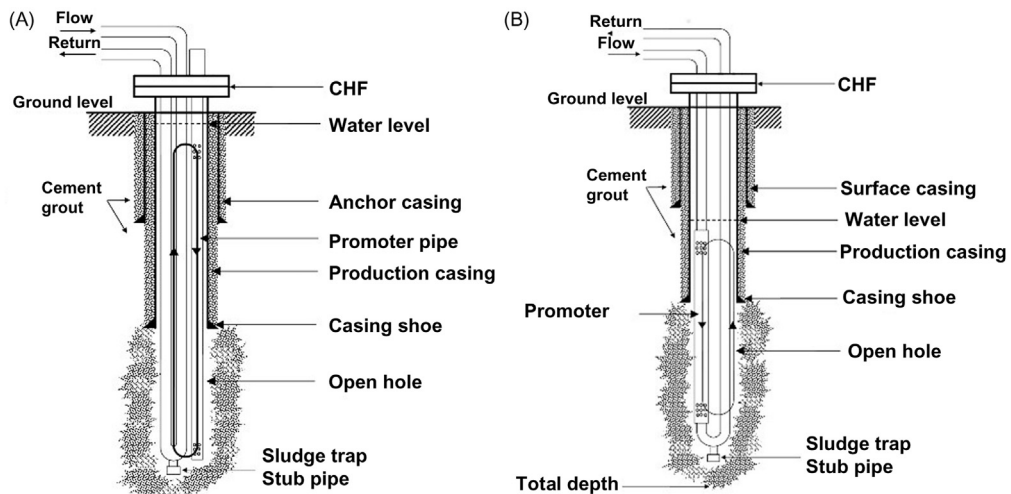


Figure 3.8 (A) Geothermal well with a DHE and a dedicated promoter pipe and (B) DHE with a built in promoter pipe around the cold flow tube. DHE, Down-hole heat exchanger. Modified after Dunstall, M.G., 1992. *Downhole Heat Exchangers Performance Analysis* (Ph.D. thesis). University of Auckland.

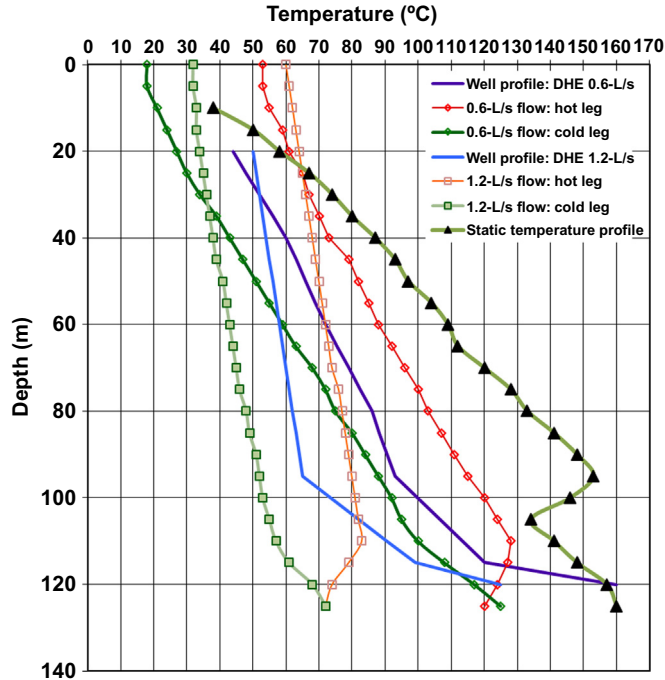


Figure 3.9 Temperature profile of a shallow lateral flow geothermal well in the Rotorua two-phase system before and after the DHE operation, also showing the hot and cold DHE legs at 0.6 and 1.2 L/s circulation. DHE, Down-hole heat exchanger. Data from Dunstall, M.G., 1992. *Downhole Heat Exchangers Performance Analysis (Ph.D. thesis)*. University of Auckland.

Dunstall (1992) reported DHE field testing results in a 125 m deep well with a maximum down-hole temperature of 160°C (Fig. 3.9). The temperature profile of the secondary fluid circulating inside the DHE (Fig. 3.9) shows the drop in temperature of the rising fluid (hot leg) as it gives some of its energy to the down flowing (cold leg) circulation water. This interference limits the amount of thermal power that can be produced by DHE. Fig. 3.9 also shows that increasing the circulation flow rate from 0.6 to 1.2 L/s increases temperature of the produced fluid and hence the thermal power recovered. Note that increasing the output temperature also resulted in high temperature for the returned fluid as more energy will be available for the load.

The well usually represents a large cost in geothermal projects, but the heat output of an individual well is usually fairly low with a DHE, typically few tens of kW_{th}. DHEs may be financially attractive under a range of situations including the following:

- When heat loads are small and widely dispersed, drilling more wells may be cheaper than distributing all the heat available from a single flowing well.
- Where mineral scaling or aggressive reservoir fluids cause expensive or frequent equipment damage.

- When unsuccessful or abandoned wells are available, these may include exhausted or dry oil wells, geothermal wells which are low volume producers, or wells with fluids considered too cold or aggressive for extraction. This would make use of an otherwise useless well.

To improve the performance of DHE, airlifting can also be used to extract some geothermal fluid and gas, which will be replaced by fresh hot fluid from the reservoir (Fig. 3.10). Steins et al. (2012) showed that air lifting improved the output of a DHE from about $20 \text{ kW}_{\text{th}}$ to about $45 \text{ kW}_{\text{th}}$ (125%) by removing 0.47 L/s of water using airlifting, while Dunstall (1992) reported an improvement of only 2% despite pumping at a higher rate of 1.2 L/s of water (see Section 9.2.2 for more detail).

The DHE with the largest reported thermal output was reported by Culver (1990) from a potentially self-discharging well in Turkey. Using a DHE, this well produced 6 MW_{th} from a 153°C hot water reservoir about 250 m deep well with 5 L/s fluid bleed (dump). Even assuming the produced fluid is at 153°C (which is unrealistic), using Eq. (2.1) and Fig. 2.2, the electrical power potential of this well will be 0.3 MWe at the most, which is relatively small. This demonstrates our earlier point that self-discharging wells produce more power than other well types.

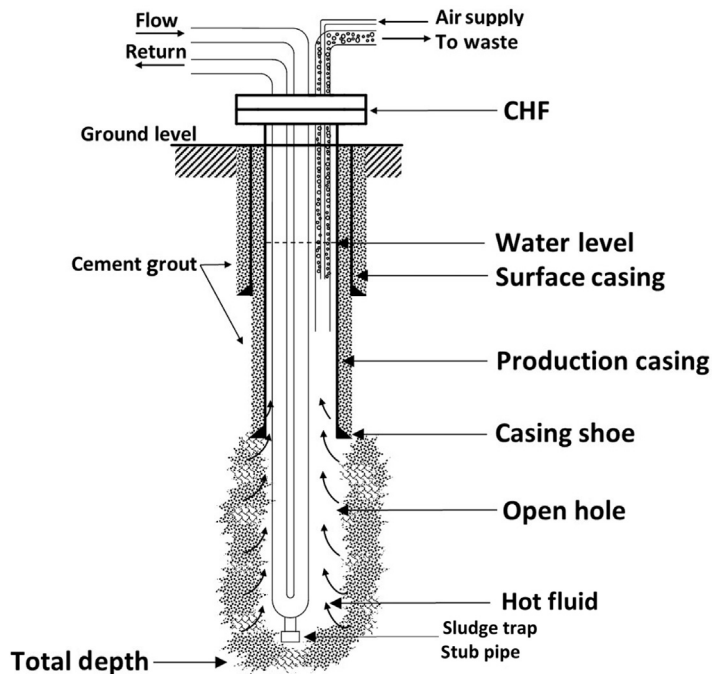


Figure 3.10 Geothermal well with air lifting for improved DHE output. DHE, Down-hole heat exchanger. After Dunstall, M.G., 1992. *Downhole Heat Exchangers Performance Analysis (Ph.D. thesis)*. University of Auckland.

Several authors and companies have proposed using DHEs for power generation from deep wells with conductive heat transfer from the surrounding formations into the well. It is our opinion that this will not be commercially feasible without the production of some fluid at the surface. The main reason is the limited energy recovery from the reservoir rock by thermal conduction and the interference between the hot and cold legs of the DHE as demonstrated in [Fig. 3.9](#).

3.6 Reinjection wells

Reinjection is the process of returning the geothermal fluids (brine, steam condensates and NCG) back into the geothermal reservoir after energy extraction. This is done for environmental considerations as surface disposal of the geothermal waste water is prohibited in most countries. Reinjection also benefits the geothermal reservoir by maintaining reservoir pressure (Kaya et al., 2011). As discussed in Chapter 2, Geothermal Systems, knowing the type of geothermal system as well as a comprehensive monitoring programme are key to the long-term success of any reinjection strategy.

Geothermal reinjection wells are generally designed and drilled to the same standards as production wells ([Fig. 3.2](#)). One reason is that it is possible for a good production target to be unexpectedly encountered while drilling for reinjection. In some fields, reinjection wells have been converted to production wells and vice versa (Diaz et al., 2016).

The preferred option is to have reinjection taking place under gravity if possible, as this reduces the risk of vertical migration of hot fluid to the surface (Kaya et al., 2011). However, reinjection pumps are used in some fields to increase the WHP and force the fluid into the reinjection wells. Having reinjection under pressure increases the risk of reinjection-induced seismic events and can result in reinjected fluid reaching the ground surface (Kaya, 2011; Diaz et al., 2016).

3.7 Monitoring wells

Monitoring wells are used to measure/monitor changes in the pressure, water level, temperature and fluid chemistry of the reservoir. These are usually dedicated shallow (<100 m) ground-water monitoring wells (4"–7" diameter), commonly drilled from the same pad used for drilling deeper wells (production or reinjection). These wells serve as a first warning system for any unusual migration of deep fluids (e.g. reinjected fluid or steam) to the ground-water aquifers. The data and interpretations from these wells are also reported periodically to the local environmental agency, for compliance monitoring.

It is not common to drill dedicated deep monitoring wells, due to the high cost. Deep monitoring wells are normally production or reinjection wells that are not in use or made redundant for some reason. They are used for long-term monitoring of

changes in the deep reservoir pressure in response to development (exploitation). In rare cases, dedicated deep monitoring wells (400–1500 m) are drilled to ensure there is no communication between different fields (Boseley et al., 2012). Dedicated deep monitoring wells have the same general casing design as production wells but are generally smaller in diameter (slim holes) to reduce cost.

High down-hole temperatures and harsh fluid chemistry limit the installation of electronic devices for long-term monitoring. The bubbler tube (capillary tube) is widely used for monitoring deep reservoir pressure at relatively low cost and with no electronics downhole (Fig. 3.11).

Capillary tubes are also used in pumped wells (Figs. 3.4 and 3.5) to monitor the reservoir pressure (water level) and make sure the pump does not run dry, as this will damage the pump.

Since 2009, down-hole seismic monitoring has helped make interesting correlations between deep and shallow microseismicity induced by production and reinjection at Wairakei (Sepulveda et al., 2016). These are dedicated monitoring wells with permanent installations of borehole seismometers, drilled in and around the bore field at depths of <150 m, with the exception of two deep (> 1000 m) preexisting wells re-purposed with seismometers (Sepulveda et al., 2015).

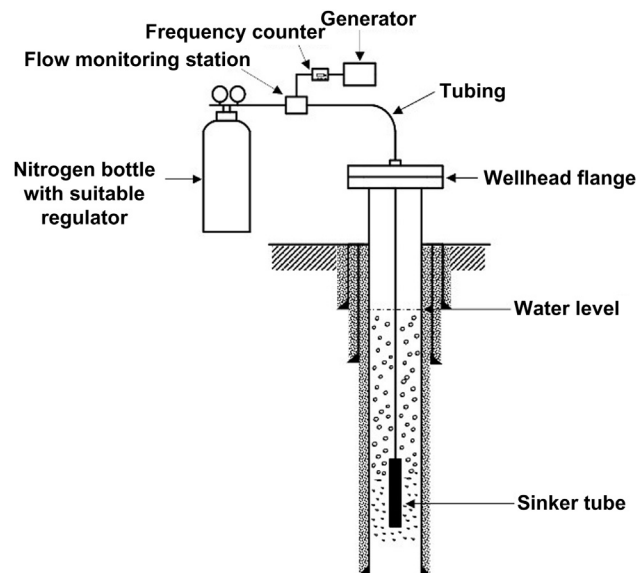


Figure 3.11 Pressure monitoring well installed with a down-hole bubbler tube. *Modified after Yalniz, M.U., 1997. Preliminary interference measurement at Te-Aroha using capillary tubing. In: Diploma in Geothermal Energy Technology Project. The University of Auckland, No. 1997-30 (Yalniz, 1997).*

3.8 Other well types

This section covers other types of wells drilled by other industries and occasionally repurposed for geothermal energy use. These include mining exploration wells that are drilled and (wire line) cored ahead of the mine workface to delineate the extent, depth and thickness of the mined minerals through the combined study of the cores and geophysical surveys. Most of these mining wells are normally abandoned (cemented) after drilling. However, abandoned and flooded underground mine workings are used to produce low-grade energy for space heating and cooling in many countries (Patsa et al., 2015). This is done by drilling dedicated wells into these workings or by using the mineshafts.

Petroleum, ground water, coal bed methane (CBM) and waste-water disposal wells can also be repurposed for geothermal, and will be discussed in detail in the following sections.

3.8.1 Petroleum wells

Petroleum wells are used for the production of petroleum from deep reservoirs with static oil and/or gas stored in sedimentary formations. These wells can be vertical or horizontal depending on the production targets. In most cases, well stimulation is essential to allow commercial levels of production. Hydraulic fracturing stimulation technology was originally developed for petroleum wells. Petroleum wells generally have small diameter production casings (5.5–7" outer diameter) compared to geothermal wells. Production from petroleum wells typically takes place through a permanent tubing installed down the well (Fig. 3.12) and some wells are installed with down-hole pumps. If required, petroleum down-hole (insert) pumps are installed at the end of this tubing and driven by a shaft (sucker rod) that runs inside the tubing. These pumps are of no use to geothermal applications because of their limited output and low operating temperatures.

Several authors investigated the production of geothermal energy from abandoned petroleum wells (Bu et al., 2012; Alimonti & Soldo, 2016; Caulk & Tomac, 2017). Petroleum reservoirs are flooded with water during the enhanced oil recovery stage before abandonment. These systems are effectively warm water systems, with thermal conduction as the main mode of heat transfer. Generally two possible designs are considered; wellbore heat exchanger (i.e. DHE) using a single well (Bu et al., 2012; Templeton et al., 2014; Alimonti & Soldo, 2016; Caulk & Tomac, 2017) and producing in a doublet arrangement (a production and reinjection well pair). The DHE has a limited power output and can mainly be used for direct-use applications as discussed in Section 3.5. The power output from a doublet can also be limited by the size of the well casing and the size of down-hole pump that can be installed. However, there are millions of abandoned petroleum wells globally (Templeton et al., 2014), which can potentially produce a significant amount of energy at relatively low cost when

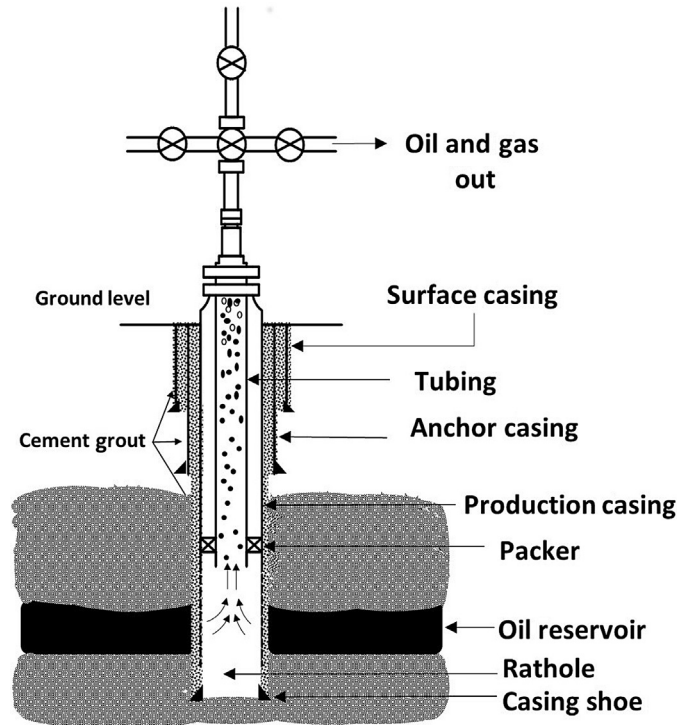


Figure 3.12 Typical petroleum well producing through a tubing with no down-hole pump. Modified after Hammadih, M.L., Al-Hosani, K., Boiko, I., 2015. Soft sensing in deep wells within artificial gas lift technology. In: SPE 177731-MS.

there are favourable economic conditions. Bertani (2016) reported a 0.2 MWe pilot in Utah, United States, and a 0.4 MWe pilot in the north oil field of China using ORC technology.

The use of abandoned petroleum wells for geothermal energy production is also confused with EGS (Toth et al., 2018). These wells are already permeable since they were used for petroleum production; hence, no permeability enhancement is needed. Also, the working fluid (water) should already be available in situ either from enhanced oil recovery (water flooding) or preexisting in the reservoir. However, casing integrity issues can arise when the well, originally designed for petroleum industry standards, gets converted for geothermal energy use later in its life. Therefore the as-built well design should be examined to make sure it is compatible with the geothermal drilling standards.

Cinar (2013) proposed burning the residual oil (in situ combustion) in those abandoned wells to generate heat and create an EGS in the abandoned oil reservoir. While this concept of fire flooding is well known for improving oil recovery and seems attractive, practically it will not work for the simple reason that the heat generated is

of short duration, relatively small and much localised. It cannot be compared in magnitude and extent with naturally occurring geothermal energy. The coal industry has been utilising underground coal gasification (UCG) for commercial use (Gregg et al., 1976) by pumping compressed air and burning the coal underground. UCG requires an air injection well and a fuel gas production well <50 m apart with combustion taking a few weeks at the most and hence the generated energy is limited in magnitude and extent.

3.8.2 Ground-water wells

This is the most common type of well, found in every country in the world, for the production of potable water for human and animal consumption and also for industrial and agricultural use. The simplest ground-water well is the dug well (below water table) normally lined with porous stone or concrete. The dug well is low cost as a drilling rig is not required, and it has a large diameter and large wellbore storage volume.

Rotary drilling is commonly used for deeper wells, which vary in design based on depth and drilling conditions. The use of nonmetallic casing is common, and wells are completed as open holes, but commonly with stainless or plastic polyvinyl chloride (PVC) continuous-slot screens in the production part of the well (Fitts, 2013).

Ground-water wells are also used for dewatering or for storing water (by injection) in winter for use in the dryer summer season. Artesian (self-discharging) wells can be encountered in confined aquifers, but down-hole pumps (with motors) are the common practice in unconfined aquifers. There are techniques used to locate drilling targets (Fitts, 2013), our recommendation is to engage the experienced local drilling contractor for setting targets, drilling and pump installation. A typical ground-water well design is similar to those shown in [Figs. 3.4A and 3.5](#).

Ground-water wells are cleaned and tested using a slug test by pumping high pressure air to air lift the water from the wellbore prior to pump installation (see Chapter 10: Field Studies) or using a pumping test after running a down-hole pump.

The main feature of ground-water well testing is that different units are used for permeability (hydraulic conductivity in m/s) which is different from all other industries, which use m^2 or Darcy as the measure for reservoir permeability. The hydraulic head is used instead of reservoir pressure when deriving the analytical solutions of the governing diffusivity equations (Chapter 4: Introduction to Pressure Transient Analysis).

Ground-water drilling rigs are used in some countries for drilling and completing direct-use geothermal wells in some warm-water sedimentary basins. Ground-water wells are also useful when investigating the signature of geothermal systems through down-hole temperature measurements and chemical analysis.

3.8.3 Coal bed methane wells

Coal bed methane (CBM) wells, also known as coal seam gas or mine gas wells, are drilled and completed into coal seams or coal measures to recover the methane gas (CH_4) that naturally occurs in coal. Historically, CBM gas was released to the atmosphere during coal mining. The CBM industry started in the early 1980s and experienced a boom in many parts of the world (e.g. United States, Canada, China, Australia, India and parts of Europe) (Zarrouk, 2008). CBM accounts for about 10% of total US gas consumption (Palmer, 2010). It is a mixture of gases dominated by CH_4 (90%–99%), with the remaining gases including C_2H_6 , CO_2 , N_2 , He, O_2 , H_2 and also some trace amounts of H_2S (Zarrouk, 2008).

Coal beds are simply a coal formation in its mid stage of maturation, with coal being both the gas source and reservoir. Commercially viable CBM reservoirs are within coals of rank ranging from subbituminous to low-volatile bituminous and are characterised by high gas content, high permeability, high reservoir pressure and large coal bed thickness.

Extracting CBM is a more environment-friendly energy resource than coal or oil. However, the CBM reservoir water is laden with high salinity, heavy metals and dissolved minerals, therefore its discharge is an environmental hazard and the water is commonly reinjected.

Unlike conventional natural gas reservoirs characterised by high discharge pressures, CBM reservoirs usually produce gas near atmospheric pressure. Therefore in most fields, gas must be compressed on site up to transmission line pressure.

Most CBM wells are relatively low-cost shallow (250–800 m) vertical wells commonly run with a 5.5" or 7" production casing size. CBM wells are commonly tested for the permeability of the target zone in open hole by using packers or a drill stem test (DST) in the open hole before running casing.

The wells are installed with down-hole pumps to dewater the coal, drop the reservoir pressure and allow the gas to be desorbed from the coal and travel in the annulus between the casing and the pump tube (Fig. 3.13). CBM wells are commonly stimulated in high permeability (> 100 mD) coal beds either through underreaming or cavitation (Fig. 3.13A), and in lower permeability (3–20 mD) coal beds through hydraulic fracturing (Fig. 3.13B) or single lateral (horizontal) wells. Relatively expensive single lateral or multilateral horizontal wells (multilateral means drilling two or more horizontal production holes from a single surface location) are used for very low permeability (< 3 mD) 'tight' seams (Palmer, 2010).

Coal has some unique properties compared with other reservoir rock types: it has lower density, low porosity and lower thermal conductivity, which makes it a good thermal insulator. For this reason, most CBM reservoirs have a relatively high temperature gradient and help identify good potential warm water aquifers (Zarrouk

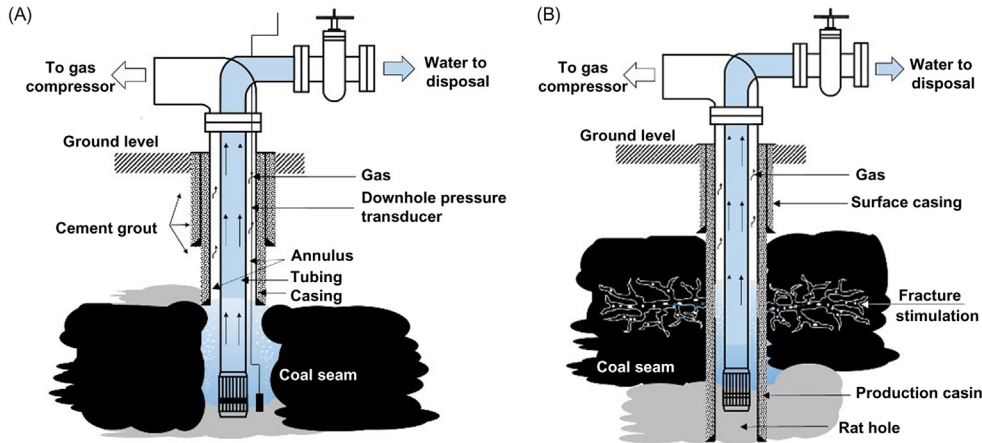


Figure 3.13 CBM wells with down-hole pumps (A) open-hole completion (cavity stimulation) (B) fracture stimulation. Modified after All, C., 2003. *Handbook on Coal Bed Methane Produced Water: Management and Beneficial Use Alternatives* (All, 2003).

and Moore, 2007). Coal is also very mechanically weak and hence can be easily fractured during injection testing.

UCG wells which are used to burn the coal underground by injecting compressed air to produce clean synthetic gas (CH_4 , H_2 , CO and CO_2) are designed and drilled to the same standard as CBM or oil wells.

3.8.4 Waste-water disposal wells

These wells are drilled by several industries for the permanent disposal of waste fluids underground (Lehr, 1986; Warner, 1977). It is called reinjection when some volume of produced water is put back into its original formation. Water injection was first employed in the petroleum industry for hydrocarbon recovery improvement in 1865 (Thakur & Satter, 1998). The application has spread into other industries such as brine disposal, liquid waste and municipal waste disposal (Brasier & Kobelski, 1996).

Some of these waste waters have poor water quality, with hazardous compositions, such as selenium, boron, high chloride and traces of hydrocarbon (Warner, 1977; Allen & Robinson, 1993; Hulme, 2005; Hodder, 2010). In many countries, it is compulsory for field operators to design the best solution to address these issues in order to protect environment. The most practical and cost-effective option is underground injection or reinjection. If these wells show elevated/commercial level temperatures with depth, they can be candidates for geothermal energy production provided that the produced fluids are reinjected back into the original reservoir.

3.9 Summary

Geothermal wells are larger in diameter than wells drilled by all other industries, and they require specialised drilling practices. Geothermal wells are also designed and completed differently depending on the type of geothermal system and the intended well utilisation. Self-discharging wells produce more mass flow rate and energy than all other wells. Nondischarging wells can also be produced by running down-hole pumps, using air lifting, installing DHEs, or used for reinjection or long-term monitoring. Abandoned mine workings and wells drilled by other industries (petroleum, CBM, ground-water and waste-water disposal wells) can also be used for geothermal energy production if commercial level temperatures are encountered.

CHAPTER 4

Introduction to pressure-transient analysis

Contents

4.1	Definition	63
4.2	Typical well test types	64
4.3	Historical overview of pressure-transient analysis	65
4.3.1	Early petroleum analytical theory and graphical semilog methods	66
4.3.2	Departures from early theory: new methods	67
4.3.3	Departures from early theory: new models and theory	68
4.3.4	Major analytical pressure-transient analysis publications	69
4.3.5	Overview of geothermal-specific analytical pressure-transient analysis	69
4.3.6	Overview of geothermal-specific numerical pressure-transient analysis	70
4.4	Fundamental concepts	71
4.4.1	Wellbore storage	71
4.4.2	Infinite-acting radial flow	72
4.4.3	Skin	72
4.4.4	Superposition	74
4.4.5	Diffusivity equation	75
4.4.6	Line-source solution	76
4.5	Analytical graphical methods	76
4.5.1	Miller—Dyes—Hutchinson semilog plot	76
4.5.2	Horner semilog plot	77
4.5.3	Multirate superposition plot	79
4.5.4	Two-rate plot	81
4.5.5	General semilog plot	82
4.5.6	Type-curve matching: log—log plot	83
4.5.7	Bourdet pressure derivative plot	86
4.6	Summary	88

4.1 Definition

The term ‘pressure transient’ is quite general and can refer to any circumstance in which pressure is changing with time. In the context of well testing a ‘pressure transient’ refers to changes in the reservoir pressure (usually measured downhole) induced by a change in flow rate. This can be a change in flow rate into the well during

injection, or out of the well during production. Pressure-transient analysis (PTA) is the analysis of the resulting pressure and flow data set, and involves matching a model (either analytical or numerical) of the well and reservoir to the data. The objective of PTA is to obtain information about the reservoir, for example typical results include: the reservoir transmissivity (kh), skin factor (s), the initial reservoir pressure (P_i) as well as other parameters describing the size of the reservoir and its boundaries (Ramey, 1975). PTA has also been described as the most powerful tool available for diagnosing well condition (Ramey, 1975). The term PTA is often used interchangeably with ‘well testing’, although this broader term encompasses a range of testing beyond PTA.

4.2 Typical well test types

The four common types of single-well testing are as follows (and shown schematically in Fig. 4.1):

1. Drawdown test: A shut-in well is suddenly opened to production flow, causing the pressure to drop from the static shut-in value.
2. Build-up test: A well on production is suddenly shut-in, after which the pressure builds up to the static shut-in value.
3. Injection test: Injection is commenced abruptly into a static well, causing the pressure to increase from the static shut-in value.
4. Fall-off test: Injection into a well is abruptly terminated, causing the pressure to decline back to its static shut-in value (Fig. 4.1).

Interference testing is also common and involves two wells. Production or injection flow changes occur in the first well, but the pressure change (drawdown, build-up, injection or fall-off) is measured in a second well some distance away. Due to the distance

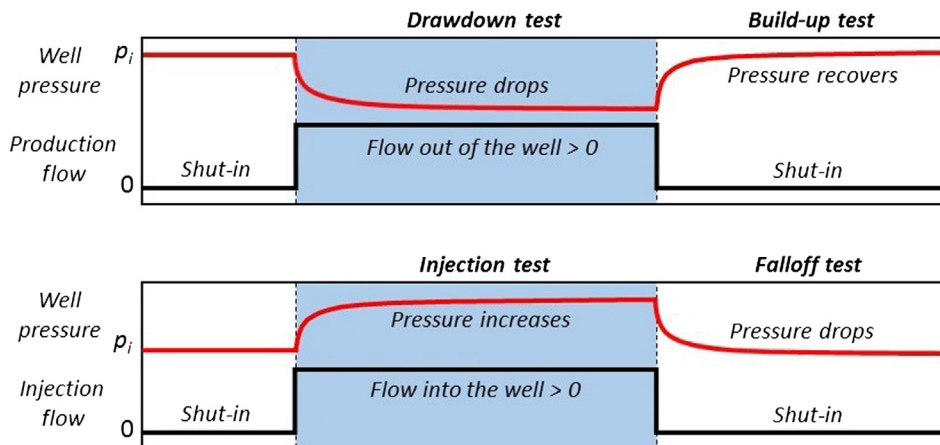


Figure 4.1 Schematic of drawdown and build-up testing (production) and injection and fall-off testing (injection).

between the wells, interference testing informs on a larger part of the reservoir than single-well testing but requires a significantly longer period of time (Earlougher, 1977).

Moreover, multirate PTA methods theoretically enable the pressure response to any change (or series of changes) in flow rate to be analysed as a well test (Earlougher, 1977).

Geothermal well tests are usually build-up or fall-off tests. Drawdown and injection tests are not usually possible as the high-temperature fluid involved does not allow for the required sudden changes in flow rate. Geothermal well testing has usually omitted multirate testing due to an absence of good-quality flow data, and fluctuations in flow rate.

There are various issues which prevent drawdown testing in most geothermal wells. The main reason is that production can initiate flashing in the reservoir, and pressure waves do not travel far in the resulting two-phase zone. Moreover, flashing means it is not possible to maintain a constant well output, and the well pressure fluctuates. Even if this was not the case, sudden production of high-temperature geothermal fluid will cause thermal shock damage to the well casing which is initially cold at shallow depths. For this reason the process of initiating production from geothermal wells is gradual. Moreover, some wells may take a while to start flowing, and some require discharge stimulation such as air compression or airlifting to initiate flow (Section 6.6.1). The exception is drawdown testing in warm and hot water wells, which do not suffer from issues relating to flashing, thermal shock or initiating flow. Downhole pumps can give a constant flow rate.

Geothermal build-up testing is practically possible as the cessation of production can be very rapid without the risk of thermal shock, and there are no issues regarding fluctuating flow rate as the well is shut in. However, analysis is still complicated by the presence of the production-induced two-phase zone in the reservoir, which persists and moves for some time after shut-in (O'Sullivan, 1987).

Injection and fall-off testing avoid the issues relating to flashing. However, an injection test is not usually possible as sudden injection of cold water at high flow rates into hot casing can cause thermal shock damage. For this reason the introduction of cold water into a geothermal well is always a gradual process called quenching, as specified in the 'Code of Practice for deep geothermal wells NZS 2403:2015' (Standards New Zealand, 2015). However, fall-off testing is possible as the cessation of injection can be very rapid without the risk of thermal shock, and this is by far the most common type of geothermal well test. Another form of testing, once injection is established, is the pressure response to step changes in flow rate (up or down).

4.3 Historical overview of pressure-transient analysis

A summary overview of the development of both analytical and numerical PTA is presented in this section, and then important concepts and methods are covered in

more detail in subsequent sections. For decades, PTA relied solely on analytical models which are a set of linear equations to describe the system behaviour. Analytical models can only represent simple systems and so the need to represent more complex systems led to the use of numerical models. Numerical models represent a system as a number of individual elements (blocks) which then interact with each other according to a set of partial differential equations. Early use of numerical methods was in combination with analytical methods, often to validate the use of an analytical model. Later the use of computers became easier and more widespread with the advent of personal computers in the 1980s, enabling the development of purely numerical methods.

4.3.1 Early petroleum analytical theory and graphical semilog methods

All analytical models are solutions to the general diffusivity equation, which governs radial fluid flow in a porous medium (Section 4.4.5). The first and simplest solution to this equation is called the ‘line-source solution’ developed in 1935 by Theis for the groundwater industry (Section 4.4.6). This was revolutionary as time was introduced as a variable factor, which had not been considered before, and so the theory of PTA began (Houzé et al., 2012).

The focus of PTA theory in the petroleum industry was on single-well testing, in contrast to the groundwater focus on multiwell interference testing (Atkinson et al., 1978a). The primary reason for the single-well focus is the high compressibility of hydrocarbons (especially natural gas) which limits the distance over which the pressure response can travel (Atkinson et al., 1978a).

One of the earliest graphical techniques was developed in 1937 by Muskat, to determine the reservoir pressure from build-up data (Ramey, 1975). The plot is the difference between reservoir pressure and downhole pressure (logarithm) versus shut-in time. The value assumed for the reservoir pressure is then adjusted by trial and error until the data forms a straight line (Muskat, 1937).

A significant advance in mathematical theory was made in 1949 by van Everdingen and Hurst with the application of the Laplace transform to transient flow problems in reservoirs (van Everdingen and Hurst, 1949), which allowed the concept of wellbore storage (Section 4.4.1) to be considered for the first time (Ramey, 1975).

It was recognised that during the main flow regime of interest [infinite-acting radial flow (IARF) – Section 4.4.2], downhole pressures change linearly with the logarithm of time, and that this relationship can be used to calculate reservoir permeability and skin. This gave rise to a series of semilog graphical techniques, on which data measured during IARF should form a straight line. The slope of the straight line can be used to calculate reservoir permeability k and skin factor s . The first of these in 1950 was the Miller–Dyes–Hutchinson (MDH) semilog plot (Miller et al., 1950; Section 4.5.1) which is technically applicable only for well tests with a single flow-step

(e.g. drawdown test). This was shortly followed by the Horner semilog plot in 1951 (Horner, 1951; [Section 4.5.2](#)) which was designed specifically to account for two flow steps (e.g. build-up test after drawdown). The MDH and Horner plots were very significant advances, considered to be the fundamental basis of analytical PTA (Ramey, 1975).

Soon afterwards in 1953, the concept of skin factor emerged to explain the apparent displacement of semilog straight lines ([Section 4.4.3](#); van Everdingen, 1953; Hurst, 1953). The displacement was hypothesised to be the result of resistance to flow in the immediate vicinity of the well and could be accounted for by adding a dimensionless pressure drop across a ‘skin’ at the well–reservoir interface (Ramey, 1975). This concept has retained its relevance through time, appearing in books on modern PTA (Horne, 1995; Houzé et al., 2012); it is widely used by the industry.

In practice both production and injection flow rates are often variable, precluding the use of MDH and Horner plots. The simplest multirate case is a two-rate flow test, for which the two-rate plot was developed in 1963 (Russell, 1963; [Section 4.5.4](#)). The multirate superposition plot was developed in 1965, capable of handling an unlimited number of flow rates (Odeh and Jones, 1965; [Section 4.5.3](#)). Both these multirate plots are still semilog plots, producing a straight line during IARF from which k and s can be calculated.

Modern use of a semilog method is via a ‘general’ semilog plot ([Section 4.5.5](#)) which accounts for the entire flow history prior to a pressure transient by using the principle of superposition in time ([Section 4.4.4](#); Houzé et al., 2012).

Application of the original semilog techniques was only successful for dry steam wells, for example at the Geysers, the United States, and Larderello, Italy (Barelli et al., 1975; Economides and Fehlbeg, 1979; Ramey, 1970), and there was difficulty in locating the correct portion of the semilog straight line for some wells (Ramey, 1975). For dry steam wells at the Matsukawa Geothermal Field, Japan, semilog techniques were applied to build-up data with mixed success (Hanano and Sakagawa, 1990).

4.3.2 Departures from early theory: new methods

Many data sets are too short for conventional semilog methods, never reaching IARF and therefore not displaying a straight line. Attempts to utilise these short data sets led to important work by Ramey (1970) on a process called type-curve matching, which was a form of manual nonlinear regression (NLR) performed by sliding tracing paper containing test data over preprinted log–log type curves. Type-curve matching allowed for the estimation of wellbore storage and skin from the data set (Ramey, 1970; [Section 4.5.6](#)). For years, type-curve matching was used in combination with other specialised plots, though it was affected by many issues including poor resolution (Ramey, 1970; Bourdet et al., 1989), complexity and difficulty of

use (Bourdet et al., 1989), and inapplicability to complex flow histories (Houzé et al., 2012). Some specialised type curves were generated numerically (Horne et al., 1983).

Another important issue with conventional semilog analysis was the identification of the semilog straight line (Atkinson et al., 1978a). This led to the Bourdet pressure derivative technique (Bourdet et al., 1983; [Section 4.5.7](#)) which was originally intended to aid identification of the IARF regime (semilog straight line) and was added to type curves to improve resolution (Bourdet, 1983). However, it was useful far beyond this purpose, as not only does the IARF regime have a characteristic pressure derivative response but so do many different flow regimes and reservoir, wellbore and boundary behaviours (Horne, 1995; Houzé, 2012). The Bourdet derivative (or ‘derivative plot’) became the key diagnostic tool for PTA data sets and is referred to as the most important advance in the history of PTA (Houzé et al., 2012).

The general technique of nonlinear regression (NLR) was a major advance relevant to PTA (and elsewhere) as it allowed the fitting of models to field data sets to be easier and more robust, less vulnerable to subjective judgement than graphical techniques (Earlougher and Kersch, 1972; [Section 5.6](#)). As computers became more widespread in the mid-1980s, software emerged for automated well test analysis, utilising NLR. Most software could handle the entire pressure and flow rate history, with a range of analytical and semianalytical models available ([Section 5.6](#)).

4.3.3 Departures from early theory: new models and theory

The early analytical models were based on various simplifying assumptions, including that the reservoir was homogenous and infinite ([Section 4.4.5](#)). As PTA theory progressed some of these assumptions were able to be abandoned. The inclusion of reservoir boundaries in 1954 was an important departure from the assumption of an infinite reservoir (Matthews et al., 1954; [Section 5.1](#)). Circular, square and rectangular reservoir boundaries could be included with different locations of the well within the boundary. This involved the important concept of superposition ([Section 4.4.4](#)), using arrays of wells to represent linear boundaries.

The assumption of a homogeneous system was relaxed in order to model naturally fractured reservoirs ([Section 5.5](#)), which occur commonly (Earlougher, 1977). Warren and Root (1963) published one of the earliest models to represent a fractured reservoir with distinct primary and secondary porosity, which was called the ‘dual-porosity’ model and is still used today. Representing fracture networks as fractals (using the ‘fractional dimension’ concept) was made possible in 1990 by modification of the diffusivity equation (Chang and Yortsos, 1990), and shortly afterwards in 1995 it was verified using numerical simulation (Acuna and Yortsos, 1995).

Relaxing the homogenous reservoir assumption also allows the fracture(s) in the vicinity of the well resulting from hydraulic fracturing operations to be accounted for.

Models to describe these were developed throughout the 1970s including the uniform flux fracture model (Gringarten et al., 1972), infinite-conductivity fracture model (Gringarten et al., 1974) and the finite-conductivity fracture model (Cinco-Ley et al., 1978) (Section 5.4).

4.3.4 Major analytical pressure-transient analysis publications

By the early 1960s, it was considered that the fundamental work for PTA was complete (Atkinson et al., 1978a), and so Matthews and Russell (1967) published the first Society of Petroleum Engineers (SPE) monograph on this topic. After another decade of advances in PTA theory, this was superseded by the Earlougher (1977) SPE monograph, with less focus on mathematical derivation and more focus on application and examples. Modern analytical PTA using software with nonlinear regression is covered by books by Horne (1995) and Bourdet (2002), and another highly useful reference is a handbook by Houz e (2012).

4.3.5 Overview of geothermal-specific analytical pressure-transient analysis

The analytical PTA theory and methods described in this overview were developed for the petroleum industry. Prior to the 1960s, PTA was rarely applied in geothermal wells, due in part to the perception that geothermal reservoirs were primarily fracture dominated and could not be represented adequately by simple porous medium models (Atkinson et al., 1978a). In fact, there are a variety of limitations to the use of analytical models in geothermal fields (Section 5.7). So geothermal-specific PTA research began in the late 1960s at Stanford University and Lawrence Berkeley Laboratory, the United States, and later at the Department of Scientific and Industrial Research, New Zealand.

Reviews of the application of early PTA methods to geothermal data sets was published by Ramey (1975) and Atkinson et al. (1978a). Both papers were published prior to the advent of computers and refer primarily to graphical analytical methods. Ramey (1975) noted that PTA might not always be practical for geothermal reservoirs due to factors including the unknown thickness (height) of the production interval and the lack of suitable analytical solutions to represent real geothermal system geometry.

Ramey (1975) noted that matches between analytical models and geothermal field data were only ‘reasonable’, and predicted that new models and downhole tools would improve this. In the late 1970s and 1980s a major area of geothermal-specific research was the derivation and validation (often numerically) of a new diffusivity equation to describe radial two-phase water/steam flow, to enable the use of two-phase PTA methods (Section 5.8.2). Another major area was the development of a

parallelepiped model to reflect the geometry of vapour-dominated reservoirs (Section 5.8.1). A third major area was research into methods to handle nonisothermal cold water injection into a hot reservoir (Section 5.8.3). Other studies considered adsorption in vapour-dominated reservoirs (Section 5.8.4) and geo-pressured reservoirs (Section 5.8.5).

There is not a consensus on whether analytical PTA methods are really applicable to geothermal wells. For example, Horne (2016) states that geothermal wells are frequently like petroleum wells and can be interpreted using standard techniques, though they are more often fractured, and the effects of two-phase fluid properties must be taken into account. A similar statement is made by Grant and Bixley (2011). On the other hand, some authors are clear that analytical models are theoretically inapplicable (O’Sullivan et al., 2005; Guerra and O’Sullivan, 2018), while others state that analytical models often do not work in practice (Ramey, 1975; McLean and Zarrouk, 2017a).

4.3.6 Overview of geothermal-specific numerical pressure-transient analysis

The limitations of analytical or semianalytical methods (Section 5.7) have led to numerical simulation for PTA. Various numerical PTA studies relevant to geothermal wells have been carried out from the 1980s onwards. Early work in the 1980s investigated wellbore storage in two-phase wells (Section 8.8.1), a number of refinements to the dual-porosity model (Section 8.8.2) and PTA in two-phase porous media and fractured reservoirs (Section 8.8.4). In the 1990s, studies examined stress-sensitive reservoirs (Section 8.8.5) and permeability change during injection (Section 8.8.6). In the 2000s were studies on non-Darcy flow (Section 8.8.3) and a case study using the fractional dimension model at Wairakei Geothermal Field (Section 8.8.7). Since 2010 the frequency of geothermal PTA studies has increased markedly, including more research on permeability change during injection (Section 8.8.6) and two-phase fractured reservoirs (Section 8.8.4), as well as research on the effect of mineral scaling (Section 8.8.8) and utilising temperature data in addition to pressure data (Section 8.8.9).

The authors of most of the studies listed above have created customised numerical models. The only software for numerical PTA, AWTAS (Section 8.3), was developed in 2005, after which numerical PTA could be performed without developing numerical models or even much knowledge of numerical modelling in general. AWTAS is a comprehensive automated well test analysis system for geothermal with model responses generated numerically using TOUGH2 (O’Sullivan et al., 2005), though it is not commercially available. In any case, AWTAS has been superseded by the power of the PyTOUGH scripting library to control TOUGH2. The utilisation of these tools for numerical PTA is guided by a framework which is the subject of Chapter 8.

4.4 Fundamental concepts

4.4.1 Wellbore storage

Though the objective of PTA is to obtain information about the reservoir, unfortunately the fluid in the wellbore is the first to respond to changes in flow rate, followed later by the fluid in the reservoir. The early-time pressure-transient response is therefore characteristic of the wellbore, and only later is characteristic of the reservoir (Horne, 1995). The early-time wellbore response is referred to as wellbore storage, which is shown schematically in Fig. 4.2.

The usual mechanism to control flow into and out of a well is the flow control valve at the wellhead. However, the permeable reservoir is usually many hundreds of metres down the well. The two are separated by a wellbore full of fluid, which means that changes in flow rate at the permeable reservoir level are not the same as the flow rate measured at the wellhead, there is a delay. For example, during a draw-down test, production will be initially from expansion of the fluid volume in the wellbore, with no element of reservoir fluid. As time progresses, the proportion of reservoir fluid increases until the entire flow is from the reservoir. Unless the flow rate is measured downhole, which is possible in the petroleum industry but not commonly done in geothermal wells, the early pressure-transient response will be dominated by the wellbore. It is necessary to measure the pressure-transient response far beyond the point when the wellbore effects become negligible in order to obtain the actual reservoir response.

The wellbore storage coefficient (C) is used to quantify the effect and is defined as the volume of fluid that the wellbore will produce per unit drop in pressure, see Eq. (4.1) (Horne, 1995).

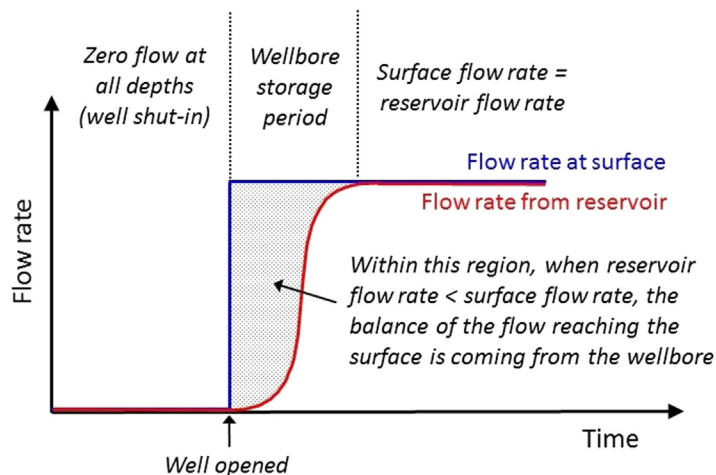


Figure 4.2 Schematic of wellbore storage concept, for a drawdown test.

$$C = \frac{V}{\Delta p} \quad (4.1)$$

where C is the wellbore storage coefficient (m^3/Pa), V is the volume of produced fluid (m^3) and p is the pressure (Pa).

During wellbore storage dominance, pressure is proportional to time and therefore plots as a unit-slope on a log–log plot (Horne, 1995). The first work on the effect of wellbore storage on well testing was as an example to demonstrate the usefulness of the Laplace transform for solving well test problems (van Everdingen and Hurst, 1949).

4.4.2 Infinite-acting radial flow

Infinite-acting radial flow (IARF) is the main flow regime of interest, occurring after the early wellbore-dominated response but before any boundary responses are seen in late time. As IARF occurs before the effects of boundaries, the response during this time behaves as if the reservoir is infinite; hence, the term infinite acting (Horne, 1995). During IARF the reservoir is effectively a flat circular disc, with horizontal flow pathways converging on the well equally from all directions. Under this flow regime the pressure response is proportional to the logarithm of time and will therefore form a straight line on a semilog plot. This fact forms the basis of various graphical semilog methods including the MDH plot, Horner plot, multirate superposition plot, two-rate plot and general semilog plot (Sections 4.5.1–4.5.5). When IARF can be identified, the slope of the semilog line can yield the average reservoir permeability (k) around the well (if the reservoir thickness is known) and the skin factor (s).

4.4.3 Skin

This terminology comes from the fact that a coating (a ‘skin’) can form at the interface between the reservoir and the wellbore. This commonly occurs when a well is drilled with mud, which inevitably penetrates some distance into the near-well reservoir rocks, blocking up the permeability and effectively damaging the reservoir. This decrease in permeability is referred to as positive skin and can also result from mineral scaling in geothermal wells after production starts. Negative skin occurs when there is a localised increase in permeability in the vicinity of the wellbore, which can occur as the result of formation collapse or fracturing during drilling, or deliberate stimulation. Early work on the skin concept was within the petroleum industry and focused on positive skin (van Everdingen, 1953; Hurst, 1953).

Skin causes a difference in pressure Δp_s between the pressure expected to be seen at the well p_{wf} under ideal conditions and the actual measured value of p_{wf} (Fig. 4.3) (Horne, 1995).

The skin factor is used to quantify this skin effect, defined in Eq. (4.2).

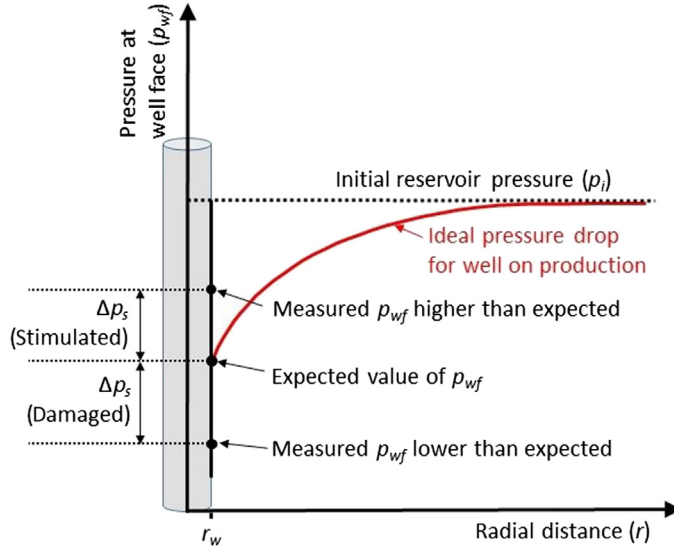


Figure 4.3 Skin effect causing pressure at well face p_{wf} to deviate from the value expected under ideal conditions.

$$s = \frac{2\pi kh}{qB\mu} \Delta p_s \quad (4.2)$$

where s is the skin factor (dimensionless), k is the reservoir permeability (m^2), h is the reservoir thickness (m), q is the flow rate (m^3/s), B is the formation volume factor (dimensionless), μ is the dynamic viscosity (Pa s) and p is the pressure (Pa).

The skin effect can be modelled in two ways, the fixed radius skin zone model and the effective wellbore radius model (Horne, 1995). The fixed radius skin zone model is a zone of radius r_s in the immediate vicinity of the wellbore (of radius r_w) with either a higher or lower permeability k_s than the reservoir permeability k , depending on whether there is stimulation or damage (Fig. 4.4). For the fixed radius skin zone model the skin factor s is given by Eq. (4.3) (Horne, 1995).

$$s = \left(\frac{k}{k_s} - 1 \right) \ln \frac{r_s}{r_w} \quad (4.3)$$

The effective wellbore radius model represents positive skin as simply the result of a smaller wellbore and negative skin as the result of a larger wellbore (Fig. 4.5). The skin factor is calculated from the actual well radius r_w and its effective radius r_{we} due to skin effect by the following equation:

$$s = - \ln \left(\frac{r_{we}}{r_w} \right) \quad (4.4)$$

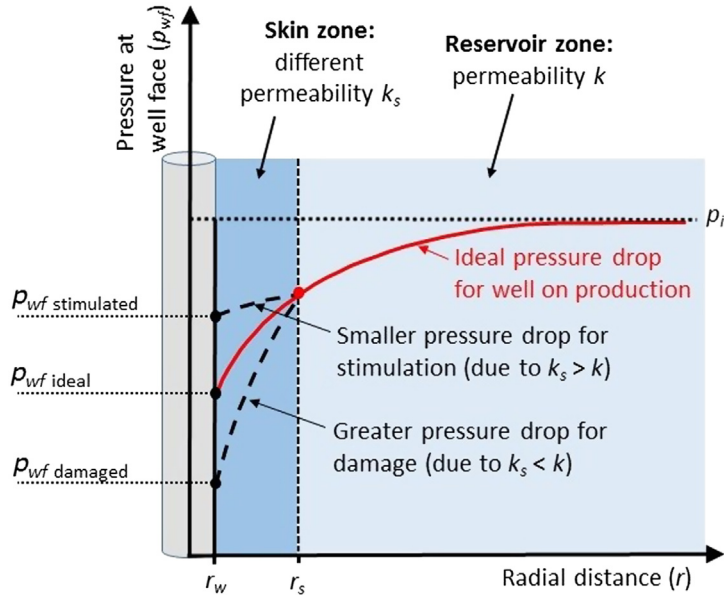


Figure 4.4 Schematic of fixed radius skin zone model.

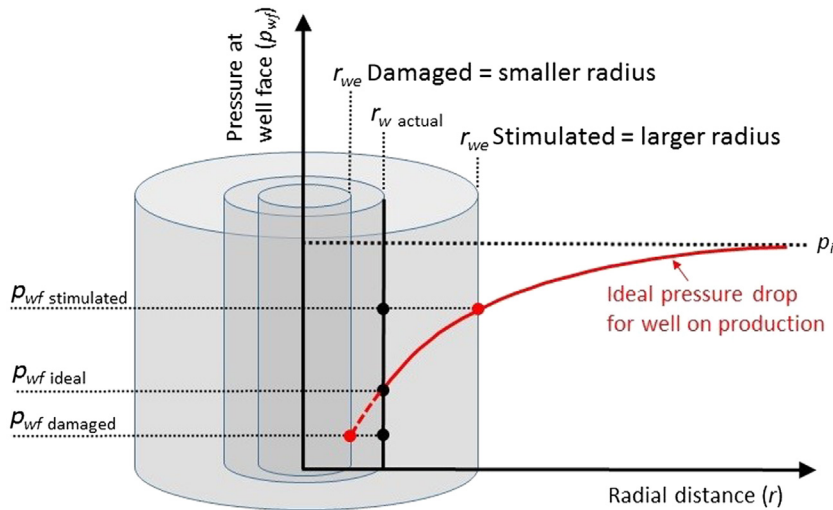


Figure 4.5 Schematic of effective wellbore radius model.

4.4.4 Superposition

Basic PTA models represent only very simple systems, for example a single well in an infinite reservoir (no boundary) and a single, constant flow rate. Complex systems with multiple wells, complex boundary geometries and variable flow rates can be represented by a combination of simple models by the principle of superposition (Horne, 1995). By this principle, if a complex system can be represented by individual

simple components, then the system response to each component can be added together to obtain the overall system response. One useful application of superposition is the ability to represent a linear boundary at some distance from a well by including a second, identical well at twice the distance of the desired boundary, a concept called an ‘image well’ (Horne, 1995; Houzé et al., 2012).

Superposition in time allows the addition of well responses at different start times. The most common application of this is the representation of complex production or injection histories as a series of flow steps each with their own simple pressure response, starting at different times and with different weights, which can be added together to give the overall system response (Houzé et al., 2012). ‘Convolution’ is the term which refers to the combination of pressure transients resulting from a variable flow rate, and ‘deconvolution’ is the extraction of a constant flow rate pressure response from the variable flow rate response (Horne, 1995). It is the principle of superposition in time which enables the graphical methods of the multirate superposition plot (Section 4.5.3) and general semilog plot (Section 4.5.5).

4.4.5 Diffusivity equation

The diffusivity equation (Eq. 4.5) is the mathematical equation governing radial flow in a porous medium filled with single-phase fluid of small and constant compressibility. Solutions to the diffusivity equation for a wide variety of reservoir and boundary scenarios are the foundation of analytical PTA. The derivation of this equation has been published by the SPE (Matthews and Russell, 1967; Earlougher, 1977).

$$\frac{\partial^2 p}{\partial r^2} + \frac{1}{r} \frac{\partial p}{\partial r} = \frac{\emptyset \mu c_t}{k} \frac{\partial p}{\partial t} \quad (4.5)$$

where p is the pressure (Pa), r is the radial distance from wellbore (m), \emptyset is the porosity (dimensionless), μ is the dynamic viscosity (Pa s), c_t is the total system compressibility (1/Pa), k is the reservoir permeability (m^2) and t is the time (second).

There are many assumptions required for the derivation of Eq. (4.5) (Matthews and Russell, 1967; Earlougher, 1977; Horne, 1995), including the following:

- Horizontal and radial flow.
- Negligible gravity effects.
- Isothermal flow.
- Applicability of Darcy’s law.
- Homogeneous and isotropic (uniform permeability in all directions) porous medium.
- Single-phase flow.
- Fluid compressibility is small and constant.
- Porosity, permeability, viscosity and compressibility are constant and therefore independent of pressure.
- Pressure gradients in the reservoir are small.

With these assumptions, Eq. (4.5) is linear in form and is easily solved for various reservoir and boundary scenarios. These solutions are referred to in this study as ‘analytical models’. Relaxing any of the assumptions may result in a nonlinear diffusivity equation requiring the use of numerical simulation to solve (Earlougher, 1977). The basic diffusivity equation can be modified to describe multiphase flow (e.g. oil, gas and water) with the inclusion of a pressure-dependent diffusivity coefficient (Matthews and Russell, 1967).

4.4.6 Line-source solution

The development of PTA theory began with the work of Theis in the groundwater industry (Theis, 1935). Prior to this, all mathematical theory was based on the equilibrium state of the well, a state in which water levels and therefore pressure are unchanging. Theis was the first to consider time as a variable and to analyse the transition between equilibrium states (the ‘pressure transient’).

It was recognised that conceptually the mathematical theory of groundwater hydrology is similar to that of heat transfer by conduction, heat sources being comparable to recharging wells and heat sinks comparable to discharging wells (Theis, 1935). The coefficient of thermal diffusivity is analogous to the permeability-thickness product kh (transmissivity) of an aquifer (Theis, 1935). The Theis solution to the diffusivity equation is the first analytical PTA model, commonly called the line-source solution as it has a wellbore of zero radius (a ‘line source’). Various other assumptions of the model include that the aquifer is homogeneous, of constant thickness, infinite in extent, fully penetrated by the well, with constant and uniform transmissivity.

4.5 Analytical graphical methods

4.5.1 Miller–Dyes–Hutchinson semilog plot

The Miller-Dyes-Hutchinson (MDH) semilogarithmic plot is a plot of pressure versus the logarithm of time (Fig. 4.6) and was originally designed for pressure build-up tests (Miller et al., 1950). It was recognised that during the IARF flow regime (Section 4.4.2), pressure change varies linearly with the logarithm of time. This linear relationship is used to estimate various reservoir parameters (Miller et al., 1950).

Eq. (4.6) (from Horne, 1995, converted to SI units) is for pressure as a function of time, the modern version using logarithm base 10 and including the effects of skin.

$$p_{wf} = p_i - 0.1832 \frac{qB\mu}{kh} \left(\log t + \log \frac{k}{\phi \mu c_t r_w^2} + 0.8686s + 0.3514 \right) \quad (4.6)$$

where p_{wf} is the flowing bottom-hole pressure (Pa) and p_i is the initial pressure (Pa).

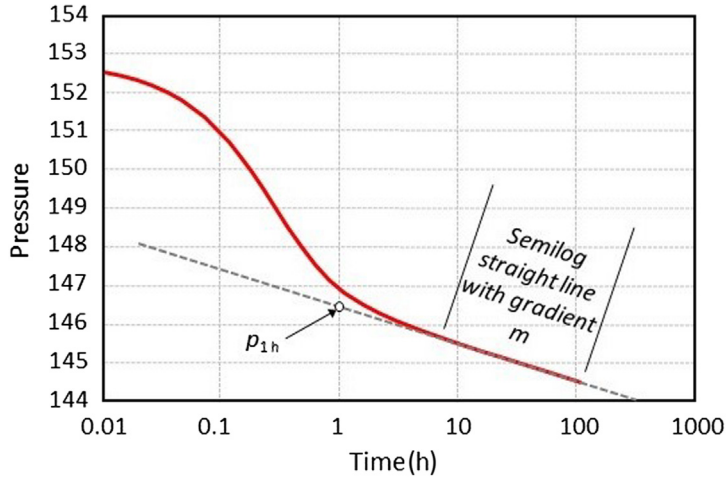


Figure 4.6 MDH semilog plot example: linear fit through semilog straight line in fall-off data set.

The gradient of the semilog straight-line m (Pa/cycle) can then be used to calculate the permeability using Eq. (4.7) (from Miller et al., 1950, converted to SI units), which has remained unchanged since the original MDH publication.

$$k = 0.1832 \frac{qB\mu}{mh} \quad (4.7)$$

The skin factor can then be estimated using the gradient m , the difference between the initial pressure p_i and the pressure at 1 hour p_{1hr} extrapolated on the semilog straight line (Fig. 4.6), using Eq. (4.8) (from Horne, 1995; converted to SI units).

$$s = 1.151 \left(\frac{p_i - p_{1hr}}{m} - \log \frac{k}{\phi \mu c_t r_w^2} - 0.3514 \right) \quad (4.8)$$

MDH is the simplest form of semilog analysis and is strictly only applicable to the pressure transient resulting from the first flow step change (e.g. the drawdown for production tests, or first build-up during injection tests). However, MDH was still widely used for build-up analysis providing the production flow period was much longer than the pressure-transient period (Earlougher, 1977).

In practice, it is not always simple to identify the correct portion of data to use (the semilog straight line), and the Bourdet pressure derivative was originally developed to assist with this issue (Section 4.5.7).

4.5.2 Horner semilog plot

Pressure build-up tests are actually a very simple multirate case with only two flow steps: production then shut-in. MDH semilog plots theoretically only apply to well tests with a single-flow step, and so are technically inapplicable for build-ups.

The Horner semilog plot was designed specifically to account for the two flow steps of pressure build-ups (Horner, 1951). In fact the Horner plot is the same as the earlier Theis pressure recovery plot for groundwater hydrology, though it was developed independently (Ramey, 1975).

The Horner plot did not in fact replace the MDH semilog plot for pressure build-up analysis. MDH was still preferred due to ease of use; however, the Horner plot did provide a useful alternative in the circumstance that production times prior to shut-in were short (Earlougher, 1977).

The Horner plot (Horner, 1951) is pressure versus the logarithm of Horner time (Eq. 4.9). It can be seen in Fig. 4.7 that while time increases from left to right, the definition of Horner time means it increases in the opposite direction. Therefore if only Horner time is plotted, increasing in the usual manner from left to right, then the shape of the pressure-transient data set will appear to be reversed.

$$\text{Horner time} = \frac{t_p + \Delta t}{\Delta t} \quad (4.9)$$

where t_p is the producing time (seconds) and Δt is the time since shut-in (seconds).

Eq. (4.10) gives the pressure during shut-in (p_{us}) as a function of time in the IARF period. This describes a straight line with slope $-m$ and intercept p_i from which the permeability k can be calculated using Eq. (4.7) in the same manner as MDH semilog analysis (Earlougher, 1977).

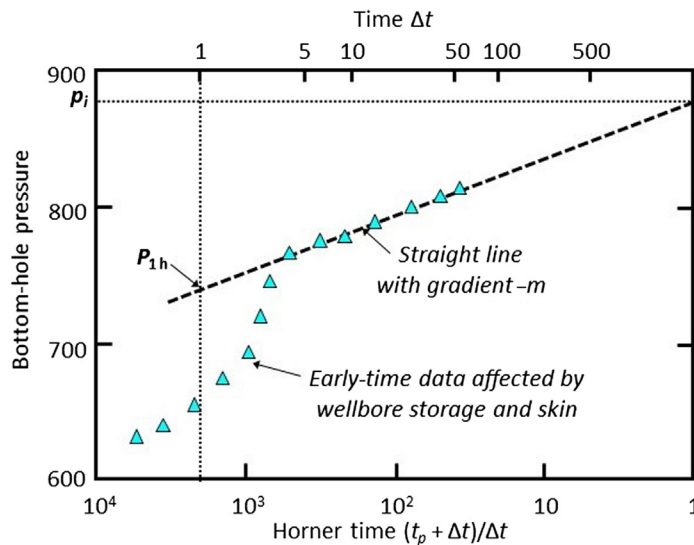


Figure 4.7 Example Horner plot for a build-up test, showing both Horner time and normal time for comparison. Data from Earlougher Jr., R.C., 1977. *Advances in Well Test Analysis*. Henry L. Doherty Memorial Fund of AIME, New York.

$$p_{ws} = p_i - m \log \left(\frac{t_p + \Delta t}{\Delta t} \right) \quad (4.10)$$

The skin factor can be estimated in a similar manner to MDH semilog analysis provided the production time t_p is $\gg 1$ hour using Eq. (4.11) (from Earlougher, 1977, converted to SI units).

$$s = 1.1513 \left(\frac{p_{1hr} - p_{wf}(\Delta t = 0)}{m} - \log \left(\frac{k}{\phi \mu c_t r_w^2} \right) - 0.3514 \right) \quad (4.11)$$

where: $p_{wf}(\Delta t = 0)$ is the downhole flowing pressure at the point of fluid flow shut-in.

If the production time t_p is on the order of 1 hour (3600 seconds) then Eq. (4.12) (from Earlougher, 1977, converted to SI units) is used to calculate skin factor.

$$s = 1.1513 \left(\frac{p_{1hr} - p_{wf}(\Delta t = 0)}{m} + \log \left(\frac{t_p + 3600}{t_p} \right) - \log \left(\frac{k}{\phi \mu c_t r_w^2} \right) - 0.3514 \right) \quad (4.12)$$

4.5.3 Multirate superposition plot

The MDH and Horner semilog methods strictly apply only when flow rates are constant (Earlougher, 1977). There are many practical reasons why flow rates may vary during a test, and many circumstances in which a test will be designed to have variable flow rates to avoid a halt in production. Variable flow rates are accounted for in a method first developed by Odeh and Jones (1965), thus allowing almost any flow rate change to be analysed as a well test (Earlougher, 1977).

A variable flow rate can be approximated by a series of flow steps (Fig. 4.8), and there can be any number of pressure data points (including zero) measured during each flow step. The pressure data are then displayed on a multirate superposition plot (Fig. 4.9), which is another form of semilog plot [also known as a 'rate-normalised plot' (Horne, 1995)]. It is defined by Eq. (4.13) and is not a plot of a single pressure transient but incorporates data from a number of pressure transients resulting from a number of flow steps.

$$\frac{p_i - p_{wf}(t)}{q_N} \text{ versus } \sum_{j=1}^N \left(\left(\frac{q_j - q_{j-1}}{q_N} \right) \log(t - t_{j-1}) \right) \quad (4.13)$$

A straight line is expected with slope m' and intercept b' (Fig. 4.9) which can then be used to calculate permeability k (Eq. 4.14) and skin factor s Eq. (4.15) (both from Earlougher, 1977, converted to SI units).

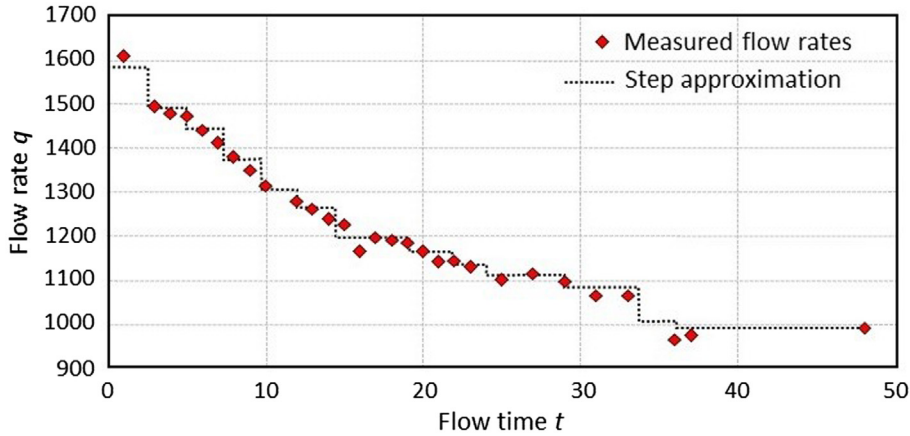


Figure 4.8 Step approximation of variable production flow rate. Data from Earlougher Jr., R.C., 1977. *Advances in Well Test Analysis*. Henry L. Doherty Memorial Fund of AIME, New York.

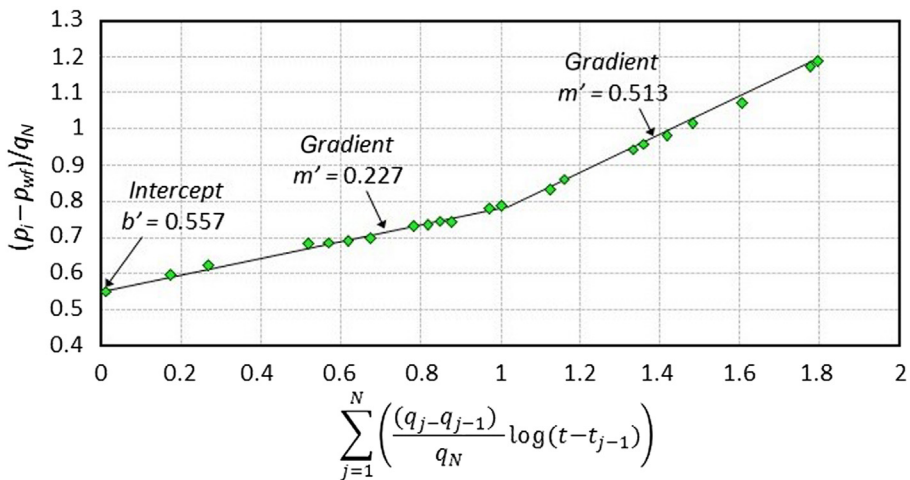


Figure 4.9 Example multirate superposition plot. Data from Earlougher Jr., R.C., 1977. *Advances in Well Test Analysis*. Henry L. Doherty Memorial Fund of AIME, New York.

$$k = 0.1832 \frac{B\mu}{m'h} \tag{4.14}$$

$$s = 1.1513 \left(\frac{b'}{m'} - \log \left(\frac{k}{\phi \mu c_r r_w^2} \right) - 0.3514 \right) \tag{4.15}$$

Interpretation is not always straightforward, for example in Fig. 4.9, there are two straight lines through the data. The first is interpreted as corresponding to the general reservoir and the second as the result of some boundary condition (Earlougher, 1977).

4.5.4 Two-rate plot

A simple case of multirate analysis (Section 4.5.3) is the two-rate flow test developed by Russell (1963). A well producing at a stable rate q_1 (usually for a few days) is changed to produce at a different rate q_2 (which can be higher or lower), and the resulting transient is analysed (Matthews and Russell, 1967). The advantages of this method are an improvement in wellbore problems and minimal disruption to production (Matthews and Russell, 1967). There has been a misconception that wellbore storage effects are eliminated by the two-rate test. In fact the duration of wellbore storage is unaffected, but a change in wellbore storage during the transient is prevented, avoiding this potential complication of the analysis (Earlougher, 1977).

A two-rate flow test plot (Fig. 4.10) is defined by Eq. (4.16) (Matthews and Russell, 1967).

$$\text{pressure versus } \left(\log\left(\frac{t + \Delta t'}{\Delta t'}\right) + \frac{q_2}{q_1} \log \Delta t' \right) \quad (4.16)$$

where $\Delta t'$ is the time after flow rate change (seconds).

This will give a straight line from which the slope m_1' can be used to determine reservoir permeability k using Eq. (4.17) and then skin factor s can be calculated using Eq. (4.18) (both from Earlougher, 1977, converted to SI units).

$$k = -0.1832 \frac{q_1 B \mu}{m_1'} \quad (4.17)$$

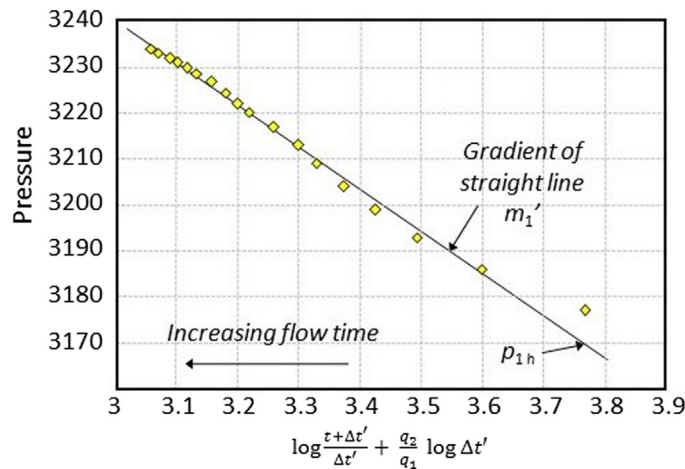


Figure 4.10 Example two-rate plot for a step decrease in flow rate. Data from Matthews, C.S., Russell, D.G., 1967. *Pressure Buildup and Flow Tests in Wells*, vol. 1. Society of Petroleum Engineers of AIME, Dallas, TX.

$$s = 1.1513 \left(\frac{q_1}{q_1 - q_2} \left(\frac{p_{wf}(\Delta t = 0) - p_{1hr}}{m_1'} \right) - \log \frac{k}{\phi \mu c_t r_w^2} - 0.3514 \right) \quad (4.18)$$

Although two-rate flow analysis has a lot of potential, geothermal examples are rare, most likely due to difficulties with flow control. However, two-rate analysis was applied to field data from geothermal wells at Cerro Prieto, Mexico, reportedly with mixed success (Rivera and Ramey, 1977; Rivera et al., 1980).

4.5.5 General semilog plot

Modern semilog plots use superposition time S_n (Eq. 4.19) which accounts for the entire flow history (production or injection) prior to a single pressure transient resulting from a single-flow step (Fig. 4.11) (Houzé et al., 2012). This ‘general’ semilog plot (Fig. 4.12) is different to Horner plots or two-rate plots which only handle two flow steps, or a multirate superposition plot which handles any number of flow steps but does not plot a single transient.

$$S_n(\Delta t) = \sum_{i=1}^{n-1} \frac{q_i - q_{i-1}}{q_n - q_{n-1}} \log(t_n - t_i + \Delta t) + \log \Delta t \quad (4.19)$$

The gradient of the straight-line section is used to calculate the permeability as for an MDH or Horner plot (Eq. 4.7). The skin factor is calculated by taking any point (X, Y) from the straight-line section and using Eq. (4.20) (from Houzé et al., 2012, converted to SI units).

$$s = 1.1513 \left(\frac{Y - p_{wf}}{m} - X - \log \left(\frac{k}{\phi \mu c_t r_w^2} \right) - \sum_{i=1}^n \left(\frac{q_i - q_{i-1}}{q_n - q_{n-1}} \log(t_{n+1} - t_i) \right) - 0.3515 \right) \quad (4.20)$$

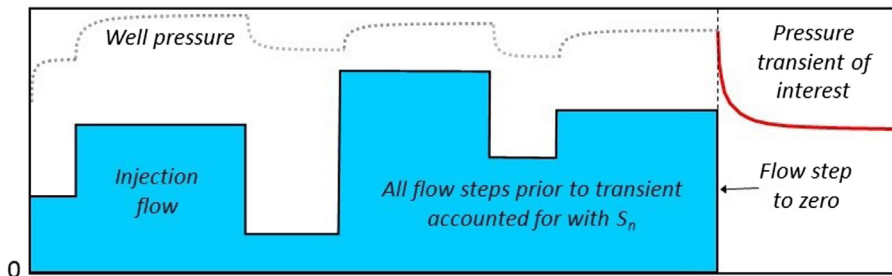


Figure 4.11 Schematic of complex injection flow history prior to a final flow step (to zero) and resulting fall-off curve.

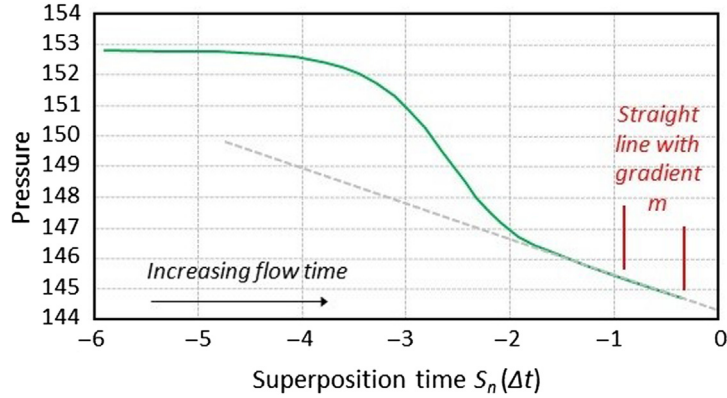


Figure 4.12 Example of general semilog plot: pressure versus superposition time for a fall-off.

The calculation of superposition time (Eq. 4.19) and skin factor (Eq. 4.20) are cumbersome to perform manually and fortunately have been enabled in modern times by the development of PTA software (Section 5.6).

4.5.6 Type-curve matching: log–log plot

Type-curve matching is a form of manual nonlinear regression (NLR), developed more than a decade before automated NLR became widespread. It is based on ‘type curves’ (Fig. 4.13), which are log–log plots of dimensionless pressure (p_D) versus dimensionless time (t_D). These were developed by Agarwal et al. (1970), demonstrating the importance of dimensionless wellbore storage (C_D) and skin (s) on the early-time pressure response. Dimensionless pressure (p_D) (Eq. 4.21), dimensionless time (t_D) (Eq. 4.22) and dimensionless wellbore storage coefficient (C_D) (Eq. 4.23) are linear functions of actual pressure, time and wellbore storage coefficient [Eqs 4.21–4.23 from Horne (1995), Eq. 4.23 converted to SI units].

$$p_D = \frac{2\pi kh}{qB\mu} \Delta p \quad (4.21)$$

where $\Delta p = (p_i - p_w)$.

$$t_D = \frac{kt}{\phi\mu c_i r_w^2} \quad (4.22)$$

$$C_D = \frac{C}{2\pi\phi c_i h r_w^2} \quad (4.23)$$

Ramey (1970) developed the procedure of matching field data to these type curves to obtain reservoir parameters. The procedure was designed to make use of ‘short-time’

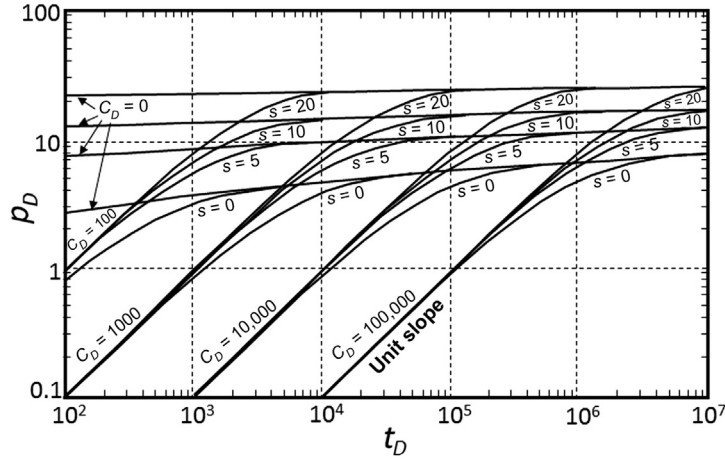


Figure 4.13 Type-curve example: dimensionless pressure (p_D) versus dimensionless time (t_D), for different values of dimensionless wellbore storage coefficient (C_D) and skin factor (s). Modified from Ramey Jr., H.J., 1970. Short-time well test data interpretation in the presence of skin effect and wellbore storage. *J. Petrol. Technol.* 22 (01), 97–104.

data, which are data sets too short to reach IARF, and therefore cannot be used for semi-log straight-line analysis (Ramey, 1970). Type-curve matching was recommended for use only when conventional straight-line semilog methods were not possible (Earlougher, 1977). Beyond 1970, many specialised type curves were generated for different models.

Type-curve matching is well described and illustrated in the Earlougher (1977) monograph. The basic method (Fig. 4.14) is to produce a log–log plot of actual measured pressure change versus time on tracing paper, using the same scale as a pre-printed set of log–log type curves of dimensionless pressure and time. The field data can then be moved around on top of the type curves until the best match is determined. Any match point between the two curves can be used to calculate reservoir parameters, and the position of the match curve used to estimate skin factor.

As Eq. (4.21) is a linear function, it follows that the difference between the logarithm of the actual pressure drop ($\log \Delta p$) and the logarithm of the dimensionless pressure drop ($\log p_D$) is constant (Eq. 4.24) from rearrangement of Eq. (4.21), and the same is true for time (Eq. 4.25) from rearrangement of Eq. (4.22).

$$\log \frac{2\pi kh}{qB\mu} = \log p_D - \log \Delta p \tag{4.24}$$

$$\log \frac{k}{\phi\mu c_t r_w^2} = \log t_D - \log t \tag{4.25}$$

Hence the vertical offset between the field data plot and the type curves, which can be assessed from any vertical match point (Fig. 4.14), can then be used with

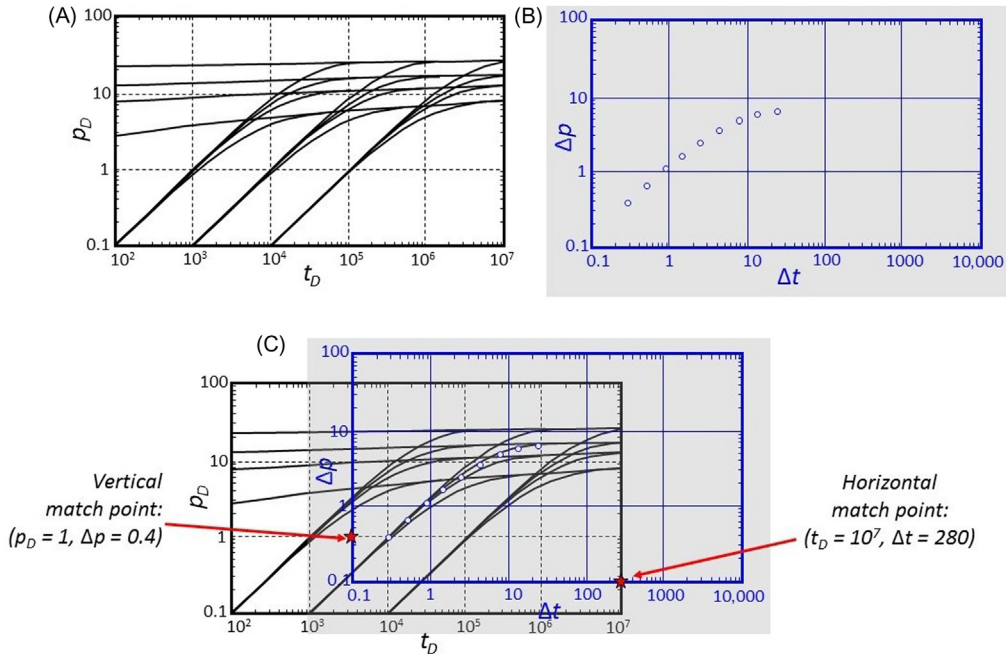


Figure 4.14 Schematic of type-curve matching procedure: (A) preprinted dimensionless type curves p_D versus t_D ; (B) field data on tracing paper Δp versus Δt and (C) match between field data and type curves yielding vertical and horizontal match points. Modified from Ramey Jr., H.J., 1970. *Short-time well test data interpretation in the presence of skin effect and wellbore storage*. *J. Petrol. Technol.* 22 (1), 97–104.

Eq. (4.24) to calculate the reservoir permeability k . Then the horizontal time offset, assessed from any horizontal match point (Fig. 4.14), can be used with Eq. (4.25) to calculate the porosity ϕ , assuming all other constant parameters in the equations are known (Horne, 1995).

One specialised type curve, described by Eq. (4.26), is used to analyse interference tests. Interference testing has advantages over single-well testing, including the minimisation of wellbore storage and skin effects (as fluid is not actually moving at the observation well) (Horne, 1995). This can also be viewed as a disadvantage, if estimating the skin factor (e.g. to evaluate the effectiveness of stimulation) is the objective. Another advantage is that storativity $\phi c_v h$ can be estimated rather than just the transmissivity kh . The main disadvantage of interference testing is that the measured pressure changes are very small (Earlougher, 1977).

$$p_D \text{ versus } \frac{t_D}{r_D^2} \quad (4.26)$$

where r_D is the dimensionless radial distance $r_D = r/r_w$.

The vertical match point (p_D and Δp) is used to calculate the reservoir permeability in the usual manner (as in Fig. 4.14 and Eq. 4.24). The horizontal match point (t_D/r_D^2 and t) is used to calculate the storativity using Eq. (4.27), where in this case r is the distance (m) between the two wells (Earlougher, 1977).

$$\phi c_t = \frac{1}{r^2} \frac{k}{\mu} \frac{t}{(t_D/r_D^2)} \quad (4.27)$$

4.5.7 Bourdet pressure derivative plot

The Bourdet pressure derivative was introduced by Bourdet (1983), around the time of the advent of computers, originally to help identify the portion of data representing the IARF flow regime (Section 4.4.2). The Bourdet pressure derivative (or just ‘pressure derivative’) is defined as the slope of the semilog plot displayed on a log–log plot, for example Fig. 4.15, which shows a simple example of a well with wellbore storage and skin, which starts in the wellbore storage flow regime (unit-slope pressure derivative) before transitioning to a period of IARF (zero slope pressure derivative). The Bourdet pressure derivative is referred to as the most important advance in the history of PTA (Houzé et al., 2012). It became useful far beyond the original scope as there are characteristic derivative shapes (some examples in Fig. 4.16) for many different flow regimes and well, reservoir and boundary behaviours (Horne, 1995; Houzé et al., 2012).

The pressure derivative (p') is taken with respect to the natural logarithm of time (Eq. 4.28) (Bourdet, 2002). As IARF is characterised by a semilog straight line, the associated characteristic pressure derivative is therefore constant, with a value equal to the slope of that straight line. Adding the Bourdet pressure derivative to type curves (Section 4.5.6) greatly improved their resolution, as barely perceptible differences in the shape of the pressure curves are greatly magnified in the pressure derivative

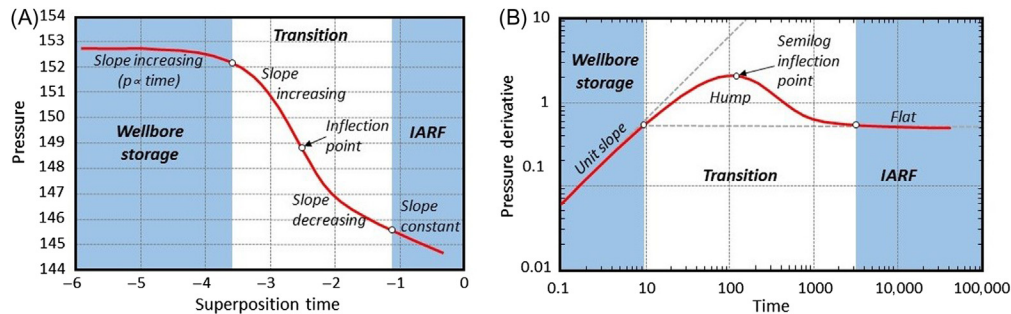


Figure 4.15 Bourdet pressure derivative example demonstrating how (A) features of the slope of the semilog plot correspond to (B) the derivative on the log–log plot.

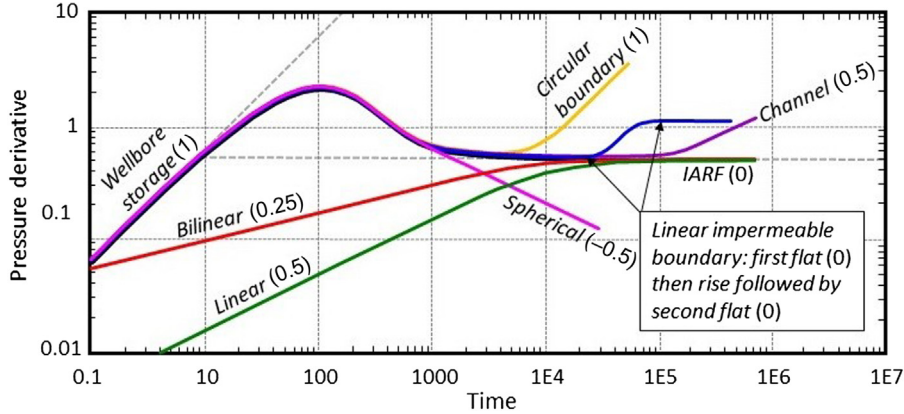


Figure 4.16 Examples of characteristic pressure derivatives: wellbore storage, bilinear and linear flow in a dominant near-well fracture, IARF, spherical flow due to partial penetration, circular boundary, channel boundary and linear impermeable boundary. *IARF*, Infinite-acting radial flow.

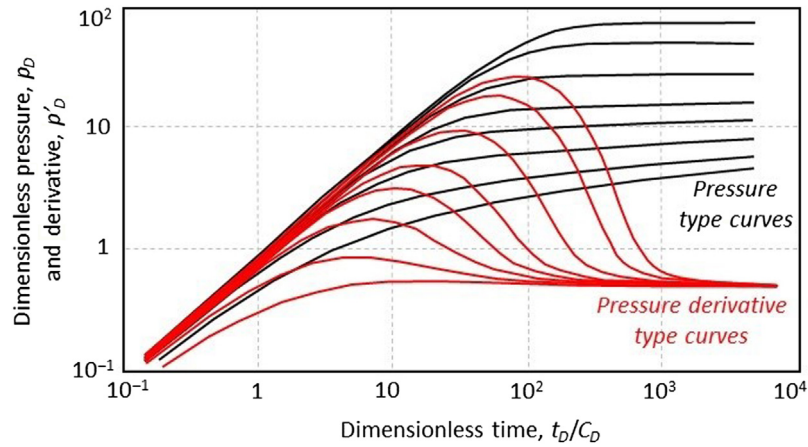


Figure 4.17 Addition of Bourdet pressure derivative to type curves: Dimensionless pressure type curves (black) look similar; however, the corresponding pressure derivative type curves (red, grey in print version) are easily distinguishable. Data from Bourdet, D., 2002. *Well Test Analysis: The Use of Advanced Interpretation Models*, vol. 3, Cubitt, J. (Ed.), Elsevier.

(Fig. 4.17) (Bourdet, 2002). The pressure derivatives effectively put pressure-transient data under the microscope to identify different wellbore and reservoir effects that are difficult to see or quantify using the other analytical methods.

$$\Delta p' = \frac{dp}{d \ln \Delta t} = \Delta t \frac{dp}{dt} \quad (4.28)$$

4.6 Summary

This chapter has covered the basics of pressure-transient well testing. The historical overview describes the emergence of analytical PTA theory from the groundwater industry and diversification into the petroleum industry. For a long time all PTA was analytical, and then numerical methods were included in combination with the analytical methods to address more complex systems, and then fully numerical PTA became possible.

This chapter has discussed the analytically-based early theory and fundamental concepts, including wellbore storage and skin, IARF and superposition in time and space. Several of the major analytical graphical methods are described in some detail, particularly the various semilog straight-line methods and type-curve matching, and lastly, the Bourdet pressure derivative, a hugely significant advance that is the cornerstone of modern PTA with computers.

All the analytical theory and methods discussed in this chapter can theoretically only be used to represent simple systems, for example radial flow in an infinite homogenous reservoir. More complex systems, such as reservoirs with boundaries and fractured reservoirs required more complex analytical models. The development of these more complex models is described in the next chapter, including some which were developed specifically for geothermal well test analysis.

Numerical methods played a role in the development of some of these more complex analytical models. Fully numerical PTA is now possible and will be discussed in Chapter 8, Numerical Pressure-Transient Analysis Modelling Framework.

CHAPTER 5

Advanced analytical pressure-transient analysis relevant to geothermal wells

Contents

5.1	Introduction	89
5.2	Reservoir boundaries	90
5.2.1	Impermeable boundaries	90
5.2.2	Constant-pressure boundaries	93
5.2.3	Caution with boundary models	93
5.3	Multiphase reservoir fluid	94
5.4	Non-Darcy flow	95
5.5	Single-fracture models	96
5.6	Fractured reservoirs	98
5.6.1	Dual-porosity model	99
5.6.2	Fractional dimension (fractal) model	102
5.7	Analytical automated well test analysis systems	103
5.8	Limitations of analytical methods in geothermal well test analysis	104
5.9	Geothermal-specific analytical methods	105
5.9.1	Parallelepiped model for vapour-dominated reservoirs	105
5.9.2	Two-phase water/steam reservoirs	106
5.9.3	Nonisothermal systems	108
5.9.4	Adsorption in vapour-dominated reservoirs	111
5.9.5	Geo-pressured geothermal systems	111
5.10	Summary	111

5.1 Introduction

All analytical models are solutions to the diffusivity equation, and many simplifying assumptions are required. The earliest and simplest models and methods are described in Chapter 4, Introduction to Pressure-Transient Analysis. In this chapter, more complex analytical models are described, in which some of the assumptions are relaxed or eliminated. Important examples are reservoir boundary models, fractured reservoir models, single-fracture models, multiphase reservoir fluid, stress-sensitive reservoirs and non-Darcy flow. These advances were made within the petroleum industry but are relevant for the geothermal industry as these are also common features of geothermal reservoirs.

5.2 Reservoir boundaries

If there is no outer confining boundary, the reservoir would be effectively infinite. While no reservoir is truly infinite in reality, the pressure response at the wellbore will behave for some period of time as if it is infinite, hence the term ‘infinite-acting’ radial flow (IARF) (Section 4.4.2). After a sufficiently long period of time, when the pressure disturbance has spread far enough from the well, the effect of boundaries can be observed. Two common types are impermeable boundaries and constant-pressure boundaries (Horne, 1995), though other less common types are sometimes found such as leaky or conductive boundaries (Houzé et al., 2012). Only the two most common boundary types are described in this section, as these are the ones mostly likely to be seen in geothermal data sets. More details regarding complex boundary types is available in Horne (1995) and Houzé et al. (2012).

5.2.1 Impermeable boundaries

The first major type of boundary is an impermeable boundary, also referred to as a ‘no-flow’ boundary, as fluid cannot flow across or along the boundary. A common example of a real-life impermeable feature in a reservoir is a fault with a well-developed impermeable fault core (gouge, cataclasite and mylonite) preventing fluid flow across the fault plane, with no significant damage zone (fracturing adjacent to the fault core) to allow fluid flow along the fault plane. A word of caution on faults — depending on the size and geometry of the fault core and damage zone, faults can be either impermeable barriers or conduits for fluid flow (Rowland and Sibson, 2004). An impermeable boundary response can arise from a real impermeable feature in the reservoir and also by interference with another well (Horne, 1995).

When a well is surrounded on all sides by impermeable boundaries, the reservoir is referred to as ‘closed’. The simplest geometry for a closed reservoir is a central well surrounded by a circular boundary (Fig. 5.1A), and a more complex example is a rectangular reservoir with the well off-centre (Fig. 5.1B). A significant early paper on boundaries by Matthews et al. (1954) presents solutions for circular, square, rectangular and triangular boundaries, with various positions of the well within the boundary. All of these simple geometries can be used as an approximation for real-life reservoirs bounded on all sides by impermeable features.

In a closed reservoir, when the well test has been running for long enough that all boundaries have been detected, then the pressure everywhere in the reservoir will decline at the same rate. This is called ‘pseudosteady state’, and the pressure drop during this period can be used to estimate the reservoir volume (Horne, 1995). The characteristic pressure derivative for pseudosteady-state flow is a unit-slope pressure derivative in late time for a drawdown test (Fig. 5.1). For circular reservoirs with the well in the centre the transition from IARF to pseudosteady-state flow is very rapid

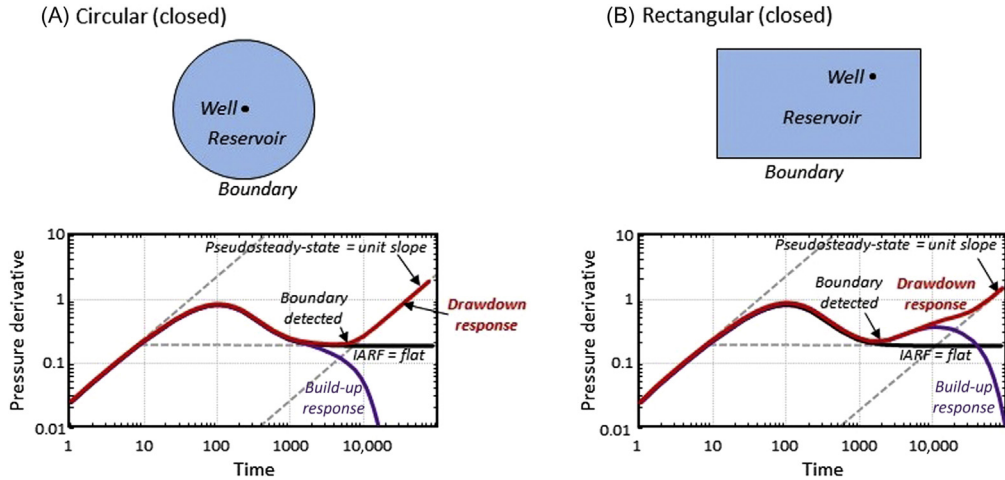


Figure 5.1 Examples of reservoirs with closed boundaries, and associated characteristic pressure derivative response for drawdowns and build-ups: (A) circular boundary with well in centre and (B) rectangular boundary with well off-centre. After Houzé, O., Viturat, D., Fjaere, O., 2012. *Dynamic Data Analysis: The Theory and Practice of Pressure Transient, Production Analysis, Well Performance Analysis, Production Logging and the Use of Permanent Downhole Gauge Data*. KAPPA Engineering.

(Fig. 5.1A) as all parts of the boundary are detected at the same time. For rectangular reservoirs where there is a different distance from the well to each of the four sides of the rectangle, this transition becomes uneven and is extended over a long period (Fig. 5.1B) as each boundary is detected at different times. Therefore care must be taken when identifying the pseudosteady-state straight line as it may not be obvious until very late time for reservoirs with complex shapes and elongated reservoirs in particular (Horne, 1995). During build-up testing in closed reservoirs the pressure derivative will drop steeply down to zero (Fig. 5.1A), as the pressure stabilises at the average reservoir pressure (Houzé et al., 2012). For more complex reservoirs such as the rectangular case, the pressure derivative can rise as the closer boundaries are detected, before the steep drop to zero (Fig. 5.1B) (Houzé et al., 2012).

It is a common mistake with closed systems to expect the build-up response to exhibit the same behaviour as a drawdown (unit-slope in late time). In the case of most other models the drawdown and build-up responses are the same or similar. However, the behaviour of a closed reservoir during the recovery from pseudosteady state (the build-up) is fundamentally different: after all the boundaries are detected the pressure stays constant, hence the pressure derivative drops to zero (Houzé et al., 2012).

Not all reservoirs are closed, and also many closed ones will not appear to be so over the usual duration of a well test, especially if the reservoir is large. In the case of a

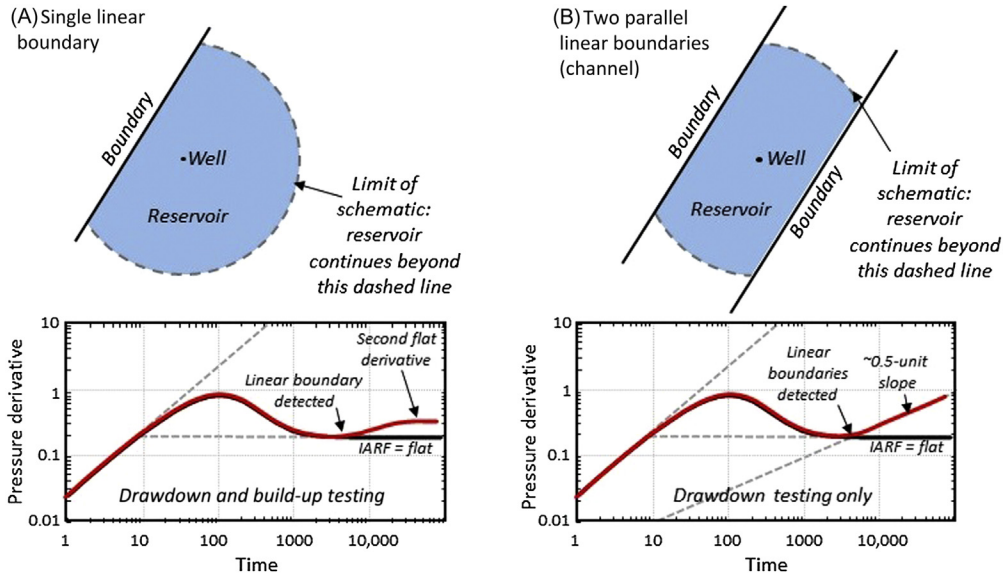


Figure 5.2 Examples of reservoirs with linear boundaries, and associated characteristic pressure derivative response: (A) single linear impermeable boundary (drawdown/build-up response) and (B) channel – two parallel linear impermeable boundaries with central well (drawdown response). After Houzé, O., Viturat, D., Fjaere, O., 2012. *Dynamic Data Analysis: The Theory and Practice of Pressure Transient, Production Analysis, Well Performance Analysis, Production Logging and the Use of Permanent Downhole Gauge Data*. KAPPA Engineering.

single linear impermeable boundary such as an impermeable fault, the boundary is not ‘closed’ as the well is not enclosed on all sides (Fig. 5.2). The response to this type of boundary is a doubling in slope of the IARF semilog straight line, which appears as an increase, followed by a second flattening of the pressure derivative, at a value twice that of IARF (Fig. 5.2A) (Home, 1995). This behaviour is the same during drawdown and build-up testing. The time at which the boundary is detected (the pressure derivative deviates from the IARF response) can be used to estimate the distance to the boundary (Home, 1995).

Two parallel linear impermeable boundaries form a channel, which gives a pressure derivative of approximately 0.5 unit-slope for a drawdown test (Fig. 5.2B). Although this is theoretically only applicable to drawdowns, in practice the buildup response is frequently similar (Houzé et al., 2012). If the well is off-centre in the channel then the transition to the 0.5 unit-slope will be extended in a manner similar to that discussed for the rectangular case (Fig. 5.1B). If the faults are intersecting (not parallel) then the response is more complex, with the pressure derivative stabilising for the second time at a level $2\pi/\theta$ greater than the IARF line, where θ is the angle between the faults (Houzé et al., 2012).

5.2.2 Constant-pressure boundaries

The other major boundary type is a constant-pressure boundary, which is a feature so permeable that the pressure disturbance from the well test has no impact upon the pressure at that feature (Horne, 1995). Rather, the long-term effect is that the well will reach the same constant pressure as the boundary. A truly constant-pressure boundary is unlikely in practice; however, scenarios such as a nearby aquifer or nearby injection wells produce a response very similar to a constant-pressure boundary (Horne, 1995). In vapour-dominated reservoirs the presence of a deep horizontal boiling surface led to the concept of a constant-pressure boundary (Cinco-Ley et al., 1979). Constant-pressure theory was included in the Society of Petroleum Engineers (SPE) monograph of Matthews and Russell (1967) and later reviewed and expanded by Ehlig-Economides (1979) and incorporated into the parallelepiped model for geothermal vapour-dominated reservoirs (Kruger and Ramey, 1979) (Section 5.9.1). A constant-pressure boundary model is still in common use today, useful in any scenario in which the reservoir pressure is supported by fluid encroachment (Horne, 1995).

Constant-pressure boundaries can be circular or linear, and both will result in a transition from the IARF flat pressure derivative to the pressure stabilising at a constant value, hence a pressure derivative of zero (Fig. 5.3) (Horne, 1995). The pressure derivative response is the same for drawdowns and build-ups (Houzé et al., 2012).

5.2.3 Caution with boundary models

The pressure derivative responses of constant-pressure boundaries (Fig. 5.3) are very similar to the build-up responses of closed reservoirs (Fig. 5.1), in both cases, the pressure derivative drops to zero as the pressure stabilises at a constant value (Houzé et al., 2012).

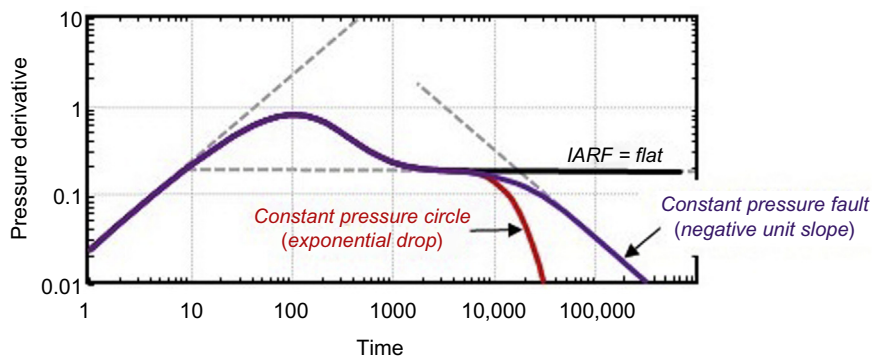


Figure 5.3 Characteristic pressure derivative response for two constant-pressure boundary examples: constant-pressure circle and single constant-pressure fault. After Houzé, O., Viturat, D., Fjaere, O., 2012. *Dynamic Data Analysis: The Theory and Practice of Pressure Transient, Production Analysis, Well Performance Analysis, Production Logging and the Use of Permanent Downhole Gauge Data*. KAPPA Engineering.

To avoid confusion between these two very different models, it can be desirable to perform a drawdown test instead of a build-up test, for which the behaviour of the two types of model are significantly different, though drawdown testing is not often possible in geothermal wells (Section 4.2). The equivalent conclusion when injecting cold water (rather than production testing) implies a preference for injection tests instead of fall-off tests.

Underestimating or overestimating the production or injection history for a test (or not including it at all) will result in a deviation from the IARF response, causing it to drift above or below the expected flat derivative response. Increases in the derivative can be indistinguishable from no-flow boundary responses, and decreases indistinguishable from constant-pressure boundary responses (Houzé et al., 2012). Therefore there is need for caution: any feature in the pressure derivative that looks like a boundary response could in fact be an artefact created by an incomplete flow history and occur when no actual boundaries are present. It is vitally important to not only accurately log the flow rate in the well but to include the entire flow history in the analysis.

Boundary responses typically appear in the pressure derivative during late time, when the actual measured change in pressure is very small. This makes them vulnerable to a variety of artefacts, which are too small to be significant earlier in the well test, but can become significant in late time. These include drift in the downhole pressure tool, large-scale reservoir trends and interference from other wells (Houzé et al., 2012). Steps can be taken to detect and measure these effects and correct the data accordingly. Some geothermal-specific artefacts affecting geothermal PTA datasets are discussed in Chapter 7, Downhole Tools and Other Practical Considerations, some of which are the direct result of the high-temperature fluid found in geothermal reservoirs.

5.3 Multiphase reservoir fluid

Single-phase fluid is one of the assumptions required for the derivation of the diffusivity equation (Section 4.4.5) and hence the simplest analytical models; however, the use of analytical techniques has been extended to certain types of multiphase petroleum systems. In this context, ‘multiphase’ refers to various combinations of oil, water and gas. It does not refer to geothermal two-phase steam/water systems, discussed in [Section 5.9.2](#). It should be noted that even within the petroleum industry, most existing multiphase techniques are of limited applicability and accuracy, and it is recommended that multiphase conditions be avoided if possible (Horne, 1995).

The approach of Perrine (1956) is the most straightforward, as total flow properties replace individual phase properties (Horne, 1995). These are the total mobility and total compressibility and are calculated from the properties of the individual phases. Assumptions required by this approach are significant, including small pressure

and saturation gradients, negligible saturation changes during the test and negligible capillary pressure (Horne, 1995). Various studies have demonstrated the limitations of this approach (Horne, 1995), including unreliability for higher gas saturations (Weller, 1966), underestimation of effective phase permeabilities (Chu et al., 1986) and overestimation of skin effect when gas near the wellbore blocks flow (Ayan and Lee, 1988).

Raghavan (1976) accounted for the pressure dependence of fluid properties and effective permeability, using a specially defined pseudopressure function. There are different pseudopressure functions for drawdown and build-up behaviour. A reservoir has absolute permeability; however, each phase experiences a different (effective) permeability depending on the abundance of each phase. Relative permeability is the ratio of the effective permeability of each phase to the absolute permeability, and relative permeability curves describe how this varies with water (liquid) saturation. It is necessary to know the relative permeability curves for the reservoir in order to apply the pseudopressure function. This is the major limitation of this approach, as the relative permeability curves are difficult to obtain in practice, and the estimated reservoir parameters are very sensitive to the relative permeability data (Horne, 1995). The relative permeability curves in two-phase and vapour-dominated geothermal reservoirs can be estimated from history matching of production data using numerical reservoir simulation.

The pressure-squared approach was developed by Al-Khalifah et al. (1987), using a pseudosteady-state solution of the diffusivity equation in terms of pressure squared (p^2) rather than pressure. It is a more general approach, of which Perrine's approach is a special case (Al-Khalifah et al., 1987). The new diffusivity equation can be solved to obtain new equations for pressure behaviour during IARF and skin factor, which allow estimation of the oil phase permeability. This approach has the advantage that it is not necessary to know the relative permeability curves in advance, and this approach has been successful in high- and low-volatility oil systems (Horne, 1995).

5.4 Non-Darcy flow

Non-Darcy flow is turbulent flow in porous media, which occurs at high flow rates, for example in natural gas wells and geothermal wells. It was examined in detail by Wattenbarger and Ramey (1968) to determine its importance for gas wells. Non-Darcy flow effects have the appearance of positive skin but are flow rate dependent (Ramey, 1965). Total skin factor will be comprised of a constant component due to actual well damage or stimulation (s'), and a flow rate variable component due to non-Darcy skin (D) (Eq. 5.1) (Horne, 1995).

$$s = s' + Dq \quad (5.1)$$

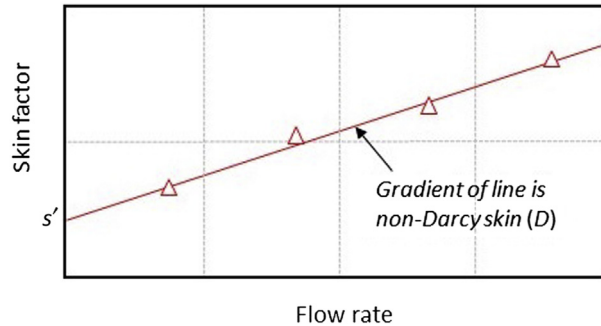


Figure 5.4 Skin factor versus flow rate graph to assess mechanical skin (s') and non-Darcy skin (D).

Therefore if pressure–transient data sets are available for more than one flow rate then the fraction of the overall effective skin factor due to non–Darcy flow can be calculated (Ramey, 1965). A practical method to handle non–Darcy flow is a graph of skin factor versus flow rate, which should be linear (Fig. 5.4). The y -intercept is the constant skin factor s' , and the slope D is the parameter describing non–Darcy skin (Horne, 1995).

Non–Darcy effects in gas wells have an effect on the skin factor significant enough to make a stimulated well appear damaged (Ramey, 1965). Benson (1982) applied this concept to pressure build-ups in a geothermal well and found that very high values for overall skin (mysterious in a fractured well drilled without mud) were explained by a significant non–Darcy skin component. Non–Darcy flow effects on geothermal pressure transients were also identified at Afyon Ömer–Gecek Geothermal Field, Turkey (Onur, 2010).

The downside to this method to assess non–Darcy skin is that it requires multiple pressure–transient datasets to be collected, at least three datasets at different flow rates, to allow the estimation of at least three total skin data points for the linear fit (Fig. 5.4). This will not always be practical due to operational constraints, cost and time.

For numerical PTA a more rigorous approach is possible by integrating the Forchheimer equation into the simulation, described in Section 8.8.3.

5.5 Single-fracture models

The objective of hydraulic fracturing is to improve the connection between the well and the reservoir to increase the well productivity, and it is extremely common in oil and gas wells (Horne, 1995). Hydraulic fracturing operations aim to produce a single vertical fracture which fully penetrates the thickness of the productive formation, to some significant distance from the well, described by the fracture half-length X_f (Fig. 5.5A).

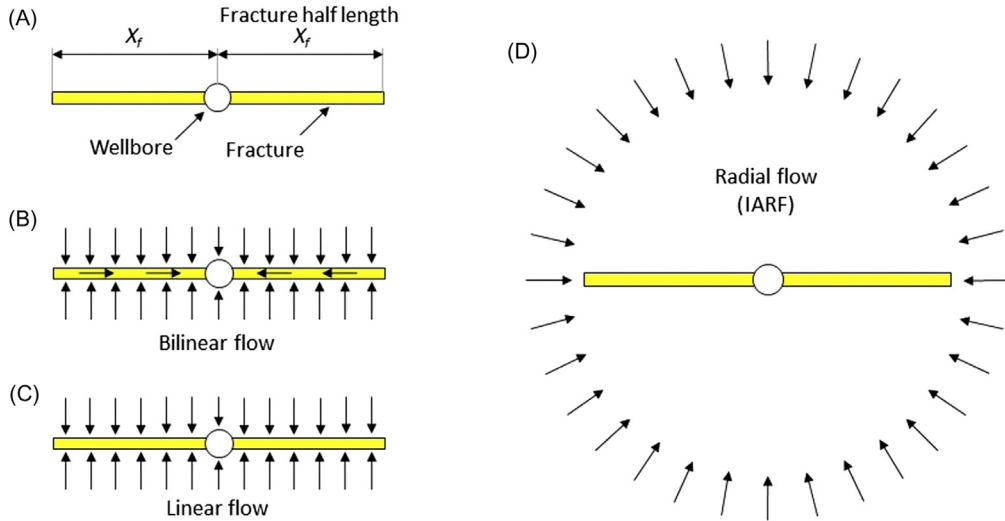


Figure 5.5 Flow regimes of interest with a single-fracture model: (A) model schematic from the perspective of looking along the vertical axis (down the wellbore); (B) bilinear flow; (C) linear flow and (D) radial (IARF) flow. After Houzé, O., Viturat, D., Fjaere, O., 2012. *Dynamic Data Analysis: The Theory and Practice of Pressure Transient, Production Analysis, Well Performance Analysis, Production Logging and the Use of Permanent Downhole Gauge Data*. KAPPA Engineering; Horne, R.N., 1995. *Modern Well Test Analysis: A Computer-Aided Approach*. Petroway Inc.

As the fracture will have much higher permeability than the formation, it will dominate the early pressure-transient response with linear flow along the fracture rather than radial flow in the reservoir. Throughout the 1970s, analytical models for various types of single fracture were developed.

The uniform flux fracture model by Gringarten et al. (1972) was one of the first solutions and requires the assumption that flow into the fracture is uniform along the length of that fracture. This is not an assumption that holds in practice, as flow into the fracture is known to be far from uniform (Horne, 1995).

The next development by Gringarten et al. (1974) was an infinite conductivity fracture model, which is applicable only to highly conductive fractures (Horne, 1995). An initial period of linear flow (Fig. 5.5C) will transition to radial flow (IARF) (Fig. 5.5D). During the linear flow period the characteristic derivative plot response is that the pressure and pressure derivative have a 0.5 unit-slope and are separated by a factor of 2 (Fig. 5.6) (Horne, 1995).

The more general finite-conductivity fracture model developed by Cinco-Ley et al. (1978) is initially a bilinear flow regime (Fig. 5.5B), followed by a linear flow regime (Fig. 5.5C), followed by radial flow (Fig. 5.5D) (Horne, 1995). The characteristic bilinear derivative plot response is that the pressure and pressure derivative have a 0.25 unit-slope and will be separated by a factor of 4 (Fig. 5.6) (Horne, 1995).

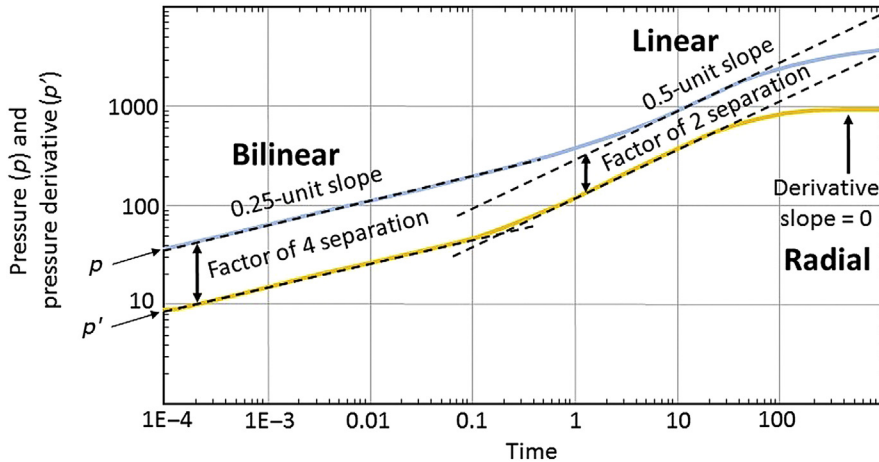


Figure 5.6 Single-fracture model: characteristic pressure and pressure derivative during the progression through bilinear, linear and radial (IARF) flow regimes as expected for a finite-conductivity fracture model. After Houzé, O., Viturat, D., Fjaere, O., 2012. *Dynamic Data Analysis: The Theory and Practice of Pressure Transient, Production Analysis, Well Performance Analysis, Production Logging and the Use of Permanent Downhole Gauge Data*. KAPPA Engineering; Horne, R.N., 1995. *Modern Well Test Analysis: A Computer-Aided Approach*. Petroway Inc.

The transitional increase in slope towards the 0.5 unit-slope linear response often begins but then transitions again into radial flow before the 0.5 unit-slope is reached; hence, this characteristic linear response is often not seen (Horne, 1995).

Recent work by Luo and Tang (2015) has moved away from the single-fracture model and allowed for patterns of multiple fractures ‘multiwing fractures’ at the wellbore. A semianalytical solution was developed and the impact of complex fracture patterns on the pressure derivative investigated, concluding that complex fracture patterns can cause humps in the pressure derivative during the fracture-controlled bilinear and linear flow periods (Fig. 5.7) (Luo and Tang, 2015).

5.6 Fractured reservoirs

Early analytical models are based on the assumption that the reservoir is a uniform porous medium, with a single value for porosity, when in fact many reservoirs (and most geothermal reservoirs) are extensively fractured. One of the earliest models to represent fractured reservoirs is the analytical ‘dual-porosity’ (matrix-fracture) model of Warren and Root (1963), requiring simplistic assumptions. A more modern representation of fractured reservoirs is the generalised radial flow (GRF) model of Barker (1988) (also called ‘fractal’ or ‘fractional dimension’).

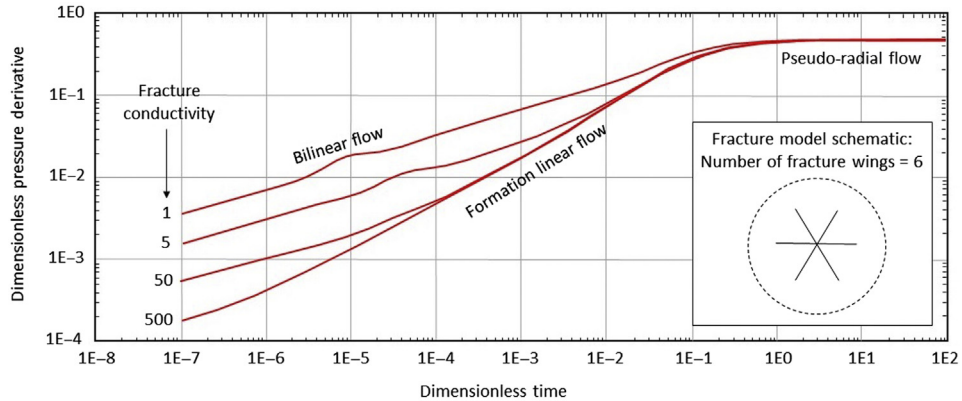


Figure 5.7 Examples of pressure derivatives generated by multiwing fracture model with six 'wings' for a range of fracture conductivity, exhibiting humps in the bilinear and linear flow periods. After Luo, W., Tang, C., 2015. *Pressure-transient analysis of multiwing fractures connected to a vertical wellbore*. *SPE J.* 20 (2), 360–367.

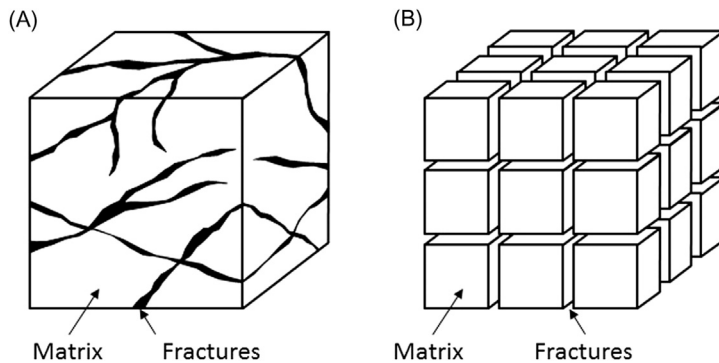


Figure 5.8 Schematic of dual-porosity concept: (A) 'actual' reservoir showing matrix and fractures and (B) dual-porosity model reservoir with matrix blocks and fractures. After Warren, J.E., Root, P.J., 1963. *The behavior of naturally fractured reservoirs*. *Soc. Pet. Eng. J.* 3(03), 245–255.

5.6.1 Dual-porosity model

Some reservoirs have distinct primary and secondary porosity. Primary porosity is the original porosity of the rock when it formed, and secondary porosity is the pore space created by subsequent processes such as fracturing. Warren and Root (1963) developed the dual-porosity (or 'double-porosity') model to represent this type of reservoir, in which there are regions that contribute to the pore space but not the flow capacity. This true in practice as not all pores are connected. A real-world reservoir cut by fractures (Fig. 5.8A) is represented by regularly spaced matrix blocks, connected by straight and evenly spaced fractures (Fig. 5.8B).

This dual-porosity model is equally applicable to fractured or vugular reservoirs. Vugular reservoirs contain many small cavities, which can either be primary, forming at the same time as the host rock, or secondary, forming due to subsequent processes. Assumptions of the dual-porosity model include pseudosteady-state matrix–fracture flow, uniform block size and uniform fracture spacing (Fig. 5.8B).

The dual-porosity model has a characteristic pressure derivative response (Fig. 5.9). The first reservoir response is from the fractures as they have greater transmissivity and are connected directly to the wellbore. There is a flat derivative associated with this (and semilog straight line). After some period the primary porosity in the matrix will begin to respond, flowing into the fractures and causing the pressure derivative to dip, though once established will return to the flat derivative (second semilog straight line) (Horne, 1995).

Two parameters are specific to the dual-porosity model: the storativity ratio ω (Eq. 5.2) and transmissivity ratio λ (Eq. 5.3 is the version for cubic or spherical matrix blocks) (Horne, 1995).

$$\omega = \frac{\phi_f c_{ff}}{\phi_f c_{ff} + \phi_m c_{fm}} \quad (5.2)$$

$$\lambda = \frac{60 k_m}{x_m^2 k_f} r_w^2 \quad (5.3)$$

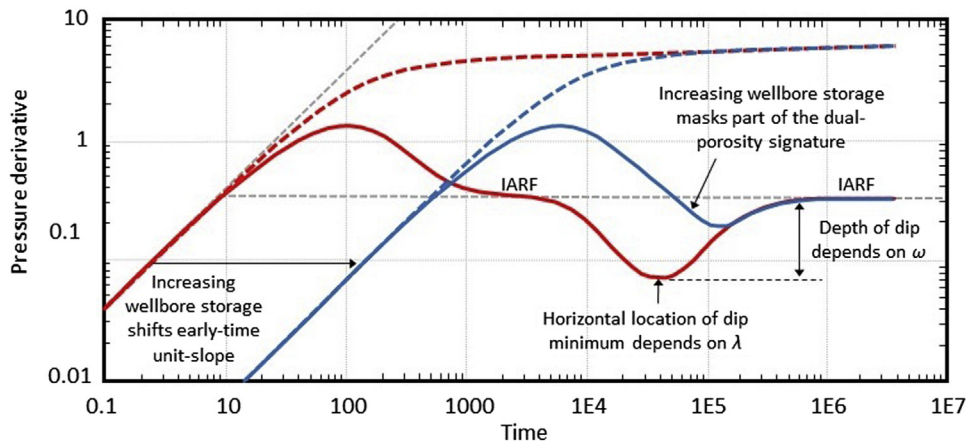


Figure 5.9 Characteristic pressure derivative for dual-porosity model: initial IARF flat derivative (flow in fractures only), followed by transition (dip) then second IARF flat derivative (flow in fractures and matrix). Tendency of first flat derivative to be masked by wellbore storage is shown. After Houzé, O., Viturat, D., Fjaere, O., 2012. *Dynamic Data Analysis: The Theory and Practice of Pressure Transient, Production Analysis, Well Performance Analysis, Production Logging and the Use of Permanent Downhole Gauge Data*. KAPPA Engineering; Horne, R.N., 1995. *Modern Well Test Analysis: A Computer-Aided Approach*. Petroway Inc.

The Warren and Root (1963) model was expanded by Mavor and Cinco-Ley (1979) to include the effect of wellbore storage and skin. In practice the earlier secondary porosity (fracture) response is often masked by wellbore storage and only the later response including the primary porosity (matrix) is observed (Fig. 5.9) (Mavor and Cinco-Ley, 1979). This makes it difficult to identify dual-porosity reservoirs.

The dual-porosity concept was later generalised for numerical simulation by Pruess and Narasimhan (1985) with the multiple interacting continua (MINC) method. The MINC method effectively takes a grid and divides each block into a group of blocks: a ‘fracture block’ and within this a number of nested ‘matrix blocks’ (up to 5 nested matrix blocks) (Fig. 5.10). The interface between block groups is by the fracture blocks only. Connections with the matrix blocks are internal within the group; matrix blocks do not connect directly with any part of a different block group. Matrix blocks are connected only to the adjacent matrix blocks, or to the fracture block in the case of the largest matrix block. Some numerical studies have used MINC to expand on the Warren and Root (1963) model (Section 8.8.2).

An experimental study by Okandan et al. (1988) reproduced drawdown behaviour of single-phase flow using three-dimensional (3D) arrangements of actual marble blocks, which represent zero matrix permeability. Experimental results conformed to dual-porosity theory (Okandan et al., 1988). However, more recently there is a consensus that exponential fracture spacing is more descriptive of reality, and the shape of the pressure derivative is significantly affected by this distribution (Spivey and Lee, 2000). In particular the classic V-shaped dip in the pressure derivative for the double-porosity model (Fig. 5.9) may not be present.

More recently, Valdes-Perez et al. (2013) have developed a new analytical dual-porosity model with a fractal fracture network, by incorporating the GRF concept

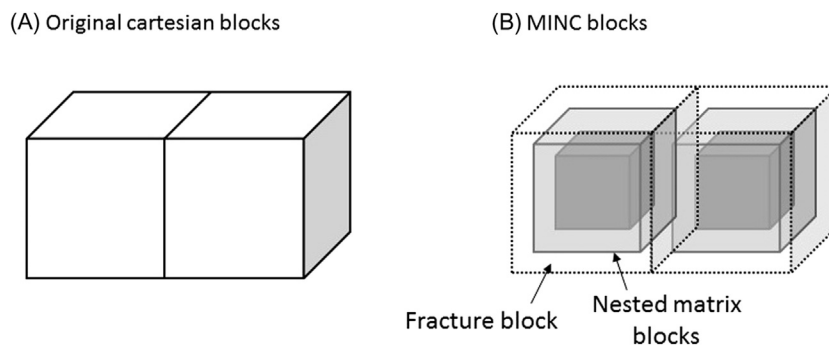


Figure 5.10 Schematic of MINC grid showing the division of original cubic blocks into groups, each containing a fracture block and a set of nested matrix blocks (more matrix blocks are possible than the two shown). *MINC, Multiple interacting continua. After Pruess, K., Narasimhan, T., 1985. A practical method for modelling fluid and heat flow in fractured porous media. J. Soc. Pet. Eng. 25 (1), 14–26.*

discussed in the next section. This new model accounts for the transient behaviour of flow between the matrix and fractures (Valdes-Perez et al., 2013).

5.6.2 Fractional dimension (fractal) model

The generalised radial flow (GRF) model of Barker (1988) was developed to account for the fact that real-world networks of fractures cannot be adequately represented by models which are strictly one-dimensional (1D), two-dimensional (2D) or three-dimensional (3D) (linear, radial or spherical flow regimes). Rather than choosing one of these integral dimensions, the fractional dimension n can take any value in the range 1–3, hence the term ‘fractional’.

The value of a fractional dimension model is clear when considering real geothermal wells, which are not uniformly permeable at all depths, but usually intersect a number of permeable fractures ‘feed zones’ which can be identified by a combination of completion testing (see Chapter 6: Completion and Output Testing) and image logs (McLean and McNamara, 2011; Massiot et al., 2017). It is possible to identify the fractures which are permeable *at the well face*; however, deeper into the reservoir the fracture network could become narrower and peter out altogether or expand greatly and become much more extensive than is apparent at the well. A 1D network is effectively a ‘slot’ (though not necessarily a straight one) and hence the volume of the feed zone increases linearly with radial distance from the well (O’Sullivan et al., 2005). A 2D network is effectively a ‘disc’, also known as penny- or pancake- shaped, where the feed zone volume increases with the square of the radial distance. A 3D network would occupy a spherical region where the feed zone volume increases with the cube of the radial distance (O’Sullivan et al., 2005). A real fracture network, however, is more likely to be something in between, and therefore is best represented by some fractional dimension.

It was determined by Barker (1988) that for constant rate well testing in infinite-acting porous media, when n is greater than two, the pressure will approach steady state, which means the pressure derivative will approach zero. When n is less than or equal to 2, the test will be transient (not steady-state), and the dimension is obtained from the slope of the log–log plot (Barker, 1988).

The fractional dimension model can be used to represent fractal fracture networks. Fractal patterns result from the repetition of a particular pattern over different length scales. Networks of natural fractures in rock have fractal characteristics and therefore cannot be fully described by random fracture networks, dual-porosity or MINC models (Acuna and Yortsos, 1995). A study of rock cores from the Kakkonda Geothermal Field, Japan, concludes that there is indeed a fractal distribution of both the location of the fractures and the fracture widths (Tateno et al., 1995).

Chang and Yortsos (1990) derived an analytical implementation of the fractional dimension concept for single-phase flow by modification of the diffusivity equation.

This was verified by Acuna and Yortsos (1995) using numerical simulation of both fractal fracture networks and flow in those networks. An important characteristic of the fractional dimension model is that the pressure derivative is linear on a log–log plot, and the slope of this linear section depends on the value of the fractional dimension n . Pressure derivative slopes of -0.5 , 0 and 0.5 correspond to conventional spherical (3D), radial (2D) and linear (1D) flow, respectively. The pressure derivative slope of the fractal model can take any value in that range -0.5 to 0.5 and thus be any dimension between 3 and 1 (Acuna et al., 1992). Similar pressure derivative behaviour is observed in the numerical version of the fractional dimension model, and is shown in Section 8.5.3. The method for implementation of the fractional dimension concept for numerical simulation is also described in Section 8.5.3.

The analytical fractional dimension model is applied to field data from the Geysers, on pressure-transient data sets from a number of wells, yielding dimensions both less than and greater than 2 (Acuna et al., 1992). Acuna et al. (1992) concluded that this is a reasonable alternative model for interpretation of well tests, which is more consistent with other field evidence, rather than simplistic single-fracture models.

5.7 Analytical automated well test analysis systems

Prior to the 1970s, PTA was restricted to graphical techniques (e.g. semilog plots or type curves) which could only represent simple cases and were vulnerable to subjective judgement (Earlougher and Kersch, 1972). The use of computers to match models to well test data was inevitable. This process is a type of inverse modelling, where models are matched to data to obtain estimates of the model parameters. Earlougher and Kersch (1972) used regression techniques with more complicated models, including an anisotropic reservoir and significant wellbore storage.

If the model is a nonlinear combination of the model parameters, the inverse modelling process is called nonlinear regression (NLR). Rosa and Horne (1983) used NLR to automate type-curve matching by transforming the model (type curves) to Laplace space. Horne et al. (1983) used NLR to incorporate spinner measurements of flow rate into geothermal PTA.

Since those early studies, a number of automated well test analysis systems (software) have been developed, with a range of analytical or semianalytical models (O’Sullivan et al., 2005). Computer-aided well test analysis was widespread by the time of a survey paper by Horne (1994) on this topic, due to both the advent of personal computers and improvement in methodologies. Important advantages of NLR over graphical methods include the ability to handle more unknown parameters, ability to calculate confidence intervals for those parameters and ability to handle variable flow rates (Horne, 1994).

Throughout the 1980s and 1990s, various software packages for automated well test analysis were developed, including ANALYZE (McEdwards and Benson, 1981), AUTOMATE (Horne, 1994) and DIAGNS (McLaughlin et al., 1995). Automated well test analysis systems are usually capable of tasks such as field data handling (import and processing), automatic graphical presentation of data in a variety of common plots, and automated matching to a variety of available reservoir models, including estimated parameters and confidence intervals (Horne et al., 1980). An automated well test analysis system in widespread use in the geothermal industry is SAPHIR, developed by KAPPA Engineering (Houzé et al., 2012).

One analytical automated well test analysis system was developed within the geothermal industry, at the Iceland GeoSurvey (ISOR), called Well Tester (Juliussón et al., 2007). This is based on the analytical models summarised by Horne (1995), originally written in Matlab (though later converted to Python), with the objective of simplifying the analysis and automating the report generation (E. Juliussón, personal communication, 2018). Well Tester has a graphical user interface, aids data processing, utilises the derivative plot and automates NLR.

5.8 Limitations of analytical methods in geothermal well test analysis

Uptake of PTA by the geothermal industry has been limited for a variety of reasons. One reason noted by Ramey (1975) has been the mistaken impression that petroleum reservoir engineering analytical methods could be applied only to closed systems, and geothermal systems are known to be open systems. Another reason is the belief that the simplifying assumptions at the root of the diffusivity equation (and therefore all analytical models) are not applicable in the geothermal environment, in particular due to fracturing (Ramey, 1975). This belief has persisted for decades (O’Sullivan et al., 2005) despite some disagreement (Atkinson et al., 1978b; Grant and Bixley, 2011).

It is true that there has been some success with analytical PTA for dry steam wells at the Geysers, California (Ramey, 1970) and the Larderello and Travale-Radicondoli fields, Italy (Atkinson et al., 1978a; Barelli et al., 1975; Celati et al., 1975); however, such vapour-dominated systems are rare. In two-phase systems such as Tongonan, Philippines, the application of conventional PTA to geothermal wells was more limited due to the uncertainty of the reservoir rock and fluid properties (Menzies, 1979). It is our experience that analytical PTA models usually do not fit geothermal data due to a combination of practical issues and theoretical ones.

In terms of theoretical issues the assumptions of the diffusivity equation (Section 4.4.5) include horizontal flow, negligible gravity effects, Darcy flow, homogeneous and isotropic porous medium, a single fluid (an isothermal system), small and constant compressibility, and that fluid and reservoir parameters are independent of pressure (Earlougher, 1977). There are major deviations from these assumptions in

geothermal wells/reservoirs. Geothermal reservoirs are not isothermal and so fluid properties are not uniform throughout the reservoir (O'Sullivan et al., 2005). Those fluid properties depend nonlinearly on thermodynamic conditions (pressure, temperature, saturation, composition). They are particularly variable when boiling and condensation are occurring (O'Sullivan et al., 2005). In terms of geometry and structure, geothermal reservoirs are usually in volcanic rock where permeability is controlled by faults/fractures in a 3D network that is connected to the wellbore only at limited points (Grant and Bixley, 2011). Therefore flow can be in any direction through the network not just the horizontal direction, and the system is anything but homogeneous.

Technically the linear diffusivity equation must therefore be replaced with a non-linear form, which requires numerical models to solve (Earlougher, 1977; O'Sullivan et al., 2005). However, not all assumptions are necessary, and many fracture systems behave as if they were ideal homogeneous systems (Ramey, 1975). In addition, considerable effort was made to extend analytical PTA methods specifically to some types of geothermal reservoirs, with the relaxation of some assumptions and development of new models (Section 5.9). Despite these efforts, numerical PTA is becoming more widespread, and the transition from analytical PTA has already begun.

Aside from the issues with the theoretical applicability of analytical models to geothermal PTA, there are common and major practical issues with gathering geothermal well test data. These are discussed in Chapter 7, Downhole Tools and Other Practical Considerations, and include slow closure of the control valve, two-stage pump shut-down, thermal expansion of the wireline and expansion/contraction of the fluid column in the well due to changes in temperature.

5.9 Geothermal-specific analytical methods

Efforts were made to extend analytical methods specifically to some types of geothermal wells starting from the late 1960s (Atkinson et al., 1978a). Many issues required attention, despite some success in the application of conventional semilog straight line methods to dry steam wells. The major advances in geothermal-specific analytical PTA models are summarised in this section.

5.9.1 Parallelepiped model for vapour-dominated reservoirs

The configuration of the rare vapour-dominated (dry steam) reservoirs such as The Geysers, California, and Larderello, Italy, precludes the use of radial models and gave rise to the parallelepiped model (Economides et al., 1982). These reservoirs are bounded by faults and overlain by impermeable formation, also a constant-pressure boundary is often observed, and large natural fractures of high conductivity can be present (Cinco-Ley et al., 1979; Economides et al., 1982). This 3D configuration can

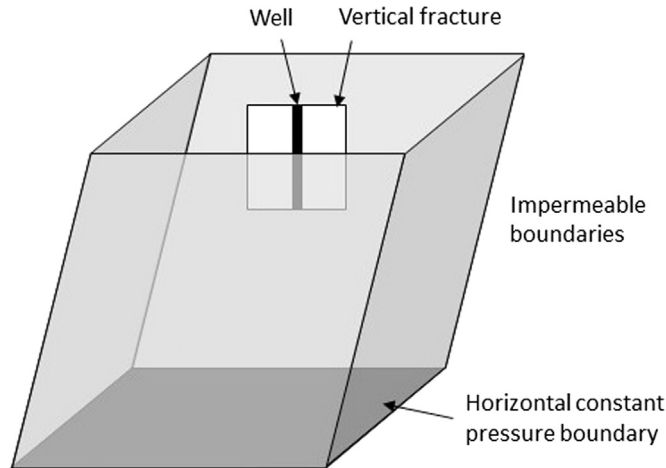


Figure 5.11 Schematic of early parallelepiped model with five planar impermeable boundaries and one constant-pressure boundary at the base. After Kruger, P., Ramey Jr., H.J., 1979. *Stimulation and reservoir engineering of geothermal resources*. In: *Second Annual Report, July 1, 1978–September 30, 1979 (SGP-TR-35), Technical Report, Stanford University Geothermal Program*.

be represented with a parallelepiped model, which is of use only for vapour-dominated reservoirs (Economides et al., 1982).

An early general form of the parallelepiped model was closed in by impermeable boundaries on five sides with a boiling surface on the bottom represented by a constant-pressure boundary, and a well intersecting a fracture represented by a rectangular source (Fig. 5.11) (Cinco-Ley et al., 1979). Type curves are generated and compared to field data in a specialised form of type-curve matching. This model was used successfully on data from Travale-Radicondoli, Italy, and The Geysers, California (Economides et al., 1982). The model was later extended to include a condensation surface at the top (Ramey et al., 1980).

5.9.2 Two-phase water/steam reservoirs

The presence of two phases (water and steam) in the reservoir is important because the mobility and compressibility of two-phase mixtures are significantly different to single-phase fluid (Cox and Bodvarsson, 1986). Hence, the pressure behaviour during well tests will not conform to simple models derived for single-phase flow. The diffusivity equation (Section 4.4.5) assumes single-phase flow and therefore research into two-phase flow requires derivation of a new diffusivity equation.

Some of the earliest two-phase flow studies in the late 1970s and early 1980s examined reservoirs that are already two-phase prior to production and derived a new diffusivity equation for two-phase flow (Grant, 1978; Garg, 1980; Moench and Atkinson, 1978). Grant (1980) applied these techniques for a two-phase well at

Kawerau Geothermal Field, New Zealand, identifying the cause of poor production as low permeability. As discussed by Grant and Sorey (1979), these methods are valid only for small changes in pressure and saturation. It was found that the slope of the semilog straight line was inversely proportional to the total kinematic mobility kh/ν . The same is true for reservoirs which start as single-phase hot water close to boiling point and evolve to become two-phase during pressure drawdown resulting from production (Garg and Pritchett, 1984). In this case a boiling front will propagate away from the wellbore and can be represented by a moving constant-pressure boundary (Garg and Pritchett, 1984).

The equation as described by Grant (1978) was later expanded by O'Sullivan and Pruess (1980) and O'Sullivan (1981) to obtain analytical solutions for constant rate drawdown and injection (O'Sullivan, 1985). It was shown that despite being based on uniform fluid properties, analytical models can give a reasonable approximation of geothermal drawdown behaviour (O'Sullivan et al., 2005). This is of limited practical use as drawdown tests in high-temperature geothermal wells are rare (Section 4.2). In addition, significant assumptions are still required: constant flow rate, line source and a uniform horizontal reservoir (O'Sullivan, 1981).

Horne et al. (1980) investigated the effect of a phase boundary at a constant radial distance from the well. This could represent boiling of a hot water reservoir during production or injection of cold water into a steam or two-phase reservoir. It was determined that an offset of the semilog straight lines and their relative slopes could be used to determine the mobility ratio. It is noted that the presence of boundaries may render the analysis impossible (Horne et al., 1980).

An important concept for two-phase flow is called "relative permeability" and addresses the fact that the permeability is not the same for different phases. For example, at high steam saturations the steam phase will flow (higher permeability) but the water phase will be immobile (no permeability). Steam and water flow will be controlled by a 'relative permeability', which is the ratio of the effective permeability of that phase to the absolute permeability measured for single-phase flow. Relative permeability curves are the relative permeabilities of steam and of water, as a function of steam saturation (or water saturation). Relative permeability curves are hard to obtain but technically can be generated from production field data (Kruger and Ramey, 1979), and this has been done for Wairakei (Horne and Ramey, 1978).

Garg and Pritchett (1984) used a numerical simulator to establish the validity of earlier analytical two-phase solutions. The study considered drawdown-build-up behaviour of initially two-phase systems and those that flash during drawdown, as well as cold water injection into two-phase reservoirs. It was found that during pressure build-up a condensation front propagates from the well outwards, eventually engulfing the two-phase zone (Garg and Pritchett, 1984). It was concluded that

drawdown/build-up data can be used to yield kinematic mobility regardless of whether the reservoir was two-phase initially or evolved to be two-phase as a result of production. Build-up data from reservoirs, which evolved to be two-phase, could also be used to obtain reservoir permeability. Considering injection of cold water, it was concluded that pressure build-ups from injection into a two-phase reservoir could be used to obtain absolute reservoir permeability. Garg and Pritchett (1984) also concluded that fall-off data is difficult to analyse in a two-phase scenario. Riney and Garg (1985a) demonstrated the build-up techniques by application to field data from Baca geothermal field, where all wells induce flashing during production.

Cox and Bodvarsson (1986) published a study with some realistic two-phase reservoir configurations, recognising that a fully two-phase reservoir is rare, and two-phase zones are usually spatially limited within the reservoir and usually located at the top. Numerical simulation was employed to assess the validity of analytical solutions. It was found that for an isolated steam zone a constant-pressure approximation is not valid, though the time of deviation from the line-source solution could be used to determine the distance to the two-phase zone (Cox and Bodvarsson, 1986). This is contrary to an earlier study by Sageev and Horne (1983) who find that the two-phase zone can be represented by a constant-pressure boundary. Cox and Bodvarsson (1986) also found that for a fully two-phase reservoir the assumptions regarding relative permeability could result in values for transmissivity and storativity that are incorrect by an order of magnitude. For a two-phase layer overlying a single-phase liquid layer, production from the liquid zone results in transients that resemble constant-pressure effects, and production from the two-phase zone is affected by the low mobility of the two-phase mixture (Cox and Bodvarsson, 1986).

A practical procedure was developed by Garg and Pritchett (1988) for analysing interference tests in reservoirs which become two-phase as a result of production, though it is noted that for an extensive two-phase zone the method will give only an approximation of reservoir transmissivity (Garg and Pritchett, 1988). This method was applied at Sumikawa Geothermal Field where it was used successfully in determining the permeability structure of the reservoir (Garg et al., 1991).

A more general diffusivity equation for radial two-phase flow is proposed by Burnell et al. (1991) and verified numerically, though this is still fundamentally based on the Theis solution and associated assumptions. Many issues still remain regarding analytical two-phase methods. While there has been some success, it is limited to particular two-phase scenarios or particular types of well testing.

5.9.3 Nonisothermal systems

Injection tests are common in geothermal wells, and there is a major problem: analytical methods assume an isothermal system, but cold water injection into a hot

geothermal reservoir is strongly nonisothermal. This is significant as it results in a large contrast in fluid viscosity, which has a major impact on fluid flow in the reservoir, and hence PTA results.

Early injection tests were analysed by simply using the hot reservoir fluid properties and ignoring the cold water, or by assuming a simple composite model with two reservoir regions of different fluid properties separated by a stationary boundary, though neither method is applicable to a real nonisothermal case (Benson and Bodvarsson, 1982). Research from the late 1970s to the early 1990s developed PTA theory to better cope with nonisothermal scenarios.

Tsang and Tsang (1978) developed a semianalytical method applicable only to the pressure build-up during injection (not the fall-off), in single-phase porous media reservoirs. The viscosity is allowed to be temperature dependent. The pressure transient thus calculated lies between the two Theis solutions calculated using cold injectate and hot reservoir fluid properties (Tsang and Tsang, 1978).

O'Sullivan and Pruess (1980) developed a semianalytical method for cold water injection into single-phase (hot water) or two-phase reservoirs, using a similarity variable. Numerical simulation is employed to verify the semianalytical results, however it is later concluded that the numerical simulator is in fact a more useful and flexible tool than the semianalytical method (O'Sullivan and Pruess, 1980).

Analytical methods were too limited to adequately represent nonisothermal scenarios, and numerical simulation was employed to this end throughout the 1980s. Benson and Bodvarsson (1982) numerically simulated nonisothermal pressure transients and then analysed them to develop methods of analysis capable of retrieving the correct reservoir properties kh and s for single-phase hot water porous media reservoirs. It was concluded that in the case of a moving thermal front the fluid properties of the cold water would control the PTA response. However, in the more common case of a well with a 'cold spot' (a region of cold water around the well from extended injection during testing, workover or drilling), the reservoir fluid properties control the response. In detail the slope of the semilog line will theoretically correspond to the cold water properties at first (Fig. 5.12), transition to the hot water properties when the pressure pulse moves beyond the cold spot into the hot reservoir, then transition back to the cold properties when the thermal front moves away from the well (Benson and Bodvarsson, 1982; Bodvarsson et al., 1984). This concept in combination with a horizontal fracture is a good match to field data from Krafla Geothermal Field, Iceland, with transmissivity of wells reported to be 1.5–2.5 Dm (Bodvarsson et al., 1984). An important concept further developed by Benson (1984) is the 'fluid skin', where cold viscous water near the well produces a PTA response with the appearance of positive skin, which can be corrected.

Garg and Pritchett (1984) investigated cold water injection into two-phase porous medium reservoirs, also using a numerical simulator to devise techniques for analysis.

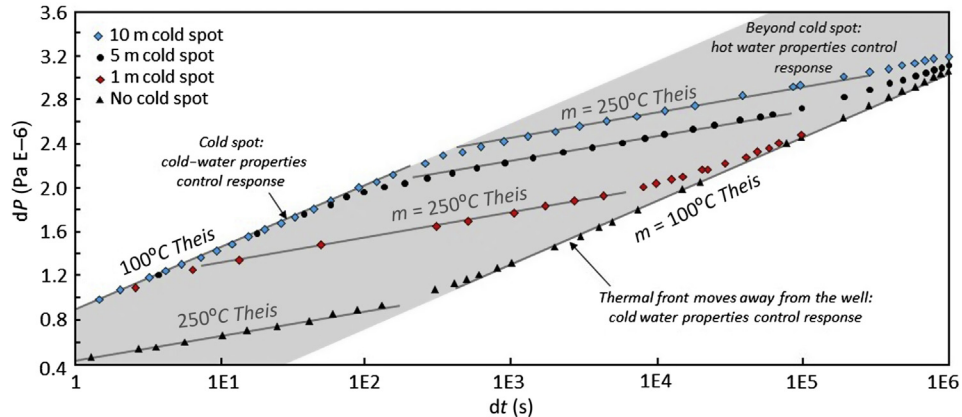


Figure 5.12 Example of semilog pressure-transient response with a cold spot around the well: injecting 100°C water into a 250°C reservoir. Data from Benson and Bodvarsson (1982). Non isothermal effects during injection and falloff tests. Technical report LBL-14270, Lawrence Berkeley Laboratory, California.

It was concluded that build-up during injection can yield the formation permeability k ; however, the fall-off data are not useful (Garg and Pritchett, 1984).

Cox and Bodvarsson (1985) investigated cold water injection into single-phase fractured reservoirs, also using numerical simulation to derive techniques for analysis. It was found that for horizontal fractures the early-time PTA data is reflective of the reservoir fluid and later is reflective of an average temperature (Cox and Bodvarsson, 1985). For vertical fractures the PTA data is always reflective of the reservoir fluid (Cox and Bodvarsson, 1985).

Garg and Pritchett (1990) derived an approximate analytical solution for cold water injection into both single-phase and two-phase porous medium reservoirs. A numerical simulator is then used to verify this solution. The assumptions include a line-source, porous medium and uniform initial temperature. It is concluded that during injection, pressure build-up behaviour is controlled by the viscosity of the cold injected fluid, regardless of whether the reservoir is single or two phase. During pressure fall-off in a single-phase reservoir the response is controlled by the viscosity of the hot reservoir fluid. However, pressure fall-off in a two-phase reservoir is too complex to be described by this analytical model (Garg and Pritchett, 1990). It was noted by the authors that the analytical solution cannot be applied to fractured reservoirs.

While there has been progress with analytical methods for nonisothermal systems, they are still of limited applicability. Recent work by Guerra and O'Sullivan (2018) showed that analytical PTA software vastly overestimated both the reservoir permeability and skin. Numerical PTA can handle the nonisothermal injection of cold water into hot reservoirs, and this is the subject of Section 8.6.

5.9.4 Adsorption in vapour-dominated reservoirs

Adsorption is the process by which ions, atoms or molecules adhere to the surface of a solid material. It differs from absorption which is when a fluid penetrates the entire volume of a material. Zarrouk (2008) showed that there can be chemical adsorption (chemisorption) which can be nonreversible and physical adsorption (physisorption) which is reversible. Water adsorbed by physisorption may exist on rock surfaces in a vapour-dominated zone, therefore adsorption effects were incorporated by Economides and Miller (1985) into the Warren and Root dual-porosity model for fractured reservoirs (Section 5.6.1). These new methods imply that adsorption has a significant effect on the interpreted extent of a vapour-dominated zone and hence reserve estimation for vapour-dominated reservoirs (Economides and Miller, 1985).

5.9.5 Geo-pressured geothermal systems

The term 'geo-pressured' refers to a zone in which formations are undercompacted and so the pore fluid bears the majority of the overburden pressure (see Section 2.3.2). The pressure of these pore fluids is usually far above the hydrostatic head of water, and the fluids are also high temperature and contain dissolved methane (Garg et al., 1978). Interest in the geo-pressured zone underlying the Gulf Coast, the United States, led to drilling and well testing starting in 1978. Garg et al. (1978) assessed whether typical PTA techniques could be applied to geo-pressured wells. A numerical model was developed capable of simulating the important relevant mechanisms of irreversible formation compaction and methane saturation. This model was used to assess the deviation from conventional analytical PTA solutions caused by these two mechanisms. It was tentatively concluded that in general the permeability (or mobility) can be obtained reliably using analytical methods despite both mechanisms. However, estimates of storativity became unreliable due to significant error in values obtained for compressibility (Garg et al., 1978).

5.10 Summary

Some of the simplifying assumptions required for analytical PTA models can be relaxed to allow for models that are more complex. Some of the general concepts from the petroleum industry are useful for geothermal reservoirs, such as reservoir boundaries, non-Darcy flow and fractured reservoirs, though the applicability of analytical PTA is still limited. Most of the geothermal-specific concepts described in this chapter are only applicable to rare geothermal reservoir types: vapour-dominated or geo-pressured systems. Numerical simulation was employed to verify analytical solutions for two-phase water/steam reservoirs and nonisothermal reservoirs; however, numerical simulation emerges as the more powerful tool for PTA in these complex systems.

CHAPTER 6

Completion and output testing

Contents

6.1	Introduction	113
6.2	Well testing during drilling	114
6.2.1	Stage testing	115
6.2.2	Static formation temperature test	116
6.2.3	Borehole imaging	119
6.3	Completion testing	121
6.3.1	Typical test design	121
6.3.2	Water loss surveys	122
6.3.3	Injectivity index	125
6.3.4	Injection pressure transient: build-up/fall-off	130
6.4	Heat-up (warm-up) surveys	130
6.5	Output (discharge) testing	133
6.6	Flow measurement methods	135
6.6.1	Vertical discharge with lip pressure	135
6.6.2	Horizontal discharge with lip pressure	136
6.6.3	Separator method	139
6.6.4	Total flow calorimeter	140
6.6.5	Tracer dilution method	142
6.6.6	Two-phase sharp edge orifice plate	144
6.6.7	Comparison between the different two-phase measurement techniques	145
6.7	Discharge prediction	145
6.7.1	Discharge stimulation	148
6.7.2	Estimated output	150
6.8	Production pressure transient: drawdown/build-up	151
6.9	Flowing down-hole surveys	152
6.10	Geothermal well abandonment	154

6.1 Introduction

In this Chapter the various stages of well testing are described, including testing during drilling, testing immediately after drilling (completion testing), testing as the well heats up once injection stops (heat-up surveys) and discharge after the well is fully heated (output testing). The term “well testing” is used in its broad sense to refer to all these activities. The particular type of well testing called pressure transient analysis (PTA) as discussed in Chapters 4 and 5 is a part of these activities, and is possible by step

changes in flow rate during completion or stage testing (injection of cold water) or output testing (production of reservoir fluid). Data gathering for any well normally starts during the drilling stage, with a host of measurements and rock samples (cuttings or core) collected. Sometimes dedicated testing is undertaken during drilling, such as stage testing, static formation temperature testing and borehole imaging. However, most quantitative data is collected once the drilling of a geothermal well is complete. At this time a host of well tests are undertaken to identify the main feed zone (loss zone) the well is going to produce from, the injectivity (water take) of the well and to measure the transmissivity of the producing formations. After this is the heat-up stage where profiles of the static temperature and pressure are measured to identify the pressure control point (PCP) which helps in identification of the major feed zone(s), and the final temperature profile of the well. After heat-up but before discharge, discharge-prediction methods are used to assess whether the well will self-discharge and to help plan intervention if required. After this several methods for output testing could be implemented to assess the productivity of the well, the selection of which will be based on availability and cost. Flowing surveys are carried out during output testing, and are useful to confirm the location of the major feed zone, and the flash point in the well.

6.2 Well testing during drilling

The drilling programme for any well will include logging of rock cuttings, which circulate to the surface with the drilling fluid, and possibly core sampling at important intervals. This information is used to update the geological model and also helps the drilling engineer in finding the permeable drilling targets, which are often a particular rock type. This information is also important when choosing good competent formations for setting casings (avoiding heaving or sloughing formations).

The drilling engineers also have an extensive measurement while drilling (MWD) programme to make sure that the well is on target, and for problem solving when needed. These parameters mainly include the drilling torque (TQ), rate of penetration (ROP), weight on bit (WOB), losses in mud circulation and many other parameters that can be used to guide the reservoir/well test engineers when planning and fine-tuning the completion/well testing programme for a given well.

Fig. 6.1 shows the ROP profile for a deep well in Tauhara Geothermal field, New Zealand. Generally, the ROP reduces with depth, as the rock is harder and more compacted under the lithostatic (overburden) pressure. However, there are depths with a sudden increase in ROP, which is an indicator of permeable/fractured formations. These depths are likely to be feed/loss zones during the completion test.

There are also dedicated well tests carried out during drilling to capture important reservoir parameters for reservoir categorisation and critical decision-making

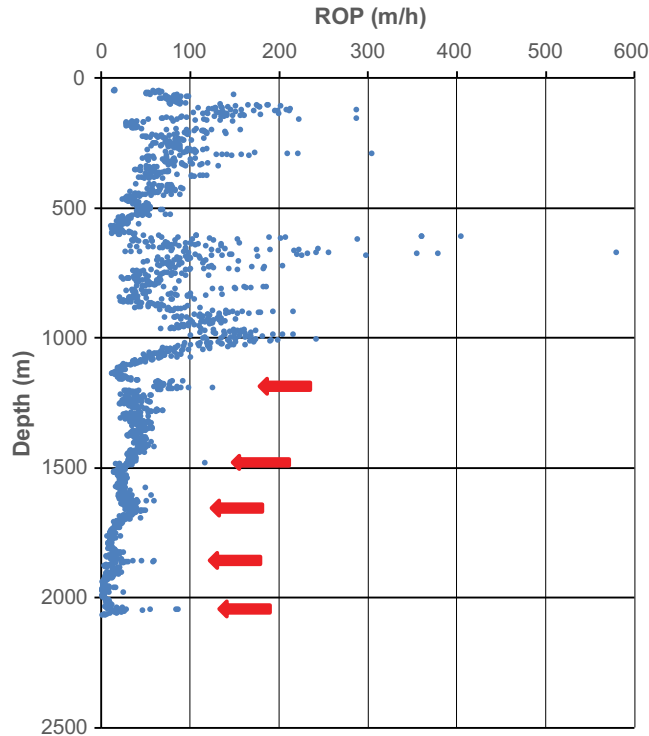


Figure 6.1 ROP of a deep well at Tauhara Geothermal field, arrows indicate sudden spikes in ROP. ROP, Rate of penetration. *From Contact Energy Ltd., with kind permission.*

while drilling. These tests and down-hole measurements require the temporary interruption/cessation of drilling operations, putting the rig on standby. These tests include stage testing to assess the injectivity index, static formation temperature testing to assess the reservoir temperature, and borehole imaging (BHI).

6.2.1 Stage testing

In some exploration programmes in new fields or in a new area/sector of an existing field, it is possible to include stage testing of the shallower parts of the reservoir before they are blocked off from the well by running/cementing the next planned casing size. Stage testing can also be carried out at different drilled depths before arriving at the final targeted depth, to evaluate the necessity of drilling deeper. This test involves measuring the injectivity of the well, which can be related to production flow rates (Grant and Bixley, 2011).

It is not common to carry out pressure-transient testing during stage testing while drilling the well, due to the high cost associated with downtime in drilling activities. There is also the risk of hole collapse since the test takes place while the

hole is open before the installation of the permanent perforated liner. For the same reason, it is not common to run a down-hole tool in the open hole, beyond the production casing shoe. The injectivity is assessed in the usual manner as for a completion test, except with the down-hole tool at the casing shoe instead of the major feed zone, from the change in pressure with change in flow rate (Section 6.2.3). The injectivity index (II) can be reported as a function of the wellhead pressure (WHP) in impermeable wells (which have positive WHP during injection), or for permeable wells (where WHP is always negative during injection) as a function of the down-hole pressure measured at the casing shoe.

6.2.2 Static formation temperature test

During the drilling in new geothermal fields, there can be conflicting results from the alteration mineralogy (geo-indicators) on whether the drilling target has high temperature or not. Since the circulating drilling fluids cool the wellbore, it takes several weeks or months for the well to heat up and reach undisturbed temperature conditions, which is too long to wait during drilling operations. This issue can be resolved by carrying out a static formation temperature test (SFTT), also known as temperature build-up test or temperature transient. Cold water is circulated for 15–20 hours, the drilling pipes are pulled up 50 m from the bottom of the hole, circulation stops, the well is allowed to heat-up, and the temperature versus time is recorded and analysed (Grant and Bixley, 2011). The SFTT is also sometimes carried out before setting the production casing (Sarmiento, 2011) to make sure that the resource has a high temperature in conventional two-phase systems. The test is not commonly used after completing the drilling of two-phase geothermal wells, but it is a standard part of enhanced geothermal systems (EGS) wells completion programme.

The temperature measurements made in a well are used to infer details about the reservoir as a whole and can substantially reduce uncertainty about the heat content, which can affect the commercial viability of a project (Sarmiento, 2011). A number of factors introduced in the drilling process affect the SFTT, including but not limited to the following (Chiang and Chang, 1979; Roux et al., 1979; Kutasov and Eppelbaum, 2005):

- The thermal properties of the drilling fluids.
- The thermal diffusivity of the reservoir.
- The difference between reservoir and drilling fluid temperatures.
- The drilling technology used.
- The amount of time drilling fluids have been circulated in a well.

Several methods have been developed over the years to analyse the temperature transient data to estimate the final formation temperature, including:

1. Horner method (Dowdle and Cobb, 1975)
2. Improved Horner method (Roux et al., 1979)

3. Brennand method (Brennand, 1984)
4. Curve-fitting method (Hyodo and Takasugi, 1995)
5. Improved Horner method (Kutasov and Eppelbaum, 2005)

All the earlier methods are based on solving the one-dimensional thermal diffusion equation in radial coordinates. When comparing these five methods using multiple field data sets, it is our recommendation that the Brennand (1984) method is the most reliable (Forsyth and Zarrouk, 2018). This is in agreement with the conclusions of Sarmiento (2011) and Horne (2016).

Brennand (1984) imposed a number of conditions when solving the diffusion equation, which is transformed into the Laplace space and linear approximation to yield the following equation:

$$T(r_w, t) = T_f - m \log\left(\frac{1}{\Delta t + pt_c}\right) \quad (6.1)$$

where T_f is the final formation temperature, t_c is the water circulation time, Δt is the time from when circulation stops (shut-in) and $p = 0.785$ is a constant empirically derived from field test data (Brennand, 1984).

Using the gradient over one log cycle (m), and the difference between circulation temperature and formation temperature ($T_f - T_c$), the thermal diffusivity (α) can be calculated using the following equations:

$$m = \lambda(T_f - T_c)n \quad (6.2)$$

$$n = \frac{c_p \rho r_w^2}{k} = \frac{r_w^2}{\alpha} \quad (6.3)$$

where $\lambda = 6.28$ is a constant empirically derived from matching field test data, T_c is circulation temperature (temperature of the returning fluids), r_w is the well radius (m), $\alpha = k/(\rho c_p)$ is the thermal diffusivity (m^2/s), k is thermal conductivity ($\text{W}/\text{m K}$) of the rock, ρ is rock density (kg/m^3) and c_p is the specific heat capacity of the rock ($\text{kJ}/\text{kg K}$).

The evaluation of T_f is made as follows:

1. Temperatures are recorded at time intervals after shut-in.
2. Plot measured temperature versus Brennand time $1/(\Delta t + pt_c)$.
3. Use a linear fit for 'all' data points.
4. The intersection of the linear fit and zero Brennand time represents the SFTT (T_f).
5. If the circulation temperature (T_c) is known, then the thermal diffusivity (α) can be calculated using Eqs (6.2) and (6.3) as a check to ensure the result is realistic.

The accuracy of the Brennand method is $\pm 5^\circ\text{C}$ and has the advantage of requiring a shorter water circulation time than the other methods, which will reduce the test and drilling rig time.

Example: For the SFTT data given by Brennand (1984) in Table 6.1. The circulation time t_c is 15 hours, $r_w = 0.108$ m and the circulation temperature $T_c = 65^\circ\text{C}$. Fig. 6.2 shows the fitting of the Brennand (1984) data and estimation of SFTT.

Using Eqs (6.2) and (6.3), the calculated thermal diffusivity of the reservoir rock $\alpha = 1.6 \times 10^{-6} \text{ m}^2/\text{s}$, which is reasonable, being within the range of $(0.4 \times 10^{-6} \text{ to } 1.6 \times 10^{-6} \text{ m}^2/\text{s})$ given by Vosteen and Schellschmidt (2003) for most rock types (magmatic, metamorphic and sedimentary) between 0°C and 300°C .

Table 6.1 Brennand (1984) SFTT data showing the calculated Brennand time.

Time (h)	Brennand time (1/s) $1/(\Delta t + p t_c)$	Temperature ($^\circ\text{C}$)
2.58	1.93×10^{-5}	93
3.58	1.81×10^{-5}	88
4.58	1.70×10^{-5}	99
5.58	1.6×10^{-5}	108
6.58	1.51×10^{-5}	112
7.58	1.43×10^{-5}	117
8.58	1.36×10^{-5}	120
9.58	1.30×10^{-5}	126
10.58	1.24×10^{-5}	133
11.48	1.19×10^{-5}	133
12.58	1.14×10^{-5}	134
13.58	1.10×10^{-5}	137
14.58	1.05×10^{-5}	141
15.58	1.02×10^{-5}	146

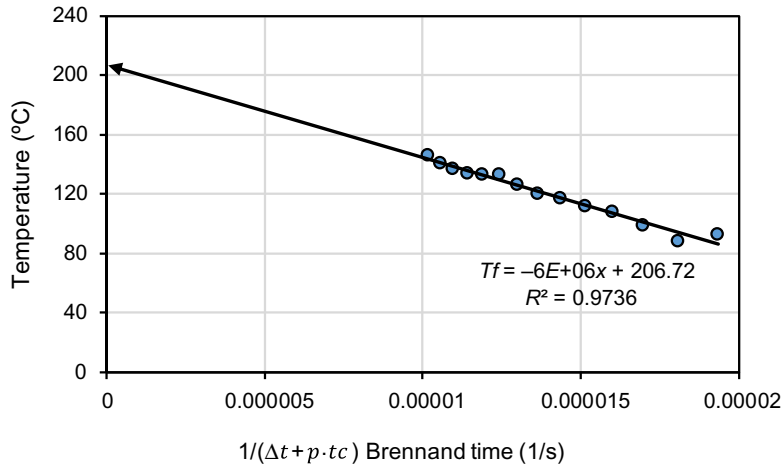


Figure 6.2 SFTT result using the Brennand method, giving a final formation temperature of 206.7°C . SFTT, Static formation temperature test.

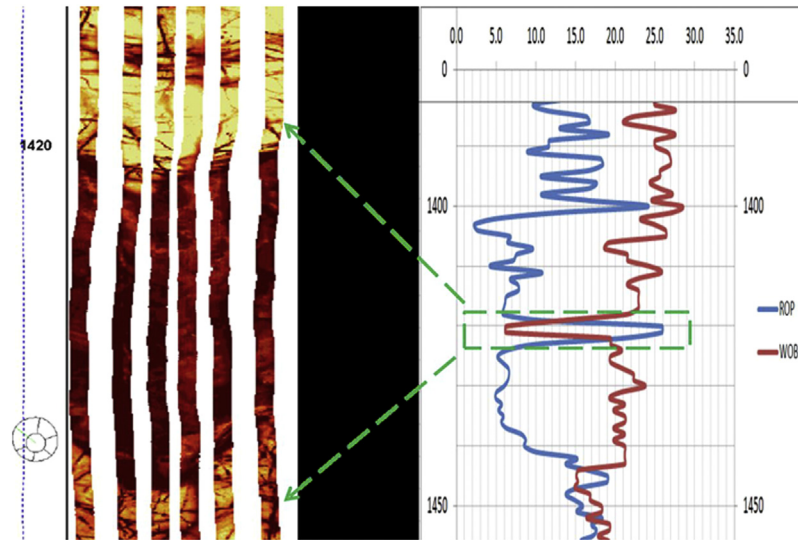


Figure 6.3 Comparison between FMI logs and drilling conditions in the production part of the well. FMI, Formation microimager. From Shanti Sugiono, Star Energy Ltd., with kind permission.

6.2.3 Borehole imaging

Borehole imaging (BHI), also called "borehole televiewer (BHTV)" logging returns an image of the cylindrical wall of the open section of the borehole, either by reflection of acoustic signals, known as acoustic formation imaging technology (AFIT), or by direct contact measurement of the resistivity of the formation, known as a formation microimager (FMI). The image of the borehole can be used to identify natural structural features and their orientation, such as fractures and faults, which are potential feed zones. Drilling-induced features, such as tensile fractures and borehole breakouts, can be used to assess the orientation of the stress field around the borehole. This technique has been used in the petroleum industry for more than 30 years and has been making some traction in the geothermal industry but is still not widely used.

Massiot et al. (2017) showed that integrating BHI data into the interpretation of completion test data increases the robustness of the feed zone interpretation (location, extent, fracture or matrix permeability components) in geothermal wells. It can identify if the well has matrix- or fracture-controlled permeability, which is valuable to know during pressure transient analysis.

Fig. 6.3 shows the BHI (FMI) of an extensive permeable fracture zone in a geothermal well, which directly correlates with an increase in the ROP in m/h and also the drop of the WOB during drilling.

Fig. 6.4 shows a small subvertical fracture captured by coring and the same fracture shown in the BHI (FMI) of the open hole.

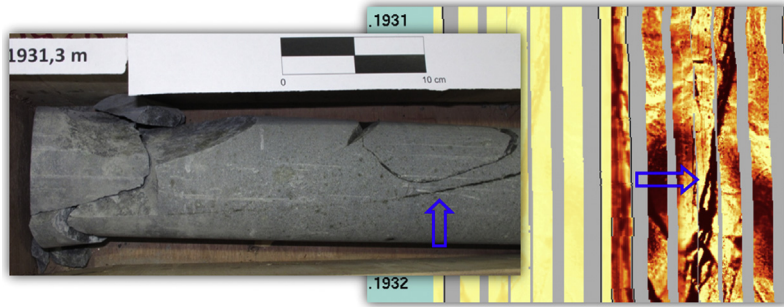


Figure 6.4 BHI of a subvertical fracture captured by core sample. *BHI*, Borehole imaging. From Shanti Sugiono, Star Energy Ltd., with kind permission.

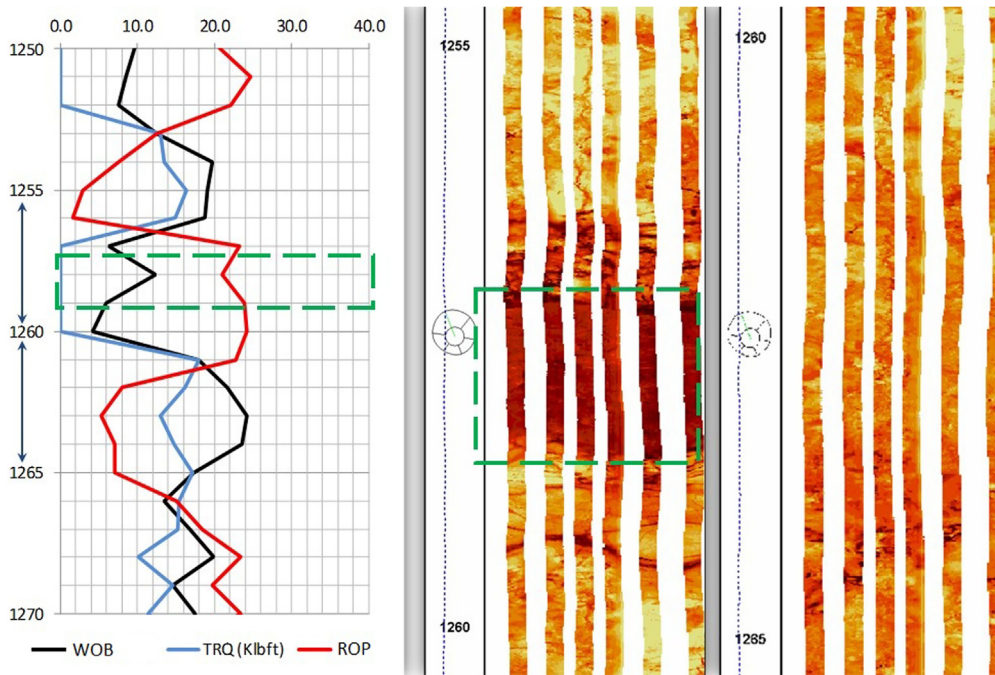


Figure 6.5 Comparison between BHI and drilling conditions in the production part of the well. *BHI*, Borehole imaging. From Shanti Sugiono, Star Energy Ltd., with kind permission.

Fig. 6.5 is another good example of changes in drilling parameters (reduction in TQ and WOB) when encountering permeable formations as demonstrated by the BHI.

The main risk associated with BHI logs is that the valuable tool must be run in the open hole before the installation of the perforated liner. The open hole could collapse and the tool and the entire well could be lost; normally drilling engineers would

prefer running the perforated liner as soon as the drilling of the production part of the well is complete to ensure the stability of the well. There is also the cost associated with the rental of the BHI tool and the drilling rig standby time, since the BHI tool is run before running (installing) the steel liner.

6.3 Completion testing

Once the drilling operations are completed by running the liner and installing the permanent master valve on the wellhead, a completion-testing programme will immediately commence. The completion testing programme includes several steps or tests that help identify the main feed zones in the well, assess the need for intervention, and estimate the future well performance from the injectivity. Predictions of productivity from the injectivity are less reliable than the results of output testing, however they are usually available several months earlier.

6.3.1 Typical test design

A typical completion test is best illustrated with a graph showing both tool depth and injection rate with time (Fig. 6.6). There are typically three injection rates, before a fall-off to either a fourth injection rate, or zero flow, followed by the first heating run. Profiles are measured at each injection rate, to yield temperature and pressure profiles, and usually multiple profiles at each rate to yield enough spinner data to allow calculation of the fluid velocity, as will be described in the following sections. The choice of injection rates, the order of these and the number/speed of the profiles measured at each rate are at the discretion of the reservoir engineer designing the test.

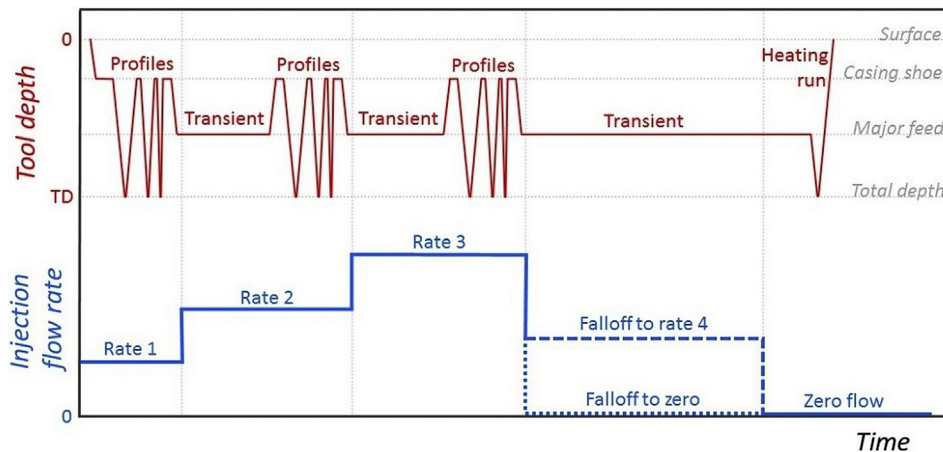


Figure 6.6 Schematic of typical completion test design: tool depth and injection flow rate versus time.

Unfortunately in reality the test design is often modified or shortened due to restricted time or other operational constraints.

If pressure-transient analysis (PTA) is a priority, and we argue that it should be a priority for all injection tests and especially the completion test, then having the tool stationary for a long time after flow changes is critical. Experience has shown that measuring profiles in the middle of a data set destined for PTA and simply returning the tool to approximately the same depth is not possible. The pressure change being measured is small and therefore sensitive to any difference in tool depth, however small, including changes in the length of the wireline which occur when it is exposed to different temperatures (Section 7.9). It is therefore recommended that for each injection rate the measurement of any pressure-transient data sets is completed first, followed by profiles (Fig. 6.6).

Ideally, the flow changes will happen and associated pressure-transient data sets will be measured with the tool located at the major feed zone. In some cases there is a clear major feed zone in the well, and this depth can be identified from the data captured during the first flow rate, allowing the tool to be positioned correctly for subsequent flow changes. In some cases the major feed zone depth is less clear and may not become apparent until more data is captured, and possibly not until the full set of heating runs reveals the pressure control point (PCP). Some wells have two strong feed zones of approximately the same permeability, complicating analysis. The positioning of the tool for the pressure-transient data set is not always certain; however, in practice it is often possible to estimate the major feed zone depth with reasonable accuracy early in the test. For impermeable wells, which remain full to the wellhead during all injection rates, the depth of the tool is not important and the pressure can even be measured at the wellhead; however, this is rare and most geothermal wells are more permeable than this.

6.3.2 Water loss surveys

The first part of the test is a water loss survey, where cold water is injected down the well commonly at three different rates (Fig. 6.6). Injection is usually via the drilling rig pumps and water supply system, while the drilling rig is demobilising from site. A pressure–temperature–spinner (PTS) tool is run up and down the well to measure various profiles during each of the three injection rates to help identify the main water loss zone(s) in the well. The main loss zone that is taking most of the injected cold water is likely to be the most permeable zone (major feed zone), where most of the hot geothermal fluid will enter the well during production. Having access to the MWD data (ROP, WOB and TQ) and possibly BHI data to consider in conjunction with the water loss survey and fluid velocity profiles will help the well test engineers to better identify the main loss zones. Final confirmation of the location of the major

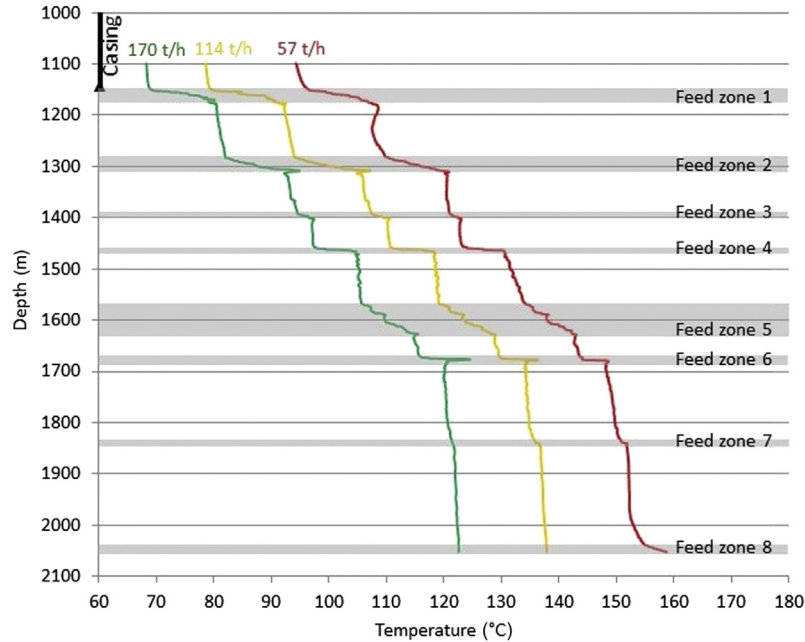


Figure 6.7 Temperature profiles of a Wairakei well during water loss surveys. *Data from Contact Energy Ltd., with kind permission.*

feed zone comes from the identification of the PCP, if present, from heat-up surveys (Section 6.3), though these are not available until many weeks after the completion test and a preliminary assessment is always required.

Fig. 6.7 shows the temperature profile of a Wairakei well for three cold water injection rates. The higher the injection rate, the lower the temperature profile during injection due to more fluid flow and more cooling. Eight loss zones are identified from sudden increases in the temperature gradient (Fig. 6.7), and it is not clear from this data alone which of the feed zones is the major one. It should be noted that the increase in injection rate and hence the injection pressure will tend suppress the lower feed zones.

Raw spinner data are profiles of the frequency at which an impeller spins as the tool travels at a given velocity up or down the well. For each flow rate, ideally a set of profiles will be measured with multiple up- and down- velocities (Fig. 6.6), which are then used to calculate a single fluid velocity profile for that injection rate. The calculation of the fluid velocity at each depth can be visualised using a ‘cross plot’ which is a plot of tool velocity versus spinner frequency (Fig. 6.8). Data are effectively extrapolated either with a linear or bilinear trend line to identify the tool velocity at which the frequency would be zero. Zero frequency means the spinner (impeller) is not turning, which only occurs when the tool is moving at the same velocity at the injected water (no relative velocity). Therefore in this circumstance the tool velocity

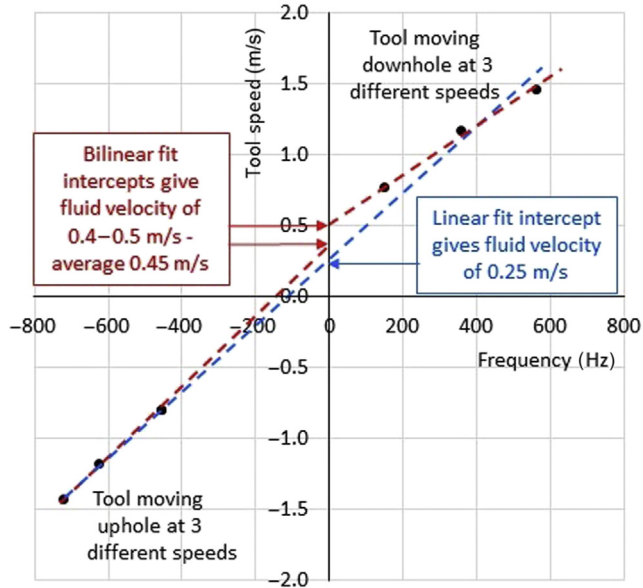


Figure 6.8 Cross plot of spinner data: tool speed versus frequency at a particular depth, showing linear and bilinear fit to data. *Data from Contact Energy Ltd., with kind permission.*

equals the fluid velocity. Each cross plot yields one data point for fluid velocity at one particular depth, and it would be impractical to process the entire data set visually in this manner. Processing can be achieved using standard functions in Excel or by using customised programmes to automate the generation of the entire fluid velocity profile.

The fluid velocity profiles for the same Wairakei well in Fig. 6.7 are given in Fig. 6.9. In theory, feed zones are identified from decreases in the fluid velocity, as fluid exits the wellbore. However, the fluid velocity is also affected by changes in borehole diameter (even in the annulus outside the perforated liner), and so there are many apparent decreases (and increases) which do not relate to feed zones. Fig. 6.9 shows data from a well with highly variable borehole diameter, and two examples are indicated of fluid velocity anomalies which do not relate to feed zones. It is possible to remove the impact of the variable borehole diameter by dividing one profile by another, by the 'spinner ratio' method (Grant et al., 2006), and for this purpose it is desirable to have at least two high quality fluid velocity profiles. The spinner ratio profile in Fig. 6.9 reveals two permeable feed zones in the well.

It would usually be expected that the fluid velocity would be zero at the base of the well, as there will be no fluid movement beyond all the permeable zones. However, in the example well in Fig. 6.9 this is not the case: there is clearly a permeable zone at the very bottom of the well, which is also apparent in the nonconvergence of the temperature profiles in Fig. 6.7.

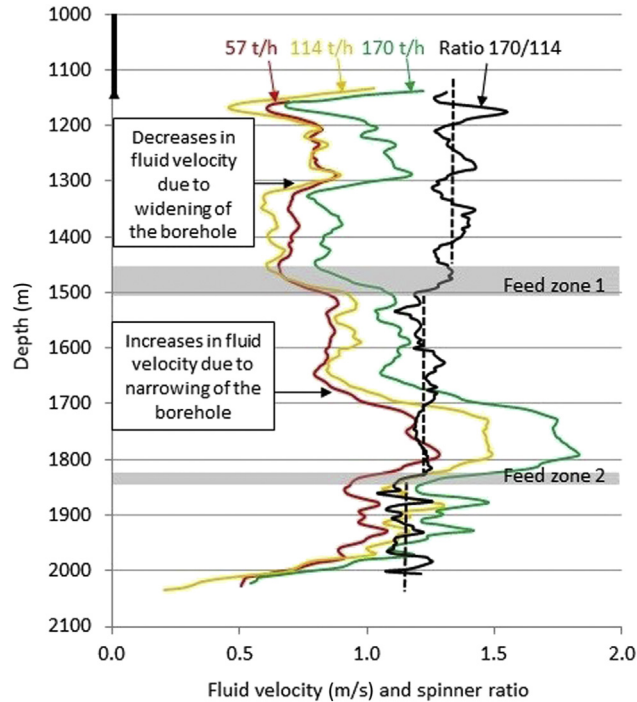


Figure 6.9 Fluid velocity profiles of a Wairakei well for three different injection rates during the water loss survey, and the ratio of two of the profiles. *Data from Contact Energy Ltd., with kind permission.*

It can be seen in [Figs 6.7 and 6.9](#) that the feed zones apparent in the injection temperature profiles are not necessarily the same as those apparent in the spinner ratio. A robust interpretation is only possible by integrating as many data types as possible, including heatup profiles ([Section 6.3](#)), drilling data ([Section 6.1](#)) and BHI ([Section 6.1.3](#)) if available. An example of an integrated feed zone interpretation is shown in [Fig. 6.10](#), incorporating data from the water loss survey, heatup and BHI.

6.3.3 Injectivity index

The injectivity index is a measure of the well fluid take at a given WHP or reservoir pressure. It is normally measured in tonne/h/bar or kg/s/kPa or kg/s/bar (Grant and Bixley, 2011).

$$\Pi = \frac{\Delta \dot{m}}{\Delta P} \quad (6.4)$$

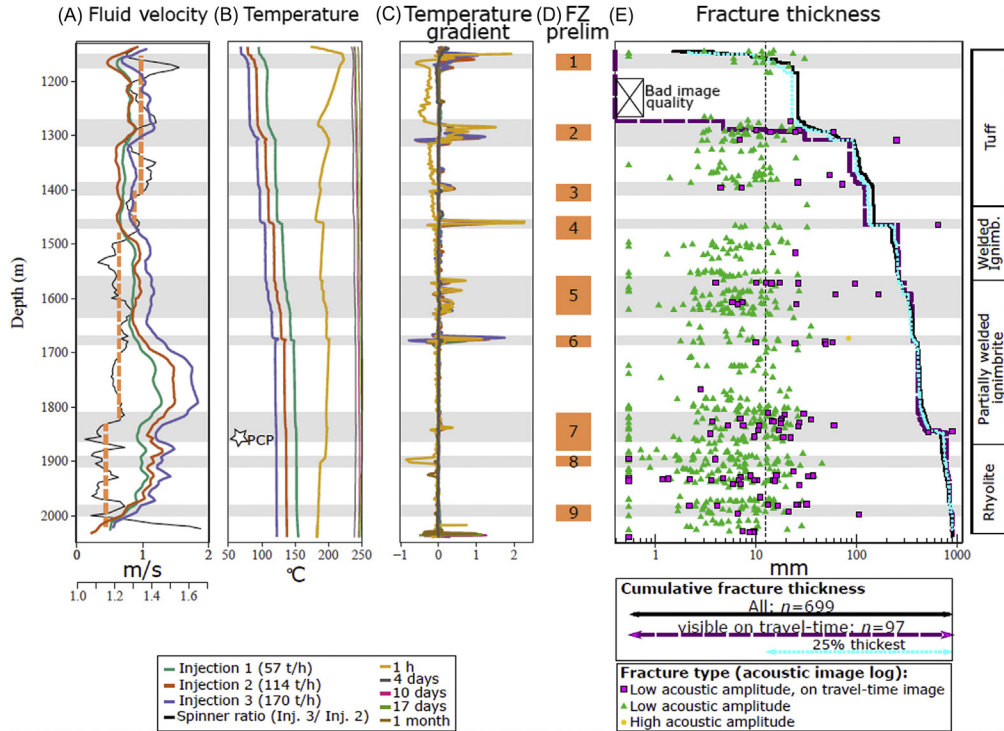


Figure 6.10 Integrated interpretation of feed zone location, for the same Wairakei well as Figs 6.7 and 6.9 including (A) fluid velocity profiles and spinner ratio; (B) temperature profiles during injection and heatup and PCP; (C) temperature gradient to highlight rapid change; (D) interpreted location of feed zones and (E) BHI fracture data. *PCP*, Pressure control point; *BHI*, borehole imaging. From Massiot, C., McLean, K., McNamara, D., Sepulveda, F., Milicich, S., 2017. Discussion between a reservoir engineer and a geologist: permeability identification from completion test data and borehole image logs integration. In: Proceedings of the 39th New Zealand Geothermal Workshop. Rotorua, New Zealand, with kind permission.

where Π is the injectivity index (tonne/h/bar), $\Delta \dot{m}$ is the change in mass flow rate (tonne/h) and ΔP is the change in pressure (bar). If the injectivity is measured using the WHP, then the well take is as follows:

$$\dot{m} = \Pi \times P_{\text{WHP}} \tag{6.5}$$

While if the reservoir pressure is used as the reference then the well take is:

$$\dot{m} = \Pi(P_{\text{Res}} - P_{\text{Well}}) \tag{6.6}$$

Table 6.2 gives a qualitative indication of the relationship between measured injectivity and two-phase well production potential.

Table 6.2 The relation between measured injectivity and the potential for fluid production for two-phase systems.

Injectivity (tonne/h/bar)	Description of production capacity
< 5	Poor producer (not useful)
10–20	Small producer
> 50	Good producer

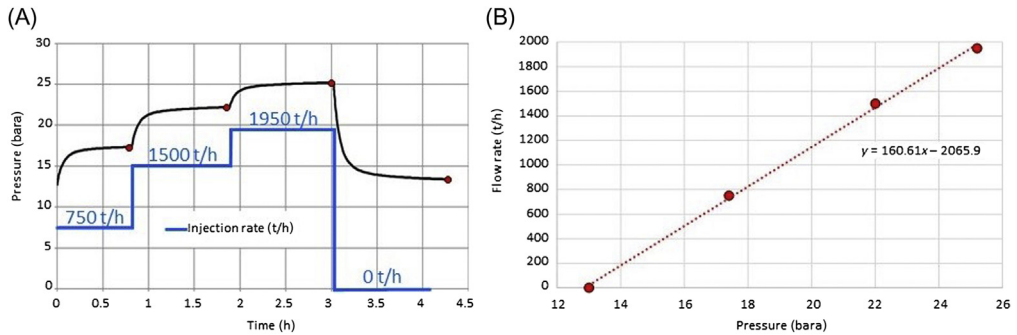


Figure 6.11 WHP response during a completion test (injection fall-off): (A) injection flow rate and pressure, showing ‘stable’ points for linear fitting [red circles (grey in print version)] and (B) linear fit through flow rate versus pressure chart of data from (A). WHP, Wellhead pressure.

Note that high injectivity does not always mean good productivity; the well also needs to have a high feed zone temperature and this might not be known at this stage of the completion testing, only becoming apparent after an extended period of heating (Section 6.3).

The fitting of the well injectivity is normally one straight line to get the average well injectivity (see Fig. 6.11 for example). Fig. 6.11 was created artificially using a simulator to show a smooth injection pressure response, which is not common in practice. It uses unrealistic injection flow rates, which are not possible to achieve in practice through a standard size production casing. The high injectivity index of 160.6 tonne/h/bar with a positive WHP at zero flow rate is also unusual. The pressure fall-off is also relatively quick to reach initial level (final reservoir pressure).

Fig. 6.12 shows an actual injection fall-off test (measured with the reservoir pressure as the reference) of a relatively low/medium injectivity well (9.3 tonne/h/bar) and a slow pressure fall-off. Note that the injectivity in Fig. 6.12 is referenced to the reservoir pressure rather than the WHP.

Many conventional wells have a pressure-dependent injectivity or what is sometimes called skin-dependent injectivity (in damaged wells), where the high positive skin controls/limits the well take. An example of pressure-dependent injectivity is a

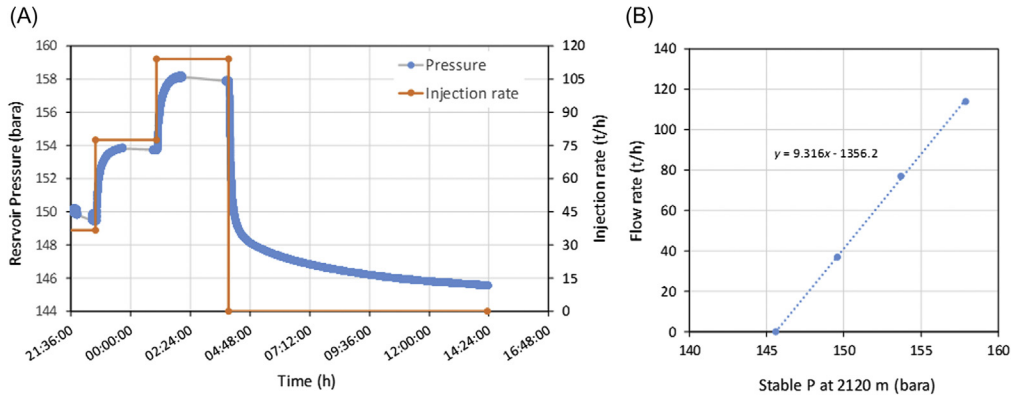


Figure 6.12 Reservoir pressure response during a completion test (injection fall-off): (A) injection flow rate and pressure and (B) linear fit through flow rate versus pressure. *Data from Contact Energy, with kind permission.*

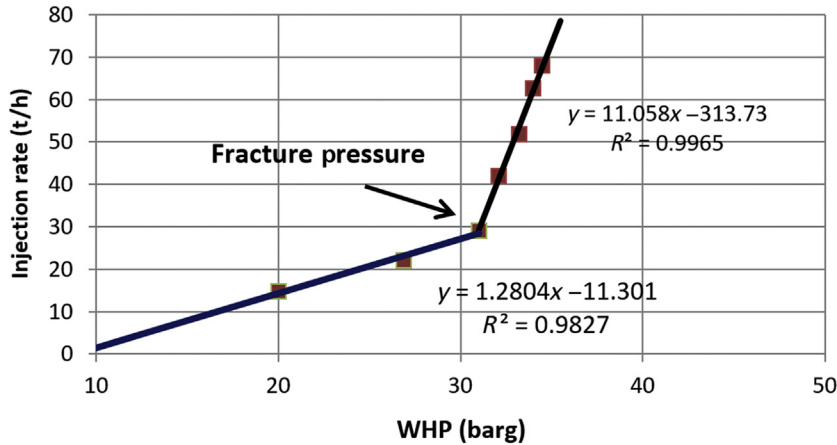


Figure 6.13 Injectivity of a hot water well showing a pressure-dependent injectivity and the fracture pressure. *Data measured by authors.*

well with an existing fracture or fracture network that opens further during high-pressure injection (Wibowo et al., 2010) or the injection of high-pressure water initiates a new fracture by exceeding the rock fracturing pressure (Fig. 6.12). This is also known as hydrofracturing or water enhancement and is used in some conventional (Aqui and Zarrouk, 2011) and EGS (Bendall et al., 2014) fields to improve the permeability of the well. It is different from hydraulic-fracturing (fracking) used in the petroleum industry and will be discussed further in Section 9.3.2.

It is our preference that the injectivity is fitted with a piece-wise linear fit (Fig. 6.13) rather than a single straight line, which will not be representative if the data points do not line up.

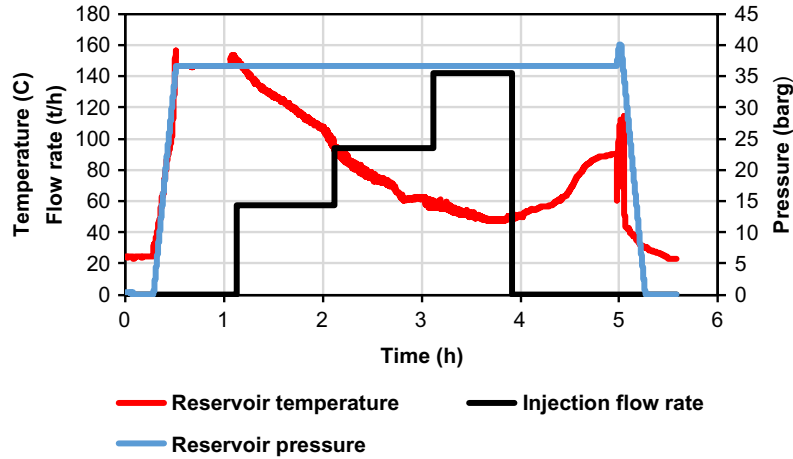


Figure 6.14 'Infinite' injectivity/permeability well. *Data provided by Mr Julian Lopez.*

It is also common to use the reservoir pressure as a reference rather than the WHP, if the reservoir is very permeable and the well cannot sustain a positive WHP during injection, which means the water level inside the well does not reach the well-head. Experience in some unique shallow and highly permeable (highly fractured) wells have shown that increasing the injection rate results in no increase in the water level in the well and so is not felt by the sensitive down-hole pressure tool, hence these wells are sometimes known as 'infinite injectivity or infinite permeability wells' (Fig. 6.14). This is because it is not possible to measure the reservoir injectivity, which will be infinity (using Eq. 6.4) when there are no changes in reservoir pressure during injection.

Fig. 6.14 shows an infinite injectivity/permeability well during injection fall-off testing in a shallow <400 m hot water system well. The down-hole reservoir pressure remains constant before and after cold water injection of up to 143 tonne/h. The down-hole transient temperature data shows the cooling effect of cold water pumped during the injection, which then heats up when the injection stops. The tool was then lowered below the test target to tag the bottom of the well (total depth) hence the slight increase in temperature and pressure before the tool was retrieved (Fig. 6.14). This well was not self-discharging and was installed with a down-hole pump, which is the only limit to productivity from such a permeable well.

The injectivity is normally estimated using cold water. However, wells that are used for hot brine reinjection will have different effective injectivity when hot water is used. Experience in many fields showed that the injectivity reduces with increase in the injection fluid temperature. This will have significant negative implications if the injectivity measured with cold water is used to design the hot brine reinjection system

(pumps etc.). For this reason, Siega et al. (2014) developed an empirical method based on field observations to correct the injectivity index for the injection fluid temperature, which is presented in Section 9.3.3. Cold fluid stimulation (thermal effects).

In very deep (e.g. EGS) wells, the friction between the injected fluid and the long well casing can result in quadratic-shaped injectivity when using the WHP. In this circumstance, it is recommended to use the reservoir pressure as the reference for the well injectivity index(II).

6.3.4 Injection pressure transient: build-up/fall-off

PTA is an extensive subject, covered in detail in Chapter 4, Introduction to Pressure-Transient Analysis, and Chapter 5, Advanced Analytical Pressure-Transient Analysis Relevant to Geothermal Wells and Chapter 8, Numerical Pressure-Transient Analysis Modelling Framework. In this section the analysis will not be discussed, only the manner in which the data collection fits into the completion test design (Section 6.2.1).

It is possible to measure pressure transients at various times throughout the completion test, whenever there is a change in flow rate. When injection rates increase, “build-ups” can be measured (not the same as a build-up after production), and when rates decrease, “fall-offs” can be measured. Ideally, both a build-up and fall-off will be measured, to yield two different types of PTA data set for comparison, and without moving the tool (as discussed in Section 6.2.1).

Unfortunately, pressure fall-offs are commonly measured as an afterthought, to zero flow, when the well is shut in and the tool is still in the well waiting for the first heatup run (often 1-hour heating). From a PTA point of view, a fall-off to zero flow should be avoided due to a range of issues that can arise when injection ceases and the temperature profile in the well changes rapidly as the well heats up. These include expansion of the fluid column (Section 7.10), expansion of the wireline (Section 7.9) and also downflows which were suppressed by injection but start again when injection stops (Section 7.8). A fall-off to a lower flow rate rather than zero flow (these two options are shown in Fig. 6.6) is strongly recommended as it avoids those issues as much as possible, by minimising the change in temperature profile of the well over the duration of the pressure transient.

6.4 Heat-up (warm-up) surveys

A typical completion test finishes with a period when injection stops and the well is allowed to heat up for some time (often 1 hour) and then the first heat-up PTS profile is measured (Fig. 6.6). The well then remains shut (no injection or production) for several weeks and a number of PTS profiles are measured at increasing time intervals. A typical set of heat-up profiles are measured at 1 hour, 1 day, 2 days, 7 days, 14 days and 28 days, though this varies due to operational constraints or if the well heats up

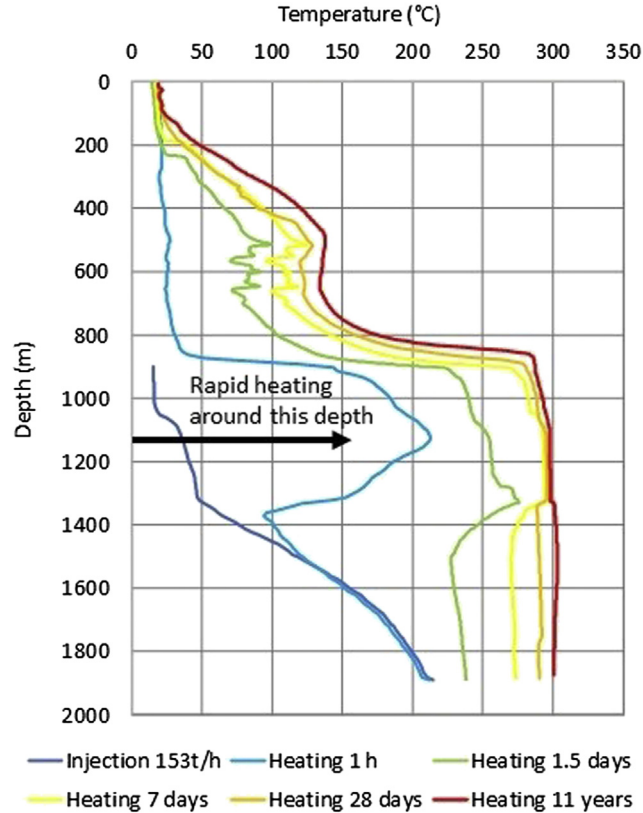


Figure 6.15 Temperature profiles of a Tauhara well during cold water injection and heat-up. Data from Contact Energy Ltd., with kind permission.

very slowly or very rapidly. These heat-up surveys help identify the main feed zone through (1) temperature profiles revealing locations of rapid heating (Fig. 6.15) and (2) pressure profiles revealing the location of the PCP (Fig. 6.16).

The PCP is a very strong indication of the major feed zone in the well. Geothermal wells typically have multiple feed zones; and the PCP will generally be near the major feed zone. However, it is not always this simple and in wells with two dominant feed zones, the PCP will lie between these feed zones. The PCP is also called the ‘pivot point’ as the set of pressure profiles appears to pivot (clockwise) at this depth as the well heats up (Fig. 6.16). This indicates a strong connection to the reservoir at this depth, which keeps the pressure constant at this depth, while it changes above and below due to changes in density of the fluid column as the temperature increases in the well.

The drawback is that the PCP does not become clear until several weeks after the completion test, and not all wells have a PCP. If the well is impermeable and has no

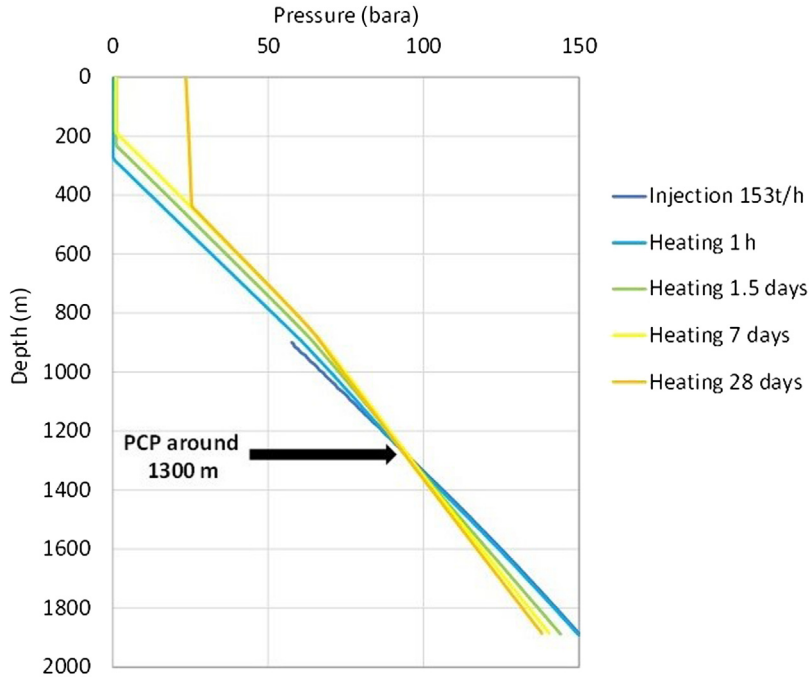


Figure 6.16 Pressure profiles of a Tauhara well during cold water injection and heatup showing a clear PCP. Data from Contact Energy Ltd., with kind permission.

strong connection to the reservoir, then there will be no PCP, and the pressure profiles will be parallel to each other. In addition, if the reservoir is not very hot, it will be difficult to observe pivoting (even if the well has a good permeable connection to the reservoir) as there will be little temperature change to alter the density of the fluid column. If the PCP shows up inside the cased part of the well and the well has high (commercial level) temperatures, it will be an indication that the well has some formation damage (+ skin).

Fig. 6.15 shows the heatup temperature profiles of a well at Tauhara Geothermal field, New Zealand. The temperature profile after 1 hour of heatup shows a major reversal below 1300 m, most of the injected water exited the wellbore above this depth and resulted in significant cooling of this upper zone with temperatures $<100^{\circ}\text{C}$. The same upper zone heated to 270°C in 1.5 days and kept on increasing. This is a clear indication of the major (permeable) feed zone of this well, expected to be the source of production. This conclusion is consistent with the location of the PCP, also located at approximately 1300 m depth (Fig. 6.16).

The Tauhara well of Figs 6.15 and 6.16 is a typical two-phase well in a medium-enthalpy system with temperatures near boiling point, anticipated to produce >20 MWe. It is important to note that not all heat-up surveys are as simple or

straightforward to analyse as in this Tauhara example. It is common to have wells with internal flow which masks the actual well behaviour (Horne, 2016), especially in reservoirs where production and drawdown in the deep reservoir initiate recharge (downflow) from shallower aquifers.

Geothermal well test analysis in general and down-hole heat-up surveys in particular are subjective. The interpretation of the surveys must consider the laws of thermodynamics, fluid mechanics and heat transfer. It is common to have more than one possible or logical interpretation of the data; this is when experience is valuable.

6.5 Output (discharge) testing

Once the well is fully heated up, it will be kept on bleed for a few days using the 1" bleed line to slowly heat up the casing before the output test (it is not advised to thermally shock the casing as this can result in casing damage).

The output test is the final and most important test carried out on the well after completion, as it will help determine the power output of the well in MWe. The test also provides the output curve of the well, which is used to estimate the well flow rate and enthalpy by knowing the WHP during the operation of the well. The measurement should be carried out from the lowest WHP (valve fully open) to the maximum discharge pressure (MDP) which is the maximum pressure that still allows the fluid to discharge to the wellhead (Fig. 6.17).

Fig. 6.17 shows that the enthalpy drops by 100 kJ/kg with the drop in mass flow rate as the well is throttled during an output test. A further loss of enthalpy of about

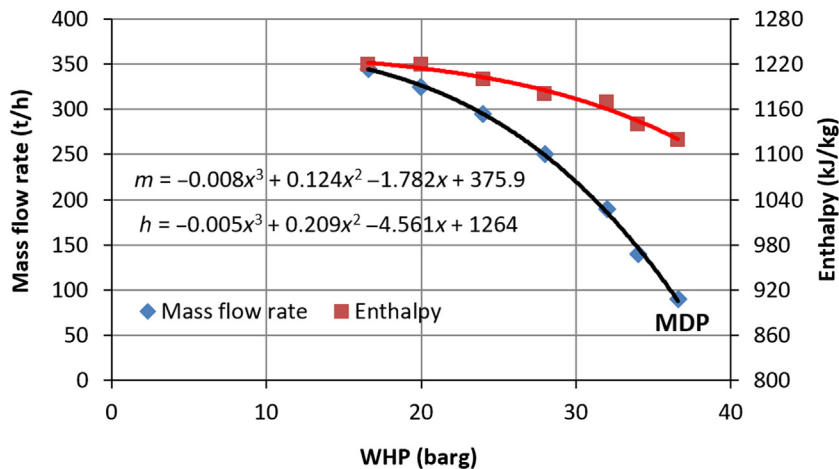


Figure 6.17 Output curve (deliverability curve) of a two-phase medium-enthalpy well. Throttling of the well increases to the right of the chart (as WHP increases). WHP, Wellhead pressure. Data from Contact Energy Ltd., with kind permission.

50–100 kJ/kg also takes place between the reservoir and the wellhead as the geothermal fluid needs to overcome the different pressure drop components (acceleration, friction and gravity) and also due to some thermal loss through the casing (Zarrouk and Moon, 2014). The output curves (mass flow rate vs WHP) of all wells will change (decline) with time and this can be modelled with the elliptical curve equation: this is presented in Section 9.2.1 Decline analysis from discharging wells. The enthalpy of the produced geothermal fluid can also change (likely to increase) with time, but this depends on the type of geothermal system. For warm and hot water systems, the enthalpy is unlikely to increase much as there is no flashing taking place in the reservoir. In two-phase systems, high enthalpy wells will experience an increase in enthalpy with time as more fluid is withdrawn from the reservoir and the pressure draws down more rapidly than low and medium-enthalpy systems due to the lower permeability. Vapour-dominated systems on the other hand can start their production life with wet steam then produce dry and later superheated steam. If the produced enthalpy of the well reduces with time, this can be related to cold water intrusion from shallow formations or reinjection returns (thermal breakthrough). Monitoring the production fluid chemistry will help identify the exact cause.

Output curves can also be generated/predicted using wellbore simulators prior to testing the well based on the well design and reservoir conditions. Wellbore simulators (e.g. WellSim) are also used to match the measured output curves to estimate reservoir (bottom-hole) conditions.

Fig. 6.17 also shows the MDP point of the well, James (1980) related the MDP with the liquid feed zone temperature using the following equation:

$$T = 99.75 \times P_{\text{MDP}}^{0.283} \quad (6.7)$$

where T is the feed zone temperature (°C) and P_{MDP} is the MDP (bara).

Example: For the data in Fig. 6.17, the MDP is 36.6 bara, using Eq. (6.7) gives a feed zone temperature of 276.3°C with a liquid enthalpy of 1217.4 kJ/kg which is very close to the measured enthalpy (well fully open) of 1220 kJ/kg in Fig. 6.17.

Eq. (6.7) can be used to estimate the feed zone temperature from output testing data when it is not possible to run a temperature tool down the well.

One of the practical challenges with output testing is the limited water storage volume for the fluid produced by the well. This should not be a problem for vertical discharge, but more of a problem in horizontal discharge testing, when the produced fluid is stored on site in the drilling pond. The various flow measurement methods are discussed in Section 6.5.

6.6 Flow measurement methods

There are several methods used for measuring well output used by the geothermal industry, which may be suitable depending on the likely size (strength) of the well, and other operational constraints. These include the measurement of the mass flow rate and enthalpy.

Note that the geothermal fluid flow is measured as mass flow rate rather than volume flow rate (e.g. m^3/s or L/min) since the volume of fluid (steam and water) expand with temperature. The mass flow rate is commonly reported in tonne/h for simplicity; however, all calculations are done in kg/s ($1 \text{ kg}/\text{s} = 3.6 \text{ tonne}/\text{h}$). The (specific) enthalpy is measured and reported in kJ/kg .

6.6.1 Vertical discharge with lip pressure

Newly drilled geothermal wells are commonly discharged vertically after completion to allow the well to clear any rock cuttings, mud and other drilling effluents. Installing a lip pressure pipe during the vertical discharge (Fig. 6.18) can also be used to measure the mass flow rate to calculate the power output of the well. The lip pressure method

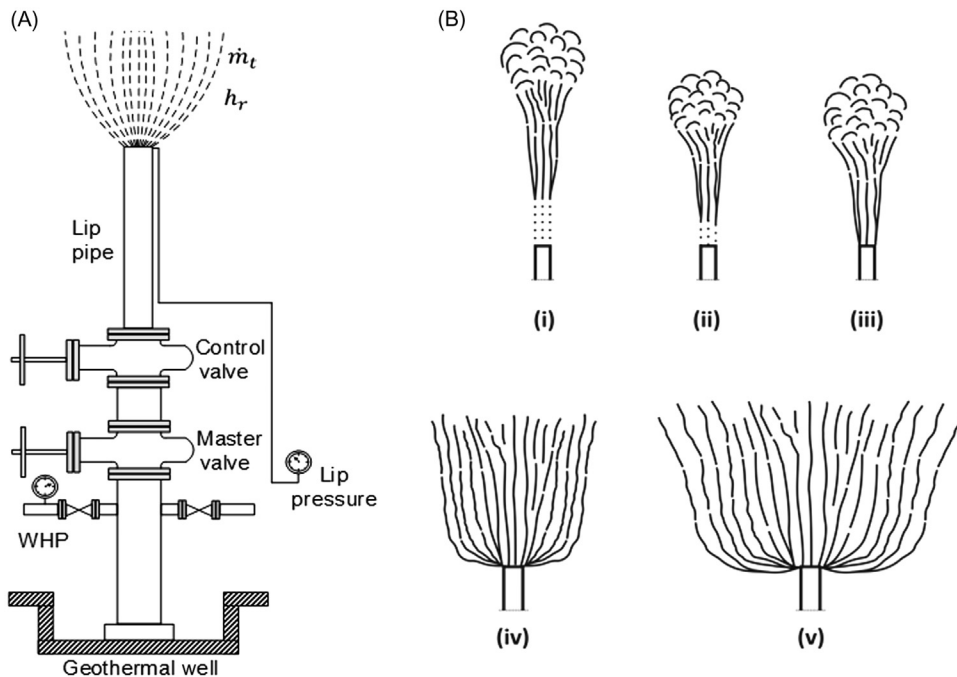


Figure 6.18 (A) Geothermal well with lip pressure pipe during vertical discharge test and (B) the shape of the discharged plume: (i) super heat steam, (ii) saturated steam, (iii) two-phase fluid with low flow rate, (iv) two-phase fluid with medium flow rate and (v) two-phase fluid with high flow rate.

was developed by James (1962), where the geothermal fluid is discharged to the atmosphere through a pipe and the pressure at the pipe-lip is measured. The empirically derived James correlation is used to calculate the two-phase mass flow rate (Eq. 6.8). This method is useful for well production testing, with good accuracy over a short period.

$$\dot{m}_t = \frac{184 \times A \times P_{\text{lip}}^{0.96}}{h^{1.102}} \quad (6.8)$$

where \dot{m}_t is the total mass flow rate (kg/s); P_{lip} is a lip pressure (bara); A is the cross-sectional area of lip pressure pipe (cm²) and h is the enthalpy (kJ/kg) of liquid at the feed zone temperature, known from the heated-up down-hole temperature profile of the well.

It is important to note that vertical discharge is only suitable for measuring geothermal wells with liquid feeds. However, experience has shown that most wells have higher enthalpy than that of saturated fluid at the feed zone temperature (Mubarok and Zarrouk, 2017), so some level of excess enthalpy is present in most two-phase wells.

Another important point to note is that Eq. (6.8) is not very sensitive to changes to the enthalpy, which is good since the enthalpy is estimated.

The major limitation of the vertical discharge method is the very high level of noise as the fluid is discharged to the atmosphere, which can be around 140–160 dB. In addition, the vertically discharged fluids spray the ground around the well with geothermal fluid rich in silica and heavy metals. For this reason, the vertical discharge method is limited in populated areas and may be subject to local environmental regulations. The major benefits of the vertical discharge method are reliability and low cost.

The shape of the fluid plume as it emerges from the lip pressure pipe visually indicates if the well is high or low enthalpy (Fig. 6.18B). Wells discharging dry steam will have a transparent zone as the steam leaves the lip pressure pipe (Armstead, 1978). High enthalpy wells will have a lower mass flow rate and a more conical shape, while lower enthalpy wells with higher mass flow rates will have a much wider base.

6.6.2 Horizontal discharge with lip pressure

In this method the geothermal two-phase fluid is discharged into a silencer (atmospheric flash vessel) through a horizontal lip pressure pipe where the water flow rate is measured using a weir box at the back of the silencer (Fig. 6.19).

The discharge enthalpy and mass flow rate for the horizontal lip pressure method can be calculated using Eqs (6.9)–(6.11) (Grant and Bixley, 2011; Mubarok et al., 2015).

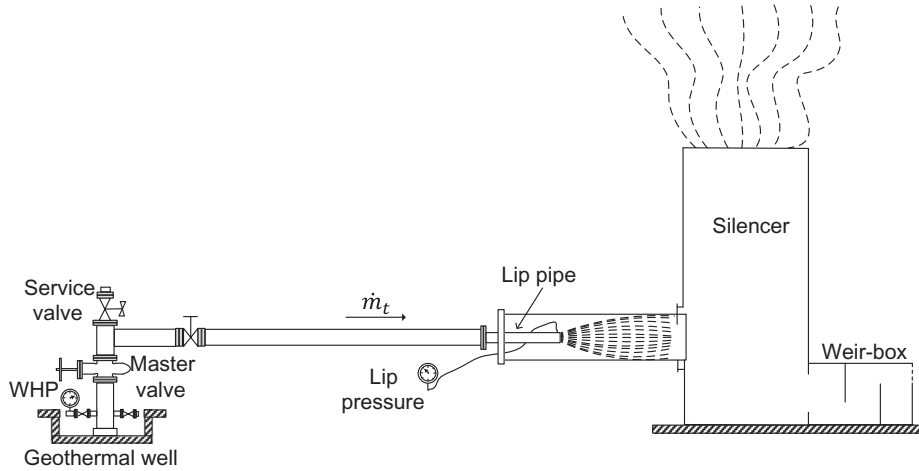


Figure 6.19 Output testing using a horizontal discharge into a silencer. Modified from Mubarok, M. H., Zarrouk S.J., Cater, J.E., 2019. Two-phase flow measurement of geothermal fluid using orifice plate: field testing and CFD validation. *Renew. Energy* 134, 927–946.

$$\dot{m}_t = \frac{\dot{m}_{w(\text{atm})} h_{fg(\text{atm})}}{h_{g(\text{atm})} - h} \quad (6.9)$$

where $\dot{m}_{w(\text{atm})}$ is the liquid mass flow rate (kg/s) at atmospheric pressure through a weir box (Fig. 6.19); $h_{g(\text{atm})}$ is the steam enthalpy at atmospheric pressure (kJ/kg); and $h_{fg(\text{atm})}$ is the latent heat at atmospheric pressure (kJ/kg).

The enthalpy h (kJ/kg) can be calculated using the following equation after Grant and Bixley (2011):

$$h = \frac{h_{g(\text{atm})} + 3329Y}{1 + 28.3Y} \quad (6.10)$$

where

$$Y = \frac{\dot{m}_{w(\text{atm})}}{A \times p_{\text{lip}}^{0.96}} \quad (6.11)$$

where P_{lip} is the lip pressure (bara), A is the lip pressure pipe cross-sectional area (cm^2) and $\dot{m}_{w(\text{atm})}$ is the mass flow rate (kg/s) in the weir box at atmospheric pressure (1 bara).

Eq. (6.10) is limited to an enthalpy range between 800 and 2200 kJ/kg (Grant and Bixley, 2011).

The horizontal discharge is more accurate for the measured mass flow rate than vertical discharge, as it measures the actual enthalpy of the well and can be used to



Figure 6.20 Horizontal atmospheric discharge of a direct use well without a lip pressure pipe (Rotorua, New Zealand). *Picture by authors.*

measure wells with two-phase feed zones (not only liquid feeds). However, the method is more expensive when compared to vertical discharge due to the additional equipment requirements and setup time.

Some geothermal field operators carry out horizontal discharge testing into the silencer without the use of a lip pressure pipe. In this case, the enthalpy is estimated based on the feed zone temperature, similar to vertical discharge testing. In this case, only Eq. (6.9) will be required to calculate the mass flow rate, and the result generally matches vertical discharge testing. However, the added cost for having a lip pressure pipe is relatively small compared with the cost of mobilising and installing a silencer. It will allow the measurement of enthalpy during the output test, which is important. Therefore horizontal discharge testing without a lip pressure pipe is not recommended.

Some low-enthalpy direct use wells producing from lateral outflows are discharged horizontally without a lip pressure pipe or a silencer (Fig. 6.20). This serves to clear the well of any build-up of silt or debris around the feed zone. It also gives the well operators a qualitative visual estimation of changes in the well output; however, it cannot quantify the output.

The main health and safety consideration during atmospheric discharge of geothermal fluids is noncondensable gas (NCG) (CO_2 and H_2S) poisoning. Normally the gas discharges in higher concentration at the start (as it accumulates in the well casing on top of the water level) and later declines depending on the NCG content in the geothermal fluid. Gases can build-up/settle in localised depressions (e.g. well cellar). Large fans could be used to disperse the gas when there is no wind and gas detectors with alarms should be carried by all personnel. Some of the symptoms of gas poisoning are headache, dizziness, nausea, eye and throat irritation, fatigue and breathing problems. Exposure to high gas concentrations may cause unconsciousness or death.

6.6.3 Separator method

The two-phase geothermal fluid is separated into steam and liquid brine in a separator vessel at a pressure higher than atmospheric pressure.

The efficiency of separation can be as high as 99.99% (Zarrouk and Purnanto, 2015). The separated steam flow can be measured using an orifice plate, while the separated liquid flow is commonly measured using a silencer with a weir box and more recently ultrasonic meters are used to measure the liquid flow rate.

Note that using a simple orifice plate for the liquid phase can induce flashing of the saturated brine leading to water hammering problems (Watson, 2013). Therefore the separated liquid is commonly measured using a silencer with a weir box (Fig. 6.21).

When the flow of separated steam and liquid has been measured, the two-phase flow rate and total enthalpy of the well can be calculated using Eqs (6.12)–(6.14).

$$\dot{m} = \dot{m}_w + \dot{m}_s \quad (6.12)$$

where \dot{m}_w is the mass flow rate of water (brine) (kg/s) and \dot{m}_s is the steam flow rate (kg/s). The dryness (x) and total enthalpy (h) of the fluid are given in the following equations:

$$x = \frac{\dot{m}_s}{\dot{m}} \quad (6.13)$$

$$h = h_f + xh_{fg} \quad (6.14)$$

where h_f is the liquid enthalpy (kJ/kg) and h_{fg} is the latent enthalpy (kJ/kg) at the separator pressure.

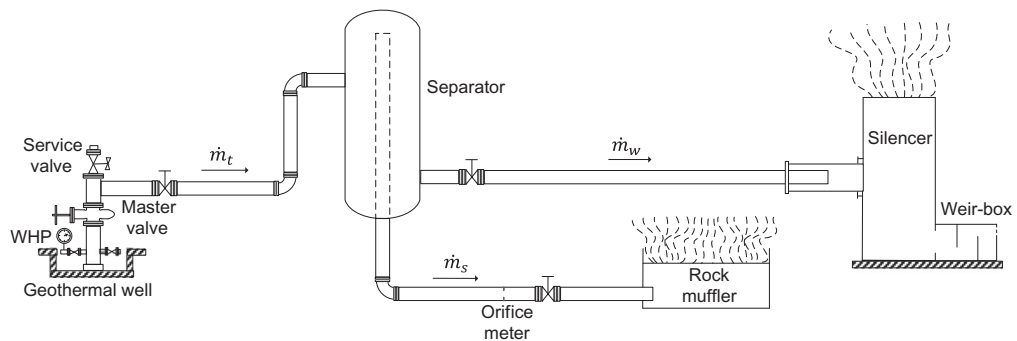


Figure 6.21 The separator method for measuring well output. Modified from Mubarak, M.H., Zarrouk S.J., Cater, J.E., 2019. Two-phase flow measurement of geothermal fluid using orifice plate: field testing and CFD validation. *Renew. Energy* 134, 927–946.

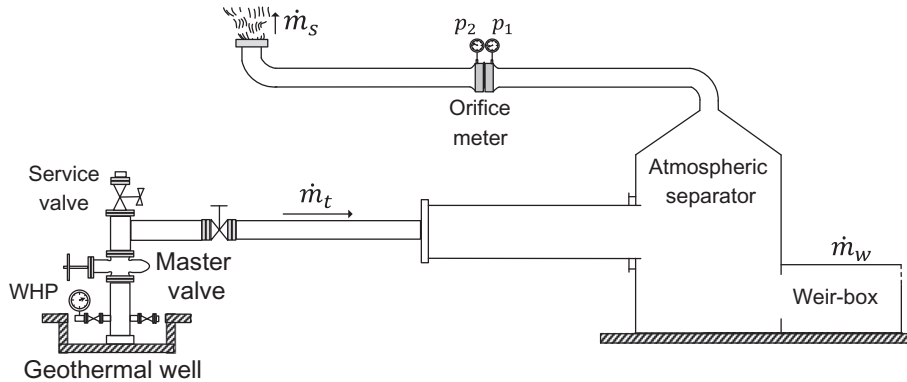


Figure 6.22 Horizontal discharge into an atmospheric separator. Modified after Khasani, I.R., Itoi, R., Zarrouk, S.J., 2015. The utilization of transient output measurement to characterize geothermal reservoir properties using AWTAS for well 2H-21 at Hatchobaru geothermal field, Japan. In: *Proceeding of the World Geothermal Congress. Melbourne, Australia.*

The separator method is the most accurate method for measuring both mass flow rate and enthalpy (Helbig and Zarrouk, 2012; Mubarok et al., 2019). However, the associated cost is high due to capital costs including separator, silencer and rock muffler, as well as transportation and installation costs.

In some Japanese fields (e.g. Hatchobaru) and the geothermal fields in Iceland, the common practice is to use an atmospheric separator (Fig. 6.22), which is a modified silencer without a lip pressure pipe, but having the steam flow leaving the silencer measured using a single-phase sharp edge orifice plate (Khasani et al., 2015). This will allow accurate measurement of the total mass flow rate and enthalpy from each well using Eqs (6.12)–(6.14).

6.6.4 Total flow calorimeter

The total flow calorimeter is a simple and practical method to measure mass flow rate and flowing enthalpy from geothermal wells (Bixley et al., 1998). Geothermal fluid is discharged into a tank (at atmospheric pressure) about half full of cold water of known volume and temperature (Fig. 6.23). The concept of this method is to measure the initial and final conditions for volume and temperature of the fluid inside the tank and convert these to a mass flow rate and flowing enthalpy. The mass flow rate and enthalpy are given by the following equations (Grant and Bixley, 2011):

$$\dot{m}_t = \frac{(\rho_{w2}V_2) - (\rho_{w1}V_1)}{\Delta t} \quad (6.15)$$

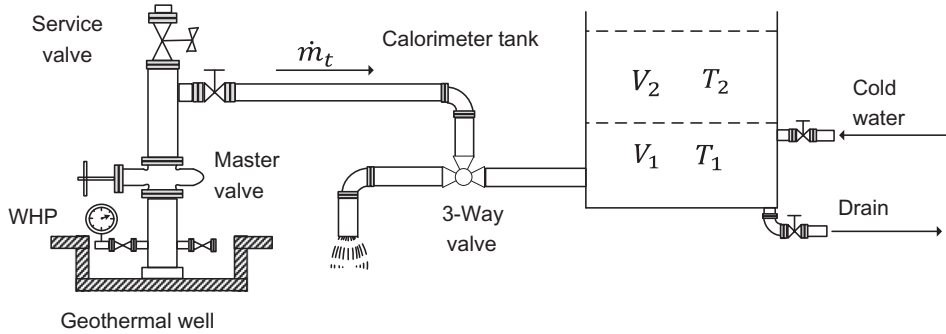


Figure 6.23 Schematic of output testing using a calorimeter. *Modified from Mubarok, M.H., Zarrouk S.J., Cater, J.E., 2019. Two-phase flow measurement of geothermal fluid using orifice plate: field testing and CFD validation. Renew. Energy 134, 927–946.*

$$h = \frac{Q}{\dot{m}_t} = \frac{(\rho_{w2} V_2 h_{w2}) - (\rho_{w1} V_1 h_{w1})}{\dot{m}_t} \quad (6.16)$$

where \dot{m}_t is the total mass flow rate (kg/s), ρ_{w1} is the density of the cold fresh water (kg/m³), V_1 is the volume (m³) of the cold water, ρ_{w2} is the density of the water–geothermal fluid mixture (kg/m³), V_2 is the volume of cold water–geothermal fluid mixture (m³), Δt is the time (in seconds) taken for the water volume in the tank to increase from V_1 to V_2 , Q is the well thermal power output (kW_{th}), h_{w1} is the specific enthalpy of the cold water (kJ/kg) at T_1 (°C), h_{w2} is the specific enthalpy of the mixture (kJ/kg) (at T_2 (°C)) and h is the measured flowing enthalpy of the well (kJ/kg).

Bixley et al. (1998) showed that the calorimeter is only practical for geothermal wells with a limited output of approximately 25 kg/s (90 tonne/h) because of the limited tank capacity. This flow rate is small for commercial electrical power production wells. In theory it is possible to increase the tank capacity in order to accommodate a larger mass flow rate; however, the tank size and increased cold water needed would make it difficult to transport the calorimeter to remote well test sites. Therefore this method is only suitable for geothermal wells with low flow rates. Calorimeters are normally used for testing small size investigation wells (slim holes) and direct use wells.

Some of the challenges include the loss of steam and water from the top of the tank, heat loss through the tank walls and the restriction in the surface pipeline connecting the well to the calorimeter, which can mask the actual well production capacity. This is a common problem that results in a quadratic-shaped well output and an enthalpy that increases with the increase in WHP (Fig. 6.24), which is unrealistic.

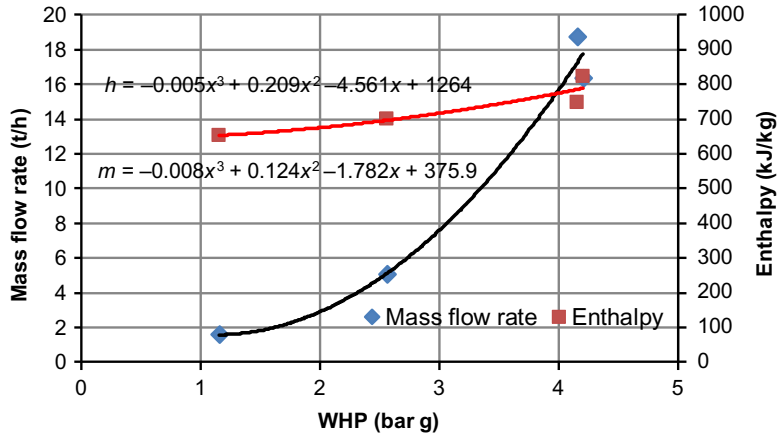


Figure 6.24 Output test of well RR778 (154 mm diameter production casing), Rotorua, through a 76 mm diameter pipeline into a calorimeter. Data from Killip, M., 1984. Report on the output test for bore 778. In: Ministry of Energy—Rotorua Geothermal Task Force, Tests 5&6 (Killip, 1984).

6.6.5 Tracer dilution method

Also known as tracer flow testing (TFT), the tracer dilution method is a chemical method where the mass flow rate and total enthalpy are calculated by injecting chemical tracers of known concentration into the two-phase pipeline (Lovelock, 2001). Steam and water samples are collected downstream then sent to the lab for analysis.

A host of chemical tracers are used in the geothermal industry. Different tracers are used for liquid and steam phases. The tracers for measuring the liquid phase include potassium fluoride (KF), sodium bromide (NaBr), fluorescein dye, sodium benzoate, rhodamine WT dye, 1,5-naphthalene disulphonate and 2,7-naphthalene disulphonate (Hirtz et al., 2001). Tracers used for the vapour phase include propane, sulphur hexafluoride (SF_6), freon-12, helium and isopropanol (Hirtz et al., 2001).

The equipment for this method consists of two parts: an injection pump setup (Fig. 6.25A) and sampling setup (Fig. 6.25B). The chemical tracers, in a tracer feed bottle, are injected at a known rate into the upstream side of a two-phase pipeline using a positive-displacement dosing pump. Then samples of the liquid and steam phases are collected at a downstream sampling point, ideally one at the top of the pipe for the steam sample and one at a 45° angle from the bottom for the liquid sample. The location of the downstream sampling point has to be far enough ($100 \times$ pipe diameter) away from the injection point to ensure that the tracers are completely mixed with the geothermal fluid.

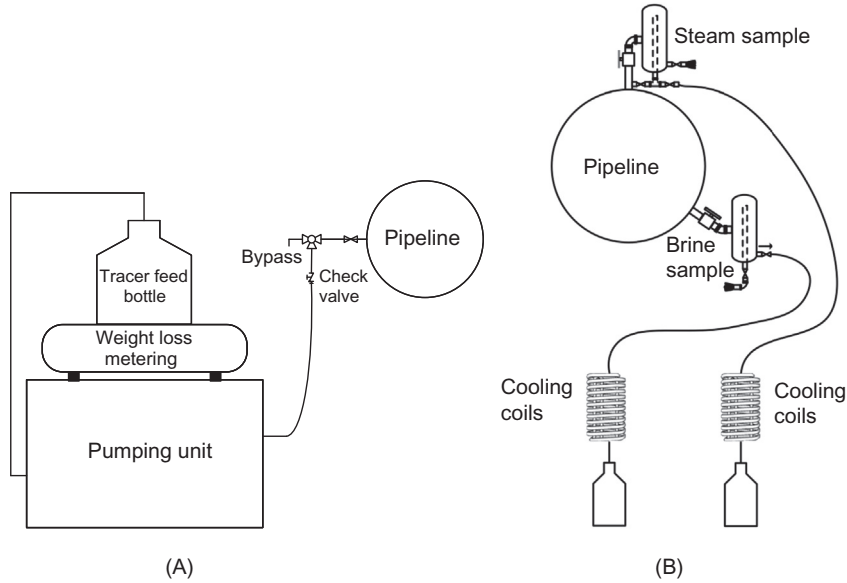


Figure 6.25 (A) Tracer injection setup and (B) downstream brine and steam sampling setup. Modified from Mubarok, M.H., Zarrouk S.J., Cater, J.E., 2019. Two-phase flow measurement of geothermal fluid using orifice plate: field testing and CFD validation. *Renew. Energy* 134, 927–946.

When lab results are available, the steam and liquid flow rate can be calculated using the following equations (Grant and Bixley, 2011; Lovelock, 2001):

$$\dot{m}_w = \frac{\dot{m}_{wt}}{\dot{C}_{wt}} \quad (6.17)$$

$$\dot{m}_s = \frac{\dot{m}_{st}}{\dot{C}_{st}}. \quad (6.18)$$

where \dot{m}_{wt} is the water tracer injection flow rate (mg/kg); \dot{C}_{wt} is the tracer concentration in water minus background concentration (mg/kg); \dot{m}_{st} is the steam tracer injection flow rate (kg/s); and \dot{C}_{st} is the tracer concentration in steam minus background concentration (mg/kg). The steam mass flow (\dot{m}_s) in Eq. (6.17) has to be corrected for the amount of steam tracer dissolved in the water (Lovelock, 2001) using the following equation:

$$\dot{m}_s = \frac{(\dot{m}_{st}C_s) - (\dot{m}_wC_w)}{C_s} \quad (6.19)$$

where C_w and C_s are the alcohol (steam tracer) concentrations in the liquid and steam (mg/kg). The steam (\dot{m}_s) and liquid (\dot{m}_w) mass flow rate (kg/s) are calculated at the

pipeline pressure. The total enthalpy (h) can be calculated from measured \dot{m}_s and \dot{m}_w values at the pipeline pressure using the following equation:

$$h = \frac{\dot{m}_s h_g + \dot{m}_w h_f}{\dot{m}_s + \dot{m}_w} \quad (6.20)$$

The results from the TFT method will not be available until a few days after the test, when the results of analysis of the tracer samples return from the laboratory. Helbig and Zarrouk (2012) showed that the TFT method is the least accurate method of output testing and requires relatively high ongoing running cost.

A study by Broaddus et al. (2010) shows that the TFT method can be used for online flow rate and enthalpy measurement using automated analysis. The challenge of this method is that it is difficult to find appropriate instrumentation for chemical tracer analysis with the required sensitivity and accuracy due to the limitations of current sensor technology.

The total flow calorimeter and lip pressure pipe methods both require the geothermal well to be taken out of production during testing. The separator and TFT methods have the benefit that they can be used while the well is online (in production); however, the separator method requires significant capital cost for infrastructure, and TFT does not provide real-time results. Real-time mass flow rate and enthalpy measurement during production is very desirable in order to minimise prediction error, loss of generation and ongoing measurement expenses.

6.6.6 Two-phase sharp edge orifice plate

This method is a simple modification of the single-phase orifice plate method, to allow the measurement of two-phase mass flow rate. The single-phase orifice plate method is widely used by the geothermal industry for measuring steam from dry wells or main headers, or water/brine.

The two-phase orifice plate (Fig. 6.26) has been reported in use in many fields around the world (Helbig and Zarrouk, 2012). Helbig and Zarrouk (2012) and Mubarak et al. (2019) tested a host of correlations for the use of the orifice plate in two-phase flow measurement. Mubarak et al. (2019) gave a simple and accurate correlation for the measurement of two-phase mass flow rate (Eq. 6.21).

$$\dot{m}_t = 970,000 \times h^{-1.72} \times \left[\left(\frac{p_1}{p_2} \right)^{D\sqrt{\Delta p/D}} \right] \times \left[\frac{(\pi d^2/4) \sqrt{2\Delta p}}{(\sqrt{1-\beta^4})} \right] \quad (6.21)$$

where p_1 is the pressure of the orifice plate (bar), p_2 is the pressure downstream of the orifice plate (bar), D is the inside pipe diameter (m), d is the orifice diameter (m)

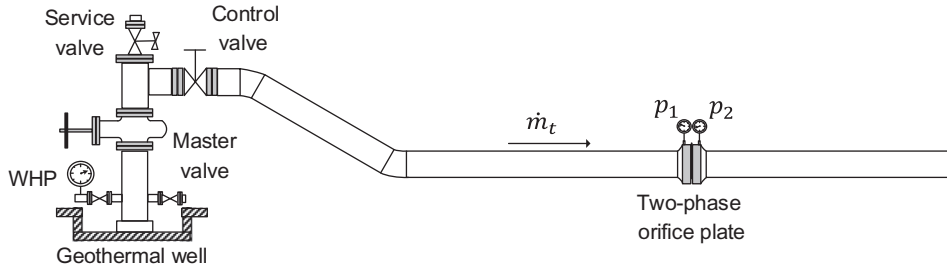


Figure 6.26 Measuring two-phase flow using the sharp edge orifice plate. Modified from Mubarak, M. H., Zarrouk S.J., Cater, J.E., 2019. Two-phase flow measurement of geothermal fluid using orifice plate: field testing and CFD validation. *Renew. Energy* 134, 927–946.

($\beta = d/D$), h is the enthalpy of the two-phase fluid (kJ/kg) and $\Delta p = (p_1 - p_2)$ (Fig. 6.26).

Eq. (6.21) requires an estimate of the enthalpy, which is considered constant. Alternatively the output curve of the well (e.g. Fig. 6.17) is used to estimate the enthalpy as a function of WHP, which will make Eq. (6.21) a function of WHP. However, this is not very accurate as the output curve of the well changes with time due to reservoir pressure drawdown. This will require remeasuring the well output using one of the methods discussed above, which may include taking the well out of production and the associated costs.

There is ongoing work to modify and improve the operation of the two-phase orifice plate method to measure enthalpy as well as mass flow rate.

6.6.7 Comparison between the different two-phase measurement techniques

Helbig and Zarrouk (2012) provided a comparison between the accuracy of some of the different two-phase measurement techniques (Table 6.3).

Several other two-phase measurement methods have been investigated using laboratory and field-testing techniques by many authors (Mubarak et al., 2019). However, none of these methods has made it to commercial or industrial use. This is due to unknown accuracy, lack of measurement repeatability, complicated setups and high costs (Mubarak et al., 2019).

6.7 Discharge prediction

As discussed earlier in Chapter 2, Geothermal Systems, conventional wells drilled in warm and hot water systems are unlikely to self-discharge unless the reservoir pressure is higher than the hydrostatic head of water. Most two-phase and dry steam wells are self-discharging; however, some geothermal two-phase wells can be left open, and

Table 6.3 Accuracy of different measurement techniques.

Method	Good (careful) test control	Average (normal) test control
Separator	$h \pm 10$ kJ/kg $\dot{m} \pm 2\%$	$h \pm 30$ kJ/kg $\dot{m} \pm 4\%$
Lip pressure pipe	$h \pm 20$ kJ/kg $\dot{m} \pm 4\%$	$h \pm 50$ kJ/kg $\dot{m} \pm 8\%$
Sharp edge weir	$\dot{m} \pm 2\%$	$\dot{m} \pm 4\%$
Tracer dilution	$h \pm 20$ kJ/kg $\dot{m} \pm 7\%$	$h \pm 50$ kJ/kg $\dot{m} \pm 10\%$
Single-phase orifice plate	$h \pm 10$ kJ/kg $\dot{m} \pm 2\%$	$h \pm 30$ kJ/kg $\dot{m} \pm 4\%$
Two-phase orifice plate	$h \pm 20$ kJ/kg $\dot{m} \pm 5\%$	$h \pm 50$ kJ/kg $\dot{m} \pm 8\%$

Source: After Helbig, S., Zarrouk, S.J., 2012. Measuring two-phase flow in geothermal pipelines using sharp edge orifice plates. *Geothermics* 44, 52–64.

even though the reservoir is hot and permeable, they will not spontaneously discharge by themselves. Mubarok and Zarrouk (2017) reported that this problem affects 15%–20% of the conventional two-phase wells and is more common in low and moderate enthalpy geothermal systems.

The causes of the wells not self-discharging are as follows (Sarmiento, 2011; Grant and Bixley, 2011; Mubarok and Zarrouk, 2017):

- Deep water levels (> 500 m) from the wellhead.
- Temperature recovery is very slow and WHP does not develop by itself.
- Cold water column (due to cold ground) on top of the hot reservoir fluid.
- Well damage (skin) during drilling.
- Poor reservoir permeability.
- High elevation terrain (lower water level).
- Small production casing size (higher pressure drop).

Another cause can be a very long workover time, during which a large volume of cold water is pumped down the well. In this case it is possible that the well would discharge by itself if it was left to heat up long enough, but this could take several years, much too long for a commercial development to wait (Watson, 2013). These wells have to be jump-started. This is called ‘discharge stimulation’, noting that the term ‘stimulation’ is also used to refer to the unrelated process of improving the permeability of the near wellbore and reservoir (discussed in Section 9.3).

Predicting if the geothermal well will self-discharge or not is very important during the planning of output testing and later during the ongoing operation of these wells. Mubarok and Zarrouk (2017) summarised five different discharging predicting methods including:

- A_f/A_c ratio method,
- liquid hold-up method,

- analytical radial flow simulation method,
- numerical simulation radial modelling and
- distance between the water level and the feed zone depth method.

The most widely used and reliable method is the A_f/A_c method developed by Sta Ana (1985) (Mubarok and Zarrouk, 2017). This method uses available data from the completion testing (Section 6.2) to predict the likelihood of self-discharge. A_f is the area between the temperature profile of the well and the BPD (boiling point for depth) curve plotted from the effective water level of the well (deep pressure profile extrapolated to $p = 1$ bara) (Fig. 6.27). A_c is the area between the 100°C line and the measured temperature profile (Fig. 6.27). The criteria for whether the well will self-discharge or not are given in Table 6.4. Fig. 6.27 shows a well with $A_f/A_c = 0.76$ for which self-discharge is uncertain.

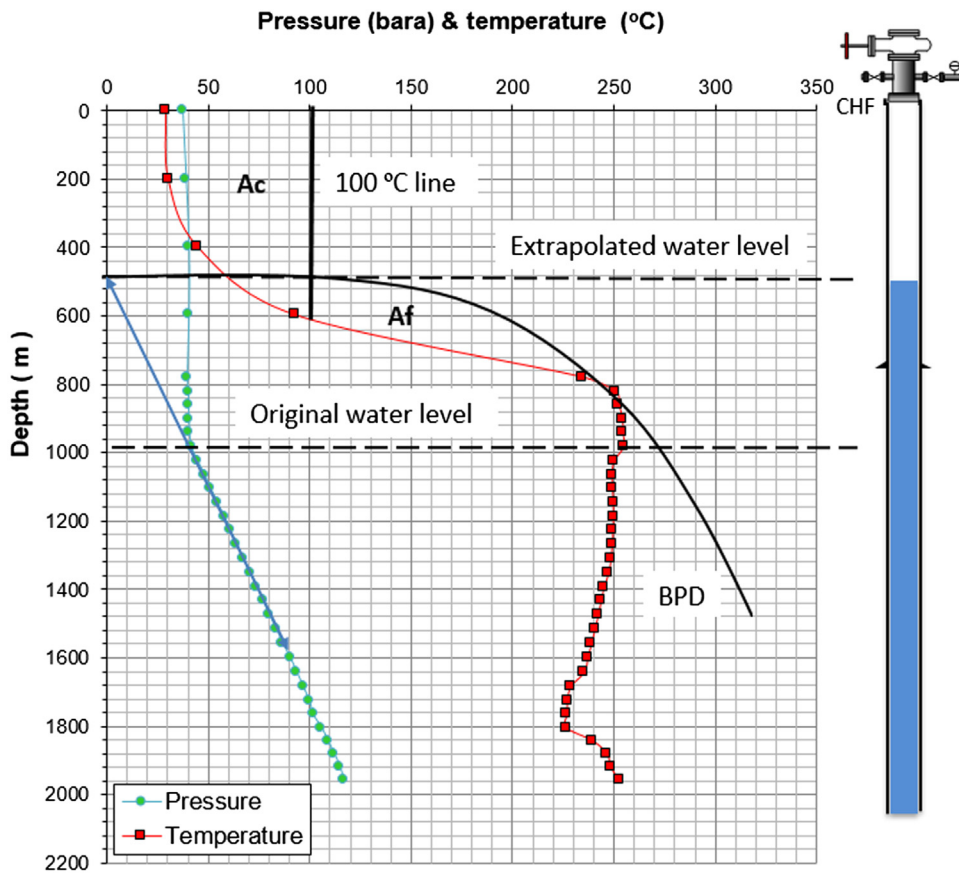


Figure 6.27 A low-enthalpy well with $A_f/A_c = 0.76$. Data from Mr. Mohamad Husni Mubarok with permission.

Table 6.4 The range of A_f/A_c ratio criteria (Sta Ana, 1985).

A_f/A_c ratio	Discharge prediction
<0.70	Little or no chance for successful self-discharge
0.70–0.85	Uncertain discharge
>0.85	Excellent chance for successful self-discharge

Another simple method is measuring the distance between the water level and the feed zone depth in the shut-in and heated up well (Mubarok and Zarrouk, 2017). For two-phase systems with feed zone temperatures $>200^\circ\text{C}$, the well will self-discharge if the distance is <600 m, while if the distance is >650 m, then the well is unlikely to self-discharge (Mubarok and Zarrouk, 2017).

6.7.1 Discharge stimulation

If the geothermal well is not predicted to self-discharge, then discharge stimulation techniques can be applied to make the well flow. Several methods can be applied to get the well discharging (Mubarok and Zarrouk, 2017):

- Soap sticks [for water level <100 m from casing head flange (CHF)]. Soap sticks contain surfactant in a solid stick, which reduces the surface tension and foams the wellbore fluid to reduce the water head and allow the well to flow. It is commonly used in oil and gas wells for the same reason.
- Air compression. The well is connected to an air compressor through the side valve. The compressed air pushes the fluid in the wellbore deep into the formations to be heated by the reservoir rock, then the well is discharged.
- Airlifting. The cold water column in the well is removed by pumping compressed air into the wellbore via a coil tubing unit. Hot water from the near wellbore will flow into the well to replace the removed water and hopefully flow to the surface.
- Well-to-well injection. Produced hot fluid from a nearby well is injected into the nondischarging well to heat the casing and the fluid in the well, to promote self-discharge.
- Injection of steam from a portable boiler. A portable boiler is transported to site and steam is injected into the well to heat the casing and fluid and promote the well to self-discharge.
- Nitrogen injection. Similar to airlifting but liquid nitrogen is used which expands when heated and pushes all the fluid inside the casing into the deep formation to heat. This is the most expensive method of discharge stimulation and the last resort. If nitrogen injection is not successful, then the well will not flow and either will be used for reinjection, monitoring or installed with a down-hole pump.

Air compression is by far the most economical for wells with a deep water level (>100 m from CHF). The A_f/A_c method was originally developed for predicting the

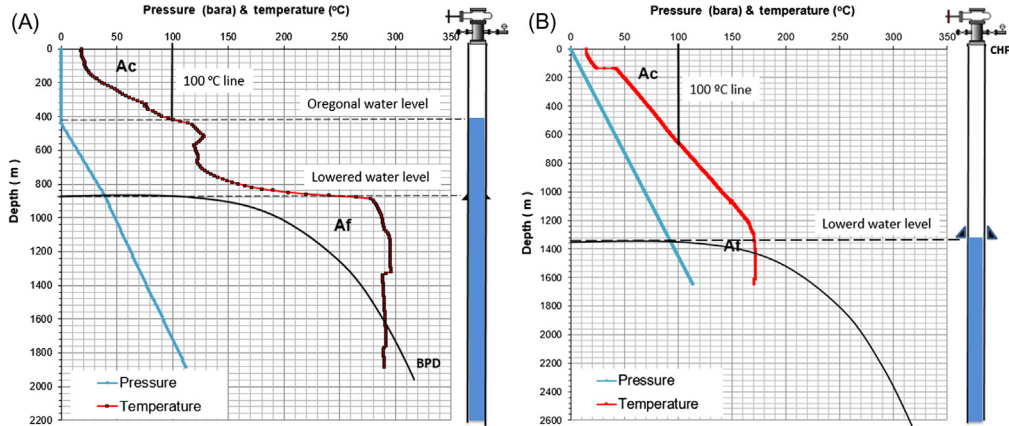


Figure 6.28 (A) A medium-enthalpy two-phase well with high chance ($A_f/A_c = 1.4$) of self-discharge after air compression and (B) a hot water well with no chance ($A_f/A_c = 0.12$) of self-discharge after air compression.

efficiency of air compression. An air compressor is connected to one of the side valves of the well, and high-pressure air is used to push the water level in the well below the casing shoe (CS) or into the main feed zone, and then that cold water (so recently close to the surface) is allowed to heat up. If the water level is lowered to the CS, then air compression can be stopped, then the well is shut off for 2 days then discharge tested. If the water level needs to drop below the CS to the feed zone depth, then air compression should continue for a day or two, then the well is discharged through a lip pressure pipe. The decision to push the water level to or below the CS depends on the depth of the feed zone and the assessment of the success of compression job using the A_f/A_c method (Fig. 6.28).

Fig. 6.28A shows a medium-enthalpy two-phase system well with the original water level at 400 m, which is lowered by air compression to the CS (~ 870 m). This well has a high chance of self-discharge after air compression. While Fig. 6.28B shows a hot water well with the original water level at the CHF, which is lowered by air compression to the CS (~ 1340 m). Even after air compression this well has no chance of self-discharging a useful level of mass flow at a reasonable WHP. This well has a WHP of about 0.45 bar gauge and can only self-discharge a limited amount of fluid because as the reservoir pressure draws down the well will stop flowing. Also, the WHP is very low to provide flowing pressure to any utilisation system. Using air compression or other discharge stimulation method in this well does not work because flashing will not take place. This well should be installed with a down-hole pump, which is a common practice for hot water wells as discussed in Chapter 2, Geothermal Systems.

Due to the high cost associated with discharge stimulation, it is a common industry practice to keep these geothermal wells discharging continually even when not in use (Mubarok and Zarrouk, 2017). This may sound wasteful; however, geothermal energy utilisation is not about thermodynamic efficiency but rather economic viability (Mubarok and Zarrouk, 2017).

6.7.2 Estimated output

If the geothermal well is expected to self-discharge, it is important to have an estimate of the expected mass flow rate to enable the planning of well discharge/output testing. This will be important for the use of correct equipment and for pipe sizing.

The well injectivity is directly related to productivity. As a rule of thumb depending on the field type, the well productivity is about three to five times less than the injectivity index (II) in two-phase geothermal systems. The ratio (productivity/injectivity) generally reduces with the increasing enthalpy, so it is lower in vapour-dominated systems and higher in hot water wells.

Grant and Bixley (2011) presented a relationship between injectivity and the maximum flow rate from the well for an 8" (0.2 m) casing size. This relation has an accuracy of 50% and is used to give a very approximate indication of the maximum production rate.

Mubarok and Zarrouk (2017) gave a similar relation for large wells with a 13³/₈" (0.32 m) size production casing (Fig. 6.29). The relation in Fig. 6.29. should also have an accuracy of $\pm 50\%$.

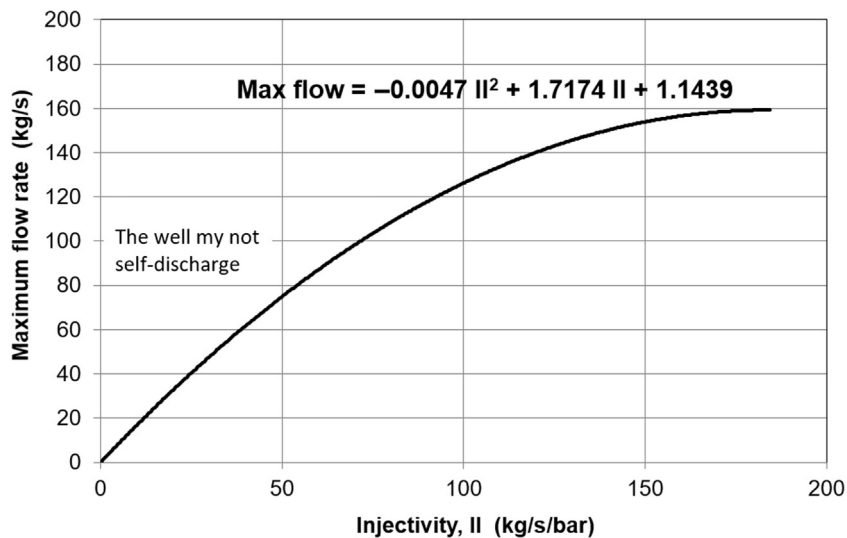


Figure 6.29 Relation between injectivity (II) and expected maximum well discharge for a large production casing size 320 mm well. After Mubarok, M.H., Zarrouk S.J., 2017. *Discharge stimulation of geothermal wells: overview and analysis. Geothermics 70, 17–37.*

6.8 Production pressure transient: drawdown/build-up

Drawdown tests are not commonly applied in geothermal wells. This is because most wells in two-phase systems have flashing taking place in the wellbore or the reservoir during drawdown, which complicates the well test analysis as discussed in Section 4.2. Most hot water and warm water wells do not self-discharge as discussed in Chapter 2, Geothermal Systems, therefore cannot be subject to a drawdown test. However, some hot water wells have a reservoir pressure higher than the hydrostatic head of water and do self-discharge. These wells are tested by flowing the wells for some time, then keeping them shut for about 8–10 times the flow test time to measure the pressure build-up.

In wells installed with a down-hole pump, using the down-hole pump for the drawdown (pumping test) can affect the build-up test since the pump tube will be full of fluid, while the annulus between the tube and casing will have a lower head (e.g. Fig. 3.13). This pressure differential can make the fluid flow from the tube back into the reservoir causing the pump to run in the opposite direction, which can be observed at the surface if a top drive pump is used. The effect will show up as a straight line during early build-up and is more prominent in low permeability wells, which take a longer time to recover (Fig. 6.30).

This will also result in an extended (> 1.5 log cycle) wellbore storage period, shown in the log-log pressure derivative plot of Fig. 6.31, which also shows that this well does not reach infinite-acting IARF behaviour even after 47 hours of pressure build-up as it has a low permeability of 1.2 mD. Additionally, the shape of the hump of pressure derivative is very steep (affected by fluid return from the pump) and will be difficult to match.

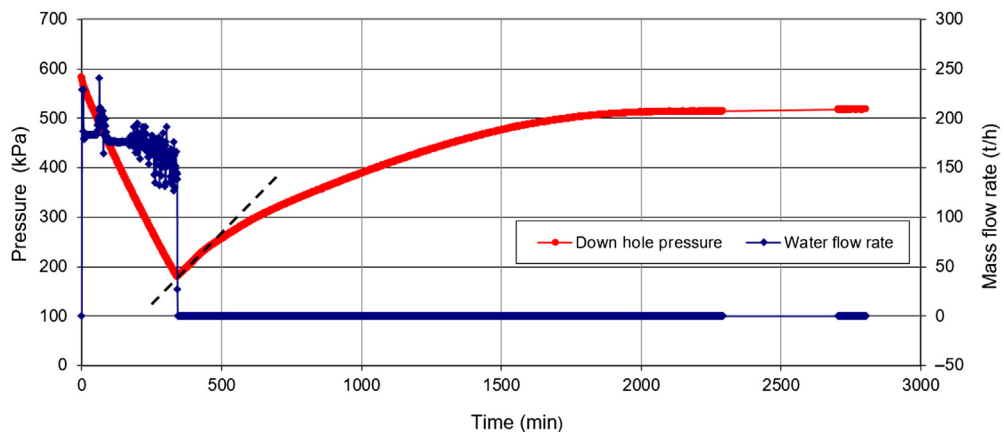


Figure 6.30 Drawdown/build-up of a well in a warm water system using the down-hole pump. Data measured by authors.

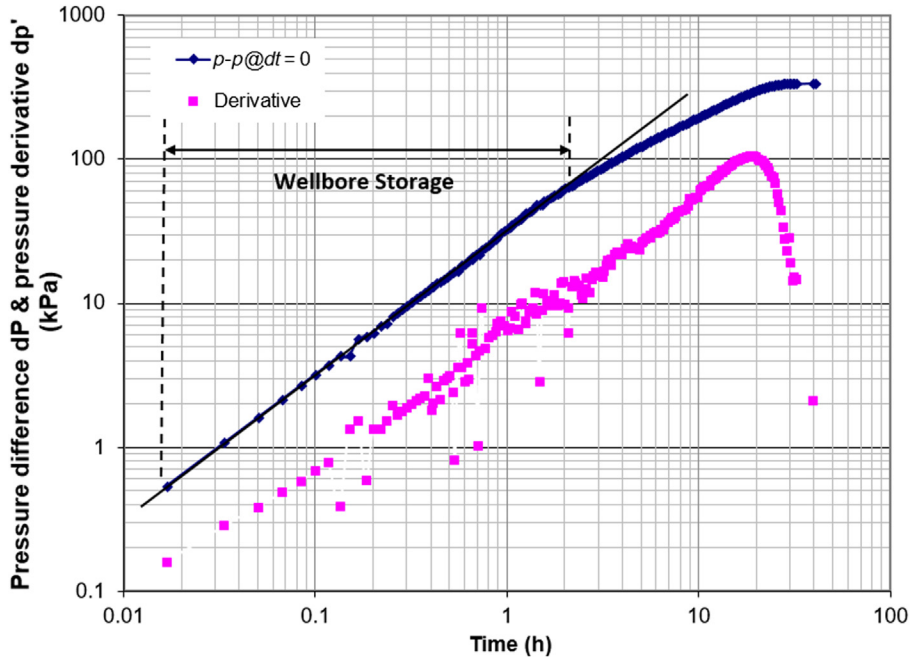


Figure 6.31 Log–log pressure derivative plot of build-up data from Figure 6.30 showing extended wellbore storage effect.

6.9 Flowing down-hole surveys

Flowing down-hole surveys are PTS surveys carried out on the production well while it is producing/flowing, which requires a counter weight to stop the fluid flow pushing the tool out of the well. Sometimes spinners are not used in flowing surveys as the very fast flowing fluids can damage them. However, there is great benefit from having a fluid velocity profile measured while the well is flowing if possible. Flowing surveys are useful to identify the major feed zone from which the flowing fluid is sourced. These are also important to monitor changes in the feed zones during the life of the well, for example, when the water level in the reservoir drops due to production and then shallow steam zones dominate production. Flowing PT surveys are also useful for measuring pressure drop in the casing that can help identify if the flow in the well is reservoir- or wellbore-limited. Flowing surveys can also be used to identify casing damage such as a hole in the casing that can form a steam thief (leak) zone (Osborn and Spielman, 1995).

Fig. 6.32 shows a flowing survey of a Tauhara well, with the extrapolated water level in the well at 200 m depth when the well is shut. The flowing temperature profile shows that the water level is at about 650 m depth, which is where flashing is first taking place (inside the production casing). The flashing temperature is about 253°C,

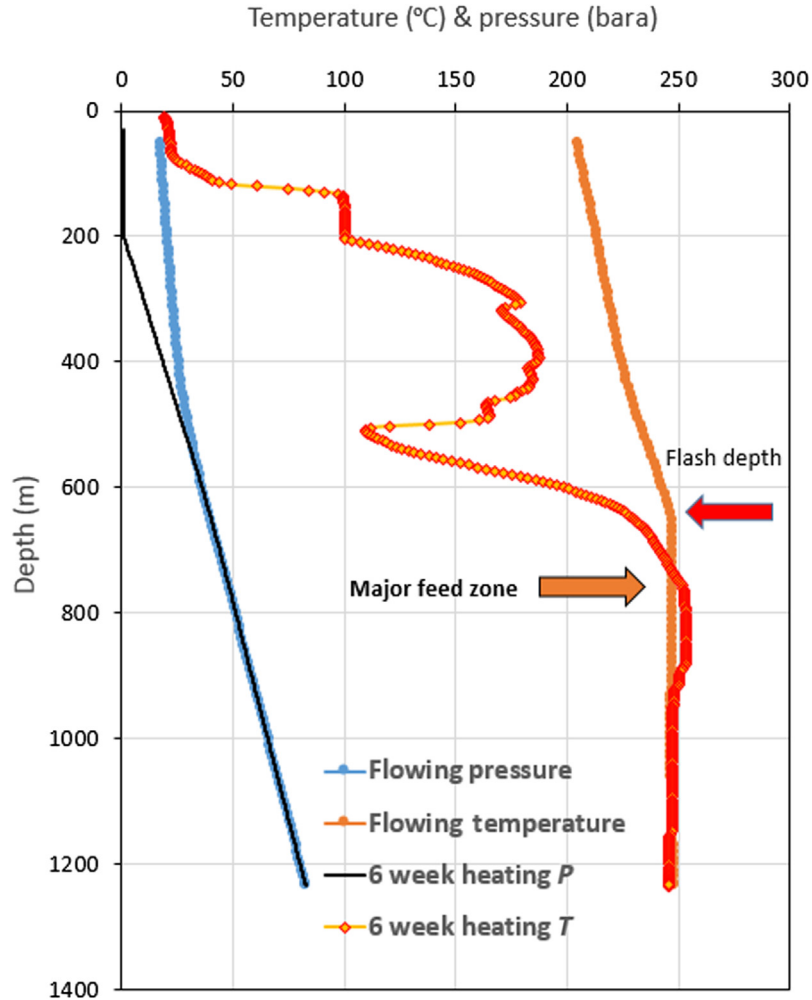


Figure 6.32 Flowing and heated-up pressure & temperature (PT) profiles of a Tauhara well. Data from Contact Energy, with kind permission.

which is consistent with the major feed zone temperature, which means the produced fluid has an enthalpy of about 1100 kJ/kg. The flash point in the well is where calcite scaling (CaCO_3) can deposit if the right chemical composition of the geothermal fluid exists. This will be further discussed in Chapter 9, Operation and Management of Geothermal Wells.

It is important to note that flowing surveys in slim holes can be significantly affected by the small clearance/annulus between the small diameter casing/perforated liner and the diameter of the PTS tool. In this case, the mass flow rate of the well will be very restricted and much lower than it would be if there was no tool in the well.

The main challenge with flowing surveys is keeping the tool down the well while the geothermal fluid is flowing. The other challenge can be having the PT tool stuck in the well when pushed (jammed) sideways by fluid forcibly entering the well from a narrow/localised feed zone.

6.10 Geothermal well abandonment

Like any piece of equipment, geothermal wells will reach the end of their operational life and will require proper abandonment. This could be due to significant drawdown or cold water intrusion in the reservoir, causing the well productivity to become sub-commercial in some cases, or due to mechanical damage (erosion, casing shear due to earthquake or subsidence) or chemical damage (corrosion) to the well casing. Some of the wells at Wairakei have been producing for nearly 60 years, but most wells will have shorter life of 20–30 years on average. The New Zealand Standard ‘Code of practice for deep geothermal wells’ (NZS 2403, 2015) outlines the main requirements for well abandonment.

Geothermal wells also require maintenance (workover), mainly to the valves in the wellhead assembly. Any workover that involves the well casing or liner will likely require a drilling rig or the coil tubing unit on the well, which will involve significant time and cost. It also involves quenching the well with cold water, which puts the casing under significant stress.

Common scenarios requiring a workover include:

1. removal of scale build-up inside the casing,
2. running a sleeve when there is a hole in the casing, a collar parting or similar and
3. well abandonment.

The worst-case scenario is having a well at risk for blow-out, which occurs when the casing damage is shallow and the high temperature fluid escapes to the ground surface. This will require a ‘killer well’, which is a targeted well drilled to the production zone of the damaged well to inject cement and stop the fluid flow. There is significant cost and risk associated with drilling killer wells, and there is the risk that the killer well may not be useable for production later. This effectively results in the loss of the original blown-out well plus the added cost of the killer well, and then a new makeup well will still be required to maintain the same level of power/energy production.

CHAPTER 7

Downhole tools and other practical considerations

Contents

7.1	Introduction	155
7.2	General downhole tools	158
7.2.1	Go-devil	159
7.2.2	Pressure, temperature and spinner tool	160
7.2.3	Borehole imaging	161
7.3	Downhole tools to assess casing condition	162
7.3.1	Cement bond logs	162
7.3.2	Downhole camera	163
7.3.3	High-temperature casing calliper	163
7.3.4	Mechanical calliper	166
7.3.5	Lead impression block	168
7.4	Tools to obtain physical samples from downhole	169
7.4.1	Downhole samplers	169
7.4.2	Downhole scrapers (scale catcher)	169
7.4.3	Wellbore debris	170
7.5	The effect of slow valve closure	171
7.6	The effect of two-stage pump shutdown	172
7.7	Flow control and metering	174
7.8	Internal flow between feed zones	176
7.9	Thermal expansion of wireline of downhole tools	177
7.10	Expansion/contraction of fluid column during heating/cooling	180
7.11	Boiling and two-phase effects inside the casing of dry steam wells	183
7.12	Reservoir boundary in enhanced geothermal system wells	186
7.13	Pressure drop inside a flowing geothermal well	188
7.13.1	Single-phase fluid	188
7.13.2	Two-phase fluid	189

7.1 Introduction

Gathering downhole well test data is a complicated and expensive exercise, requiring specialised tools and equipment not readily available in many parts of the world. The running of these downhole tools requires trained professionals and is commonly performed by specialised contractors.

Performing a geothermal well test centres around recording and capturing all the data and events during the test. The recording of all field data should be completed using real local time to allow for correlation between the different events and the measured data. This assists with the test interpretation in the event that the data does not follow the predicted or standard response.

Running downhole tools in a geothermal well with high wellhead pressure (WHP) requires significant preparations, health and safety (H&S) assessment and installation of additional equipment (e.g. lubricator tube), and in most cases, it involves taking the well out of production. It also involves using a specialised logging truck and one or more cranes. Fig. 7.1 shows the usual well setup during the running of the downhole tool (bleed valve closed, master valve open, and side valves open or closed depending on whether there is any injection), while Fig. 7.2 shows the retrieval/recovery of the downhole tool after logging and pressure bleeding of the lubricator tube (bleed valve open, master valve closed and side valves closed). The lubricator tube may not technically be required when the well does not sustain WHP, simplifying the process and reducing risk and cost. However, from an H&S point of view, it is safer to have a lubricator tube installed when logging all wells in two-phase systems.

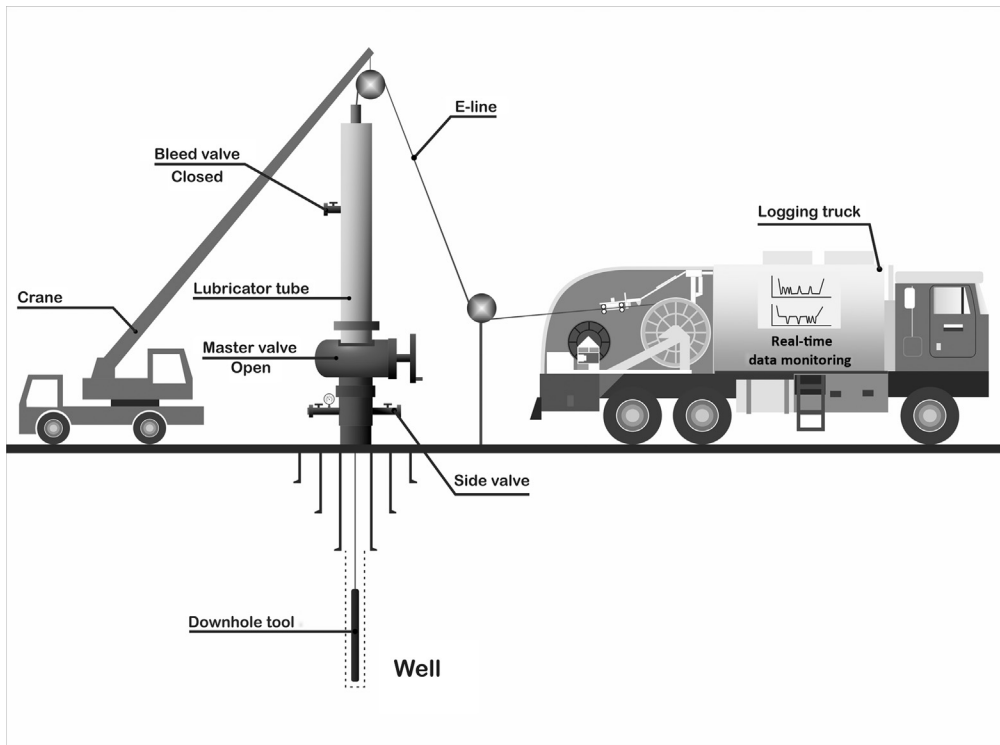


Figure 7.1 Wellhead setup during downhole logging with tool down the well.

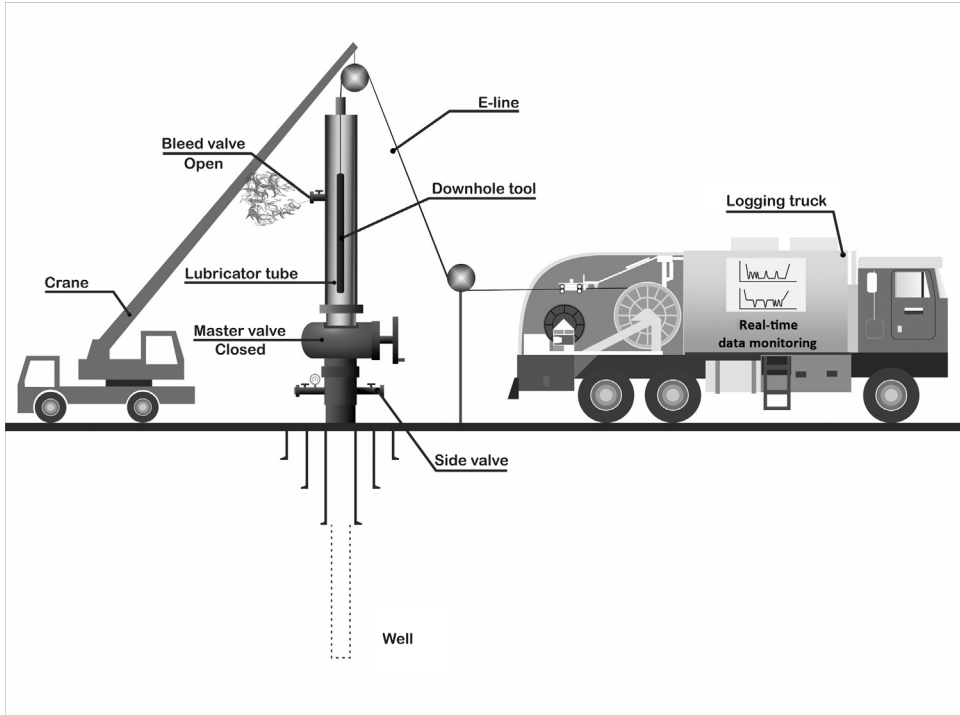


Figure 7.2 Wellhead setup during tool retrieval from the well.

There is less risk when logging warm and hot water systems since these wells are unlikely to be pressurised ($WHP = 0$).

Downhole logging tools can be run into the well attached to either a ‘slick-line’ which is a single solid stainless steel wire or an electronic line ‘e-line’. The slick-line cannot be used to send signals or information to the surface while the tool is logging and hence the downhole tool must run in memory mode, storing the information, which is later downloaded at the surface when the tool is recovered at the end of the test. The e-line on the other hand is made from multiple carbon steel wires, which form a protective sheath (armour) around a core of Teflon-insulated conductive copper wires, which transmit electronic signals to the surface for real-time data monitoring (Fig. 7.1). The slick-line has a higher temperature limit of up to 400°C – 600°C (depending on the type of stainless steel), is low cost to run and generally has a longer life. E-lines on the other hand are rated up to 315°C (but normally operated only up to 280°C to extend life), are much more expensive to use and have a shorter life than the slick-line (private communications with Richard Adams, MB Century Ltd.).

Figs 7.1 and 7.2 show the setup during the logging of a well that is not in service and not connected to the steam-field pipeline network, allowing the lubricator tube

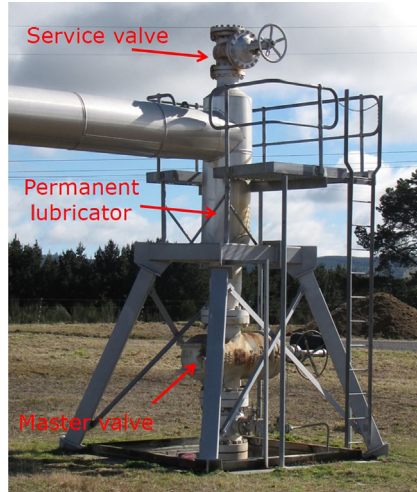


Figure 7.3 Production well with a permanent (built-in) lubricator tube. (Picture by authors).

to be connected to the master valve. Wells that are in service are connected to the system and should be isolated using the control (production) valve, and the lubricator tube is usually connected above the service valve. Therefore it is very important to have a service valve large enough ($> 6''$) installed on all wells to facilitate downhole logging. It is a common problem that only a smaller service valve is used, which complicates well logging. Some wells requiring frequent ongoing logging may be installed with a permanent lubricator tube below the service valve (Fig. 7.3). Note that in Fig. 7.3 the control valve is located out of the frame along the pipeline to the left.

7.2 General downhole tools

There are a wide variety of downhole tools potentially available for testing geothermal wells. Note that most downhole geophysical logs (e.g. spontaneous potential logs, gamma ray logs, porosity logs, resistivity logs and magnetic resonance imaging logs) are not commonly used in geothermal wells. This especially is the case in the higher temperature environments of two-phase and vapour-dominated systems. The reasons for this include:

- Most of these tools are not designed/rated for the high-temperature geothermal conditions, often with a maximum temperature rating of around 80°C – 150°C depending on the tool supplier.
- The high risk of losing the tools downhole while running logs in open holes (most cannot be run after the installation of the perforated liner) in a fractured geothermal environment.
- High cost.

It is important to note that all the downhole tools should be calibrated in the laboratory before transportation to the well test site. The downhole tools commonly used by the geothermal industry include those described in the following subsections.

7.2.1 Go-devil

The simplest tool is the ‘go-devil’ or ‘sinker bar’, used to investigate if the casing/liner is obstructed prior to running any valuable downhole tools into the well. Since the go-devil does not measure any data, it does not require an e-line and can be run using a slick-line from a small trailer-mounted winch. Major obstructions will prevent the go-devil from moving down the well, and a skilled operator will be able to identify minor obstructions from bumps recorded while travelling down and then up the well. Fig. 7.4 shows two common go-devil designs, both with holes to allow fluid flow as the go-devil travels up or down the well. Go-devils are normally made from a drillable material (e.g. aluminium or brass) in case they become stuck in the well (Fig. 7.4).



Figure 7.4 Common designs of go-devils (aluminium on the left, brass on the right) used by the geothermal industry. *From MB Century Ltd., with kind permission.*

7.2.2 Pressure, temperature and spinner tool

The pressure, temperature and spinner (PTS) tool is the most important and commonly used geothermal well testing tool, designed to continuously measure and record down-hole temperatures, pressures and spinner rotation with depth in the geothermal well (Fig. 7.5). It is the only tool used to assess the thermodynamic state, heat transfer and fluid mechanics (thermofluid) conditions inside the well. The spinner is an impeller which measures the frequency of rotation, usually as revolutions per minute, and this data can be processed to obtain the fluid velocity profile of the well (Section 6.2.2). The PTS tool is essential for completion/injection testing, stage testing, flowing surveys, and for logging shut geothermal wells. The interpretation of the PTS data for these purposes is discussed in detail in Chapter 6, Completion and Output Testing.

The data is stored electronically inside the tool and can be made available in real time via an e-line to the surface when using a logging truck (Fig. 7.1). Note that while the slick-line is lower cost to run and has higher temperature tolerance, it does not offer real-time data monitoring from the surface, and so tool failures can go undetected for many hours. The PTS tool main body/housing is an insulating stainless steel Dewar flask to protect the battery and electronic circuits from damage by the high temperatures downhole. The Dewar flask significantly reduces the rate of temperature build-up inside the tool once down the well. However, the heat transfer from the ends of the Dewar flask and the heat generated by the tool's battery cause the internal temperature to rise. Therefore the tool has a temperature limit on its electronic components, so monitoring the internal tool temperature is important to ensure the tool does not sustain thermal damage during the test. Sisler et al. (2015) gave an insight on

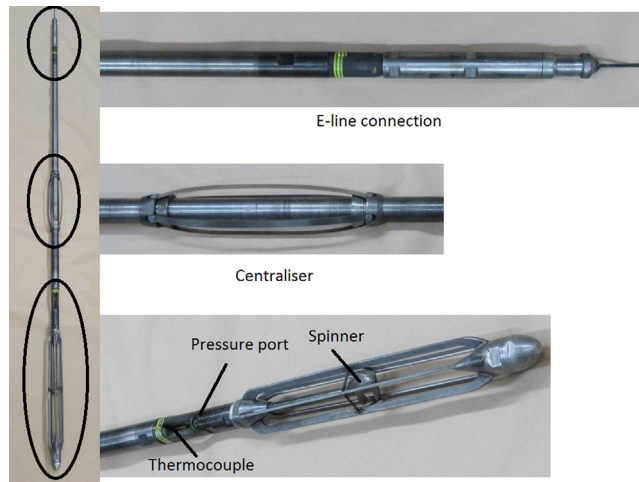


Figure 7.5 PTS tool (2.6 m long) with the main components indicated. *PTS*, Pressure, temperature and spinner. Pictures kindly provided by MB Century Ltd.

optimising the PTS tool downhole run time; this is by cooling the heat sink bar inside the PTS tool or simply freezing the entire tool, before running down the well.

It is important to point out that when performing flowing (discharging) surveys using the PTS tool, a counterweight is placed in front of the tool to make sure it is not carried out of the well with the flowing geothermal fluid travelling to the surface. The safe practice is to first run a dummy tool (same size and weight as the PTS tool) with the calculated counterweight, then retrieve the dummy tool and run the actual tool if the dummy tool run is successful. This will require additional preparations, time and cost which are not required when testing static (nonflowing) wells.

7.2.3 Borehole imaging

There are two types of borehole imaging (BHI) tools, otherwise known as borehole televiewer (BHTV) tools, which work by detecting physical properties of the reservoir formation. These tools do not measure an ‘image’ in an optical sense; rather they provide a ‘map’ of various physical properties, over almost the entire surface of the borehole wall. One type is the acoustic formation imaging tool (AFIT) which works by sending an ultrasonic acoustic signal towards the borehole wall and then measuring the travel time and amplitude of the reflected signal. The acoustic source and detector rotate, allowing the image to cover 360 degrees of the borehole wall (Fig. 7.6A). The use of AFIT technology in geothermal wells has been enabled in recent years by the development of tools able to withstand high temperatures up to 300°C (McLean and McNamara, 2011).

The other type of BHI is the formation microimager (FMI) which provides a microresistivity map of the borehole wall by measuring the microresistivity of the formation via direct contact of pads with the borehole wall. Features in the subsurface

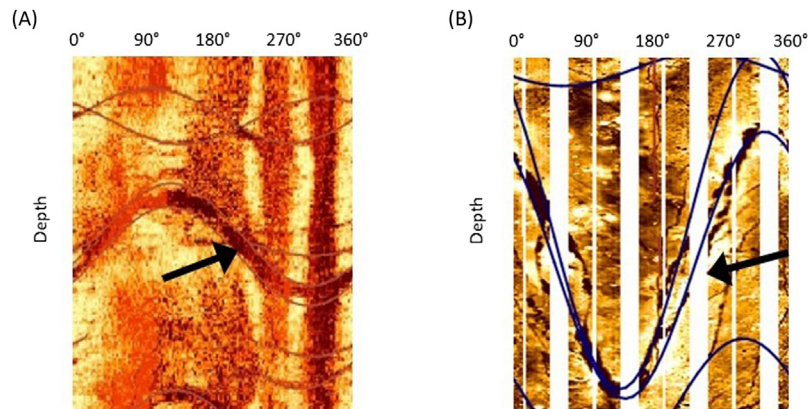


Figure 7.6 Examples of wide planar fractures which appear as sinusoidal features in the 360-degree image: (A) AFIT acoustic amplitude and (B) FMI resistivity. *AFIT*, Acoustic formation imaging tool; *FMI*, formation microimager. *With kind permission from Contact Energy Ltd.*

with a microresistivity contrast, such as fractures, bedding and lithological features can be identified in the image. The FMI image is distinctive as the image is obtained only where the pads make contact with the borehole wall, and the data gaps in-between the pads mean the image appears in long stripes (Fig. 7.6B).

Note that BHI logs are different to resistivity logs, which are commonly used in the mining and petroleum industries for determining hydrocarbon-bearing versus water-bearing formation, qualitative indication of permeability zones, and to determine porosity (Asquith and Krygowski, 2004).

BHI are best used in conjunction with other downhole data such as cuttings, cores, PTS, and production data (Hurley et al., 2004; Massiot et al., 2017).

7.3 Downhole tools to assess casing condition

The integrity of the geothermal well casing is critically important for the safe operation of geothermal wells. Any casing damage can introduce a risk to the operation of the well and may result in geothermal fluid leaking to the shallow aquifers and ground surface. This results in lost well output and in the worst case scenario can cause an uncontrolled discharge of geothermal fluid at the ground surface (a 'blowout'), in which case a 'killer' well (Section 6.9) will be needed (King and Robson, 1998). Casing condition monitoring is also important when wells change hands from one developer/operator to the next, as it describes the condition of an important asset.

There are a few different ways to measure casing condition in high-temperature wells: mechanical, electromagnetic, acoustic and optical (Williams et al., 2016). The downhole monitoring tools used for casing condition monitoring are discussed in the following sections.

7.3.1 Cement bond logs

This tool evaluates the quality of the bond between the cement and the casing and the cement and the formation. The tool measures the cement bond amplitude through near- and far- sonic receivers to assess the quality of the cement job. Cement bond logs (CBL) are commonly used in the petroleum industry and have become more commonly used for testing the production casing of geothermal wells in the past 10 years. CBL are normally run during drilling operations, after cementing the casing, to make sure the cement is where it should be around the casing, and so the casing will be able to withstand the mechanical and thermal stresses during operation of the well. Poor cement jobs will require intervention before the well is produced, because any water trapped in the cement around the casing is a hazard which can result in casing implosion as the water expands due to heating when the well is produced (Section 9.6.2). The intervention may involve making perforations in the casing, installing a bridge plug inside the well below the perforations and squeeze cementing

to fix the cement job. The casing is then pressure-tested to make sure that the cement went to the correct location behind the casing, and the perforations are plugged with cement. This intervention is particularly important if the well is going to be fracture stimulated (Chapter 9: Operation and Management of Geothermal Wells) since fracture jobs will put high pressure on the target formations (and sometimes the casing).

7.3.2 Downhole camera

The downhole camera (DHC), also known as a borehole viewer, is simply an optical video camera that is run down the well to capture images of the casing. This tool is gaining popularity as it provides visual inspection of the casing conditions in real time. Glynn-Morris et al. (2009) showed DHC images of casing damage including bent casing, broken casing with formation fill, and remnants of tools lost inside the casing. These images are important for decision-making and when designing the appropriate workover, to make sure all necessary equipment is brought to site during mobilisation. It should be noted that optical methods do not work when the well fluid is not transparent (Williams et al., 2016) and/or at high temperatures ($> 125^{\circ}\text{C}$). Therefore cameras are usually run with the well under cold water injection to keep the fluid in the well cold and protect the camera.

DHCs currently in use have two lenses, one at the front of the tool and the other one on the side. Figs 7.7–7.9 show some DHC images inside the liner and casing. Fig. 7.9 shows a side camera image of the perforated liner with some debris partially blocking one of the perforations.

7.3.3 High-temperature casing calliper

The high-temperature casing calliper (HTCC), also known as hot hole casing corrosion (Stevens, 2000), is a noncontact electromagnetic tool used to measure the thickness of the casing and the internal diameter. Thickness measurement is important to determine (quantitatively) if any corrosion is occurring on the outside of the casing. The HTCC tool applies electromagnetic principles: generating oscillating currents in

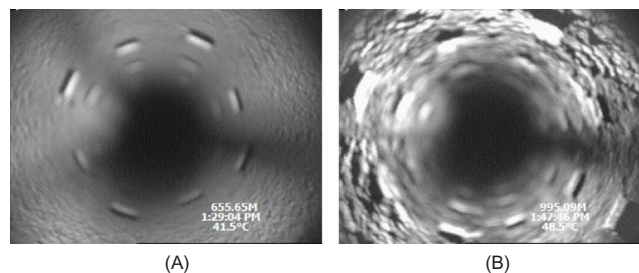


Figure 7.7 (A) Minor scaling deposition inside the liner. (B) Corrosion inside the perforated liner. With kind permission from MB Century Ltd.

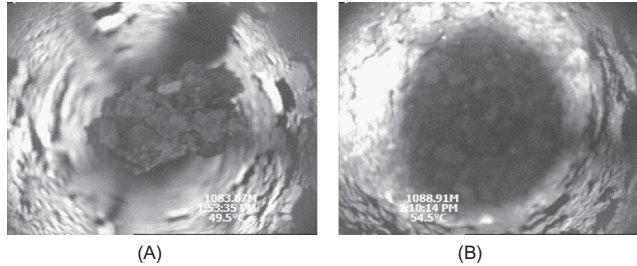


Figure 7.8 (A) Partially blocked liner. (B) Well blocked with corrosion and scale flakes. *With kind permission from MB Century Ltd.*

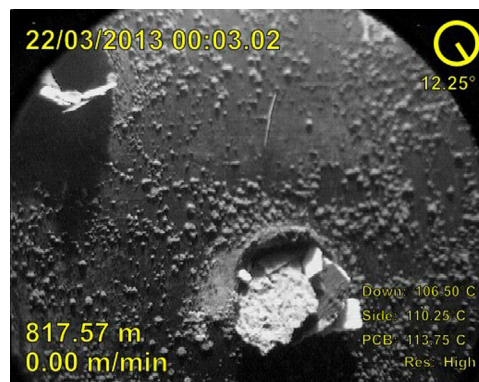


Figure 7.9 Side camera image showing partially blocked perforated liner hole. *With kind permission from MB Century Ltd.*

several coils to create several magnetic fields that generate eddy currents in the steel casing. The eddy currents generate their own magnetic fields, but there will be a shift in phase and the detection of this shift in phase is used to determine the condition (thickness) of the steel in the casing (Stevens, 2000; Williams et al., 2016). The tool also has an electromagnetic internal diameter proximity sensor (differential calliper) and a roughness indicator (RI).

External casing corrosion (ECC) is inferred from the phase shift and the differential calliper. If the phase changes indicate a change in the mass of metal, then the differential calliper will show if the metal loss is from the internal walls of the casing. If the metal loss is from external corrosion then the differential calliper reading of the internal diameter of the casing will remain constant (Stevens, 2000). Stevens (2000) provided good examples of the use of the HTCC tool; Fig. 7.10 shows internal metal loss at depths of 398 and 405 m inside a $9\frac{5}{8}$ " production casing, this is evident from the phase shift and changes in internal diameter and increases in RI. Fig. 7.11 shows external metal (ECC) loss at depths of 248–250 m in the $13\frac{3}{8}$ " anchor casing, where there

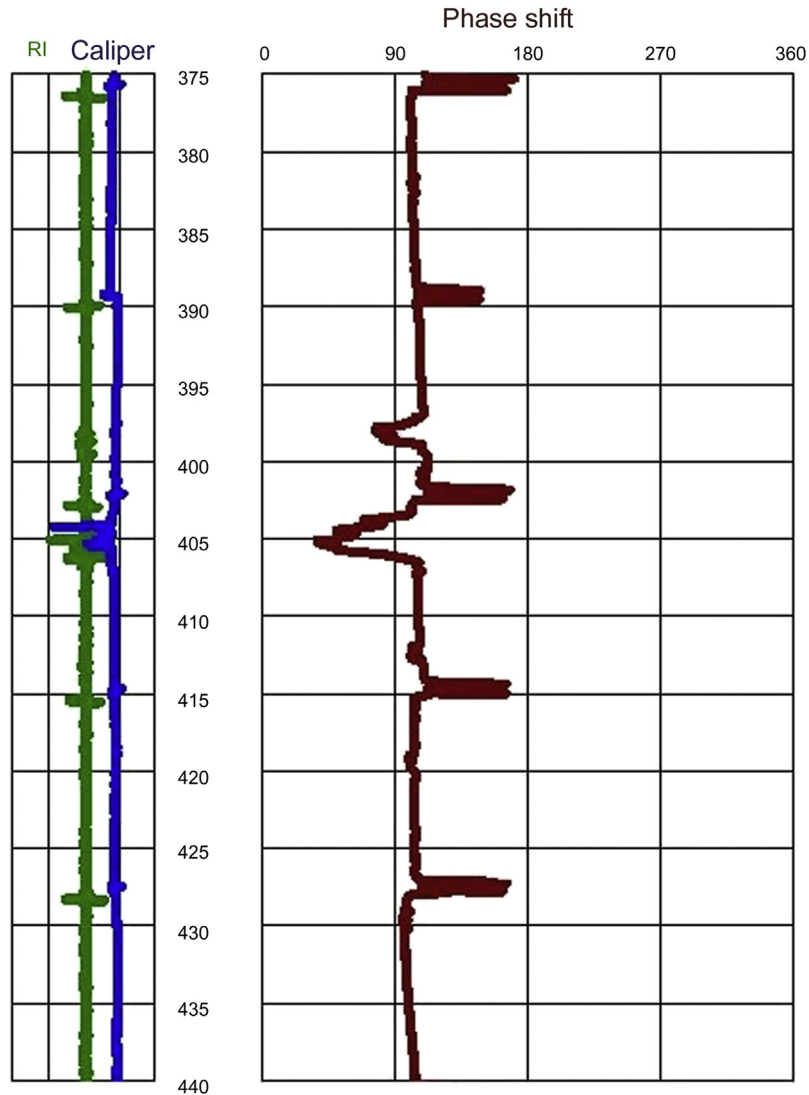


Figure 7.10 ICC inside the 9 $\frac{5}{8}$ " production casing. ICC, Internal casing correction. With kind permission from MB Century Ltd.

is a phase shift but the internal diameter and RI remain unchanged. Fig. 7.11 also shows that the 13 $\frac{3}{8}$ " anchor casing extends to the depth of 270 m then only the 9 $\frac{5}{8}$ " production casing continues beyond that depth as shown from the changes in phase shift. Fig. 7.12 shows a parted (split) collar in the 9 $\frac{5}{8}$ " production casing. This is evident from the changes in phase shift, internal diameter and RI at the collar depth.

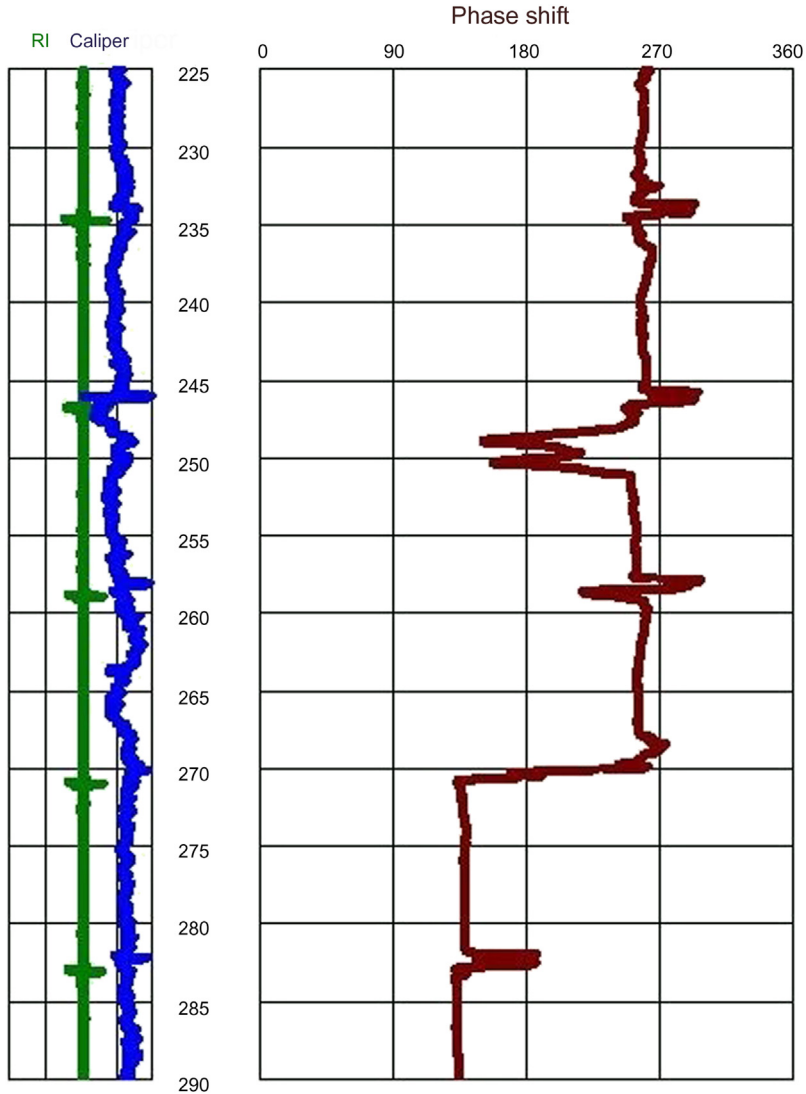


Figure 7.11 ECC outside the 13 $\frac{3}{8}$ " anchor casing. ECC, External casing corrosion. *With kind permission from MB Century Ltd.*

7.3.4 Mechanical calliper

The multifinger (MF) mechanical calliper is a contact tool that provides a measurement of the internal casing diameter and helps identify anomalies, which can be due to build-up of mineral scale or due to casing collapse or damage. As many as 60 small mechanical fingers survey the well casing for possible change in diameter (Fig. 7.13). This tool has been in use by the geothermal industry since the 1980s but became less

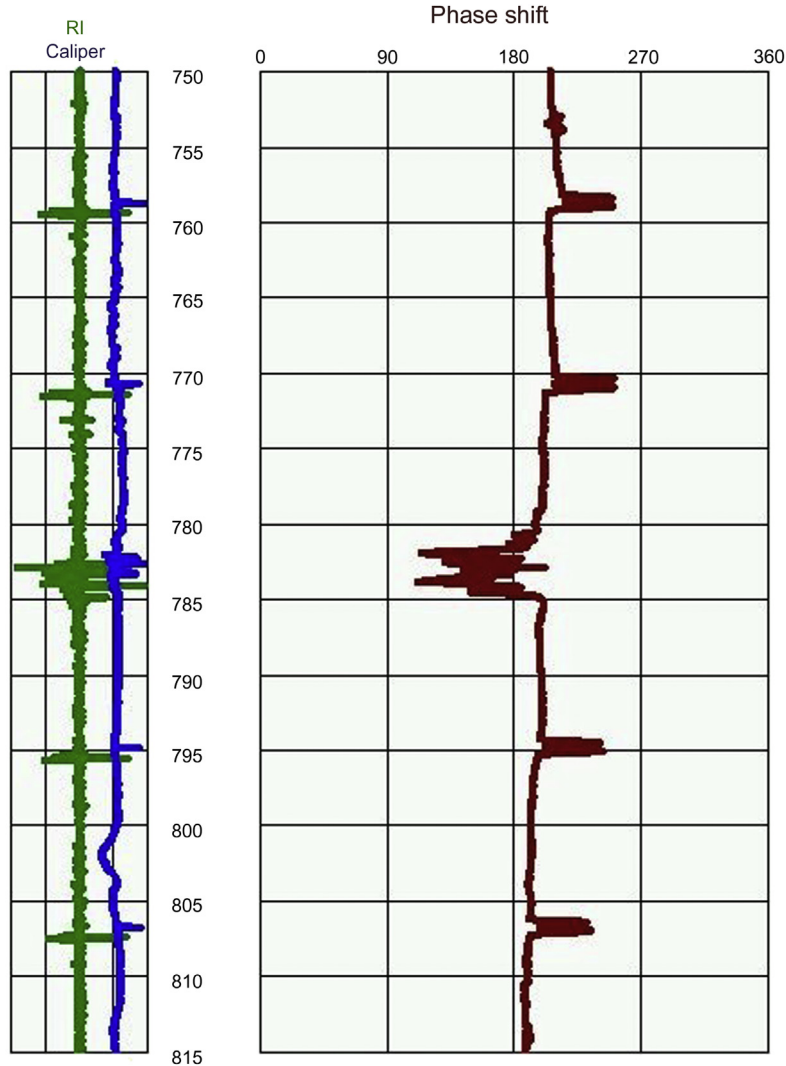


Figure 7.12 Split collar in the 9 $\frac{5}{8}$ " production casing. *With kind permission from MB Century Ltd.*

commonly used in the late 1990s and early 2000s with the introduction of the HTCC tool. In recent years the MF mechanical calliper is making a comeback as it can survey mineral scaling, which the HTCC tool cannot detect. The tool is lowered to the bottom of the well, and then the fingers are extended to survey the diameter of the hole on the way up.

Williams et al. (2016) discussed MF calliper tools operating in tandem with HTCC. This combined survey should provide a full assessment of the condition of the inside and outside of the casings in one run.



Figure 7.13 Mechanical calliper showing the extended multiple fingers. *With kind permission from MB Century Ltd.*

7.3.5 Lead impression block

This tool has been around for a long time and has been widely used by the petroleum industry. It is simply a lead plate attached to the front of heavy steel weight (Fig. 7.14). The tool is attached to a slick-line and dropped inside the well to impact possible obstructions inside the well casing and leave an impression of that obstruction on the lead plate. When the tool is retrieved at the surface, visual examination of the impression will give an indication of the cause of the obstruction, which is a subjective process of interpretation. It cannot distinguish between mineral scale inside the casing or a casing break, and in some cases, it can raise more questions than provide answers. Therefore the lead impression block is not commonly used in geothermal wells, as it does not provide much information when compared with DHCs discussed earlier. However, this tool is relatively low cost to run and can be of use when the other tools are inaccessible or when the fluid inside the well is too murky (opaque) for the DHC. The tool is often used during drilling operations.



Figure 7.14 Lead impression block 5½" diameter. *With kind permission from MB Century Ltd.*

7.4 Tools to obtain physical samples from downhole

7.4.1 Downhole samplers

The flow-through sampler is used to take a fluid (liquid and/or gas) sample inside the wellbore at the reservoir depth. The tool is open at the front and back, allowing the fluid to flow in and out while the tool is running down the well, normally using a slick-line. The tool is triggered with a sudden jolt at the desired (reservoir) depth and the canister closes, trapping the fluid at that depth. The common sample size is 600–1000 mL (information provided by MB Century, Ltd.). These samples are captured at high pressure and temperature, and care should be taken when releasing the canister pressure after retrieval.

The important consideration is that the fluid inside well could be influenced by the drilling fluids and/or the water injected during completion testing. This can affect the sample quality; samples more representative of the reservoir fluid will be obtained if the well is produced (if possible) and the samples are taken at the surface. However, if the well cannot be produced then the downhole sample might be the only option. Downhole samples are more suitable for wells that are on bleed or have been shut for a long time (not recently drilled). The information usually obtained from the downhole fluid sample is the chemistry of the reservoir fluid or the mud/sludge in damaged wells.

7.4.2 Downhole scrapers (scale catcher)

Solid scale can form inside the casing or liner of geothermal wells by the deposition of minerals normally dissolved in the geothermal fluid. These minerals can deposit

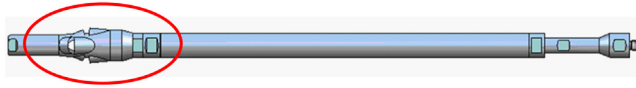


Figure 7.15 Schematic of scale catcher showing the jaws. *With kind permission from MB Century Ltd.*

(precipitate) in both production and reinjection wells, causing reduction in the cross-sectional area of the wellbore and a restriction to the flow rate. The common minerals in production wells are calcite and anhydrite, while silica is the most common scale in reinjection wells (Chapter 9: Operation and Management of Geothermal Wells).

The scale catcher consists of a scale collection bowl with a number of openings with upper sharp and hardened jaws designed to scrape out samples of scale as the sampler is moved up or down along the scale surface (Fig. 7.15). The scale catcher can also be used to sample potential sludge build-up in the bottom of the well in the case of mud- or cement- damaged wells.

The tool is lowered into the well to the desired sampling zone, and the sample is collected. The recovered sample is retrieved from the bowl of the tool for chemical analysis. The scale catcher is normally made of carbon steel, is completely mechanical, and can be exposed to any well conditions (information provided by MB Century Ltd.).

7.4.3 Wellbore debris

If for some reason the geothermal well is not discharged after drilling, there will be a build-up of debris at two main locations inside the wellbore:

1. The first is debris floating on top of the water at the water level in the well; this debris is mainly made up of drill pipe joint lubricating oil (grease) that solidifies with time as it traps other floating material, making it difficult to run downhole tools. It can also trap some gases underneath which are health risk to the well test team. A solid 2" go-devil should be used to pierce through this material before any downhole tool is used.
2. The second and more common form of debris is drilling fluid/chemicals (mud) mixed with finely crushed rock and possibly some cement, which settles at the bottom of the well in the form of thick sludge that can trap downhole tools. In this scenario the weight of the downhole tool drops as it travels down through this material. Submerging the tool in the sludge should be avoided, and in the event that the tool does become submerged then care should be taken when pulling the tool out of the well, which should be at a reduced speed with short stops to use the spring action of the long wireline to help retrieve the tool from the well.

As with most wells, geothermal wells are drilled with a 'rat hole' (~100 m) beyond the deepest feed zone at the bottom of the well, to allow any falling debris/-sludge to accumulate without interfering with the operation of the well. This debris could be sludge as discussed earlier, rock particles from the formation or falling tools

and logging equipment. However, above the rat hole, equipment/debris stuck or jammed inside the liner or production casing cannot be ignored. It can cause throttling of the flow, which is undesirable as it limits the well output, makes it difficult to operate/manage the well, and also prevents downhole tools from investigating depths beyond the obstruction.

7.5 The effect of slow valve closure

In some circumstances the flow into a well will be controlled by a control valve (or even the master valve) rather than a pump, for example during an injection test into an injection well using the operational brine reinjection system. Valves do not open or close instantaneously, and changing the valve position may take several minutes, regardless of whether the valve is automated or operated manually.

Pressure-transient analysis (PTA) theoretically requires instantaneous steps in flow rate, which cannot be achieved in reality. The effect of slow valve closure on PTA is distortion of the early-time data, for example a fall-off which is rounded instead of dropping sharply, and can be smooth (Fig. 7.16A) or incremental (Fig. 7.16C) (McLean

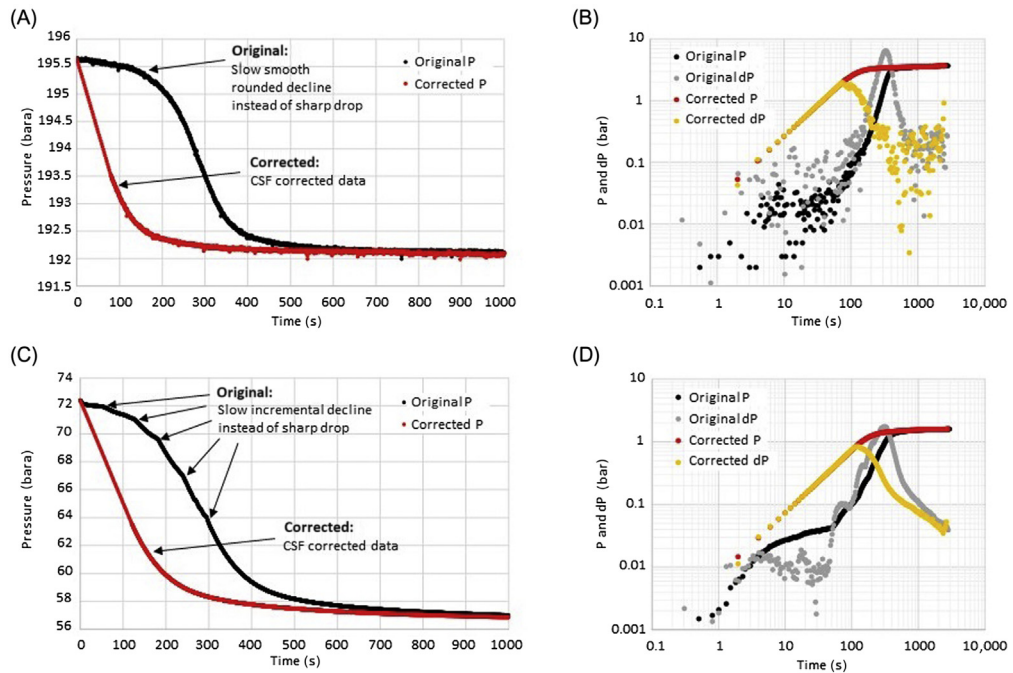


Figure 7.16 Examples of distortion of early-time data by slow valve closure, for two injection wells: WK317 example of smooth closure shown in (A) history plot (first 1000 s) and (B) derivative plot, and WK318 example of incremental closure shown in (C) history plot (first 1000 s) and (D) derivative plot. From Contact Energy Ltd. with kind permission.

and Zarrouk, 2015a). The effect of this distortion can be seen in the derivative plot in the early-time derivative, which is shifted to the right (time delayed), rises too steeply (slope \gg unit slope) and then drops very steeply during the transition to the reservoir response, resulting in a derivative hump which has been distorted into a sharp peak (Fig. 7.16B and D) rather than the expected typical smaller rounded hump (see Chapter 4, Introduction to Pressure-Transient Analysis, Fig. 4.15B). Incremental valve closure also results in multiple humps in the steep early-time derivative (Fig. 7.16D).

It has been shown that it is not possible to simply ignore the early-time distortion and fit models to the intermediate-time reservoir response, as this introduces significant error into the results of PTA, which will massively overestimate reservoir permeability and skin factor (McLean and Zarrouk, 2015a). It is possible to correct the distortion, and McLean and Zarrouk (2015a) demonstrated a technique for this called ‘cut–shift–fill’ (CSF) which effectively removes the rounded early portion of the data set and shifts the remaining data back in time so it can connect via a linear fit with the first data point (Fig. 7.17). It has been demonstrated that the CSF method significantly improves the distortion of the derivative plot and corrects the estimated values for reservoir permeability and skin factor to within a reasonable error from known values (McLean and Zarrouk, 2015a). CSF has been demonstrated to be valid for cases where the valve closure occurred over an interval of ~ 10 minutes, it is not known whether the method is valid for significantly longer time intervals.

7.6 The effect of two-stage pump shutdown

Pressure transients are often measured during completion testing (Chapter 6: Completion and Output Testing) immediately after drilling, with injection achieved using the rig pumps. The drilling rig pump system usually has at least two pumps, and sometimes more for redundancy. In older pump systems, in the absence of a modern

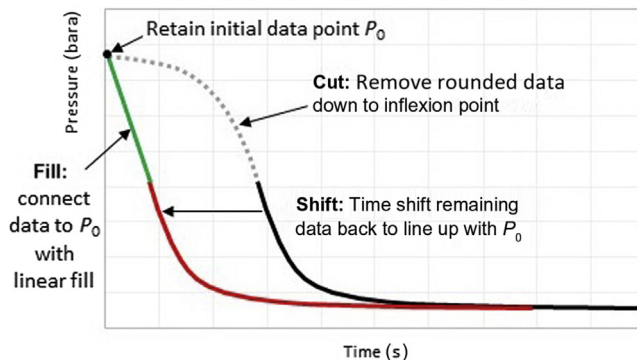


Figure 7.17 Schematic of CSF method to correct for distortion of early-time data by slow valve closure. CSF, Cut-shift-fill. After McLean, K., Zarrouk, S.J., 2015a. *Geothermal well test analysis using the pressure derivative: Some common issues and solutions*. *Geothermics*, 55, 108–125.

control system, the individual pumps may have to be shut down one at a time. Thus the cessation of flow for the pressure fall-off is not a single step straight to zero flow; instead, there is an intermediate flow step in-between. This results in a common artefact which is a fall-off that appears to occur in two stages: the pressure drops and begins to level out before dropping a second time (Fig. 7.18A and C). This is apparent in the pressure derivative as a small spike in the derivative which is far more apparent when it occurs later in the transient (Fig. 7.18B) and quite subtle when occurring earlier in the transient when wellbore storage dominates (Fig. 7.18D).

This artefact can be corrected by using the CSF method (Section 7.5, Fig. 7.17) and removing all the data in the first stage. The effectiveness of this method in returning the derivative to the expected shape depends on the time delay between the first and second stage, and the duration of wellbore storage. In the case of a longer delay (> 2 minutes) and shorter wellbore storage period, the CSF method is less effective, and the resulting derivative remains partially distorted (Fig. 7.18B). However, in the case of a shorter delay (~ 1.5 minutes) and a longer wellbore storage period, the CSF method is more effective in correcting the derivative (Fig. 7.18D).

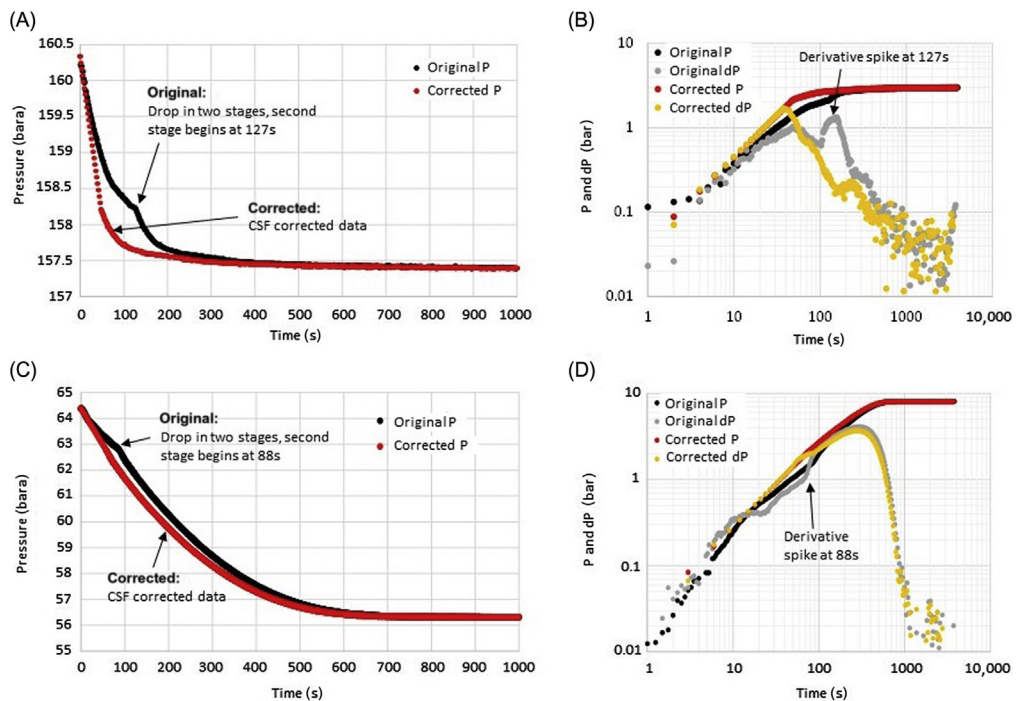


Figure 7.18 Examples of distortion of early-time data by two-stage pump shutdown, for two wells: WK410 example of relatively late second stage (127 s) in (A) history plot (first 1000 s) and (B) derivative plot; and WK686 example of earlier second stage (88 s) shown in (C) history plot (first 1000 s) and (D) derivative plot. *Data from Contact Energy Ltd. with kind permission.*

McLean and Zarrouk (2015a) modelled a two-stage drop and demonstrated that significant error is introduced into the results of PTA by ignoring this artefact and modelling the distorted data set. The CSF method was shown to be effective in correcting a data set with high permeability, short wellbore storage and the second stage as late as 127 seconds, returning values of reservoir permeability and skin within an acceptable margin of error, and that this error decreases significantly as the second stage starts earlier (McLean and Zarrouk, 2015a). It follows that the CSF will also be effective for data sets with low permeability and/or longer wellbore storage.

7.7 Flow control and metering

PTA requires two sets of data: pressure and flow rate with time. In geothermal PTA the pressure data set is typically very good, usually captured with a downhole PTS tool with data points at least once per second and sometimes up to four times per second. However, the importance of the flow rate data set is frequently overlooked. Many geothermal data sets have only three data points for flow rate, corresponding to the start of each of the three flow rates in the injection/completion test programme. Or if there is a more detailed flow log, it often only contains data points every minute or two and only during the transient of interest, with even sparser flow data covering the rest of the injection period.

One reason that pressure fall-offs to zero flow are the most common type of geothermal well test is that it is relatively easy to obtain a smooth pressure curve when there is no injection into the well, because there is no noise or variation in the pump rate to distort the curve, and no flow log required. However, there are a variety of reasons to avoid fall-offs to zero flow, as the heat up of the well during the test causes thermal expansion of the wireline (Section 7.9), pivoting of the pressure profiles in the well (Section 7.10), and also internal flows suppressed during injection can start flowing again (Section 7.8). To avoid these issues and obtain meaningful PTA results, it is necessary to capture pressure transients between two non-zero injection rates, both during the 'build-ups' after increases in flow rate and also during fall-offs after decreases in flow rate.

Pressure transients captured during injection into the well require not only a detailed and accurate flow log but also good flow control to keep the flow rate constant. Some noise in the flow data can be managed and is inevitable; however, drift in the flow rate (Fig. 7.19) when it is supposed to be constant will hinder analysis. Good flow control is clearly a critical element of the well test and when it is recognised as such, there is no practical reason that a good test with constant rates and fast flow changes cannot be achieved.

Personnel on site during a pumping operation must also ensure that air is not being sucked into the pump, which can happen when there is insufficient head (pressure) at the pump inlet, for example if the water level in the tank drops too low or the pump inlet is not set deep enough into a river or storage pond. Air in the water will cause

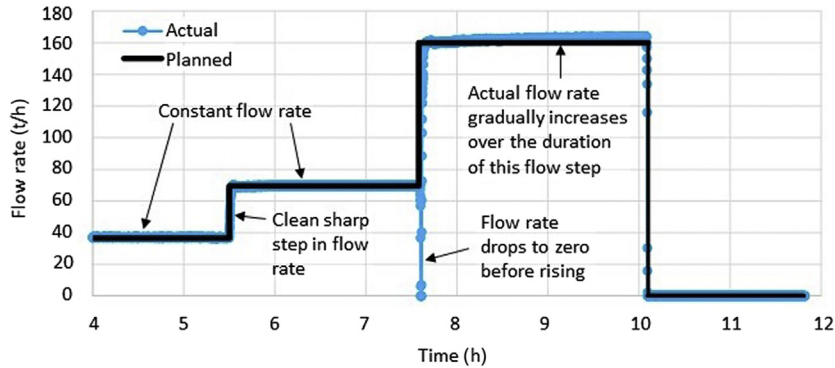


Figure 7.19 Example of actual flow rate versus planned flow rate, showing examples of good flow control at lower flow rates and poor flow control at higher flow rate. Data with kind permission from Contact Energy Ltd.

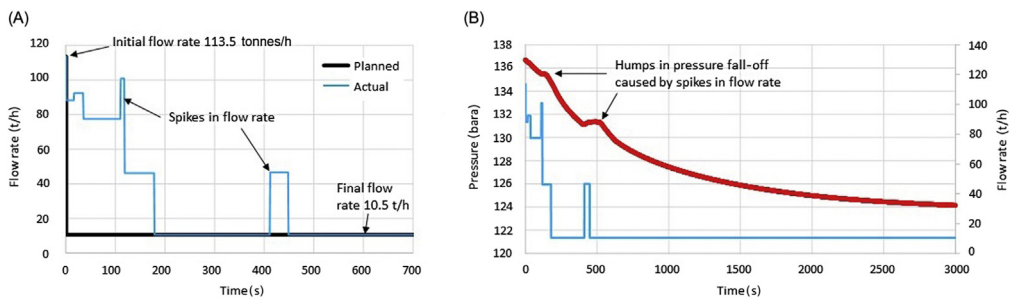


Figure 7.20 Example of poor flow control during a fall-off: (A) planned single step flow change from 113.5 to 10.5 tonnes/h compared to messy actual flow and (B) anomalous pressure fall-off data showing correlation between anomalies and spikes in flow rate. Data with kind permission from Contact Energy Ltd.

long-term damage to the pump (cavitation) and can also render the pressure transients useless. Air in the injected water means two things: the measured fluid flow (injection) rate will be inaccurate, but also that compressible air down in the wellbore will affect the pressure and so the measured pressure fall-off will be distorted, resulting in a more rapid pressure fall-off and higher permeability estimates. It is difficult to observe and isolate this effect on the PTA data once it takes place. Therefore care should be taken to make sure that it does not happen in the first place.

Fig. 7.20 shows an example of poor flow control during a fall-off test. It clearly demonstrates that a clean flow step is necessary to produce a smooth transient, and that an accurate and frequent flow log is necessary to identify deviations in the actual flow rate from the planned flow rate. Without the good flow log in the Fig. 7.20 example, which easily explains the anomalies in the pressure fall-off, time could have been wasted in attempting to explain these as wellbore or reservoir effects.

7.8 Internal flow between feed zones

It is typical for geothermal wells to have permeable feed zones along the length of the open hole, which can be identified during completion testing (Chapter 6: Completion and Output Testing). In some cases, when these different permeable levels in the reservoir are connected via the wellbore, a feed zone at a higher pressure will spontaneously flow through the wellbore and into a feed zone at a lower pressure, even when the well is shut in at the surface. This is particularly common in developed reservoirs where pressure drawdown due to production at deep reservoir levels encourages internal flow downwards (downflows) from feed zones above.

These downflows are sometimes very strong and cannot be suppressed even at maximum injection rates. They are apparent as isothermal sections in temperature logs and also can be seen in fluid velocity profiles. Wells with very strong downflows make PTA impossible, though the good news is that they are very permeable and can make good production or injection wells.

Some downflows are weak and are not seen during completion testing, as the injection rates used are sufficient to suppress the downflow. However, these downflows start up again when injection stops, and if a downflow starts up during a pressure fall-off, it will distort the data set. This is a good reason not to design a well test with a fall-off to zero flow, instead pressure transients should be measured due to steps between two non-zero injection rates (increasing or decreasing). Other good reasons to avoid pressure fall-offs to zero flow include the effects of pivoting (Section 7.10) and thermal expansion of the wireline (Section 7.9).

Downflows appear in the history plot of a fall-off as a slowing down of the pressure decline (Fig. 7.21A) as the flow becomes nonzero within the well. This appears in the derivative plot (Fig. 7.21B) as a dip in the derivative. This effect is less obvious when it occurs earlier in the test, when it can be partially masked by wellbore storage

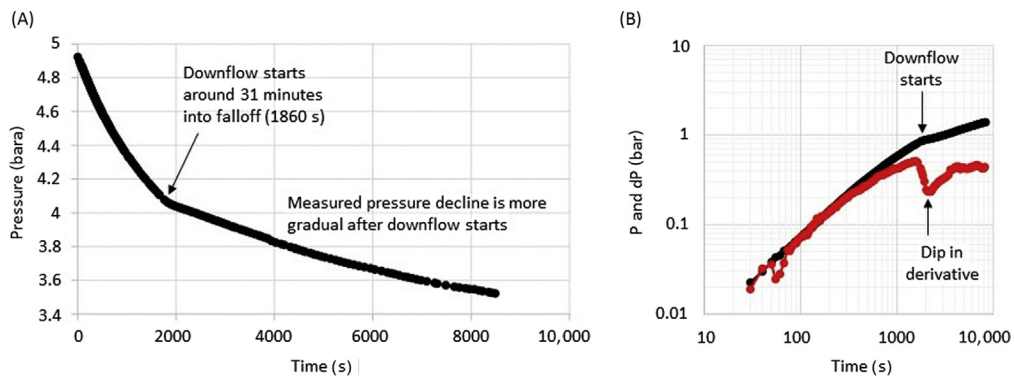


Figure 7.21 Example of downflow starting during a fall-off in a shallow well: (A) history plot and (B) derivative plot. *Data with kind permission from Contact Energy Ltd.*

(McLean and Zarrouk, 2015a). Conversely, it is more obvious when it occurs later in the fall-off test, when it can easily cause the pressure to start increasing in late-time (when it should be decreasing), which causes the derivative to become negative (McLean and Zarrouk, 2015a).

7.9 Thermal expansion of wireline of downhole tools

The length of a wireline (slick-line or e-line) at the surface is not equal to its length when it is downhole. Elongation of the wireline has several components: thermal expansion of the metal due to high temperatures; elastic stretch from weight on the wireline both from the tool and the weight of the wireline itself; and elastic stretch due to force on the tool due to the movement of fluid in the well. The consequence of this is that the 'measured depth' recorded during wireline operations is only an indication of the actual depth in the well. For most practical purposes, the measured depth is sufficient, but in some cases, these variations in depth become significant, for example when perforating the casing or for PTA.

Calculating the actual depth of the tool in the well with high accuracy would require some impossibilities: the temperature profile in the entire well at all times (the downhole tool effectively measures only the temperature at the end of the wireline) and the velocity of fluid at all depths in the well at all times. In addition, the elongation of the wireline changes with depth as the weight of wireline present in the well changes. Also, the rate of elastic stretching and thermal expansion must be accounted for, as the wireline will not be at equilibrium at all times. Any calculation of actual depth would be the result of a complex modelling process and therefore still only an estimate.

Some idea of the general magnitude of the elongation of the wireline comes anecdotally from geothermal wireline operators. It is usual to design a logging programme so that the deepest measured depth is 20 m above the total depth (TD) of the well in order to prevent the tool at the end of the wireline (which is really longer than the measured depth indicated at the surface) from bumping into the bottom of the well. When removing a slick-line from a deep hot geothermal well, it is not unusual for it to be several meters (up to ~ 10 m) longer than when it went in, and this effect is less for e-line. During shut (static) PTS runs the pressure profile measured while the tool is moving down (shorter colder wireline, less time exposed to hot conditions in the well) is often offset by up to 1 bar from the pressure profile when the tool is moving up (longer hotter wireline, more time exposed to heat in the well). An offset of +1 bar is approximately equivalent to the tool being 10 m deeper, depending on the density of fluid at that depth.

The good news for pressure transients is that only *changes* in elongation of the wireline over the duration of the pressure transient are relevant, as these effectively

represent drift in the pressure gauge as the tool moves deeper (even while the wireline and tool appear stationary at the surface). While capturing a pressure transient, the tool does not move and the injection rate does not change, and so the only potential change to the elongation of the wireline comes from thermal expansion, if the temperature profile in the well is changing. There will be relatively small changes in temperature profile in the well as injection rates change, and the major change occurs when injection stops and the well begins to heat up.

For pressure fall-off tests to zero flow, there is often a significant change in temperature profile over the length of the wireline as the well heats up (Fig. 7.22), which will cause thermal expansion. The impact of this thermal expansion on a pressure transient depends on its magnitude (greater for deep wells with rapid heating), and its relative magnitude compared to the reservoir response. A ‘larger’ reservoir response (impermeable well will have a greater pressure change ΔP during the test) which may render the wireline expansion insignificant, while it may be significant in the case of a ‘smaller’ reservoir response (very permeable well with small pressure change).

The expansion of the wireline is effectively a form of gauge drift, which theoretically can be removed from the original data set prior to PTA. In practice, this is difficult as the linear coefficient of thermal expansion (α_L) must be known for that particular wireline, and these are not always available. This is theoretically easier for slick-lines, which are a single strand of solid stainless steel, but the value of α_L depends on the exact type (chemical composition and crystalline structure). A typical slick-line suitable for the corrosive conditions in geothermal wells is the Sandvik SAF 2507 which is a duplex stainless steel, with austenitic and ferritic crystalline structure, containing chromium, nickel and molybdenum, with an average value of $\alpha_L = 14.0 \times 10^{-6}/^\circ\text{C}$ in the temperature range relevant to geothermal reservoirs (30°C – 300°C) (Sandvik, 2018).

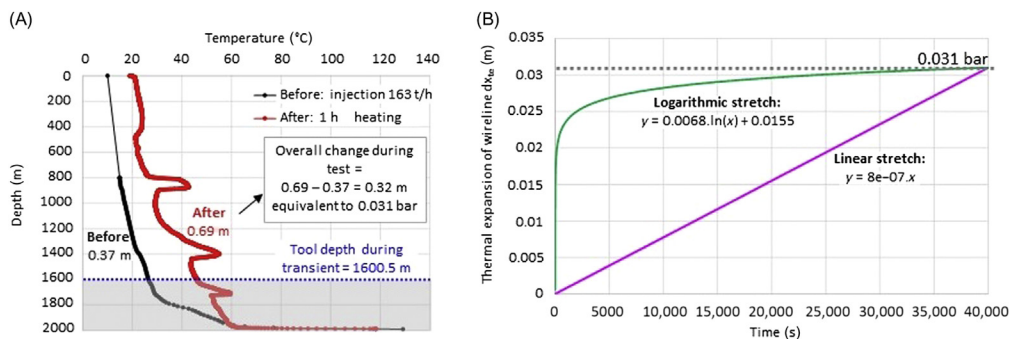


Figure 7.22 (A) Temperature profiles used to assess overall change in thermal expansion of wireline during a pressure transient in a Tauhara well (B) Linear and logarithmic models for the time-dependence of the thermal expansion, each resulting in a final pressure difference of 0.031 bar. (A) Data with kind permission from Contact Energy Ltd.

On the other hand, e-lines are a type of wire rope, and typical geothermal e-lines are made of galvanised improved plow steel which is a type of carbon steel, despite issues with hydrogen embrittlement. E-lines have a complex structure usually with two layers of steel wires forming a sheath (armour) which protects a core of insulated conductive copper wires, which transmits electrical signals to the surface. The complex structure may be the reason for the lack of available α_L values.

Another practical difficulty is the time-dependence of the change in temperature profile and the equilibrium between the wireline length and the temperature profile. Despite these challenges, it is still useful to estimate the thermal expansion using a few assumptions, in order to assess whether this effect has a significant impact on the shape of the pressure derivative and then remove this drift from the data set if necessary.

Temperature profiles measured at the start and finish of a pressure-transient data set (Fig. 7.22A) can theoretically be used to estimate the change in thermal expansion of the wireline over this time. The change in length of an interval x along the wireline (relative to a temperature of 0°C) is given by Eq. (7.1). The sum of all these changes along the entire length of the wireline will give the total change in length due to thermal expansion.

$$dx_{te} = \alpha_L \cdot x \cdot T_{av} \quad (7.1)$$

where dx_{te} is the change in length of wireline due to thermal expansion (m), α_L is the linear thermal expansion coefficient ($1/^\circ\text{C}$), x is the depth interval between downhole data points (m) and T_{av} is the average temperature over this interval ($^\circ\text{C}$).

For the example in Fig. 7.22 the total thermal expansion has been assessed using Eq. 7.1, using the temperature profiles measured immediately before – and after – the pressure transient. Only the temperature profiles above the transient tool depth are relevant, as these are the temperatures the wireline is exposed to. The change in wireline length due to thermal expansion over the duration of the pressure-transient test is $0.69 - 0.37 = 0.32$ m. This change in depth converts to a change in pressure of 0.031 bar by using the density of fluid at the tool depth (994 kg/m^3). This sounds like a small number, but the impact is significant when applied to a simulated fall-off data set in a

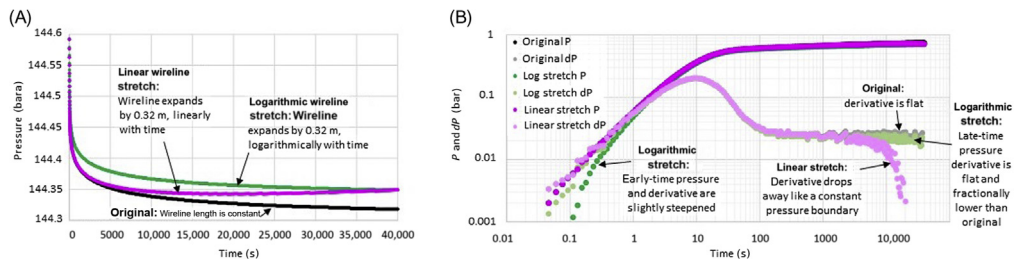


Figure 7.23 Modelling of the impact of wireline thermal expansion on a fall-off test in a permeable well, using the linear and logarithmic models in B: (A) history plot and (B) derivative plot. *From Contact Energy Ltd. with kind permission.*

permeable well ($200 \times 10^{-15} \text{m}^2$) (Fig. 7.23). If the tool deepens linearly during the test, the fall-off flattens and then rises slightly (Fig. 7.23A) and is very apparent in the pressure derivative which declines rapidly in late time (Fig. 7.23B) in a manner resembling a constant pressure boundary response (Section 5.1.2). The effect is much more subtle if the tool deepens logarithmically during the test, producing only a very minor distortion of the early-time section of the derivative plot (Fig. 7.23B), and no noticeable effect on the derivative in late time or in the history plot (Fig. 7.23A). Clearly, the shape of the function describing the wireline expansion with time has a major impact on the appearance and severity of this artefact in the history and derivative plots. The effect is very apparent when significant wireline expansion is occurring relatively late in the data set and could be missed completely when most of the wireline expansion occurs earlier.

In summary, the thermal expansion of the wireline is difficult to assess and model; however, if this is done carefully and assumptions are justified then the drift in the pressure-transient data set can be removed prior to PTA. The good news is that effects of thermal expansion on the pressure-transient data set can be easily minimised/avoided by avoiding fall-offs to zero flow. It is only when injection into the well ceases that significant heating (and hence wireline expansion) will take place. This does not occur during injection pressure transients (increasing injection rate) or for fall-offs to a lower injection rate (instead of zero flow). By maintaining injection, albeit at a different rate, the temperature profile in the well remains similar (relative to the very large temperature differences possible during heatup), and wireline stretch is minimised along with the effects of pivoting (Section 7.10) and internal flow (Section 7.8). This is also a good reason to start injecting cold water into the well for as long as possible (at the first planned flow rate) prior to commencing the official completion testing program.

7.10 Expansion/contraction of fluid column during heating/cooling

In a permeable well the water level is often below the master valve, and the fluid column inside the well expands during heating (Fig. 7.24A) and contracts during cooling due to injection, simply as a result of the changing temperature and therefore density of the fluid column. In permeable wells there is a good connection to the reservoir and this results in pivoting of the pressure profiles around the pressure control point (PCP) (Section 6.3) (Fig. 7.24B). This effect is confined within the wellbore and is not representative of conditions in the reservoir beyond the well. This effect will only be present during fall-off tests (the most common type of geothermal well test), it will not be significant during injection tests, drawdown tests, or build-up tests, as there is no heating of the fluid column during these tests. The effect can be minimised by avoiding fall-offs to zero flow, and instead performing fall-offs between two non-zero injection rates, which minimises the change to the temperature profile of the well, avoiding not only pivoting but thermal expansion of the wireline (Section 7.9) and some internal flows (Section 7.8).

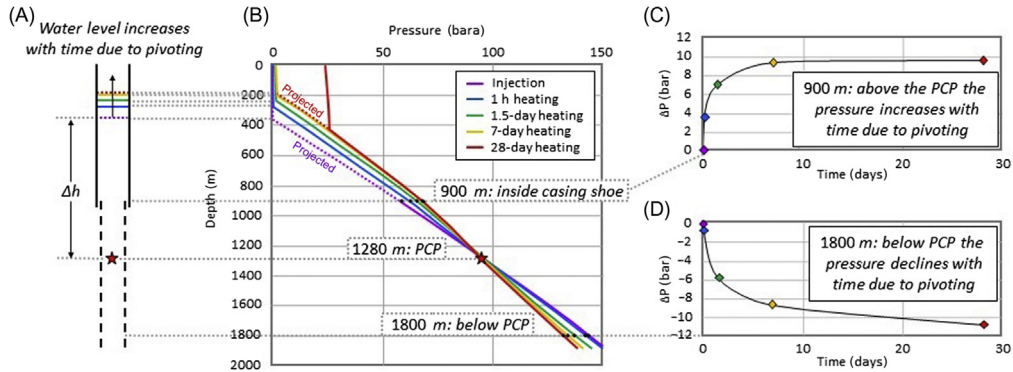


Figure 7.24 Schematic demonstrating the effect of pivoting on the pressure measured at a particular depth, using a real set of heatup profiles: (A) well schematic showing increase in water level during heatup, (B) pressure profiles showing pivoting around the PCP (1280 m) over a 28-day period, (C) pressure change versus time as measured above the PCP at the casing shoe (tool depth = 900 m) and (D) pressure change versus time as measured below the PCP (tool depth = 1800 m). *PCP*, Pressure control point. *Data with kind permission from Contact Energy Ltd.*

If a downhole tool is stationed at the PCP during a fall-off test then the pressure change due to pivoting will be zero, and so the pressure change measured in this location will be the response of the reservoir. However, if the downhole tool is not at the PCP then the measurement will be a combination of the pivoting effect and the reservoir response. It is relatively common to position the downhole tool at the casing shoe if the liner has not yet been installed to eliminate the risk of losing the tool due to formation collapse (e.g. during stage testing). In this scenario the downhole tool will be above the PCP and the pivoting will result in an increase in pressure with time (Fig. 7.24C). If the tool is stationed below the PCP, for example at a deeper minor feed zone, the pivoting will result in a decrease in pressure with time (Fig. 7.24D).

The magnitude of the pivoting effect can be significant, for example it can be seen in Fig. 7.24C that at the casing shoe after 1 hour heating, ΔP due to pivoting will be 3.7 bar, and in Fig. 7.24D near the bottom of the well it will be -0.6 bar. The exact magnitude of the pivoting effect depends on the distance from the PCP, the greater the distance, the greater the magnitude. The rate of heating is also important as slow heating means the effect will be less noticeable over the typical duration of a well test. The overall temperature differential is also important because without a temperature difference there will be no heating, no density change and no pivoting.

The effect of this pressure pivoting on the history and derivative plot are shown in Fig. 7.25 (for the downhole tool positioned above and below the PCP at 900 and 1800 m as in Fig. 7.24C and D), assuming the pressure change due to pivoting is linear with time over the duration of the test. It is necessary to make this assumption as it is not possible to measure heatup profiles during a fall-off without disturbing the fall-off data set (Section 6.2.1). While the relationship is likely to be more complex than a

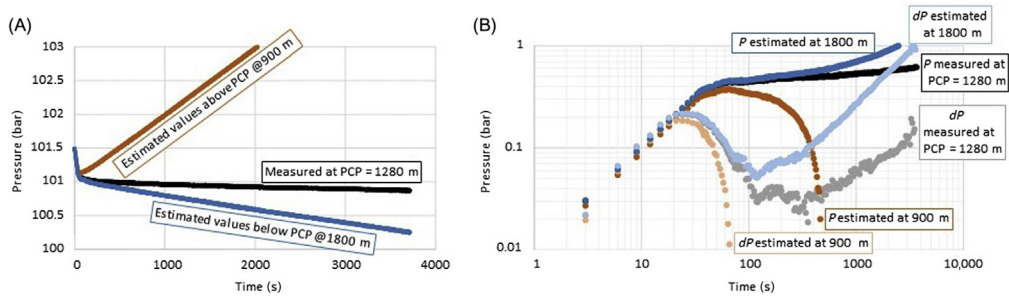


Figure 7.25 Demonstration of the effect of pivoting on the pressure-transient data, showing actual measured fall-off data at the PCP (= 1280 m) and also the estimated shape of the falloff as if measured above the PCP at 900 m and below the PCP at 1800 m, assuming the ΔP due to pivoting is linear with time: (A) history plot and (B) derivative plot. PCP, Pressure control point. From *Contact Energy Ltd. with kind permission*.

simple linear relationship, the lack of data precludes a more complex model, and the results (Fig. 7.25) provide a useful estimate of the likely magnitude of the effect, even if the shape is likely to differ slightly in reality.

During a fall-off test, positioning the downhole tool above the PCP causes the pressure to rise in the history plot when it should be decreasing (Fig. 7.25A), which in the derivative plot means the pressure and derivative become negative and drop away (Fig. 7.25B), resembling a constant pressure boundary. The effect of positioning the downhole tool below the PCP in the history plot is the pressure decreases more than it should (Fig. 7.25A), which in the derivative plot means the pressure and derivative bend upwards (Fig. 7.25B), in this case giving the appearance of a closed boundary (approximately unit-slope derivative in late time). The actual measured data with the tool at the PCP has the appearance of a channel boundary (~ 0.5 unit-slope derivative in late time). Therefore care must be taken to avoid confusing the effect of pivoting above the PCP with constant pressure boundary effects (Section 5.1.2) and the effect of pivoting below the PCP with impermeable boundary effects (Section 5.1.1).

This example represents an extreme case of distortion of the pressure-transient data by pivoting, as this well is very permeable and so the magnitude (overall ΔP) of the reservoir response during the test is only ~ 0.6 bar (Fig. 7.25A) which is small and easily overwhelmed by the ΔP due to pivoting. The high permeability and also the high temperature mean the well heats up fast and so the pivoting effect is significant over the duration of the test even though it is only ~ 1 hour. It can be expected that the effect of pivoting on other data sets can be more subtle than this example.

The good news is that this pivoting artefact in the data can be completely avoided by locating the downhole tool at the PCP. The bad news is that the location of the PCP is not always known at the time of testing. However, in practice, it is often possible to locate the tool at (or very close to) the PCP by interpreting the major feed zone in the well during the completion test (Chapter 6: Completion and Output

Testing), though the apparent major feed zone does not always correspond with the PCP, and in some cases, there is more than one major feed. The only definitive method to locate the PCP is heatup runs over several weeks. For a new well the pressure transient will be measured prior to the heatup runs, during the completion test, and some offset between the downhole tool and the PCP is common. However, for any later pressure transients (injection or production) measured after the heatup runs, the tool can and should be located at the PCP.

While it is possible to estimate the effect of pivoting using the pressure profiles before and after the pressure transient, an assumption of the relationship between the pivoting ΔP and time must be made. This assumed relationship can be used to estimate and remove the effect of pivoting from the data prior to PTA; however, the 'corrected' data set and results of PTA then rely on that assumption. While in some cases this may be the only alternative, it is highly desirable to avoid this process by correctly positioning the downhole tool. For some very important wells, it may be justified to retest the well after the PCP has been located, if there is a large discrepancy between tool depth and PCP and the magnitude of the pivoting effect is estimated to be significant, particularly if identification of boundaries is an important objective of the well test.

7.11 Boiling and two-phase effects inside the casing of steam wells

Dry steam wells are generally difficult to test especially high-temperature permeable wells, because of the two-phase effects taking place in the wellbore and the near-wellbore reservoir. Some wells will have internal circulation and boiling at multiple points in the well during injection (Fig. 7.26). Fig. 7.26 shows the water level under injection is 710 m below casing head flange (CHF) with an unusually nonlinear pressure profile indicating internal circulations inside the casing at multiple depths.

Fig. 7.27 shows the transient temperature and pressure measured downhole during injection of first 25 L/s and then 35 L/s when the PTS tool was located at 1090 m. Fig. 7.28 shows the transient temperature and pressure during injection of 45 and 60 L/s for the same tool depth. Note that the intensity of internal circulations changes with the cold water injection rate. The cold water causes condensation of the shallow steam zones, which results in a pressure drop, allowing the other feed zones to kick in, causing the cycling effect in Figs 7.27 and 7.28. Note that this undesirable behaviour helps identify all the feed zones as shown in Fig. 7.26.

The temperature and pressure behaviours of Figs 7.27 and 7.28 are common when the PTS tool is placed above most of the feed zones. This problem can be resolved by quenching the well for a few days and placing the PTS tool deeper into the well.

The final warmed up temperature and pressure profiles of this well are given in Fig. 7.29. Fig. 7.29 shows that there are four distanced zones; the first zone (0–730 m) is a gas column, which can be identified from the cooler temperature

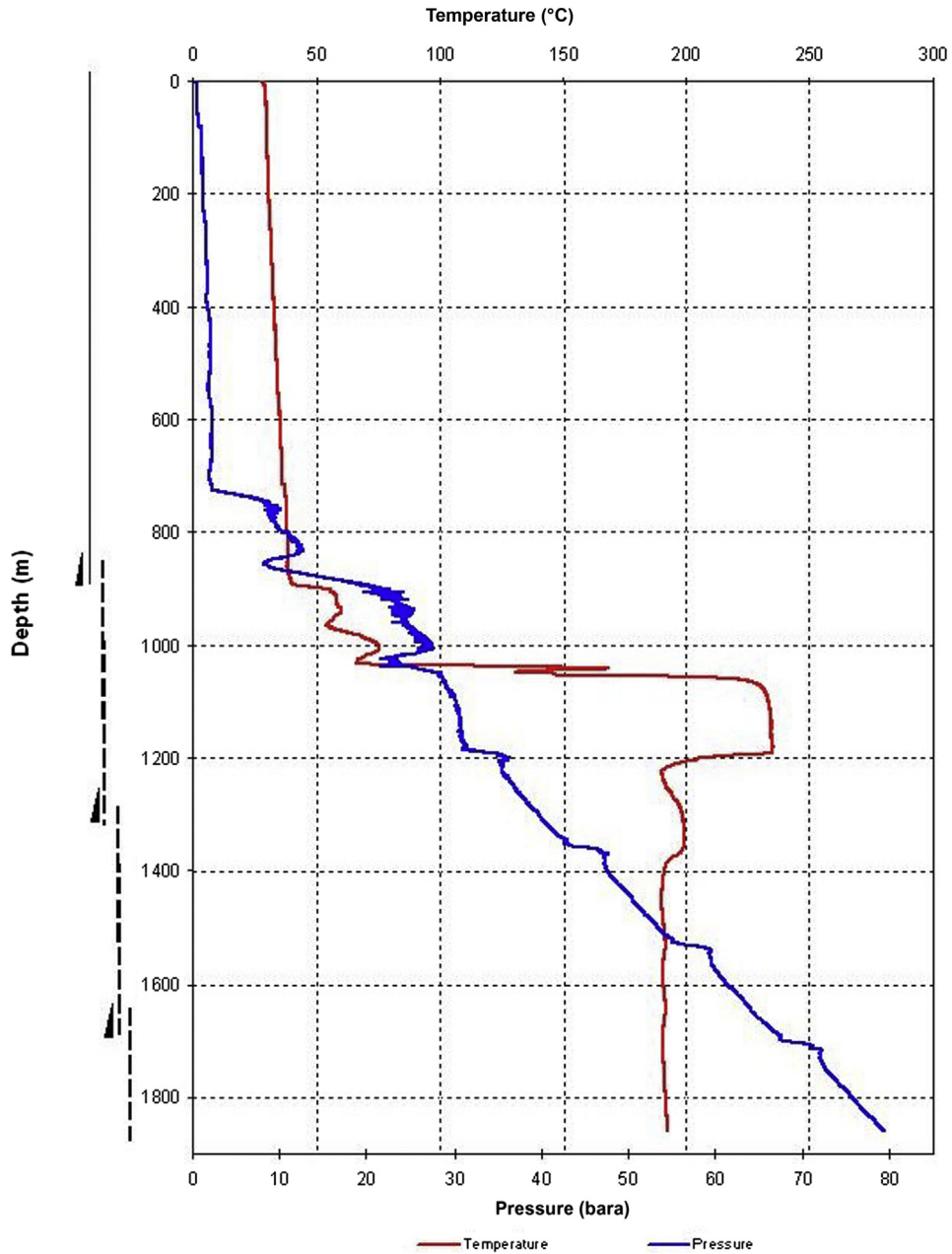


Figure 7.26 Temperature and pressure profiles under injection. From Mr. Mulyadi, Star Energy, with kind permission.

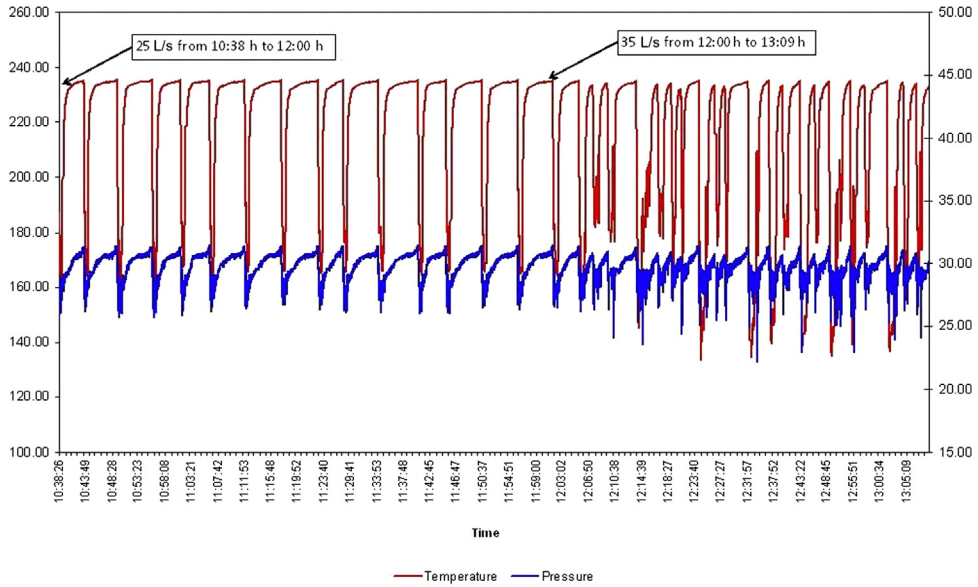


Figure 7.27 Temperature and pressure profiles at 1090 m depth during injection rates 25 and 35 L/s. From Mr. Mulyadi, Star Energy, with kind permission.

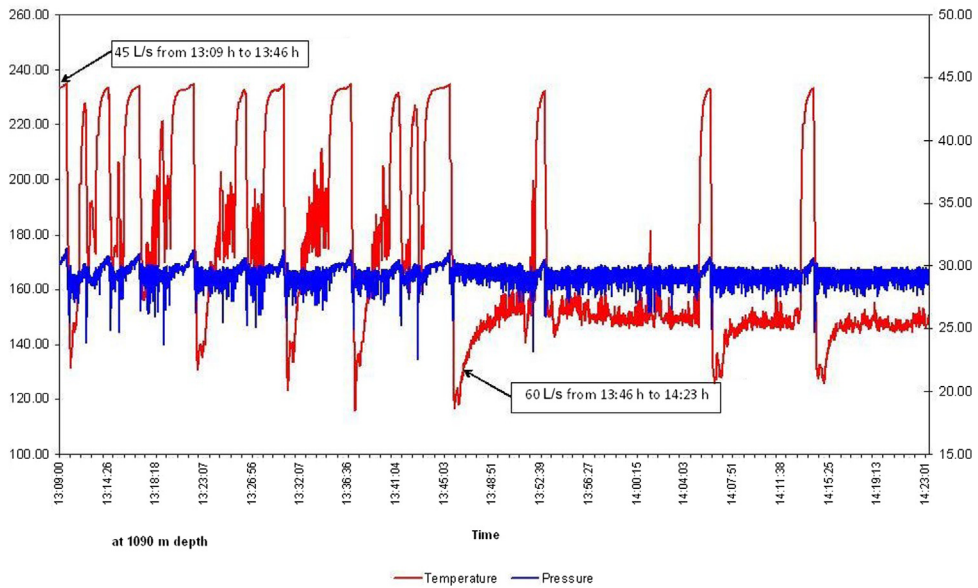


Figure 7.28 Temperature and pressure profiles at 1090 m depth during injection rates 45 60 L/s. From Mr. Mulyadi, Star Energy, with kind permission.

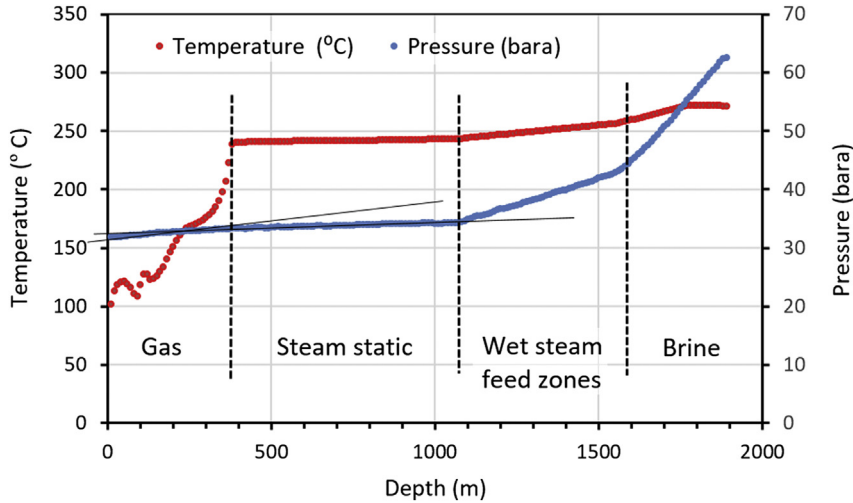


Figure 7.29 Fully heated up shut-in pressure and temperature profiles of the well. *From Mr. Mulyadi, Star Energy, with kind permission.*

profile and relatively high-pressure gradient than the lower zone. The second zone (730–1080 m) is a static steam zone with temperatures corresponding to the saturation pressure. The third zone (1080–1585 m) is a wet steam zone with higher pressure gradient than the saturated steam static but still at saturation temperatures for the given pressures. The final and fourth zone (1585 m to TD) is a liquid (brine) with temperatures at or below the liquid water saturation pressures.

The output testing of dry steam wells or almost dry (> 2600 kJ/kg) wells are generally carried out using a single-phase orifice plate into a rock muffler or a silencer to measure the mass flow rate and enthalpy.

7.12 Reservoir boundary in enhanced geothermal system wells

In recent years injection fall-off tests have been performed in low-permeability deep (> 3000 m) EGS wells with no free gas content. If the well maintains a high WHP long after the injection has stopped, and if the WHP is measured/sampled at high frequency (every second or less) using a sensitive digital pressure transducer then it is possible to observe an oscillating pressure response immediately after injection stops, and the testing wellhead valve is suddenly shut (Fig. 7.30). The pressure behaviour of Fig. 7.30B is consistent with a water hammer effect, where the pressure wave travels at the speed of sound in water to the end of the reservoir and back multiple times until full attenuation. This phenomena only lasts for 2–3 minutes and does not have much effect on the long-term PTA data, but can possibly be used to estimate the distance to the reservoir boundaries from the time taken to reach this boundary and knowing the speed of sound in water (~ 1500 m/s). It is important to note that the

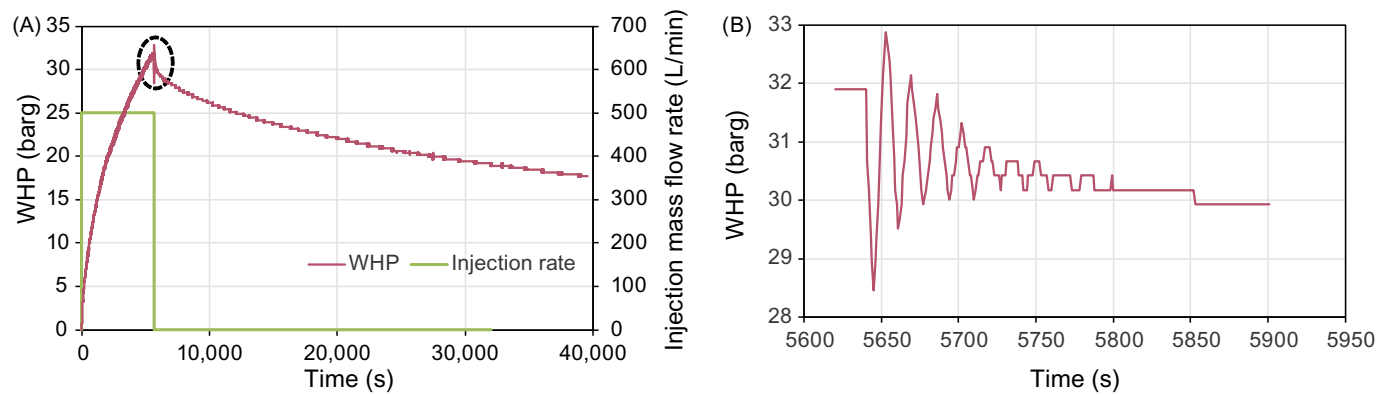


Figure 7.30 (A) Schematic of injection fall-off test. (B) Oscillating pressure response after injection valve closure. *Data from VITO, with kind permission.*

speed of sound in water is a function of water temperature, pressure and salinity (concentration of dissolved NaCl). The pressure increase after the valve shut-in is also a function of valve closure time and initial injection fluid velocity. The speed of sound in the wellbore water can be estimated, but the speed of sound in the water-saturated porous or fractured reservoir rock is different. Further work is needed to investigate the prospect of utilising such data in PTA.

7.13 Pressure drop inside a flowing geothermal well

Quantifying the pressure drop inside geothermal wells as the fluid moves up the casing to the surface is very important. This is to understand whether the fluid flow emerging from the wellhead is reservoir-controlled or wellbore-controlled, when there is no reliable well test data (e.g. injectivity index I and transmissivity kh), which is common in many cases.

Geothermal wells with reservoir pressure higher than the hydrostatic head of cold water (Llanos et al., 2015) will always flow by themselves when opened (self-discharging). Dry steam wells also always flow even when the reservoir pressure is much lower than the local hydrostatic head as explained in Chapter 6, Completion and Output Testing.

The pressure drop inside the wellbore is the difference between reservoir pressure and WHP:

$$\text{WHP} = P_{\text{res}} - \Delta P_{\text{well}} \quad (7.2)$$

where P_{res} is the measured reservoir pressure and P_{well} is the pressure drop inside the well (casing and liner) from the feed zone to the wellhead.

7.13.1 Single-phase fluid

For geothermal wells producing single-phase (liquid or steam) flow, the pressure drop comes from two components, which are friction and gravity:

$$P_{\text{well}} = \Delta P_f + \Delta P_g \quad (7.3)$$

where ΔP_g is the pressure drop due to gravity and ΔP_f is pressure drop due to friction in a pipe:

$$\Delta P_g = \rho g L \quad (7.4)$$

$$\Delta P_f = f \frac{L \rho v^2}{D} \quad (7.5)$$

where ρ is the density of the fluid (kg/m^3), g is the gravitational acceleration (9.81 m/s^2), L is length of the casing (m), v is the average fluid velocity (m/s), D is the internal diameter (m) and f is the friction factor (dimensionless).

It is clear from Eq. (7.4) that the gravitational pressure drop is much higher for liquid than steam. Eq. (7.5) indicates that the fluid velocity dominates the friction pressure drop, and from experience, steam velocity should be <40 m/s and liquid velocity should be <5 m/s to maintain realistic (manageable) pressure drop.

The friction factor (f) can be calculated from the Moody diagram (chart) using the Reynolds number ($Re = \rho Dv/\mu$) and the effective roughness (ε/D), where μ is the dynamic viscosity of the fluid (kg/m s) and ε is the casing roughness height or absolute roughness (mm). The Moody diagram covers all types of single-phase flow regimes: laminar, transitional and completely turbulent flows (Dougherty et al. 1985).

When the Moody diagram is not available and for a standard casing size ($9\frac{5}{8}$ " geothermal well ($\varepsilon/D = 0.0002$) use the Colebrook equation ($3000 < Re < 2 \times 10^8$):

$$\frac{1}{\sqrt{f}} = -2 \log \left(\frac{\varepsilon/D}{3.7} + \frac{2.51}{Re\sqrt{f}} \right) \quad (7.6)$$

Note that we do not recommend using the explicit Haaland equation (Dougherty et al. 1985) for calculating the friction factor since it is not very accurate.

The Karman equation ($Re > 2 \times 10^8$) is as follows:

$$f = \frac{1}{[2 \log(D/\varepsilon) + 1.14]^2} \quad (7.7)$$

Note that having $Re > 2 \times 10^8$ requires very high and unrealistic velocities; therefore only the Colebrook equation Eq. (7.6) should be of use. However, the implicit Colebrook equation should be solved iteratively to obtain the friction factor (f).

Note that the casing will have at least two different sections (production casing and perforated liner), each with a different internal diameter. While the roughness height (ε) of the casing is similar to that in commercial steam pipelines (0.046 mm), it is different in the perforated liner, which has undergone machining or gas cutting to make the perforations (holes), and also, through this section the fluid could flow in the annulus between the perforated liner and open hole. Experience has shown that a roughness height of ($\varepsilon = 0.138$ mm) could be used for the perforated liner.

In rare cases of self-discharging warm and hot water wells producing very low velocity laminar flow ($Re < 3000$), normally at very low (near atmospheric) WHP, the friction factor becomes (Dougherty et al., 1985):

$$f = \frac{64}{Re} \quad (7.8)$$

7.13.2 Two-phase fluid

Geothermal wells producing from two-phase reservoirs have a much more complicated pressure drop. The reservoir pressure is commonly lower than the hydrostatic

head of water, but the flashing of the geothermal fluid into steam and water drives the flow inside the well to the surface. The low density (high specific volume) of steam results in significant volumetric expansion that results in a drop in the density of the steam–water mixture, which drives the flow from the well. The average (steam–water) velocity inside the well will increase with the drop in pressure as the fluid travels up the well. Three pressure drop components will form during two-phase flow in the wellbore (Watson, 2013); these components are friction, acceleration and gravity:

$$\frac{dP}{dz} = \left(\frac{dP}{dz}\right)_{\text{fric}} + \left(\frac{dP}{dz}\right)_{\text{accel}} + \left(\frac{dP}{dz}\right)_{\text{grav}} \quad (7.9)$$

All these three pressure drop components act against the reservoir pressure. The acceleration (momentum) pressure drop is a result of the increase in the fluid (steam and water) velocity after the flash point, which increases as the fluid travels to the surface (wellhead). The friction component also increases with the fluid velocity and hence increases towards the wellhead. While the gravitational pressure drop starts as the dominant component below the flash point then reduces from the flash point upwards as the average density of the two-phase fluid reduces.

It is important to note that in some rare cases the two-phase flow up through the geothermal well is not driven by boiling or flashing, but simply by gas lifting due to the high gas (CO₂) content. Watson (2013) provided a good example of these wells, which discharge intermittently (cycle) in their output.

Depending on the fluid dryness fraction, several two-phase flow regimes (patterns) can form (Fig. 7.31) inside the wellbore; each flow regime will have a different pressure drop component for friction, acceleration and gravity. There are hosts of empirical, phenomenological and analytical correlations that have been developed by different authors for handling these pressure components. Discussing these correlations

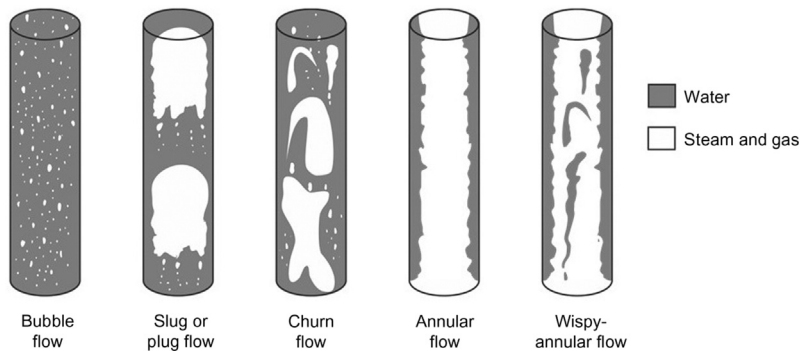


Figure 7.31 Two-phase flow regimes in a vertical upward flow in geothermal wells. After Butterworth, D., Hewitt, G.F., 1978. *Two-phase flow and heat transfer*. In: *Harwell Series*. Oxford University Press.

is outside the scope of this book. Therefore pressure drop calculations are commonly carried out using wellbore simulators to estimate the pressure drop inside the wellbore and the contribution of each pressure component from the bottom up, if the reservoir conditions are known, to estimate the wellhead conditions (WHP, temperature and enthalpy). If the wellhead conditions are known, the wellbore simulator can be used to estimate reservoir conditions (e.g. enthalpy, temperature and flowing pressure). Some wellbore simulators have a coupled reservoir simulator, which can be used to predict the mass flow rate the well can produce. Other simulators simply model the wellbore flow only. Some wellbore simulators can handle high gas (CO_2) content, deviated well profiles and multiple (more than two) casing sizes, with the provision for heat loss from the casing to the surrounding rock formation, while other simulators are much simpler, treating the geothermal fluid as pure water and can only simulate flow in vertical wells.

It is difficult to observe and distinguish between the different two-phase flows regimes of Fig. 7.31 during well testing or when the well is on production. However, slug/plug and to a lesser extent churn flows will result in significant vibration and periodic shake on the two-phase pipelines and result in much higher pressure drop. It can be felt by simply placing the hand on the pipe, but wellbore simulators are the best tool to predict flow regime. Note that there are similar two-phase flow regimes for geothermal fluid flowing in horizontal (steam-field) pipelines at the ground surface. While there will be no gravitational component, the pressure drop calculations are more complicated as flow regimes are highly affected by the pipeline diameter (Rizaldy and Zarrouk, 2016). Discussing this further is outside the scope of this book.

For example, a geothermal well with 1000 m TD, 9 $\frac{5}{8}$ " production casing 500 m deep, and 7" perforated liner from 500 m to TD. The well produces 50 kg/s from a 280°C and 65 bar liquid feed zone at TD. Using the simulator by Brennand and Watson (1987), we can get the temperature, pressure and dryness fraction profile inside the wellbore as the fluid travels to the surface (Fig. 7.32A). Since no heat loss was considered, there is only 12 kJ/kg of enthalpy drop from the bottom of the well to the surface. The fluid will arrive at the ground surface at 220°C with a WHP of 23.2 bar with a dryness fraction $x = 0.152$. Knowing the fluid conditions at the wellhead is important when choosing the appropriate power plant technology (binary, single or multiple flash) and for the design of the surface facility to avoid slug flow in the surface pipelines.

Wells with high flowing WHP theoretically allow the use of multiple flash (two or three) plant design. However, in many cases the choice of the geothermal power plant technology is based on commercial and financial considerations.

The pressure drop components are given in Fig. 7.32B, which show the increase in friction and acceleration as the gravitational pressure drops and the fluid travels to the surface. Note that there is a sudden change in pressure at the casing shoe (500 m)

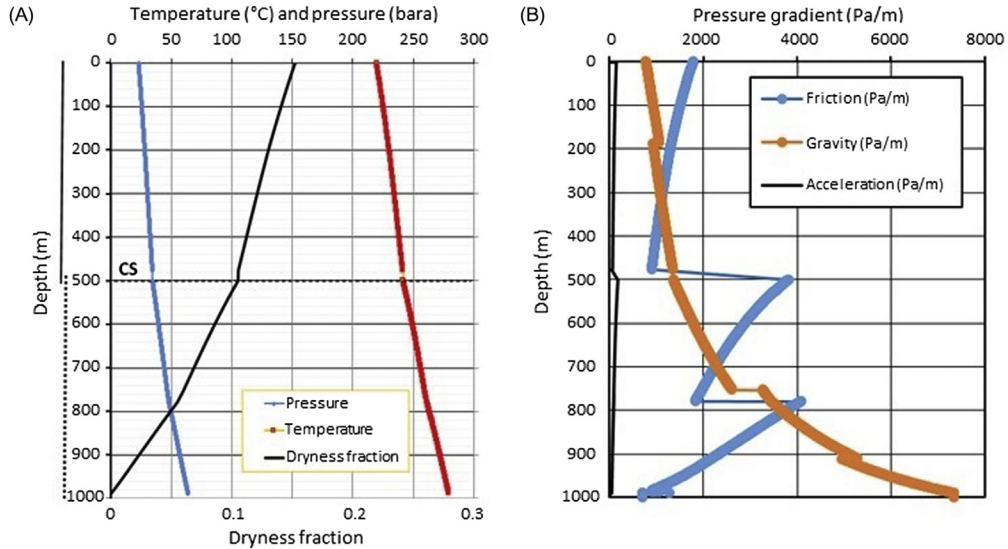


Figure 7.32 (A) Pressure, temperature and dryness fraction. (B) Friction, acceleration and fraction pressure drop components.

when there is a change in casing size from the 7" liner to the larger 9⁵/₈" production casing, also there are changes in pressure drop due to change in flow regime as the simulator switches from one correlation to another.

Wellbore simulators have many applications including:

- Predicting the output curves, prior to testing the well.
- Matching measured output curves to estimate wellbore conditions (friction factor).
- Estimating the reduction in the well output when the well undergoes casing modifications [e.g. running a smaller casing (sleeve) or installing an antiscalant dosing tube].
- Identifying the flashing point/depth for setting antiscalant tubing.
- Modelling/estimating pressure drop inside the casing.

CHAPTER 8

Numerical pressure-transient analysis modelling framework

Contents

8.1	Introduction	193
8.2	Reservoir simulators	194
8.3	Geothermal numerical well-test software	196
8.4	Numerical pressure-transient analysis modelling framework	196
8.4.1	General model setup	197
8.4.2	Well block parameters	199
8.4.3	Fixed radius skin zone	201
8.4.4	Time stepping	201
8.5	Other reservoir and boundary models	202
8.5.1	Linear impermeable boundary	203
8.5.2	Channel boundary	203
8.5.3	Fractional dimension	205
8.6	Injectate temperature effect	206
8.7	Effect of CO ₂ content	208
8.8	Overview of historical geothermal numerical pressure-transient analysis studies	209
8.8.1	Wellbore storage in two-phase reservoirs	209
8.8.2	Developments to dual-porosity model	209
8.8.3	Non-Darcy flow	210
8.8.4	Fractured two-phase reservoirs	211
8.8.5	Stress-sensitive reservoirs	211
8.8.6	Permeability change during injection	211
8.8.7	Production testing using reservoir models	213
8.8.8	Effect of scaling on geothermal pressure-transient analysis	214
8.8.9	Estimating reservoir parameters using temperature and pressure profiles	215

8.1 Introduction

Numerical pressure-transient analysis (PTA) refers to when the PTA model response is calculated using a numerical simulator, with a grid of interconnected blocks, rather than by the analytical solutions to the diffusivity equation discussed in Chapter 4, Introduction to pressure-transient analysis, and Chapter 5, Advanced analytical

pressure–transient analysis relevant to geothermal wells. The numerical PTA model response is then matched to field data using nonlinear regression (NLR) in the same manner as for analytical PTA, to obtain estimated model parameters such as reservoir permeability and skin factor.

Numerical methods are powerful and have the ability to handle issues beyond the reach of analytical (and semianalytical) models (Earlougher, 1977; O’Sullivan et al., 2005; Houzé et al., 2012). Numerical models have been used by both the petroleum and geothermal industries to address complex nonlinear issues such as multiphase systems, injection testing, non-Darcy flow, and complex geometries both within the wider reservoir and at the wellbore (Houzé et al., 2012).

Early use of numerical techniques was in combination with analytical techniques. In some cases, numerical techniques were used to validate an analytical solution. For example, a study of nonisothermal effects by Benson and Bodvarsson (1982) uses a numerical simulator to generate synthetic data against which the applicability of semianalytical techniques is tested (Section 5.8.3). In other cases the agreement of numerical results with analytical solutions was used to validate the use of numerical models for well testing.

Many of the combined analytical–numerical studies are described in Chapter 5, Advanced analytical pressure–transient analysis relevant to geothermal wells. This chapter on numerical PTA focuses on fully numerical studies.

8.2 Reservoir simulators

A numerical simulator is required, and there are various simulators with two-phase fluid modelling capability. These include TOUGH2 (integrated finite difference method) (Pruess, 1991); TETRAD (finite difference method) (Vinsome, 1991); FEHM (control volume finite element method) (Zyvoloski, 2007); and STAR (finite difference method) (Pritchett, 1995), all of which have the ability to handle fluid flow in geothermal reservoirs (O’Sullivan and O’Sullivan, 2016).

Most widely used in the geothermal industry is the simulator TOUGH2 (O’Sullivan and O’Sullivan, 2016). TOUGH2 is accompanied by PyTOUGH, a Python scripting library that can be used to automate all aspects of TOUGH2 simulations including generating grids and input files, running simulations and extraction of results (Croucher, 2011).

The integrated finite difference method (of which TOUGH2 is one example) is a first-order solver method which can be prone to numerical artefacts (dispersion). However, as the well-test modelling grid is a one-dimensional radial grid, a very fine computational mesh can be used when required (Section 8.4.1), which overcomes the effects of numerical dispersion. This ensures that most first-order reservoir simulators (e.g. TOUGH2 and STAR) can provide accurate estimations of reservoir properties.

The TOUGH2 simulator was used to develop the only *numerical* automated well-test analysis system (AWTAS) for geothermal PTA (Section 8.3).

Numerical PTA would theoretically benefit from coupling a wellbore simulator to the reservoir simulator, as a wellbore is not porous media, and a reservoir simulator designed for porous media can only approximate the behaviour of the wellbore. However, there is currently no established wellbore simulator capable of capturing transient behaviour; all readily available wellbore simulators are steady state (O’Sullivan, personal communication, 2018). Also the coupling of wellbore and reservoir simulators is a nontrivial process and the subject of ongoing research.

Reservoir processes are typically long term (hours to decades), and wellbore processes are typically short term (seconds to tens of minutes); however, in the near-well region of the reservoir the response timescales overlap, and coupled simulation is required (da Silva and Jansen, 2015). In a review of coupled reservoir-well simulation, da Silva and Jansen (2015) identify various PTA problems, which require coupled simulation to solve, including wellbore storage and changing skin.

There are a number of approaches to coupled simulation, which will no doubt be enabled in the future by the development of a transient wellbore simulator. The fully implicit method merges the two sets of underlying partial differential equations, which implies rewriting the simulators and is often not practical (da Silva and Jansen, 2015). A more practical approach uses predefined time synchronisation points to swap information between the simulators, and the swapping can be implicit or explicit. Implicit in this case means that at each time step the flow rates and pressures are computed alternately between the two simulators until there is convergence (da Silva and Jansen, 2015). Explicit swapping means the results from the wellbore simulator for the previous time step are used by the reservoir simulator in the current time step, the wellbore simulator in the current time step then uses those reservoir results and so the process repeats (da Silva and Jansen, 2015).

In an early geothermal example, Miller et al. (1982) couple a transient wellbore simulator WELBORE (Miller, 1980) to a version of the reservoir simulator GEOTHNZ (Zyvoloski et al., 1979) to investigate wellbore storage in two-phase water/steam reservoirs (Section 8.8.1), though the method of coupling is not described. Another geothermal example is Murray and Gunn (1993) who investigate indirect coupling of the reservoir simulator TETRAD (Vinsome, 1991) with the wellbore simulator WELLSIM (Gunn and Freeston, 1991) via the simple interface of a wellbore lookup table, which is produced by WELLSIM and used by TETRAD. The method is presented as a viable alternative to direct wellbore–reservoir coupling to improve issues related to efficiency and nonconvergence (Murray and Gunn, 1993).

8.3 Geothermal numerical well-test software

O'Sullivan et al. (2005) developed a *numerical* automated well-test system called AWTAS for geothermal PTA, using the TOUGH2 simulator. It is the first and only geothermal well-test analysis software to be developed and published which calculates the model response numerically rather than analytically. Equivalent *analytical* software is discussed in Section 5.6. The objective of AWTAS was to create something accessible to non-TOUGH2 users, by means of a graphical user interface, with a range of models already set up and with NLR capability. These models included homogeneous porous media, skin, wellbore storage, leaky aquifer, fractional dimension and various other models to represent different reservoir types (O'Sullivan et al., 2005).

AWTAS was never widely utilised as it was developed for a private client, and the user interface was required to be written in a programming language which is now obsolete (O'Sullivan, personal communication, 2014). It is also now considered to have been superseded by the capabilities of PyTOUGH, which automates TOUGH2 (Section 8.2). However, while PyTOUGH is a powerful tool, the advances toward user-friendliness made by AWTAS are lost, in particular the built-in NLR, predefined models and graphical user interface. Although access to AWTAS is limited, it has been used for a small number of academic studies (Khasani and Zarrouk, 2015; Villacorte and O'Sullivan, 2011; Zarrouk et al., 2007).

Ide et al. (2000) mention numerical PTA software preceding AWTAS, associated with a hardware control system for well testing at the New Energy and Industrial Technology Development Organisation in Japan. This software was created for the same reasons as AWTAS, due to the limitations of conventional analytical PTA in geothermal wells (Ide et al., 2000). The combined hardware/software system was capable of a sinusoidal injection test, stepped constant rates test and triangular air pattern test (Ide et al., 2000), though little information is available about the numerical PTA software.

8.4 Numerical pressure-transient analysis modelling framework

The only numerical PTA software (AWTAS) is mostly inaccessible and has been superseded (Section 8.3), and so in order to generate a numerical PTA model response, the reservoir engineer must set up the simulation themselves. There are many decisions to be made regarding the grid setup and other simulation parameters; in fact, there are theoretically an unlimited number of ways to set up the simulation, and the model results can be sensitive to details of the grid design or other parameters. To address this issue a framework for numerical PTA modelling using TOUGH2 and PyTOUGH has been created, explaining and justifying details of the grid design, which has also been tested for undesirable sensitivities (McLean and Zarrouk, 2017a).

The simulator TOUGH2 has been chosen due to widespread use in the geothermal industry; however, there is the potential for the framework to be implemented with other simulators.

The framework increases the user-friendliness of numerical PTA, by making the time-consuming decisions regarding model design, and provides comparability between numerical PTA results for different wells/tests, by ensuring the same design is used for different analyses. The framework has not yet been implemented into any software and is not yet user-friendly to that level; however, the use of PyTOUGH greatly improves the user-friendliness as a single script can set up the model, run it, extract the results and present them in any required format (graphical or otherwise).

The pressure derivative can be automatically calculated and plotted using standard Python functions, and remains the key diagnostic tool for numerical PTA, due to its sensitivity and characteristic shapes, greatly assisting in the selection of a suitable model to match the field data. Calculation of the pressure derivative plot must be made using superposition time (Section 4.4.4) in order to avoid false boundary effects which arise when the injection or production history is not taken into account (Houzé et al., 2012). While the superposition time concept is only technically valid for linear systems and IARF, in practice the characteristic shape of many different flow regimes/models is retained despite superposition, and the derivative plot is still an important diagnostic tool (Houzé et al., 2012).

The numerical PTA framework is based on a radial grid and in its simplest form is equivalent to the analytical infinite uniform porous reservoir model (IARF). Numerical equivalents to several of the analytical reservoir and boundary models are created by modifications to the basic radial grid (Section 8.4.1), and presented later in this chapter. Even more versions of the numerical model are possible, and can be implemented by the reservoir engineer once the standard framework is set up.

8.4.1 General model setup

The general setup is a radial grid with a single layer and three main components: (1) well block, (2) skin zone and (3) reservoir zone (Fig. 8.1). The radius of the well block is the actual drilled well radius, the skin zone then extends out to 5 m, and the outer radius of the reservoir zone is 20 km which is effectively infinite as it is likely to be beyond the extent of any pressure or temperature disturbance related to well testing.

The grid needs to be very fine in the skin zone close to the well where the pressure will be changing the most rapidly and can be coarser in the reservoir zone where pressure changes will be slower. This is achieved using a logarithmic radial block spacing, with 50 blocks in the skin zone from the well radius to 5 m, and then 100 blocks in the reservoir zone from 5 m to 20 km, which is the fixed outer radius of the model (McLean and Zarrouk, 2017a). A sensitivity analysis concluded that the number of

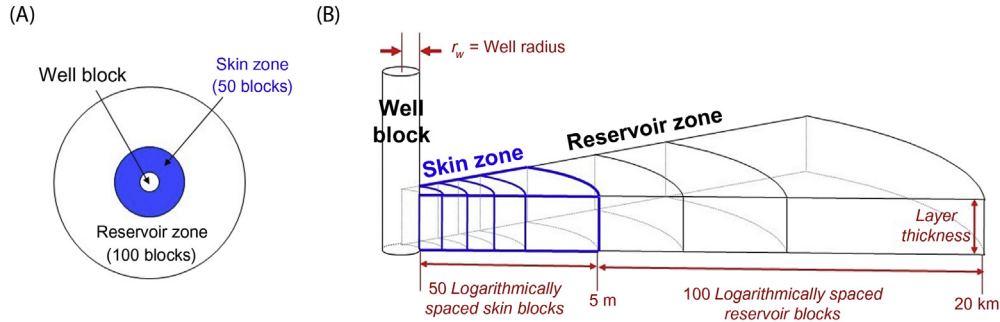


Figure 8.1 Schematic of radial grid design showing the well block, skin zone and reservoir zone: (A) plan view and (B) partial side view in 3D. Not to scale and does not show all blocks. After McLean, K., Zarrouk, S.J., 2017a. *Pressure transient analysis of geothermal wells: a framework for numerical modelling*. *Renew. Energy* 101, 737–746.

skin zone and reservoir zone blocks could be decreased without affecting the model results, but considering that the model is already very small (151 blocks) and in the absence of an imperative to decrease the number of blocks, this is not recommended (McLean and Zarrouk, 2017a).

The model has a single layer, with a thickness equal to that of the permeable reservoir intersected by the well (McLean and Zarrouk, 2017a). This is often – but not necessarily – equal to the vertical thickness of the entire open-hole section in the well. Usually there is a distribution of feed zones over the length of the open hole, in which case the entire thickness would be used for the model. However, in some cases the permeability is clearly localised in one part of the well, and part of the open hole can be excluded with confidence. An example of this would be an impermeable section at the base of the well (‘rat hole’ in drilling terminology), which can sometimes be relatively long, and is clearly identifiable during injection testing as it is not penetrated by the cooler injected water. By default the entire open-hole thickness must be used if no data is available to locate the feed zones, which is sometimes the case for older data sets, though this should not be the case for a properly designed modern injection/completion test (Chapter 6: Completion and output testing).

In the case of deviated wells the vertical reservoir thickness should be used rather than the measured depth along the well track. As the reservoir thickness h is typically large for geothermal wells, it is unlikely that the deviation will affect the model results (McLean and Zarrouk, 2017a), which in any case can be considered in terms of kh rather than k alone. However, consider a deviated well and a vertical well penetrating through the same vertical thickness of the same reservoir. The deviated well will have a longer well track and higher probability of intersecting permeable fractures, which tend to be subvertical in volcanic geothermal systems (McLean and McNamara, 2011). It is therefore likely the deviated well will return a higher value for permeability than

the vertical well. This must be kept in mind when considering and comparing the results of the well testing and is likely an area of future research.

8.4.2 Well block parameters

TOUGH2 is for the simulation of fluid flow through porous media, and a well is not a porous medium, so in theory a coupled wellbore/reservoir simulator should be used; however, this is not available or practical at this point in time (Section 8.2). It is possible to represent the well as a TOUGH2 block with special properties, as was done by O’Sullivan et al. (2005) for AWTAS (Section 8.3), which provides a reasonable approximation of the well behaviour.

The radius of the well block should be the actual drilled radius of the well, which can be estimated as the size of the drill bit used (McLean and Zarrouk, 2017a). In reality the radius of the hole is often bigger than this and variable over the length of the well due to formation collapse and washout, though in the absence of open-hole calliper logs (which are rarely done) the drill bit provides a practical estimate of the average radius. Note that there will be a perforated liner inside the open hole, which should reduce the average radius; however, McLean and Zarrouk (2017a) effectively ignore the perforated liner.

The ‘porosity’ of a well is effectively 1.0, as a well is really just a vertical pipe; however, TOUGH2 is not designed to deal with a value this high. A porosity of 0.9 is large enough to reflect the well geometry while still allowing TOUGH2 to run in a stable manner. The reduction of porosity to 0.9 instead of 1.0 does not significantly affect the model results (McLean and Zarrouk, 2017a).

The initial volume of the well block automatically created in the model is calculated from the well radius and model layer thickness. However, the actual volume of fluid in the well will be greater than this, as it must include the fluid within the casing (above the reservoir). Moreover, for the actual volume of fluid in the well to be represented in the model, it must be equal to the volume of the *pore space* of the well block (not the total volume of the well block). A practical way to estimate the required total volume of the well block (which can then be updated in the TOUGH2 input file via PyTOUGH) is to divide the volume of all the water in the well from the static water level down to the base of the permeable reservoir interval, by the porosity (0.9). The connection area between the well block and the first block in the skin zone does not change.

The concept of ‘permeability’ does not apply to a wellbore, which is effectively a vertical pipe with unlimited permeability. TOUGH2 requires a finite value for permeability and so this can be automatically set to be three orders of magnitude greater than that of the reservoir. Experience has shown that any greater permeability contrast will make negligible difference to the model results and may lead to convergence problems (O’Sullivan, personal communication, 2015).

A large pore compressibility must be specified for the well block, in order to approximate the large change in water level that can occur during injection testing, especially in relatively impermeable wells (McLean and Zarrouk, 2017a). For most geothermal wells the permeability is sufficiently high that the well is not filled with fluid throughout the duration of a well test; instead, the water level is usually somewhere down in the casing. The water level changes with injection rate, hence the volume of fluid present in the wellbore changes (Fig. 8.2). The compressibility to use in the model can be estimated from the change in fluid volume ΔV (calculated from the change in water level Δh) and the change in pressure Δp between two injection rates (O’Sullivan, personal communication, 2014) (Eqs. 8.1 and 8.2). For an impermeable well filled all the way up to the wellhead at all injection rates, there is no volume change and so the compressibility will be zero.

$$C = \frac{\Delta V}{\Delta P} \frac{1}{V} \quad (8.1)$$

$$\Delta V = \pi r_w^2 \Delta h \quad (8.2)$$

where C is the compressibility (1/Pa), ΔV is the change in volume (m^3) calculated from change in water level, ΔP is the change in pressure (Pa) measured at the transient depth, V is the total volume of fluid (m^3) under static conditions, r_w is the well radius (m) and Δh is the change in water level (m).

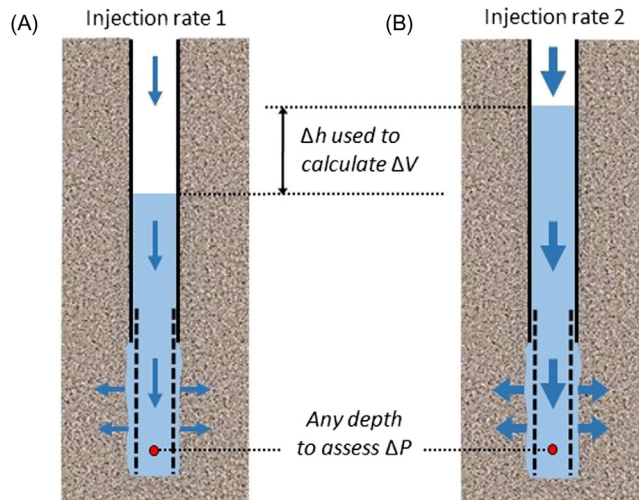


Figure 8.2 Schematic of injection into a permeable geothermal well: (A) initial rate and (B) second, higher rate; showing associated change in water level and definition of Δh and ΔP to be used for the estimation of well compressibility.

8.4.3 Fixed radius skin zone

The skin effect (Section 4.4.3) is represented by a zone with a fixed radius of 5 m and variable permeability. The assumption of 5 m is a reasonable estimate of the extent of ingress of material such as mud or cuttings into the reservoir (positive skin) or fracturing/hole collapse (negative skin) during drilling. Alternatively it is possible to define the radius as a variable parameter; however, the results become nonunique, and many combinations of radius and permeability in the skin zone would produce the same model results. A model sensitivity analysis completed with iTOUGH2 (Finsterle, personal communication, 2014) using a model with variable skin zone radius found that the correlation between the skin zone radius and skin zone permeability was almost one, too high to determine these parameters independently.

The radius is therefore fixed, and the skin factor s is the variable parameter, the value of which is used to calculate the permeability in the skin zone using the following equation (Horne, 1995):

$$k_s = \frac{k_r}{1 + \left(s / \left(\ln \left(\frac{r_s}{r_w} \right) \right) \right)} \quad (8.3)$$

where k_s is the skin zone permeability (m^2), k_r is the reservoir zone permeability (m^2), s is the skin factor (dimensionless), r_s is the skin zone radius = 5 (m) and r_w is the well radius (m).

8.4.4 Time stepping

It is not possible to specify a constant time step suitable for the whole simulation. Rapid pressure change occurs during the early-time of the pressure-transient behaviour, therefore closely spaced logarithmic time steps are required at this time. Further into the pressure transient, the pressure change is more gradual, therefore longer time steps can be used, which decreases the model running time and the size of the final data set.

TOUGH2 allows nonconstant time steps to be specified, though the input format only allows the first 104 time steps to be specified, after which the time step remains constant at the last specified value until the end of the simulation. It is recommended that 104 logarithmically spaced time steps are used, starting at 0.01 seconds and ending with 100 seconds.

The closely spaced time steps will always appear at the start of the simulation, which is an issue because the simulation does not usually start at the same time as the pressure transient of interest, but rather with the period of injection or production flow prior to the transient. This is especially true for geothermal well tests, which are most commonly fall-offs after some period of injection, or build-ups after production. If the closely-spaced time steps are located at the start of the injection (or production)

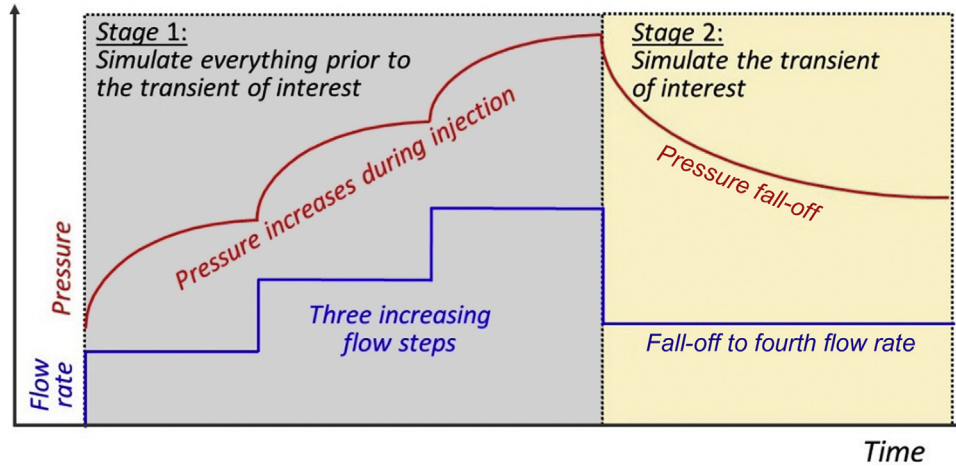


Figure 8.3 Schematic of two-stage simulation process, using a common geothermal injection/fall-off example. After McLean, K., Zarrouk, S.J., 2017a. *Pressure transient analysis of geothermal wells: a framework for numerical modelling*. *Renew. Energy* 101, 737–746.

period, then the time step will be large and constant (100 seconds) by the time the pressure transient of interest is reached, which is too large to capture early-time behaviour. The issue can be resolved by running the simulation as two linked simulations, with the second simulation starting at the transient of interest:

- Stage 1: Simulate the injection or production flow history of the well, up to the pressure transient of interest.
- Stage 2: Simulate the pressure transient of interest.

Fortunately, this can be achieved easily by using PyTOUGH, which can automatically save the conditions in the blocks (pressure, temperature, saturation) at the end of the first simulation and use them as initial conditions for the second simulation. The two stages of simulation are shown schematically in Fig. 8.3.

8.5 Other reservoir and boundary models

The basic numerical PTA modelling framework described in the preceding sections is effectively the equivalent of the analytical infinite uniform porous reservoir model, for modelling infinite-acting radial flow (IARF) (Sections 4.4.2 and 4.5.7). In analytical PTA, there are also a range of impermeable boundary models available (Section 5.1.1). Boundaries can be implemented in the basic radial numerical PTA framework (Section 8.4) by modification of the block volumes and connection areas.

Some of the simplest and most useful of these boundary models have been demonstrated with the numerical PTA framework, including a single linear impermeable boundary, and two parallel linear impermeable boundaries (channel). It is theoretically possible to implement boundaries of any shape into the numerical PTA framework.

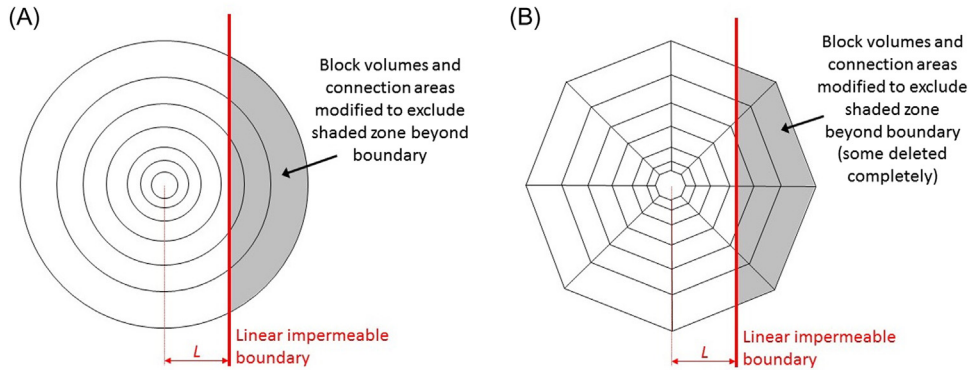


Figure 8.4 Schematic of implementation of linear impermeable boundary into the model grid, at a distance (L) from the well centre: (A) radial one-dimensional grid and (B) two-dimensional ‘spiderweb’ grid. After McLean, K., Zarrouk, S.J., 2017a. *Pressure transient analysis of geothermal wells: a framework for numerical modelling*. *Renew. Energy* 101, 737–746.

8.5.1 Linear impermeable boundary

The basic radial numerical PTA grid can be modified to include a single linear impermeable boundary, by the reduction of block volumes and connection areas in the region beyond the boundary (Fig. 8.4A). This can be achieved by using basic geometry calculations and automated using PyTOUGH so the user specifies only the perpendicular distance L from the well centre to the boundary (McLean and Zarrouk, 2015b).

The validity of modifying the radial grid, which is mathematically one dimensional (in the sense that the radial distance from the well is the dimension), as if it contains a two-dimensional linear feature, is debatable. McLean and Zarrouk (2017a) compared the response of an equivalent two-dimensional ‘spiderweb’ grid (Fig. 8.4B) to the modified radial grid (Fig. 8.4A), and the simulated pressure transients were indistinguishable. Therefore the use of the modified radial grid is justified and is preferred for simplicity.

The implementation of the linear impermeable boundary model in the numerical PTA framework produces a similar pressure derivative response to that expected from analytical theory (Section 5.1.1), which is a flattening of the derivative, followed by a rise and second flattening of the derivative (Fig. 8.5A). It can be seen in Fig. 8.5B that as the boundary approaches the well (as L decreases), the effect of the boundary is seen earlier. When the boundary is very close to the well, the first flattening of the derivative is obscured by wellbore storage, and the boundary is not apparent in the data.

8.5.2 Channel boundary

Two parallel linear impermeable boundaries form a channel along which the flow becomes linear after both boundaries are detected. The theory and calculation of the

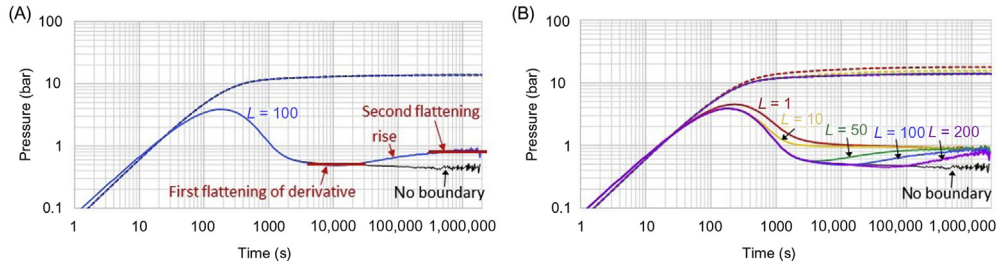


Figure 8.5 Pressure derivative plot of a fall-off simulated with the linear impermeable boundary model: (A) characteristic shape demonstrated for a boundary at 100 m and (B) effect of varying the distance to the boundary (pressure derivatives as *solid lines* and corresponding pressure as *dashed lines*).

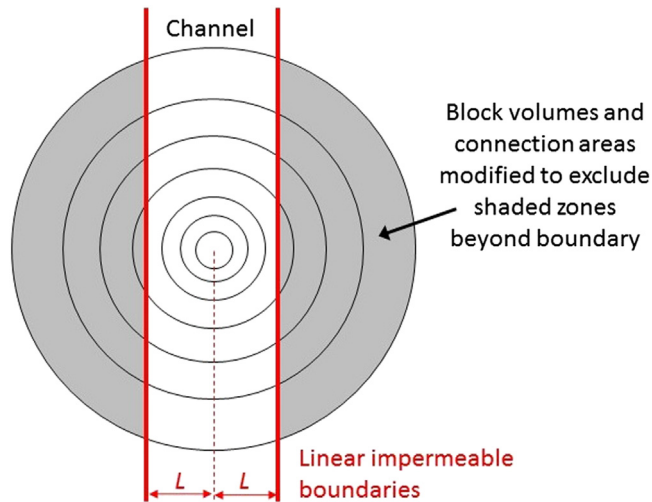


Figure 8.6 Schematic of implementation of channel model as two linear impermeable boundaries, at a distance (L) from the well centre.

modifications to the block volumes and connection areas is exactly the same as for a single linear boundary (Section 8.5.1), but the volume removed from each block and area removed from each connection is doubled (Fig. 8.6). This is equivalent to the analytical channel model with the well in the centre of the channel. It is also possible to specify the two linear boundaries at different distances from the well.

The characteristic response of the channel model is a pressure derivative of 0.4–0.5 unit-slope (Fig. 8.7). There is no particular behaviour for the corresponding pressure curves, though when the channel is very narrow, the pressure and pressure derivative are almost parallel (McLean and Zarrouk, 2017b). The channel boundary model response is similar to that expected from analytical PTA theory (Section 5.1.1).

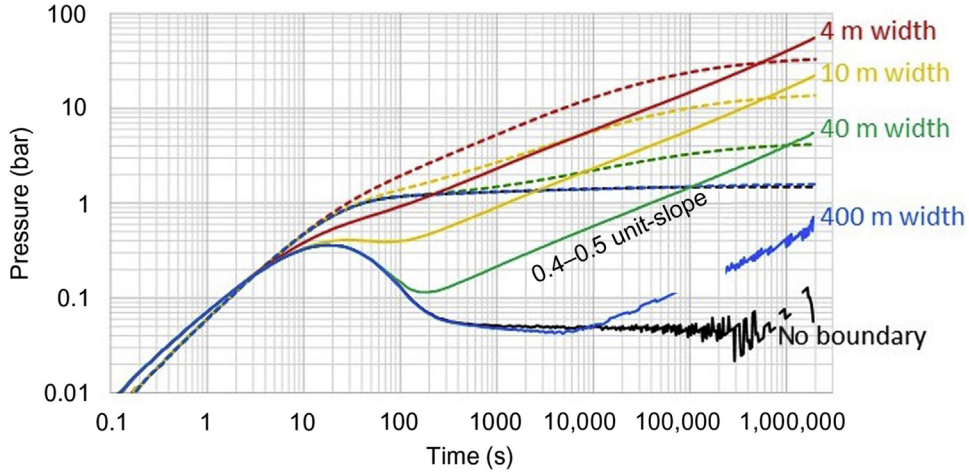


Figure 8.7 Simulated pressure derivative plot of a fall-off, showing the effect of varying the distance to the channel boundaries (L), pressure derivatives as *solid lines* and corresponding pressure as *dashed lines*.

Table 8.1 Equations to calculate volume of the i th block (V_i) and connection area to the next largest block ($A_{i+1/2}$) for a specified fractional dimension (n) in a radial model (O’Sullivan et al., 2005).

Dimension	Volume of i th block (V_i)	Connection area to next largest block ($A_{i+1/2}$)
1	$2h^2(r_{i+1/2} - r_{i-1/2})$	$2h^2$
2	$\pi h(r_{i+1/2}^2 - r_{i-1/2}^2)$	$2\pi h r_{i+1/2}$
3	$\frac{4\pi}{3}(r_{i+1/2}^3 - r_{i-1/2}^3)$	$4\pi r_{i+1/2}^2$
N	$\frac{\alpha_n h^{3-n}}{n}(r_{i+1/2}^n - r_{i-1/2}^n)$	$\alpha_n h^{3-n} r_{i+1/2}^n$

8.5.3 Fractional dimension

The fractional dimension model is useful to represent fractured reservoirs, without having to go into explicit details of the fracture network, with a noninteger dimension in the range 1.0–3.0 (Section 5.5.2). The fractional dimension concept can be implemented analytically, or in the case of numerical simulation by using a radial grid and modification of the block volumes and surface areas (O’Sullivan et al., 2005).

The fractional dimension concept was implemented into the AWTAS software for numerical geothermal PTA (Section 8.3) via the equations in Table 8.1, where α_n is defined by the following equation (Barker, 1988):

$$\alpha_n = \frac{2\pi^{n/2}}{\Gamma(n/2)} \quad (8.4)$$

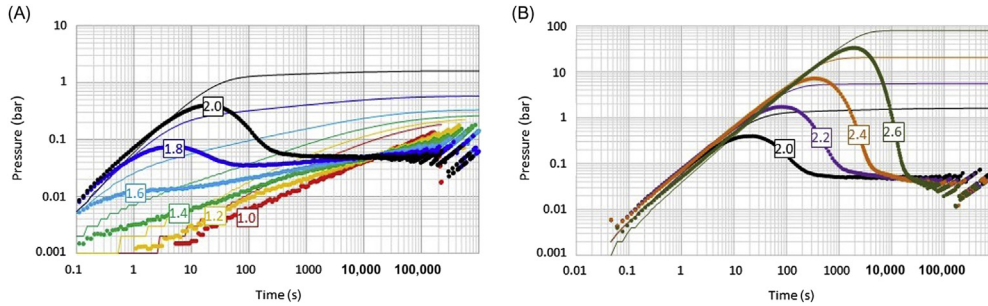


Figure 8.8 Derivative plots demonstrating the impact of varying n when all other model parameters are constant: (A) n in range 1.0–2.0 and (B) n in range 2.0–2.6.

The derivative plots of Fig. 8.8 show the effect of varying the fractional dimension n while keeping all other parameters in the numerical model constant. It can be seen that the pressure derivative becomes noisy in late time as the magnitude of the pressure change becomes very small, which is due to the limit in significant figures available to calculate pressure in TOUGH2 and similar simulators, and cannot always be removed by widening the differentiation interval while calculating the derivative. Regardless of this very late-time effect, the model response is clear at earlier times, and some familiar responses can be seen, similar to their analytical equivalents. When $n = 2.0$ (Fig. 8.8A and B), the typical shape of the infinite acting radial flow (IARF) flow response is seen, with the pressure derivative flattening (Section 4.5.7). When $n = 1.0$ (Fig. 8.8A), the response has the shape of linear flow in a near-well fracture with the pressure derivative rising in a ~ 0.5 unit-slope parallel to the pressure response (Section 5.4). The intermediate dimensions between 2.0 and 1.0 show the continuity between the two responses, and the tendency for the effects of wellbore storage and skin (the early-time unit-slope and hump in the derivative) to disappear as the fractional dimension decreases. This is due purely to the geometry of the system and not to any actual change in wellbore storage or skin, and this concept is called geometrical skin (Houzé et al., 2012). As n increases above 2.0, there is a dramatic increase in the duration of wellbore storage and apparent skin to the extent that the reservoir response only emerges during the noisy very late-time stage, making simulations for this model with $n > 2.6$ pointless (Fig. 8.8B). Again, this is purely a geometrical effect.

The numerical implementation of the fractional dimension model in the AWTAS software (Section 8.3) has been applied to production data from dry steam wells at the Wairakei geothermal field (Zarrouk et al., 2007), and output testing of a two-phase well at Hatchobaru geothermal field (Khasani and Zarrouk, 2015) (Section 8.8.7).

8.6 Injectate temperature effect

One of the big issues with using analytical PTA for geothermal data is that analytical models assume only one set of fluid properties, which means the test is isothermal

(Section 5.7). This assumption does not hold for the majority of geothermal pressure transients, which are usually from injection tests, and are very much nonisothermal. During injection testing, cold water of approximately ambient temperature is injected into a hot reservoir, which can be in excess of 300°C. The two fluids (injectate and reservoir) have significantly different properties, and while it can be demonstrated that using the properties of the hot reservoir fluid will give more realistic results than using the cold fluid properties (Grant and Bixley, 2011), this does not solve the problem.

For numerical PTA, the two fluids are not an issue, as no decision needs to be made between the two sets of fluid properties, as both are specified during the model setup. The reservoir fluid properties are set by the initial temperature and pressure of the reservoir, and the cold injectate fluid properties are set by the enthalpy of the injection into the well block.

The numerical PTA framework specified in this chapter has been used to demonstrate the impact of the injectate temperature effect on the results of PTA (McLean and Zarrouk, 2015c). There is a major impact on the result for skin factor, and a minor impact on the result for reservoir permeability. This makes sense, as the cold injectate near the well is much more viscous than the hot reservoir fluid, so it does not move as easily, producing an additional pressure drop in the vicinity of the well which resembles positive skin. In a derivative plot the similarity between changing the injectate temperature and changing the skin factor is easily apparent (Fig. 8.9).

In the absence of a model able to incorporate the injectate temperature effect, the analysis will return a positive value for skin factor even if there is no actual skin in the well (McLean and Zarrouk, 2015c). The ‘injectate temperature effect’ (McLean and Zarrouk, 2015c) is conceptually the same as the ‘fluid skin’ discussed by Benson (1984) in an analytical study of nonisothermal systems (Section 5.8.3), though it was discovered independently.

When comparable analytical and numerical PTA analyses are performed on field data (McLean et al., 2016; McLean and Zarrouk, 2017b), the analytical results for skin

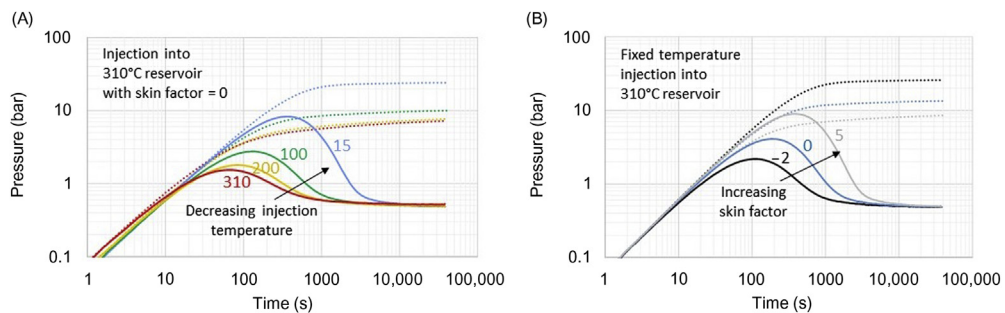


Figure 8.9 Derivative plots demonstrating the similarity between: (A) decreasing the injectate temperature and (B) increasing the skin factor. (A) After McLean, K., Zarrouk, S.J., 2015c. *Impact of cold water injection on geothermal pressure transient analysis: a reservoir modelling assessment*. In: *Proceedings of the 37th New Zealand Geothermal Workshop*. Taupo, New Zealand.

factor are systematically higher by a value of approximately 3–4, sufficient to make a stimulated well appear damaged.

The injectate temperature effect was investigated in detail by Guerra and O’Sullivan (2018). Pressure–transient data were simulated using TOUGH2 and then analysed using the software SAPHIR (analytical models) to determine if there were any circumstances in which analytical PTA would be able to reproduce the known parameters k and s (reservoir permeability and skin factor). Various reservoir types (homogenous, fractured and layered) were considered as well as a range of temperature contrast between the injectate and reservoir. There were no circumstances in which analytical PTA returned the correct values for k and s , both parameters were significantly overestimated to varying degrees (Guerra and O’Sullivan, 2018).

8.7 Effect of CO₂ content

As many geothermal reservoirs contain significant amounts of CO₂, the potential effect of that CO₂ content on the shape of pressure transients was investigated by Adityatama et al. (2018). Adityatama et al. (2018) used a TOUGH2 model similar to the numerical PTA framework in this chapter to simulate pressure–transient data sets, then attempted to analyse these using analytical models (SAPHIR). CO₂ was included in the simulation with the use of the water–CO₂ (EOS2) module of TOUGH2.

Adityatama et al. (2018) showed that the CO₂ content has no effect on the pressure derivative plot of fall-off data (Fig. 8.10) as long as the CO₂ remains dissolved

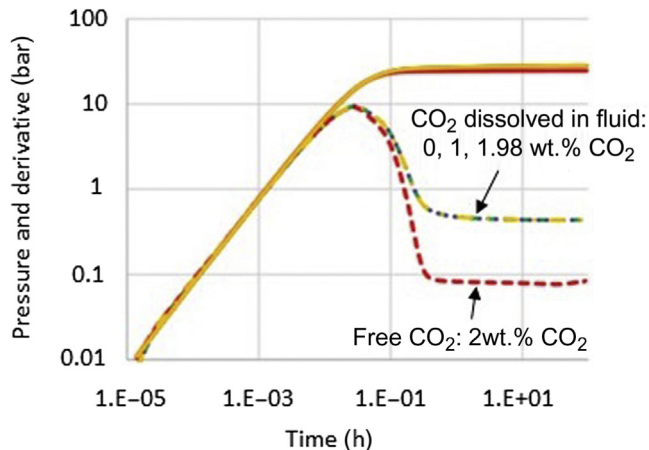


Figure 8.10 Effect of CO₂ content on a pressure derivative plot of simulated fall-off data. After Adityatama, D.W., Kaya, E., Zarrouk, S.J., 2018. Investigation of pressure transient analysis methods for CO₂ rich geothermal reservoirs. In: Proceedings of the 40th New Zealand Geothermal Workshop. Taupo, New Zealand.

in the reservoir fluid, which is the case up to 1.98 wt.% CO₂ in their scenario. Once the solubility of CO₂ is exceeded even slightly (2 wt.% CO₂), there is a significant impact on the shape of the pressure derivative. The section of flat derivative (representing IARF) is shifted significantly lower, and the transition hump becomes so steep (Fig. 8.10); it cannot be matched by analytical PTA models (Adityatama et al., 2018).

8.8 Overview of historical geothermal numerical pressure-transient analysis studies

Early use of numerical simulation for PTA was in support of, or in combination with, analytical PTA. Some of this combined work is described in Chapter 5, Advanced analytical pressure–transient analysis relevant to geothermal wells, though soon numerical PTA became a tool in its own right, considered by some to be more useful and flexible than analytical tools (O’Sullivan and Pruess, 1980). In this section an historical overview of some major numerical geothermal PTA studies is given, starting in the early 1980s. A number of modern examples with associated field data are presented in Chapter 10, Field studies.

8.8.1 Wellbore storage in two-phase reservoirs

Miller et al. (1982) use coupled wellbore–reservoir simulation (Section 8.2) to investigate the effect of wellbore storage on two-phase geothermal drawdown tests. Numerical simulation was used because deriving an analytical solution required the assumption of a uniform steam saturation, which is not representative of real reservoirs (Miller et al., 1982). A major issue involved with this type of well testing is that the high compressibility of the two-phase fluid results in extended wellbore storage effects, which can last for several hours and completely dominate the pressure response (Miller et al., 1982).

Various scenarios were considered, including a hot water reservoir with flashing in the wellbore, a hot water reservoir with flashing in the reservoir, a two-phase reservoir that is liquid dominated (low steam saturation of 0.19), and a two-phase reservoir that is vapour dominated (high steam saturation of 0.78). It was concluded that with good design and sufficient duration, drawdown pressure transients can be analysed to obtain total kinematic mobility (Miller et al., 1982). One build-up test was also simulated, concluding that while wellbore storage effects are shorter for build-ups, the analysis is difficult. Injection testing was not considered.

8.8.2 Developments to dual-porosity model

Over the period 1978–83, there were various developments to the dual-porosity model (Section 5.5.1), enabled by numerical simulation. Moench and Atkinson (1978)

used numerical simulation to investigate the effects of phase change in a homogeneous reservoir. This model was further developed by Moench (1978) for a fractured reservoir, with impermeable matrix blocks and thermal conduction from the matrix blocks to the fractures. This model was used successfully for PTA of a steam well at Larderello, Italy (Moench and Neri, 1979). The Moench and Neri (1979) model was further expanded by Moench and Denlinger (1980) to include steam vaporisation and flow within the matrix blocks. This was necessary in order to account for the longevity of production wells at The Geysers, the United States. The issue of mineral deposition at the matrix–fracture interface (fracture skin) was examined by Moench (1983), and new type curves were generated.

8.8.3 Non-Darcy flow

An early paper on numerical simulation of non-Darcy flow in geothermal reservoirs by Zvyoloski (1982) concluded that the effects of non-Darcy flow are significant and can be modelled, though the study did not consider well testing specifically. Non-Darcy flow affects pressure–transient well testing by appearing as positive skin, with a skin factor increasing as flow rate increases. Analytical well testing methods cope with non-Darcy flow by assessing and removing the flow rate–dependent component of the apparent skin, leaving the actual mechanical skin (Section 5.3).

Numerical models enable a more rigorous approach by incorporating non-Darcy flow directly into the model. Darcy’s law for the flow of fluid through porous media (Eq. 8.5) can be modified with the addition of a turbulence component called the Forchheimer’s term to account for non-Darcy flow (Eq. 8.6) (Houzé et al., 2012).

$$\frac{\partial P}{\partial x} = \frac{\mu}{k} u \quad (8.5)$$

$$\frac{\partial P}{\partial x} = \frac{\mu}{k} u + \beta \rho u^2 \quad (8.6)$$

where P is the pressure (Pa), x is the distance (m), μ is the dynamic viscosity (Pa s), k is the permeability (m^2), u is the velocity (m/s), β is the Forchheimer coefficient ($1/\text{m}$) and ρ is the density (kg/m^3).

Wu (2000) used this approach to numerically simulate non-Darcy flow for both single-phase and multiphase flow, through both porous and fractured reservoirs, developing type curves for well-test analysis. It was found that drawdown tests are sensitive to non-Darcy flow behaviour but build-up tests are not (Wu, 2000), and injection tests were not investigated. Zhang and Xing (2012) numerically simulated a series of drawdown tests to investigate further, concluding that the ratio of fluid density to viscosity significantly affects the non-Darcy flow behaviour.

8.8.4 Fractured two-phase reservoirs

O'Sullivan (1987) investigated the impact of fracturing on the results of well testing in two-phase reservoirs. Drawdown/build-up and injection/fall-off tests were simulated using TOUGH2, for both uniform porous reservoirs and fractured reservoirs (represented using the MINC method, Section 5.5.1). No wellbore simulator is used, and the well is represented as a single block in the radial model (as per Section 8.4.2).

Various scenarios were considered including a drawdown/build-up test in an initially two-phase reservoir, a drawdown/build-up test in a hot water reservoir which flashes during drawdown, and an injection/fall-off test into a two-phase reservoir. It was concluded that fracturing can confuse the results of geothermal well tests, and that in some cases the distortion caused by fracturing will prevent identification of a straight line for kh calculation (O'Sullivan, 1987). The results of this study do not provide a method to analyse well-test data with these effects but are useful to demonstrate their impact, which could aid in the identification of these effects in field data.

8.8.5 Stress-sensitive reservoirs

Conventional PTA assumes that permeability is constant; however, in some petroleum and geothermal reservoirs, it is pressure dependent (stress sensitive). Numerical simulation has enabled the study of this issue, in particular the stress sensitivity of naturally fractured reservoirs. Ambastha and Zhang (1996) used a FORTRAN-based programme to calculate stress-sensitive pressure-transient responses, concluding that significant errors occur in parameter estimation if stress sensitivity is not taken into account.

Later work by Samaniego and Villalobos (2003) defines a pseudo-pressure to account for stress-sensitive behaviour in drawdown/build-up tests, which can be incorporated into a simulation. This pseudo-pressure is a function of the specific fluid and fracture properties in the reservoir, therefore these properties must be known for each reservoir, and the equation will differ between reservoirs. Application of this method to field data showed that if stress sensitivity is not taken into account then analysis of the drawdown would estimate a significantly lower value for reservoir permeability than analysis of the build-up. However, if stress sensitivity is accounted for, then a single model with a built-in function for pressure-dependent reservoir permeability can match both the drawdown and build-up (Samaniego and Villalobos, 2003).

8.8.6 Permeability change during injection

Nakao and Ishido (1998) studied the apparent increase in permeability that can occur during injection, using field data from an injection test in well YT-2 in Yutsubo geothermal field, Japan. It is expected that a step increase in the injection rate will result in an increase in the downhole pressure, which will then stabilise at a higher value.

However, in some cases the pressure initially increases but then declines with time, even if the injection rate is stable. This pressure decline with time can be attributed to an increase in permeability due to the injection of cold water. It should be noted that this effect is not always a result of increasing permeability: it can also be an artefact in the data resulting from contraction of the fluid column as it cools during injection, if the downhole tool is positioned above the PCP (see Section 7.10). This behaviour is more likely to be observed during stage testing, where the downhole tool is positioned at the casing shoe. It can be avoided by positioning the tool deeper in the well at the PCP, and ensuring a reasonable period of cold water injection before the actual injection/completion test starts, which will ensure the fluid column in the well has already been cooled to a great extent and is relatively stable.

In the Nakao and Ishido (1998) study, this effect was investigated using the numerical simulator STAR, and the permeability and porosity were calculated as a function of the local instantaneous temperature and pressure. The Nakao and Ishido (1998) model is radial with a central well block and fixed radius skin zone. Closer to the well, the reservoir blocks are fractured dual-porosity (MINC) type, but beyond a fixed radius (97.2 m), the reservoir is a porous medium and has a different thickness. The reasoning for this composite model with two distinct reservoir zones is not given. The lack of wellbore storage in this model was considered by the authors to be an obstacle in improving the match further (Nakao and Ishido, 1998). It is concluded that an increase in porosity (due to cooling and increased pressure) results in a drastic increase in permeability in the fractured zone around the well, and that this effect is reversible (Nakao and Ishido, 1998).

A major assumption in this modelling process is the function used to calculate porosity from pressure and temperature, and also the function to calculate permeability from porosity. Riffault (2014) revisited the same data set used by Nakao and Ishido (1998), investigating a number of different relationships for the dependence of porosity and permeability on pressure and temperature, establishing a new relationship in the process. The model geometry was a complex radial model with 47 layers, and blocks to represent the well, casing, liner, different reservoir lithologies, nonreservoir lithologies and a thin fracture.

Villacorte and O'Sullivan (2011) investigated the same phenomenon in a comprehensive study based on field data from injection tests in two unidentified wells. Model results were simulated using both TOUGH2 and FEHM, and NLR was achieved using both iTOUGH2 (Finsterle, 2000) and PEST (Doherty, 2010). Comparison was made to results from the analytical PTA software package SAPHIR (Houzé et al., 2012) and the numerical PTA software AWTAS (Section 8.3).

Villacorte and O'Sullivan (2011) considered the field data in various stages, corresponding to the different injection rates, allowing a different permeability (and other model parameters) to be calculated for each stage. The permeability was found to

increase with increasing injection rate and then decrease for the fall-off stage. These ‘stage-wise’ simulations fit very well to the pressure field data during the increasing injection steps, but not well during the fall-off (Villacorte and O’Sullivan, 2011).

Villacorte and O’Sullivan (2011) did not mention wellbore storage, other than a ‘well’ block appearing in the schematic. It was found that without a skin zone, most of the initial simulations did not match the field data, and so a fixed radius skin zone was then included. Various values were used for the skin zone radius but no conclusions were drawn as to the best value to use; however, the presence of a skin zone was found to improve the match (Villacorte and O’Sullivan, 2011). No conclusions are drawn on the relative merits of the different simulators, inversion modelling packages, or PTA software.

8.8.7 Production testing using reservoir models

Zarrouk et al. (2007) developed radial models for four shallow dry steam production wells at the Poihipi power station, located on the margins of the low-enthalpy Wairakei geothermal field, New Zealand. A variety of pressure-transient behaviour was available in the production data set, created inadvertently by cyclic daily production of the wells (Fig. 8.11), which was done for operational reasons (Zarrouk et al., 2007). Wellhead pressure (WHP) measurements and mass flow rates were converted into downhole pressures using the steady-state wellbore simulator WELLSIM (Gunn and Freeston, 1991). The calculated downhole pressures were then used as input to model the reservoir, using the numerical PTA software AWTAS (Section 8.3).

The model grids are radial, with a single layer 150 m thick and an outer radius of sufficient extent to be considered infinite. AWTAS was used and therefore the simulator was TOUGH2, with a framework similar to that described in this chapter (Section 8.4). Wellbore storage and skin models were not used as their impact on this production field data is assumed to be minor (Zarrouk et al., 2007) since the wells were never shut in. Three different reservoir model types were employed: uniform porous media, dual-porosity and fractional dimension. The fractional dimension model (Section 8.5.3) provided the best fit to the field data (Fig. 8.11), with a fractional dimension of approximately $n = 2.5$, implying a significant component of vertical flow in the reservoir with flow pathways converging towards the open-hole section of the well from above or below, rather than simple two-dimensional horizontal radial flow (IARF, as would be the case if $n = 2.0$).

Khasani and Zarrouk (2015) arrived at the same conclusion regarding the fractional dimension model when modelling output test data from well 2H-21 at the Hatchobaru geothermal field, Japan. The Khasani and Zarrouk (2015) study is conceptually similar to the Zarrouk et al. (2007) study, except that measurements of two-phase flow during output testing were used to constrain the reservoir models, rather

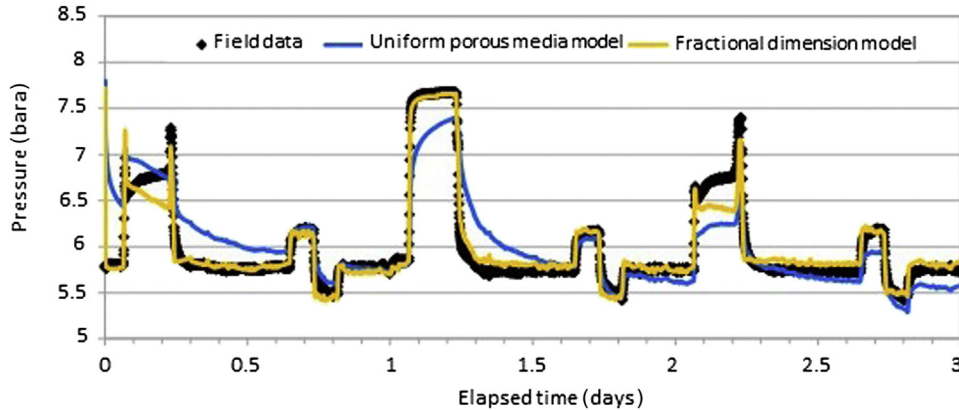


Figure 8.11 Match between the uniform porous media model, the fractional dimension model and 3 days of the production history. Data from Zarrouk S.J., O'Sullivan, M., Croucher, A., Mannington, W., 2007. Numerical modelling of production from the Pohipi dry steam zone: Wairakei geothermal system, New Zealand. *Geothermics* 36(4), 289–303.

than single-phase steam flow only. The results of the output testing (mass flow and WHP at the wellhead) were converted into downhole pressure using the transient wellbore simulator WELBORE (Miller, 1980), then these downhole pressures are used as input for AWTAS to model the reservoir. Khasani and Zarrouk (2015) considered three reservoir model types: uniform porous media, dual-porosity and fractional dimension, obtaining the best fit with the fractional dimension model, with a fractional dimension of $n = 2.8$.

8.8.8 Effect of scaling on geothermal pressure-transient analysis

When the equilibrium between reservoir fluid and mineral phases is disturbed (by production or injection), precipitation or dissolution of minerals can result, which affects the reservoir permeability. Akin (2012) investigates precipitation of minerals in the wellbore, which is a relatively long-term process called ‘scaling’, to see if it can affect the results of PTA which are measured over a relatively short timescale.

This requires coupling of a chemical reaction model with a model for the relationship between porosity and permeability. Numerical simulation was carried out using STARS (CMG, 2003) which handles both the transport and reaction equations (Akin, 2012). We recommend against the use of this coupled approach, as it complicates the solution and requires additional input parameters that are not available. This is regardless of whether the coupling is done internally within the reservoir simulation software or using an external coupling with another chemical reaction simulator. In this case the grid used was of square Cartesian form, which is a departure from the usual radial grid used for well-test modelling.

PTA of the simulated pressure–transient data sets was carried out using the analytical model software SAPHIR. The study is relatively inconclusive; stating that while changing deposition and dissolution rates leads to changes in wellbore storage, scatter induced in the pressure derivative prevents rigorous analysis (Akin, 2012).

8.8.9 Estimating reservoir parameters using temperature and pressure profiles

The objective of two separate but concurrent studies by Kusumah (2014) and Seto (2014) was to obtain estimates of reservoir permeability and porosity using both pressure and temperature profiles from completion and heatup testing of the well THM15 in Tauhara geothermal field, New Zealand. This is a deviation from other transient studies, which typically only use pressure data, and from a single depth.

The simulator used in both studies was TOUGH2, and NLR was completed using iTOUGH2. Kusumah (2014) concluded that manual model matching was the superior inversion method, while Seto (2014) obtained the best results with iTOUGH2. Kusumah (2014) did not obtain good matches with the temperature data, and this is tentatively attributed to the absence of a skin effect in the model. Seto (2014) found matching data from heatup runs to be problematic near the feed zones, which are areas of localised rapid change.

The Kusumah (2014) grid was complex with 40 different layers with 17 different rock types, corresponding to the geology of the reservoir near the well. The casing, liner and well are also represented with different ‘rock types’. The grid is radial, 200 m thick, with 99 blocks of increasing radius out to 15 km. No details were given on the parameters of the well block, and no skin zone is included.

Seto (2014) used two grids: a complex radial grid with 40 layers and 5 rock types, and then an even more complex grid with 14 rock types. There are also ‘rock types’ for the casing, liner and well. The grid is 200 m thick, the well block is described as being highly permeable but no other details are given, and no reference is made to the skin effect.

Despite these very complex and well-specific models, the temperature behaviour was not adequately reproduced in either study; however, good matches to the pressure profiles were obtained in both studies.

CHAPTER 9

Operation and management of geothermal wells

Contents

9.1	Introduction and steam gathering system	217
9.2	Production data analysis	219
9.2.1	Decline analysis from discharging wells	219
9.2.2	Production from downhole heat exchangers	222
9.3	Stimulation of geothermal wells	226
9.3.1	Acidising	227
9.3.2	Hydraulic fracturing	231
9.3.3	Cold fluid stimulation (thermal effects)	234
9.3.4	Deflagration stimulation	237
9.3.5	Other geothermal stimulation techniques	239
9.3.6	Recommendations for geothermal stimulation	239
9.4	Scaling in geothermal wells	240
9.4.1	Calcite scaling	240
9.4.2	Anhydrite scaling	244
9.4.3	Silica scaling	244
9.5	Corrosion in geothermal wells	247
9.5.1	External casing corrosion	247
9.5.2	Internal casing corrosion	249
9.5.3	Stress corrosion cracking	249
9.6	Casing damage	250
9.6.1	Internal casing wear	250
9.6.2	Casing implosion	250
9.6.3	Casing coupling compression failure	252
9.6.4	Casing shear or buckle	254

9.1 Introduction and steam gathering system

This chapter covers the use of geothermal wells beyond the initial drilling and completion/output testing discussed in the early chapters. Several technical challenges can arise as we start to operate the geothermal well. The major topics/sections here: sizing pipelines and connecting the well to the piping network, two-phase and

single-phase flow issues, production data analysis, decline analysis, downhole heat exchangers, permeability enhancement/stimulation, scaling, corrosion and different mechanical casing damage. Geothermal production wells are connected to the steam gathering system — also known as the production facility or the system above-ground — through a network of long pipelines. Fig. 9.1 shows a simplified steam gathering system where two-phase geothermal fluid from different wells is collected in the main header and sent to a cyclone separator (Zarrouk and Purnanto, 2015). The separator produces dry steam at a set pressure, which is normally sent to the steam power plant (or possibly to a binary plant evaporator), while the brine on the other hand is either flashed to produce steam at lower pressure or used in a heat exchanger to extract more thermal power using another working fluid (Fig. 9.1). In most hot water systems and in all warm water systems, only heat exchangers are used (no steam separation or flashing), and the fluid is then reinjected back into the reservoir.

The pipelines follow the ground topography to the separator station in both steam or binary power plants in two-phase systems. The diameter/size of the horizontal pipeline from each well depends on the well production casing size and the mass flow rate of fluid produced by the well. Hence, it is recommended to measure the well output prior to sizing or running the pipelines. For a standard size ($9\frac{5}{8}$ ") production casing, the common production pipeline sizes are 8", 10" or 12" depending on the total mass flow rate from the well. Note that 8" pipelines (commonly used in the past) are likely to restrict the flow and are not recommended for use with standard size wells. For the large size ($13\frac{3}{8}$ ") production casing (big wells), the common production pipeline size is 14", and some large output wells are installed with 20" production pipeline. The main consideration is to make sure that the pipeline size is not restricting fluid production, and that it will not result in slug flow and water hammer effects (Watson, 2013).

If single-phase fluid is produced from the well (in warm and hot water systems), then sizing the pipe diameter and calculating pressure drop is a relatively simple fluid

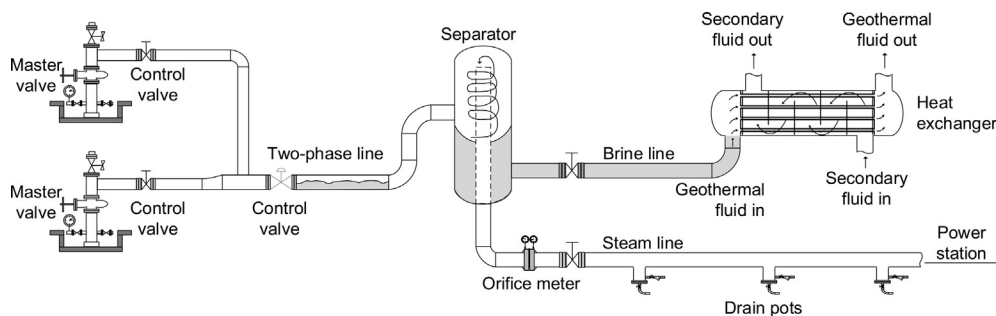


Figure 9.1 Simplified above-ground system showing two production wells connected to one main header, which sends two-phase geothermal fluid to a separator that produces dry steam to the turbine and brine which is used in a shell and tube heat exchanger.

mechanics exercise. However, when two-phase fluid is produced, the pressure drop calculations are much more complicated as there are a host of factors which affect the various pressure drop correlations applicable to different pipeline sizes and the two-phase flow regimes (Rizaldy and Zarrouk, 2016).

One of the common problems encountered in large ($\geq 8''$) diameter geothermal two-phase flow pipelines is the slug flow regime which causes major water hammer effects and vibration, resulting in high pressure drop, and damage to the pipeline and the support structure. This is more of a problem when the two-phase geothermal fluid has low enthalpy (low dryness fraction), flows downhill, and in proximity to bends, valves and reducers. Unfortunately, due to the thermal expansion of geothermal pipelines between cold shut down and hot flowing conditions, the steam field piping system is designed with multiple thermal expansion loops to safely manage thermal expansion between cold and hot conditions. This will result in longer pipeline runs and multiple bends and additional fittings, which can increase the risk of slug flow conditions.

Single-phase steam pipelines leaving the separator (Fig. 9.1) are installed with a steam flow meters (e.g. orifice plate) and drain pots with steam traps (Arifien et al., 2015; Arifien and Zarrouk, 2015) to remove steam condensates and ensure that clean and dry steam is sent to the steam turbines at the power station. Any moisture carried with the steam can cause mineral scaling in the steam turbine nozzles and erosion to the turbine blades (Rizaldy et al., 2016). The build-up of condensates at low points (e.g. faulty drain pots) in the steam line can result in turbine water flooding and water hammer risks/effects.

Single-phase brine pipelines leaving the separator are at risk of steam flashing if the pressure suddenly drops, which can cause separator flooding (sending brine with the steam) and water hammer effects (Watson, 2013). Therefore it is desirable to increase the pressure of the separated brine (e.g. flowing downhill) or to cool the brine by removing the thermal power in heat exchangers (Fig. 9.1).

9.2 Production data analysis

The output of a geothermal production well is usually characterised by the output curve (deliverability curve) at the original output test shortly after completion testing (Chapter 6: Completion and output testing). The output of the well changes with time, usually declining, and the methodology for characterising this is outlined in this section, for both discharging wells and production from downhole heat exchangers (DHEs) (nondischarging).

9.2.1 Decline analysis from discharging wells

The output of most geothermal production wells will progressively decline with time; the two most common causes are scaling and decreased reservoir pressure. Early in the

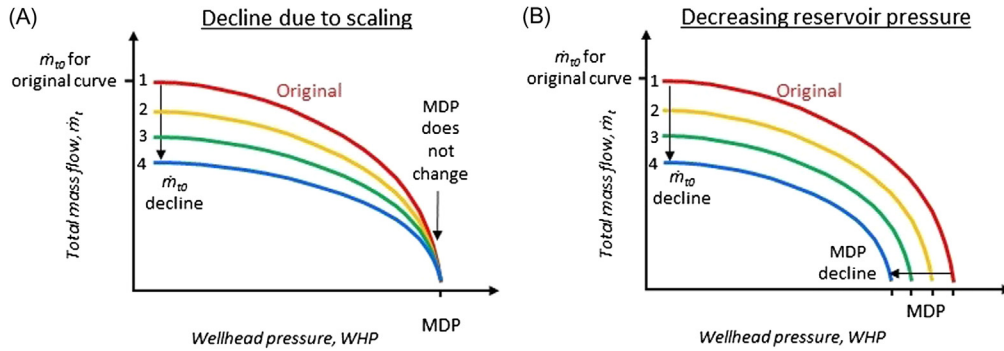


Figure 9.2 Schematic of progressive change to output curves as the result of: (A) scaling in the wellbore and (B) decreasing reservoir pressure. After Grant, M.A., Bixley, P., 2011. *Geothermal Reservoir Engineering*. Elsevier.

life of a well, the output is characterised by the output curve (or ‘deliverability curve’, Section 6.4) which shows total mass flow rate versus wellhead pressure (WHP). The shape of the output curve can then change over the life of the well due to a variety of processes (Grant and Bixley, 2011). The expected changes in shape due to scaling or decreasing reservoir pressure are shown in Fig. 9.2. The main difference is that the maximum discharge pressure (MDP) (the theoretical highest WHP at which the well will discharge) does not change as the result of scaling (Fig. 9.2A), but changes with reservoir pressure (Fig. 9.2B).

When analysing long-term production data, it is difficult to visualise or quantify the change with time using an output curve plot as each data point effectively represents a slightly different output curve. The mass flow is dependent on the control valve opening (and hence WHP) and so the mass flow data must be normalised to a single WHP to make the values comparable, and then observe trends with time. This is achieved using Eq. (9.1) which is an elliptical model commonly used for modelling output curves.

$$\dot{m}_t = \dot{m}_{t0} \sqrt{1 - \left(\frac{\text{WHP}}{\text{MDP}}\right)^2} \quad (9.1)$$

where \dot{m}_t is the total mass flow rate (kg/s); \dot{m}_{t0} is the maximum total mass flow rate (kg/s) as WHP approaches zero; WHP is the wellhead pressure (Pa) and MDP is the maximum discharge pressure (Pa).

The process effectively models each data point (mass flow/WHP) as an entire elliptical output curve and then takes the mass flow value on that curve for a fixed WHP (Fig. 9.3A), usually the separation pressure (though it is not important which fixed WHP is chosen). All the mass flow values at the fixed WHP (standardised) are then

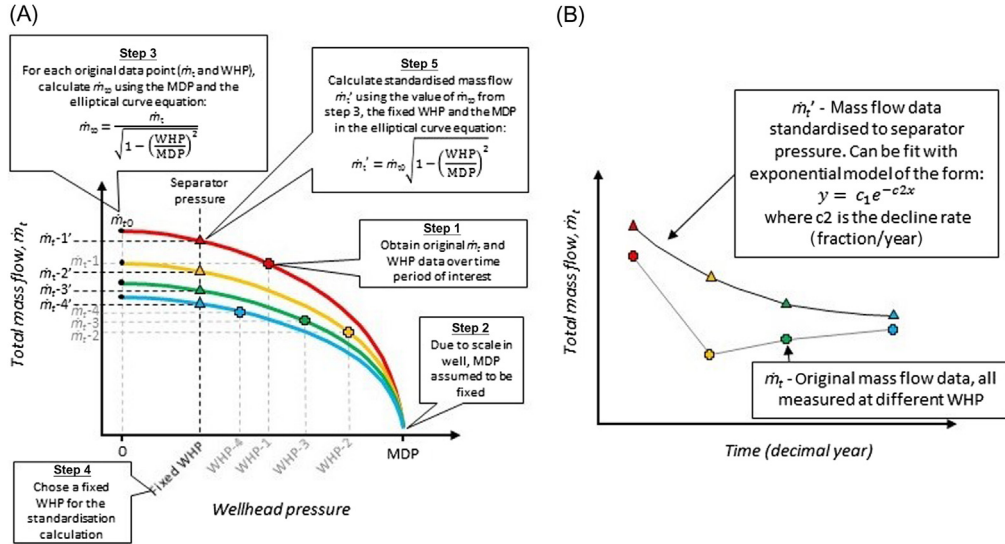


Figure 9.3 Schematic demonstration of standardisation of mass flow to WHP = separator pressure, for a well affected by scaling: (A) graph of mass flow versus WHP, showing original data, projected curves and standardised data and (B) graph of mass flow versus time, showing original data and standardised data used to assess the decline rate. *WHP*, Wellhead pressure.

plotted versus time in decimal years, to assess the exponential decline rate, which is a fixed fraction per year (Fig. 9.3B). While this process appears cumbersome schematically (Fig. 9.3), the calculations are straightforward. It can be seen in Fig. 9.3B that the assessment of decline from the original mass flow data is not valid and can be very misleading – in this example the mass flow from the well is increasing between the last three data points, even though the well is actually declining, because the data is measured at progressively lower WHP. However, the decline is clear in the standardised data, which accounts for the different WHP.

Fig. 9.4 is a field example of decline analysis from a well in New Zealand. This well declines very rapidly due to scaling in both the wellbore and the formation. The well used to require regular workovers and acidising until the installation of an antiscalant dosing system. The early decline rate is high at 0.92/year, before accelerating to a massive 13.7/year in the last days of production (Fig. 9.4). The output of the well is then partially recovered by mechanical workover and acidising. The installation of an antiscalant dosing system has prevented recurrence of scaling/decline, and has in fact resulted in progressive recovery of the well output, at a recovery rate of 0.18/year over the 4 years post-installation (Fig. 9.4). The data in Fig. 9.4 is presented with a logarithmic y-axis, which is not strictly necessary, but can aid the presentation of the data in some cases.

In the case of Fig. 9.4 the mass flow is standardised to WHP = 18 barg. The original data (mass flow rate, WHP) from which the standardised mass flow is calculated is

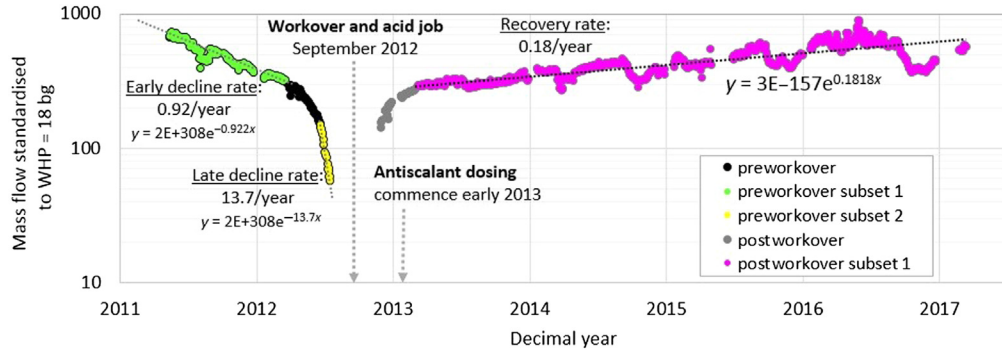


Figure 9.4 Example of production well decline due to calcite scaling, and recovery due to mechanical workover/acidising, followed by progressive recovery due to antiscalant dosing. *Data from Contact Energy, with kind permission.*

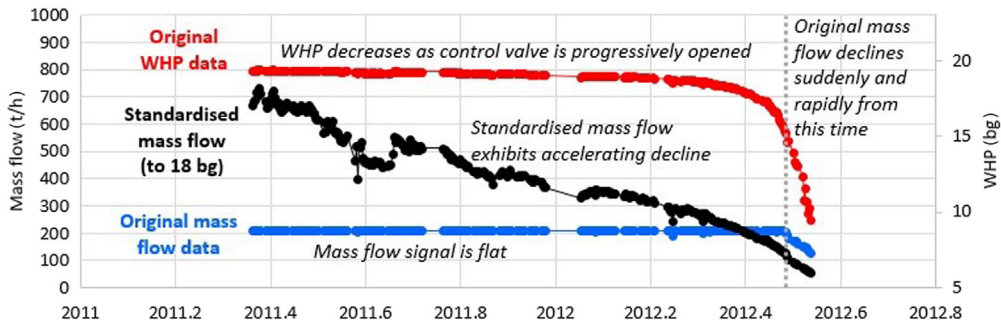


Figure 9.5 Original data (mass flow and WHP) and standardised mass flow (to 18 barg) from the pre-workover section of Fig. 9.4. Note this well is operating close to the MDP and so standardisation to a lower WHP results in a very large increase in mass flow value. *MDP, Maximum discharge pressure; WHP, wellhead pressure. Data from Contact Energy, with kind permission.*

presented in Fig. 9.5, for the pre-workover period. This has been shown as a cautionary example – the original mass flow data is almost completely flat until it declines suddenly and rapidly in the last 2 weeks. Monitoring of the mass flow rate alone is not sufficient to identify decline. The decline is visible throughout that time period in the slow decreasing of the WHP, as the control valve is progressively opened to maintain a constant mass flow. The decline is immediately apparent in the standardised mass flow, and this should always be used to monitor well decline.

9.2.2 Production from downhole heat exchangers

DHEs are used when it is not desirable to produce the geothermal fluid, or when the geothermal well does not self-discharge. DHEs do not require reinjection wells as there is no production of the geothermal fluid. To extract the energy, a secondary or

working fluid (normally fresh water) is pumped down to the DHE in the well, then up to the surface systems (Section 3.5).

It is difficult to predict the thermal power output of DHEs until the well is production-tested by connecting the DHE to the duty (thermal load). The thermal power output of the DHE is affected by: the temperature distribution in the well, the mixing ratio (ratio of fresh fluid entering the well to the total fluid circulating), the depth of the U-tube, the water level in the well and the secondary fluid circulation flow rate. As discussed in Chapter 3, Geothermal wells, DHEs are mainly suitable for direct-use applications, with a thermal power output of less than 1.0 MWth for DHEs with well depth of up to about 150 m (Lund, 2003). However, they may be commercially viable down to a depth of 500 m under certain conditions (Lund, 2003).

The flow rate of the secondary fluid circulating inside the DHE is limited by the maximum velocity of the fluid inside the 1" (nominal bore) U-tube pipeline (2.2–2.5 m/s) (Dunstall, 1992). Stable thermal power output is reached after a few hours or a few days of operation, depending on the dominant heat transfer mechanism. Dunstall (1992) reported the long-term operation (6-day test) of a 1" U-tube DHE installed in RR679, a 121 m deep well in Rotorua, New Zealand, with a 4" well casing. The thermal power output stabilised in 1 hour, which is very fast, along with the temperatures of the DHE inlet and outlet, and feed zone (Fig. 9.6). The data in Fig. 9.6 is for the DHE installed at 121 m depth. The DHE was relocated from

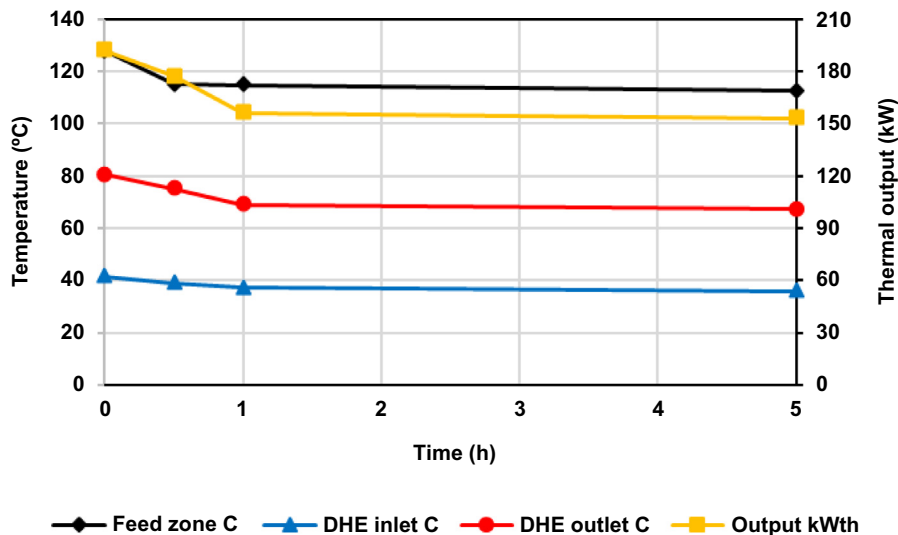


Figure 9.6 Heat load and temperature variation during a long-term test of well RR679 installed with a 121 m DHE. DHEs, Downhole heat exchangers. Data from Dunstall, M.G., 1992. *Downhole Heat Exchangers Performance Analysis (Ph.D. thesis)*. University of Auckland.

65 m depth, resulting in an increase in thermal power output from 9 kWth to more than 150 kWth.

Airlifting through the injection of air into the well to remove some of the geothermal fluid (Fig. 3.10) can increase the thermal power output of a DHE. In the case of well RR679 with the DHE at 121 m depth, the increase in thermal power output due to airlifting was relatively low at 5%–9% (Dunstall, 1992). When the DHE was at 65 m depth a $\frac{3}{4}$ " promoter pipe (Fig. 3.8) installed down to 120 m depth to enhance circulation (convective heat transfer), resulted in a large increase in output of 78%.

Steins et al. (2012) reported results from another Rotorua well with 1" NB and DHE installed at 54 m depth, showing that airlifting increased the thermal power output by 125% from 20 to 45 kWth.

Table 9.1 provides a comparison between the reported operating parameters of different U-tube DHE setups.

It can be concluded from Table 9.1 that the performance of the DHE is affected by the temperature profile in the well, and the depth/length of the heat exchanger in relation to the depth of the feed zone.

It is important to note that the quality of the thermal power produced by the DHE is also very important for the particular direct-use application. From the examples in Table 9.1 the 30 kWth at DHE outlet temperature of 32°C (highlighted

Table 9.1 Comparison between different U-tube downhole heat exchangers (DHE) setups.

Data	Dunstall (1992)	Dunstall (1992)	Steins et al. (2012)	Chuanshan et al. (2011)
Well drilled depth (m)	123	123	55	117.5
Production casing depth (m)	112	112	40	55
Production casing diameter (mm)	100	100	150	280
DHE U-tube diameter (mm)	25.4	25.4	25.4	50
Feed zone depth (m)	120	120	50	55–100
Feed zone temperature (°C)	157.2	157.2	138.1	51
DHE outlet temperature (°C)	66	—	62	32
DHE inlet temperature (°C)	35.4	—	52	19.4
DHE circulation rate (L/s)	1.2	0.44	0.47	0.7
DHE installed depth (m)	121	65	54	115
Power output without airlift (kW)	143.5	9	20	30
Water level from the wellhead (m)	10	10	10	—
Airlift tube installed depth (m)	12	N/A	30	N/A
Submergence ratio (%)	17	N/A	67	N/A
Water removed by airlift (L/min)	1.3–1.5	N/A	10	N/A
Promoter pipe diameter (mm)	N/A	19	N/A	N/A
Promoter pipe depth (m)	N/A	120	N/A	N/A
Power output with airlift (kW)	146	N/A	45	N/A
DHE performance improvement (%)	2	78	125	N/A

column) was used as part of a heat pump system, and it has less value/applications than the 20 kWth at DHE output temperature of 62°C which was used to supplement an existing (gas fired) space heating system at a local motel.

DHEs are usually employed for direct-use applications; however, there has been some interest in the possibility of using DHEs for electrical power generation. Lienau and Lund (1991) and Morita et al. (1992) reported the field testing of an annular (or ‘coaxial’) DHE (Fig. 9.7) for this purpose. Annular DHE is made of two concentric tubes with the fluid flowing down the annulus and rising in the central tube (Fig. 9.7). It is different from the U-tube, where the heated fluid flows down and then up the well in one smaller-diameter pipe (Fig. 3.7). The annular DHE experiment was conducted in the upper part of the 1962 m deep HGP-A well at Puna, Hawaii. An insulated pipe of 5 cm (2") internal diameter was installed to a depth of 876.5 m inside a larger pipe of 16 cm (6¼") diameter, to form an annular DHE. Water at 30°C was pumped down the annulus and heated to 43.6°C at a flow rate of 80 L/min with a power output of 76 kWth (Morita et al., 1992). This was significantly less than the original prediction which was that steam at temperatures exceeding 100°C would be produced, and it was proposed that this steam could be used in a conventional steam

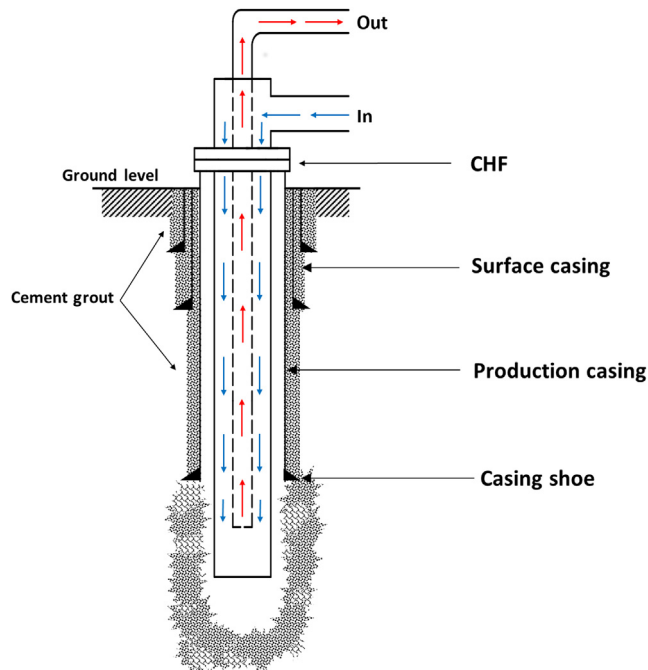


Figure 9.7 Annular (coaxial) DHE tested for electric power generation. DHEs, Downhole heat exchangers. After Lienau, P.J., Lund, J.W., 1991. Downhole heat exchanger technology being considered for electric power generation in Hawaii. *GHC Q. Bull.* 13(4), 1–11.

cycle or binary cycle, with the condensate being pumped back down the well to complete the loop (Lienau and Lund, 1991).

Morita et al. (2005) further investigated the use of deep coaxial DHE, in high-temperature wells in Japan, for power generation using small-scale binary plants. There were two deep DHEs, one at a depth of 2100 m and 269°C at Hijiori, and the other at a depth of 2000 m and 322°C at Toyaha. Morita et al. (2005) concluded that the Hijiori well could generate 40–50 kWe, while the well in Toyaha can generate up to 70 kWe for about 15 years. There is no reported commercial implementation or demonstration project of electrical power generation using DHE. It is very unlikely that a DHE can be implemented ‘commercially’ for power generation, for the following reasons:

- The limited possible flow rate that can be achieved through the DHE tubes or annulus, when compared with flow rates during production from self-discharging wells through the full bore of the production casing.
- The limited heat transfer coefficient between the well and formation to the DHE, which can only be maximised by bleeding the well under certain conditions. Heat transfer by conduction alone will not be sufficient and will cool the reservoir around the well.
- The limited DHE (outer tube) surface area available for the heat transfer. and the same time.
- Fluid rising in the central tube will lose some of the heat it gained to the cooler downflowing fluid in the DHE annulus (Fig. 9.7). This concept was clearly demonstrated in Fig. 3.9 for the U-tube DHE.

9.3 Stimulation of geothermal wells

Conventional geothermal developments generally rely on the natural in-situ primary and/or secondary reservoir permeability for production, often large fractures and faults. Common practice in the past was to abandon the well or use it for monitoring if there was no commercial level of permeability after completion testing. However, the increase in drilling cost in conventional geothermal developments and the drilling of deep enhanced geothermal systems (EGS) wells, which generally have lower permeability, have pushed most developers towards applying permeability stimulation/enhancement techniques. Another motivation is that in some fields the drilling engineers have no option but to drill with mud (heavy fluids) in the production zone to maintain hole stability, which will result in major skin and permeability damage.

The importance of well stimulation was recognised in the 1930s by the petroleum industry for solving the problem of limited well productivity (Economides et al., 2000). Since then the technology has advanced, allowing the extraction of

hydrocarbons from low-permeability rock formations efficiently and economically. Stimulation was later investigated by the geothermal industry, with the primary objective to remedy and/or improve connection of the wellbore with the natural fractures or faults in the geothermal reservoir, to improve permeability and therefore well productivity (Aqui, 2012).

In the geothermal industry the predominant well stimulation techniques in use or under consideration are as follows:

- acid injection, also known as ‘acidising’
- hydraulic fracturing
- deflagration
- thermal fracturing

Published reports of well stimulation using these techniques have been very scarce in the early years of application in the geothermal industry, due to technical issues associated with the high-flow and high-temperature nature of geothermal systems, particularly for hydraulic fracturing. However, these techniques – particularly acidising – later gained wide acceptance in the late 1980s (Malate, 2003). A relatively new technique in stimulating geothermal wells known as ‘thermal fracturing’ shows promising potential, despite inadequate understanding of the mechanism at work (Flores et al., 2005; Grant and Bixley, 2011).

9.3.1 Acidising

With the increase in drilling costs, many developers these days apply acid injection treatment to improve the permeability of wells during completion. It is by far the most commonly used and successful stimulation method for geothermal production and reinjection wells.

The history of acid injection is well documented in the petroleum industry, and it is the oldest well stimulation technique, predating hydraulic fracturing by about half a century. Herman Frasch, the chief chemist of the Solar Refinery of the Standard Oil Company, was credited for the development of the acidising technique when he proposed the use of hydrochloric acid (HCl) to treat oil wells as far back as 1895 (Kalfayan, 2008). Despite significant success in improving production, acidising did not gain popularity due to an innate corrosion problem that affects the well casings. It was only in 1932 that the use of acid became mainstream with the introduction of arsenic as a corrosion inhibitor. Since then commercial acidising in the petroleum industry has resulted in an average production increase of 412% in the United States (Economides and Nolte, 2000). Acidising technology has advanced through the years with the development of additives, methods and systems to address various problems relating to acid injection, and to improve zone coverage during the acidising process (Economides and Nolte, 2000).

The use of acidising as a well stimulation technique in the geothermal industry came much later. The earliest documented and perhaps the first application of chemical stimulation was in 1977 when sodium carbonate solution (Na_2CO_3) was used to dissolve quartz in the Fenton Hill Hot Dry Rock (EGS) project in New Mexico, the United States (Mortensen, 1978). It was then reported by: Campbell et al. (1981) and Portier et al. (2007) in the Geysers and Beowawe geothermal fields, the United States; Gomez et al. (2009) in the Ahuachapan, Berlin and the Momotombo geothermal fields in Central America; Malate (2003) in the BacMan, Leyte and Tiwi geothermal fields in the Philippines and by Portier et al. (2009) in the Salak geothermal field in Indonesia, Los Azufres geothermal field in Mexico and Larderello in Italy. The reported improvement in the injectivity index (II) of the wells varied from 40% up to 900% (Aqui, 2012).

One advantage of acidising geothermal wells as compared to petroleum wells is that the high production flow rates make it unnecessary to dissolve all the mineral deposits during stimulation. Undissolved precipitates loosened or softened by the acid reaction are cleared when production recommences.

There are two acidising treatment techniques used in the petroleum industry, which have been applied in the geothermal industry: matrix acidising and acid fracturing (also known as ‘fracture acidising’). The major difference between the two is the pressure at which acid is pumped into the formation relative to the ‘fracturing pressure’ of the reservoir formation.

In matrix acidising, acid is injected at pressures below the formation fracturing pressure. This treatment is designed to remove skin damage caused by drilling mud and cement during drilling operations, as well as other formation damage that may occur during well operation (Portier et al., 2007; Kalfayan, 2008).

It is important to assess the formation damage before any acid treatment. Aside from skin damage, the presence of mineral deposits within the production liner and in the near-wellbore formation is of interest in the stimulation of geothermal wells, particularly in the acid treatment of reinjection wells (Kalfayan, 2008). In such cases the acid dissolves the mineral deposits (i.e. silica scale) that plug the natural permeability/fractures, thus re-establishing the flow of reinjected brine into the reservoir.

Matrix acidising in geothermal wells is usually conducted in three stages (Malate, 2003), which are as follows:

1. *Preflush* – Usually 5%–15% concentration hydrochloric acid (HCl) is injected. This is designed to dissolve carbonate minerals in the formation that would react with the HCl.
2. *Main-flush* – It is a mixture of HCl and HF known as ‘mud acid’. The usual concentrations are 10% HCl and 5% HF in the mixture used for geothermal wells. HCl is effective in dissolving limestone and dolomites, while HF is effective in dissolving siliceous minerals such as clays, feldspar and silica sands. HF also dissolves calcium and magnesium fluorides.

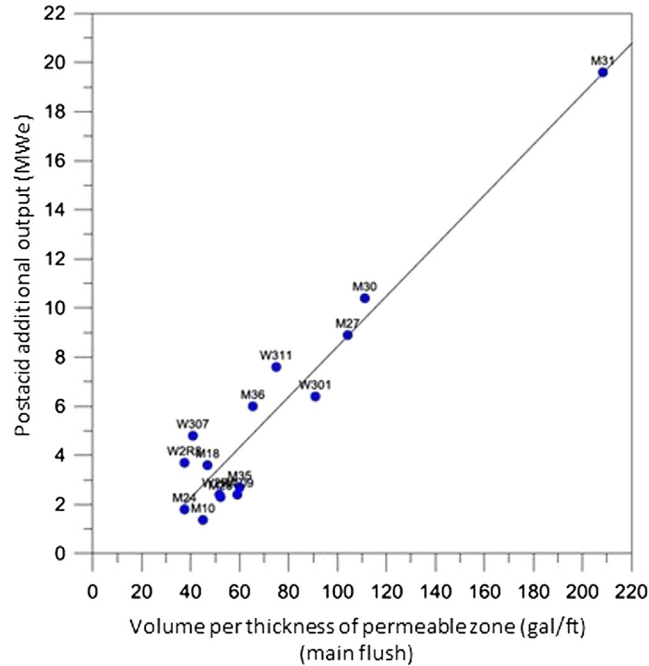


Figure 9.8 The relation between acid dosing rate and output gains. From Morente, C.P.P., 2013. *Evaluation of acid stimulation experience of production wells at EDC. In: Project Report for Postgraduate Certificate in Geothermal Energy Technology. University of Auckland, New Zealand (Confidential Report), Energy Development Corporation, with kind permission.*

3. *Postflush (also known as overflush)* — It serves to push the main-flush acid mixture further into the formation and minimises inevitable precipitation reactions from taking place near the wellbore. In oil well stimulation, weak hydrochloric acid (HCl), ammonium chloride, diesel (for oil wells and only following a water or weak acid overflush) and nitrogen gas (for gas wells and only following a water or weak acid overflush) are usually used (Economides et al., 2000). In geothermal wells, however, it is a common practice to use fresh water for the overflush.

Morente (2013) carried out a detailed evaluation of matrix acidising experience in production wells from several geothermal fields in the Philippines. The study showed that the gains in productivity after acidising clearly increase with the main-flush dosing rate (Fig. 9.8).

Morente (2013) also concluded the following:

- It is highly recommended to carry out a PTS (pressure–temperature–spinner) survey when designing the acid treatment jobs, to help identify the thickness of the permeable zone and therefore the calculation of the required acid volumes.

- The optimum acid dosing rate is yet to be fully established with more data, but at this time, it appears to be at least 50 gal/ft (621 L/m) for the preflush (10% HCl) and 75 gal/ft (931 L/m) for the main-flush (10% HCl + 5% HF).
- Dosing rates higher than the conventional 50 gal/ft of preflush and 75 gal/ft of main-flush could potentially yield better results (Fig. 9.8).
- Wells that did not increase in productivity after acidising were mechanically damaged prior to the acid treatment.

Coutts et al. (2018) presented the results of acidising the well PK4a at Kawerau geothermal field, New Zealand. This well is used for the reinjection of brine, which is supersaturated with amorphous silica, with a silica saturation index (SSI) of 1.7 (see Section 9.4.3). The acid treatment resulted in a 90% improvement in the II of the well. However, the high SSI meant that the injectivity decline after acidising is very rapid, occurring in three stages:

1. Initial rapid decline marking the end of thermal stimulation (see Section 9.3.3) for approximately 10 days.
2. A period of higher than normal (pre-acidising) decline for approximately 50 days.
3. Return to a more typical long-term decline rate.

Coutts et al. (2018) made an interesting point of considering a higher HF concentration to increase the reaction rate, which we feel is something worthwhile to investigate in the future.

Fig. 9.8 shows that higher acid volume per reservoir thickness will result in greater improvement in well output. Experience also shows that the higher the well permeability preacid job, the greater the improvement in productivity, postacid job.

Wells with low pre-acid permeability may be stimulated using acid fracturing (or ‘fracture acidising’), which is designed to stimulate undamaged formation and is conducted above the formation fracturing pressure. Acid is injected to create fractures or is injected into a fracture created by a viscous fluid, for example gel known as a ‘pad’. After pressures return to normal the conductivity of the fracture is retained by the asperities of the fracture surfaces resulting from dissolution etching of the passing acid (Kalfayan, 2008).

Acidising of geothermal wells is related to sandstone acidising as most geothermal reservoirs are associated with silica-based formation. However, actual field practice in the geothermal industry does not strictly follow the matrix acidising concept as acid injection is usually conducted at high pumping pressures regardless of the formation fracturing pressure, and at relatively high rates because of the need to extend the reaction process beyond the wellbore (Aqui, 2012). Bakar and Zarrouk (2018) showed that it is common to fracture or extend natural fractures in conventional geothermal reservoirs during injection testing. Therefore it is not surprising that most reported geothermal acid treatment jobs are effectively a mix of matrix and fracture acidising.

Acid fracturing with the specific objective of creating new fractures has been rarely used in low-permeability geothermal reservoirs. The high temperatures and the highly consolidated nature of the geothermal formation limit the penetration of the live acid deep into the formation, as it neutralises quickly, resulting in relatively short conductive flow paths or channels (Campbell et al., 1981). However, acid fracturing in lower-temperature warm and hot water EGS remains a possible option that could be integrated with hydraulic fracturing.

9.3.2 Hydraulic fracturing

Hydraulic fracturing evolved from the acidising technology when Grebe and Stoesser (1935) observed that the formation ‘lifting pressure’ was sometimes obtained during acid injection, indicating that the formation was also being fractured. It is closely related to acid fracturing, with the same basic fracturing objectives: creating or propagating long, open, conductive channels extending beyond the wellbore, deeper into the formation. Hydraulic and acid fracturing differ in how the fracture is created and maintained. Acid fracturing depends on dissolution etching to create fractures and relies largely on the resulting asperities on the fracture surfaces to maintain conductivity (Aqui, 2012), while hydraulic fracturing is a mechanical process.

The hydraulic fracturing process involves exerting hydraulic pressure on the rock formation until the formation fracturing pressure or ‘breakdown pressure’ is reached (Adachi et al., 2007; Guo et al., 2007). It is usually conducted in the following stages:

1. *Pad stage* – Only the hydraulic fracturing fluid, mainly water, is injected into the well to break down the formation and to initiate fractures and to reduce fluid loss into the immediate wellbore formation when preparing the succeeding injection stage.
2. *Slurry stage* – Once pad stage is completed, the slurry, a mixture of the fracturing fluid and solid material to prop the fractures open (called ‘proppant’) is injected into the wellbore and into the fractures.
3. *Flush stage* – Final pumping into the well of one wellbore volume of fluid, intended to sweep the wellbore clean of any proppant. The well is then shut to allow fluid leak off into the formations and allow fractures to close on the proppants.

The new fractures formed during the pad stage are kept open by the fracturing fluid pressure. These fractures tend to close when pumping is stopped, rendering the newly fractured formation unavailable for production (Economides et al., 2000). Full closure of the fractures is prevented by the proppant, usually sand, bauxite or ceramic spheres mixed into the fluid injected during the slurry stage.

Three hydraulic fracturing concepts exist for stimulating tight petroleum wells, which depend on rock, formation and fluid properties (Reinicke et al., 2010), namely:

1. *Hydraulic proppant fracturing (HPF)* – This is the conventional method, which uses highly viscous gel as the fracturing fluid, with a high proppant concentration. This method creates conductive yet relatively short fractures in porous matrix formations, and the use of gel also reduces the amount of water required. It is suitable for reducing permeability damage (i.e. ‘skin’) in the direct vicinity of the wellbore. The well is shut after the fracturing process to allow the fractures to close on the proppants in place.
2. *Water fracturing (WF) (also called ‘self-propped fracs’ or ‘water fracs’)* – This uses water as the fracturing fluid, containing friction-reducing chemicals partially modified with the addition of proppant in low concentrations. This method creates long and narrow fractures to connect the wellbore to the main reservoir, which may be at some distance. The ‘unpropped fracture conductivity’ induced by the WF stimulation is maintained by the self-propping ability of the reservoir rock. Self-propping is the non-closure of the fracture due to fracture erosion, disaggregation and/or shear stress dislocation of the fracture surfaces, resulting in permanent opening of the fracture.
3. *Hybrid fracturing (also called ‘hybrid fracs’)* – This is a combination of fracture stimulations using different gels and slick (treated) water fluids as the fracturing fluid. This concept utilises the advantages of both the HPF and WF processes in creating the fracture geometry and in the effective placement of the proppant into the far end of the induced fracture.

Although proven successful in improving petroleum well production, these hydraulic fracturing methods experience several technical issues:

- HPF stimulations are prone to leave gel residues or may result in the precipitation of minerals that may affect the performance of the stimulated well (Reinicke et al., 2010).
- Since WF stimulations are dependent on the self-propping ability of the reservoir formation, fracture closure is likely to occur rapidly as a result of pressure solution processes eroding the asperities that are essential for keeping the hydraulic fractures from closing.
- The low viscosity of water makes it difficult to effectively transport proppants into the newly created hydraulic fractures.
- Another potential problem particular to fracturing of geothermal wells using proppants is that the most widely used proppant is quartz sand, which is silica and can dissolve in hot water (unsaturated with silica) over time, hence non-quartz sand proppant should be considered (e.g. ceramic proppant).

Experiments by Fredd et al. (2001) on the mechanism of water frac (WF) and of the conventional hydraulic proppant frac (HPF) confirmed that fracture displacement

is necessary for surface asperities to provide residual fracture width and sufficient conductivity. The presence of proppants increases fracture conductivity and reduces the impact of formation properties (contacting asperities and tortuosity). The success of water frac – the creation of the necessary level of conductivity – is largely controlled by formation properties, and these are difficult to predict.

In naturally fractured reservoirs such as tight, fissured oil and gas formations, there can be problems with excessive leak-off, resulting in low propagation of hydraulic fractures, which have to be resolved before any fracturing stimulation can be done (Warpinski, 1991; Britt et al., 1994). Geothermal reservoirs are generally associated with natural fractures and faults, which provide the necessary reservoir permeability. These natural fracture networks and faults are the pathways by which the wellbore is connected to hot geothermal fluids in the reservoir. Hydraulic fracturing in geothermal reservoirs is generally performed to connect these natural flow paths to the wellbore, and hence leak-off (bleeding of the well pressure after the hydraulic fracturing) is not a problem, rather it is a good indication that significant connection has been attained. Geothermal well completion using slotted liner over a long interval of open hole, however, makes it difficult to control the point of fracture initiation (Flores et al., 2005).

Grant and Bixley (2011) proposed that fracture initiation during hydraulic fracturing in geothermal wells is most likely to occur just below the production casing shoe, at which point the fracturing pumping pressure will overcome the formation fracturing gradient. The exact location nonetheless depends on formation geology or on the presence of existing natural fractures (Grant and Bixley, 2011). Hydraulic fractures tend to orient vertically (Fink, 2011) upward, because the least principal stress (where fracture initiation occurs) is generally one of the horizontal confining stresses (in x or y directions). The successful fracturing treatment of wells at the Nigorikawa geothermal field in Hokkaido, Japan, closely demonstrates this concept (Niitsuma et al., 1985).

Published reports of hydraulic fracturing of geothermal wells have been very limited. Fracturing experiments conducted at the Raft River in Idaho in 1979, at the Imperial Valley, East Mesa, California in 1980, and at Baca, New Mexico in 1981, are the earliest records of this stimulation method (Entingh, 2000). Remarkable improvements were achieved, particularly in the case of the East Mesa wells.

Around the same time, wide-ranging laboratory and field-scale experimental works were also conducted to evaluate the effectiveness of hydraulic fracturing in stimulating EGS (or ‘hot dry rock’) systems to create artificial fractures that could provide the necessary permeability to mine the heat from the rocks. A considerable amount of literature can be found describing the results of experiments in EGS systems: in the United States at Fenton Hill, New Mexico (Mortensen, 1978; Duchane and Brown, 1995; Murphy et al., 1999) and Coso, California (Rose et al., 2005); and in France at Soultz-sous-Forêts (Baria et al., 1999; Durst and Vuataz, 2000; Dezayes et al., 2005; Schindler et al., 2008). Similar studies have been pursued in Japan

(Matsunaga et al., 2005), Germany (Rummel and Kappelmeyer, 1982), and Australia (Wyborn et al., 2005). While the application of hydraulic fracturing is well established in the petroleum industry, there is no clear guideline for its application in stimulating geothermal wells, and it is rarely used in conventional geothermal wells. However, growing interest in EGS has triggered ongoing efforts to assess potential use of hydraulic fracturing in: India (Chandrasekharam and Chandrasekhar, 2010), Korea (Lee et al., 2010), the United Kingdom (Law et al., 2010), Lithuania (Sliupa et al., 2010) and the Philippines (Bayrante et al., 2010).

The limited field-testing results on hydraulic fracturing stimulation specifically for geothermal applications means that most operators resort to the use of fracturing techniques designed for petroleum reservoirs despite the very different high-temperature geothermal environment (Flores et al., 2005). This technical drawback was exemplified in the three-well HPF stimulation conducted at the Leyte (conventional) geothermal field in the Philippines using propped viscous gel. The results were only an average improvement of the injection capacities of two wells, while the third well showed no improvement (Malate, 2003). Despite the lack of an industry-specific procedure, 'brute-force' WF fracturing treatments in geothermal wells have been undertaken usually after the completion of tight wells as practised in Iceland, Philippines and elsewhere in attempts to enhance permeability (Aqui, 2012). These fracturing treatments (also known as water enhancement) are usually performed using fresh water pumped into the well at high rates above the formation fracturing pressure and usually without proppants.

9.3.3 Cold fluid stimulation (thermal effects)

Cold fluid stimulation is a variation of the conventional hydraulic fracturing concept differing in the mechanism by which permeability is enhanced. Instead of the hydraulic pressure 'breaking the rock formation' by injecting fluid at sufficiently high pumping rates to overcome the formation fracturing pressure, cold fluid stimulation is conducted far below the formation fracturing pressure for an extended period of time and relies on thermal effects to increase permeability (Benson et al., 1987). Thermal effects could be due to single or multiple mechanisms, including, 'thermal cracking' of the formation, mineral dissolution, and thermal contraction of the rock matrix. In a study investigating the effects of cold fluid injection on the permeability in a fractured rock formation, it was shown that thermal stress and chemical reaction have significant influence on well permeability (Ghassemi and Suresh Kumar, 2007).

The concept and efficacy of cold fluid stimulation is well recognised, but the mechanism is still poorly understood (Grant and Bixley, 2011). Several studies related to this concept have put forward a number of theories for the mechanism by which cold-water injection affects formation permeability. Prevailing theories drawn from

analytical and numerical models derived from actual field and laboratory experiments include the following:

- The increase in permeability around the injection well is due to the increase in the thermally induced fracture aperture combined with the increase in the permeability-thickness product brought about by the downward flow of the cold water with greater density through the fractures (Cox and Bodvarsson, 1985; Ariki and Hatakeyama, 1998).
- Permeability reduces for higher temperature injection but then permeability increases again when temperature reverts to low temperature, a reversible mechanism based on laboratory experiments (Contreras, 1990). The reversibility between temperature and the injectivity index (II) (Section 6.2.3) of the well was demonstrated by Siega et al. (2014) with geothermal field data, though the mechanism remains unknown. Siega et al. (2014) derived a very practical empirical equation for the correction of II for changes in injectate temperature (Fig. 9.9). For example, this is very useful to correct the II from its relatively high value measured during cold water injection at the completion test, to the value of II that will be active during hot brine reinjection (the II will be lower).
- Permeability increase is due to thermal contractions of the rock matrix that develop fractures with relatively large apertures (Kitao et al., 1990). Numerical models confirm the increase in the fracture aperture in the field tests to be the result of thermal contractions (Pruess and Enedy, 1993; Ariki and Akibayashi, 2001). Radial flow models also showed that improvement in permeability is strongly influenced by

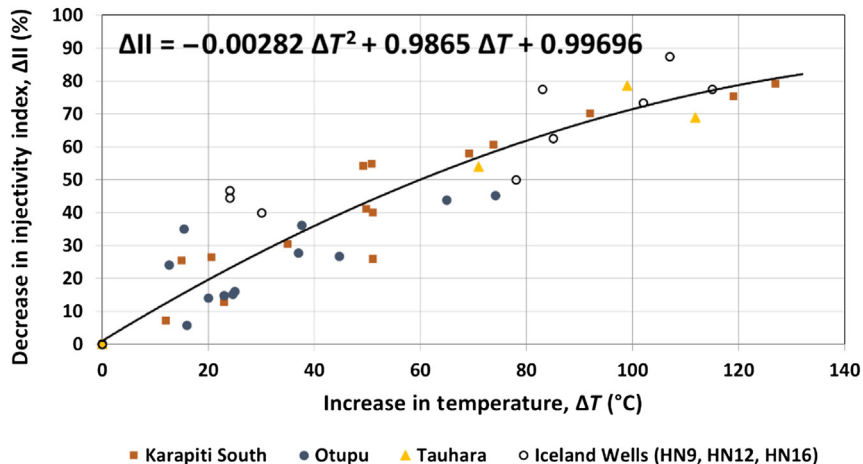


Figure 9.9 Percentage decrease in injectivity index (ΔII) versus increase in formation temperature. From Siega, C., Grant, M.A., Bixley, P.F., Mannington, W., 2014. Quantifying the effect of temperature on well injectivity. In: *Proceedings of the 36th New Zealand Geothermal Workshop, Auckland, New Zealand*, with kind permission.

changes in fracture porosity as a result of both cooling and pressure build-up near the wellbore (Nakao and Ishido, 1998).

- Cooling gives rise to tensile stress components near the borehole wall, which will decrease the internal fluid pressure required for hydraulic fracture. In extreme cases the sum of thermal and regional stresses can become tensile to the point of exceeding the tensile strength of the rock, even without internal pressurisation of the hole. In contrast, heating induces compressive stresses near the borehole wall, and the internal pressurisation required to overcome the sum of regional and thermal stresses is correspondingly higher. In extreme cases, these compressive stresses could match the uniaxial (or biaxial) compressive strength of the rock (Stephens and Voight, 1982).

Cold fluid stimulation is relatively common in geothermal wells, and there are many published examples. One of the earliest documented examples was the discontinuous injection of cold water (intermittent injection with heatup in between), conducted in the Sumikawa geothermal field in the Akita Prefecture, Japan (Kitao et al., 1990). The targeted three wells were stimulated with cold river water forced by reciprocating pumps, which resulted in increases to the II of between 33% and 64%.

In the past decade, several other injection tests have been reported using intermittent injection or cycling between cold-water injection and heatup, which successfully improved the wellbore connection with the major fracture networks of the reservoir. At the Hellisheidi geothermal field in Iceland a cooling/warm-up cycle was started in the well HE-8 upon its completion (Bjornsson, 2004). This was done using the Icelandic practice known as ‘cooling string approach’, which involves cooling the well rapidly by pumping 50–60 kg/s of cold water through the drill pipes for a period of 10–20 hours (depending on circulation losses) and then allowing the well to warm up for 12–24 hours, and then repeating the cycle once or twice. At the end of the stimulation the II of the well had increased from 4 kg/s/bar to a maximum of 7 kg/s/bar, an improvement of around 75%. In Salak geothermal field, Indonesia, cold fluid stimulation was conducted as part of its well stimulation programme to improve the permeability connections between the wells and the reservoir, particularly those wells located in the outer boundaries of the resource (Yoshioka et al., 2009; Pasikki et al., 2010). The cold fluid stimulation was able to increase the II of three out of four wells but the improvements were not sufficient to support commercial steam production. Similar cold fluid stimulation was conducted in Los Humeros geothermal field, Mexico, which successfully improved the injection capacity (injectivity) of a former production well turned into a reinjection well (Flores-Armenta and Tovar-Aguado, 2008).

The warming stage (cycling) is not necessarily required, and permeability improvements have been achieved even if the warming stage has been omitted during the stimulation process. The temperature difference between the cold injection fluid

(20°C–25°C), and the hot reservoir formation (over 200°C) alone can induce a more permeable connection between the wellbore and the geothermal reservoir. This is supported by various published examples: the improved productivity of a well with continuous cold seawater injection in the Bouillante geothermal field, Guadeloupe, West Indies (Sanjuan et al., 2000); the enhanced permeability and productivity after cold-water injection into a well in Borinquen geothermal field, Costa Rica; and the increase in the capacity of injection wells after sustained cold river water injection in the Rotokawa and Kawerau geothermal fields, New Zealand (Siega et al., 2009). The early reinjection of waste brine in the Palinpinon and Tongonan geothermal fields in the Philippines also showed improved injectivity and hence injection capacity in two wells, proving the effectiveness of the technique even when the temperature contrast is less, for a relatively high injection temperature of 150°C (Dobbie et al., 1982).

Notably, the effectiveness of the cold fluid stimulation technique has been prolific despite the diversity in the geological settings of the fields and chemistry of the injected fluid, not to mention the apparent dissimilarity in the injection methodology. Experimental studies on cold fluid stimulation at a laboratory scale have been very scarce but in a study at the Stripa Iron Ore Mine in Sweden (Lee and Farmer, 1993) using warm water in granites, and a study using the in situ test results on fractured gneiss (Barton and Lingle, 1982) it was indicated that the permeability of the rock mass decreased with increase in temperature 4- and 10-fold, respectively. Basic questions, such as ‘Which injection fluid is most effective?’ or ‘How long a cooling or warming period is required for an effective stimulation?’ are yet to be addressed. Many more questions than these must be well understood for an effective and scientific approach to this stimulation technique (Aqui, 2012).

9.3.4 Deflagration stimulation

Deflagration, also known as high-energy gas fracturing, creates a rapidly expanding gas cloud downhole, which delivers a high-pressure impulse with the potential to create new fractures or enhance existing fractures (McLean et al., 2016). Deflagration can also clean out the perforations in petroleum wells (Aqui, 2012). If there is formation damage, the high-energy gas wave generated from the vaporising propellant breaks through the formation damage, creating small fractures near the perforation channel. When the pressure dissipates, the gas surges back, carrying with it fine particles from the formation (Aqui, 2012). The deflagration tool is run on an E-line and consists of a perforated hollow steel carrier, which houses the solid propellant charge (solid rocket fuel), a detonator and a casing collar locator. The setup is similar to a wireline-deployed perforating gun, used to perforate casing (McLean et al., 2016).

The subsonic timescale over which the high-pressure impulse is delivered is the key to deflagration technology. It is different to an explosive, which creates supersonic

shock waves on a very short timescale, and hydraulic fracturing which creates a pressure impulse over a relatively long timescale, rather it is something intermediate between the two.

Due to the high temperatures of geothermal wells and the instability of the propellant and detonator the well needs to be quenched below 204°C during operations (McLean et al., 2016). Therefore high-temperature wells must have at least sufficient permeability to allow the pumping of cooling water beyond the targeted depth, to prevent premature triggering of the deflagration gun. Otherwise, the well must be cooled by circulation through the drill pipe or coil tubing unit before running the deflagration gun. However, this option has higher associated cost and risk.

While deflagration technology can theoretically create new fractures in unfractured rock, application of the technique in geothermal reservoirs has aimed to stimulate existing permeable fractures, at known feed zones. Therefore accurate location of the tool at clearly identified feed zones is critical, as the deflagration is effective only over the length of the tool (a typical length is ~ 10 m) and a few metres above and below. A matrix has been developed by the Energy Development Corporation (EDC), Philippines, to facilitate the selection of candidate wells for deflagration, ranking wells based on factors such as position within the geothermal field, proximity and capacity of nearby wells, temperature, permeability and skin factor (Aspiras et al., 2015). The selection of target feed zones in those wells are ranked based on factors such as lithology, rock compressive strength and fracture interconnectivity (if known).

Ohren et al. (2011) reported on deflagration in three wells at Soda Lake, the United States. Improvements were reported in all three wells, though the effect of deflagration could not be isolated from other performance-enhancing operations which occurred around the same time, including liner removal, casing perforation and cold fluid stimulation (McLean et al., 2016). For example, an increase in injectivity of two orders of magnitude was reported in one of the wells, which was due to the combined effect of deflagration and 5 days of cold-water injection.

Deflagration was trialled in four wells at Reykjanes geothermal field, Iceland (Sigurdsson, 2015). In two wells the results were inconclusive due to unstable or limited well testing conditions. In the remaining two wells the increase in overall II was small, 30% in one well after eight shots at seven depths, and 7% in the other after five shots at four depths. It was concluded that deflagration does increase the near-well permeability, but not significantly, though it may have been hampered by difficulty with accurately locating feed zones in the wells (Sigurdsson, 2015).

Deflagration was trialled in three wells in Ohaaki geothermal field, New Zealand (Bixley et al., 2016; McLean et al., 2016). Increases in the overall II were quite small, consistent with the experience of deflagration in Iceland (McLean et al., 2016). However, Bixley et al. (2016) showed that in multi-feed zone wells (which comprise the majority of geothermal wells) the overall II of the well is not a good measure of

deflagration success, as it may not be sensitive to large changes in injectivity at an individual feed zone. As an example, an increase in overall injectivity of 70% can result from an increase in II at the actual deflagrated feed zone of 300%. Bixley et al. (2016) concluded that definitive proof of an improvement in permeability due to deflagration would be an increase in production flow rate, though this will only become evident after weeks and months when the temperature of the well fully recovers, and the flow rate stabilises.

We believe that in geothermal wells, deflagration has the potential to remediate wells with skin damage (although this condition is rare due to aerated drilling), to clear perforations in the liner blocked by mineral scaling, and to further enhance the near-wellbore permeability (negative skin).

9.3.5 Other geothermal stimulation techniques

Other novel well stimulation techniques have been discussed by Chu et al. (1987), Tambini (2003) and Malate (2003), including acoustic (active cavitation and ultrasonic) stimulation, electric stimulation (Baterbaev et al., 2002) and lateral laser drilling from a vertical well (Ezzedine et al., 2012; Bajcsi et al., 2015). Most of these stimulation techniques are still in the research and development stage; more testing is needed before they can be implemented on a field scale.

It is our recommendation that field developers and investors consider proven tested methods only, unless the project financial model accommodates testing new techniques. This level of testing is normally undertaken in research-driven projects with some government or industry funding/subsidies.

9.3.6 Recommendations for geothermal stimulation

We have some general recommendations for stimulation using current proven technology to improve the permeability of geothermal production and reinjection wells, particularly deep EGS wells, where drilling commonly utilises mud in low-permeability reservoir rock and stimulation is common:

- To minimise the requirement for stimulation, if possible do not drill the productive part of the well with mud, thus eliminating the primary cause of skin damage in geothermal wells.
- If stimulation is required after drilling, first use deflagration ([Section 9.3.4](#)) to improve the near-wellbore permeability, initiate fractures, and remove skin damage, especially in perforated targets where cement invasion reduces the near-well permeability.
- Carry out an extended cold-water stimulation ([Section 9.3.3](#)) for example using the cooling string approach, to improve permeability further out into the reservoir.

- Then flow up with an extensive wellhead (bullhead) acidising operation, exceeding the recommended/standard acid pumping volumes discussed in Section 9.3.1, and also considering concentrations of HF higher than the standard 5%.

For low-permeability low-temperature EGS wells, a possibility is to consider extended hydraulic fracturing and/or acid fracturing operations (large flow rate for a considerable time), if there are encouraging economic incentives with the availability of fracturing equipment and experienced personnel. Also there should be good environmental controls, public consultation and acceptance for the application of hydraulic fracturing.

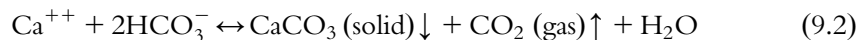
If a stimulation job following these guidelines does not produce the desired permeability/productivity enhancement, then no other ‘existing/proven’ method is likely to work. Ultimately, there is a limit to the funds and time a developer will be prepared to invest to make the well productive, and there will be a point in time when the well has to be abandoned.

9.4 Scaling in geothermal wells

Generally, all the natural elements of the periodic table can be found in the geothermal fluid, in different proportions between different wells and fields. Some of these elements form solid minerals, which deposit inside the geothermal well casing or liner, where they are referred to as ‘scale’ and effectively reduce the diameter of the casing, restricting flow of production or reinjection fluid through the casing.

9.4.1 Calcite scaling

Calcium carbonate (CaCO_3) – also known as calcite – is the most common type of scale in production wells. The scale forms when there are calcium ions (Ca^{++}) in the reservoir rock and high CO_2 gas dissolved in the geothermal fluid, governed by the reaction described by Eq. (9.2):



Calcite scale (CaCO_3) has a retrograde solubility (solubility decreases with an increase in temperature) (Fig. 9.10). The significance of this is that higher temperature wells will have fewer issues with calcite scaling, while colder wells have more issues, but that it can change if there are induced cool downflows in high temperature wells.

The solubility of calcite also increases with increasing CO_2 partial pressure and salinity (e.g. NaCl). Scaling (deposition) takes place at the flash point (when brine first boils) due to loss of gas (CO_2) from the liquid, forming localised scale that can rapidly result in a major constriction (Fig. 9.11).

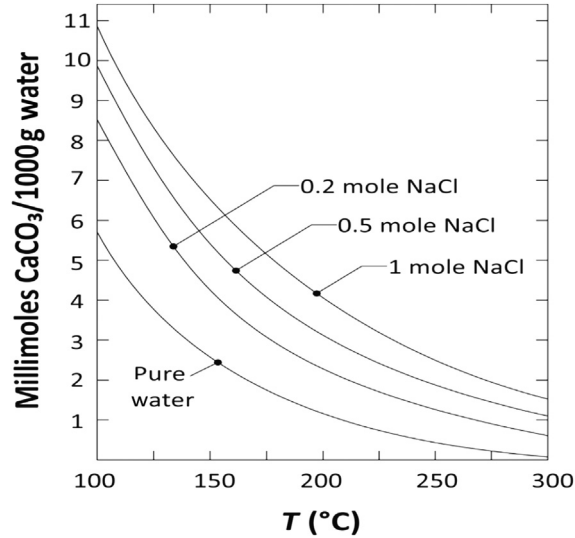


Figure 9.10 Solubility of calcite at CO² partial pressure of 12 bar. After Ellis, A.J., 1963. The solubility of calcite in sodium chloride solutions at high temperatures. *Am. J. Sci.* 261, 259–267 (Ellis, 1963).

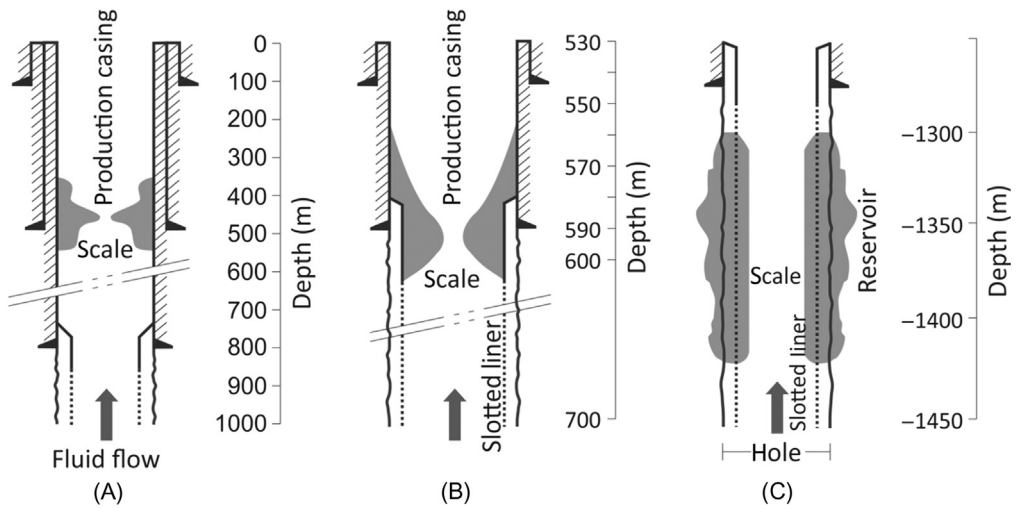


Figure 9.11 Schematic of calcite scaling in different parts of the geothermal wells: (A) in the production casing; (B) at the top of the liner and (C) within the liner. After Ocampo-Díaz, J.D.D., Valdez-Salaz, B., Shorr, M., Saucedo-M, I., Rosas-González, N., 2005. Review of corrosion and scaling problems in Cerro Prieto geothermal field over 31 years of commercial operations. In: *Proceedings of the World Geothermal Congress, Antalya, Turkey* (Ocampo-Díaz et al., 2005).

Fig. 9.12 shows downhole camera images (Section 7.3.2) of localised calcite scale deposition in a geothermal well in New Zealand. Scaling starts at about 529 m depth, increasing in thickness between 571 m and 601 m, while deeper there is no scaling in the perforated liner at 626 m.

Calcite scaling can also form inside reinjection wells when the injected fluid heats up inside the casing, due to the retrograde solubility (Fig. 9.10) of calcite. However, this is uncommon.

Long-term trends in a geochemical plot of Cl/Ca ratio versus silica (quartz) temperature (Fig. 9.13) can reveal calcite scaling over time. As the temperature decreases, the Cl/Ca ratio increases as Ca is lost from the fluid when it precipitates as scale in the well.

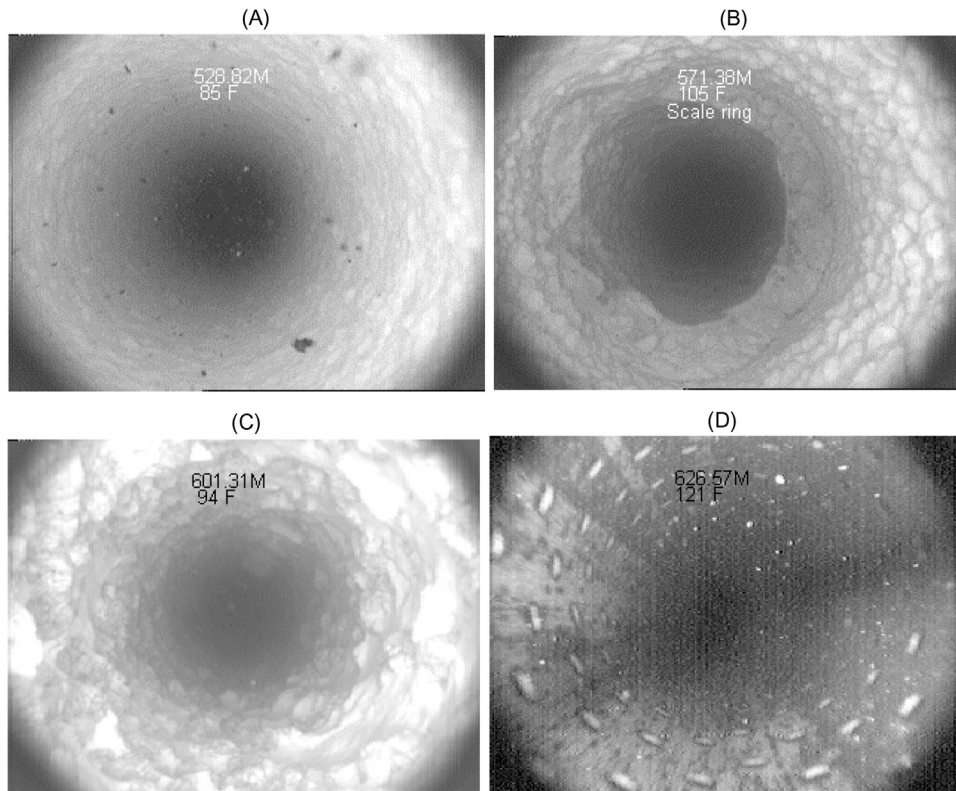


Figure 9.12 Downhole camera images of calcite scaling inside the production casing and liner: (A) thin scale at 529 m, (B) thick scale at 571 m with a sudden reduction (scale ring) in diameter, (C) thicker scale at 601 m likely the first flash point and (D) no scaling at 626 m in the perforated liner (below the flash point). *Images from Contact Energy Ltd., with kind permission.*

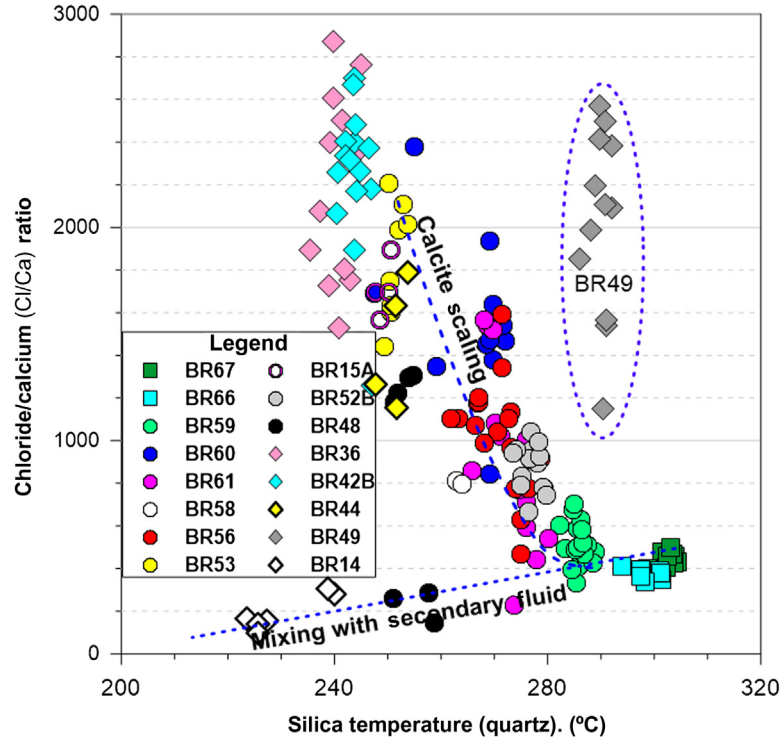


Figure 9.13 Cross-plot of chloride/calcium ratio and silica (quartz) temperature of Ohaaki production wells 2015–17. From McLean, K., McDowell, J.M., Sepulveda, F., Seastres, J., Zarrouk, S.J., Alcaraz, S., 2018. Upflow along a basement fault revealed by geothermal numerical pressure transient analysis. In: *Proceedings of the 40th New Zealand Geothermal Workshop, Taupo, New Zealand* (McLean et al., 2018).

There are various common solutions (mechanical and chemical) for calcite scaling, which can be chosen based on factors such as cost, tool availability and severity of scaling:

- Broaching (mechanical scale removal) using a broaching tool, which has sharp cutting edges and is run on a wireline and is repeatedly hoisted up and dropped onto the scale (Wilson et al., 2015). It is more effective in vertical than deviated wells, as friction with the deviated casing will slow the tool as it drops.
- Using a workover rig to drill out the scale (mechanical scale removal).
- Water blasting and acid cleaning with a coiled tubing unit, with the tubing positioned at the depth of the scale.
- Prevention of scale by injection of antiscalant into the fluid flow in the well, below the flash point, using downhole capillary tubing with a sinker bar, and a dosing pump at the surface.
- Using a rig to pull the perforated liner, water blasting at the surface before reinstalling the liner in the well.

9.4.2 Anhydrite scaling

Anhydrite (CaSO_4) scale forms in the presence of acid sulphide water and calcium ions. Similar to calcite, anhydrite has retrograde solubility and also forms in production wells but is less common than calcite. Anhydrite solubility is independent of pH and generally forms close to the wellhead. Anhydrite scaling has been reported in several production wells in Japan (Fukuda et al., 2010). It can also form inside geothermal wells when the well is shut, if there are internal flows/mixing. Anhydrite scaling in wells is localised (Fukuda et al., 2010) similar to that of calcite (Fig. 9.11) and can result in a major restriction to fluid flow.

Anhydrite generally dissolves when the well is kept on bleed while not in use. Fukuda et al. (2010) used the EDTA (ethylenediaminetetraacetic acid) chelating agent, to dissolve anhydrite scale in two wells at the Mori geothermal field in Japan.

9.4.3 Silica scaling

The chemical compound silica (SiO_2), in a crystalline form called quartz is one of the most abundant minerals in the Earth's crust, and also exists in the geothermal reservoir rock as quartz but deposits in surface equipment as amorphous (non-crystalline) silica (Opal-A). Fig. 9.14 shows the solubility of quartz and amorphous silica with temperature, and the path taken by a geothermal fluid (starting at 250°C) through the separator (due to steam loss, silica concentration increases in the remaining brine, which becomes saturated with amorphous silica at a relatively high temperature of $\sim 180^\circ\text{C}$) or through the heat exchangers (no steam loss, therefore silica concentration does not

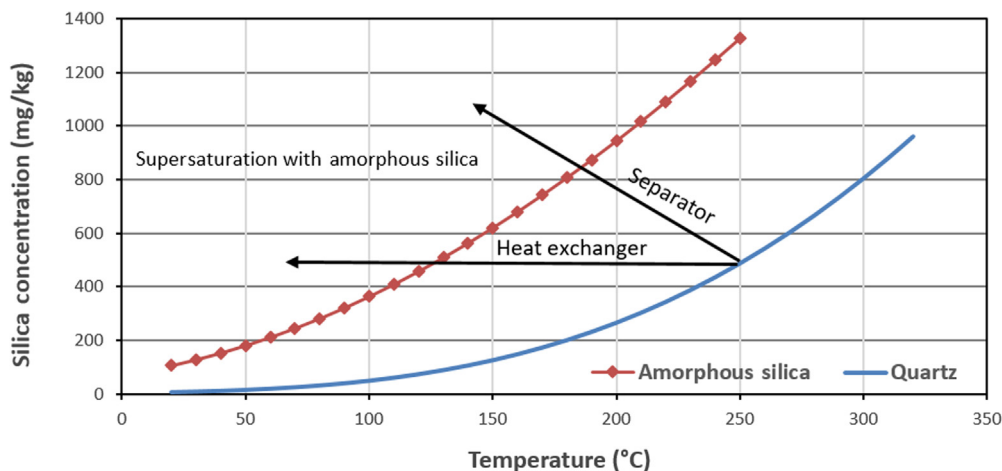


Figure 9.14 Solubility of quartz and amorphous silica with temperature. Modified from Zarrouk S.J., Woodhurst, B.C., Morris C., 2014. Silica scaling in geothermal heat exchangers and its impact on pressure drop and performance: Wairakei Binary Plant, New Zealand. *Geothermics* 51, 445–459.



Figure 9.15 Silica scaling in reinjection well perforated liner showing many blocked perforations due to silica scaling (pictures by authors).

change, and saturation with amorphous silica occurs at a relatively low temperature of $\sim 125^{\circ}\text{C}$). The large gap between the quartz and amorphous silica solubility curves, has effectively enabled geothermal development, as without it any decrease in geothermal fluid temperature would immediately result in silica scaling.

Silica scaling is the most common type of scale in geothermal surface facilities, normally forming inside the separator after flashing, as the steam is removed from the two-phase geothermal fluid and the silica is concentrated in the separated brine (Fig. 9.14). It is also common in geothermal heat exchangers (Zarrouk et al., 2014) and brine lines (e.g. for transport of brine to reinjection areas). Therefore it is the most common scale in reinjection wells (Fig. 9.15) and often reduces injectivity of the well (Coutts et al., 2018).

Silica scaling has also been reported in some high-enthalpy vapour-dominated production wells where the geothermal fluid totally dries inside the casing, forming both scaling on the walls and silica sand particles travelling in the steam which can damage the turbine blades. This was observed in some of the shallow dry steam wells in Wairakei and also reported in Kamojang, Indonesia (Nugroho and Hendriana, 2018).

Experience has shown that geothermal developments can tolerate some degree of silica supersaturation without scaling. However, silica scaling is affected by many factors including (Brown, 2011):

- degree of supersaturation,
- acidity (pH),
- temperature,
- flow rate,
- aeration and
- other ions in solution (mainly Fe, Mg and Al).

The degree of silica saturation in the geothermal fluid is measured through the silica saturation index (SSI) Eq. (9.3).

$$\text{SSI} = \frac{\text{Concentration of silica in solution}}{\text{Equilibrium solubility of amorphous silica (at same temperature and pH)}} \quad (9.3)$$

When $\text{SSI} = 1$ this means the fluid is just at the point of saturation, and an SSI of greater than 1 means the fluid is supersaturated with amorphous silica and will have a higher risk of unmanageable scale build-up. Experience has shown that depending on the fluid chemistry, it is possible to tolerate some level of supersaturation (Zarrouk et al., 2014; Zarrouk and Moon, 2014). The presence of some ions (Al in particular) can result in the formation of Al-silicate at SSI less than 1.0 (Newton et al., 2018).

The treatment of silica scaling in reinjection wells mainly involves drilling with a workover rig and acidising (Zarrouk et al., 2014). For production wells a common method is water blasting, using a 45-degree nozzle for the production casing and 90-degree nozzle for the liner (Nugroho and Hendriana, 2018).

Due to the generally high scaling potential of geothermal fluids, silica in particular, only two types of heat exchangers are used for the extraction of thermal power from geothermal fluid. This is relevant to direct-use applications and in binary plants which extract heat from two-phase geothermal liquid after the separator (Fig. 9.1).

Once-through (straight tube) shell and tube heat exchangers (Fig. 9.1) are used for high-pressure and high-temperature applications, with the geothermal fluid always flowing in the tube side, and the cleaner secondary fluid flowing in the shell side. Note that U-bend tubes are not recommended for use in geothermal applications, as it is not possible to clean them out once mineral deposition takes place. For once-through heat exchangers the common recommended tube diameter is 1" (25.4 mm) to allow the cleaning of mineral scale: smaller diameter tubes should only be considered when there is no scaling potential in the geothermal fluid.

Plate type heat exchangers are used for lower pressures (<20 bar) and lower temperatures (<150°C) in direct-use applications only (Thain et al., 2006), but not in binary plants. Plate type heat exchangers are lower in cost, more compact, easily cleaned, adaptive to duty change and more efficient than shell and tube heat exchangers. Their use is restricted to geothermal fluid that is single-phase liquid only, with no gas or steam. Scaling in plate type heat exchangers is less common because the geothermal fluid used is cooler and generally less saturated with silica or other minerals. However, scaling can take place when the system is shutdown if the geothermal fluid is not drained/removed from the heat exchangers, by circulating fresh clean water. There can also be a build-up of slit and sand if the geothermal fluid carries solid particles, hence some geothermal heating systems use particle filters (see Section 2.2.1).

While on the secondary fluid (heated) side, growth of organic matter (e.g. Alga) can block the heat exchanger if the secondary fluid is not treated (Chlorinated).

9.5 Corrosion in geothermal wells

Geothermal fluid contains many chemical impurities, in both the liquid and vapour phase, which can be corrosive to the well construction materials (casing and cement). Corrosion can result in loss of casing material, which can threaten the integrity of the casing and result in a hole or casing break. This can result in the loss of geothermal fluid to the surrounding formation, drop in the flowing well pressure and the migration of hot geothermal fluids to the ground surface where there will be a risk of blow-out. In some cases when the pressure inside the well is less than that of the surrounding formation, there could be an inflow of cooler fluid (of different chemistry) into the well, this fluid can potentially quench (cool) the well or possibly cause the formation of calcite or anhydrite scale, which can lead to well blockage.

The geothermal corrosion environment mostly affects the above-ground (steam field and power station) equipment (Nogara and Zarrouk, 2018a) and is beyond the scope of this book. Nogara and Zarrouk (2018a) discussed different classification systems for the geothermal fluid corrosivity indexes used in the industry. This book focuses on the geothermal well, where the carbon steel casing of geothermal wells is susceptible to corrosion attack: both internally by the deep geothermal reservoir fluid and externally by the shallow fluids in the formations penetrated by the casing.

Nogara and Zarrouk (2018b) evaluated the performance and corrosion behaviour of 172 carbon steel and corrosion-resistant alloys (CRA) in different geothermal wells and surface facilities and also discussed the corrosion evaluation methods and factors controlling corrosion rate for different geothermal fluid chemistry. Nogara and Zarrouk (2018b) concluded that the main factors that influence corrosion in the geothermal fluid environment include high salinity, pH, high temperature, fluid velocity, high concentration of dissolved gases and lack of stable corrosion products; the combination of these factors increases the corrosion rate. Nogara and Zarrouk (2018b) recommended carrying out material field testing when possible, prior to material selection for highly corrosive fluid environments.

9.5.1 External casing corrosion

External casing corrosion (ECC) refers to casing being attacked by corrosive fluids from the outside. ECC is common in petroleum wells and has been reported in many fields worldwide (Gordon et al., 1984; Crolet and Bonis, 1986; Rahman, 1989; Talabani et al., 2000; Lopez et al., 2003). Gordon et al. (1984) found that there are two causes for ECC in petroleum wells: in the upper 60 m of wells, ECC is mainly caused by oxidation, enhanced by the high chloride, sulphate and salt (e.g. NaCl)

concentrations of the ground waters. Below 60 m, ECC is associated with CO₂-rich (carbonic acid H₂CO₃) solutions, which accounts for approximately 60% of oilfield casing failures (Lopez et al., 2003). Poor cementing jobs are often the main contributors to ECC in petroleum wells, as the casing is left exposed to shallow reservoir fluids (Gordon et al., 1984; Talabani et al., 2000). ECC due to CO₂-rich water is also a problem associated with CO₂ injection for enhanced oil recovery (Ikeda et al., 1985). The most common type of corrosion in geothermal wells is ECC near the surface (<60 m) in hot moist soil or cement where oxygen can reach the steel casing (Thorhallsson, 2003). Exposed annuli can also trap water and oxygen in wells on standby and reinjection wells (Thorhallsson, 2003).

In andesitic geothermal systems, such as in the Philippines and some Indonesian geothermal systems like Karaha-Telaga (Moore et al., 2002), most cases of ECC are caused by acid-sulphate-rich waters. These waters form from the oxidation of H₂S to form sulphuric acid, which can descend through highly permeable structures to as deep as 2500 m in the Philippines (Rosell and Ramos, 1998; Moore et al., 2002).

Three wells at the BacMan field, Philippines (Rosell and Ramos, 1998) and several in Palinpinon (Zaide-Delfin, unpublished results, 1988) and Cerro Prieto, Mexico (Dominguez, 1980) suffered from casing penetration due to ECC by acid-sulphate fluids. A consequence of casing penetration is blockage of the well by anhydrite deposition due to mixing of acid-sulphate water with upflowing neutral Cl waters during discharge (also a downflow of acid fluids while the well is shut, mixing with reservoir Cl waters) (Zaide-Delfin, unpublished results, 1988; Rosell and Ramos, 1998; Sugiama et al., 2004).

Neutral to slightly acid pH CO₂-rich waters are extremely corrosive to the steel casing at high temperatures in geothermal systems (Bixley and Wilson, 1985; Hedenquist and Stewart, 1985). Cement failure due to CO₂-rich waters was reported to occur in less than 5 years and, in one case, resulted in a collapsed well casing within 90 days (Kukacka and Sugama, 1995). Zarruk (2004) reported ECC taking place between the depths 200 and 600 m due to CO₂-rich waters in many geothermal fields in New Zealand.

ECC can manifest itself in the cellar through a steam leak from an exposed annulus between casings, or steaming ground around or near the well. In many cases the corrosion remains undetected until a significant loss in production is noticed. It is common practice to grout (abandon) a well once a hole is detected in the casing, to prevent blowouts and to stop cold downflow through the casing hole when the well is shut (Zarruk, 2004).

Detailed and well-calibrated numerical reservoir models can be a useful tool for monitoring the existence and migration of corrosive fluids during the life of the field (Zarruk, 2004).

9.5.2 Internal casing corrosion

Internal casing corrosion (ICC) is the corrosion that takes place inside the casing due to reaction between the geothermal fluid and the well casing material.

The common fluid that causes ICC is acid-sulphate waters, commonly reported in young volcanic (sulphur-rich) areas (Ellis and Mahon, 1977). In Matsukawa, Japan, acid-sulphate-rich waters with pH ranging from 3.7 to 5.5 caused ICC during early production (before well drying). Similar casing corrosion was reported at Tiwi, Philippines where caustic injection is used to increase the pH from 3 to 5 (Sugiaman, 2004) to prevent ICC. The worst reported case of ICC was in the Tatun geothermal field in Taiwan, with average fluid pH ranging between 2 and 3.5. Liquid sulphur was encountered along with the hot water in some wells (Ellis and Mahon, 1977). The carbon steel casing corrosion in Tatun was very rapid, causing total corrosion of the casing within hours during output testing and resulting in the abandonment of field development since 1971 (Armstead, 1978; Zarrouk, 2004). Nogara and Zarrouk (2015) tested several CRA in acid-sulphate geothermal fluid (pH 3.54–3.72) and reported several CRA and metal alloys able to withstand acid-sulphate water corrosion.

The hydrothermal minerals typically formed during the interactions of rock with acid-sulphate fluids (cation depleted) include: kaolinite, dickite, pyrophyllite, illite, sulphur, natroalunite, alunite, jarosite, anhydrite, andalusite, tourmaline, diaspore, pyrite, marcasite and enargite (Moore et al., 2002). These minerals can be identified during drilling, which should give indication of the presence of acid-sulphate fluids in the reservoir fluid.

At the Salton Sea, the United States, Grade 29 Titanium was used for casing material to resist chloride crevice corrosion and pitting attack from highly saline (hypersaline) brine with total dissolved solids of greater than 100,000 ppm (Thomas, 2003). Thomas (2003) concluded that Grade 29 Titanium has the potential to be used in the construction of EGS wells recharged with sea water, and also for hypersaline fluid found in some of the sedimentary basins in Europe. However, this comes at a very high cost. Nogara and Zarrouk (2014) gave a cost ratio of Titanium Grade 29 to commercial carbon steel casing material (e.g. L80, K55) of about 31 times.

9.5.3 Stress corrosion cracking

Stress corrosion cracking (SCC) results from the combined action of mechanical stress, such as static or applied tensile stress, and a corrosive environment (Nogara and Zarrouk, 2018a). There are different types of SCC including (Nogara and Zarrouk, 2018a):

- chloride-SCC, which affects stainless steel under certain conditions,
- ammonia-SCC, which attacks some copper alloys and
- sulphide-SCC also known as sulphide stress cracking (SSC) when the geothermal fluid has high hydrogen sulphide (H_2S) content.

SSC limits the options for geothermal well casing materials to the lower strength steels (Nogara and Zarrouk, 2018a), because higher strength steels will fail by SSC, due to the presence of H₂S. Therefore SSC is not common in geothermal wells due to the use of lower-strength casing (K55 and L80 grade). However, evidence of SSC is observed when using the C95 casing grade.

Keeping wells hot on a heavy bleed line greater than 1" is recommended for all hot wells with high H₂S content so that H₂S does not build up in the casing and causes problems like SSC.

9.6 Casing damage

Unlike petroleum wells which generally are abandoned when the resource is depleted, most geothermal wells are abandoned due to casing integrity damage rather than lack of energy or fluid in the reservoir. Damage to geothermal production and reinjection wells means:

- expensive repairs,
- expensive abandonment,
- drilling of replacement wells,
- substantial decrease in power generation and
- risk of a blowout.

In addition to corrosion (discussed in [Section 9.5](#)), there are hosts of reasons that can cause casing damage, and the various forms of casing damage are discussed in the following sections.

9.6.1 Internal casing wear

Geothermal wells can sustain casing damage very early, even during drilling operations, due to internal casing wear. This can be related to drilling pipe rubbing against the casing, which occurs mainly in deviated/directional wells when the rate of angle change with depth is greater than 5 degrees/33 m ([Fig. 9.16](#)). Snyder (1979) reported that internal casing wear commonly affects two drill pipe joints ([Fig. 9.16](#)). This can result in severe metal loss from the casing walls and possibly results in a hole in the casing. This will allow the geothermal fluid to leak to the surrounding formation and form a steam thief zone, which if not monitored can result in surface blowout.

9.6.2 Casing implosion

Casing implosion can occur due to a poor cementing job where there is trapped water due to cement-slurry placement problems. When water is trapped within the cement between two casings or between the casing and an impermeable formation, the inner casing can preferentially implode. This can manifest as necking of inner casing or violent implosive tear ([Fig. 9.17](#)). Normally, there is no evidence of damage to the outer

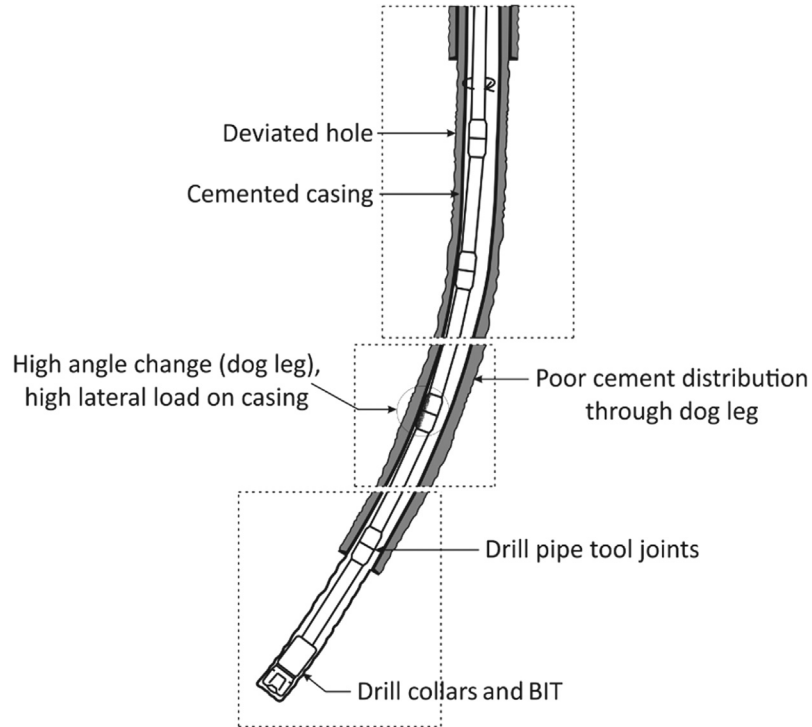


Figure 9.16 Internal casing wear. After Snyder, R.E., 1979. *Casing failure modes in geothermal wells. Geotherm. Resour. Council Trans. 3, 667–670.*

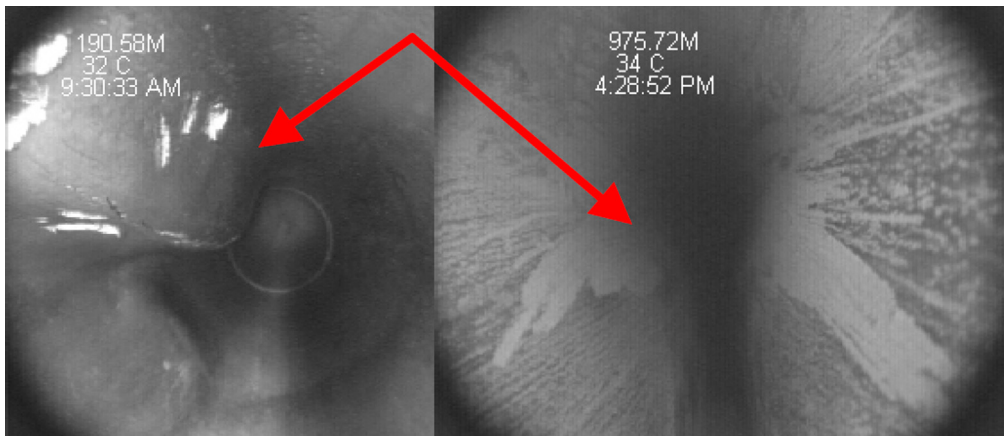


Figure 9.17 Casing implosion damage in two wells: (left) necking of inner casing and (right) total casing implosion from two sides (no tear). From Dr Ramonchito Cedric M. Malate, with kind permission.

casing but it can cause leaking in the outer casing coupling (Jacobs, 2016). Casing implosion normally occurs the first time the well heats up after drilling, due to the high thermal expansion coefficient of water which can result in high pressure in the trapped volume of water, sufficient to collapse 9 $\frac{3}{8}$ " and 13 $\frac{3}{8}$ " casing. If the implosion takes place between two casing strings, then measuring the total volume of implosion (if possible) can be used to estimate the mass of trapped water by knowing the difference in temperature between shut and flowing conditions Eq. (9.4).

$$\Delta V = m \times \left(\frac{1}{\rho_{\text{final}}} - \frac{1}{\rho_{\text{initial}}} \right) \quad (9.4)$$

where ΔV is the change in volume (m^3) of the casing (volume of the implosion), m mass of the trapped water (kg), ρ_{final} the density of liquid water at the flowing temperature at the casing implosion depth and ρ_{initial} in the density of liquid water at the warmed up temperature at the casing implosion depth. Experience has shown that casing implosion can take place with as little as 100 kg of liquid water trapped in the cement between 9 $\frac{3}{8}$ " and 13 $\frac{3}{8}$ " casings.

Liner-tieback well construction, which involves cementing the production casing in two stages, will reduce the risk as it can ensure a better cement job, but failure was reported in some cases (Jacobs, 2016).

Solutions to casing implosion damage are as follows:

1. The best solution to casing implosion is prevention by ensuring a good-quality cement job. This normally means pumping up to five times the annulus space volume and ensuring cement return at the surface.
2. Tapered chisel dropped repeatedly to straighten out the hump, for minor implosion (Thorhallsson, 2003).
3. Mill (machine) the implosion/hump and run and cement a smaller sleeve (patch) production casing. However, this will result in a loss in well productivity as part of the production casing will reduce in diameter.
4. Abandon the well and drill a new well (if there are multiple implosions), after risk and cost analysis.

9.6.3 Casing coupling compression failure

In high-temperature production wells the production casing heats and thermally expands due to the thermal expansion of the steel. However, the cement and the surrounding rock formation resist casing expansion. This can cause weak points in the casing to yield and deform, normally this takes place at the casing joints where the (buttress) threads jump (Fig. 9.18). This damage is more likely to take place at high formation temperatures ($> 300^\circ\text{C}$) and is more common near the ground surface where the casing is relatively cold (when the well is shut), and therefore the

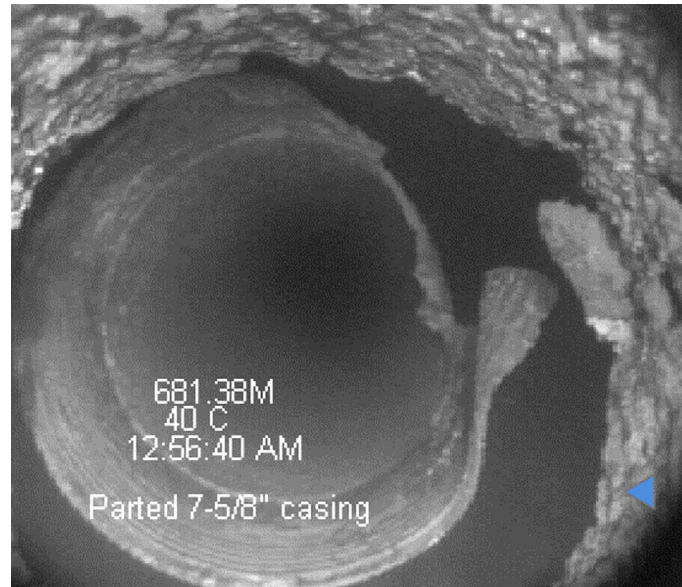


Figure 9.18 Production casing joint parting at the joint. From Dr Ramonchito Cedric M. Malate, with kind permission.

temperature difference and heating rate during production will be the greatest. It is more common in long casing runs than short production casing strings.

The following considerations apply to high-temperature geothermal fields (Jacobs, 2016):

- Design must allow for plastic behaviour in pipe body.
- Casing pretensioning (staged cemented/liner-tieback strings) — some pretensioning is better than none.
- Use casing couplings with greater compression efficiency (not buttress threads).
- Slow down the initial temperature increase of the well (initiate production flow gradually) to break the casing cement bond and allow the casing to move.
- For wells that cannot self-discharge, it is recommended to use hot geothermal fluid from another well or a portable boiler (Section 6.6.1), to prevent thermal shock during discharge stimulation. Avoid using the air compression stimulation method, to prevent a sudden geothermal fluid release and associated very rapid heating. For the same reason also avoid using liquid nitrogen injected through tubing (within a few minutes of steam discharge at the surface), there have been a number of instances of sudden catastrophic failure of casing, trapping the tubing.

Thermal expansion of the casing can also result in the extension of the well production casing and master valve assembly above-ground (Fig. 9.19), which will require the extension of the thrust frame and possibly adjustment of the above-ground pipe work. This is more common with production wells with relatively shallow production casing.

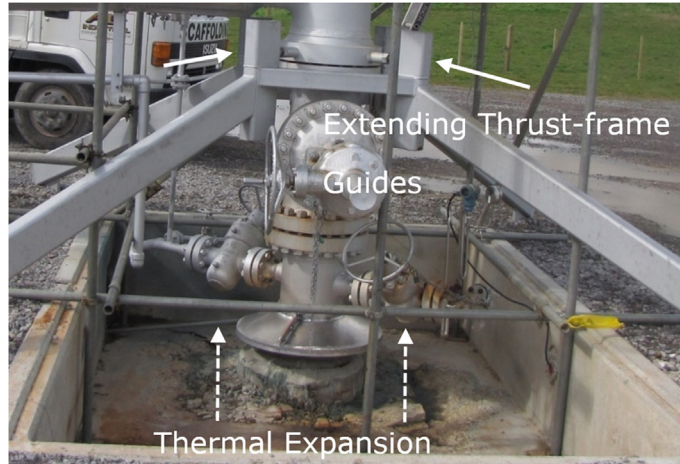


Figure 9.19 Extension of the well production casing and master valve assembly aboveground due to thermal expansion (picture by authors).

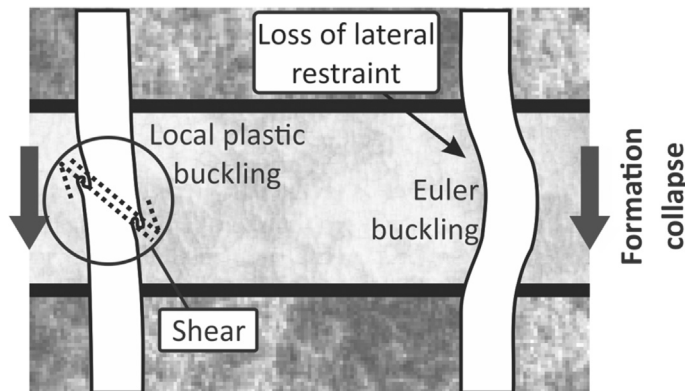


Figure 9.20 Casing shear (plastic buckling) and Euler buckling (no shear) due to subsidence. After Dusseault, M.B., Bruno, M.S., Barrera, J., 2001. *Casing shear: causes, cases, cures*. In: *SPE Drill 16*, 98–107, SPE 72060-PA.

9.6.4 Casing shear or buckle

Formation compaction (e.g. subsidence) associated with ongoing fluid withdrawal and reservoir pressure depletion is reported in many fields around the world and can cause the casing to shear or buckle (Dusseault et al., 2001). Casing shear commonly takes place just below the anchor casing shoe, where the production casing is left alone to withstand all the shear stresses, without support from larger casings, which can result in casing failure. Subsidence of tough formations can result in plastic buckling while soft formations can result in Euler buckling where the casing is deformed but does not sustain a mechanical shear (Fig. 9.20). Euler buckling can result in a dogleg in the

casing, which can cause problems during workover and when running downhole tools, but the casing can still be safe for production from the well.

Casing shear can also be caused by seismic events, which can result in permanent casing damage. It is interesting to note that seismic events can also result in the improvement of well productivity if it improves fracture/fault permeability in the productive part of the reservoir, so long as it does not result in production casing damage. Both casing shear and improvement in productivity can occur in different wells within the same geothermal field, as the result of the same seismic event (author's experience).

CHAPTER 10

Field studies

Contents

10.1	Introduction and overview of published geothermal PTA field studies	257
10.2	Single linear impermeable boundary	259
10.3	Two linear impermeable boundaries (channel)	262
10.4	Permeable fault (narrow channel)	264
10.5	Fracture closure	266
10.6	Cement damage and recovery	268
10.6.1	Presence of a linear impermeable boundary (fault)	270
10.6.2	Suppression of two-phase feed zones	271
10.6.3	Other data features	273
10.7	Permeability enhancement by deflagration	274
10.8	Permeability enhancement by cold water injection	277
10.9	Pumped wells	280
10.10	Tracer testing	282

10.1 Introduction and overview of published geothermal PTA field studies

There are a wide variety of practical applications for pressure–transient analysis (PTA) techniques in geothermal wells, alone or in combination with other types of data and analysis. These include: assessment of well condition (damage or stimulation), quantification of reservoir parameters (such as permeability or transmissivity), identification of reservoir–scale structural features (such as flow pathways and boundaries), and assessment of fractures created in enhanced geothermal systems (EGS). Despite the limitations of analytical PTA (Section 5.7), it is still in widespread use in the geothermal industry, and a number of geothermal analytical PTA field studies have been published, as listed below. Some of the more recent studies utilise numerical PTA, some using the framework described in Chapter 8 (or similar), or other forms of numerical modelling.

One of the most common applications of PTA in the geothermal industry is the assessment of reservoir parameters such as transmissivity and structure, which can be used as inputs to the conceptual model of the geothermal field. Historically, the majority of these types of studies have been completed using analytical PTA techniques, and despite the limitations of analytical PTA have yielded useful results. The following examples span around 50 years and are from geothermal fields all over

the world: in Japan, Sumikawa (Garg et al., 1991; Ishido et al., 1992), Matsukawa (Hanano and Sakagawa, 1990), Okuaizu (Ishido, 1985) and Uenotai (Menzies et al., 1990); in Turkey, Afyon Ömer-Gecek (Onur, 2010), Balçova-Narlıdere (Onur et al., 2002) and Kizildere (Onur et al., 2003); in Iceland, Hellisheidi (Björnsson, 2004) and Krafla (Bodvarsson et al., 1984); in Italy, Larderello (Celati et al., 1975) and Travale-Radicondoli (Atkinson et al., 1978a,b); in the United States, Dixie Valley (Morin et al., 1998), Baca (Riney and Garg, 1985b) and The Geysers (Acuna et al., 1992); in New Zealand, Wairakei (Zarrouk et al., 2007) and Ohaaki (McLean et al., 2018); in Mexico, Cerro Prieto (Rivera-R et al., 1980); in Republic of Djibouti, the Asal region (Elmi, 2005); in Iran, Sabalan (Khosrawi, 2015; Porkhial et al., 2015); in Republic of Georgia, Zugdidi-Tsaishi (Sanyal et al., 2000); in Indonesia, Kamojang (Aprilian et al., 1993); in Philippines, Tongonan (Menzies, 1979).

PTA results useful for the conceptual model potentially have the ability to constrain the field-scale numerical reservoir model, as is done in the petroleum industry (Putriyana and Syihab, 2013). This is very rarely used in the geothermal industry due to the numerous practical issues and general lack of confidence in geothermal PTA. This is also due to the fact that geothermal reservoir thickness is not clearly constrained in most cases and fluid production comes from localised feed zones in the large open-hole section of the well.

PTA is also a useful tool for the assessment of wellbore condition: stimulation or damage in the immediate vicinity of the well. There is the ability to quantify the effect of damage such as mineral scaling (Arkan et al., 2002; Onur et al., 2003) or cement invasion (Malibiran and Zarrouk, 2014). And there is the ability to quantify the effect of recovery efforts such as acidising and/or mechanical cleaning (Arkan et al., 2002; Barrios et al., 2007; Eker et al., 2017; Malate et al., 1998), or the effect of stimulation by deflagration (McLean et al., 2016).

The effect of injection temperature and cumulative injection on permeability-thickness and skin factor can also be assessed (Ariki and Akibayashi, 2001; Bixley and Grant, 1979; Horne, 1982; McLean and Zarrouk, 2015c; Villacorte and O'Sullivan, 2011).

The nature of fractures in EGS may be assessed, for example in Switzerland at Basel (Haring et al., 2008) and St Gallen (Wolfgang et al., 2015), in France at Soultz-sous-Forêts (McClure and Horne, 2011), Rittershoffen (Baujard et al., 2017) and the Carnmenellis Granite in England (Pine, 1983).

Some of the more recent geothermal field studies are presented in the following sections, comprising mostly examples of numerical PTA using TOUGH2 and PyTOUGH (the same or similar to the framework in Chapter 8), some analytical PTA, and also including examples of other types of well test data and analysis.

10.2 Single linear impermeable boundary

At Ohaaki geothermal field, New Zealand, in the well BR66, two pressure transients were measured during two separate (but very similar) injection tests in 2015 (McLean et al., 2016). The injection tests were pre- and post- deflagration of the well, as part of a larger programme to evaluate the effectiveness of deflagration. There are two aspects to the McLean et al. (2016) study: the shape of the pressure-transient data sets, and the difference between the two data sets. The shape of those pressure transients informs on the structure of the reservoir, a single linear impermeable boundary, and is discussed in this section. The difference between the two pressure transients is the result of permeability enhancement by deflagration and will be discussed in [Section 10.7](#).

For comparability the two injection tests have the same design: three increasing flow rates (37, 77 and 113 t/h) followed by a fall-off to zero flow (McLean et al., 2016). This is not the currently recommended practice for measuring pressure fall-offs, which should be to a lower flow rate (instead of zero) to avoid a variety of practical issues (Section 6.2.4). The data sets ([Fig. 10.1](#)) have been corrected using the cut-shift-fill (CSF) method (Section 7.5) to remove minor rounding in very early time. A period of data is missing from the late-time period of the pre-deflagration data set, as the tool was moved up and down the well to measure a heating profile, a practice that should be avoided due to the sensitivity of the pressure-transient data set, and the practical impossibility of returning the tool to exactly the same depth (Section 6.2.1).

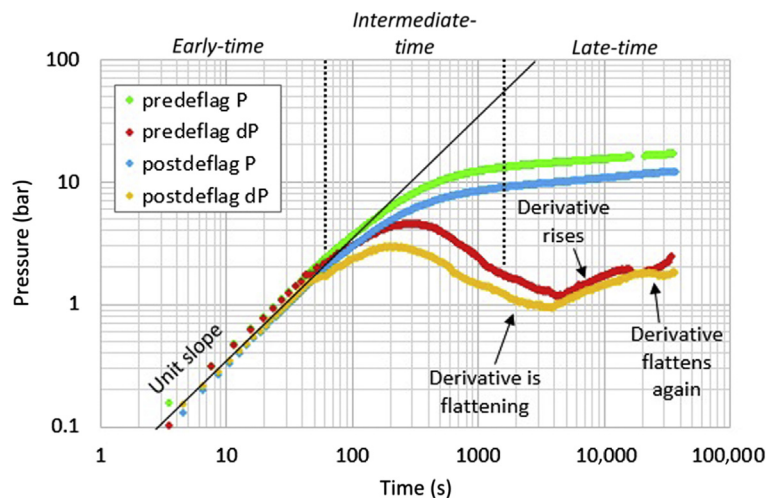


Figure 10.1 BR66 fall-off data from pre- and post-deflagration injection testing. *Modified from McLean, K., Zarrouk, S.J., Wilson, D., 2016. Application of numerical methods for geothermal pressure transient analysis: a deflagration case study from New Zealand. In: Proceedings 41st Workshop on Geothermal Reservoir Engineering, Stanford University, Stanford, CA.*

Due to this anomaly, confidence in the later data is lowered, and the upwards bend at the end of that derivative is questionable.

It can be seen in Fig. 10.1 that the two injection tests produced pressure transients of a very similar shape, indicating that the test is repeatable, which increases confidence in the results. The slight differences in shape (the smaller hump and downwards shift of the late-time data) are the result of actual changes near the well as a result of the deflagration operation and will be discussed in Section 10.7.

The shape of the pressure-transient data in the derivative plot (Fig. 10.1) is similar to the shape of a single linear impermeable boundary response, where the derivative flattens, rises and then flattens at a higher level (Sections 5.1.1 and 8.5.1). These pressure-transient data sets were analysed using both numerical and analytical PTA methods (McLean et al., 2016). Analytical PTA was completed using the software SAPHIR, and numerical PTA was completed using the numerical framework discussed in Chapter 8, Numerical pressure-transient analysis modelling framework, with non-linear regression using model-independent parameter estimation (PEST). Three models were considered: an infinite uniform porous reservoir (just for interest/comparison, not because the shape of the derivative would match this model), a single linear impermeable boundary, and the other possibility to match this derivative shape which is a dual-porosity reservoir. It was concluded that the best match to the data was from the single linear impermeable boundary model, though a dual-porosity model was also a reasonable match. There is little difference in the shapes of the numerical and analytical models when matched to the pre-deflagration data Fig. 10.2 and post-deflagration data Fig. 10.3.

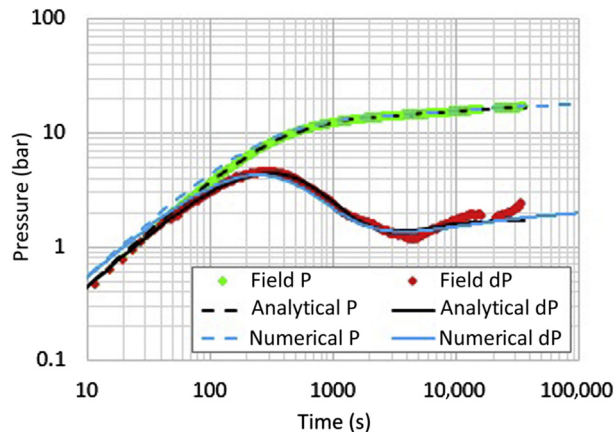


Figure 10.2 Match between pre-deflagration fall-off data and linear impermeable boundary models (numerical and analytical). Modified from McLean, K., Zarrouk, S.J., Wilson, D., 2016. *Application of numerical methods for geothermal pressure transient analysis: a deflagration case study from New Zealand*. In: *Proceedings 41st Workshop on Geothermal Reservoir Engineering, Stanford University, Stanford, CA*.

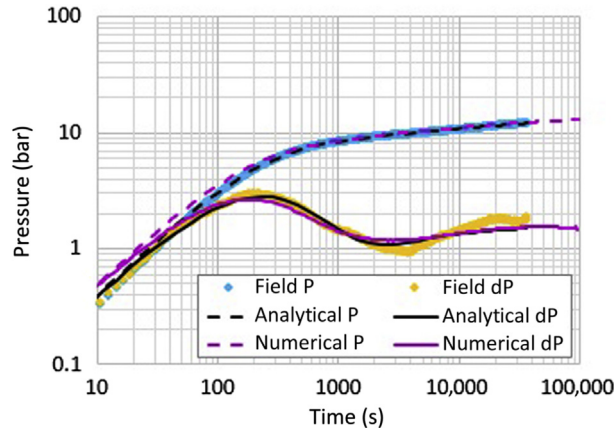


Figure 10.3 Match between post-deflagration fall-off data and linear impermeable boundary models (numerical and analytical). Modified from McLean, K., Zarrouk, S.J., Wilson, D., 2016. Application of numerical methods for geothermal pressure transient analysis: a deflagration case study from New Zealand. In: Proceedings 41st Workshop on Geothermal Reservoir Engineering, Stanford University, Stanford, CA.

Table 10.1 Summary of estimated parameters for the linear impermeable boundary model, from numerical and analytical PTA of pre- and post-deflagration field data (McLean et al., 2016).

	Estimated parameters		
	k (mD)	s	L (m)
<i>Analytical</i>			
Pre-deflag	3.8	2.4	19.9
Post-deflag	4.5	0.7	22.5
<i>Numerical</i>			
Pre-deflag	4.3	− 2.4	30 ^a
Post-deflag	4.8	− 3.1	30 ^a

^aThis parameter was fixed during the inversion process, to improve the late-time match.

A comparison of the estimated parameters from the numerical and analytical PTA is given in Table 10.1. The shapes of the numerical and analytical models are very similar, with similar estimated values for reservoir permeability of around 4–5 mD. In addition, both models estimate the boundary to be nearby, at a distance (L) of 20–30 m. However, there is an important difference in the estimated values for skin factor: the analytical model values are positive, indicating damage, and the numerical values are negative, indicating stimulation (Section 4.4.3). Analytical PTA will always overestimate the skin factor in cold water injection tests, as it cannot account for the temperature contrast between the cold injectate and hot reservoir fluid (McLean and Zarrouk, 2015c) (Section 8.6). Numerical PTA does account for this contrast, and

produced negative values for the skin factor in this case, which are more realistic. Negative values for skin factor are expected as BR66 was drilled with aerated water (not mud) and into fractured volcanic rock.

10.3 Two linear impermeable boundaries (channel)

The response of two parallel linear impermeable boundaries has been identified in Well-X in New Zealand (McLean and Zarrouk, 2017b). Together these two boundaries form a channel (Section 8.5.2), within which flow to the well is initially radial, before transitioning to linear flow.

The injection/fall-off test had three increasing flow rates (46, 93 and 139 m³/h) followed by a fall-off to zero flow (Fig. 10.4A), see Section 6.2.4 for a discussion of the drawbacks of zero-flow fall-offs. As the well had an open hole with no perforated liner during this test, the tool is located at the casing shoe rather than at the major feed zone within the permeable reservoir. Usually this would be expected to cause drift in the data set as the water column in the well expands during heating (Section 7.10); however, in this case the reservoir temperature is relatively low (172°C) and there is no obvious rebound in the fall-off (McLean and Zarrouk, 2017b). Minor rounding at the start of the pressure fall-off is corrected using the CSF method (Fig. 10.4B).

Inspection of the pressure data (Fig. 10.4A) shows three potential pressure transients for analysis: two build-ups and the fall-off. However, the lack of detailed flow rate data precludes analysis of the build-ups (McLean and Zarrouk, 2017b), as the flow rate data shown in Fig. 10.4A are not logged but consist of a single flow rate value at the

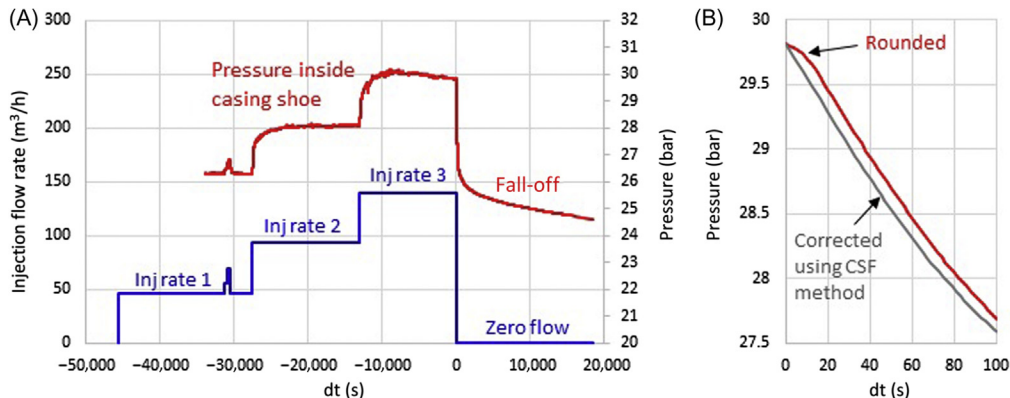


Figure 10.4 Well-X injection test: (A) Injection flow rate and pressure in casing shoe versus time; (B) CSF correction of rounding at the start of the pressure fall-off. Modified from McLean, K., Zarrouk, S.J., 2017b. Geothermal reservoir channel located by pressure transient analysis: a numerical simulation case study. *Geotherm. Resour. Council Trans.* 41, 2780–2797.

beginning of each step (with the exception of a brief period during the first injection rate). Therefore, it is not known whether the small fluctuations and drift in the pressure build-ups are the result of actual reservoir/wellbore processes, or simply the result of fluctuations and drift in the injection flow rate. Adequate flow rate logging and flow control (Section 7.7) is essential to enable both the PTA of build-ups and also fall-offs, which are no longer recommended to be to zero flow (Section 6.2.4).

The derivative plot of the fall-off data (Fig. 10.5) reveals a period of radial flow (flat derivative) followed by a period of linear flow in late time (0.4–0.5-unit-slope derivative). Numerical and analytical models have been matched to this field data, and their shapes are very similar. Neither of the models can reproduce the steepness of the derivative hump, but provide a good match in later time.

The estimated parameters associated with each model are also included in Fig. 10.5 and have similar values for reservoir permeability (k) and initial pressure (P_i). The numerical value for skin is negative (-2.2) while the analytical value for skin is positive (1.3). This is expected as the analytical model cannot account for the temperature contrast when injecting cold water into a hot reservoir, as discussed in Section 8.6 (McLean and Zarrouk, 2015c). A negative value for skin is expected as this well was drilled with aerated water into fractured volcanic rock.

The estimated parameters describing the width of the channel are also similar, the difference being that the analytical PTA (using SAPHIR) estimates the distance to each of the two boundaries separately (L_1 and L_2) while the numerical PTA model is

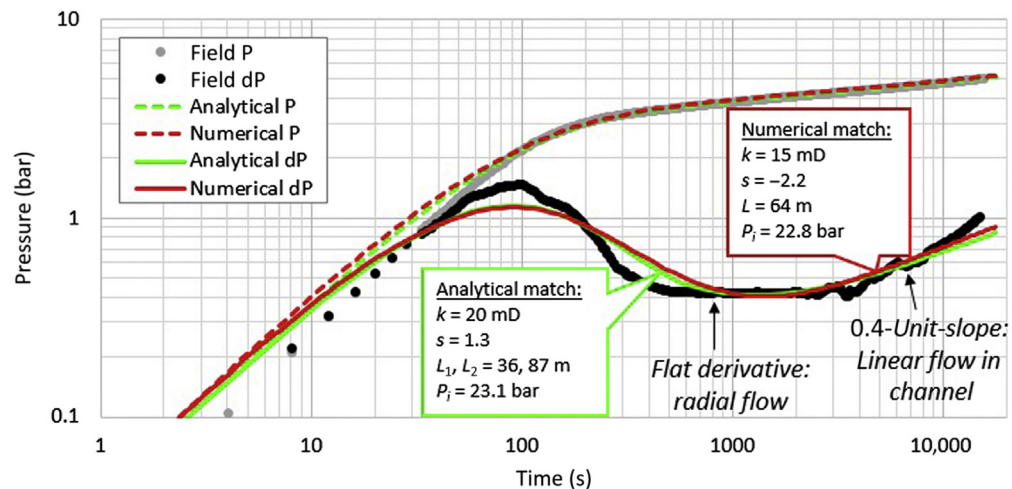


Figure 10.5 Derivative plot of Well-X pressure fall-off data, with best-match numerical and analytical models and associated estimated parameters. Modified from McLean, K., Zarrouk, S.J., 2017b. Geothermal reservoir channel located by pressure transient analysis: a numerical simulation case study. *Geotherm. Resour. Council Trans.* 41, 2780–2797.

designed with the well in the centre of the channel and therefore estimates the distance to the two boundaries as a single value (L). A simple modification of the PyTOUGH code would allow the numerical model to estimate the values separately; however, the quite sharp transition between the flow regimes (around 4000 seconds) is not indicative of a significant offset of the well from the centre of the channel, and so this modification was considered unnecessary (McLean and Zarrouk, 2017b).

Despite this difference in the model setup, the numerical and analytical models both estimate approximately the same total width for the channel: 123 m in the analytical case and 128 m in the numerical case (McLean and Zarrouk, 2017b). The presence of boundaries controlling flow within this channel is very important for the conceptual understanding of the reservoir.

10.4 Permeable fault (narrow channel)

In the previous field study (Section 10.3) the numerical channel model has been applied to field data, revealing the presence of a channel 120–130 m wide, which controls flow in the reservoir near the well. The relatively wide channel from that case allows a radial flow regime to develop, and then boundaries are detected and the flow regime becomes linear. The channel model has another useful application: when the channel is very narrow, there is no time to establish radial flow, and so linear flow dominates the pressure response, as might be observed along a permeable fault in the reservoir. McLean et al. (2018) apply a very narrow channel model to field data from the well BR49 at Ohaaki geothermal field, New Zealand. The major feed zone in BR49 is located in the greywacke basement (which underlies the volcanic units in this area), and numerical PTA reveals that the flow to BR49 is dominated by linear flow, indicating a permeable fault within the basement. This corroborates the current conceptual model of the Ohaaki geothermal field (Mroczek et al., 2016), which indicates a secondary upflow along faults through the basement in this area.

The pressure derivative plot of some narrow channel model pressure responses (Fig. 10.6) shows that when the channel is narrow, the response apparently transitions from wellbore storage directly into the linear flow response, and no radial flow response (flat derivative) is observed. In fact, radial flow does occur very briefly, as the channel does not have zero width, but it is entirely masked by wellbore storage. During the linear flow response, the pressure and derivative are almost parallel for a significant period of time, with an approximately 0.4-unit-slope.

The injection test into BR49 had three increasing flow rates (39, 57 and 71 t/h) followed by a fall-off to the first flow rate (39 t/h). Zero flow during the fall-off was avoided to prevent heating in the wellbore during the test, and associated distortion of the data set (see Section 6.2.4). Despite the careful test design, the fall-off data exhibited a significant rebound, which was initially attributed to pressure recovery in the

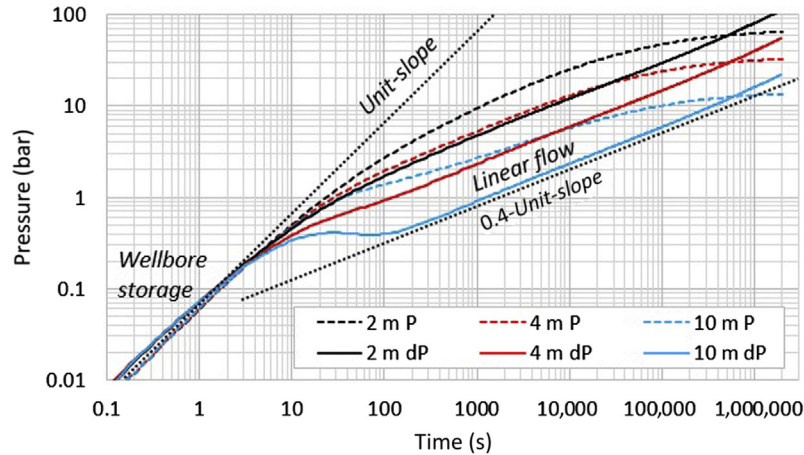


Figure 10.6 Derivative plot of numerically modelled response of a narrow channel with widths of 2, 4 and 10 m. After McLean, K., McDowell, J.M., Sepulveda, F., Seastres, J., Zarrouk, S.J., Alcaraz, S., 2018. Upflow along a basement fault revealed by geothermal numerical pressure transient analysis. In: *Proceedings 40th New Zealand Geothermal Workshop, Taupo, New Zealand.*

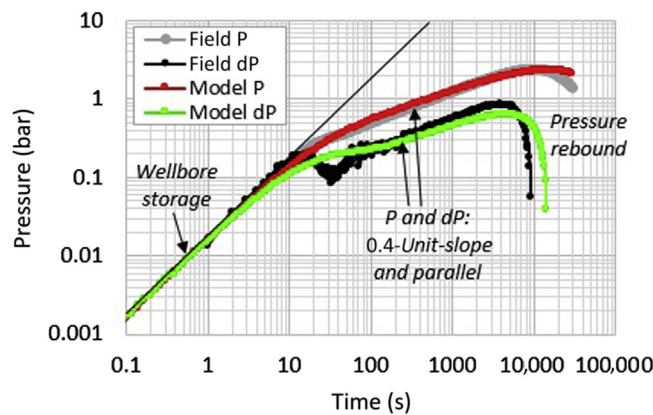


Figure 10.7 Derivative plot showing BR49 field data, with best fit numerical PTA narrow channel model. After McLean, K., McDowell, J.M., Sepulveda, F., Seastres, J., Zarrouk, S.J., Alcaraz, S., 2018. Upflow along a basement fault revealed by geothermal numerical pressure transient analysis. In: *Proceedings 40th New Zealand Geothermal Workshop, Taupo, New Zealand.*

nearby reservoir as several production wells in the vicinity were shut in at this time due to a flash plant outage (McLean et al., 2018). While the pressure recovery does affect the field data (especially in late time), the earlier part of the field data reveals a relatively uncommon and distinctive response (Fig. 10.7). The pressure and pressure derivative transition rapidly from the wellbore storage unit-slope into a 0.4-unit-slope parallel response, characteristic of a narrow channel (Fig. 10.6).

McLean et al. (2018) carried out numerical PTA on the BR49 field data, using the numerical PTA framework (Chapter 8: Numerical pressure-transient analysis modelling framework) and inversion using PEST. The model match (Fig. 10.7) is good, especially considering that the wider pressure recovery of the reservoir (due to the flash plant outage) is not accounted for by the model. The model does in fact produce some rebound in the pressure, which is the result of superposition of pressure transients from the earlier injection steps and is unrelated to the wider pressure recovery. The best fit numerical model is a channel 5 m wide, with permeability (k) of 66 mD and effectively no skin ($s = 0.2$) (McLean et al., 2018).

For BR49, in the context of the Ohaaki reservoir conceptual model, any further work to include the pressure recovery in the model would have been superfluous. The key point from BR49 was already made: the flow to the well is not radial, as is usually expected, but is dominated by linear flow. In the impermeable greywacke basement where the BR49 feed zone is located, the only geological feature likely to be responsible for such a flow pathway is a permeable fault. An examination of the conceptual model and its contributing data all corroborate this hypothesis (McLean et al., 2018). While the presence of permeable faults (and secondary upflow along them) under the BR49 area had been inferred from other long-term data sources (Mroczek et al., 2016), PTA is a powerful tool that could have indicated this very early in the life of the well (immediately after well completion) and at low cost (McLean et al., 2018).

10.5 Fracture closure

A behaviour sometimes observed in geothermal pressure transients is a bend in the measured pressure during fall-off, as observed in a well at Soda Lake, United States (Fig. 10.8A) (Bakar and Zarrouk, 2018). One hypothesis to explain this behaviour is a

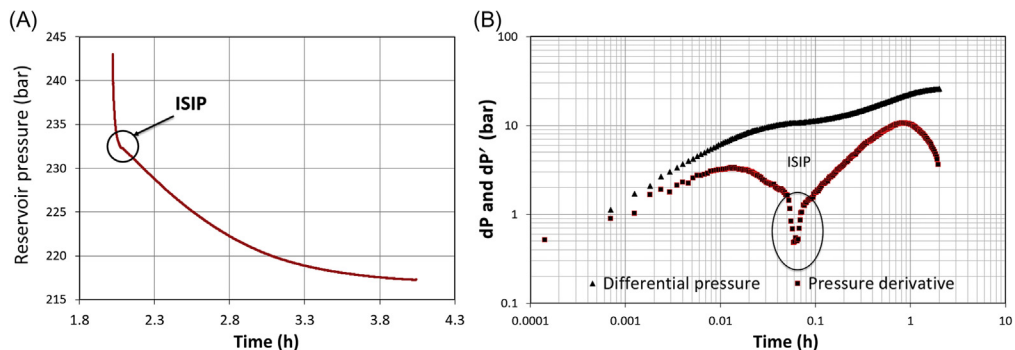


Figure 10.8 Pressure fall-off after injection exhibiting a bend at the ISIP: (A) History plot and (B) Pressure derivative plot. *ISIP*, instantaneous shut-in pressure. After Bakar, H.A., Zarrouk, S.J., 2018. *Transient pressure analysis of geothermal wells fractured during well testing. Geothermics* 76, 26–37.

sudden decrease in permeability as a fracture that was stimulated during injection closes again (or partially closes) as pressure in the well drops. This is more likely to occur in wells with relatively low permeability, where the pressure differential induced by injection can be large enough to exceed the fracturing stress/pressure of the reservoir rock.

Similar behaviour is observed during mini-frac testing, which is carried out prior to fracture stimulation in the petroleum and coalbed methane industries. When injection stops during the mini-frac test, the pressure initially falls off very rapidly, indicating high permeability. Then when the pressure drops to a certain value, the fracture starts to close [this is known as the instantaneous shut-in pressure (ISIP)], reducing the rate of pressure fall-off (Fig. 10.8A). This is followed by the final closure pressure (FCP) when the fracture fully closes. It is difficult to observe the FCP in Fig. 10.8A as it took place over a longer time, as will be demonstrated in the numerical simulation below. Mulyadi (2010) reported similar fracture behaviour during water fracturing/enhancement of geothermal wells at Wayang Windu, Indonesia.

The first part of the pressure response (before the bend) is known as ‘fracture dominated’, while the second part of the pressure response (after the bend) is known as ‘reservoir dominated’ and is made up of pseudo-linear flow and finally pseudo-radial flow. The pressure response of Fig. 10.8A cannot be matched using any standard PTA method and the shape of the pressure derivative (Fig. 10.8B) shows a unique response during early time.

Numerical simulation is the only option for data sets like these. In theory, the numerical simulation of this scenario would require coupling of a rock mechanics simulator to a flow simulator; however, the parameters required for rock mechanics modelling are typically unknown in geothermal reservoirs (Bakar and Zarrouk, 2018). In addition, there will be complications when trying to couple (parallelise) different simulators with different numerical grid systems. Hence, Bakar and Zarrouk (2018) have approached this problem by using the TOUGH2 flow simulator, and by explicitly implementing a fracture into a square Cartesian grid, adjacent to the well, for both a horizontal fracture case and a vertical fracture case.

A very good match is obtained between the explicit vertical fracture model and the Soda Lake field data (Fig. 10.9A) using an automated process of adjusting the fracture half-length and fracture permeability in the model (Bakar and Zarrouk, 2018). To match the field data, the fracture half-length and permeability decrease rapidly and then increase slightly, which implies the fracture is closing and then opening a little, before closing at the end (Fig. 10.9B): this process has been named ‘fracture clapping’ (Van der Baan et al., 2016; Bakar and Zarrouk, 2018). The mechanism to explain this behaviour is not fully understood, and it is masking the FCP commonly observed in mini-frac test. The shape of the Soda Lake field data could not be matched with the horizontal fracture model, indicating that the actual fracture is likely to be vertical.

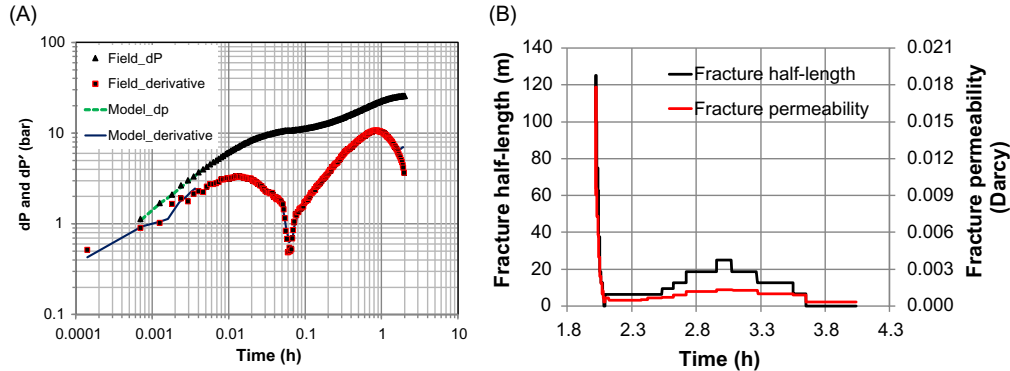


Figure 10.9 (A) Log–log plot showing the match between model and field data and (B) modelled fracture permeability and fracture half-length during pressure fall-off. After Bakar, H.A., Zarrouk, S.J., 2018. *Transient pressure analysis of geothermal wells fractured during well testing. Geothermics* 76, 26–37.

This methodology can be applied to any fracture shape to match well test data. Bakar and Zarrouk (2018) showed field data from other geothermal wells with very similar fracture closure behaviour and pointed out that in some cases this can be masked/complicated by other well effects.

A scenario similar to this often occurs during cementing of geothermal wells. The rock fracture pressure is exceeded when the high pumping pressure plus the cement head breaks the rock, causing the cement to go into the created fractures. This can lead to a poor cement job (Bakar and Zarrouk, 2018), particularly when cementing deep production casings. Drilling engineers attempt to avoid this by using light cement or by cementing the casing in two stages (liner tie-back system).

10.6 Cement damage and recovery

Malibiran and Zarrouk (2014) described a detailed case study of cement damage in the well T4 in the two-phase Mount Apo geothermal field, Philippines. The cement damage took place during the drilling/cementing of the nearby well T7. It is a common mistake to keep the nearby wells on production while cementing (or in some cases stimulating) a new well. T4 suddenly ceased producing, and the output of the power plant reduced from 42.6 to 37.9 MWe. Direct evidence of cement damage in T4 came from downhole camera runs, which showed a large quantity of cement on the lower side of the deviated production casing, and also liner slots blocked with cement (Fig. 10.10). Also, cement was ejected from the well during discharge testing. Cement was even found in the cooling water system of the power plant, requiring the cement to have travelled from the well through the above-ground separation system, the power plant (including turbine) and into the condenser and cooling water system.

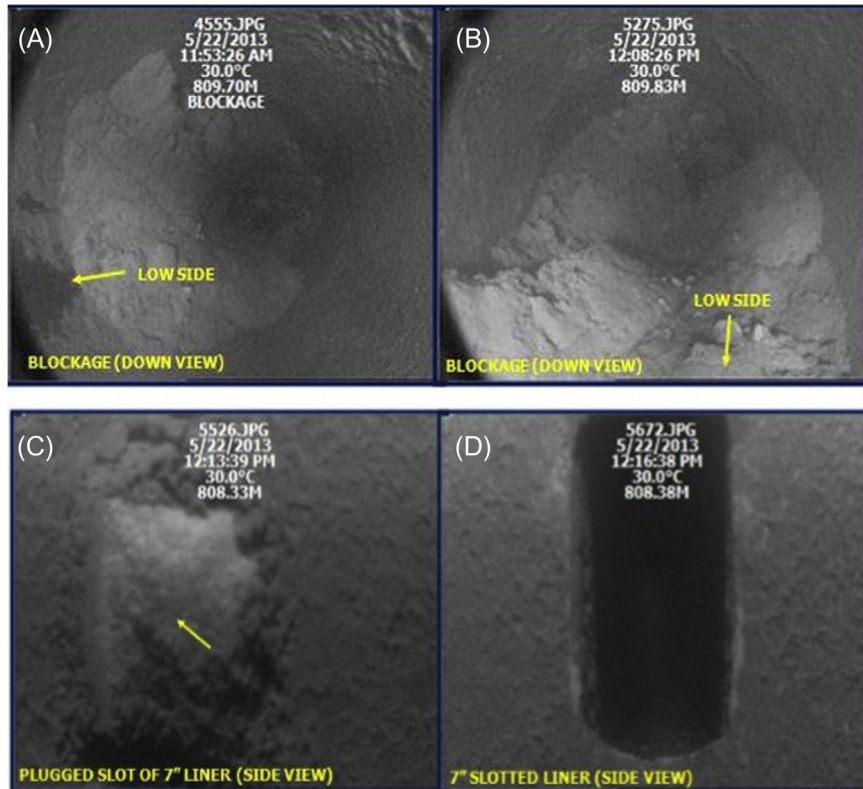


Figure 10.10 Downhole camera images showing cement in T4 near the casing shoe: (A) cement sitting on low side of deviated liner; (B) close-up of (A); (C) liner slot plugged with cement; (D) clean liner slot for comparison. From Malibiran, M.A., Zarrouk, S.J., 2014. *Modelling pre and post acid stimulation of well T4, Mt. Apo geothermal field, Philippines*. In: *Proceedings the 36th New Zealand Geothermal Workshop, Auckland, New Zealand with permission*.

Once it was established that T4 had cement damage, a workover drilling rig was mobilised to drill the cement-damaged zone through both the production casing and the slotted liner. T4 was then stimulated with acid to dissolve any remaining cement that might be causing skin damage, and to improve the reservoir permeability beyond the wellbore.

Injection fall-off tests were performed at the following important stages in the life of T4:

1. post-drilling
2. after cement damage
3. after mechanical clearing
4. after acidising

Table 10.2 Comparison of results of analytical PTA of fall-off data sets at the various stages of the process with T4.

Results of analytical PTA				
Estimated parameter	Stage 1: Postdrilling	Stage 2: Cement-damaged	Stage 3: Postmechanical workover	Stage 4: Postacidising
Reservoir permeability k (mD)	16.0	6.7	201	217
Skin	- 2.0	14.9	- 2.6	- 4.0

Source: From Malibiran, M.A., Zarrouk, S.J., 2014. Modelling pre and post acid stimulation of well T4, Mt. Apo geothermal field, Philippines. In: Proceedings the 36th New Zealand Geothermal Workshop, Auckland, New Zealand.

PTA of the fall-offs from these tests was completed using analytical methods/software, and despite the limitations of these, yielded results were consistent with the condition of the well at the various stages (Table 10.2). The results in Table 10.2 show the reservoir permeability decreasing as a result of cement damage, then increasing (far beyond the original value) as a result of mechanical workover and acidising operations. Also, the results for skin factor are consistent, as the original negative skin (stimulation) becomes a very large positive skin after cement damage, which then becomes negative again after the mechanical workover and even more negative after acidising.

Numerical modelling of the downhole pressure data was also carried out, though this was prior to the numerical PTA framework described in this book and would not be described as 'numerical PTA'. Radial grids were embedded into a Cartesian grid and the entire pressure history matched. The primary conclusion by Malibiran and Zarrouk (2014) regarding the numerical modelling was that the simplest radial model (homogenous porous media) produced a better match to the field data than two more complex models intended to represent fracturing in the reservoir [fractured media (3-layer) model, and fractional dimension].

10.6.1 Presence of a linear impermeable boundary (fault)

Malibiran and Zarrouk (2014) use a single linear impermeable boundary model for all the fall-off data sets from T4. The single linear impermeable boundary model has a characteristic shape, where the pressure derivative flattens, before rising and flattening again at a higher level (Sections 5.1.1 and 8.5.1). This characteristic derivative shape is observed in only one of the field data sets, the fall-off from Stage 4: post-acidising (Fig. 10.11B). This boundary response is apparent prior to two-phase effects which

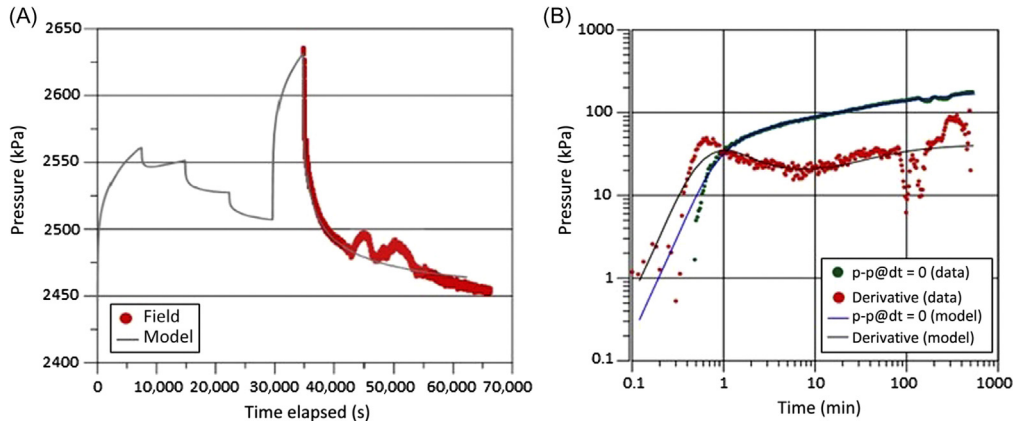


Figure 10.11 Field data from Stage 4: postacidising T4 pressure fall-off, with analytical PTA models: (A) history plot; (B) pressure derivative plot. After Malibiran, M.A., Zarrouk, S.J., 2014. *Modelling pre and post acid stimulation of well T4, Mt. Apo geothermal field, Philippines*. In: *Proceedings the 36th New Zealand Geothermal Workshop, Auckland, New Zealand*.

distort the data set beyond 90 minutes, which can be seen as spikes/oscillations in the fall-off in Fig. 10.11A.

The use of the linear impermeable boundary model for the data sets from all four stages is a reasonable approach, even though it is only identified in one. The data sets from the other three stages are of lower quality or have other issues preventing the identification of the boundary response; however, they do exhibit other features of interest (see Sections 10.6.2 and 10.6.3). The identification of a linear impermeable boundary in the vicinity of T4 has a high level of uncertainty, as the response is seen only once, and there is the possibility it is due to subtle two-phase distortions, prior the obvious two-phase oscillations.

10.6.2 Suppression of two-phase feed zones

During injection testing of two-phase wells, the injection rates need to be high enough to suppress all the two-phase feed zones. This leads to a variant of the usual completion/injection test design (Section 6.2.1): in high enthalpy wells the injection steps are different (Fig. 10.12), starting at the highest flow rate, with injection steps downwards, then returning to the highest flow rate for a period of time prior to the fall-off, to ensure the two-phase feeds remain quenched. The fall-off is never to zero flow, this is not possible in two-phase wells, as some flow is required at all times to keep the well under control.

Two factors control whether two-phase feed zones “kick” (flow) during the fall-off: the injection rate during the fall-off, and the duration and magnitude of the injection prior to the fall-off. It can be difficult to judge the times and

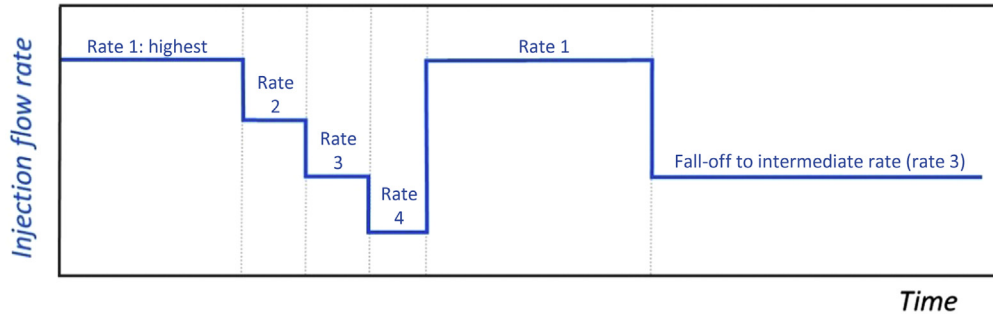


Figure 10.12 Typical flow rate steps during testing of two-phase wells: design to maintain control of two-phase feed zones.

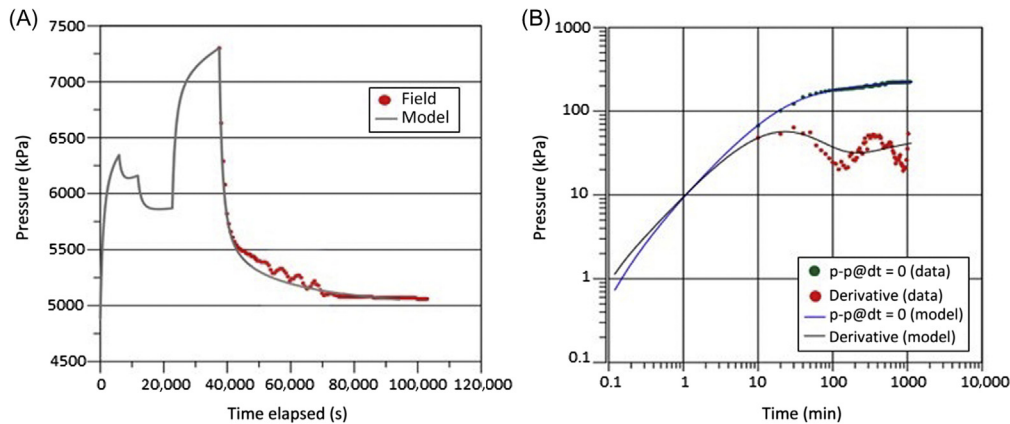


Figure 10.13 Field data from Stage 1: postdrilling T4 pressure fall-off, with analytical PTA models: (A) history plot; (B) pressure derivative plot. After Malibiran, M.A., Zarrouk, S.J., 2014. *Modelling pre and post acid stimulation of well T4, Mt. Apo geothermal field, Philippines*. In: *Proceedings the 36th New Zealand Geothermal Workshop, Auckland, New Zealand*.

durations of the flow steps, and the result is distortions to the fall-off data set, as two-phase feed zones kick. The effect can be seen in the Stage 4 data set (Fig. 10.11) with spikes/oscillations starting at approximately 90 minutes, and also in the Stage 1 data set (Fig. 10.13) where oscillations are apparent beyond approximately 200 minutes.

To avoid these issues while testing wells with two-phase feed zones, it is recommended to concentrate on the pressure transients between increasing injection steps instead of fall-offs. If fall-offs are necessary, it is recommended to maximise injection at the highest flow rate (immediately prior to the fall-off) and to inject at a reasonably high rate during the fall-off.

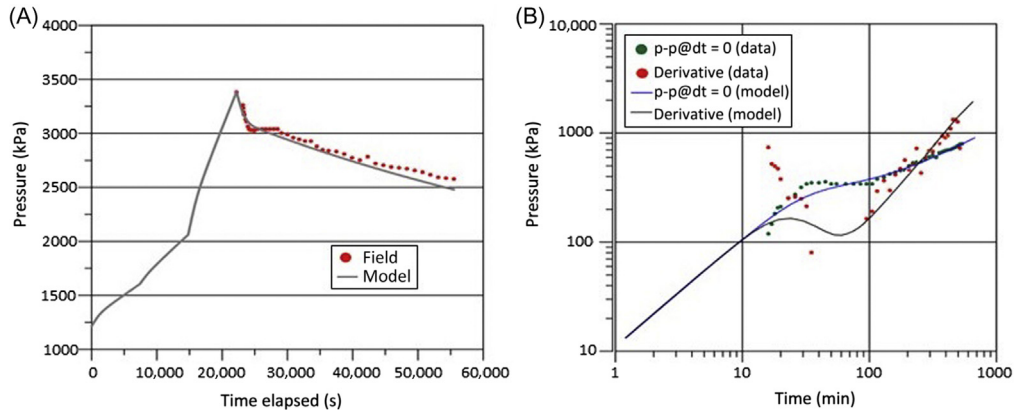


Figure 10.14 Field data from Stage 2 cement-damaged T4 pressure fall-off, with analytical PTA models: (A) history plot; (B) pressure derivative plot. After Malibiran, M.A., Zarrouk, S.J., 2014. *Modelling pre and post acid stimulation of well T4, Mt. Apo geothermal field, Philippines. In: Proceedings the 36th New Zealand Geothermal Workshop, Auckland, New Zealand.*

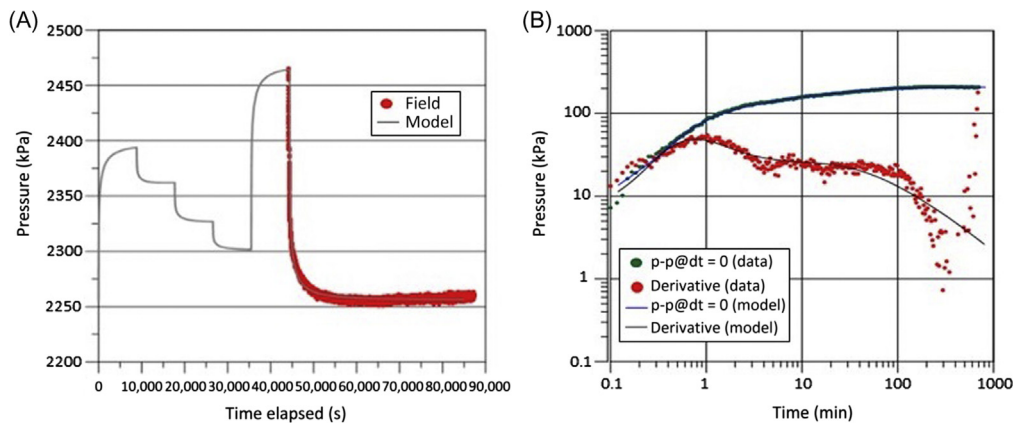


Figure 10.15 Field data from Stage 3 postmechanical workover T4 pressure fall-off, with analytical PTA models: (A) history plot; (B) pressure derivative plot. After Malibiran, M.A., Zarrouk, S.J., 2014. *Modelling pre and post acid stimulation of well T4, Mt. Apo geothermal field, Philippines. In: Proceedings the 36th New Zealand Geothermal Workshop, Auckland, New Zealand.*

10.6.3 Other data features

In the Stage 2 cement-damaged data set (Fig. 10.14) there are very few data points and the derivative is very scattered. The reasons for this, and the different test design (pressure appears to be increasing in steps before the fall-off) are not discussed by Malibiran and Zarrouk (2014).

In the Stage 3 postmechanical workover data set there is a slight rebound in the pressure fall-off (Fig. 10.15A), which causes the pressure derivative to drop away in

late time (Fig. 10.15B) in a manner reminiscent of a constant pressure boundary response (Section 5.1.2). This is a feature of the data commonly seen when heating occurs during the fall-off, resulting in drift in the pressure data due to pivoting of the pressure profile in the well (Section 7.10) and/or expansion of the wireline during the fall-off (Section 7.9). In the case of T4, heating in the wellbore could result from insufficient suppression of the feed zones in the well (the flow rate during the fall-off was the lowest of all the flow rates in this test), causing this rebound in the fall-off, which is a much more subtle distortion than the oscillations in Figs. 10.11 and 10.13.

10.7 Permeability enhancement by deflagration

In 2015 deflagration was carried out in the well BR66 at Ohaaki geothermal field, New Zealand (McLean et al., 2016). The well had a low injectivity index at completion, and deflagration stimulation (Section 9.3.4) was carried out in an attempt to improve the injectivity – and ultimately the productivity – of the well. Pre-deflagration and post-deflagration injection tests were carried out in order to assess the effect of deflagration on the well. This effect was quantified by changes in the injectivity index, skin factor and reservoir permeability. Also the shape of the pressure transients was consistent with a linear impermeable boundary in close proximity to the well. While this is not directly relevant to the evaluation of the effect of deflagration, the presence of boundaries is significant to the conceptual understanding of the reservoir and was discussed in that context in Section 10.2. In this section the focus is on the effect of deflagration.

The well BR66 has an average deviation of 13 degrees and the open-hole section of perforated liner extends from 1498 m to the total drilled depth of 2783 m. Within this open-hole section, feed zones were identified from the completion test data (Fig. 10.16) to be around 1880, 2120, 2270 and 2470 m, identified from injection temperature profiles, fluid velocity profiles (calculated from spinner data), spinner ratio, heatup pressure profiles, heatup temperature profiles and borehole image data (AFIT). The spinner data in this case are very noisy and harder to interpret than usual, particularly the spinner ratio, though regardless of this there is sufficient consistency between the various data sets to identify likely feed zones. The pressure control point (PCP) in this case lies between two feed zones (1880 and 2120 m) (Fig. 10.16). The interpretation of feed zone depths was carried out with extra care, as correct positioning of the deflagration tool at an existing feed zone is critical to the success of the operation (Section 9.3.4). The pressure wave from deflagration was intended to affect and stimulate an existing feed zone; not to create a new feed zone.

The feed zone at 2120 m was selected as the target for deflagration, as it is the clearest of the feed zones and an associated fracture system can be pinpointed in the borehole image (Fig. 10.17). Two shots were planned at this depth, each shot

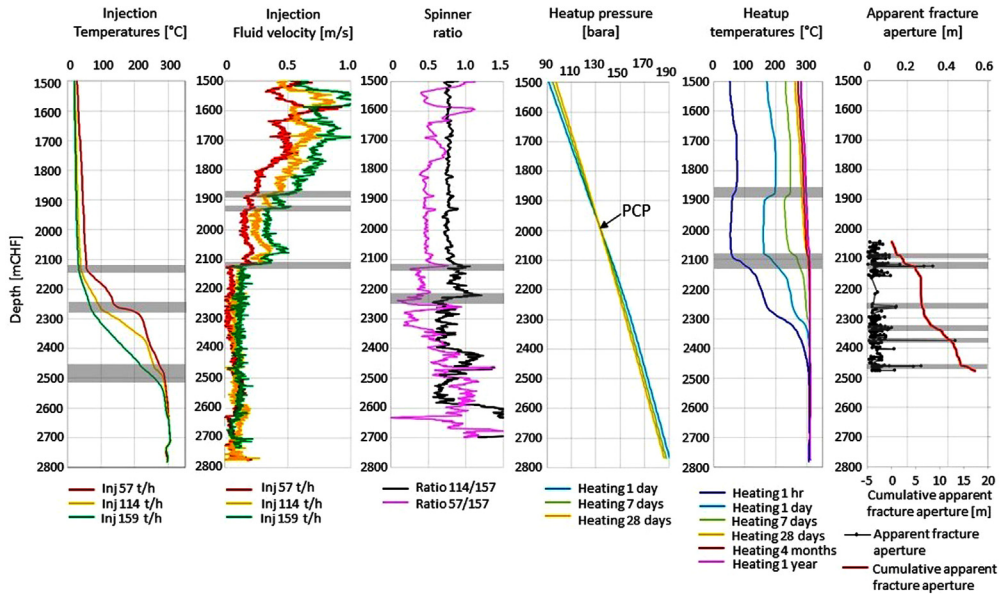


Figure 10.16 Summary of completion test data from BR66, profiles of injection temperatures, fluid velocity, spinner ratio, heatup pressures, heatup temperatures, AFIT fracture data. Indicators of potential feed zones in each data set are shaded with grey. *AFIT*, Acoustic formation imaging technology. From Contact Energy Ltd., with kind permission.

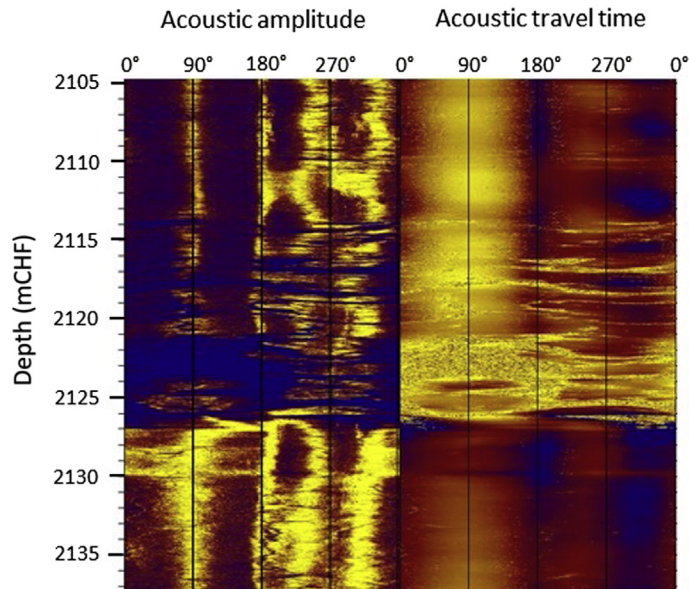


Figure 10.17 Acoustic formation image (AFIT) of fracture zone at 2120 mChF, the first target for deflagration. *AFIT*, Acoustic formation imaging technology.

involving twelve 33 MJ fuel units in two carriers, for a total energy per shot of 392 MJ (McLean et al., 2016). The first shot at 2120 m resulted in only a small change in injectivity, and so the second shot was moved to 1880 m, which was interpreted to be the other major feed zone as the PCP sits between the 2120 and 1880 m feeds (Fig. 10.16).

The entire deflagration programme involved the following steps over several days: quench, pre-deflagration injection/fall-off test, deflagration shot at 2120 m, brief intermediate injection test, deflagration shot at 1880 m and post-deflagration injection/fall-off test. The pre- and post-deflagration injection/fall-off tests had the same design, with three increasing injection steps (around 37, 77, 113 t/h) of the same duration, followed by a fall-off to zero flow. The brief injection test between the two shots had the same injection rates but much shorter steps, intended only to give a quick estimate of injectivity index but no other information.

The injectivity index (II) of the well increased by 17% after the first shot at 2120 m, from 5.9 to 6.8 t/h/bar. After a second shot at 1880 m, the II increased further, to 9.3 t/h/bar, an increase of 57% compared to the pre-deflagration test (Fig. 10.18).

It was later concluded by Bixley et al. (2016) that the II is not the best indicator of permeability improvement by deflagration, as the overall II is not sensitive to large changes in the injectivity of a single feed zone. Changes in the productivity are a better indicator (Bixley et al., 2016).

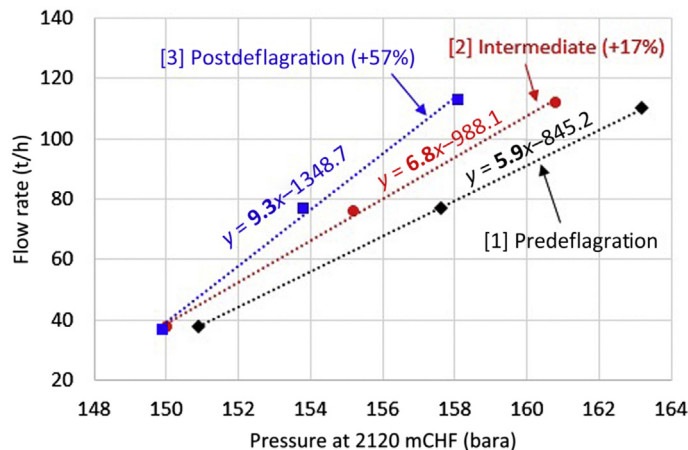


Figure 10.18 Flow rate versus pressure at 2120 m, showing increase in injectivity from the pre-deflagration injection test, to the intermediate test, to the post-deflagration test. Modified from McLean, K., Zarrouk, S.J., Wilson, D., 2016. Application of numerical methods for geothermal pressure transient analysis: a deflagration case study from New Zealand. In: Proceedings 41st Workshop on Geothermal Reservoir Engineering, Stanford University, Stanford, CA.

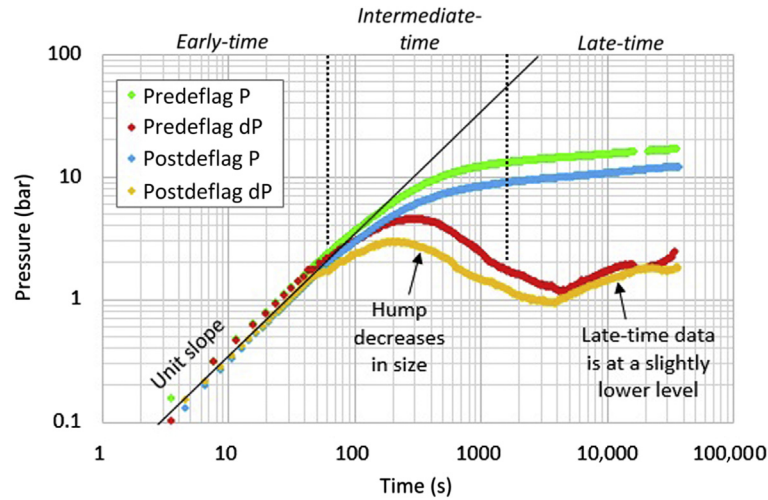


Figure 10.19 BR66 fall-off data showing changes between pre- and post-deflagration data sets. Modified from McLean, K., Zarrouk, S.J., Wilson, D., 2016. *Application of numerical methods for geothermal pressure transient analysis: a deflagration case study from New Zealand*. In: *Proceedings 41st Workshop on Geothermal Reservoir Engineering, Stanford University, Stanford, CA*.

Assessment of the impact of deflagration is also possible by PTA. The high pressure wave created by deflagration is expected to stimulate existing permeable fractures in the immediate vicinity of the wellbore, which is expected to decrease the skin factor. This was observed by comparison of the PTA results from the pre- and post-deflagration fall-offs. As a result of deflagration, the hump in the pressure derivative in intermediate-time is decreased, and the late-time data have shifted to a slightly lower level (Fig. 10.19).

When subjected to numerical PTA, this change in shape results in the following changes to the estimated parameters (summarised in Table 10.1): the reservoir permeability increases slightly from 4.3 to 4.8 mD, and the skin factor decreases from -2.4 to -3.1 . The decrease in skin factor is a quantitative assessment of the effect of deflagration on the near-well permeability. The results are similar when using analytical PTA techniques, except that the observed decrease in skin factor (from 2.4 to 0.7) is between two erroneous positive values (McLean et al., 2016).

10.8 Permeability enhancement by cold water injection

Aqui (2012) simulated cold condensate injection in the well TC5RD in Southern Negros geothermal field, Philippines, as part of a wider study into permeability enhancement. The TOUGH2 simulator was used in combination with PyTOUGH, and inverse modelling was achieved using a built-in Python optimisation code. This study pre-dates the numerical PTA framework presented in Chapter 8, Numerical pressure-transient analysis modelling framework.

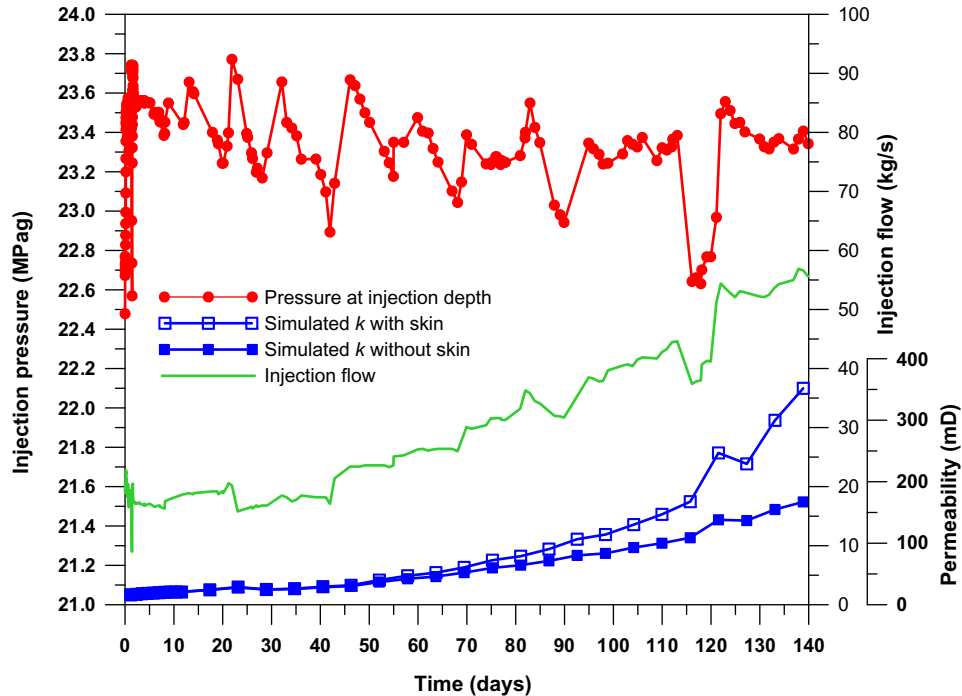


Figure 10.20 Measured condensate injection rate and reservoir pressure with time at TC5RD and the simulated increase in permeability with and without reduction in the near wellbore skin. From Aqiu, A.R., 2012. *Permeability Enhancement of Conventional Geothermal Wells* (Master's thesis). University of Auckland, Auckland, New Zealand with kind permission.

The radial model grid has a thickness of 100 m and 86 blocks of incrementally increasing radius. Various scenarios were considered, some without a skin zone, and some with a fixed radius skin zone. The field data used for model matching was 5 months of injection flow rate and pressure at the injection depth (Fig. 10.20), which shows the water take increasing from 19 to 57 kg/s with no apparent change in injection pressure. This corresponds to an increase in water take of about 0.3 kg/s (or an injectivity index of 1.1 t/h/bar) a day, which is substantial. To account for this increase in injectivity, the numerical modelling requires the reservoir permeability to progressively increase by about two orders of magnitude (Fig. 10.20). Aqiu (2012) hypothesised that this permeability increase is primarily the result of chemical reaction, as the clean and relatively cold steam condensate dissolves minerals from the andesite reservoir rock (previously in equilibrium with reservoir fluid at 230°C).

This hypothesis was investigated further by Aqiu (2012) with a laboratory experimental study of the fluid–rock interaction between the host rock and the injected condensates, using a flow-through (physical) apparatus. The results (Fig. 10.21) show

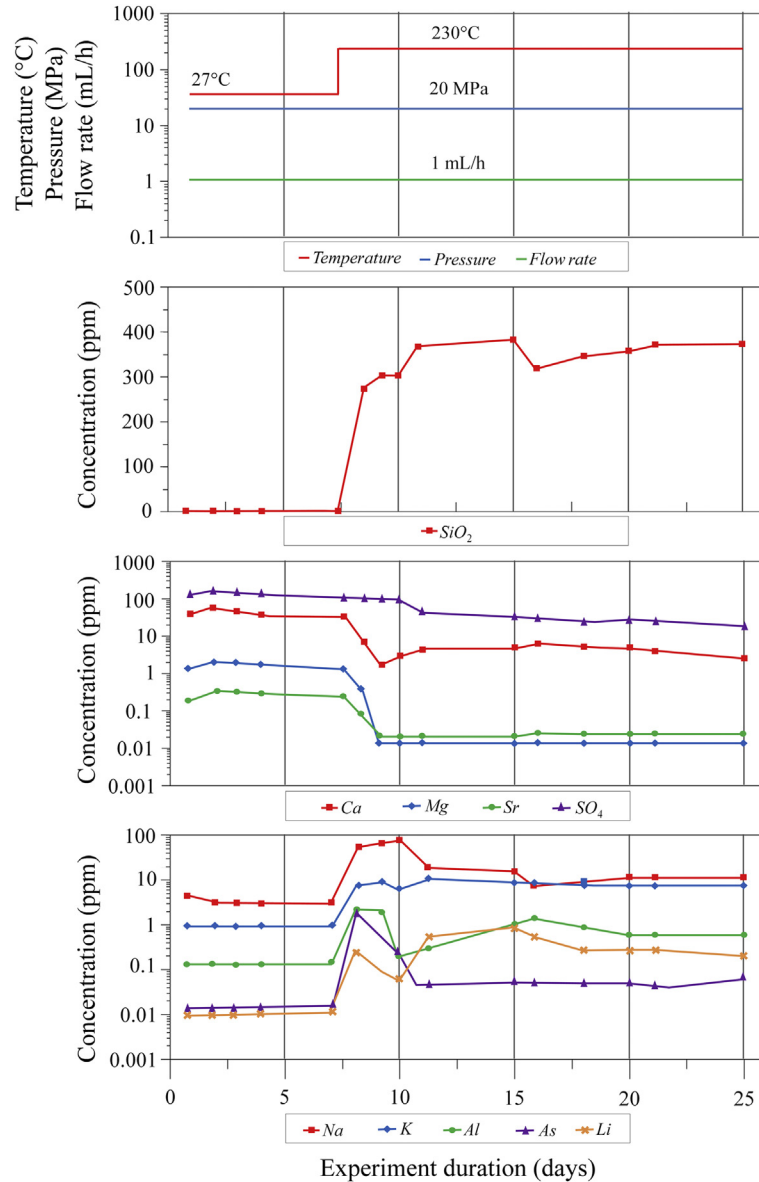


Figure 10.21 The fluid–rock interaction laboratory experimental results showing that increasing temperature and time results in dissolution (evidenced by an increase in concentration in the fluid) of reservoir rock minerals containing (SiO^2 , Na, K, Al, As and Li); and the precipitation of minerals containing (Ca, Mg, Sr and SO^4). From Aqiu, A.R., 2012. *Permeability Enhancement of Conventional Geothermal Wells (Master's thesis)*. University of Auckland, Auckland, New Zealand with kind permission.

that increasing temperature will cause dissolution of minerals with solubility that increases with temperature (e.g. SiO_2), and precipitation of secondary minerals with retrograde solubility (e.g. CaCO_3 , CaSO_4).

Aqui (2012) concluded that the combined effects of dissolution and precipitation will result in a net reduction in rock mass and increases in porosity and permeability. It was also concluded that thermal effects (cooling/thermal cracking) in this case had only a minor contribution to permeability enhancement, and the dominant cause of permeability enhancement is rock dissolution.

In a separate study of production wells, Malibiran and Zarrouk (2014) showed that in some geothermal production wells in two-phase systems, the permeability (also the injectivity) of the well increases with time by more than an order of magnitude due to fluid production only. This may be because the produced geothermal fluid helps clean the wellbore from any mud or drilling damage. An increase in permeability such as this is possible only in the absence of mineral scaling in the wellbore/reservoir. The other possible explanation is similar to the conclusions of Aqui (2012): the reservoir fluid recharging this well is undersaturated with dissolved minerals, and as it heats up near this well, it will dissolve some of the reservoir rock, increasing the porosity and permeability.

10.9 Pumped wells

Pumped wells in hot water systems generally undergo completion testing similar to two-phase flowing wells. The main test is an injection/fall-off test for measuring the transmissivity (kh) of the well. If the well can sustain production/flow when using a pump, a drawdown/build-up test can be performed instead, using temporary pumps. It is not common to use the permanent downhole pump for the drawdown/build-up testing because generally once that pump is installed, the well will be put on production. However, in some low temperature warm water systems, which are managed or tested by the local hydrologist or the drilling contractor, the permanent downhole pump is used to test the well. This test is known as the pumping test.

The drawdown/build-up test is normally performed by removing water from the well either by installing a temporary pump, or air-lifting the water (a process called a 'slug test'), and then allowing the well to recover (pressure build-up). The slug test is carried out after completing the drilling of non-pressurised wells while the drilling rig still on site. A small diameter (1" or 1½") pipe is run in the well to a depth of <100 m below the water level, then compressed air is used to remove the water down to the depth of the pipe. A portable downhole pressure transducer on a cable is normally positioned below the depth of the air-lift pipe, to measure the increasing pressure as the water head builds up (Fig. 10.22). Air-lifting has the advantage that it will clear some of the drilling debris from the well, and quickly draw down the water level.

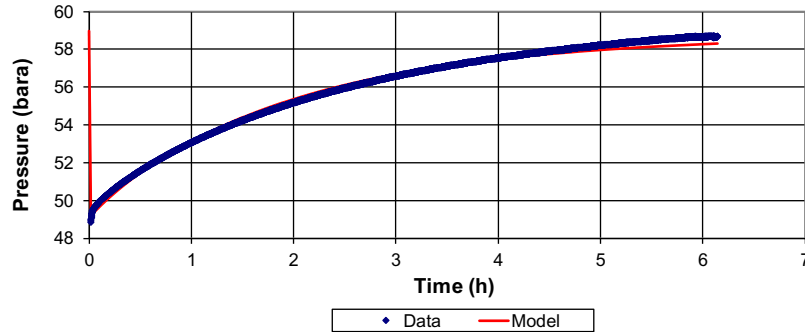


Figure 10.22 History plot of pressure drawdown and build up during a slug test of a warm water well (data measured by authors).

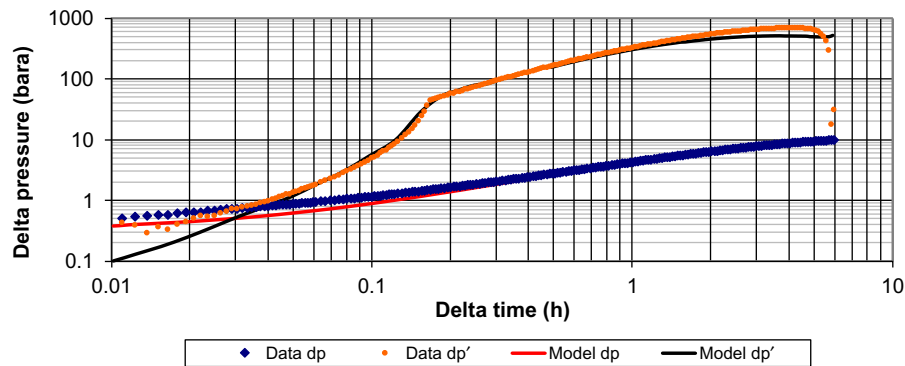


Figure 10.23 Log–log pressure derivative plot showing both field data and model of the slug test (same dataset as shown in the history plot in Fig. 10.22).

Fig. 10.22 shows data from a slug test in a warm water system well, during which air-lifting removed the water column in approximately 66 seconds, and the recovery (pressure build-up) of the well is recorded for approximately 6.1 hours. After this time, the well was still not fully recovered, but the drilling rig had to demobilise, so the test was terminated. The same data set is shown in a log–log pressure derivative plot in Fig. 10.23, which exhibits a sharp change in pressure derivative at an elapsed time of between 0.1 and 0.2 hours. This feature is attributed to a complicated well-bore effect: ‘wall flow’ which is a flow of fluid down the internal surface of the casing when the injection of compressed air stops.

Analytical PTA (an infinite acting homogenous porous media model) shows that the reservoir has skin damage ($s = + 4.98$) with a moderate reservoir permeability of 16.8 mD.

It is possible to use the numerical PTA framework described in this book to analyse the data, though this work has not been completed. It will be of interest to see how numerical PTA and analytical PTA compare for warm water wells, which have much lower temperatures than most geothermal wells, and theoretically less PTA issues. The slug test is a relatively simple test, and it is not a replacement for an extended injection/fall-off or drawdown/build-up test, though it does have the advantage of producing very little fluid at the surface.

Note that groundwater engineers (hydrologists), civil/soil (geotechnical) engineers, and some mining engineers use the hydraulic conductivity (K) as the measure of permeability (for underground flow). To convert the hydraulic conductivity to permeability, use the following equation:

$$k = \frac{K\nu_l}{g} \quad (10.1)$$

where k = permeability (m^2); K = hydraulic conductivity (m/s); g = gravitational acceleration (9.81 m/s^2); ν_l = kinematic viscosity (μ/ρ) in (m^2/s) for the liquid water at reservoir temperature.

Therefore, it is important to note that the ‘transmissivity’ based on the hydraulic conductivity $T = Kh$ (m^2/s) is different from the ‘transmissivity’ used in petroleum and geothermal reservoir engineering $T = kh$ (m^3).

10.10 Tracer testing

Tracer testing is the injection of a chemical or radioactive tracer in one well and observing the arrival of the chemical signature of this tracer in one or more observation wells. Normally the observation wells are on production. The chemical or radioactive tracers are selected to not react with the reservoir rock as they travel between wells. They are also selected to decay with time, so they do not leave a long-lasting signature that can interfere with and confuse future tracer testing. For radioactive tracers, a short half-life is chosen while chemical tracers degrade kinetically with temperature (Zarrouk, 2008). Tracer testing helps provide information on the permeability and porosity of the part of the reservoir between the injection and production wells.

There are a host of chemical and radioactive tracers used in the industry including the following:

Chemical tracers:

Naphthalene sulphonate (Akin and Gulgor, 2018)

Naphthalene disulphonate (Sanjuan et al., 2016)

Naphthalene trisulphonate (Llanos et al., 2015)

*Radioactive tracers:*Tritium ^3H (Christi et al., 2015)Iodine ^{131}I (Dennis et al., 1981; Barry et al., 1982)Barium ^{82}Br (Dennis et al., 1981)

Commonly, the analysis of tracer testing is carried out using analytical solutions to the transient advection/diffusion equation of tracer concentration with sorption/adsorption (in rock) and reaction (tracer concentration decay) terms (Zarrouk, 2008).

However, with the wide use of numerical reservoir models, the industry is increasingly using numerical models rather than analytical models when matching the tracer-testing data. The reasons being that analytical solutions are relatively simple (similar to analytical PTA) also since numerical reservoir models provide a three-dimensional and transient representation of tracer migration in the reservoir, which can help calibrate the permeability structure of the model. This is especially the case when using inverse modelling tools, which automate the match between the field data and the numerical model.

Llanos et al. (2015) built a three-dimensional (Cartesian grid) model using the TOUGH2 geothermal reservoir simulator for matching field data (Fig. 10.24) from the chemical tracer testing of the Habanero geo-pressured EGS system, Australia. The inverse modelling process provided a good match between the measured field data

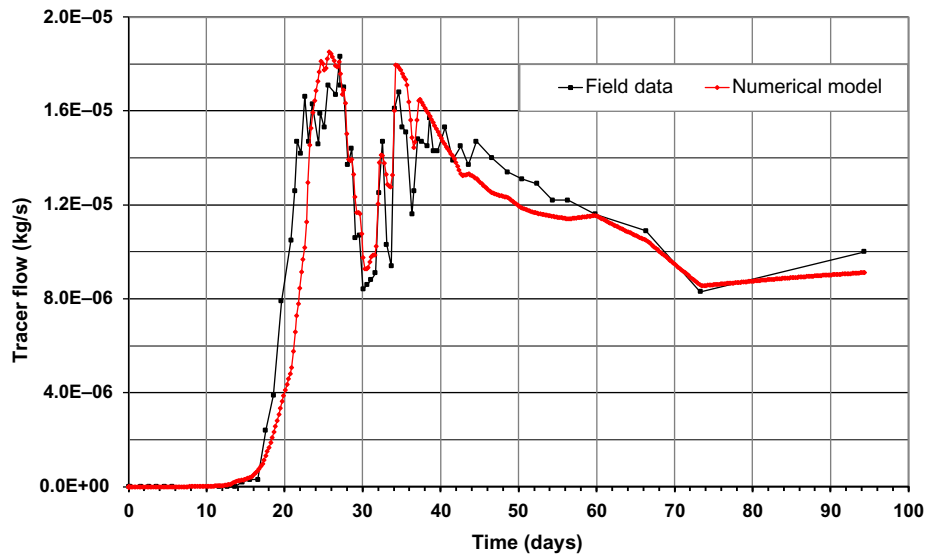



Figure 10.24 Tracer return between wells H01 and H03 at the Habanero geo-pressured EGS project. EGS, Enhanced geothermal systems. After Llanos, E.M., Zarrouk, S.J., Hogarth, R., 2015. Simulation of the Habanero geothermal reservoir, Australia. *Geothermics* 53, 308–319.

and the numerical model (Fig. 10.24). The result was a calibrated model with estimated parameter values from the inversion process such as porosity and stimulated fracture zone permeability. The calibrated reservoir model was then used to model future production scenarios and optimise the location of new/future wells (Llanos et al., 2015).

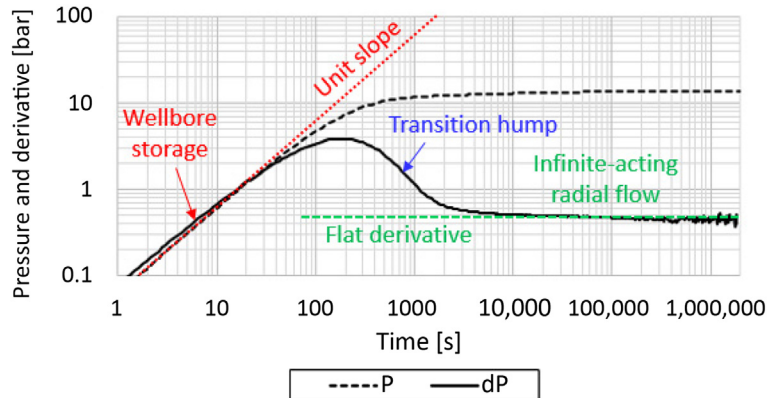
Appendix 1: Quick reference guide to characteristic pressure transient features in geothermal wells

A.1.1 Common geothermal reservoir and boundary responses

A.1.1.1 Infinite-acting radial flow

Description	Model schematic
<p>There are effectively no reservoir boundaries (infinite) and two-dimensional radial flow converges on the well horizontally, through a homogenous porous media reservoir. This is simulated using the basic numerical Pressure Transient Analysis (PTA) framework as described in Section 8.4.</p>	
<p><i>Relevant book sections:</i> Section 8.4 (numerical), Section 4.4.2 (analytical)</p>	

Derivative plot



Characteristic features of the pressure derivative

- The pressure derivative is flat during IARF (slope = 0), beyond the wellbore storage period and transition. There is no characteristic shape in the pressure data.
- During wellbore storage, the pressure and derivative have a unit slope and are coincident.
- In this example, there is no skin and so the transition hump is a 'normal' size.

Key numerical model parameters for this example

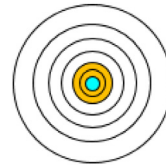
Reservoir permeability (k) = 10 mD; layer thickness (h) = 600 m; transmissivity (kh) = 6000 mD m = 6 D m; skin factor (s) = 0

A.1.1.2 Effect of skin

Description

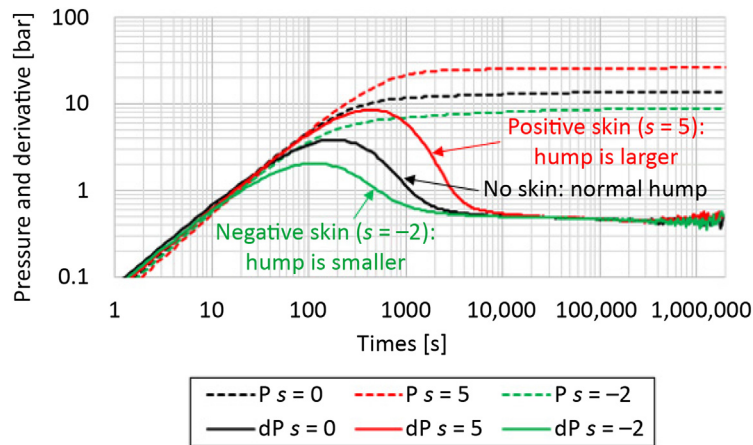
Skin means there is a contrast in the permeability close to the well, compared to the wider reservoir. This skin can be positive (damage) which means a decrease in near-wellbore permeability, or negative (stimulation) which means an increase in near-wellbore permeability. This is simulated using the basic numerical PTA framework as described in Section 8.4.

Model schematic



Relevant book sections: Section 8.4 (numerical), Section 4.4.3 (analytical)

Derivative plot



Characteristic features of the pressure derivative

- The effect of skin is in early-time during the wellbore storage period and transition. The part of the response revealing the nature of the reservoir (IARF in this case) is unaffected, although positive skin delays the time at which the reservoir response is observed.
- Negative skin decreases the size of the transition hump, shortening wellbore storage and transition.
- Positive skin increases the size of the transition hump, lengthening wellbore storage and transition.
- There is no characteristic shape in the pressure data.

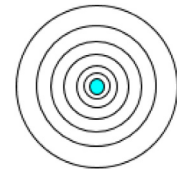
Key numerical model parameters for these examples

Reservoir permeability (k) = 10 mD; layer thickness (h) = 600 m; transmissivity (kh) = 6000 mD m = 6 D m; skin factor (s) = 0 (black), $s = 5$ (red), $s = -2$ (green)

A.1.1.3 Effect of cold water injection into hot reservoir

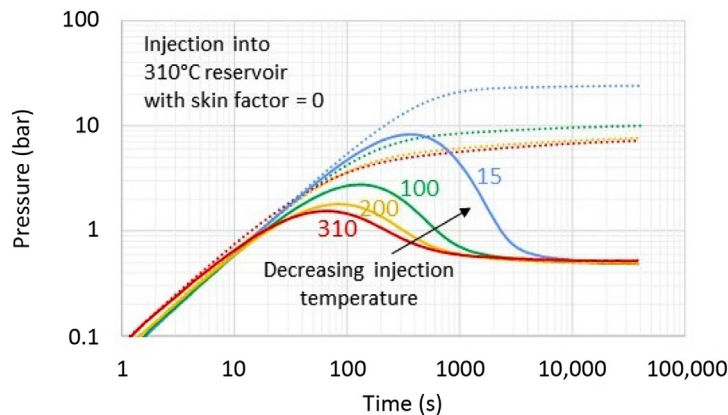
Description

During an injection/falloff test, cold water is injected into the well. There is a large contrast in temperature (and therefore fluid properties) between the cold water (injected at ambient temperature $\sim 20^\circ\text{C}$) and the hot reservoir fluid (sometimes $>300^\circ\text{C}$). The cold water in and around the well is much more viscous than the hotter reservoir fluid and produces an effect with the appearance of positive skin. This is called the 'injectate temperature effect'.



Relevant book sections: Section 8.6 (numerical), Section 5.8.3 (analytical)

Derivative plot (Fig. 8.9)



Characteristic features of the pressure derivative

- As the temperature contrast between the cold injectate and hot reservoir increases, the duration of wellbore storage increases and the size and steepness of the transition hump increase.
- This response is not unique: it has the same appearance as positive skin.
- In order to accurately estimate the actual skin factor, the injectate temperature effect must be accounted for and can be by using the numerical PTA framework in Chapter 8, Numerical PTA Modelling Framework. Analytical models/software cannot account for this and will significantly overestimate the skin factor.

Key numerical model parameters for these examples

Reservoir permeability (k) = 10 mD; reservoir permeability (k) = 600 m; transmissivity (kh) = 6000 mD m = 6 D m; skin factor (s) = 0; reservoir temperature = 310°C ; injectate temperature = 310, 200, 100, 15°C

A.1.1.4 Fractional dimension ($n = 1-2$)

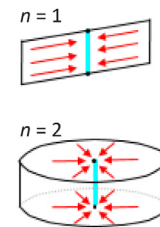
Description

Radial flow (as in the IARF flow regime) means that fluid flow is converging on the well radially, from all directions, and that flow is horizontal. The shape of the reservoir is effectively a disc. In this case, the dimension of the flow is 2.

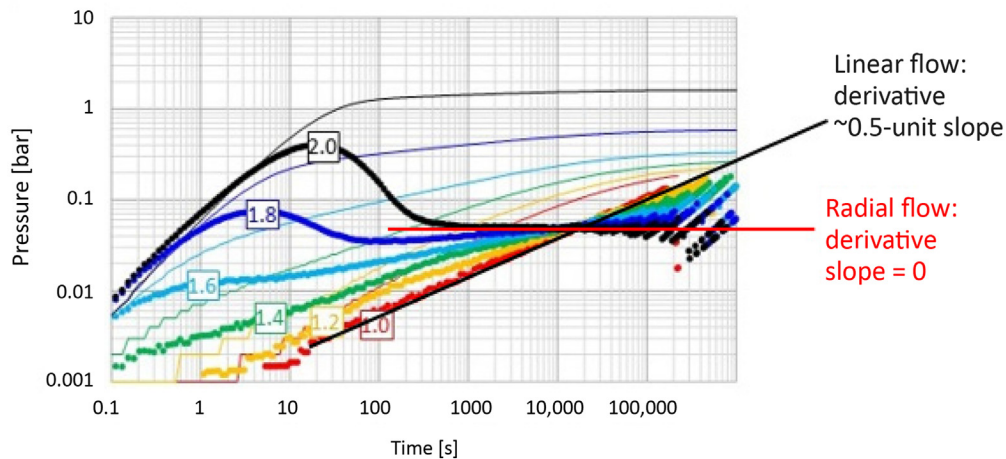
Linear flow has a dimension of 1, which means the flow is approaching the well along a plane. The fractional dimension model allows for the variability in flow dimension with a single parameter ' n ', which can have the value $n = 1.0$ for linear flow, $n = 2.0$ for radial flow or any value in the range $n = 1.0-2.0$ for some intermediate flow regime between these two end members.

Relevant book sections: Section 8.5.3 (numerical), Section 5.5.2 (analytical)

Model schematic



Derivative plot



Characteristic features of the pressure derivative

- When $n = 2.0$ (radial flow), the pressure derivative is flat (slope = 0) beyond wellbore storage and transition effects.
- When $n = 1.0$ (linear flow), the pressure derivative rises with an approximately 0.5-unit slope, even in early time, and the effects of wellbore storage cannot be seen.
- As n incrementally decreases from 2.0 to 1.0, the slope of the reservoir response incrementally increases from 0 to 0.5.
- Also as n incrementally decreases from 2.0 to 1.0, the effects of wellbore storage diminish until the unit slope and transition hump cannot be seen. The effect has the appearance of negative skin (stimulation) though it is due purely to the geometry of the flow. This is referred to as 'geometrical skin'.

Key numerical model parameters for these examples

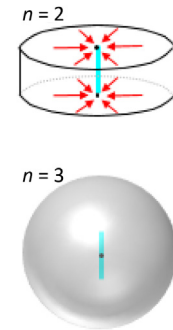
Reservoir permeability (k) = 100 mD; layer thickness (h) = 600 m; transmissivity (kh) = 60,000 mD m = 60 D m; skin factor (s) = 0; fractional dimension (n) = 2.0 (black), $n = 1.8$ (blue), $n = 1.6$ (light blue), $n = 1.4$ (green), $n = 1.2$ (yellow), $n = 1.0$ (red)

A.1.1.5 Fractional dimension ($n = 2-3$)

Description

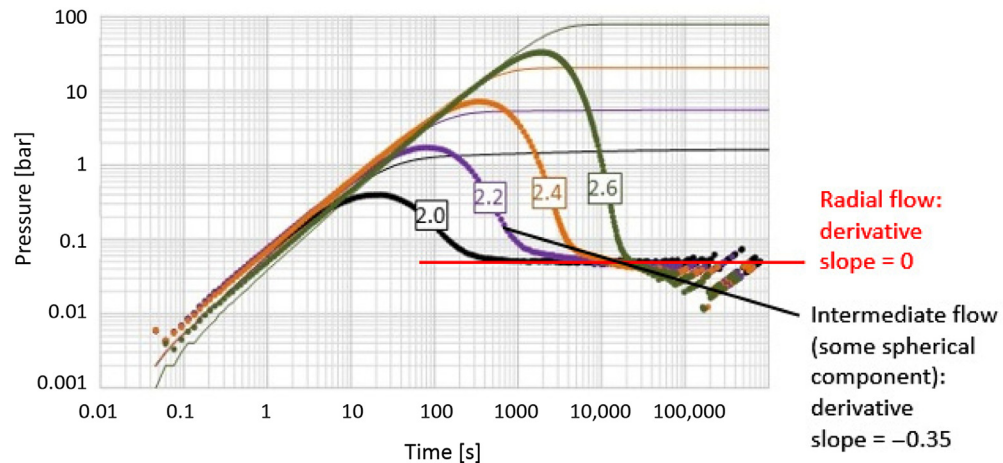
Radial flow (as in the IARF flow regime) means that fluid flow is converging on the well radially, from all directions, the flow pathways are horizontal and the shape of the reservoir is effectively a disc. In this case, the dimension of the flow is $n = 2$. Spherical flow has a dimension of $n = 3$, which means the flow pathways converge on the well from every direction in three dimensions (including vertically), as if the well is the centre of the sphere. The fractional dimension model allows for variability in the flow dimension with a single parameter ' n ', which can have the value $n = 2.0$ for radial flow, $n = 3.0$ for spherical flow or any value in the range $n = 2.0-3.0$ for some intermediate flow regime between these two end-members.

Model schematic



Relevant book sections: Section 8.5.3 (numerical), Section 5.5.2 (analytical)

Derivative plot



Characteristic features of the pressure derivative

- When $n = 2.0$ (radial flow), the pressure derivative is flat (slope = 0) beyond wellbore storage and transition effects.
- As n increases beyond 2.0, the slope of the reservoir response incrementally decreases, becoming negative. When $n = 3.0$, the theoretical derivative slope of the reservoir response is -0.5 ; however, the response cannot be simulated for a value of n this high, due to the geometrical skin (see next).
- As n increases beyond 2.0, the effects of wellbore storage increase until the unit slope and transition hump dominate the response. This has the appearance of extreme positive skin (damage) though it is due purely to the geometry of the flow. This is called 'geometrical skin'.

Key numerical model parameters for these examples

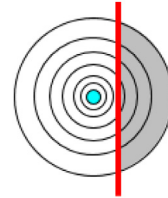
Reservoir permeability (k) = 100 mD; layer thickness (h) = 600 m; transmissivity (kh) = 60,000 mD m = 60 D m; skin factor (s) = 0; fractional dimension (n) = 2.0 (black), $n = 2.2$ (purple), $n = 2.4$ (orange), $n = 2.6$ (olive green)

A.1.1.6 Linear impermeable boundary (single)

Description

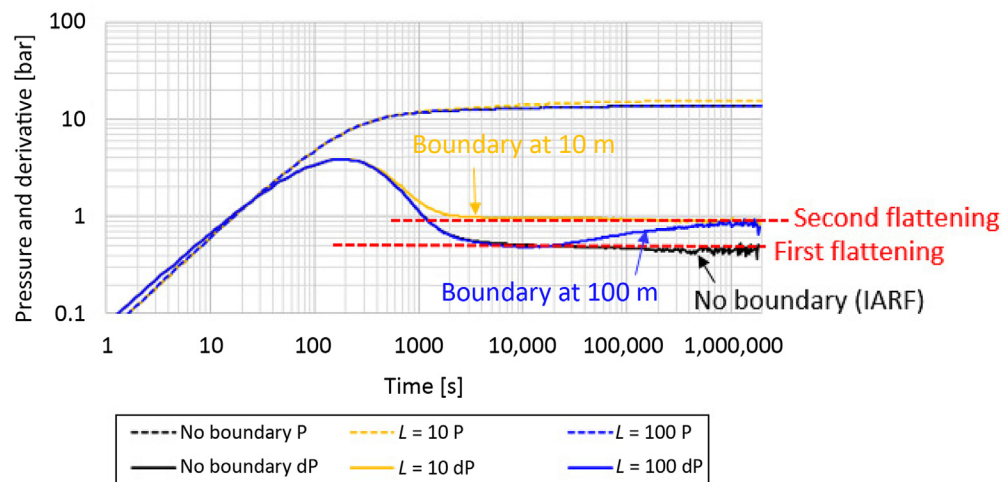
The reservoir is not infinite but contains an impermeable zone, separated from the permeable reservoir by a linear boundary at some distance from the well. A geological feature likely to be responsible for this kind of response is an impermeable fault.

Model schematic



Relevant book sections: Section 8.5.1 (numerical), Section 5.1.1 (analytical)

Derivative plot



Characteristic features of the pressure derivative

- The derivative flattens (slope = 0) before the boundary is detected and it rises and flattens a second time at a higher level (e.g. blue data for $L = 100$ m).
- This full response is only seen if there is sufficient time to see the reservoir response (flat derivative) before the boundary is detected. This may not be the case if wellbore storage is long, or if the boundary is close (e.g. yellow data for $L = 10$ m).
- A cautionary note: if the first derivative flattening is completely masked (as is the case for the orange data example), then the response will appear like a normal IARF response. Any field data with this appearance is unlikely to be associated with a boundary model, though there could in fact be a linear impermeable boundary very close to the well.
- There is no characteristic shape in the pressure data.

Numerical model parameters for these examples

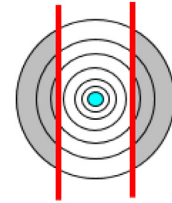
Reservoir permeability (k) = 10 mD; layer thickness (h) = 600 m; transmissivity (kh) = 6000 mD m, = 6 D m; skin factor (s) = 0; well-boundary distance (L) = 100 m (blue), $L = 10$ m (yellow), no boundary (black)

A.1.1.7 Wide channel

Description

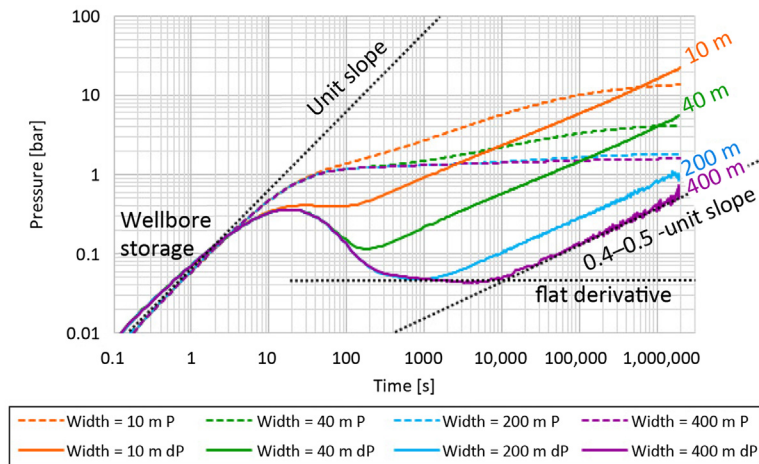
The reservoir is not infinite but contains impermeable zones, separated from the permeable reservoir by two parallel linear boundaries at some distance from the well. Within the wide channel, there is time for some radial flow to develop, before the boundaries are detected and the flow becomes linear along the channel. A geological feature likely to be responsible for this kind of response is a pair of parallel impermeable faults.

Model schematic



Relevant book sections: Section 8.5.2 (numerical), Section 5.1.1 (analytical)

Derivative plot



Characteristic features of the pressure derivative

- The derivative flattens (slope = 0) before the boundaries are detected, after which it rises with a $\sim 0.4-0.5$ unit slope, increasing slightly in very late time.
- This full response is only seen if there is sufficient time to see the reservoir response (flat derivative) before the boundaries are detected (e.g. purple data, width = 400 m). This may not be the case if wellbore storage is long or if the boundaries are close (e.g. orange data, width = 10 m).
- Unlike the single linear impermeable boundary, the presence of the boundaries will be apparent even if the flat derivative section is masked by wellbore storage, as the $0.4-0.5$ -unit slope response is characteristic.
- There is no characteristic shape in the pressure data.

Key numerical model parameters for these examples

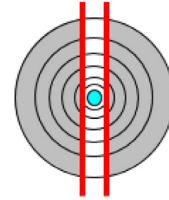
Reservoir permeability (k) = 100 mD; layer thickness (h) = 600 m; transmissivity (kh) = 60,000 mD m = 60 D m, skin factor (s) = 0; well-boundary distance (L) = half channel width = 5 m (orange), $L = 20$ m (green), $L = 100$ m (blue), $L = 200$ m (purple)

A.1.1.8 Narrow channel

Description

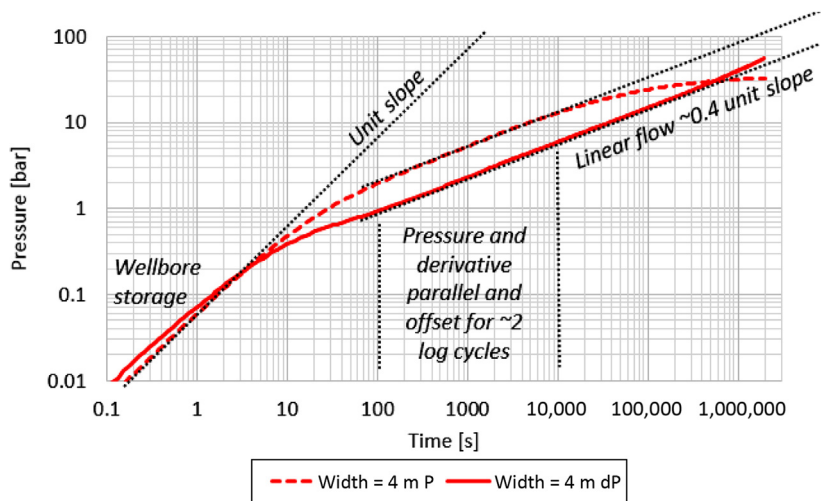
Flow to the well is restricted to a narrow channel. This is the same as the wide channel boundary model, except that the linear boundaries are very close together. There is no time for radial flow to develop around the well, and the flow is dominated by linear flow along the channel. A geological feature likely to be responsible for this kind of response is a permeable fault, with fluid flow dominantly along the fault.

Model schematic



Relevant book sections: Section 8.5.2 (numerical), Section 5.1.1 (analytical)

Derivative plot



Characteristic features of the pressure derivative

- The response transitions from wellbore storage directly into a linear flow response, where the derivative has a ~ 0.4 – 0.5 -unit slope.
- The difference from the wide channel response is that when the channel is very narrow, the pressure becomes parallel to the derivative (and offset) for a significant period, before diverging in very late time.
- This is not quite the same as a true ‘linear flow’ response (e.g. fractional dimension $n = 1.0$) as the channel still has some width, and the wellbore storage response is still apparent (unit slope and convergence of pressure and derivative).

Key numerical model parameters for these examples

Reservoir permeability (k) = 100 mD; layer thickness (h) = 600 m; transmissivity (kh) = 60,000 mD m = 60 D m, skin factor (s) = 0; well-boundary distance (L) = half channel width = 2 m (red)

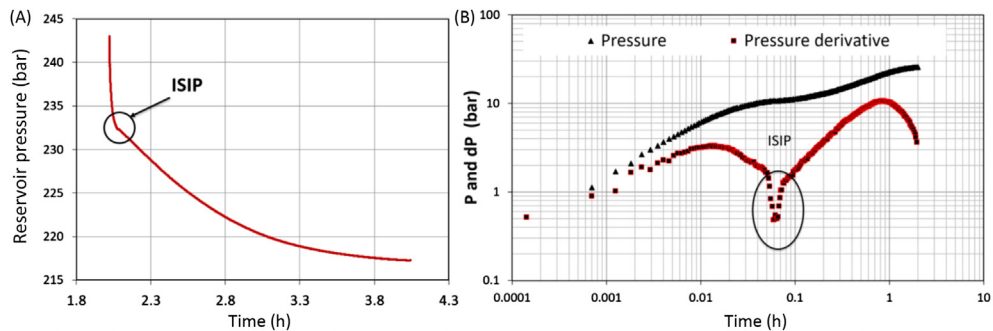
A.1.1.9 Fracture closure after injection

A behaviour sometimes observed in geothermal pressure transients is a significant bend in the measured pressure during falloff. One hypothesis to explain this behaviour is a sudden decrease in permeability as a fracture that was stimulated during injection closes again (or partially closes) as pressure in the well drops. This is more likely to occur in wells with relatively low permeability, where the pressure differential induced by injection can be large enough to exceed the fracture stress/pressure of the reservoir rock.

Similar behaviour is observed during mini-frac testing which is carried out prior to fracture stimulation in the petroleum and coalbed methane industries. When injection stops during the mini-frac test, the pressure initially falls off very rapidly, indicating high permeability. Then when the pressure drops to a certain value, the fracture starts to close (this is known as the instantaneous shut-in pressure—ISIP) reducing the rate of pressure falloff.

Relevant book sections: Section 10.5

History plot (A) and derivative plot (B)



Characteristic features of the history plot (A)

- The rate of decline of the falloff decreases when the fracture starts to close (ISIP): the falloff appears to have a sharp bend in it (circled data).
- This has the same appearance as a sudden decrease in reservoir permeability during a falloff and also similar to internal flow (downflow) during the test.

Characteristic features of the derivative plot (B)

- The bend in the history plot will appear in the derivative as a significant dip in the derivative (red data).
- The bend is also apparent in the log–log pressure data (black data).

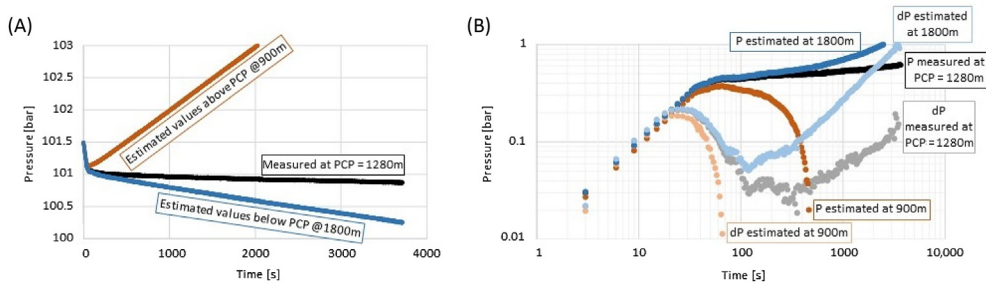
A.1.2 Common artefacts in geothermal PTA field data

A.1.2.1 Pressure pivoting

When there is significant change to the temperature profile of the fluid column in the wellbore during a test, the pressure profile of the column will be affected. Of particular relevance to injection/falloff tests in geothermal wells is the pivoting of the pressure profiles when heating takes place during the falloff. If the downhole tool is positioned at the pressure pivot point (PCP), then the falloff data will be unaffected. However, in practice, the pivot point is not actually known until weeks after the completion test, and the position of the tool for the falloff during the completion test is usually at what appears at the time to be the major feed zone. Positioning of the tool above or below the pivot point will result in drift in the data. To avoid this issue (and other issues related to heating in the wellbore), it is not recommended to design falloff tests with an injection flow of zero, but rather a falloff between two flow rates.

Relevant book sections: Sections 7.10 and 6.2.1

History plot (A) and derivative plot (B)



Characteristic features of the history plot (A)

- If the tool is positioned above the PCP, the pressure will appear to rebound in a history plot (brown data). The exact shape of this rebound is indicative only, in reality it depends on the rate of pivoting/heating during the falloff, which is unknown.
- If the tool is positioned below the PCP, the pressure will appear to drift downwards in the history plot (blue data).

Characteristic features of the derivative plot (B)

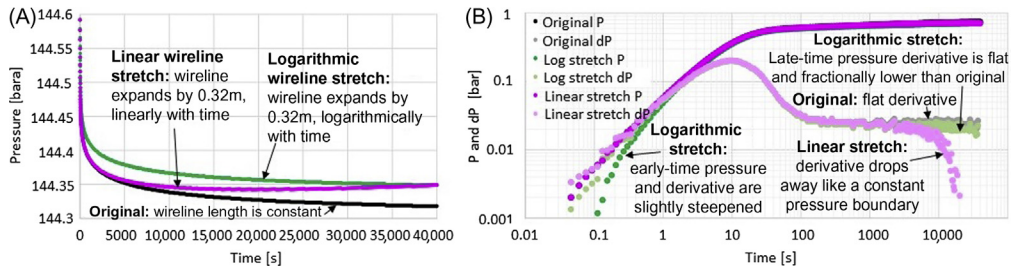
- The appearance of the pressure rebound in the derivative plot (tool above the PCP) is the pressure and derivative bend downwards quickly, becoming negative (brown and light brown data). This can resemble the constant pressure boundary response.
- The appearance of downwards drift (tool below the PCP) in the derivative plot is that the pressure and derivative bend upwards (blue and light blue data). In this example, the data have the appearance of a closed boundary.
- The actual field data set in this case (P = black, dP = grey) was measured at the PCP, where it shows the true reservoir response: a channel boundary as revealed by the 0.4–0.5-unit slope derivative.

A.1.2.2 Wireline stretch

When the temperature profile in the wellbore changes during a test (e.g. significant heating during a falloff), the wireline will expand. The amount of expansion can be significant (up to 10 m) for hot and deep wells (long wirelines). The expansion of the wireline will move the tool deeper into the well, increasing the head of water over the tool and hence the pressure. To avoid this issue (and other issues related to heating in the wellbore), it is not recommended to design falloff tests with an injection flow of zero, but rather a falloff between two flow rates.

Relevant book sections: Sections 7.9 and 6.2.4

History plot (A) and derivative plot (B)



Characteristic features of the history plot (A)

- Expansion of the wireline may or may not be apparent in the history plot, it depends on the rate of heating during the falloff (which in practice is not known).
- If the heating is approximately linear, the effect may be apparent as a slight rebound (pink data).
- If the heating is logarithmic (green data)—more rapid at first and then slowing down—then the effect may not be apparent.

Characteristic features of the derivative plot (B)

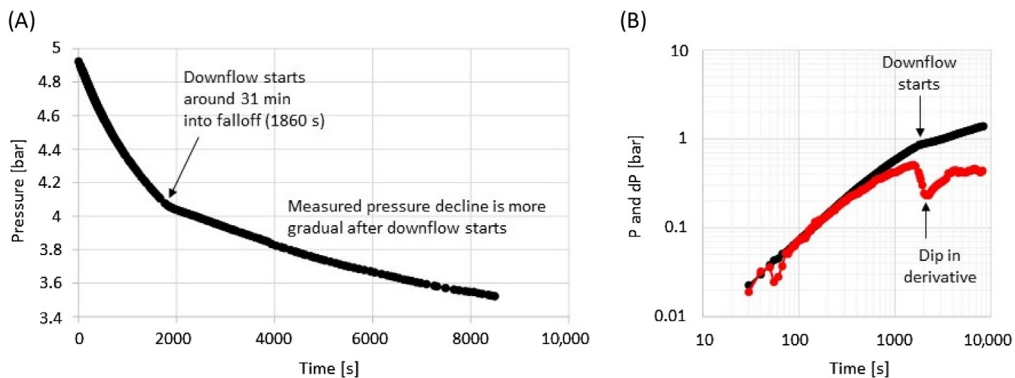
- A slight rebound in the history plot (linear heating) will appear as a downturn in the pressure derivative (pink and light pink data). This has a similar appearance to a constant pressure boundary response. If the 'constant pressure boundary response' disappears with a nonzero flow rate falloff test, or a pressure build-up test, it was probably due to wireline stretch and possibly also pressure pivoting.
- Logarithmic heating has no obvious impact on the history plot or the derivative plot (green and light green data). The very slight steepening of the early-time response and slight offset of the late-time flat derivative will not be detectable and will not have a significant impact on the estimated parameters.

A.1.2.3 Internal flow between feed zones

Geothermal wells usually have several localised feed zones where there is a permeable connection to the reservoir and fluid can enter or exit the wellbore during well testing. In some wells, a deep feed zone is underpressured compared to the shallower feed zone, and the shallow feed zone will flow into the well and down to the deep feed zone, this is called a ‘downflow’. PTA is not possible in these cases as downflows disrupt the pressure response. Sometimes downflows can be more subtle and are overlooked: a downflow may be suppressed during injection of cold water into the well, but then reactivate during the falloff. Careful examination of the temperature and spinner profile as the PTS tool is removed from the well will reveal the presence of a downflow. The downflow will also affect the falloff data set, though the effect can be confused with other responses. There is no known correction for when downflows start during the falloff and downflow conditions should be avoided. To avoid this issue (and others), it is not recommended to design falloff tests with an injection flow of zero, but rather a falloff between two flow rates.

Relevant book sections: Sections 7.8 and 6.2.4

History plot (A) and derivative plot (B)



Characteristic features of the history plot (A)

- The rate of decline of the falloff decreases when the downflow starts: the falloff appears to have a bend in it (black data).
- This has the same appearance as a sudden decrease in reservoir permeability during a falloff (as in the case of a fracture closing during the test).

Characteristic features of the derivative plot (B)

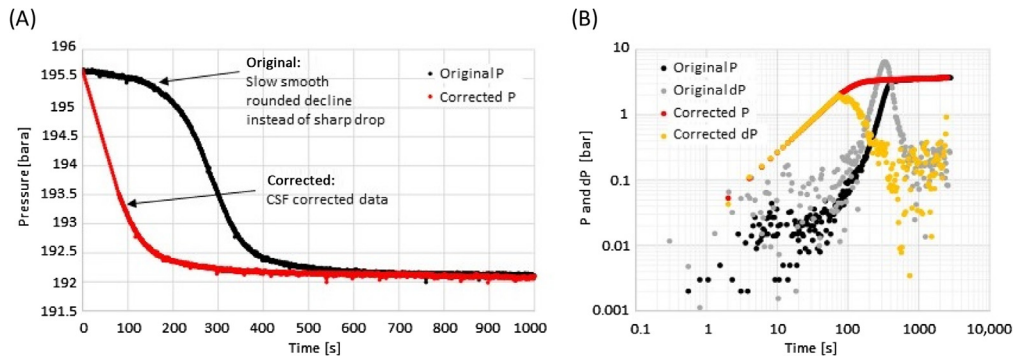
- The bend in the history plot will appear in the derivative as a small dip in the derivative (red data).
- The bend is also apparent in the log–log pressure data (black data).

A.1.2.4 Slow valve closing

Often the changes in flow rate into—or out of—a well during a test are controlled by the position of a valve, unless there is some custom-designed flow control system. Some valves are difficult to close and even with enthusiastic operators, the process can take a few minutes, and in extreme cases, up to 10 min. Pressure transients are worked into a completion test or output test design with step changes in the flow rate. A real-world flow change will never be a step change, and some correction is usually required. Slow valve closing over time periods of up to 10 min can be corrected in the raw data set using the cut-shift-fill (CSF) method, prior to PTA.

Relevant book sections: Section 7.5

History plot (A) and derivative plot (B)



Characteristic features of the history plot (A)

- During a falloff, the pressure will not drop rapidly in the expected manner but decline very slowly at first. The result is that the early part of the falloff is rounded, and the remainder of the falloff appears delayed in time (black data). The effect is the same for a build-up.
- The rounded falloff may be relatively smooth if the valve closes smoothly (black data) or it can appear scalloped (looks like several tiny falloffs) if the valve is closed incrementally.
- Correction with the CSF method (removal of the rounded portion) will restore the history plot to the expected shape (red data).

Characteristic features of the derivative plot (B)

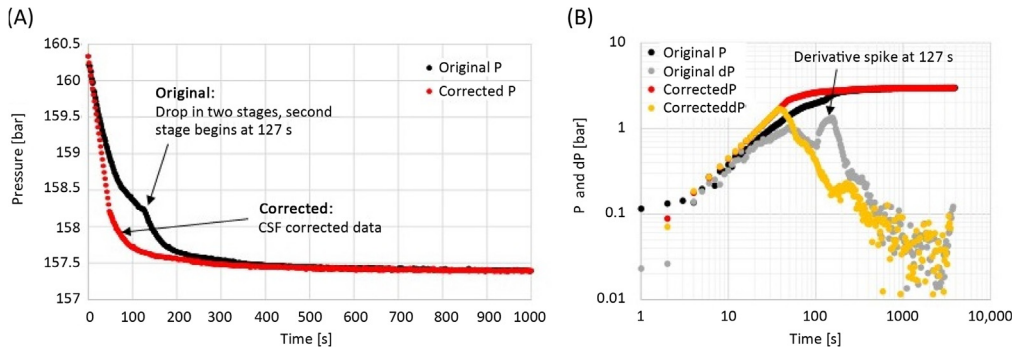
- During early time, the pressure and derivative will usually be very scattered (black and grey data).
- Ignoring the scatter, the slope of the pressure and derivative will initially be very low, increasing rapidly with time to much steeper than a unit slope (black and grey data).
- The derivative hump during the transition from wellbore storage to reservoir response has the appearance of a sharp peak (grey data).
- The CSF method usually mostly restores the shape of the early-time data to the expected shape (red and yellow data).

A.1.2.5 Two-stage pump shut down

Injection/Falloff tests are often performed using more than one pump. If the pumps are not shut down at the same time, then the single large falloff designed in the test becomes a combination of two (or more) smaller falloffs. Provided that the time delay between the pump shut downs is not too long, the effect can be removed from the data set using the CSF method. This artefact in falloff data is completely avoidable with clear instructions to the pump operators.

Relevant book sections: Section 7.6

History plot (A) and derivative plot (B)



Characteristic features of the history plot (A)

- The falloff occurs in two stages (black data).
- The effect is very obvious when the delay between pump shut downs is quite large (> 2 min in the example above: black data). When the delay is smaller, the effect is less obvious in the history plot.
- Correction with the CSF method (removal of the first stage) will restore the history plot to approximately the expected shape (red data).

Characteristic features of the pressure derivative (B)

- The second stage of the falloff appears in the derivative as a narrow spike (grey data).
- The CSF method removes the derivative spike and approximately restores the shape of the derivative (yellow data).

Appendix 2: Glossary of common terms used in geothermal energy technology

- Acidising** The practice of applying acids into a well in order to make it more permeable by removing acid-soluble material (e.g. calcite) which obstructs the flow of fluids. The common acids used are HCl for dissolving carbonates or a mixture of HCl and HF for dissolving silicates. Acidising is the most successful and widely used method for geothermal well stimulation
- Acid sulphate** Surficial waters low in chloride and with a pH in the range 0–5 may form from condensation of geothermal steam and gases at the ground surface, during which process the H_2S oxidises to sulphate
- Adiabatic** A change acted upon a system at constant total heat (constant enthalpy). An action or a process during which no heat is added or taken from a system. Flow up the geothermal well is often assumed to be adiabatic; however, in reality, there is some heat loss
- Advection** The process by which fluids and solutes are transported by the bulk motion of flowing deep groundwater under gravity. Counterflow is a form of advection
- Airlift** An apparatus used for pumping water from wells either temporarily (during discharge stimulation) or for a permanent water supply (direct-use wells). In operation, compressed air enters the reduction pipe and mixes with the water. As the water and air rise, the air expands and is practically at atmospheric pressure at the top of the discharge pipe. The efficiency of the airlift is calculated on the basis of the work done in lifting the water, divided by the isothermal work required to compress the air. Airlifting introduces oxygen into the well which will enhance oxidation/corrosion of the carbon steel casing
- Alteration** Change in the mineralogical composition of a rock typically brought about by reaction with hydrothermal fluids or meteoric groundwater. Sometimes classed as a phase of metamorphism but usually distinguished from it because it is more localised and involves water. The original (primary) mineralogy may be partially or fully replaced by secondary minerals. A common example in geothermal systems is an alteration of primary volcanic minerals to clays
- Amorphous silica** A form of silica, SiO_2 , which does not have a regular crystal structure; usually deposited at the surface from deep geothermal waters; commonly found as terraces (silica sinter) around boiling hot springs and geysers. It is the form of silica that deposits in geothermal pipelines and reinjection wells when the fluid is supersaturated with silica
- Analytical models** In the context of pressure transient analysis (PTA), this refers to relatively simple systems of equations which can be used to describe fluid flow and the pressure response of the system. All early PTAs (and still much of petroleum PTA) are based on analytical models. Geothermal PTA is too complex for analytical models and requires numerical simulation to solve (see 'numerical PTA' and 'PTA')
- Anhydrite** Calcium sulphate, $CaSO_4$. Anhydrite occurs as a secondary mineral in some geothermal fields at shallow depths and is likely to coincide with the occurrence of acid sulphate fluids. Can form as a scale inside shut geothermal wells when there are internal flows/mixing
- Anion** A negatively charged ion, such as bicarbonate (HCO_3^-)
- Anisotropic** Having a physical or optical property that varies with the direction (e.g. permeability). The permeability of geothermal reservoirs is generally anisotropic
- Annulus** The ring-shaped space between two concentric circles. In geothermal wells, this refers to the space between the drill string or smaller casing and the borehole wall or outer (larger) casing.

Although 'annulus' strictly describes an area in common geothermal usage, the term is often used to refer to the volume contained within the annular space over a depth interval

Aquifer (1) A formation, a group of formations or a part of a formation that is water bearing. (2) A stratum or zone below the surface of the Earth that is capable of producing water, as from a well. (3) An underground stratum that will yield water in sufficient quantity to be of value as a source of supply. An aquifer is not a stratum that merely contains water, for this would apply to all strata in the groundwater area. An aquifer must yield water

Bar absolute (or 'bara', or 'bar abs') A measure of pressure, relative to a vacuum (zero pressure)

Bar gauge (or 'bar g', or 'bg') A measure of pressure, relative to atmospheric pressure (which is ~1 bar absolute). Hence, equivalent readings of bar gauge are about 1 bar lower than bar absolute. The atmospheric pressure can be less than 1 bar at high elevations.

Bicarbonate waters CO₂-rich waters, containing low chloride, with bicarbonate (HCO₃⁻) as the major anion plus variable sulphate. Bicarbonate waters typically form in the marginal and shallow subsurface region where CO₂ gas is absorbed and steam is condensed into cool groundwaters; the condensation of steam heats the groundwaters, hence the term *steam-heated*

Bit The cutting tool attached to the bottom of the drill string and used to drill the well

Blowdown Also known as condensates, the water discharged from the geothermal power plant cooling tower basin to control the concentration of salts and other impurities present in circulating water. Normally this water is injected back into the reservoir

Blowout A sudden violent escape of gas, steam and water from a well when high pressure gas and steam are encountered during drilling, or if there is a breach of the casing integrity. Uncontrolled discharge can cause major damage to the drilling rig and personnel

Blowout preventers (BOP) High pressure valves, usually hydraulically operated, fitted to the top of the casing series of a drilling well to prevent a blowout. Three types of BOP valves are used in geothermal drilling: annulus, blind rams and pipe rams. Note that shear rams are not used in geothermal well control

Boiling point temperature Temperature at which water boils as a function of pressure

Boiling point with depth The temperature distribution with depth, which corresponds to a water column, which is just on the point of boiling (for the local pressure)

Borehole A term used to describe the actual hole created through the rock by the drilling rig e.g. 'borehole wall' refers to the interface between the rock formations and the empty space, an approximately cylindrical shape. Also called 'wellbore' or 'well bore'

Bottom-hole differential pressure A numerical expression to denote the difference between the reservoir pressure and the pressure at the bottom of a producing well. This determines the rate of fluid flow towards the wellbore

Binary cycle This system consists of two cycles operating on two different fluids interconnected at some stage for conversion of heat energy into mechanical work

Build-up A PTA data set measured when downhole pressure increases after production stops, or after there is a step down in production rate. Also used to refer to a PTA data set measured when downhole pressure increases after a step increase in injection rate

Bursting disk A thin diaphragm attached to a pipeline as a deliberate weakness so that it preferentially bursts if the pressure rises above the design pressure, preventing the rest of the pipe from bursting/damage (e.g. during water hammer)

Calcite Calcium carbonate (CaCO₃): A common nonsilicate mineral, colourless or white, occasionally tinged with impurities (grey, yellow, pink, green or blue) and colourless in thin section, with a trigonal crystal system. It is a principal constituent of sedimentary limestone and found in most sedimentary rocks, it also occurs in metamorphic and igneous rocks and is a common hydrothermal mineral in vugs/cavities or veins as well as a product of the alteration of other minerals. Calcite becomes more soluble in water when its temperature is lowered (retrograde solubility). Commonly forms as scale within geothermal production wells/surface equipment

- Calliper logging** An operation to determine the diameter of the wellbore with depth or the internal diameter of a casing, drill pipe or tubing
- Calliper tool** A surface-readout instrument that is lowered into a well to measure the diameter of its production casing or uncased wellbore in competent rock
- Casing** Pipe cemented in a well bore to support the walls of the hole, isolate potential producing zones and protect ascending thermal water from contamination. Generally, several strings of casing are set during the drilling of a well. The integrity of the casing/cement is essential to control the flow of fluid from the reservoir to the surface
- Casing head flange (CHF)** The flange that is welded or screwed to the production or anchor casings at the ground surface. It is used as a reference (zero depth) for all downhole measurements e.g. depth expressed as mCHF = metres below CHF
- Casing shoe** A steel sleeve protecting the lower end of the casing string when inserted into the well. Often provided with a drillable back-pressure valve when it is called a cement float shoe. Its depth is used as a reference point for the bottom of the production casing
- Casing string** Refers to different sizes of the concentric casing (pipe): there will be several sizes in a geothermal well, each string will be smaller and longer than the last
- Cation** A positively charged ion, such as sodium (Na^+)
- Cementing** The operation whereby cement slurry (see 'grout') is forced down through the well casing, out at the lower end, and then upwards to fill the annular space between the casing and the sides of the well bore. It secures the casing and excludes water and other fluids from the well bore
- Chloride water** The predominant fluid composition in many conventional geothermal reservoirs. Chloride is the principal anion which constitutes between 0.1 and 1.0 wt.% of the fluid. Chloride waters are characteristically of near neutral pH; springs which discharge chloride waters may deposit silica sinter around the mouth. Chloride water is the chemical signature of the deep fluid in the upflow part of the convective reservoir
- Circulation (drilling)** The journey cycle of the drilling mud from surface tanks, through the drill pipe and bit to the subsurface. Much then goes back again to the surface through the annular space between the drill pipe and wall of the drilled hole
- Circulation rate** The rate at which the water taken from the cooling tower basin circulates through the condenser system
- Clay minerals** Hydrated aluminosilicate minerals whose structures are sensitive to changes in both temperature and chemical environment. They are used as sensitive mineral geothermometers (during drilling) and as indicators of changes in the chemical environment e.g. the presence of acid fluids in an otherwise relatively neutral chemical environment
- Completion test** A suite of well testing carried out immediately after completing the drilling of the geothermal well including water-loss survey (injection), injectivity test, pressure transient testing (build-ups and/or falloffs), heat up surveys and initial output test including discharging survey. Possibly also includes casing integrity surveys, cement bond logs, electrical or mechanical casing calliper runs and downhole camera surveys
- Condenser** A cooled vessel into which steam is discharged, where it condenses, usually under vacuum. A condenser is a heat exchanger, which can involve mixing of the two fluids (direct contact condenser) or through a shell and tube heat exchanger (surface condenser)
- Conduction** Heat diffusing through solid bodies or through stagnant fluids (e.g. warm water systems)
- Confined aquifer** A formation in which the groundwater is isolated from the atmosphere at the point of discharge by impermeable formations; confined groundwater is generally subject to a pressure greater than atmospheric
- Convective system** A heat-transfer system in the upper crust of the Earth where heat is transferred by fluid moving from a heat source to a heat sink (ground surface). Convection ensures maximum heat transfer and is the dominant heat-transfer mechanism in hot water and two-phase geothermal systems

- Conventional geothermal system** A generic term used to refer to non-Enhanced Geothermal Systems (EGS) that have been successful in commercial use for decades and generally do not require permeability enhancement
- Core** In rotary drilling, special bits are employed to cut cylindrical samples of the formations penetrated. These samples, known as ‘cores’, are examined to obtain geological and petrophysical information. Deep cores are expensive when using large drill rigs and not commonly taken during commercial geothermal drilling
- Corrosion** The act or process of dissolving or wearing away metals or minerals. In geothermal wells, fluid can attack the casing from the inside (internal casing corrosion – ICC) or the outside (external casing corrosion – ECC)
- Counterflow** This term generally refers to any situation in which two fluids are flowing past each other but in different directions. In the underground geothermal reservoir, ‘counterflow’ refers to the upwards flow of hot steam (or two-phase fluid), opposite to the downwards flow of cooler recharge fluid (or condensate) under the force of gravity (this is a form of advection). This occurs at the top of two-phase and vapour-dominated geothermal systems. Counterflow is the dominant heat-transfer mechanism in vapour-dominated systems, where there is no natural convection. In mechanical terms, inside geothermal power station cooling towers, ‘counterflow’ refers to the upwards flow of air (by natural convection or fan-forced), opposite to the downwards flow of water, which is sprayed and falls under the force of gravity, being cooled in the process
- Crown block** The pulley at the top of the drilling tower (mast). Used for hoisting and lowering of equipment in drilling and serving a well
- Cut-shift-fill** A technique used to preprocess pressure transient data prior to PTA, for when the well-head valve closure is slow or the pump shutdown is not simultaneous, affecting the quality of the data. The technique involves cutting/removing the affected early data, shifting the remaining data set earlier in time and filling the early-time gap with a straight line. It is not an ideal solution, but the best fix to make affected data useable. Avoiding this early distortion in the data is greatly preferable and is often possible e.g. using a customised flow control system with ball valves will allow for very rapid changes in flow rate (almost a step change)
- Cuttings** Small chips or slivers of rock, which are produced as the drill bit grinds through rock as it penetrates downwards, which are carried to the surface by the circulating fluid and collected for examination by geologists
- Darcy’s law** A derived equation for the flow of fluids in porous and fractured media on the assumption that the flow is laminar and that inertia can be neglected
- Decline analysis** Monitoring and quantification of the change in well output with time (see ‘output test’). Mass flow decline is often assessed as a fixed fraction per year. The most common reasons for the decline are drop in reservoir pressure, scaling or cooling
- Development well** A well that is being drilled in an already discovered geothermal field
- Directional drilling** Drilling a well at an angle from vertical (deviated well). This is generally done to sidetrack obstructions, to drill wells under inaccessible surface locations e.g. swamps and protected areas, to correct irregular bottom-hole spacing and to minimise the number of well pads at the surface
- Direct use** The use of geothermal energy for all applications other than electrical power generation. Direct-use applications work with the first law of thermodynamics only hence can achieve high conversion efficiency (80–90%). Some of the common direct-use applications include space heating, industrial use, green house heating, aquaculture and others
- Discharge prediction** The well test methods and techniques used to predict if the geothermal well is going to self-discharge or not, after heat up surveys. If the well is not predicted to self-discharge, then discharge stimulation techniques should be considered

- Discharge stimulation** The processes and techniques used to get the geothermal well to produce continually; effectively, it is jump-starting the production well. Discharge stimulation techniques include using soap sticks, airlifting, air compression, well-to-well hot fluid injection, injection of hot fluid from a portable boiler and nitrogen injection. If the geothermal well cannot be discharge-stimulated, then it can only be made to produce fluid by using a downhole pump (if permeable). Discharge stimulation should not be confused with permeability stimulation (see stimulation)
- Dog-leg** A sharp or sudden change of direction in a borehole. This could have a geological significance e.g. proximity of an unconformity or merely a drilling lapse
- Downflow** A term used to describe internal flow between feed zones in a well, where fluid is flowing into the well from a shallower feed zone, then down the well and out at a deeper feed zone
- Downhole** A general term that can be applied to the following: equipment physically located down the well (e.g. downhole tools suspended on wirelines), samples retrieved from depth (e.g. downhole sampling) or data measured at depth (e.g. downhole pressure)
- Downhole heat exchanger (DHE)** A heat exchanger located at a depth within a geothermal well, to which a secondary fluid (usually water) travels downwards, and then back to the surface. A DHE is used to recover thermal power, commonly without producing the deep geothermal fluid. Typically used for low thermal load direct-use applications. There are different designs of DHE but mainly U-tube or annular construction, with some DHE's run with a promoter pipe to enhance internal heat transfer (natural convection). Other well constructions allow a small bleed of geothermal fluid to increase the thermal output of the DHE. DHEs are not recommended for use in electricity production
- Downhole sampling** This is important where variations in chemistry occur either with depth or with time. The essential features of any downhole sampler are (1) it must hold vacuum and pressure, (2) not open prematurely, (3) remain open for a designated time, (4) be inert to acid solutions, (5) be inert to fluids of high salinities and (6) perform at high temperatures
- Downtime** Time lost during drilling either due to repairs on machinery, waiting on equipment or bad weather
- Drawdown** When a well is discharged at a constant rate, this term may refer to either the total downhole pressure drop or for PTA it refers to the pressure transient with time as the downhole pressure changes between flow rates
- Drift (drift rate)** The water lost from the power station cooling tower as droplets are entrained in the effluent airstream. Typical values are 0.001%–0.2% of the circulation water rate
- Drill collar** A heavy length of pipe: several of these are placed directly above the bit and serve to concentrate the weight of the drill string on the bit
- Drill string** The whole assembly of drill pipes, drill collar and bit that is down the well during drilling
- Drill tower** The framework (also known as mast or derrick) with a pulley block at the top that acts as a crane to lift the drill string and other drilling equipment
- Drilling mud** A carefully concocted mixture of clays (bentonite) and other minerals, mixed with water, pumped down the drill pipe to lubricate and cool the bit, flush out cuttings, provide a wall to the open hole and balance formation pressures. Used during drilling through shallow formations, to be sealed off behind production casing, but not used in modern drilling operations during drilling of deep productive formations, due to the potential for formation damage (positive skin)
- Drill pipe** The steel pipe that is used for carrying and rotating the drilling tools and for permitting the circulation of the drilling mud
- Drill-stem testing** A controlled blowout in which a small amount of reservoir fluid is produced into the drill pipe through a special tool. It is generally run in open hole for a tentative test of the fluid content and calibre of the reservoir prior to undertaking a full-scale production test. Not commonly applied to geothermal wells

- ECC** Corrosion attack that takes place from the outside of the casing, mainly related to acid sulphide or carboic acid (CO₂ rich) fluids and can result in casing penetration and possibly the formation of a steam thief zone
- EGS** A very loose definition of nonconventional geothermal systems. It effectively refers to geothermal systems with high temperatures but without sufficient permeability, where stimulation (permeability enhancement) is required
- Enthalpy (*h*)** A measure of the sum of the internal energy and an amount due to work stored by the action of pressure, normally reported/used per unit mass (kJ/kg)
- E-line** Electronic-line is a specially designed multistrand cable with an insulated and electrically conductive core, used to run downhole tools and send the measured data to the surface instantly (in real time). This allows real-time monitoring of the downhole data and the tool condition, therefore allowing better and more prompt/flexible decisions and intervention. However, using the E-line is much more expensive than the single-strand wireline (also called 'slick-line'). The E-line also has temperature limits and in some cases, the wireline is the safer option
- Exploration** In general terms, this refers to the entire breadth of search for geothermal resources with the help of geological, geochemical and geophysical surveys, integrated interpretation with laboratory data back up, selection of suitable locations for exploratory test drilling and well testing of these wells
- Exploration well** A well that is being drilled in a new and relatively unknown geothermal field to gather information but also can be used for production or reinjection in the future
- Falloff** A PTA data set measured when downhole pressure decreases after a step down in injection flow rate. Sometimes falloffs are measured after a step down to zero injection, though this is not recommended in geothermal wells
- Fault** A planar fracture along which rocks have been displaced. Faults are usually *normal*, *reverse* or *strike-slip* (or a combination), depending on the direction of displacement. Faults can be permeable pathways for fluid flow (conductive faults) or if they are impermeable, they can form a reservoir boundary (sealing faults). Some geothermal systems are fault dominated, where fluid flow is concentrated along the fault, making them easy to identify and target
- Feed zone** A particular depth (or a wider interval) in the well at which there is a permeable connection between the wellbore and the reservoir. Most geothermal wells have more than one feed zone. Often one feed zone has a much better connection to the reservoir and clearly dominates the well response: this is called the 'major feed zone'. Not all wells have a major feed zone
- Field** A geographic area containing one or more geothermal reservoirs
- Fishing** Operation on the drilling rig for the purpose of retrieving casing or other items from the well bore. Fishing also applies to recovering downhole tools that were lost accidentally down the well
- Fishing tools** Tools used to pick up pieces of drill pipe, casing or downhole tools that have fallen into the hole accidentally
- Flash point** In wells drilled into a liquid-dominated reservoir, fluid will enter the well in a liquid phase, and at some point during its ascent to the surface, the pressure will become low enough for it to begin to boil (flash). The location of the flash point depends on the production flow rate/control valve opening. Calcite scaling in production wells is commonly concentrated around the flash point
- Flowing surveys** Also called 'discharging surveys': the downhole measurements [normally with a pressure, temperature and spinner (PTS) tool] carried out while the geothermal well is on production (self-discharging). A counterweight is attached in front of the tool to prevent it from being thrown out of the well by the flowing fluids. The test can help identify the major feed zone, changes in the feed zone contribution, the flash point in the well and also possible leaks in the casing
- Fluid inclusion** Small, usually microscopic, volumes of fluid trapped within hydrothermal crystals during their growth from fluids. They provide us with a sample of the fluid at the time of growth (or healing) of the crystal, and on many occasions allow us to determine rather accurately the temperature at the time of their formation

- Fluid velocity profile** The velocity of fluid as it moves up (or down) the well, entering or exiting at permeable feed zones. Calculated from spinner profiles, measured using the PTS tool (see 'PTS tool', 'spinner', 'spinner ratio')
- Formation** A succession of sedimentary or volcanic beds that were deposited continuously and under the same geological conditions. It may consist of one type of rock or combinations of types
- Fumarole** A fumarole is a natural geothermal surface feature: a vent discharging steam and other gases but not liquid water. This steam discharge is typically audible indicating velocities of 20 m/s or greater (see 'steam vent')
- Generator** An electrical machine that produces either alternating or direct current when rotated/driven by the turbine (a general term — all generators in geothermal power stations are alternators)
- Geophysics** The study of variations in physical properties of the Earth such as the pull of gravity, intensity of the magnetic field, susceptibility of rocks to electrical currents and speed of acoustic waves within the crust
- Geothermal gradient** A measure of the conductive rise of rock temperature with depth below the Earth's surface. Usually expressed in °C per 1000 m (km). The world average is between 25 and 30°C/km. In geothermal areas, this can be in excess of 100°C/km, above convective geothermal systems and at their margins
- Geothermal system** A connected region of the Earth where solid rocks by natural processes have been raised to an elevated temperature with respect to neighbouring regions. The rocks may or may not contain significant proportions of fluid. Geothermal systems can be classified both geologically or based on the dominant type of heat transfer. In this book, we presented a reservoir engineering—based classification that is based on geothermal fluid enthalpy which is driven by the combination of reservoir permeability and the heat-transfer mechanisms (also known as hydrothermal system)
- Geothermal reservoir** A zone of permeable rock within a geothermal system, which contains hot fluid. Most geothermal reservoirs (with the exception of warm water and vapour-dominated systems) have two distanced regions of interest, the upflow and outflow regions. The upflow region is targeted for geothermal fluid production during electrical power production. Locating the upflow region during exploration is the main challenge
- Geothermometry** The estimation of subsurface temperatures from the concentration of the chemical constituents present in a fluid
- Geo-pressured system** Geothermal systems under very high pressure (much higher than the hydrostatic head of a cold-water column) with temperatures up to 250°C, at depths of >2500 m and some in situ permeability. Some geo-pressured systems have a high dissolved gas (methane) content (e.g. Gulf of Mexico). Very high risk of blowout during drilling if not prepared, no reported 'commercial' utilisation yet
- Geyser** A hot spring characterised by intermittent discharge of mostly boiling water that is ejected turbulently and is often cyclic so that the manifestation is a periodic one (also called 'spouting spring')
- Go-devil** Also known as a 'sinker bar': this is effectively a go or no-go gauge used to check the open diameter of the production casing and liner before running any tool down the well. Go-devils are made of aluminium or brass so that it can be drilled through in the event that it becomes stuck and blocks the well
- Grout** A fluid mixture of cement and water (neat cement) of a consistency that can be forced through a pipe and placed as required (see 'cementing'). Various additives, such as sand, bentonite, slag and hydrated lime, may be included in the mixture to meet certain requirements. Bentonite and water are sometimes used for grout
- Hardness** A property of water causing formation of an insoluble residue when the water is used with soap. It is primarily caused by calcium and magnesium ions
- Water head** Energy contained in a water mass, produced by elevation, pressure or velocity

- Head loss** The portion of water head energy which is lost due to friction as water flows
- Heat load** The thermal power required for direct use applications. Also, refers to the heat removed from the circulating water in the cooling tower, it usually expressed in thermal megawatts (MWth). Also called 'duty'
- Heat exchanger: shell and tube** A type of heat exchanger that passes heat from a hot fluid to a cold one, one fluid being in a tube (many parallel tubes usually) and the other fluid in a shell (vessel) around the tubes. The fluids are thus kept separate
- Heat exchanger: plate** A type of heat exchanger where two fluids are separated by thin plates through which the heat passes from one fluid to the other
- Hot spring** A natural discharge of water at a temperature exceeding the average ambient value. Often hot springs are found associated with faults in or near topographic lows
- Hydraulic conductivity** The rate of flow of water in cubic metres per unit time through a cross-section of one square metre under a unit pressure gradient, at the prevailing temperature
- Hydraulic proppant fracturing (HPF)** Stimulation of production wells using highly viscous gel as the fracturing fluid, with a high proppant concentration. It is suitable for reducing permeability damage (i.e. positive 'skin') in the direct vicinity of the wellbore. The well is shut after the fracturing process to allow the fractures to close with proppants in place. Not commonly used in geothermal well stimulation.
- Hydraulic gradient** The rate of change in total head per unit of distance of flow in a given direction
- Hydrology** The science dealing with water standing or flowing on or beneath the surface of the Earth
- Hydrocarbons** Organic chemical compounds made up predominantly of carbon and hydrogen, but sometimes with sulphur, oxygen or nitrogen, typically forming chain-like molecules. Those with up to 4 carbon atoms are gaseous, those with 20 or more are solid and those in between are liquids
- Hydrothermal eruption** Eruption of rock, mud, steam and water associated with relatively sudden flashing of liquid to steam and the associated rapid expansion of the fluid volume. It is different from a volcanic eruption
- Injectivity index (II)** During injection testing, this is the ratio of the mass flow rate to reservoir pressure [or well head pressure (WHP) in less-permeable wells which do not have a vacuum at the surface during injection testing], commonly reported in t/h/bar or kg/s/MPa. Prior to production/output testing, the II can be used to estimate the well productivity index, which has the same units and is always less than the II
- Interference** The scenario in which the area influenced by one well comes into contact with, or overlaps, that of a neighbouring well e.g. when two wells are producing from the same aquifer and are located near each other
- ICC** Corrosion that attacks the geothermal well casing from the inside, mainly related to low-pH acid sulphite-rich fluid in young volcanic systems
- Isothermal** Any process within the system taking place at constant temperature
- Kelly** A square or hexagonal hollow shaft, which engages in the rotary table imparting rotation to the drill pipe. Not commonly used these days as most drill rigs have a top drive, which is connected directly to the drill pipe
- Killing a well** Reversing and halting the tendency of a geothermal well to flow (self-discharge) by pumping cold water into the well bore. During drilling, it refers to pumping suitable fluid (mud) of high specific gravity during well control
- Killer well** A geothermal well drilled to target the production zone of a nearby damaged well, to pump mud and cement and stop uncontrolled discharge from the damaged well. Killer wells are the last resort to prevent full-scale well blowout: they are expensive to drill and unlikely to be used for production in the future

- Liner** The last piece of casing placed in the hole, which has holes (perforations or slots) in it to allow the fluid to flow out of the reservoir and up the well. It is not cemented in place and in most geothermal wells not hanged to the production casing
- Lip pressure** The pressure at the outlet (the lip) of a pipe, which can be used to calculate the mass flow rate if the flow is supersonic, using an empirical relationship
- Lip pressure pipe** A pipe specially made to allow lip pressure measurement. The lip pressure pipe is used to measure mass flow rate of two-phase geothermal fluid during output testing. It can be connected to the wellhead either vertically or horizontally
- Logging** A term often used to encompass the running of downhole tools, presentation of the data (logs), analysis and interpretation. Also used more generally to describe the process of recording any data (as in data 'logs' and data 'loggers')
- Lost circulation** The result of drilling fluid escaping from the borehole into the formation by way of fractures or any permeable feature. It is an early indication of the location of feed zones during drilling
- Lubricator tube** A pipe assembly temporarily attached to the master valve of the geothermal well to allow the safely running (logging) of downhole tools in self-discharging wells with some WHP
- Magma** A molten fluid composed of a complex mixture of molten silicates with water and other gaseous material in solution, formed within the crust or upper mantle of the Earth. If magma reaches the Earth's surface, it is called lava and can form extrusive igneous rocks such as basalt or rhyolite. If it does not reach the surface, it cools more slowly and forms a pluton, a body of intrusive igneous rock such as granite (see 'pluton')
- Magnetotelluric (MT) method** A geophysical method in which orthogonal components of the horizontal electric and magnetic fields induced by natural fluctuations in the Earth's magnetic field are measured simultaneously as a function of frequency. This method provides a means of interpreting resistivity structure at much greater depths than is possible with conventional electromagnetic (e.g. electrical resistivity) methods and usually requires only a single station to produce a result. MT is the most commonly used method during geothermal field exploration
- Make-up water** The water added to the cooling tower basin to replace that water lost by evaporation, drift, blowdown and leakage. Also used to refer to the water needed for reinjection in vapour-dominated geothermal systems to ensure the sustainability of the resource
- Maximum discharge pressure (MDP)** The highest WHP at which a well will discharge, during output testing
- Memory tool** A downhole tool such as a PTS tool that measures and stores data electronically in internal memory storage for later download, when real-time data at the surface are not required or are not possible. These instruments can have internal cooling via a heat sink (also see wireline and E-line)
- Meteoric water** Water that originates as any form of precipitation (rain or snow), including rainwater and snow/glacial melt water. Meteoric water mostly runs off the land surface, collecting in lakes and rivers and ending up in the sea; however, it also infiltrates the shallow subsurface via any permeable pathway, where it comprises the majority of groundwater
- Micro-earthquake** A discrete earthquake event of low magnitude (moment magnitude <2). Can occur due to natural seismic events or due to reinjection of geothermal fluid
- Monitoring well** A well that is not used for production or reinjection of the geothermal fluid but rather for collecting reservoir data with time (e.g. pressure, temperature)
- Noncondensable gases (NCG)** Engineering term referring to the gases in steam, which do not condense into liquid e.g. CO₂, H₂S. NCG originate in the reservoir fluid where they can be dissolved in the reservoir water or already exist in gaseous form in steam. NCG dissolved in the liquid are released into the steam within the above-ground separator/flash plant. They travel with the steam through

the turbine and into the condenser where they would build-up (because they cannot condense back into liquid here) unless they are removed via pumps/compressors. NCG from the condensers are usually released to atmosphere but are reinjected into the reservoir in a few fields

Numerical PTA The methodology of analysing PTA field data sets by matching to a model response which is generated numerically, using a simulator with a grid of blocks which exchange heat and mass. Geothermal PTA data sets require numerical PTA due to the complexity of geothermal systems. More conventional analytical PTA methods do not apply to geothermal data sets (see 'analytical PTA' and 'PTA')

Orifice plate A specially shaped plate with a hole (an orifice) installed in a pipeline, forming a restriction through which fluid (water, steam or two-phase) must travel. The small pressure drop from upstream to downstream of the orifice is measured and used to calculate flow rate empirically. The use of orifice plates for single-phase flow is well established and accurate. In the past, the use of orifice plate data for two-phase flow calculation has been inaccurate; however, this has been overcome very recently

Outflow The convective upflow of a geothermal system will usually reach an impermeable barrier and begin to move laterally, though still slightly upwards: this is called the outflow of the system. The primary direction of fluid movement is horizontal. An outflow cannot be angled downwards, unless there is advection by gravity-controlled groundwater flow in that direction (see 'geothermal reservoir')

Output test The final and most important well test (after completion/injection testing and heat up), which measures the production capacity of the geothermal well in MWth and/or MWe. The test involves measuring both the mass flow rate and the enthalpy of the produced geothermal fluid at different valve openings. The results are used to produce the output curve which provides a relation between the WHP and the produced fluid mass flow rate and enthalpy. The decline in well output with time during long-term production is an important aspect of well monitoring (see 'decline analysis')

Perched water Also called 'perched aquifer': a groundwater aquifer located above – and separated from – the underlying main body of groundwater. In order for a perched aquifer to form, the water must be prevented from percolating down to the main body of groundwater by an impermeable barrier such as a layer of clay

Perforation A method of making holes through the casing in order to access a potentially productive formation, allowing the geothermal fluid to flow into the well and eventually to the surface. Done retro-actively, if a geothermal well has insufficient output as completed, and there are data indicating a hot/productive formation behind the casing

Permeability A measure of the relative ability of a rock to permit the flow of fluids through its pores. S.I. units are m^2 , though the non-S.I. unit Darcy (D) or milli-Darcy (mD) is in common usage in the geothermal industry (and petroleum industry). One Darcy (1 D) is equal to $9.87\text{E} - 13 \text{ m}^2$

pH A measure of the acidity or alkalinity of a solution, numerically equal to 7 for neutral solutions at 22°C , increasing with alkalinity and decreasing with acidity. pH modification of geothermal fluid is a common method of controlling corrosion and mineral scaling in geothermal wells

Piezometric surface The surface of uniform atmospheric pressure to which the water from an aquifer or reservoir will rise under its full head. Note the piezometric surface and the water table surface can be similar though they have distinct definitions (see 'water table')

Plate tectonics A theory of global tectonics in which the lithosphere is divided into a number of plates whose pattern of horizontal movement is that of torsionally rigid bodies that interact with one another at their boundaries, causing seismic and tectonic activity along these boundaries

Pluton Large-scale mass of intrusive igneous rock which forms when magma does not reach the Earth's surface (see 'magma').

- Pore** The void space between adjacent grains or crystals within a rock, in fractures or in vesicles (former location of gas bubbles during formation). When rocks are in situ, the pores are normally liquid or gas filled
- Porosity** A measure of how much pore space exists in rock as a percentage of its total volume
- Pressure** Defined as the perpendicular force per unit area exerted on a surface with which a fluid is in contact. The S.I. unit for pressure is the Pascal (Pa) which is defined as 1 Newton per square metre (1 N/m^2). It is simple to measure and commonly used to calculate temperature and mass flow rate in geothermal applications
- Pressure control point (PCP)** Also known as the ‘pressure pivot point’, this is the point on the pressure with depth diagram at which the different heat up pressure surveys intersect with each other. This is an indication of the depth of the best permeable connection with the reservoir (the major feed zone in the well), if there is one dominant feed zone. If there are two dominant and relatively equal feed zones, then the PCP will be located between them
- PTS tool** A downhole tool runs into the well on a wireline or E-line, controlled by a winch at the surface. Used to measure pressure, temperature and fluid flow during completion testing, heat up runs and discharging PTS runs (see ‘spinner’, ‘wireline’ and ‘E-line’).
- PTA** Analysis of downhole pressure data containing pressure transients (pressure changes with time) recorded as the result of step changes in flow rate in a well (injection or production). In geothermal wells, PTA data should be analysed by numerical methods: matching numerical models to field data to reveal information on the well condition and the nature of flow in the reservoir
- Production casing** The inner (smallest diameter) cemented casing of the well, through which the geothermal reservoir fluid flows up the well to the surface. Only the liner is smaller than the production casing (see ‘liner’)
- Promoter** A pipe or a casing design feature of a geothermal well, used to enhance heat transfer (natural convection) and thermal power output of a DHE
- Pumped well** A well installed with a downhole pump to produce the geothermal fluid. This is necessary when the well will not self-discharge, which is common in warm and hot water systems
- Quartz** An abundant and naturally occurring mineral form of silicon dioxide (silica), SiO_2 . When it forms relatively slowly and unconfined, it can form large euhedral crystals with a six-sided prismatic shape. It is very common as a geothermal reservoir mineral
- Quartz geothermometer** Aqueous geothermometer based on the silica concentration that is controlled by quartz solubility. Good for assessing reservoir temperatures in fluids from production wells but can be problematic in application to hot springs (see ‘geothermometry’)
- Recharge** The natural addition of deep groundwater to the geothermal reservoir, it is drawn in to replace the geothermal fluid discharged by the natural features or the mass produced by the production wells. Recharge is controlled by the permeability of the reservoir and hence it is directly related to the type of the geothermal system. Reinjection of waste geothermal fluids can supplement the natural recharge of the geothermal reservoir
- Reconstituted well** A well that was originally designed for one use (e.g. petroleum) but was modified to be used for geothermal applications
- Reinjection** Returning the geothermal fluid (steam condensates, brine or NCG) back into the reservoir through dedicated reinjection wells. This is to maintain pressure in the reservoir and as an environment-friendly method for waste fluid disposal
- Reserves** The definition of this is the subject of debate within the geothermal industry, but it is generally accepted as the quantity of energy yet unproduced but commercially recoverable with present-day techniques
- Reservoir** See ‘geothermal reservoir’

- Reservoir rock** Any porous and permeable rock of any type (often volcanic or sedimentary) containing thermal fluids
- Reynold's number** In pipe/well flow, the transition from laminar to turbulent flow is characterised by well-known values of Reynold's number which expresses the ratio of the inertia forces to the viscous forces
- Rotary drilling** A method of drilling which depends upon the rotation of a bit and constant circulation of fluid to remove the cuttings. All deep (geothermal and petroleum) wells are drilled with this method
- Rotary table** A circular platform on a drilling-rig floor through which the drill pipe passes; the table turns to rotate the drill pipe during drilling (also see 'Kelly')
- Salinity** The total content of dissolved salts present in water, commonly expressed in mg/kg of water or ppm
- Sandstone** A sedimentary rock composed of abundant rounded or angular fragments of sand set in a fine-grained matrix (silt clay) and more or less firmly united by a cementing material. It is a common reservoir rock in warm and hot water systems, in nonvolcanic settings
- Saturation temperature** At the saturation temperature and pressure, both water and steam phases are present
- Scaling** The deposition of minerals, e.g. silica or calcite, in well casing, above-ground steam field equipment and power plants, which can cut off fluid flow and cause damage
- Scraper** Also called a 'scratcher', this is a downhole mechanical tool used to collect solid scale samples from the internal walls of the geothermal well
- Sedimentary** Rocks composed of clastic and precipitated materials, which may be unconsolidated or welded together by pressure or by cementing into a solid rock
- Self-propping** The nonclosure of the fracture created after water fracturing (WF) due to fracture erosion, disaggregation and/or shear stress dislocation of the fracture surfaces resulting in permanent opening of the fracture
- Separator vessel** The container in which the geothermal two-phase mixture is separated into water and steam. There are two main separator designs in the geothermal industry: vertical (centrifugal principle) and horizontal (settling principle). The separator is also used to accurately measure the well output (total mass flow rate and enthalpy)
- Shaker** The filter to remove cuttings from the mud flowing out of the well during drilling. The cuttings can be analysed by geologists, while the mud falls into the mud tank where it is cooled and recirculated
- Silica saturation index (SSI)** In a fluid containing silica, this is the ratio of the measured silica content (concentration) to the calculated amorphous silica concentration at saturation conditions (for the fluid temperature). Super saturated fluid ($SSI > 1$) can result in deposition of amorphous silica (see 'silica scaling')
- Silica saturation temperature** This is the temperature at which the separated water reaches saturation with respect to amorphous silica ($SSI = 1$). If the geothermal fluid is below this temperature, silica will start to deposit
- Silica scaling** Silica deposition from geothermal fluid on the bore walls, pipes, pressure reducing valves, silencers, heat exchanger and field drains. Silica scaling occurs during steam-water separation or heat exchange below the temperature at which the water becomes saturated with amorphous silica
- Sinter** A chemical sediment deposited by a mineral spring, either hot or cold. Siliceous sinter consists of silica while carbonate sinter is made of calcium carbonate (also termed 'travertine'). Silica sinter deposits are an indication that the deep geothermal system is $>240^{\circ}\text{C}$
- Skin** A change in the near-wellbore permeability, as compared to the wider reservoir. Reduced permeability is called 'positive skin' and is often caused by infiltration of drilling mud into the formations

near the wellbore. Increased permeability is called 'negative skin' and often results from drilling-induced fracturing near the well, or deliberate stimulation (see 'stimulation')

Slick-line See 'wireline'

Slim hole Small diameter exploration well drilled to confirm the reservoir temperature and sample the chemistry of the geothermal fluid. Slim holes are generally <1200 m deep and may not be used for long-term production

Slips Wedges for holding the drill string while removing the drill string from the well so that each piece of drill pipe can be unscrewed

Specific capacity The rate of discharge of water from a drillhole which is not being pumped

Specific heat A measure of the amount of heat energy which must be supplied to raise a unit mass of a material by 1°C. A typical value for a rock is 1000 J/kg

Spinner The impeller located at the base of the PTS tool. The frequency at which the impeller spins during profiles at different speeds is used to calculate the fluid velocity profile in the well (see 'PTS tool' and 'fluid velocity profile')

Spinner ratio The result of dividing one fluid velocity profile by another, to remove the effects of the hole diameter (e.g. washouts) from the profiles (see 'fluid velocity profile')

Spudding Refers to the act of hoisting the drill pipe and permitting it to fall freely so that the drill bit strikes the bottom of the well bore with considerable force

Spudding in A term borrowed from cable tool drilling days to denote the commencement of well drilling operations

Steam main A (header) pipe carrying a high mass flow rate of steam from several wells

Steam jet ejector A nozzle through which steam passes at high speed and creates a vacuum to remove NCG from the condenser

Steaming ground Diffusive heat transfer by thermal conduction where steam rises to shallow depths but does not discharge because of relatively low permeabilities resulting from acid alteration. Vapour condenses to liquid and drains away, producing steep thermal gradients of 100°C/m in the top 15 cm and raising the temperature above ambient. Conductive heating of moist air produces a thin diffuse layer of steam that explains the name. Steaming ground is an important signature of heat transfer over high temperature systems with two-phase fluid flow

Steam thief zone A hole in the production casing that results in the loss of geothermal fluid to the surrounding rock. This can form a steam zone that can travel to the ground surface possibly causing well blowout. A steam thief zone can be identified from a sudden loss of WHP and well output, it can also be identified from a downhole camera survey (of the casing damage) and changes in the well flowing temperature and pressure profile

Steam vent Relatively quiet steam discharge from a hole in the ground at velocities less than 20 m/s (see 'fumarole')

Stimulation The term refers to the technique by which formation permeability around the well bore can be increased (negative skin), resulting in higher injection/production rates

Surface activity Visual active surface manifestations of a deep geothermal system expressed by such natural phenomena as hot springs, geysers, fumaroles, steaming ground, perched pond, mud pool and mud volcano

Thermal conductivity A measure of the ability of a material to transfer heat energy by conduction alone, when stressed by a thermal gradient. Typical values are in the range 2–2.5 W/m K

Total dissolved solids (TDS) The amount of TDS in the geothermal fluid, usually expressed as ppm or mg/kg, contained in water

Transmissivity (*kh*) In the most common usage, this refers to the product of reservoir permeability (*k*) and the thickness of the reservoir (*h*). It is a parameter estimated by PTA. Common units are Darcy-metres (D m) or m3. It is an overall measure of the potential of the reservoir in a given location. A *kh* > 10 D m generally indicates a good/productive well

- Turbine-back pressure** A type of steam turbine in which the steam emerges from the last stage into the atmosphere (no condenser)
- Turbine condensing** A type of steam turbine in which the steam emerges from the last stage into a condenser (vacuum pressure)
- Turbine** Steam moves through the turbine, which converts the energy in the steam into mechanical work (rotational) which rotates the generator to produce electricity. The turbine is made up of several sets of rotating blades attached to the turbine shaft and stationary blades (nozzles) attached to turbine housing
- Turbine nozzle** The flow passage between a pair of stationary blades. Mineral scaling will take place at the first set of nozzles if the geothermal steam carries mineral-rich droplets
- Turbine rotor** The turbine shaft that rotates and carries the blades
- Turbulent flow** Fluid flow in which the flow lines are complex and heterogeneously mixed. It is the typical flow in geothermal wells and above-ground system/pipelines resulting in higher pressure drop than laminar flow
- Upflow** The part of the underground geothermal convection cell where hot water is rising upwards, due to buoyancy forces (natural convection) as the hot fluid is less dense than surrounding fluid. The primary direction of fluid movement is vertically upwards. Ideally, geothermal wells will be drilled into the upflow of a geothermal system, though production is also possible from the system outflow (see 'geothermal reservoir')
- Vapour-dominated (dry) system** The best type of geothermal system, which produces dry saturated or slightly superheated steam at pressures above atmospheric. Wells in vapour-dominated systems produce high enthalpy, low mass flow rate with high gas content and low WHP, reservoir temperature 220°C–300°C. The reservoir generally has low permeability and surrounded by even lower permeability formation. Heat transfer by conduction (no natural convection) with some counterflow from the top of the system. Require infield reinjection and may run out of water with time. External make-up water will be required to keep these systems producing sustainably
- Viscosity (μ)** Also called 'dynamic viscosity'. The property of a substance/fluid used to offer internal resistance to flow; specifically, the ratio of shearing stress applied to the rate at which the liquid deforms in response to the stress. It is possibly the most important physical aspect of magmas. The S.I. units of viscosity are Pascals per unit time (Pa s). Another measure of viscosity is the 'kinematic viscosity' (ν), defined as the ratio of the dynamic viscosity to the density of the fluid, with S.I. units m^2/s
- Warm ground** Product of diffuse heat transfer by thermal conduction. It can be the dominant mode of heat transfer to the surface under natural conditions in hot water geothermal systems. It can also be important in two-phase systems where relatively impermeable rocks occur in the shallow subsurface preventing hot water or steam discharge
- Warm water systems** The most abundant geothermal systems, heated through the thermal gradient (conduction only) with temperatures <125°C. Some may have advective deep subhorizontal flow in tilted reservoirs. Can be found around the world and have limited natural thermal signature (thermal springs). Downhole pumps are commonly required to produce the geothermal fluid
- Water-dominated (wet) system** A geothermal system producing pressurised water at temperatures exceeding 100°C; as the water rises to the surface and its pressure is reduced, a small fraction of it flashes into steam but most remains as boiling water
- Water fracturing** Also known as water enhancement is the use of high pressure water only to fracture the geothermal reservoir and improve the fracture permeability. It is simple, low cost and more environment-friendly. However, it is less effective than HPF stimulations, as the fractures may not remain open

- Water loss survey** The first test carried out during completion testing to identify the main water loss zones in the well. Cold water is injected at two or three different flow rates while the PTS tool is moved up and down the well to identify permeable feed zones. Geothermal fluid will be produced from some of these feed zones, when the well is fully warmed up (see 'PTS tool' and 'feed zones')
- Water table** The surface between the unsaturated (vadose) zone and the body of groundwater; that surface of a body of unconfined groundwater at which the pressure is equal to that of the atmosphere (see 'piezometric surface')
- Weir plate** A restriction in a stream of water flowing in a channel, designed so the change in level of the water from upstream to downstream of the restriction can be used empirically to measure flow rate. Commonly found in geothermal silencers (atmospheric flash vessels)
- Wellbore (or 'well bore')** A term used interchangeably with 'borehole'
- WHP** The well pressure measured just below the master valve, it is used as a reference for the well performance (e.g. output curves, II). Shut in WHP is higher than flowing WHP. Medium and high enthalpy two-phase wells have higher WHP than low enthalpy wells, while vapour-dominated steam wells have lower WHP
- Wild cat** A well drilled without sufficient geological and physical data (taking high risk). This is very uncommon in geothermal exploration
- Wireline** Also called 'slick-line': this is a solid steel wire that is used to run downhole tools. Wireline cannot be used to send electronic signals to the surface. Therefore, the downhole data are not received in real time and the tools have to run in 'memory mode': data are stored within the tool and later downloaded after the tool is retrieved at the surface
- Workover** A term applied to any operation performed on a well subsequent to completing it, e.g. cleaning casing, running a sleeve, deepening, casing repairs, plugging back etc.

List of symbols

A	Cross-sectional area (m^2)
a	Pressure coefficient of modified correlation
B	Formation factor
b'	Intercept
C	Compressibility ($1/\text{Pa}$)
\dot{C}	Concentration (g/t)
c	Circulation
cp	Specific heat capacity (kJ/kg K)
D	Diameter (m), non-Darcy skin [Eq. (5.1)]
d	Orifice diameter (m)
e	Specific exergy (kJ/kg)
f	Friction factor [Eq. (7.5)]
G	Gas (NCG) content % by weight in the geothermal steam
g	Gravitational acceleration ($g = 9.81 \text{ m/s}^2$)
h	Enthalpy (kJ/kg)
II	Injectivity index (t/h/bar) [Eq. (6.4)]
k	Permeability (m^2); thermal conductivity (W/m K) in Chapter 6, Completion and Output Testing
K	Hydraulic conductivity (m/s) [Eq. (10.1)]
L	Pipe length (m)
m	Mass (kg)
\dot{m}	Mass flow rate (kg/s)
m'	Slop of similog
MDP	Maximum discharge pressure (Pa or bar)
n	Fractional dimension (1–3)
P	Pressure (Pa)
p	Constant ($p = 0.785$) [Eq. (6.1)]
p'	Pressure derivative
p_1	Pressure upstream of the orifice plate (Pa)
p_2	Pressure downstream of the orifice plate (Pa)
PI	Productivity index (t/bar h)
Q	Volume flow rate (m^3/s)
q	Volume flow rate (m^3/s)
r	Radius (m)
Re	Reynolds number ($Re = \rho Dv/\mu$)
s	Skin; specific entropy (kJ/kg K)
SFC	Specific fluid production ($(\text{t/h})/\text{MWe}$)
SPO	Specific power output (kWe/kg)
T	Temperature ($^{\circ}\text{C}$); transmissivity $T = kh$ (m^3)
t	Time (s)
v	Specific volume (m^3/kg)
v	Velocity (m/s)
x	Dryness fraction; horizontal direction (Chapter 8: Numerical PTA Modelling Framework)

u	Velocity on the x direction (m/s)
V	Volume (m^3)
w	Storativity ratio [Eq. (5.2)]
W	Power (kW)
wf	Flowing bottom-hole conditions
WHP	Well head pressure (Pa or bar)
Y	Lip pressure variable [Eq. (6.11)]
z	Depth (m)

Greek letters

α	Thermal expansion coefficient (m/mK); fractional dimension parameter [Eq. (8.4)]; thermal diffusivity $\alpha = k/(\rho cp)$ [Eq. (6.3)]
ε	Roughness height (mm) [Eq. (7.7)]
β	Forchheimer coefficient (1/m) in Chapter 8, Numerical PTA Modelling Framework, $\beta = (d/D)$ in Chapter 6, Completion and Output Testing
Δ	Differential
Γ	Gamma function [Eq. (8.4)]
μ	Dynamic viscosity (kg/m s)
ρ	Density (kg/m^3)
λ	Empirical constant [Eq. (6.2)]; transmissivity ratio [Eq. (5.3)]
η_u	Utilisation efficiency (%)
η_c	Conversion efficiency (%)
ω	Specific dissipation rate (1/s)
ϕ	Porosity
ν	Kinematic viscosity (μ/ρ) (m^2/s)

Subscripts

atm	Atmospheric condition
av	Average
accel	Acceleration
c	Condensation; circulation (Chapter 6: Completion and Output Testing)
D	Dimensionless radial distance (Chapter 4: Introduction to Pressure Transient Analysis)
e	Electrical
f	Flow; fracture of fisher (Chapter 5: Advanced Analytical PTA Relevant to Geothermal Wells)
final	Final condition
fg	Latent heat
fric	Friction
g	Gaseous/Steam phase
grav	Gravitational
i	Initial; block number [Eq. (8.4)]
initial	Initial conditions
lip	Lip pressure
m	Mixture, matrix blocks (Chapter 5: Advanced Analytical PTA Relevant to Geothermal Wells)
p	Production
r	Reservoir
res	Reservoir
s	Skin; steam

<i>st</i>	Steam tracer
<i>t</i>	Total; two phase
<i>te</i>	Thermal expansion
<i>th</i>	Thermal
0	Initial
<i>w</i>	Well; water
<i>we</i>	Equivalent well
<i>wt</i>	Water tracer

References

- Acuna, J.A., Yortsos, Y.C., 1995. Application of fractal geometry to the study of networks of fractures and their pressure transient. *Water Resour. Res.* 31 (3), 527–540.
- Acuna, J.A., Ershaghi, I., Yortsos, Y.C., 1992. Fractal analysis of pressure transients in the geysers geothermal field. In: Proceedings 17th Workshop on Geothermal Reservoir Engineering, Stanford University, Stanford, CA.
- Adachi, J., Siebrits, E., Peirce, A., Desroches, J., 2007. Computer simulation of hydraulic fractures. *Int. J. Rock Mech. Min. Sci.* 44 (5), 739–757.
- Adityatama, D.W., Kaya, E., Zarrouk, S.J., 2018. Investigation of pressure transient analysis methods for CO₂ rich geothermal reservoirs. In: Proceedings 40th New Zealand Geothermal Workshop, Taupo, New Zealand.
- Agarwal, R.G., Al-Hussainy, R., Ramey Jr., H.J., 1970. An investigation of wellbore storage and skin effect in unsteady liquid flow: I. Analytical treatment. *Soc. Pet. Eng. J.* 10 (3), 279–290.
- Aleman, E.T., Saw, V.S., 2000. An assessment of the impact of in-field injection at the Malitbog sector, Tongonan, Philippines. In: Proceedings the World Geothermal Congress, Kyushu-Tohoku, Japan.
- Alimonti, A., Soldo, E., 2016. Study of geothermal power generation from a very deep oil well with a wellbore heat exchanger. *Renew. Energy* 86, 292–301.
- Al-Khalifah, A.J., Aziz, K., Horne, R.N., 1987. A new approach to multiphase well test analysis. In: Proceedings SPE Annual Technical Conference and Exhibition, SPE 16743-MS.
- All, C., 2003. Handbook on Coal Bed Methane Produced Water: Management and Beneficial Use Alternatives. <http://www.all-llc.com/publicdownloads/CBM_BU_Screen.pdf>.
- Allen, R.M., Robinson, K., 1993. Environmental aspects of produced water disposal. In: Paper Presented at the Middle East Oil Show, Bahrain. SPE 25549-MS.
- Ambastha, A.K., Zhang, M.Y., 1996. Iterative and numerical solutions for pressure-transient analysis of stress-sensitive reservoirs and aquifers. *Comput. Geosci.* 22 (6), 601–606.
- Antics, M.A., 1998. Computational modelling of an over pressured medium enthalpy geothermal reservoir located in deep sedimentary basin. In: Proceedings 23rd Workshop on Geothermal Reservoir Engineering, Stanford University, Stanford, CA.
- Akin, S., 2012. Temperature induced dissolution or precipitation in geothermal reservoirs and their effects on pressure transient analysis. In: Proceedings 37th Workshop on Geothermal Reservoir, Stanford University, Stanford, CA.
- Akin, S., Gulgor, A., 2018. Comprehensive tracer testing in the Germencik field. In: Proceedings the 43rd Workshop on Geothermal Reservoir Engineering Stanford University, Stanford, CA.
- Aksoy, N., 2007. Optimization of downhole pump setting depths in liquid-dominated geothermal systems: a case study on the Balcova-Narlidere field, Turkey. *Geothermics* 34, 436–458.
- Aqui, A.R., 2012. Permeability Enhancement of Conventional Geothermal Wells (Master's thesis). University of Auckland, Auckland, New Zealand.
- Aqui A.R., Zarrouk, S.J., 2011. Permeability enhancement of conventional geothermal wells. In: Proceedings the 33rd New Zealand Geothermal Workshop, Auckland, New Zealand.
- Aprilian, S., Abdassah, D., Mucharam, L., Sumatri, R., 1993. Application of fractal reservoir model for interference test analysis in Kamojang geothermal field (Indonesia). In: Proceedings SPE Annual Technical Conference and Exhibition (ATCE '93), Houston, TX, SPE 26465-MS.
- Arifien, B.N., Zarrouk, S.J., 2015. Moisture removal system in geothermal steam plants. In: Proceedings the 37th New Zealand Geothermal Workshop, Taupo, New Zealand.
- Arifien, B.N., Zarrouk, S.J., Kurniawan, W., 2015. Scrubbing lines in geothermal power generation systems. In: Proceedings the 37th New Zealand Geothermal Workshop, Taupo, New Zealand.
- Ariki, K., Akibayashi, S., 2001. Effects of the injection temperature on injection-capacity of geothermal wells—numerical study. *Geotherm. Resour. Council Trans.* 25, 445–454.

- Ariki, K., Hatakeyama, K., 1998. Effects of injection temperature on the injectivity of a geothermal well. *Geotherm. Resour. Council Trans.* 22, 539–545.
- Arkan, S., Akin, S., Parlaktuna, M., 2002. Effect of calcite scaling on pressure transient analysis of geothermal wells. In: *Proceedings 27th Workshop on Geothermal Reservoir Engineering*, Stanford University, Stanford, CA.
- Armstead, H.C.H., 1978. *Geothermal Energy: Its Past, Present and Future Contributions to the Energy Needs of Man*. E. & F.N. Spon, London, ISBN 10: 0419112405.
- Aspiras, A.H., Braganza, J.S., Morente, C.P., Austria Jr., J.J.C., 2015. Selection of candidate geothermal well for deflagration. In: *Proceedings the 37th New Zealand Geothermal Workshop*, Taupo, New Zealand.
- Asquith, A., Krygowski, D., 2004. Basic well log analysis, second ed. In: *Methods in Exploration No. 16*. The American Association of Petroleum Geologists. ISBN: 0-89181-667-4.
- Atkinson, P., Barelli, A., Brigham, W., Celati, R., Manetti, G., Miller, F.G., et al., 1978a. Well-testing in Travale-Radicondoli field. Part I. Geothermal well test analysis, principles and practice. *Geothermics* 7 (2), 145–150.
- Atkinson, P., Barelli, A., Brigham, W., Celati, R., Manetti, G., Miller, F.G., et al., 1978b. Well-testing in Travale-Radicondoli field. Part V. Concluding statement on pressure transient studies made from well tests in the Travale-Radicondoli reservoir. *Geothermics* 7 (2–4), 151–157.
- Ayan, C., Lee, W.J., 1988. Multiphase pressure buildup analysis: field examples, In: *Proceedings of the SPE California Regional Meeting*, SPE 17412-MS.
- Bachu, S., 1994. Geothermal regime in the Western Canada sedimentary basin. In: Mossop, G.D., Shetsen, I. (Comp.), *Geological Atlas of the Western Canada Sedimentary Basin*. Canadian Society of Petroleum Geologists and Alberta Research Council. <<http://ags.aer.ca/publications/chapter-28-geological-history-of-the-peace-river-arch.htm>>.
- Bajcsi, P., Bozso, T., Bozso, R., Czinkota, I.M., Toth, T.M., Schubert, F., et al., 2015. Geothermal well completion technology using high power laser device. In: *Proceeding the World Geothermal Congress*, Melbourne, Australia.
- Bakar, H.A., Zarrouk, S.J., 2018. Transient pressure analysis of geothermal wells fractured during well testing. *Geothermics* 76, 26–37.
- Bär, K., Welsch, B., Schulte, D., Rühaak, W., Sass, I., 2017. Seasonal high temperature heat storage with middle deep borehole heat exchangers – a coupled-modeling study. In: *Proceedings the 42nd Workshop on Geothermal Reservoir Engineering* Stanford University, Stanford, CA.
- Barelli, A., Celati, R., Manetti, G., Neri, G., 1975. Horner method applied to build-up tests on Travale 22 well. In: *Proceedings First Workshop on Geothermal Reservoir Engineering*, Stanford University, Stanford, CA.
- Baria, R., Baumgärtner, J., Gérard, A., Jung, R., Gamish, J., 1999. European HDR research programme at Soultz-sous-Forêts (France) 1987–1996. *Geothermics* 28 (4–5), 655–669.
- Barker, J.A., 1988. A generalized radial-flow model for pumping tests in fractured rock. *Water Resour. Res.* 24 (10), 1796–1804.
- Barrios, L.A., Quijano, J., Guerra, E., Mayorga, H., Rodriguez, A., Romero, R., 2007. Injection improvements in low permeability and negative skin wells, using mechanical cleanout and chemical stimulation, Berlin geothermal field, El Salvador. *Geotherm. Resour. Council Trans.* 31, 141–146.
- Barry, B.J., McCabe, W.J., Marmont, K.B., 1982. Radioactive tracing tests at Ngawha, 1981. In: *Proceedings the Fourth New Zealand Geothermal Workshop*, Auckland, New Zealand.
- Barton, N., Lingle, R., 1982. Rock mass characterization methods for nuclear water disposal in jointed rock. In: *International Society for Rock Mechanics and Rock Engineering (ISRM) International Symposium*, Aachen, Germany.
- Baterbaev, M.D., Bulavin, V.D., Seljakov, V.I., Savchenko, A.F., 2002. Application of Technology of Electroinfluence for Intensification of an Oil Recovery in Russia and Abroad. *Neftyanoe Khozyaistvo Oil Industry*, pp. 92–95.
- Baujard, C., Genera, A., Dalmassa, E., Maurera, V., Hehna, R., Rosillettea, R., et al., 2017. Hydrothermal characterization of wells GRT-1 and GRT-2 in Rittershoffen, France: Implications on the understanding of natural flow systems in the Rhine Graben. *Geothermics* 65, 255–268.

- Bayrante, L.F., Caranto, J.A., Malate, R.C.M., 2010. EGS, the energy for the next millennium: potential sites in the Philippines. In: Proceedings World Geothermal Congress, Bali, Indonesia.
- Bendall, B., Hogarth, R., Holl, H., McMahon, A., Larking, A., Reid, P., 2014. Australian experiences in EGS permeability enhancement – a review of 3 case studies. In: Proceedings 39th Workshop on Geothermal Reservoir Engineering, Stanford University, Stanford, CA.
- Benderitter, Y., Cormy, G., 1990. Possible approach to geothermal research and relative cost estimate. In: Dickson, M.H., Fanelli, M. (Eds.), *Small Geothermal Resources*. UNITAR/UNDP Centre for Small Energy Resources, Rome, Italy, pp. 61–71.
- Benson, S.M., 1982. Well test data analysis from a naturally fractured liquid-dominated hydrothermal system. *Geotherm. Resour. Council Trans.* 6, 237–240.
- Benson, S.M., 1984. Analysis of Injection Tests in Liquid-Dominated Geothermal Reservoirs (Master's thesis). Lawrence Berkeley Laboratory, Berkeley, CA.
- Benson, S.M., Daggett, J.S., Iglesias, E., Arellano, V., Ortiz-Ramirez, J., 1987. Analysis of thermally induced permeability enhancement in geothermal wells. In: Workshop on Geothermal Reservoir Engineering, Stanford University, Stanford, CA.
- Bertani, R., 2016. Geothermal power generation in the world 2010–2014 update report. *Geothermics* 60, 31–43.
- Bixley, P.F., Grant, M.A., 1979. Reinjection testing at broadlands. In: Proceedings Fifth Workshop on Geothermal Reservoir Engineering, Stanford University, Stanford, CA.
- Bixley, P.F., Wilson, D.M., 1985. Rapid casing corrosion in high temperature liquid dominated geothermal fluid. In: Proceedings of the 10th Workshop on Geothermal Reservoir Engineering, Stanford University, Stanford, CA.
- Bixley, P., Dench, N., Wilson, D., 1998. Development of well testing methods at Wairakei 1950–1980. In: Paper Presented at the Proceedings 20th Geothermal Workshop, Auckland, New Zealand.
- Bixley, P., Mclean, K., Lim Y.W., Wilson, D., 2016. Assessing the effectiveness of declaration in multiple-feedzone wells. In: Proceedings the 38th New Zealand Geothermal Workshop, Auckland, New Zealand.
- Bjornsson, G., 2004. Reservoir conditions at 3–6 km depth in the Hellisheidi geothermal field, SW-Iceland, estimated by deep drilling, cold water injection and seismic monitoring. In: Proceedings 29th Workshop Geothermal Reservoir Engineering, Stanford University, Stanford, CA.
- Bodvarsson, G.S., Benson, S.M., Sigurdsson, O., Stefansson, V., Eliasson, E.T., 1984. The Krafla geothermal field, Iceland: 1. Analysis of well test data. *Water Resour. Res.* 20 (11), 1515–1530.
- Boseley, C., Bignall, G., Rae, A., Chambefort, I., Lewis, B., 2012. Stratigraphy and hydrothermal alteration encountered by monitor wells completed at Ngatamariki and Orakei Korako in 2001. In: Proceedings the 34th New Zealand Geothermal Workshop, Auckland, New Zealand.
- Bourdet, D., 2002. In: Cubitt, J. (Ed.), *Well Test Analysis: The Use of Advanced Interpretation Models*, vol. 3. Elsevier.
- Bourdet, D., Whittle, T.M., Douglas, A.A., Pirard, Y.-M., 1983. A new set of type curves simplifies well test analysis. *World Oil* 196 (6), 95–106.
- Bourdet, D., Ayoub, J.A., Pirard, Y.-M., 1989. Use of pressure derivative in well test interpretation. *SPE Form. Eval.* 4 (2), 293–302.
- Brasier, F.M., Kobelski, B., 1996. Injection of industrial wastes in the United States. Deep injection of disposal of hazardous industrial waste. *Scientific and Engineering Aspects*. Academic Press, San Diego, CA, pp. 1–8.
- Brennand, A.W., 1984. A new method for the analysis of static formation temperature tests. In: Proceedings the Sixth New Zealand Geothermal Workshop, Auckland, New Zealand.
- Brennand, A.W., Watson, A., 1987. Use of ESDU compilation of two-phase flow correlations for the prediction of well discharge characteristics. In: Proceedings the Ninth New Zealand Geothermal Workshop, Auckland, New Zealand.
- Britt, L.K., Hager, C.J., Thompson, J.W., 1994. Hydraulic fracturing in a naturally fractured reservoir. In: International Petroleum Conference and Exhibition of Mexico. Veracruz, Mexico.

- Broaddus, M., Katz, J.I., Hirtz, P., Kunzman, R., 2010. Advancements in tracer flow testing: development of real-time technology for flow and enthalpy measurement. *Geotherm. Resour. Council Trans.* 34, 1005–1010.
- Brown, K., 2011. Thermodynamics and kinetics of silica scaling. In: *Proceedings International Workshop on Mineral Scaling*, Manila, Philippines.
- Bu, X., Ma, W., Li, H., 2012. Geothermal energy production utilizing abandoned oil and gas wells. *Renew. Energy* 41, 80–85.
- Burnell, J.G., Weir, G.J., Young, R., 1991. Self-similar radial two-phase flows. *Transp. Porous Media* 6 (4), 359–390.
- Butterworth, D., Hewitt, G.F., 1978. *Two-Phase Flow and Heat Transfer*. Oxford University Press (Harwell Series).
- Campbell, D.A., Morris, C.W., Verity, R.V., 1981. Geothermal well stimulation experiments and evaluation. In: *SPE Annual Technical Conference and Exhibition*. San Antonio, TX, SPE 10316-MS.
- Candra, S.A., Zarrouk, S.J., 2013. Testing direct use geothermal wells in Rotorua, New Zealand. In: *Proceedings the 35th New Zealand Geothermal Workshop*, Rotorua, New Zealand.
- Caulk, R.A., Tomac, I., 2017. Reuse of abandoned oil and gas wells for geothermal energy production. *Renew. Energy* 112, 388–397.
- Cei, M., Barelli, A., Casini, M., Romagnoli, Bertani, R., Fiordelisi, A., 2009. Numerical model of the Travale geothermal field (Italy) in the framework of the I-GET European project. *Geotherm. Resour. Council Trans.* 33, 1041–1045.
- Celati, R., Squarci, P., Neri, G., Perusini, F., 1975. An attempt to correlate Kh distribution with geological structure of Larderello geothermal field. In: *Proceedings First Stanford Workshop on Geothermal Reservoir Engineering*, Stanford, CA.
- Chandrasekharam, D., Chandrasekhar, V., 2010. Hot dry rock potential in India: future road map to make India energy independent. In: *Proceedings World Geothermal Congress*, Bali, Indonesia.
- Chang, J., Yortsos, Y.C., 1990. Pressure transient analysis of fractal reservoirs. *SPE Form. Eval.* 5 (01), 31–38. SPE 18170-PA.
- Chiang, C.Y., Chang, C.R.Y., 1979. Application of the Horner method to the estimation of static reservoir temperature during drilling operations. In: *Proceedings the Third Workshop on Geothermal Reservoir Engineering*, Stanford University, Stanford, CA.
- Cho, N.C., Hwang, I.J., Lee, C.L., Park, J.W., 2009. An experimental study on the airlift pump with air jet nozzle and booster pump. *J. Environ. Sci.* 21, 19–23.
- Christi, L.F., Itoi, R., Tanaka, T., Atmogo, J.P., 2015. Characterization of fluid flow system between injection and production wells by tritium tracer test analysis. In: *Proceedings 40th Workshop on Geothermal Reservoir Engineering*, Stanford University, Stanford, CA.
- Chu, W.-C., Reynolds, A.C., Raghavan, R., 1986. Pressure transient analysis of two-phase flow problems. *SPE Form. Eval.* 1 (02), 151–164.
- Chu, T.Y., Jacobson, R.D., Warpinski, N.R., 1987. Geothermal well stimulation using high energy gas fracturing. In: *12th Workshop on Geothermal Reservoir Engineering*, Stanford University, Stanford, CA.
- Cinar, M., 2013. Creating enhanced geothermal systems in depleted oil reservoirs via in situ combustion. In: *Proceedings 38th Workshop on Geothermal Reservoir Engineering*, Stanford University, Stanford, CA.
- Cinco-Ley, H., Samaniego-V, F., Dominguez-A, N., 1978. Transient pressure behavior for a well with a finite-conductivity vertical fracture. *Soc. Pet. Eng. J.* 18 (04), 253–264.
- Cinco-Ley, H., Brigham, W.E., Economides, M., Miller, F.G., Ramey Jr., H.J., Barelli, A., et al., 1979. A parallelepiped model to analyze the pressure behavior of geothermal steam wells penetrating vertical fractures. In: *Proceedings SPE Annual Technical Conference and Exhibition*. SPE 8231-MS.
- CMG, 2003. *CMG STARS User's Guide*. Computer Modelling Group Ltd, Calgary, AB, Canada.
- Contreras, E.A., 1990. Permeability changes during the flow of distilled water and brine through geothermal sandstones at temperatures of 25°C–270°C. *Geotherm. Resour. Council Trans.* 14, 1183–1192.
- Coutts, C., Richardson, I., Quinao, J., Goh, O., 2018. Acid stimulation of Kawerau injection well PK4A using hydrofluoric acid. In: *Proceedings the 40th New Zealand Geothermal Workshop*, Taupo, New Zealand.

- Cox, B.L., Bodvarsson, G.S., 1985. Nonisothermal injection tests in fractured reservoirs. In: Proceedings 10th Workshop Geothermal Reservoir Engineering, Stanford University, Stanford, CA.
- Cox, B.L., Bodvarsson, G.S., 1986. Preliminary studies of two-phase effects on pressure transient data, In: Proceedings 11th workshop on geothermal reservoir engineering, Stanford University, Stanford, CA.
- Crolet, J.L., Bonis, M.R., 1986. Alternative method for predicting the corrosivity of wells in new CO₂ fields. *Mater. Performance* 25, 41–49.
- Croucher, A.E., 2011. PyTOUGH: a Python scripting library for automating TOUGH2 simulations. In: Proceedings 33rd New Zealand Geothermal Workshop, Auckland, New Zealand.
- Culver, G.G., 1990. Downhole Heat Exchanger. Geo Heat Center, Oregon Institute of Technology, November, 1990.
- Da Silva, D.V.A., Jansen, J.D., 2015. A review of coupled dynamic well-reservoir simulation. *IFAC-PapersOnLine* 48 (6), 236–241.
- Darwis, R.S., Tampublon, T., Simatupang, R., Asdassah, D., 1995. Study of water reinjection on the Kamojang Geothermal Reservoir performance, Indonesia. In: Proceedings 17th New Zealand Geothermal Workshop, Auckland, New Zealand.
- Dennis, B.R., Potter, R., Kolar, J., 1981. Radioactive tracers used to characterize geothermal reservoirs. *Geotherm. Resour. Council Trans.* 5, 329–332.
- Dezayes, C., Genter, A., Hooijkaas, G.R., 2005. Deep-seated geology and fracture system of the EGS Soutz Reservoir (France) based on recent 5 km depth boreholes. In: Proceedings World Geothermal Conference, Antalya, Turkey.
- Diaz, A.R., Kaya, E., Zarrouk, S.J., 2016. Reinjection in geothermal fields – a worldwide review update. *Renew. Sustain. Energy Rev.* 53, 105–162.
- Dickson, M., Fanelli, M., 2003. Geothermal background. In: Dickson, M., Fanelli, M. (Eds.), *Geothermal Energy Utilization and Technology*. Published by: United Nations Educational, Scientific and Cultural Organization, ISBN 92-3-103915-6.
- DiMarzio, G., Angelini, L., Price, B. Harris, S., Chin, C., 2015. The stillwater triple hybrid power plant: integrating geothermal, solar photovoltaic and solar thermal power generation. In: Proceedings World Geothermal Congress, Melbourne, Australia.
- DiPippo, R., 2015. Geothermal power plants: evolution and performance assessments. *Geothermics* 53, 291–307.
- Doobie, T.P., Maunder, B.R., Sarit, A.D., 1982. Reinjection experience in the Philippines. In: Proceedings the Fourth New Zealand Geothermal Workshop, Auckland, New Zealand.
- Doherty, J., 2010. PEST: Model-Independent Parameter Estimation User Manual. *Watermark Numerical Computing*.
- Dougherty, R.L., Franzini, J.B., Finnemore, E.J., 1985. *Fluid Mechanics With Engineering Applications*, eighth ed. McGraw Hill, ISBN 0-07-Y66267-3.
- Dowdle, W.L., Cobb, W.M., 1975. Static formation temperature from well logs – an empirical method. *J. Pet. Technol.* 27 (11), 1326–1330.
- Drew, S.R., 1988. Direct-use projects equipment and controls. *Geothermics* 17, 141–171.
- Duchane, D., Brown, D., 1995. Hot dry rock geothermal energy development in the USA: moving toward practical use. In: Proceedings World Geothermal Congress, Florence, Italy.
- Dunstall, M.G., 1992. Downhole Heat Exchangers Performance Analysis (Ph.D. thesis). University of Auckland.
- Durst, P., Vuataz, F.-D., 2000. Fluid-rock interactions in hot dry rock reservoirs, a review of the HDR sites and detailed investigations of the Soutz-sous-Forets System. In: Proceedings World Geothermal Conference, Kyushu-Tohoku, Japan.
- Dusseault, M.B., Bruno, M.S., Barrera, J., 2001. Casing shear: causes, cases, cures. In: SPE Drill 16, 98–107, SPE 72060-PA.
- Earlougher Jr., R.C., 1977. *Advances in Well Test Analysis*. Henry L. Doherty Memorial Fund of AIME, New York.
- Earlougher Jr., R.C., Kersch, M.K., 1972. Field examples of automatic transient test analysis. *J. Pet. Technol.* 24 (10), 1271–1277.

- Economides, M.J., Fehlbeg, E.L., 1979. Two short-time buildup test analyses for Shell's Geysers Well D-6, a year apart. In: Proceedings Fifth Workshop on Geothermal Reservoir Engineering, Stanford University, Stanford, CA.
- Economides, M.J., Miller, F.G., 1985. The effects of adsorption phenomena in the evaluation of vapour-dominated geothermal reservoirs. *Geothermics* 14 (1), 3–27.
- Economides, M.J., Nolte, K.G., 2000. *Reservoir Stimulation*, third ed. Wiley, ISBN 0 471 491926.
- Economides, M.J., Ogbe, D., Miller, F.A., Cinco-Ley, H., Fehlbeg, E.L., 1982. Pressure buildup analysis of geothermal steam wells with a parallelepiped model. *J. Pet. Technol.* 34 (04), 925–929.
- Ehlig-Economides, C.A., 1979. *Well Test Analysis for Wells Produced at Constant Pressure* (Ph.D. thesis). Stanford University, Stanford, CA.
- Eker, A.M., Yal, G.P., Cambazoglu, S., Şen, O., Dünya, H., 2017. Enhancement of geothermal reservoir through varying acidizing operation procedures in Aydın Kuyucak geothermal field. In: Proceedings 42nd Workshop on Geothermal Reservoir Engineering, Stanford University, Stanford, CA.
- Elders, W.A., Fridleifsson, G.O., 2009. The Iceland Deep Drilling Project (IDDP): deep drilling at Krafla to investigate supercritical geothermal resources. *Geotherm. Resour. Council Trans.* 33, 611–616.
- Ellis, A.J., 1963. The solubility of calcite in sodium chloride solutions at high temperatures. *Am. J. Sci.* 261, 259–267.
- Ellis, A.J., Mahon, W.A.J., 1977. *Chemistry and Geothermal Systems*. Academic Press, New York.
- Elmi, D., 2005. *Analysis of Geothermal Well Test Data From the Asal Rift area*. United Nations University, Republic of Djibouti.
- Entingh, D.J., 2000. Geothermal well stimulation experiments in the United States. In: Proceedings World Geothermal Conference 2000, Kyushu-Tohoku, Japan.
- Ezzedine, S., Rubenchik, A., Yamamoto, R., Vorobiev, O., 2012. Laser-enhanced drilling for subsurface EGS applications. *Geotherm. Resour. Council Trans.* 36, 287–290.
- Fajardo, V.R., Malate, R.C.M., 2005. Estimating the improvement of Tanawon production wells for acid treatment, Tanawon Sector, Bacman geothermal production field, Philippines. In: Proceedings World Geothermal Congress, Kyushu-Tohoku, Japan.
- Febrianto, R., Thain, I., Zarrouk, S.J., 2016. The geothermal heating system at Taupo Hospital, New Zealand. *Geothermics* 59, 347–356.
- Fink, J.K., 2011. *Fracturing Fluids. Petroleum Engineer's Guide to Oil Field Chemicals and Fluids*. Gulf Professional Publishing, Boston, MA, pp. 519–583.
- Finsterle, S., 2000. iTOUGH2 user's guide. In: Technical Report, Lawrence Berkeley National Laboratory, CA, Report LBNL-40040.
- Fitts, C., 2013. *Groundwater Science*, second ed. Elsevier 978-0-12-384705-8.
- Flores, M., Davies, D., Couples, G., Palsson, B., 2005. Stimulation of geothermal wells, can we afford it?. In: Proceedings the World Geothermal Congress, Antalya, Turkey.
- Flores-Armenta, M., Tovar-Aguado, R., 2008. Thermal fracturing of Well H-40, Los Humeros geothermal field. *Geotherm. Resour. Council Trans.* 32, 445–448.
- Forsyth, J., Zarrouk, S.J., 2018. A review of static formation temperature test evaluation methods. In: Proceedings 40th New Zealand Geothermal Workshop.
- Fredd, C.N., McConnell, S.B., Boney, C.L., England, K.W., 2001. Experimental study of fracture conductivity for water-fracturing and conventional fracturing applications. *SPE J.* SPE 74138-PA.
- Friðleifsson, G.O., 2017. IDDP-2 drilling into the supercritical at Reykjanes. In: Proc. 39th New Zealand Geothermal Workshop, Rotorua, New Zealand.
- Fukuda, D., Watanabe, M., Arai, F., Sasaki, S., Sako, O., Matsumoto, Y., et al., 2010. Removal of anhydrite and Mg-silicate scales from production wells using chemical agents at the Mori geothermal field in Hokkaido, Japan: an application of chemical well stimulation. In: Proceedings the World Geothermal Congress, Bali, Indonesia.
- Garg, S.K., 1980. Pressure transient analysis for two-phase (water/steam) geothermal reservoirs. *Soc. Pet. Eng. J.* 20 (03), 206–214.
- Garg, S.K., Pritchett, J.W., 1984. Pressure transient analysis for two-phase geothermal wells: some numerical results. *Water Resour. Res.* 20 (7), 963–970.

- Garg, S.K., Pritchett, J.W., 1988. Pressure interference data analysis for two-phase (water/steam) geothermal reservoirs. *Water Resour. Res.* 24 (6), 843–852.
- Garg, S.K., Pritchett, J.W., 1990. Cold water injection into single-and two-phase geothermal reservoirs. *Water Resour. Res.* 26 (2), 331–338.
- Garg, S.K., Riney, T.D., Pritchett, J.W., 1978. Pressure transient analysis for geopressed geothermal wells. Second Invitational Well-Testing Symposium Proceedings. Lawrence Berkeley National Laboratory, Berkeley, CA.
- Garg, S.K., Riney, T.D., Wallace Jr., R.H., 1986. Brine and gas recovery from geo-pressured systems. *Geothermics* 15 (1), 23–48.
- Garg, S.K., Pritchett, J.W., Ariki, K., Kawano, Y., 1991. Pressure-interference testing of the Sumikawa geothermal field. In: Proceedings 16th Workshop on Geothermal Reservoir Engineering, Stanford University, Stanford, CA.
- Ghassemi, A., Suresh Kumar, G., 2007. Changes in fracture aperture and fluid pressure due to thermal stress and silica dissolution/precipitation induced by heat extraction from subsurface rocks. *Geothermics* 36 (2), 115–140.
- Glynn-Morris, T., King, T., Winmill, R., 2009. Drilling history and evolution at Wairakei. *Geothermics* 31 (1), 30–39.
- Goldstein, E.N., Carle, S., 1986. Faults and gravity anomaly over the east mesa hydrothermal-geothermal system. *Geotherm. Resour. Council Trans.* 10, 223–228.
- Gomez, J.R., Pachon, L.F., Barrios, L., Porras, E., 2009. Acid stimulation of geothermal wells in Central America. In: Latin American and Caribbean Petroleum Engineering Conference, Cartagena de Indias, Colombia.
- Gordon, B.A., Grimes, W.D., Treseder, R.S., 1984. Casing corrosion in the south Belridge field. *Mater. Performance* 23 (3), 9–14.
- Grant, M.A., 1978. Two-phase linear geothermal pressure transients: a comparison with single-phase transients. *N.Z. J. Sci.* 21, 355–364.
- Grant, M.A., 1980. The testing of KA-28—pressure analysis in a two-phase reservoir. In: Proceedings Sixth Workshop Geothermal Reservoir Engineering, Stanford University, Stanford, CA.
- Grant, M.A., Bixley, P., 2011. *Geothermal Reservoir Engineering*. Elsevier.
- Grant, M.A., Sorey, M.L., 1979. The compressibility and hydraulic diffusivity of a water-steam flow. *Water Resour. Res.* 15 (3), 684–686.
- Grant, M.A., Wilson, D., Bixley, P.F., 2006. Spinner data analysis to estimate wellbore size and fluid velocity. In: Proceedings 28th New Zealand Geothermal Workshop, Auckland, New Zealand.
- Grebe, J., Stoesser, M., 1935. Increasing crude production 20,000,000 bbl. from established fields. *World Pet. J.* August, 473–482.
- Gregg, D.W., Olness, D.U., Hill, R.W., 1976. An overview of the soviet effort in underground gasification of coal. In: Technical Report No. Uclrl-52004. Lawrence Livermore Laboratory, University of California, Berkeley, CA.
- Grijalva, R.L., 1978. The fossil fuel/geothermal hybrid cycle applied to marginally useful liquid dominated hydrothermal resources. *Trans. Geotherm. Resour. Council* 2, 227–231.
- Gringarten, A.C., Ramey Jr., H.J., Raghavan, R., 1972. Pressure analysis for fractured wells. In: Proceedings SPE Annual Technical Conference and Exhibition.
- Gringarten, A.C., Ramey Jr., H.J., Raghavan, R., 1974. Unsteady-state pressure distributions created by a well with a single infinite-conductivity vertical fracture. *SPE J.* 14 (04), 347–360.
- Guerra, R.J.A., O'Sullivan, J., 2018. Investigating the effects of non-isothermal reservoir conditions on pressure transient analysis of an injection/falloff test using numerical modelling. In: Proceedings 40th New Zealand Geothermal Workshop, Taupo, New Zealand.
- Gunn, C., Freeston, D., 1991. An integrated steady-state wellbore simulation and analysis package. In: Proceedings 13th New Zealand Geothermal Workshop, Auckland, New Zealand.
- Guo, B., Lyons, W.C., Ghalambor, A., 2007. *Hydraulic Fracturing*. Petroleum Production Engineering. Gulf Professional Publishing, Burlington, pp. 251–265.
- Hammadih, M.L., Al-Hosani, K., Boiko, I., 2015. Soft sensing in deep wells within artificial gas lift technology. In: SPE 177731-MS.

- Hanano, M., Matsuo, G., 1990. A summary of recent study on the initial state of the Matsukawa geothermal reservoir. In: Proceedings 15th Workshop on Geothermal Reservoir Engineering, Stanford University, Stanford, CA.
- Hanano, M., Sakagawa, Y., 1990. Lateral steam flow revealed by a pressure build-up test at the Matsukawa vapor-dominated geothermal field, Japan. *Geothermics* 19 (1), 29–42.
- Haring, M.O., Schanz, U., Ladner, F., Dyer, B.C., 2008. Characterisation of the Basel 1 enhanced geothermal system. *Geothermics* 37 (5), 469–495.
- Hedenquist, J.W., Stewart, M., 1985. Natural CO₂-rich steam heated waters in the Broadlands-Ohaaki geothermal system, New Zealand: their chemistry, distribution and corrosive nature. *Trans. Geotherm. Resour. Council* 9, 245–250.
- Heijnen, L., Richard Rijkers, R., Te Gussinklo Ohmann, R., 2015. Management of Geological and Drilling Risks of Geothermal Projects in the Netherlands. In: Proceedings of the World Geothermal Congress, Melbourne, Australia.
- Helbig, S., Zarrouk, S.J., 2012. Measuring two-phase flow in geothermal pipelines using sharp edge orifice plates. *Geothermics* 44, 52–64.
- Held, S., Genter, A., Kohl, T., Kölbl, T., Sausse, J., Schoenball, M., 2014. Economic evaluation of geothermal reservoir performance through modeling the complexity of the operating EGS in Soultz-sous-Forêts. *Geothermics* 51, 270–280.
- Hernandez, D., Clearwater, J., Burnell, J., Franz, P., Azwar, L., Marsh, A., 2015. Update on the modeling of the Rotokawa Geothermal System: 2010–2014. In: Proceedings World Geothermal Congress, Melbourne, Australia.
- Herras, E.B., Licup Jr., A.C., Vicedo, R.O., Parilla Jr., E.V., Jordan, O.T., 1996. The Hydrological Model of the Mahanagdong sector, great Tongonan geothermal field, Philippines. *Trans. Geotherm. Resour. Council* 20, 681–688.
- Hirtz, P.N., Kunzman, R.J., Broaddus, M.L., Barbitta, J.A., 2001. Developments in tracer flow testing for geothermal production engineering. *Geothermics* 30, 727–745.
- Hochstein, M.P., 1988. Assessment and modelling of geothermal reservoirs (small utilization schemes). *Geothermics* 17 (1), 15–49.
- Hochstein, M.P., Sudarman, S., 2010. Monitoring of LUSI mud-volcano – a geo-pressured system, Java, Indonesia. In: Proceedings of the World Geothermal Congress, Bali, Indonesia.
- Hochwimmer, A., Urzua, L., Ussher, G., Parker, C., 2015. Key performance indicators for pumped well geothermal power generation. In: Proceedings of the World Geothermal Congress, Melbourne, Australia.
- Hodder, A.P.W., 2010. Geothermal waters: a source of energy and metals. In: XIII-Water-AGeothermal-10, lien. Department of Earth Sciences, University of Waikato.
- Hodson-Clarke, A., Rudoff, R., Bour, D., Russell, P., 2016. Key factors to successful drilling and completion of EGS well in Cooper Basin. In: Proceedings 41st Workshop on Geothermal Reservoir Engineering, Stanford University, Stanford, CA.
- Hogarth, R., Baur, D., 2015. Flow performance of the Habanero EGS closed loop. In: Proceedings of the World Geothermal Congress, Melbourne, Australia.
- Hole, H., 2013. Geothermal drilling-keep it simple. In: Proceedings the 35th New Zealand Geothermal Workshop, Rotorua, New Zealand.
- Horne, R.N., 1982. Effects of water injection into fractured geothermal reservoirs: a summary of experience worldwide. In: Technical Report, Stanford Geothermal Program, Interdisciplinary Research in Engineering and Earth Sciences, Stanford University, Stanford, CA.
- Horne, R.N., 1994. Advances in computer-aided well-test interpretation. *J. Pet. Technol.* 46 (7), 599–606.
- Horne, R.N., 1995. *Modern Well Test Analysis: A Computer-Aided Approach*. Petroway Inc.
- Horne, R.N., 2016. Characterization, evaluation, and interpretation of well data. In: DiPippo, R. (Ed.), *Geothermal Power Generation: Developments and Innovation*. Elsevier Inc, pp. 141–163.
- Horne, R.N., Ramey Jr., H.J., 1978. Steam/water relative permeabilities from production data. *Geotherm. Resour. Council Trans.* 2, 291–293.

- Horne, R.N., Satman, A., Grant, M.A., 1980. Pressure transient analysis of geothermal wells with phase boundaries. In: Proceedings Second New Zealand Geothermal Workshop, Auckland, New Zealand.
- Horne, R.N., Guillot, A., Rosa, A., 1983. Computerized well test analysis to utilize simultaneous pressure and flowrate measurements. In: Proceedings of the Fifth New Zealand Geothermal Workshop, Auckland, New Zealand.
- Horner, D.R., 1951. Pressure build-up in wells. In: Third World Petroleum Congress.
- Houzé, O., Viturat, D., Fjaere, O., 2012. Dynamic Data Analysis: The Theory and Practice of Pressure Transient, Production Analysis, Well Performance Analysis, Production Logging and the Use of Permanent Downhole Gauge Data. KAPPA Engineering.
- Hudson, R.B., 1988. Technical and economic overview of geothermal atmospheric exhaust and condensing turbines, binary cycle and biphasic plant. *Geothermics* 17 (1), 51–74.
- Hulen, J.B., Norton, D.L., Moore, J.N., 2001. Initial insight into the nature, origin, configuration and thermal-chemical evolution of the Adilin steam reservoir, northwest Geysers steam field, California. *Geotherm. Resour. Council Trans.* 25, 345–352.
- Hulme, D., 2005. CBM Co-Produced Water Management, Disposal, Treatment and Use. Technical Report. <http://www.uwyo.edu/haub//_files/_docs/ruckelshaus/pubs/2005-cbm-water-management-hulme.pdf>.
- Hurley, N., Borehole Images in Asquith, A., Krygowski, D., 2004. Basic well Log Analysis, Methods in Exploration No. 16, second ed. The American Association of Petroleum Geologists, 0-89181-667-4pp. 151–163.
- Hurst, W., 1953. Establishment of the skin effect and its impediment to fluid flow into a wellbore. *Pet. Eng.* 25 (11), 6–16.
- Hyodo, M., Takasugi, S., 1995. Evaluation of the curve-fitting method and the Horner-plot method for estimation of the true formation temperature using temperature recovery logging data. In: Proceedings the 20th Workshop on Geothermal Reservoir Engineering, Stanford University, Stanford, CA.
- Ide, T., Yamazawa, S., Tosha, T., 2000. The development of a computerized pressure transient test system (Part 1). In: Proceedings 25th Workshop on Geothermal Reservoir Engineering, Stanford University, Stanford, CA.
- IGA-UNFC, 2016. Specifications for the Application of the United Nations Framework Classification for Fossil Energy and Mineral Reserves and Resources 2009 (UNFC-2009) to Geothermal Energy Resources. International Geothermal Association.
- Ingason, K., Kristjánsson, V., Einarsson, K., 2014. Design and development of the discharge system of IDDP-1. *Geothermics* 49, 58–65.
- Ishido, T., 1985. Pressure transient tests at the Okuaizu geothermal field in Japan. *Geotherm. Resour. Council Trans.* 9 (2), 521–526.
- Ishido, T., Kikuchi, T., Yano, Y., Miyazaki, Y., Nakao, S., Hatakeyama, K., 1992. Analysis of pressure transient data from the Sumikawa geothermal field. In: Proceedings 17th Workshop on Geothermal Reservoir Engineering, Stanford University, Stanford, CA.
- Jacobs, 2016. Geothermal Well Design and Drilling. Lecture notes to the University of Auckland Students by Jacobs Ltd.
- James, R., 1962. Steam-water critical through pipes. *Proc. Inst. Mech. Eng.* 176 (26), 741–748.
- James, R., 1980. Deductions of the character of steam-water wells from the shape of the output curve. In: Proceedings Second New Zealand Geothermal Workshop, Auckland, New Zealand.
- Jaupart, C., Labrosse, S., Mareschal, J.C., 2007. Temperatures, heat and energy in the mantle of the earth. *Treatise Geophys* 7, 253–303.
- Johannesson, Th., 2015. Low temperature geothermal wells. In: Lecture at the IGA academy, World Geothermal Congress, Melbourne, Australia.
- Juliusson, E., Gretarsson, G.J., Jonsson, P., 2007. Well tester 1.0b user's guide. In: Technical Report. ISOR, Reykjavik, Iceland.
- Kalfayan, L.J., 2008. Production Enhancement With Acid Stimulation. PennWell, Tulsa, OK.

- Kaspereit, K., Osborn, W.L., 2017. Improved test method for slim hole and microborer drilling. In: Proceedings 42nd Workshop on Geothermal Reservoir Engineering, Stanford University, Stanford, CA.
- Kaya, E., Zarrouk, S.J., 2017. Reinjection of greenhouse gases into geothermal reservoirs. *Int. J. Greenhouse Gas Control* 67, 111–129.
- Kaya, E., Zarrouk, S.J., O'Sullivan, M.J., 2011. Reinjection in geothermal fields: a review of worldwide experience. *Renew. Sustain. Energy Rev.* 15 (1), 47–68.
- Khasani, I.R., Zarrouk, S.J., 2015. The utilization of transient output measurement to characterize geothermal reservoir properties using AWTAS for well 2H-21 at Hatchobaru geothermal field, Japan. In: Proceeding World Geothermal Congress, Melbourne, Australia.
- Khosrawi, K., 2015. Geothermal resource assessment by well testing methods, case study on NW Sabalan geothermal field, Iran. In: Proceedings of the World Geothermal Congress, Melbourne, Australia.
- Killip, M., 1984. Report on the output test for bore 778. In: Ministry of Energy—Rotorua Geothermal Task Force, Tests 5&6.
- King, T.R., Robson, Q.J., 1998. The drilling history of Wiarakei. In: Proceedings of the 20th New Zealand Geothermal Workshop, Auckland, New Zealand.
- Kitao, K., Aiki, K., Hatakeyama, K., Wakita, K., 1990. Well stimulation using cold-water injection experiments in the Sumikawa geothermal field, Akita prefecture, Japan. *Geotherm. Resour. Council Trans.* 14 (2), 1219–1224.
- Kruger, P., 1995. Heat Extraction from HDR Geothermal Reservoirs. In: Proceedings the World Geothermal Congress, Florence, Italy.
- Kruger, P., Ramey Jr., H.J., 1979. Stimulation and reservoir engineering of geothermal resources. In: Second Annual Report, July 1, 1978–September 30, 1979 (SGP-TR-35), Technical Report, Stanford University Geothermal Program.
- Kukacka, L.E., Sugama, T., 1995. Lightweight CO₂-resistant cements for geothermal well completions. In: Proceedings of the World Geothermal Congress, Florence, Italy, pp. 1439–1444.
- Kusumah, M.W., 2014. Model of a Completion Test (Master's thesis). University of Auckland, New Zealand.
- Kutasov, I., Eppelbaum, L., 2005. An improved Horner method for determination of formation temperature. In: Proceedings the World Geothermal Congress, Turkey.
- Law, R., Batchelor, T., Ledingham, P., 2010. Revisiting deep geothermal power in the United Kingdom. In: Proceedings World Geothermal Congress, Bali, Indonesia.
- Lee, K.C., 2001. Classification of geothermal resources by exergy. *Geothermics* 30 (4), 431–442.
- Lee, C.H., Farmer, I.W., 1993. *Fluid Flow in Discontinuous Rocks*, first ed. Chapman and Hall, London; New York.
- Lee, Y., Park, S., Kim, J., Kim, H.C., Koo, M.H., 2010. Geothermal resource assessment for EGS in Korea. In: Proceedings World Geothermal Congress, Bali, Indonesia.
- Lehr, J.H., 1986. Underground injection—a positive advocate. In: Proceedings of the International Symposium on Subsurface Injection of Liquid Wastes, pp. 51–56.
- Lienau, P.J., Lund, J.W., 1991. Downhole heat exchanger technology being considered for electric power generation in Hawaii. *GHC Q. Bull.* 13 (4), 1–11.
- Llanos, E.M., Zarrouk, S.J., Hogarth, R., 2015. Simulation of the Habanero Geothermal Reservoir, Australia. *Geothermics* 53, 308–319.
- Lovelock, B.G., 2001. Steam flow measurement using alcohol tracers. *Geothermics* 30, 641–645.
- Lund, J.W., 2003. The use of down-hole heat exchangers. *Geothermics* 32, 535–543.
- Lund, J.W., Boyd, T., 2016. Direct utilization of geothermal energy 2015 worldwide review. *Geothermics* 60, 66–93.
- Luo, W., Tang, C., 2015. Pressure-transient analysis of multiwing fractures connected to a vertical wellbore. *SPE J.* 20 (02), 360–367.
- Malate, R.C.M., 2003. *Well Intervention Techniques*, Lectures at the Geothermal Training Programme. The United Nations University, Reykjavík, Iceland.

- Malate, R.C.M., Austria Jr., J.J.C., Sarmiento, Z.F., Di Lullo, G., Sookprasong, A., Francia, E.S., 1998. Matrix stimulation treatment of geothermal wells using sandstone acid. In: Proceedings 23rd Workshop on Geothermal Reservoir Engineering, Stanford University, Stanford, CA.
- Malibiran, M.A., Zarrouk, S.J., 2014. Modelling pre and post acid stimulation of well T4, Mt. Apo geothermal field, Philippines. In: Proceedings the 36th New Zealand Geothermal Workshop, Auckland, New Zealand.
- Massiot, C., McLean, K., McNamara, D., Sepulveda, F., Milicich, S., 2017. Discussion between a reservoir engineer and a geologist: permeability identification from completion test data and borehole image logs integration. In: Proceedings 39th New Zealand Geothermal Workshop, Rotorua, New Zealand.
- Matsunaga, I., Niitsuma, H., Oikawa, Y., 2005. Review of the HDR development at Hijiori Site, Japan. In: Proceedings World Geothermal Congress, Antalya, Turkey.
- Matthews, C.S., Russell, D.G., 1967. *Pressure Buildup and Flow Tests in Wells*, vol. 1. Society of Petroleum Engineers of AIME, Dallas, TX.
- Matthews, C.S., Brons, F., Hazebroek, P., 1954. A method for determination of average pressure in a bounded reservoir. *Trans. AIME* 201, 182–191.
- Mavor, M.J., Cinco-Ley, H., 1979. Transient pressure behaviour of naturally fractured reservoirs. In: Proceedings SPE Annual California Regional Meeting. SPE 7977-MS.
- McClure, M.W., Horne, R.N., 2011. Pressure transient analysis of fracture zone permeability at Soultz-sous-Fortks. *Geotherm. Resour. Council Trans.* 35, 1487–1498.
- McEdwards, D.G., Benson, S.M., 1981. User's Manual for ANALYZE, a Multiple-Well, Least Squares Matching Routine for Well-Test Analysis. Rept. LBL-10907. Lawrence Berkeley Laboratory, p. 70.
- McLaughlin, K.L., Barker, T.G., Owusu, L.A., Garg, S.K., 1995. DIAGNS: an interactive workstation-based system for well test data diagnostics and inversion. In: Proceedings of the World Geothermal Congress, Florence, Italy.
- McLean, K., McNamara, D., 2011. Fractures interpreted from acoustic formation imaging technology: correlation to permeability. In: Proceedings 36th Workshop on Geothermal Reservoir Engineering, Stanford University, Stanford, CA.
- McLean, K., Zarrouk, S.J., 2015a. Geothermal well test analysis using the pressure derivative: Some common issues and solutions. *Geothermics* 55, 108–125.
- McLean, K., Zarrouk, S.J., 2015b. Linear impermeable boundary in geothermal pressure transient analysis: a reservoir modelling assessment. In: Proceedings 37th New Zealand Geothermal Workshop, Taupo, New Zealand.
- McLean, K., Zarrouk, S.J., 2015c. Impact of cold water injection on geothermal pressure transient analysis: a reservoir modelling assessment. In: Proceedings 37th New Zealand Geothermal Workshop, Taupo, New Zealand.
- McLean, K., Zarrouk, S.J., 2017a. Pressure transient analysis of geothermal wells: a framework for numerical modelling. *Renew. Energy* 101, 737–746.
- McLean, K., Zarrouk, S.J., 2017b. Geothermal reservoir channel located by pressure transient analysis: a numerical simulation case study. *Geotherm. Resour. Council Trans.* 41, 2780–2797.
- McLean, K., Zarrouk, S.J., Wilson, D., 2016. Application of numerical methods for geothermal pressure transient analysis: a deflagration case study from New Zealand. In: Proceedings 41st Workshop on Geothermal Reservoir Engineering, Stanford University, Stanford, CA.
- McLean, K., McDowell, J.M., Sepulveda, F., Seastres, J., Zarrouk, S.J., Alcaraz, S., 2018. Upflow along a basement fault revealed by geothermal numerical pressure transient analysis. In: Proceedings 40th New Zealand Geothermal Workshop, Taupo, New Zealand.
- Menzies, A.J., 1979. Transient pressure testing. In: Proceedings the First New Zealand Geothermal Workshop, Auckland, New Zealand.
- Menzies, A.J., Antunez, E.U., Sanyal, S.K., Naka, T., Takeuchi, R., Iwata, S., et al., 1990. A case history of a multi-well interference test program at the Uenotai geothermal field, Akita prefecture, Japan. *Geotherm. Resour. Council Trans.* 14 (2), 1241–1248.
- Miller, C.W., 1980. *Wellbore User's Manual*. Lawrence Berkeley Laboratory, University of CA, p. 48p.

- Miller, C.C., Dyes, A.B., Hutchinson, C.A., 1950. The estimation of permeability and reservoir pressure from bottom hole pressure build-up characteristics. *J. Pet. Technol.* 2 (4), 91–104.
- Miller, C.W., Benson, S.M., O'Sullivan, M.J., Pruess, K., 1982. Wellbore effects in the analysis of two-phase geothermal well tests. *Soc. Pet. Eng. J.* 22 (3), 309–320.
- Moeck, I.S., 2014. Catalog of geothermal play types based on geologic controls. *Renew. Sustain. Energy Rev.* 37, 867–882.
- Moeck, I.S., Beardmore, G., Harvey, C.C., 2015. Cataloging worldwide developed geothermal systems by geothermal play type. In: *Proceedings of the World Geothermal Congress*, Melbourne, Australia.
- Moench, A.F., 1983. Well test analysis in naturally fissured, geothermal reservoirs with fracture skin. In: *Proceedings Ninth Workshop on Geothermal Reservoir Engineering*, Stanford University, Stanford, CA.
- Moench, A.F., Atkinson, P.G., 1978. Transient-pressure analysis in geothermal steam reservoirs with an immobile vaporizing liquid phase. *Geothermics* 7 (2–4), 253–264.
- Moench, A.F., Denlinger, R., 1980. Fissure-block model for transient pressure analysis in geothermal steam reservoirs. In: *Proceedings Sixth Workshop on Geothermal Reservoir Engineering*, Stanford University, Stanford, CA.
- Moench, A.F., Neri, G., 1979. Analysis of Gabbro 1: steam pressure buildup test. In: *Proceedings Fifth Workshop on Geothermal Reservoir Engineering*, Stanford University, Stanford, CA.
- Moore, J.N., Christenson, B.W., Browne, P.R.L., Lutz, S.J., 2002. The Mineralogic consequences and behavior of acid-sulphate waters: an example from the Karaha-Telaga Bodas geothermal system, Indonesia. In: *Workshop on Geothermal Reservoir Engineering*, Stanford University, Stanford, CA.
- Morente, C.P.P., 2013. Evaluation of acid stimulation experience of production wells at EDC. In: *Project Report for Postgraduate Certificate in Geothermal Energy Technology (Confidential Report)*. University of Auckland, New Zealand.
- Morin, R.H., Hickman, S.H., Barton, C.A., Shapiro, A.M., Benoit, W.R., Sass, J.H., 1998. Hydrologic properties of the Dixie Valley, Nevada, geothermal reservoir from well-test analyses. In: *Proceedings 23rd Workshop on Geothermal Reservoir Engineering*, Stanford University, Stanford, CA.
- Morita, K., Bollmeier-II, W.S., Mizogami-II, H., 1992. Analysis of the results from the downhole coaxial heat exchanger (DCHE) experiment in Hawaii. *Geotherm. Resour. Council Trans.* 16, 17–23.
- Morita, K., Makoto, T., Ehara, S., 2005. Case studies on small-scale power generation with the down-hole coaxial heat exchanger. In: *Proceedings of the World Geothermal Congress*, Antalya, Turkey.
- Mortensen, J.J., 1978. Hot dry rock: a new geothermal energy source. *Energy* 3 (5), 639–644.
- Mroczek, E., Milicich, S., Bixley, P., Sepulveda, F., Bertrand, E., Soengkono, S., et al., 2016. Ohaaki geothermal system: refinement of a conceptual reservoir model. *Geothermics* 59, 311–324.
- Mubarok, M.H., Zarrouk, S.J., 2017. Discharge stimulation of geothermal wells: overview and analysis. *Geothermics* 70, 17–37.
- Mubarok, M.H., Cahyono, Y.D., Patangke, S., Siahaan, E.E., 2015. A statistical analysis for comparison between lip pressure and separator in production well testing at Lahendong and Ulubelu field. In: *Proceedings of the World Geothermal Congress*, Melbourne, Australia.
- Mubarok, M.H., Zarrouk, S.J., Cater, J.E., 2019. Two-phase flow measurement of geothermal fluid using orifice plate: field testing and CFD validation. *Renew. Energy* 134, 927–946.
- Muffler, P., Cataldi, R., 1978. Methods for regional assessment of geothermal resources. *Geothermics* 7, 53–89.
- Mulyadi, 2010. Case study: hydraulic fracturing experience in the Wayang Windu geothermal field. In: *Proceedings of the World Geothermal Congress*, Bali, Indonesia.
- Murphy, H., Brown, D., Jung, R., Matsunaga, I., Parker, R., 1999. Hydraulics and well testing of engineered geothermal reservoirs. *Geothermics* 28, 491–506.
- Murray, L., Gunn, C., 1993. Toward integrating geothermal reservoir and wellbore simulation: TETRAD and WELLSIM. In: *Proceedings 15th New Zealand Geothermal Workshop*, Auckland, New Zealand.
- Muskat, M., 1937. Use of data on the build-up of bottom-hole pressures. *Trans. AIME Soc. Pet. Eng.* 44–48.

- Nakao, S., Ishido, T., 1998. Pressure-transient behavior during cold water injection into geothermal wells. *Geothermics* 27 (4), 401–413.
- Narasimhan, T.N., Witherspoon, P.A., 1979. Geothermal well testing. *J. Hydrol.* 43 (1), 537–553.
- Newton, C.J., Zarrouk, S.J., Lawless, J., Rowe, M.C., Guidos, J.A., Brown, K.L., 2018. Aluminum-rich silica scaling: San Jacinto-Tizate geothermal power project, Nicaragua. In: Proceedings the 40th New Zealand Geothermal Workshop, Taupo, New Zealand.
- Nielson, D.L., Garg, S.K., 2016. Slim hole reservoir characterization for risk reduction. In: Proceedings 41st Workshop on Geothermal Reservoir Engineering, Stanford University, Stanford, CA.
- Niyazi, A., 2007. Optimization of downhole pump setting depths in liquid dominated geothermal systems: a case study on the Balcova-Narlidere field, Turkey. *Geothermics* 36, 436–458.
- Nogara, J., Zarrouk, S.J., 2018b. Corrosion in geothermal environment: Part 2: Metals and alloys. *Renew. Sustain. Energy Rev.* 82 (1), 1347–1363.
- Nogara, J., Zarrouk, S.J., 2018a. Corrosion in geothermal environment: Part 1: Fluids and their impact. *Renew. Sustain. Energy Rev.* 82 (1), 1333–1346.
- Nogara, J., Zarrouk, S.J., Seastres, J., 2018. Surface analysis of metal alloys exposed to geothermal fluids with high non-condensable gas content. *Geothermics* 72, 372–399.
- Nugroho, S.I., Hendriana, S., 2018. Production improvement through scale removal by Jetwash, Kamojang geothermal field. In: Proceedings 40th New Zealand Geothermal Workshop, 14–16 November 2018, Taupo, New Zealand.
- NZS 2403, 2015. New Zealand Standards, Code of Practice for Deep Geothermal Wells.
- Ocampo-Diaz, J.D.D., Valdez-Salaz, B., Shorr, M., Saucedo-M, I., Rosas-Gonzalez, N., 2005. Review of corrosion and scaling problems in Cerro Prieto geothermal field over 31 years of commercial operations. In: Proceedings of the World Geothermal Congress, Antalya, Turkey.
- Odeh, A.S., Jones, L.G., 1965. Pressure drawdown analysis, variable-rate case. *J. Pet. Technol.* 17 (8), 960–964.
- Ohren, M., Benoit, D., Kumataka, M., Morrison, M., 2011. Permeability recovery and enhancements in the Soda Lake geothermal field, Fallon, Nevada. *Geotherm. Resour. Council Trans.* 35, 493–497.
- Okandan, E., Ongen, J., Arpacı, M., 1988. Transient behavior in fractured media with zero matrix permeability. In: Proceedings 13th Workshop on Geothermal Reservoir Engineering, Stanford University, Stanford, CA.
- Onur, M., 2010. Analysis of Well Tests in Afyon Ömer-Gecek geothermal field, Turkey. In: Proceedings of the World Geothermal Congress, Bali, Indonesia.
- Onur, M., Aksoy, N., Serpen, U., Satman, A., 2002. Analysis of pressure transient tests in Balcova-Narlidere geothermal field. *Turkey J. Oil Gas* 8, 20–36.
- Onur, M., Zeybek, A.D., Serpen, U., Gok, I.M., 2003. Application of modern well test analysis techniques to pressure transient tests in Kizildere geothermal field, Turkey. *Geothermics* 32 (2), 147–170.
- Osborn, W.L., Spielman, P., 1995. Measurement of velocity profiles in production wells using wireline spinner surveys and rhodamine WT fluorescent tracer; Coso geothermal field (California). In: Proceedings of the World Geothermal Congress, Florence, Italy.
- O’Sullivan, M.J., 1981. A similarity method for geothermal well test analysis. *Water Resour. Res.* 17 (2), 390–398.
- O’Sullivan, M.J., 1985. Geothermal reservoir simulation. *Int. J. Energy Res.* 9 (3), 319–332.
- O’Sullivan, M.J., 1987. Aspects of geothermal well test analysis in fractured reservoirs. *Transp. Porous Media* 2 (5), 497–517.
- O’Sullivan, M.J., O’Sullivan, J.P., 2016. Reservoir modeling and simulation for geothermal resource characterization and evaluation. In: DiPippo, R. (Ed.), *Geothermal Power Generation: Developments and Innovation*. Elsevier Inc, pp. 165–199.
- O’Sullivan, M.J., Pruess, K., 1980. Analysis of injection testing of geothermal reservoirs. *Geotherm. Resour. Council Trans.* 4, 401–404.
- O’Sullivan, M.J., Croucher, A.E., Anderson, E.B., Kikuchi, T., Nakagome, O., 2005. An automated well-test analysis system (AWTAS). *Geothermics* 34 (1), 3–25.
- Palmer, I., 2010. Coalbed methane completions: a world view. *Int. J. Coal Geol.* 82 (3–4), 184–195.

- Patsa, E., Van Zyl, D., Zarrouk, S.J., Arianpoo, N., 2015. Geothermal energy in mining developments: Synergies and opportunities throughout a mine's operational life cycle. In: Proceeding World Geothermal Congress. Melbourne, Australia.
- Perrine, R.L., 1956. Analysis of pressure-buildup curves. *Drilling and Production Practice*. American Petroleum Institute, pp. 482–509, Report No. API-56-482.
- Pine, R.J., 1983. Pressure transient analysis for large scale hydraulic injections in the Carnmenellis Granite, England. In: Proceedings Ninth Workshop Geothermal Reservoir Engineering, Stanford University, Stanford, CA.
- Porkhial, S., Abdollahzadeh, F., Radmehr, B., Sefid, P.J., 2015. Interpretation of the injection and heat up tests at Sabalan geothermal field, Iran. In: Proceedings of the World Geothermal Congress, Melbourne, Australia.
- Portier, S., André, L., Vuataz, F.D., 2007. Review on Chemical Stimulation Techniques in Oil Industry and Applications to Geothermal Systems. Deep Heat Mining Association, DHMA, Switzerland.
- Portier, S., Vuataz, F.-D., Nami, P., Sanjuan, B., Gérard, A., 2009. Chemical stimulation techniques for geothermal wells: experiments on the three-well EGS system at Soultz-sous-Forêts, France. *Geothermics* 38 (4), 349–359.
- Pruess, K., 1991. TOUGH2: A general-purpose numerical simulator for multiphase fluid and heat flow. In: Lawrence Berkeley Report No. LBL-29400. Berkeley, CA.
- Pruess, K., 2006. Enhanced geothermal systems (EGS) using CO₂ as working fluid—a novel approach for generating renewable energy with simultaneous sequestration of carbon. *Geothermics* 35, 351–367.
- Pruess, K., Eneidy, S., 1993. Numerical modeling of injection experiments at the geysers. In: Proceedings 18th Workshop on Geothermal Reservoir Engineering, Stanford University, Stanford, CA.
- Pruess, K., Narasimhan, T., 1985. A practical method for modelling fluid and heat flow in fractured porous media. *J. Soc. Pet. Eng.* 25 (1), 14–26.
- Putriyana, L., Syihab, Z., 2013. Interpretation of well test analysis for reservoir simulation with a dual porosity model. In: Proceedings 35th New Zealand Geothermal Workshop.
- Quinao, J.J., Zarrouk, S.J., 2018. Geothermal resource assessment using experimental design and response surface methods: the Ngatamariki geothermal field, New Zealand. *Renew. Energy* 116, 324–334.
- Quinao, J.J., Singer, M., Askari, M., Azwar, L., Hall, M., Ahsan, S., 2015. Well testing and modelling of discharging big bore and 'super' big bore wells. In: Proceeding World Geothermal Congress, Melbourne, Australia.
- Raghavan, R., 1976. Well test analysis: wells producing by solution gas drive. *Soc. Pet. Eng. J.* 16 (4), 196–208.
- Rahman, S.S., 1989. Cement slurry system for controlling external casing corrosion opposite fractured and vugular formations saturated with corrosive water. *J. Pet. Sci. Eng.* 3, 255–265.
- Raman, N., Lapanji, A., Prestor, J., O'Sullivan, M.J., Brencic, M., 2015. Effects of regional production of thermal water on low-temperature geothermal aquifers in North-East Slovenia. In: Proceedings World Geothermal Congress, Melbourne, Australia.
- Ramey Jr., H.J., 1965. Non-Darcy flow and wellbore storage effects in pressure build-up and drawdown of gas wells. *J. Pet. Technol.* 17 (2), 223–233.
- Ramey Jr., H.J., 1970. Short-time well test data interpretation in the presence of skin effect and wellbore storage. *J. Petrol. Technol.* 22 (01), 97–104.
- Ramey Jr., H.J., 1975. Pressure transient analysis for geothermal wells. In: Proceedings of the Second UN Symposium on the Development and Use of Geothermal Resources, pp. 1749–1757.
- Ramey Jr., H.J., Horne, R.N., Miller, F.G., Brigham, W.E., 1980. Well test analysis research. In: Proceedings Sixth Workshop on Geothermal Reservoir Engineering, Stanford University, Stanford, CA.
- Ramos, S.G., 2002. Potential constraints to the development of the Rangas sector based on petrologic evaluation of the Bacman geothermal field, Philippines. In: Proceedings, 27th Workshop on geothermal reservoir engineering, Stanford University, Stanford, CA.
- Ravier, G., Graff, J.J., Villadangos, G., 2015. Operating a lineshaft production pump in a small pump chamber under highly aggressive geothermal fluid conditions: results from the Soultz EGS site. In: Proceedings, World Geothermal Congress, Melbourne, Australia.

- Reinicke, A., Rybacki, E., Stanchits, S., Huenges, E., Dresen, G., 2010. Hydraulic fracturing stimulation techniques and formation damage mechanisms—implications from laboratory testing of tight sandstone–proppant systems. *Chem. Erde Geochem.* 70 (3), 107–117.
- Riffault, J., 2014. Modelling of the Injection of Cold Water Into a Hot Reservoir (Master's thesis). University of Auckland, New Zealand.
- Rigby, F.A., 1979. Thermodynamics of geothermal hybrid binary cycles. *Geotherm. Resour. Council Trans.* 3, 573–576.
- Riney, T.D., Garg, S.K., 1985a. Geopressured geothermal design well test results. *Geotherm. Resour. Council Trans.* 9 (II), 565–568.
- Riney, T.D., Garg, S.K., 1985b. Pressure buildup analysis for two-phase geothermal wells: application to the Baca geothermal field. *Water Resour. Res.* 21 (3), 372–382.
- Rivera R.J., Ramey Jr., H.J., 1977. Application of two-rate flow tests to the determination of geothermal reservoir parameters. In: *SPE Annual Fall Technical Conference and Exhibition*. SPE 6887-MS.
- Rivera, R.J., Samaniego, V.F., Schroeder, R.C., 1980. Pressure transient testing at Cerro Prieto geothermal field. *Geothermics* 9 (1), 189–196.
- Rizaldy, R., Zarruk, S.J., 2016. Pressure drop in large diameter geothermal two-phase pipelines. In: *Proceedings the 38th New Zealand Geothermal Workshop*, Auckland, New Zealand.
- Rosa, A., Horne, R.N., 1983. Automated type curve matching in well test analysis using Laplace space determination of parameter gradients. In: *Proceedings of SPE Annual Fall Meeting*, CA. SPE 12131-MS.
- Rose, P., Sheridan, J., McCulloch, J., Moore, J.N., Kovac, K., Weidler, R., et al., 2005. An enhanced geothermal system at Coso, California—recent accomplishments. In: *Proceedings World Geothermal Congress*, Antalya, Turkey.
- Rosell, J.B., Ramos, S.G., 1998. Origin of acid fluids in the Cawayan sector Bacman Geothermal Production Field. In: *Proc. 23rd Workshop on Geothermal Reservoir Engineering*. Stanford University, Stanford, CA.
- Rosen, M.A., Koohi-Foyegh, S., 2017. *Geothermal Energy: Sustainable Heating and Cooling Using the Ground*. John Wiley & Sons, Inc, United Kingdom.
- Roux, B., Sanyal, S.K., Brown, S., 1979. An improved approach to estimating true reservoir temperature from transient temperature data. In: *Proceedings Fourth Workshop on Geothermal Reservoir Engineering*, Stanford University, Stanford, CA.
- Rowland, J., Sibson, R., 2004. Structural controls on hydrothermal flow in a segmented rift system, Taupo Volcanic Zone, New Zealand. *Geofluids* 4, 259–283.
- Rudesill, J.M., 1978. A case history, completion of a shallow over-pressured geothermal well. *Geotherm. Resour. Council Trans.* 2, 587–590.
- Rummel, F., Kappelmeyer, O., 1982. The Falkenberg Geothermal Frac-Project: concepts and experimental results. In: *Proceedings of the First Japan–United States Joint Seminar on Hydraulic Fracturing and Geothermal Energy*, Tokyo, Japan.
- Russell, D.G., 1963. Determination of formation characteristics from two-rate flow tests. *J. Pet. Technol.* 15 (12), 1347–1355.
- Rybach, L., 1981. Geothermal systems, conductive heat flow, geothermal anomalies. In: Rybach, L., Muffler, L.J.P. (Eds.), *Geothermal Systems: Principles and Case Histories*. John Wiley, New York, pp. 3–36.
- Sageev, A., Horne, R.N., 1983. Drawdown pressure transient analysis of a well near a steam cap. *Geotherm. Resour. Council Trans.* 7, 473–476.
- Samaniego, V.F., Villalobos, L.H., 2003. Transient pressure analysis of pressure-dependent naturally fractured reservoirs. *J. Pet. Sci. Eng.* 39 (1), 45–56.
- Sandvik, 2018. Sandvik SAF 2507 for Wirelines, Materials Datasheet.
- Sanjuan, B., Lasne, E., Brach, M., 2000. Bouillante geothermal field (Guadalupe West Indies): geochemical monitoring during thermal stimulation operation. In: *25th Workshop on Geothermal Reservoir Engineering*, Stanford University, Stanford, CA.
- Sanjuan, B., Scheiber, J., Gal, F.; Touzelet, S., Genter, A., Villadangos, G., 2016. Inter-well chemical tracer testing at the Rittershoffen geothermal site (Alsace, France). In: *European Geothermal Congress*, Strasbourg, France.

- Sanyal, S.K., 2005. Classification of geothermal systems—a possible scheme. In: Proceedings 30th Workshop on Geothermal Reservoir Engineering, Stanford University, Stanford, CA.
- Sanyal, S.K., Granados, E.E., Brown, P.J., Hallberg, J., Menteshashvili, Z., Bachakashvili, D., et al., 2000. Results of a comprehensive well test program to assess the Zugdidi-Tsaishi geothermal field, Republic of Georgia. In: Proceedings of the World Geothermal Congress, Kyushu-Tohoku, Japan.
- Sarmiento, Z.F., 2011. Application of Well Testing in Assessing Geothermal Resources. Paper Presented at Short Course on Geothermal Drilling, Resource Development and Power Plants, San Tecla, El Salvador.
- Schindler, M., Nami, P., Schellschmidt, R., Teza, D., Tischner, T., 2008. Summary of hydraulic stimulation operations in the 5 km deep crystalline HDR-EGS reservoir at Soultz-sous-Forets. In: 33rd Workshop on Geothermal Reservoir Engineering, Stanford University, Stanford, CA.
- Sepulveda, F., Andrews, J., Kim, J., Siega, C., Milloy, S.F., 2015. Spatial-temporal characteristics of micro-seismicity (2009-2014) of the Wairakei geothermal field, New Zealand. In: Proceedings, World Geothermal Congress, Melbourne, Australia.
- Sepulveda, F., Siega, C., Lin, Y.W., Urgel, A., Boese, C., 2016. Observations of deep and shallow seismicity within the Wairakei-Tauhara Geothermal System. In: Proceedings the 38th New Zealand Geothermal Workshop, Auckland, New Zealand.
- Seto, S., 2014. Transient Flow in a Geothermal Well (Master's thesis). University of Auckland, New Zealand.
- Siega, C.H., Grant, M.A., Powel, T., 2009. Enhancing injection well performance by cold water stimulation in Rotokawa and Kawerau geothermal fields. In: 30th Annual EDC Geothermal Conference, Manila, Philippines.
- Siega, C., Grant, M.A., Bixley, P.F., Mannington, W., 2014. Quantifying the effect of temperature on well injectivity. In: Proceedings 36th New Zealand Geothermal Workshop, Auckland, New Zealand.
- Sigurdsson, O., 2015. Experimenting with deflagration for stimulating geothermal wells. In: Proceedings, World Geothermal Congress, Melbourne, Australia.
- Simatupang, C.H., Intani, R.G., Suryanta, M.R., Irfan, R., Golla, G. Cease, C., et al., 2015. Evaluation of water produced from a steam dominated system, a case study from the Darajat field. In: Proceedings, World Geothermal Congress, Melbourne, Australia.
- Sisler, J.R., Zarrouk, S.J., Adams, R., 2015. Improving the performance of geothermal pressure, temperature and spinner (PTS) tools used in down-hole measurements. In: Proceedings, World Geothermal Congress, Melbourne, Australia.
- Skiba, P.A., 1985. Artesian flow testing of the geothermal production wells WEN-1 and WEN-2, Honey lake hybrid power plant project, California. *Geotherm. Resour. Council Trans.* 9, 585–589.
- Sliaupa, S., Motuza, G., Korabliova, L., Ciuraitė, K., Purnas, V., 2010. Geothermal potential of hot granites of Lithuania. In: Proceedings World Geothermal Congress, Bali, Indonesia.
- Snyder, R.E., 1979. Casing failure modes in geothermal wells. *Geotherm. Resour. Council Trans.* 3, 667–670.
- Spivey, J.P., Lee, W.J., 2000. Pressure transient response for a naturally fractured reservoir with a distribution of block sizes. In: SPE Rocky Mountain Regional/Low-Permeability Reservoirs Symposium and Exhibition, SPE-60294-MS.
- Sta Ana, F.X.M., 1985. A study on stimulation by air compression on some of the Philippine geothermal wells. In: Project for Diploma in Energy Technology (Geothermal). Geothermal Institute, The University of Auckland, New Zealand.
- Sta Ana, F.X.M., Hingoyon-Siega C.S., Andrino, R.P., 2002. Mahanagdong geothermal sector, great Tongonon field, Philippines: reservoir evaluation and modelling update. In: Proceedings, 27th Workshop on Geothermal Reservoir Engineering, Stanford University, Stanford, CA.
- Standards New Zealand, 2015. Code of Practice for Deep Geothermal Wells (NZS2403:2015). Standards New Zealand, Wellington, NZ.
- Steins, C., Zarrouk, S.J., 2012. Assessment of the geothermal space heating system at Rotorua Hospital, New Zealand. *Convers. Energy Manage.* 55, 60–70.

- Steins, C., Bloomer, A., Zarrouk, S.J., 2012. Improving the performance of the down-hole heat exchanger at the Alpine Motel, Rotorua, New Zealand. *Geothermics* 44, 1–12.
- Stephens, G., Voight, B., 1982. Hydraulic fracturing theory for conditions of thermal stress. *Int. J. Rock Mech. Min. Sci. Geomech. Abstr.* 19 (6), 279–284.
- Stevens, L., 2000. Monitoring of casing integrity in geothermal wells. In: *Proceedings, World Geothermal Congress, Paper R0253*.
- Sugiama, F., Sunio, E., Mollin, P., Stimac, J., 2004. Geochemical response to production of the Tiwi geothermal field, Philippines. *Geothermics* 33, 57–86.
- Sutherland, R., Townend, J., Toy, T., Upton, Ph, Coussens, J., Allen, M., et al., 2017. Extreme hydro-thermal conditions at an active plate-bounding fault. *Nature* 546 (7656), 137–140.
- Talabani, S., Atlas, B., Al-Khatiri, M.B., Islam, M.R., 2000. An alternate approach to downhole corrosion mitigation. *J. Pet. Sci. Eng.* 26, 41–48.
- Tambini, M., 2003. Beyond acidizing and fracturing. In: *SPE European Formation Damage Conference*. The Hague, Netherlands, SPE 82573-MS.
- Tateno, M., Watanabe, K., Nakatsuka, K., Takahashi, H., 1995. Fractal characterization of the fracture distribution and the permeability in geothermal reservoirs. In: *Proceedings of the World Geothermal Congress, Florence, Italy*.
- Templeton, J.D., Ghoreishi-Madiseh, S.A., Hassani, F., Al-Khawaja, M.J., 2014. *Energy* 70, 366–373.
- Thain, I., DiPippo, R., 2015. Hybrid geothermal-biomass power plants: applications, designs and performance analysis. In: *Proceedings, World Geothermal Congress, Melbourne, Australia*.
- Thain, I., Reyes, A., Hunt, T., 2006. A Practical Guide to Exploiting Low Temperature Geothermal Resources. Technical Report. Institute of Geological and Nuclear Sciences Limited, Lower Hutt. Available from: https://datospdf.com/download/a-practical-guide-to-exploiting-low-temperature-geothermal-resources-_5a4b94d5b7d7bcb74fbbdc50_pdf.
- Thakur, G.C., Satter, A., 1998. *Integrated Waterflood Asset Management*. PennWell Books, Tulsa, OK.
- Theis, C.V., 1935. The relation between the lowering of the piezometric surface and the rate and duration of discharge of a well using ground-water storage. *Trans. Am. Geophys. Union* 16 (2), 519–524.
- Thomas, R., 2003. Titanium in the geothermal industry. *Geothermics* 32, 679–687.
- Thorhallsson, S., 2003. Geothermal well operation and maintenance. In: *IGC2003-Short Course, Geothermal Training Programme, Orkustofnun, Grensasvegur 9, IS-108 Reykjavik, Iceland*.
- Tiangco, V., McCluuar, P., Hughes, E., 1996. Investigation of geothermal energy technologies and gas turbine hybrid systems. *Geotherm. Resour. Council Trans.* 20, 195–201.
- Toth, A.N., 2010. Steam blowout from an over-pressured geothermal reservoir in Hungary. *Geotherm. Resour. Council Trans.* 34, 211–213.
- Toth, A.N., Szucs, P., Pap, J., Nyikos, A., Fenerty, D.K., 2018. Converting abandoned Hungarian oil and gas wells into geothermal sources. In: *Proceedings, 43rd Workshop on Geothermal Reservoir Engineering, Stanford University, Stanford, CA*.
- Tsang, Y.W., Tsang, C.F., 1978. *An Analytic Study of Geothermal Reservoir Pressure Response to Cold Water Reinjection*. Lawrence Berkeley Laboratory.
- UNFC, 2009. *United Nations Framework Classification for Fossil Energy and Mineral Reserves and Resources 2009*. United Nations.
- United States Energy Information Administration (USEIA), 2017. Primary Energy Overview. <http://www.eia.gov/beta/MER>.
- Valdes-Perez, A.R., Pulido, H., Cinco-Ley, H., Larsen, L., 2013. A new double porosity fractal model for well test analysis with transient interporosity transference for petroleum and geothermal systems. In: *Proceedings 38th Workshop on Geothermal Reservoir Engineering, Stanford University, Stanford, CA*.
- Van der Baan, M., Eaton, D.W., Rreisig, G., 2016. Stick-split mechanism for anthropogenic fluid-induced tensile rock failure. *Geol. Soc. Am.* 4 (7), 503–506. Available from: <https://sites.ualberta.ca/~vanderba/papers/VEP16.pdf>.
- van Everdingen, A.F., 1953. The skin effect and its influence on the productive capacity of a well. *Trans. J. Pet. Technol.* 5 (6), 171–176.

- van Everdingen, A.F., Hurst, W., 1949. The application of the Laplace transformation to flow problems in reservoirs. *J. Pet. Technol.* 1 (12), 305–324.
- Varney, J., Zarrouk, S.J., Bean, N., Bendall, B., 2017. Performance measures in geothermal power developments. *Renew. Energy* 101, 835–844.
- Vernier, R., Laplaige, P., Desplan, A., Boissavy, C., 2015. France country update. In: Proceedings the World Geothermal Congress, Melbourne, Australia.
- Villacorte, J.D., O'Sullivan, M.J., 2011. A numerical study of the effects of cold water injection on the pressure transient response and injection capacity of geothermal wells. In: Proceedings 33rd New Zealand Geothermal Workshop, Auckland, New Zealand.
- Vinsome, P.K.W., 1991. *TETRAD User's Manual*. Dyad Engineering, Calgary, AB, Canada.
- Vosteen, H.-D., Schellschmidt, R., 2003. Influence of temperature on thermal conductivity, thermal capacity and thermal diffusivity for different types of rock. *Phys. Chem. Earth, Parts A/B/C* 28 (9), 499–509.
- Wallis, I.C., Rowland, J.V., Cumming, W., Dempsey, D., 2017. The subsurface geometry of a natural geothermal reservoir. In: Proceedings 39th New Zealand Geothermal Workshop, Rotorua, New Zealand.
- Warner, D.L., 1977. *An Introduction to the Technology of Subsurface Wastewater Injection*. Municipal Environmental Research Laboratory, Office of Research and Development, US Environmental Protection Agency, EPA/600/2-77/240.
- Warpinski, N.R., 1991. Hydraulic fracturing in tight, fissured media. *SPE J. Pet. Technol.* 43 (02), 146–151.
- Warren, J.E., Root, P.J., 1963. The behavior of naturally fractured reservoirs. *Soc. Pet. Eng. J.* 3 (03), 245–255.
- Watson, A., 2013. *Geothermal Engineering*. Springer, New York.
- Wattenbarger, R.A., Ramey Jr., H.J., 1968. Gas well testing with turbulence, damage and wellbore storage. *J. Pet. Technol.* 20 (8), 877–887.
- Weller, W.T., 1966. Reservoir performance during two-phase flow. *J. Pet. Technol.* 18 (2), 240–246.
- Wibowo, D.J.S., Nordquist, G.A., Stimac J., Suminar, A., 2010. Monitoring microseismicity during well stimulation at the Salak geothermal field, Indonesia. In: Proceedings World Geothermal Congress, Bali, Indonesia.
- Williams, R., Erstich, E., Diaz, A.R., 2016. High temperature casing condition – multi finger (HTCC-MF) tool. In: Proceedings the 38th NZ Geothermal Workshop, Auckland, New Zealand.
- Wilson, D., Gilliland, J., Austin, A., 2015. Broaching, an effective method of wireline intervention for calcite scale removal. In: Proceeding World Geothermal Congress, Melbourne, Australia.
- Wolfgang, M., Bloch, T., Bartels, J., Heuberger, S., Kuhn, P., Naef, H., et al., 2015. Reservoir-geological characterization of a fractured limestone: results obtained from the Geothermal Well St. Gallen GT-1 (Switzerland). In: Proceedings of the World Geothermal Congress, Melbourne, Australia.
- Wu, Y.-S., 2000. Numerical simulation of non-Darcy flow in porous and fractured media. *Geotherm. Resour. Council Trans.* 24, 641–646.
- Wyborn, D., de Graaf, L., Davidson, S., Hann, S., 2005. Development of Australia's first hot fractured rock (HFR) underground heat exchanger, cooper basin, South Australia. In: Proceedings World Geothermal Congress, Antalya, Turkey.
- Yalniz, M.U., 1997. Preliminary interference measurement at Te-Aroha using capillary tubing. In: Diploma in Geothermal Energy Technology Project. The University of Auckland, No. 1997-30.
- Yanagisawa, N., Muraoka, H., Sasaki, M., Sugita, H., Sato, M., Osato, K., 2013. Geochemical properties of geo-pressured reservoir for binary system. In: Proceedings the 35th NZ Geothermal Workshop, Rotorua, New Zealand.
- Yoshioka, K., Pasikki, R.G., Suryata, I., Riedel, K.L., 2009. Hydraulic stimulation techniques applied to injection wells at the Salak geothermal field, Indonesia. SPE Western Regional Meeting, San Jose, CA. SPE 121184-MS.
- Zarrouk, S.J., 2004. External casing corrosion in New Zealand Geothermal Wells. In: Proceedings of the 26th New Zealand Geothermal Workshop, Taupo, New Zealand.

- Zarrouk, S.J., 2008. *Reacting Flows in Porous Media: Complex Multi-Phase, Multi-Component Simulation*. VDM Verlag Dr. Müller, ISBN-10: 3639099850.
- Zarrouk, S.J., 2017. Postgraduate geothermal energy education worldwide and the New Zealand experience. *Geothermics* 70, 173–180.
- Zarrouk, S.J., Moon, H., 2014. Efficiency of geothermal power plants: a worldwide review. *Geothermics* 51, 142–153.
- Zarrouk, S.J., Moon, H., 2015. Response to the Comments by Ronald DiPippo on “Efficiency of geothermal power plants: a worldwide review”. *Geothermics* 53, 550–553.
- Zarrouk S.J., Moore T., 2007. Preliminary assessment of the geothermal signature and ECBM potential of the Huntly Coal bed methane field, New Zealand. In: *Proceedings the 29th NZ Geothermal Workshop*, Auckland, New Zealand.
- Zarrouk, S.J., Purnanto, M.H., 2015. Geothermal steam-water separator: a design overview. *Geothermics* 53, 236–254.
- Zarrouk, S.J., Simiyu, F., 2013. A review of geothermal resource estimation methodology. In: *Proceedings the 35th NZ Geothermal Workshop*, Rotorua, New Zealand.
- Zarrouk, S.J., O’Sullivan, M., Croucher, A., Mannington, W., 2007. Numerical modelling of production from the Poihipi dry steam zone: Wairakei geothermal system, New Zealand. *Geothermics* 36 (4), 289–303.
- Zarrouk, S.J., Woodhurst, B.C., Morris, C., 2014. Silica scaling in geothermal heat exchangers and its impact on pressure drop and performance: Wairakei Binary Plant, New Zealand. *Geothermics* 51, 445–459.
- Zenz, F.A., 1993. Explore the potential of airlift pumps and multiphase. *Chem. Eng. Prog.* 89, 51–56.
- Zhang, J., Xing, H., 2012. Numerical modeling of non-Darcy flow in near-well region of a geothermal reservoir. *Geothermics* 42, 78–86.
- Zyvoloski, G., 1982. Non-Darcy flow in geothermal reservoirs. *Geotherm. Resour. Council Trans.* 6, 325–328.
- Zyvoloski, G., 2007. FEHM: A Control Volume Finite Element Code for Simulating Subsurface Multi-Phase Multi-Fluid Heat and Mass Transfer. Document: LAUR-07-3359. Technical Report. Los Alamos National Laboratory.

